

**University of Alberta**

Alkali Metal C<sub>1</sub>-C<sub>12</sub> n-alkanoates

by

Ly Huong Bui

A thesis submitted to the Faculty of Graduate Studies and Research  
in partial fulfillment of the requirements for the degree of

Master of Science

in

Chemical Engineering

Department of Chemical and Materials Engineering

©Ly Huong Bui

Spring 2013

Edmonton, Alberta

Permission is hereby granted to the University of Alberta Libraries to reproduce single copies of this thesis and to lend or sell such copies for private, scholarly or scientific research purposes only. Where the thesis is converted to, or otherwise made available in digital form, the University of Alberta will advise potential users of the thesis of these terms.

The author reserves all other publication and other rights in association with the copyright in the thesis and, except as herein before provided, neither the thesis nor any substantial portion thereof may be printed or otherwise reproduced in any material form whatsoever without the author's prior written permission.

## **ABSTRACT**

Phase transitions of the alkali metal carboxylates have been explored by many researchers. A fair amount of scatter can also be observed in the published data. The aim of this study was to systematically study the thermal behavior of lithium, sodium, potassium, cesium and rubidium carboxylates, although only lithium, sodium and potassium carboxylates are industrially relevant. The success of the synthesis and purification of the carboxylates were confirmed by the infrared spectroscopy. The carboxylates were pure enough for further thermal study. Thermal analyses were performed using the cryogenic differential scanning calorimeter and the thermogravimetric analyzer. The nature of transition phases were investigated by microscopic differential scanning calorimeter. A critical evaluation of the present data in relation to literature values is included.

## TABLE OF CONTENTS

1. Introduction .....	1
2. Lithium C <sub>1</sub> -C <sub>12</sub> <i>n</i> -alkanoates: Thermal behavior from –30 to 600 °C .....	3
3. Sodium C <sub>1</sub> -C <sub>12</sub> <i>n</i> -alkanoates: Thermal behavior from –30 to 600 °C .....	20
4. Potassium C <sub>1</sub> -C <sub>12</sub> <i>n</i> -alkanoates: Thermal behavior from –30 to 600 °C.....	33
5. Rubidium C <sub>1</sub> -C <sub>12</sub> <i>n</i> -alkanoates: Thermal behavior from –30 to 600 °C.....	45
6. Cesium C <sub>1</sub> -C <sub>12</sub> <i>n</i> -alkanoates: Thermal behavior from –30 to 600 °C.....	56
7. Conclusions and Recommendations .....	67
References .....	70
Supporting Information .....	73

## LIST OF FIGURES

FIGURE 2-1. METAL CARBOXYLATE BONDING CONFIGURATIONS (I) IONIC (II) MONODENTATE (III) BIDENTATE (IV) BRIDGING <sup>19</sup> .....	8
FIGURE 2-2 INFRARED SPECTRUM OF LITHIUM UNDECANOATE IN THE WAVENUMBER RANGE 1350-1650 CM <sup>-1</sup> BEFORE AND AFTER HEATING TO 300 °C SHOWING THE PERSISTENCE OF SPLITTING OF THE CARBOXYLATE ABSORPTION. ....	9
FIGURE 2-3. RAMAN SPECTRUM OF LITHIUM UNDECANOATE IN THE WAVENUMBER RANGE 1350-1650 CM <sup>-1</sup> SHOWING SPLITTING OF THE CARBOXYLATE ABSORPTION.....	10
FIGURE 2-4 INFRARED SPECTRUM OF THE SOLID RESIDUE AFTER THERMAL DECOMPOSITION OF LITHIUM UNDECANOATE AND THAT OF LITHIUM CARBONATE SHOWED FOR COMPARISON. (AS SHOWN SMALLER IMAGE ON THE LEFT HAND SIDE CORNER) .....	12
FIGURE 2-5 TYPICAL PHASE TRANSITIONS OF LI-CARBOXYLATES. FROM LEFT TO RIGHT: LI-CARBOXYLATES AT AMBIENT TEMPERATURE, AT MELTING TEMPERATURE, AND AT DECOMPOSITION TEMPERATURE. ....	14
FIGURE 2-6 ONSET TEMPERATURES OF SOLID-TO-LIQUID PHASE TRANSITION AND DECOMPOSITION OF LI-CARBOXYLATES AS REPORTED BY TGA AND DSC ANALYSIS.....	15
FIGURE 2-7 ENTHALPY OF PHASE TRANSITION (SOLID-TO-LIQUID) OF LITHIUM ALKANOATES AND THEIR CORRESPONDING ACIDS. ENTHALPY VALUES OF ALKANOIC ACIDS WERE OBTAINED FROM NIST <sup>35</sup> . ....	16
FIGURE 3-1. EXAMPLE OF IR SPECTRUM WHERE SPLITTING OF ASYMMETRIC STRETCHING VIBRATION OF COO <sup>-</sup> WAS OBSERVED UPON MELTING AND SPLITTING OF SYMMETRIC STRETCHING VIBRATION OF COO <sup>-</sup> WAS NO LONGER OBSERVED UPON MELTING. ....	23
FIGURE 3-2. INFRARED SPECTRUM OF THE SOLID RESIDUE AFTER THERMAL DECOMPOSITION OF SODIUM UNDECANOATE AND THAT OF SODIUM CARBONATE SHOWED FOR COMPARISON .....	25
FIGURE 3-3. PHASE TRANSITIONS OF NA-OCTANOATE. FROM LEFT TO RIGHT: THE SAMPLE AT SOLID PHASE, AT LIQUID-CRYSTALLINE PHASE, AND AT SOLID-LIQUID TRANSITION PHASE.....	28
FIGURE 3-4. ONSET TEMPERATURES OF SOLID-TO-LIQUID (MELTING) AND DECOMPOSITION OF NA-CARBOXYLATES AS REPORTED BY TGA AND DSC ANALYSIS.....	29

FIGURE 3-5. ENTHALPIES OF PHASE TRANSITIONS OF SODIUM ALKANOATES AND THEIR CORRESPONDING ACIDS. ENTHALPY VALUES OF ALKANOIC ACIDS WERE OBTAINED FROM NIST <sup>35</sup> .	30
FIGURE 4-1 INFRARED SPECTRUM OF THE SOLID RESIDUE AFTER THERMAL DECOMPOSITION OF POTASSIUM UNDECANOATE AND THAT OF POTASSIUM CARBONATE SHOWED FOR COMPARISON	37
FIGURE 4-2. ONSET TEMPERATURES OF SOLID-TO-LIQUID (MELTING) AND DECOMPOSITION OF K-CARBOXYLATES AS REPORTED BY TGA AND DSC ANALYSIS.	40
FIGURE 4-3. ENTHALPIES OF PHASE TRANSITIONS OF POTASSIUM ALKANOATES AND THEIR CORRESPONDING ACIDS. ENTHALPY VALUES OF ALKANOIC ACIDS WERE OBTAINED FROM NIST <sup>35</sup> .	41
FIGURE 5-1. INFRARED SPECTRUM OF THE SOLID RESIDUE AFTER THERMAL DECOMPOSITION OF RUBIDIUM UNDECANOATE AND THAT OF RUBIDIUM CARBONATE SHOWED FOR COMPARISON	49
FIGURE 5-2. ONSET TEMPERATURES OF SOLID-TO-LIQUID (MELTING) AND DECOMPOSITION OF RB-CARBOXYLATES AS REPORTED BY TGA AND DSC ANALYSIS.	52
FIGURE 5-3. ENTHALPIES OF PHASE TRANSITIONS OF RUBIDIUM ALKANOATES AND THEIR CORRESPONDING ACIDS. ENTHALPY VALUES OF ALKANOIC ACIDS WERE OBTAINED FROM NIST <sup>35</sup> .	53
FIGURE 6-1. INFRARED SPECTRUM OF THE SOLID RESIDUE AFTER THERMAL DECOMPOSITION OF CESIUM UNDECANOATE AND THAT OF CESIUM CARBONATE SHOWED FOR COMPARISON.	60
FIGURE 6-2. ONSET TEMPERATURES OF SOLID-TO-LIQUID (MELTING) AND DECOMPOSITION OF CS-CARBOXYLATES AS REPORTED BY TGA AND DSC ANALYSIS.	63
FIGURE 6-3. ENTHALPIES OF PHASE TRANSITIONS OF CESIUM ALKANOATES AND THEIR CORRESPONDING ACIDS. ENTHALPY VALUES OF ALKANOIC ACIDS WERE OBTAINED FROM NIST <sup>35</sup> .	64
FIGURE 7-1. COMPARISON OF ONSET MELTING TEMPERATURES	67
FIGURE 7-2. COMPARISON OF ONSET DECOMPOSITION TEMPERATURE OF THE CARBOXYLATES	68

## LIST OF TABLES

TABLE 1-1 METAL CONTAMINANTS FROM INDUSTRIAL FIXED BED FE-LTFT SYNTHESIS <sup>3</sup> .....	2
TABLE 2-1. TEMPERATURE AND CALORIC CALIBRATION OF DSC BASED ON THE MELTING TEMPERATURE ( $T_M$ ) AND HEAT OF MELTING ( $\Delta H_M$ ) OF HIGH PURITY COMPOUNDS. TEMPERATURE VALUES WERE CORRECTED FOR HEATING RATE (DT/DB) AT EACH TEMPERATURE. AVERAGE (X) AND SAMPLE STANDARD DEVIATIONS (S) ARE REPORTED. ....	6
TABLE 2-2 TEMPERATURE AND CALORIC CALIBRATION OF TGA BASED ON THE MELTING TEMPERATURE ( $T_M$ ) AND HEAT OF MELTING ( $\Delta H_M$ ) OF HIGH PURITY COMPOUNDS. ....	6
TABLE 2-3 STRONG CARBOXYLATE STRETCHING VIBRATIONS IN THE IR AND RAMAN SPECTRA OF THE LI-CARBOXYLATES .....	7
TABLE 2-4 HIGH INTENSITY $\pi \rightarrow \pi^*$ TRANSITIONS OF THE CARBOXYLATE GROUP IN THE UV-VIS SPECTRA OF THE LI-CARBOXYLATES. ....	10
TABLE 2-5 ONSET TEMPERATURE OF DECOMPOSITION AND MASS LOSS OF LI-CARBOXYLATES DETERMINED BY TGA, AS WELL AS THE CALCULATED MASS LOSS ASSUMING THAT THE SOLID RESIDUE IS $Li_2CO_3$ . ....	11
TABLE 2-6 PHASE TRANSITIONS OF THE LI-CARBOXYLATES DETERMINED BY DSC OVER THE TEMPERATURE RANGE – 30°C TO THE DECOMPOSITION TEMPERATURE. ....	13
TABLE 2-7 COMPARISON OF THE PHASE TRANSITIONS OF THE LI-CARBOXYLATES REPORTED IN THIS STUDY WITH THAT REPORTED IN LITERATURE.....	16
TABLE 2-8 CONSTANT PRESSURE HEAT CAPACITY VERSUS TEMPERATURE CORRELATIONS OF THE SOLID $C_1$ - $C_{12}$ LI-CARBOXYLATES IN THE TEMPERATURE RANGE –30 TO +150 °C. GAPS IN THE TEMPERATURE REGION COVERED INDICATE SOLID-SOLID PHASE TRANSITIONS. ....	17
TABLE 3-1. STRONG CARBOXYLATE STRETCHING VIBRATIONS IN THE IR SPECTRA OF THE NA-CARBOXYLATES.....	22
TABLE 3-2. CARBOXYLATE HIGH INTENSITY $\pi \rightarrow \pi^*$ TRANSITIONS IN THE UV-VIS SPECTRA OF THE NA-CARBOXYLATES. ....	23
TABLE 3-3. ONSET TEMPERATURE OF DECOMPOSITION AND MASS LOSS OF LI-CARBOXYLATES DETERMINED BY TGA, AS WELL AS THE CALCULATED MASS LOSS ASSUMING THAT THE SOLID RESIDUE IS $Na_2CO_3$ . ....	24

TABLE 3-4. PHASE TRANSITIONS OF THE NA-CARBOXYLATES DETERMINED BY DSC OVER THE TEMPERATURE RANGE –30°C TO THE DECOMPOSITION TEMPERATURE.....	26
TABLE 3-5. COMPARISON OF THE PHASE TRANSITIONS OF THE NA-CARBOXYLATES REPORTED IN THIS STUDY WITH THAT REPORTED IN LITERATURE.....	30
TABLE 3-6. CONSTANT PRESSURE HEAT CAPACITY VERSUS TEMPERATURE CORRELATIONS OF THE SOLID C <sub>1</sub> -C <sub>12</sub> NA- CARBOXYLATES IN THE TEMPERATURE RANGE –30 TO +150 °C. GAPS IN THE TEMPERATURE REGION COVERED INDICATE SOLID-SOLID PHASE TRANSITIONS. ....	31
TABLE 4-1. STRONG CARBOXYLATE STRETCHING VIBRATIONS IN THE IR SPECTRA OF THE K-CARBOXYLATES .....	35
TABLE 4-2. CARBOXYLATE HIGH INTENSITY $\pi \rightarrow \pi^*$ TRANSITIONS IN THE UV-VIS SPECTRA OF THE K-CARBOXYLATES. .....	35
TABLE 4-3. ONSET TEMPERATURE OF DECOMPOSITION AND MASS LOSS OF K-CARBOXYLATES DETERMINED BY TGA, AS WELL AS THE CALCULATED MASS LOSS ASSUMING THAT THE SOLID RESIDUE IS K <sub>2</sub> CO <sub>3</sub> .....	36
TABLE 4-4. PHASE TRANSITIONS OF THE K-CARBOXYLATES DETERMINED BY DSC OVER THE TEMPERATURE RANGE – 30°C TO THE DECOMPOSITION TEMPERATURE.....	37
TABLE 4-5. COMPARISON OF THE PHASE TRANSITIONS OF THE K-CARBOXYLATES REPORTED IN THIS STUDY WITH THAT REPORTED IN LITERATURE.....	41
TABLE 4-6. CONSTANT PRESSURE HEAT CAPACITY VERSUS TEMPERATURE CORRELATIONS OF THE SOLID C <sub>1</sub> -C <sub>12</sub> K- CARBOXYLATES IN THE TEMPERATURE RANGE –30 TO +150 °C. GAPS IN THE TEMPERATURE REGION COVERED INDICATE SOLID-SOLID PHASE TRANSITIONS. ....	42
TABLE 5-1. STRONG CARBOXYLATE STRETCHING VIBRATIONS IN THE IR SPECTRA OF THE RB-CARBOXYLATES .....	47
TABLE 5-2. CARBOXYLATE HIGH INTENSITY $\pi \rightarrow \pi^*$ TRANSITIONS IN THE UV-VIS SPECTRA OF THE RB- CARBOXYLATES. ....	47
TABLE 5-3. ONSET TEMPERATURE OF DECOMPOSITION AND MASS LOSS OF RB-CARBOXYLATES DETERMINED BY TGA, AS WELL AS THE CALCULATED MASS LOSS ASSUMING THAT THE SOLID RESIDUE IS RB <sub>2</sub> CO <sub>3</sub> . ....	48
TABLE 5-4. PHASE TRANSITIONS OF THE RB-CARBOXYLATES DETERMINED BY DSC OVER THE TEMPERATURE RANGE –30°C TO THE DECOMPOSITION TEMPERATURE.....	49

TABLE 5-5. COMPARISON OF THE PHASE TRANSITIONS OF THE RB-CARBOXYLATES REPORTED IN THIS STUDY WITH THAT REPORTED IN LITERATURE.....	53
TABLE 5-6. CONSTANT PRESSURE HEAT CAPACITY VERSUS TEMPERATURE CORRELATIONS OF THE SOLID C <sub>1</sub> -C <sub>12</sub> RB-CARBOXYLATES IN THE TEMPERATURE RANGE -30 TO +150 °C. GAPS IN THE TEMPERATURE REGION COVERED INDICATE SOLID-SOLID PHASE TRANSITIONS. ....	54
TABLE 6-1. STRONG CARBOXYLATE STRETCHING VIBRATIONS IN THE IR SPECTRA OF THE CS-CARBOXYLATES.....	58
TABLE 6-2. CARBOXYLATE HIGH INTENSITY $\pi \rightarrow \pi^*$ TRANSITIONS IN THE UV-VIS SPECTRA OF THE CS-CARBOXYLATES. ....	58
TABLE 6-3. ONSET TEMPERATURE OF DECOMPOSITION AND MASS LOSS OF CS-CARBOXYLATES DETERMINED BY TGA, AS WELL AS THE CALCULATED MASS LOSS ASSUMING THAT THE SOLID RESIDUE IS CS <sub>2</sub> CO <sub>3</sub> ,.....	59
TABLE 6-4. PHASE TRANSITIONS OF THE CS-CARBOXYLATES DETERMINED BY DSC OVER THE TEMPERATURE RANGE -30°C TO THE DECOMPOSITION TEMPERATURE. ....	61
TABLE 6-5. COMPARISON OF THE PHASE TRANSITIONS OF THE CS-CARBOXYLATES REPORTED IN THIS STUDY WITH THAT REPORTED IN LITERATURE.....	64
TABLE 6-6. CONSTANT PRESSURE HEAT CAPACITY VERSUS TEMPERATURE CORRELATIONS OF THE SOLID C <sub>1</sub> -C <sub>12</sub> CS-CARBOXYLATES IN THE TEMPERATURE RANGE -30 TO +150 °C. GAPS IN THE TEMPERATURE REGION COVERED INDICATE SOLID-SOLID PHASE TRANSITIONS. ....	65

## 1. Introduction

Alkali metal alkanooates or alkali metal carboxylates are called “soaps”. Their general formula is  $C_nH_{2n+1}COOM^+$ , where M = Li, Na, K, Rb, Cs, the elements of Lithium, Sodium, Potassium, Cesium, and Rubidium.

The study of alkali metal carboxylates is of considerable interest for various reasons:

i) The Fischer-Tropsch (FT) process for the conversion of synthesis gas (CO and H<sub>2</sub>) to liquid products is well known. The products from this process contains predominantly linear hydrocarbons, but also includes oxygenates like carboxylic acids, esters, alcohols and carbonyls. Most of the short chain oxygenates (C<sub>1</sub>-C<sub>4</sub>) end up in the aqueous product phase, but the partition between the aqueous and organic phases is such that some of the short chain oxygenates also end up in the organic product phase<sup>1</sup>. During the refining of the organic product, it is consequently necessary to deal with a wide range of oxygenates, of which short chain carboxylic acids are the most deleterious<sup>2</sup>. A number of oxygenate related production challenges were noted such as equipment corrosion/fouling and catalyst leaching due to the presence of carboxylic acids in syncrude as well as adsorption of oxygenates on either metal or acid sites, thereby changing the metal-to-acid site ratio of bi-functional catalysts<sup>2</sup>. Although this does not result in deactivation, carboxylic acids can lower the effective metal-to-acid site ratio, which may cause an increase in the rate of deactivation by the formation of carbonaceous deposits. This restricts the refiner in terms of plant metallurgy, choice of catalysts and choice of solvents<sup>3</sup>.

One of the processing options for the removal of carboxylic acids is by a carbonate wash. Alkali metal salts of the carboxylic acids are readily formed and can in principal be completely removed as part of the aqueous effluent from the wash. However, in practice, some of the alkali metal carboxylates may remain in the organic product and be deposited as solids if the downstream processing includes evaporative steps<sup>4</sup>. Metal carboxylates are also produced during corrosion and catalyst leaching as mentioned above. Removal of the metal carboxylates does not require hydrogenation but follows a thermal decomposition pathway. At temperatures below their decomposition temperature, metal carboxylates can cause scaling in preheaters and result in catalyst bed plugging<sup>2</sup>. This is a clear justification for this work.

ii) The gas-phase products from FT process consist only of hydrocarbons, with very little oxygenates. This product gas undergoes a water wash to ensure that no water-soluble oxygenates especially carboxylic acids are carried over in the condensate stream to the CO<sub>2</sub> removal steps. The removal efficiency depends on the water temperature; the washing efficiency at the PetroSA refinery was higher than at the Synfuels facility due to lower water temperature (25-28°C)<sup>1</sup>. The foaming problem was reported in the Benfield process, which uses an activated, inhibited hot potassium carbonate solution to remove CO<sub>2</sub>, H<sub>2</sub>S and other acid gas components<sup>4</sup>. Carboxylic acids, which remained in the condensate stream due to the inefficient washing process, were noted to be partially responsible for the foaming problem in the Benfield process<sup>5</sup>.

iii) Traces of metals are usually present in the iron-based low temperature Fischer-Tropsch (LTFT) wax<sup>3</sup> (Table 1-1). Various methods for removing metals from LTFT wax that cause

problems with blockage of downstream refinery units have been suggested in both the journal and patent literature<sup>3</sup>.

**Table 1-1 Metal contaminants from industrial fixed bed Fe-LTFT synthesis<sup>3</sup>**

Metal	Concentration ( $\mu\text{g g}^{-1}$ )
Na	0.5
K	0.2
Fe	4.3
Cu	< 0.1

iv) Since 2001, many papers have been published that detail the different types of production processing problems caused by oilfield soaps and discuss various methods used for soap mitigation and control<sup>6,7,8,9</sup>. For example, sodium emulsion soaps, which are common to fluids produced from the Kutei Basin of Indonesia, can create severe oil dehydration problems and lead to excessive slop oil/sludge volumes at crude-oil terminals. Their properties and operational consequences were outlined in the paper by D.L.Gallup<sup>10</sup>. The source of these soaps is thought to be precursor organic acids in crude oils.

v) The phase transitions of the alkali metal carboxylates have been explored by different researchers, but most of the effort was directed at lithium, sodium and potassium carboxylates<sup>11,12,13,14,15,16,17,18</sup>. A fair amount of scatter can also be observed in the published data.

### **Objective and scope of work**

The objective of this work was mainly to obtain accurate phase transition/decomposition data suitable for design and operation, and fill the gap in the literature data for the alkali metal carboxylates of the C<sub>1</sub>-C<sub>12</sub> linear carboxylic acids. Rubidium and cesium carboxylates were also included in this study although lithium, sodium and potassium carboxylates are considered to be industrially relevant. The phase transition data of interest includes: the nature of the phase transitions (solid-solid, solid-liquid and such), their associated onset temperatures and enthalpies of phase transitions, heat capacity data, and especially decomposition onset temperatures/enthalpies of decomposition. In order to obtain the phase transition/decomposition data, we used some of the following techniques: Fourier Transform Infrared Spectroscopy (FTIR), Thermogravimetric analysis (TGA), Differential Scanning Calorimetry (DSC). The obvious challenges of this work were to successfully synthesize and purify the carboxylates, and to interpret FTIR/TGA/DSC analysis.

## 2. Lithium C<sub>1</sub>-C<sub>12</sub>*n*-alkanoates: Thermal behavior from -30 to 600 °C

### 2.1 Introduction

Lithium *n*-alkanoates (carboxylates) are the lithium salts of the corresponding linear carboxylic acids. Unlike the other Group 1 alkali metal carboxylates, the lithium carboxylates have considerable covalent character<sup>19</sup>. The short chain Li-carboxylates have some commercial application, such as lithium methanoate (Li-formate) for electron paramagnetic resonance (EPR) dosimeters<sup>20</sup>, and lithium ethanoate (Li-acetate) as buffer for gel electrophoresis of DNA and RNA<sup>21</sup>. The longer chain detergent-range Li-carboxylates find application as greases, for example lithium-12-hydroxy-octanoate (Li-12-hydroxystearate)<sup>22</sup>. Lithium stearate is also employed in cosmetics and as lubricant in plastics production<sup>23</sup>. As is often the case with the carboxylates, there are much fewer applications for carboxylates of intermediate chain length which are lighter than the detergent-range (usually C<sub>12</sub> and heavier) carboxylates. However, it has been suggested that some of these intermediate chain length carboxylate may be important for the development of lithium-ion batteries<sup>24</sup>.

Our interest in this class of compounds is the use of lithium carboxylates as intermediates in the reactive removal of carboxylic acids from dilute solutions and the subsequent recovery of the organic matter by thermal decomposition. Conceptually this is a three-step process that involves neutralization, foam fraction and thermal decomposition. Lithium has two potential advantages as counter-ion compared to other ions for this process:

(a) Lithium is a monovalent ion. The cross-linking tendency of multivalent ions to yield finely dispersed insoluble matter is thus avoided. Foam fractionation is therefore more likely to enable high recovery rates.

(b) Lithium soaps have lower water solubility than the soaps of other alkali metals<sup>22</sup>.

This thesis is concerned only with the third step in the process, namely, the thermal decomposition of the Li-carboxylates and the thermally induced changes that occur before decomposition. Such a quantitative description of the thermal behavior of the Li-carboxylates is necessary for future engineering design and development. Reports on the thermal analysis of only some Li-carboxylates was found in literature. The aim of this work is to present a systematic investigation of the thermal behavior of the C<sub>1</sub>-C<sub>12</sub>*n*-alkanoates, as well as a review of previous studies in this field.

### 2.2 Experimental

#### 2.2.1 Materials

The high purity reference materials employed for temperature and enthalpy calibration of the differential scanning calorimeter were commercially obtained and used as received. These were: indium (Impag AG, supplied by Mettler-Toledo ME-119442, indium pills, 99.999%), tin (Alfa Aesar, #11013, 99.995% metal basis), lead (Alfa Aesar, #42928, 99.999% metal basis) and zinc (Impag AG supplied by Mettler-Toledo ME-119441, 99.999%) for the differential scanning calorimeter calibration; indium (supplied by Mettler-Toledo ME – 119442), zinc (supplied by

Mettler-Toledo ME-119441), Aluminum (supplied by Mettler-Toledo ME-51119701) and Gold (supplied by Mettler-Toledo ME-51140816) for Thermogravimetric Analyzer Calibration.

Praxair's Ultra High Purity 5.0 nitrogen (99.999%) was used to maintain the inert atmospheric conditions during calorimetric runs.

The lithium carboxylates employed in this study were prepared from commercially obtained lithium hydroxide monohydrate (Cryst./Laboratory, Fisher Chemical, CAT No L127-500) and the linear carboxylic acids in the C<sub>1</sub>-C<sub>12</sub> range. Methanoic acid (99%), nonanoic acid (97%) and undecanoic acid (99%) were supplied by Acros Organics. Ethanoic acid (99.7%), propanoic acid (99.5%), butanoic acid (+99%), pentanoic acid (99%) and hexanoic acid (99%) were supplied by Aldrich. Heptanoic acid (+97%), octanoic acid (+99%), decanoic acid (96%) and dodecanoic acid (+99%) were supplied by Sigma. Lithium carbonate (purum, ≥ 99% supplied by Sigma-Aldrich) was used as spectroscopic standard to confirm the nature of the Li-carboxylates decomposition products.

The solvents that were used in the study were methanol (98%, Sigma-Aldrich), ethyl ether anhydrous (>99%, Fisher Chemical). Deionized water was prepared in the laboratory using a Millipore water purification system.

### 2.2.2 Analytical equipment and procedure

The thermal behavior of the lithium carboxylates was studied primarily with a heat flux (disk-type) differential scanning calorimeter (DSC), Mettler Toledo DSC 1 with 400W power amplifier and FRS-5 sensor with 56 thermocouples. The DSC was equipped with a Haakeintracooler, which enabled measurement of below ambient temperatures. All experiments were conducted in a dynamic atmosphere of nitrogen gas. A sheathing N<sub>2</sub> flow rate of minimum 100 mL/min was maintained and controlled through a gas flow meter (Cole Palmer PMR1-010750) and a sample chamber N<sub>2</sub> flow rate of 100 mL/min was maintained and controlled through the Mettler GC 10 gas controller. All thermal analyses were performed at a heating rate of 10 K/min in the temperature range -30 to 600 °C.

Standard 40 µl aluminum crucibles (Mettler, #51119870) without pin and with domed aluminum lids (Mettler, #51119871) were employed. Standard procedure was to pierce the lid of the crucible with a needle on a clean rubber surface (needle diameter about 1 mm) and to cold-weld the lid to the crucible using a Mettler crucible sealing press.

Samples were weighed on a XS105 Dual Range Analytical Balance from Mettler Toledo, maximum capacity 41 g at 0.01 mg readability and 120 g at 0.1 mg readability. FACT (fully automatic calibration technology) was responsible for calibration of the balance under full automatic control on the basis of the factory selected temperature criterion. Sample sizes were maintained in the range 1-10 mg.

An Olympus BX51 microscope and Mettler FP84HT TA Microscopy Cell (DTA/DSC sensor) with FP90 central processor simultaneously allowed visual phase transition observations and DSC heat flow measurements. The sample was placed in a transparent crucible (glass cover

disks diameter 7 mm, Mettler, # 17782 and glass crucibles diameter 7 mm Mettler, # 17780) and together with an inert reference crucible, the sample is subjected to a temperature program. The sample was observed visually under polarized and non-polarized light and can be photographed or filmed by video camera. The temperature difference (DTA signal) between the transparent glass sample pan and an inert reference pan was measured and recorded at the same time as the observations are made. Temperature measurement ranged from room temperature to 375 °C.

Decomposition and associated mass loss was determined by thermogravimetric analysis (TGA) using a Mettler Toledo TGA/DSC1 with LF 1100 furnace, sample robot and MX5 internal microbalance (5g measuring cell with 1µg resolution). Cooling of the instrument was performed with a Julabo circulator and the bath temperature was set at 22 °C. A sheathing N<sub>2</sub> flow rate of minimum 20 mL/min was maintained and controlled through a gas flow meter (Cole Palmer PMR1-010750). Alumina 70 µL crucibles (supplied by Mettler-Toledo ME-24123) with lid were employed. Samples were weighed using both external and internal METTLER balances to ensure accuracy. The external balance was described earlier. FACT automatic weight calibration is integrated in the micro and ultra micro balances of the TGA.

Infrared spectroscopy was employed to confirm the syntheses and for analysis of the products obtained at different temperatures during the thermal analysis. Infrared spectra were collected using an ABB MB3000 Fourier Transform Infrared spectrometer with Horizon MB™ FTIR software. Spectra were collected at a resolution of 2 cm<sup>-1</sup> and the average of 150 scans over the spectral region 4000-500 cm<sup>-1</sup>. The spectrometer was equipped with a MIRacle™ Reflection Attenuated Total Reflectance (ATR) diamond crystal plate and pressure clamp.

Raman spectra were collected using a Sierra Series Raman System from Snowy Range Instruments, which is equipped with a 100 mW laser (785 nm wavelength). SnRI Investigator™ Software was used for data acquisition. During analysis a laser power of 35mW was employed with a spectral acquisition time of 5 s. An average of 120 spectra was taken.

Ultraviolet and visible (UV-Vis) spectra were collected from 185 to 800 nm, using a Shimadzu UV-2700 UV-Vis spectrometer, using quartz cuvette with 1 cm path length. Samples were prepared in deionized water and deionized water was employed as background.

### **2.2.3 Calibration**

Temperature and caloric calibration of DSC was performed using the high purity reference materials. The onset temperature of melting was employed for temperature calibration and the heat of melting was employed for caloric calibration (Table 2-1)<sup>25</sup>. The temperature measurements were corrected for the heating rate ( $\beta$ ) by performing the temperature calibration at different heating rates and extrapolating to close-to-zero heating rate ( $\beta \rightarrow 0$ ). The heating rate correction ( $dT/d\beta$ ) was determined for each calibration substance.

**Table 2-1. Temperature and caloric calibration of DSC based on the melting temperature ( $T_m$ ) and heat of melting ( $\Delta H_m$ ) of high purity compounds. Temperature values were corrected for heating rate ( $dT/d\beta$ ) at each temperature. Average ( $\bar{x}$ ) and sample standard deviations ( $s$ ) are reported.**

Material	Experimental $T_m$ ( $^{\circ}\text{C}$ )		Experimental $\Delta H_m$ (J/g)		Literature values <sup>26</sup> $dT/d\beta$ ( $\text{K}/\text{K}\cdot\text{min}^{-1}$ )		
	$\bar{x}$	$s$	$\bar{x}$	$s$	$T_m$ ( $^{\circ}\text{C}$ )	$\Delta H_m$ (J/g)	
In	156.75	0.09	29.3	0.3	156.60	28.6	0.03
Sn	231.91	0.15	59.6	0.6	231.93	60.3	-0.01
Pb	327.33	0.14	23.4	0.2	327.47	23.0	0.04
Zn	419.45	0.26	109.8	1.4	419.53	108.6	-0.01

Temperature and caloric calibration of TGA was performed once with each of the high purity reference materials. The results showed that the system was within specification at In, Al, and Au melting points (Table 2-2).

**Table 2-2 Temperature and caloric calibration of TGA based on the melting temperature ( $T_m$ ) and heat of melting ( $\Delta H_m$ ) of high purity compounds.**

Material	TGA Specifications		Experimental	
	$T_m$	$\Delta H_m$	$T_m$	$\Delta H_m$
In	156.6 $^{\circ}\text{C} \pm 1.5^{\circ}\text{C}$	-28.5J/g $\pm 15\%$	156.44 $^{\circ}\text{C}$	-30.42J/g
Al	660.3 $^{\circ}\text{C} \pm 2.5^{\circ}\text{C}$	-397.0J/g $\pm 20\%$	661.55 $^{\circ}\text{C}$	-394.07J/g
Au	1064.2 $^{\circ}\text{C} \pm 3.0^{\circ}\text{C}$	-63.7J/g $\pm 20\%$	1064.03 $^{\circ}\text{C}$	-62.30J/g

The heat capacity calibration was performed according to the ASTM E 1269 standard test method<sup>27</sup>, using a synthetic sapphire (NIST, 100% purity) as reference material. The DSC was purged with dry nitrogen and a flow rate of 100 mL/min was maintained during all analyses. An empty crucible with pierced lid (loose, i.e. not cold welded) was used to determine background heat flow, which was subtracted from subsequent measurements. The same crucible was used for the standard sapphire and a sample of interest. The weights of the empty crucible, the sapphire and the sample of interest were recorded before and after each measurement. A maximum difference of 0.03 % of the weight before and after each measurement was acceptable, otherwise the results were discarded. The temperature program employed was -30  $^{\circ}\text{C}$  isothermally for 10 min, ramping from -30 to 150  $^{\circ}\text{C}$  at 10  $^{\circ}\text{C}/\text{min}$  and then isothermally at 150  $^{\circ}\text{C}$  for 10 minutes. Heat capacity was calculated using Equation 1.

$$C_{p,s} = C_{p,r} \frac{h_s m_r}{h_r m_s}$$

$C_{p,s}$ : Heat capacity of the sample of interest (J/g.K)

$C_{p,r}$ : Heat capacity of the sapphire reference as provided in ASTM E 1269-01 (J/g.K)

$h_s$ : Difference in heat flow of the sample of interest and the empty pan (mW)

$h_r$ : Difference in heat flow of the sapphire and the empty pan (mW)

$m_s$ : Mass of the sample of interest (mg)

$m_r$ : Mass of the standard sapphire (mg)

## 2.2.4 Synthesis of lithium alkanooates

The synthesis and purification of Li-carboxylates were based on the work of Franzosini et al<sup>15</sup>. Li-carboxylates were prepared by mixing lithium hydroxide (in deionized water) with a slight excess amount (2% molar excess) of carboxylic acids. The mixture was stirred for several hours without heating to allow sufficient time for the neutralization reaction to be complete, using a Heidolph MR Hei-Standard hot plate (heating power of 800W, maximum temperature of 300 °C, 30-1400 rpm at an accuracy of  $\pm 1\%$ ). Solid Li-carboxylates were recovered by evaporation of the solvent and excess acid at 60 °C under reduced pressure at 9.6 kPa (absolute), using a Heidolph Hei-VAP Precision with glassware set G3 rotary evaporator. The Li-carboxylates were purified by dissolution in methanol and fractional precipitation with ethyl ether and were further dried under vacuum at approximately 100 °C until they reached constant mass. The final products were finely ground before being used for thermal analysis.

## 2.3 Results & Discussion

### 2.3.1 Infrared and Raman Spectroscopy

The infrared spectra of metal carboxylates in general are characterized by the strong asymmetric stretching of the carboxylate,  $\nu_{as}(\text{CO}_2^-)$ , around 1600-1550  $\text{cm}^{-1}$  and the somewhat weaker symmetrical stretching of the carboxylate,  $\nu_s(\text{CO}_2^-)$ , around 1400  $\text{cm}^{-1}$ <sup>28,29,30,31</sup>. The asymmetric stretching of the carboxylate,  $\nu_{as}(\text{CO}_2^-)$ , is weak to very weak in the Raman spectrum, but the symmetrical stretching of the carboxylate,  $\nu_s(\text{CO}_2^-)$ , is pronounced in the Raman spectrum<sup>32</sup>.

Infrared spectroscopy was used primarily to confirm synthesis of the Li-carboxylates and provide information on structural changes that were observed during calorimetry. The IR spectra of the Li-carboxylates are provided in the supporting information (Figures S1-S12). No bands corresponding to the acid in any of the Li-carboxylates are observed which shows the high purity of the samples. The wavenumbers of the strong carboxylate stretching vibrations in the IR spectra of the Li-carboxylates are listed in Table 2-3.

**Table 2-3 Strong carboxylate stretching vibrations in the IR and Raman spectra of the Li-carboxylates**

Li-carboxylates	Carboxylate stretching vibrations ( $\text{cm}^{-1}$ )				Raman, symmetric $\text{cm}^{-1}$	$\Delta\nu$ ( $\text{cm}^{-1}$ ) standard	$\Delta\nu$ ( $\text{cm}^{-1}$ ) alternate
	IR, asymmetric		IR, symmetric				
Methanoate	1586	-	1366	-		220	-
Ethanoate	1561	-	1439	-	1417	122	-
Propanoate	1578	1559	1436	1411	1434	148	142
Butanoate	1577	1557	1436	1419	1432	138	141
Pentanoate	1577	1557	1440	1411	1431	146	137
Hexanoate	1577	1557	1439	1414	1428	143	138
Heptanoate	1579	1557	1440	1404	1422	153	139
Octanoate	1578	1556	1442	1406	1429	150	136
Nonanoate	1578	1555	1439	1404	1423	151	139
Decanoate	1579	1556	1442	1402	1424	154	137
Undecanoate	1578	1556	1444	1403	1423	153	134
Dodecanoate	1578	1556	1442	1403	1424	153	136

In general, bands corresponding to aliphatic CH<sub>2</sub> and CH<sub>3</sub> stretching vibrations are observed below 3000cm<sup>-1</sup>. The difference between Li-methanoate and heavier carboxylates lies in the intensity of the aliphatic CH<sub>2</sub> and CH<sub>3</sub> stretching vibrations, the longer the aliphatic chain of the carboxylates is, the more intense it is. Methyl and methylene bending and rocking vibrations are measured between 500 and 1400cm<sup>-1</sup>.

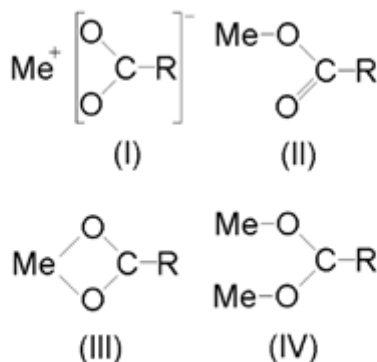


**Figure 2-1. Metal carboxylate bonding configurations (I) ionic (II) monodentate (III) bidentate (IV) bridging**  
 19

Four metal-carboxylate configurations are possible (Figure 2-1). The carboxylates of highly electropositive elements such as sodium and potassium are ionic in nature. The other bonding modes are observed for most other metals. Monodentate coordination is found in lithium and cobalt acetate<sup>19</sup>.

The work of Nakamoto<sup>29</sup> suggested that the separation of the bands (i.e.  $\Delta\nu = \nu_{\text{asym}}(\text{COO}^-) - \nu_{\text{sym}}(\text{COO}^-)$ ) is the indication of the structure of a given carboxylate, since the frequencies of the bands are highly sensitive to the structure of the carboxylate group, the nature of the solvent, the nature of the ligand and the identity of the metal ion. Ionic and bridging carboxylate structures cannot be distinguished from  $\Delta\nu$ , since the values for these two configurations overlap. Monodentate bonding, where the Li-O bond has covalent character, results in a much larger  $\Delta\nu$  than the ionic form, typically 200-300 cm<sup>-1</sup>. Conversely, bidentate bridging results in a much smaller  $\Delta\nu$  than the ionic form, typically <100 cm<sup>-1</sup>. Spectroscopic evidence for a more covalent character of the Li-O bond was found only for lithium methanoate, which has  $\Delta\nu = 220$  cm<sup>-1</sup> or more (Table 2-3). The C<sub>2</sub>-C<sub>12</sub> Li-carboxylates all have  $\Delta\nu$  values in the range typical of ionic structures and no spectroscopic evidence was found to indicate covalent character of the Li-O bond. This was supported by the UV-Vis spectroscopy, with only the lithium methanoate showing evidence of non-equivalence of the C-O bonds (Table 2-3)

At a 2 cm<sup>-1</sup> wave number resolution, splitting of the asymmetric and symmetric stretching of the carboxylate was observed in the IR spectra most of the compounds. The splitting of the carboxylate stretching vibrations persisted in the IR spectra collected after melting of the Li-carboxylates (Figure 2-2). The splitting of the  $\nu_{\text{as}}(\text{CO}_2^-)$  and  $\nu_{\text{s}}(\text{CO}_2^-)$  absorptions could suggest that Li-carboxylates existed in two different configurations but the equivalence of the C-O bonds are retained.

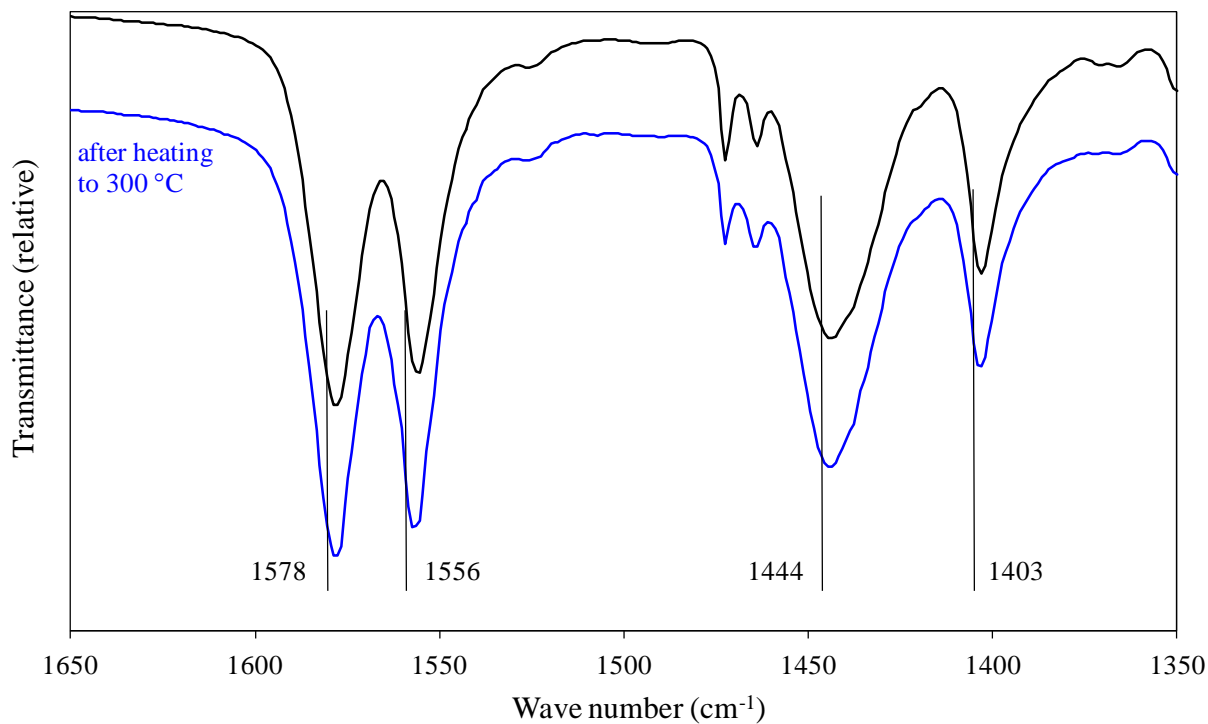


**Figure 2-2 Infrared spectrum of lithium undecanoate in the wavenumber range 1350-1650 cm<sup>-1</sup> before and after heating to 300 °C showing the persistence of splitting of the carboxylate absorption.**

The Raman spectra of the Li-carboxylates are provided in the supporting information (Figures S13-S24). The Raman spectra did not exhibit clear splitting of the symmetrical stretching of the carboxylate (Table 2-2). However, it must be noted that the peak base was much broader in the Raman spectra than in the IR spectra and in some instances a small peak adjacent to the main symmetrical stretching could be observed (Figure 2-3).

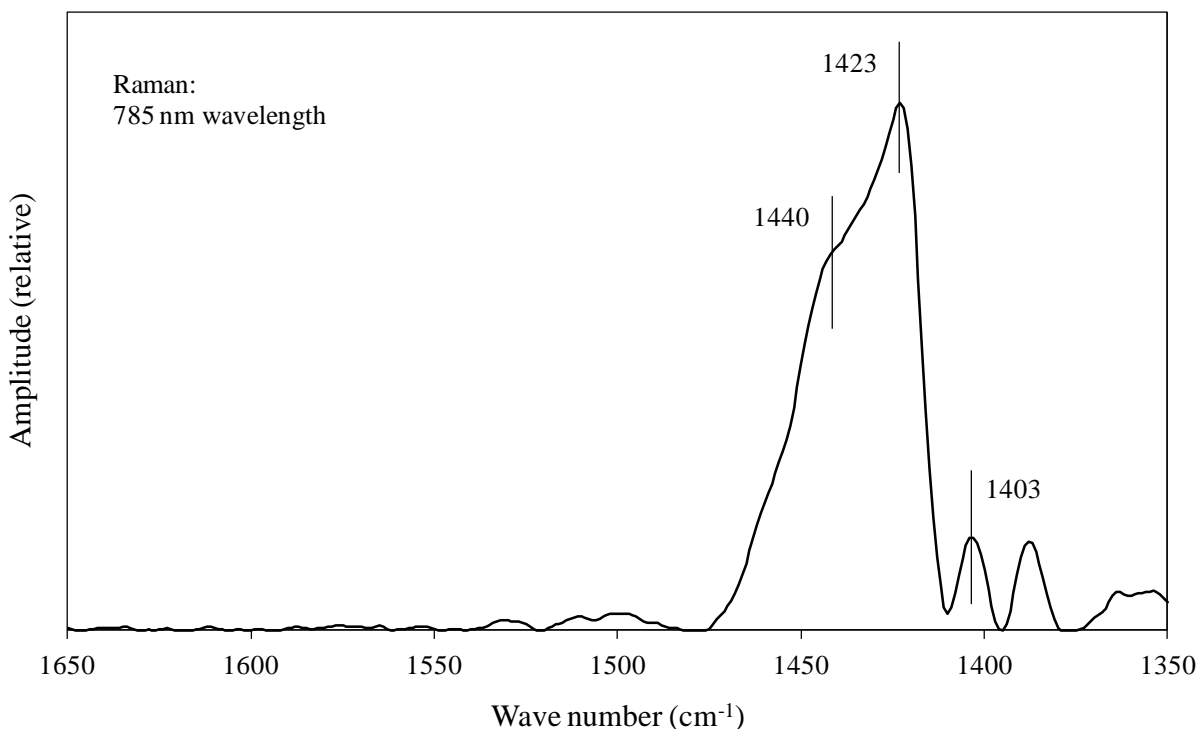


**Figure 2-3. Raman spectrum of lithium undecanoate in the wavenumber range 1350-1650  $\text{cm}^{-1}$  showing splitting of the carboxylate absorption.**

The low frequency region ( $800\text{-}200\text{ cm}^{-1}$ ) of the infrared and Raman spectrum contains carboxylate bending vibrations and metal-oxygen stretching vibrations<sup>29</sup>. In the infrared spectrum carboxylate scissoring,  $\delta(\text{CO}_2^-)$ , is around  $800\text{-}600\text{ cm}^{-1}$ <sup>28,29</sup>, but it is infrequently reported and used for carboxylate characterization. In the Raman spectrum the in-plane bending of the carboxylate group by scissoring,  $\delta(\text{CO}_2^-)$ , as well as by rocking,  $\rho(\text{CO}_2^-)$  can be clearly observed<sup>32</sup>. The anticipate absorption in the Raman spectra for the methanoate and ethanoate were observed at  $768$  and  $649\text{ cm}^{-1}$  respectively.

### 2.3.2. Ultraviolet-visible spectroscopy

The UV-Vis spectrum of carboxylate group is characterized mainly by a high intensity  $\pi \rightarrow \pi^*$  transition at around  $200\text{ nm}$ ; the  $\pi \rightarrow \pi^*$  transition at longer wavelength is weak<sup>33</sup>. It was noted that Li-carboxylates have more covalent character than the other alkali metal carboxylates<sup>19</sup>. If this is indeed the case, the equivalence of the C–O bonds will be lost, which should be reflected in the UV-Vis spectrum.

The UV-Vis spectra of the Li-carboxylates are provided in the supporting information (Figures S25-S36). The  $\pi \rightarrow \pi^*$  transitions are listed in Table 2-4. All of the values were in a narrow range, with only lithium methanoate that showed a marginally higher value.

**Table 2-4 High intensity  $\pi \rightarrow \pi^*$  transitions of the carboxylate group in the UV-Vis spectra of the Li-carboxylates.**

Li-Carboxylates	Carboxylate $\pi \rightarrow \pi^*$ transition (nm)
Methanoate	192
Ethanoate	189
Propanoate	189
Butanoate	189
Pentanoate	188
Hexanoate	188
Heptanoate	187
Octanoate	189
Nonanoate	187
Decanoate	186
Undecanoate	188
Dodecanoate	188

### 2.3.3 Decomposition by thermogravimetric analysis

The decomposition temperature and mass loss during decomposition was determined by TGA in an inert atmosphere (Table 2-5). The TGA curves over the temperature range of 150 to 600 °C (423 to 873 K) are provided in the supporting information (Figure S37). With the exception of lithium methanoate and lithium ethanoate that both decomposed around 385 °C, the heavier Li-carboxylates were thermally stable to temperatures above 400 °C.

**Table 2-5 Onset temperature of decomposition and mass loss of Li-carboxylates determined by TGA, as well as the calculated mass loss assuming that the solid residue is  $\text{Li}_2\text{CO}_3$ .**

Li-carboxylates	Onset of decomposition (K)	TGA mass loss (%)	Calculated mass loss (%)
Methanoate	659.6	26.6	28.9
Ethanoate	661.5	45.9	44.0
Propanoate	726.4	53.8	53.8
Butanoate	756.1	61.2	60.7
Pentanoate	749.9	65.8	65.8
Hexanoate	743.0	69.9	69.7
Heptanoate	741.6	72.4	72.8
Octanoate	740.5	74.8	75.4
Nonanoate	733.7	76.0	77.5
Decanoate	734.3	77.0	79.3
Undecanoate	731.9	79.6	80.8
Dodecanoate	730.5	81.8	82.1

Ethanoate and heavier carboxylates generally decompose via the formation of the metal carbonate and an organic component ketone, with the exception of lithium methanoate. The metal carbonate decomposes further into carbon dioxide and the oxide of the metal.



The temperature at which metal carbonate decomposes further depends on the electropositive nature of the metal. Alkaline metals are most electropositive of all because they have a single electron in their outer shell; as a result, carbonates of alkali metals are stable to the highest

temperature. At the final temperature of 600°C in this work, it is expected metal carbonate is the final product rather than the oxide of the metal. The ketone is generally oxidized by atmospheric oxygen to carbon dioxide and water at a temperature which is characteristic of a specific ketone. The decomposition of methanoate however follows a different course than other carboxylates. It consists of the formation of either  $H_2 + CO + Li_2CO_3$  or/and  $H_2 + Li_2C_2O_4$  (which will decompose further to form carbonate and carbon dioxide). It is likely that lithium formate decomposed directly to form lithium carbonate in this study, since only one stage of decomposition was observed from TGA results.

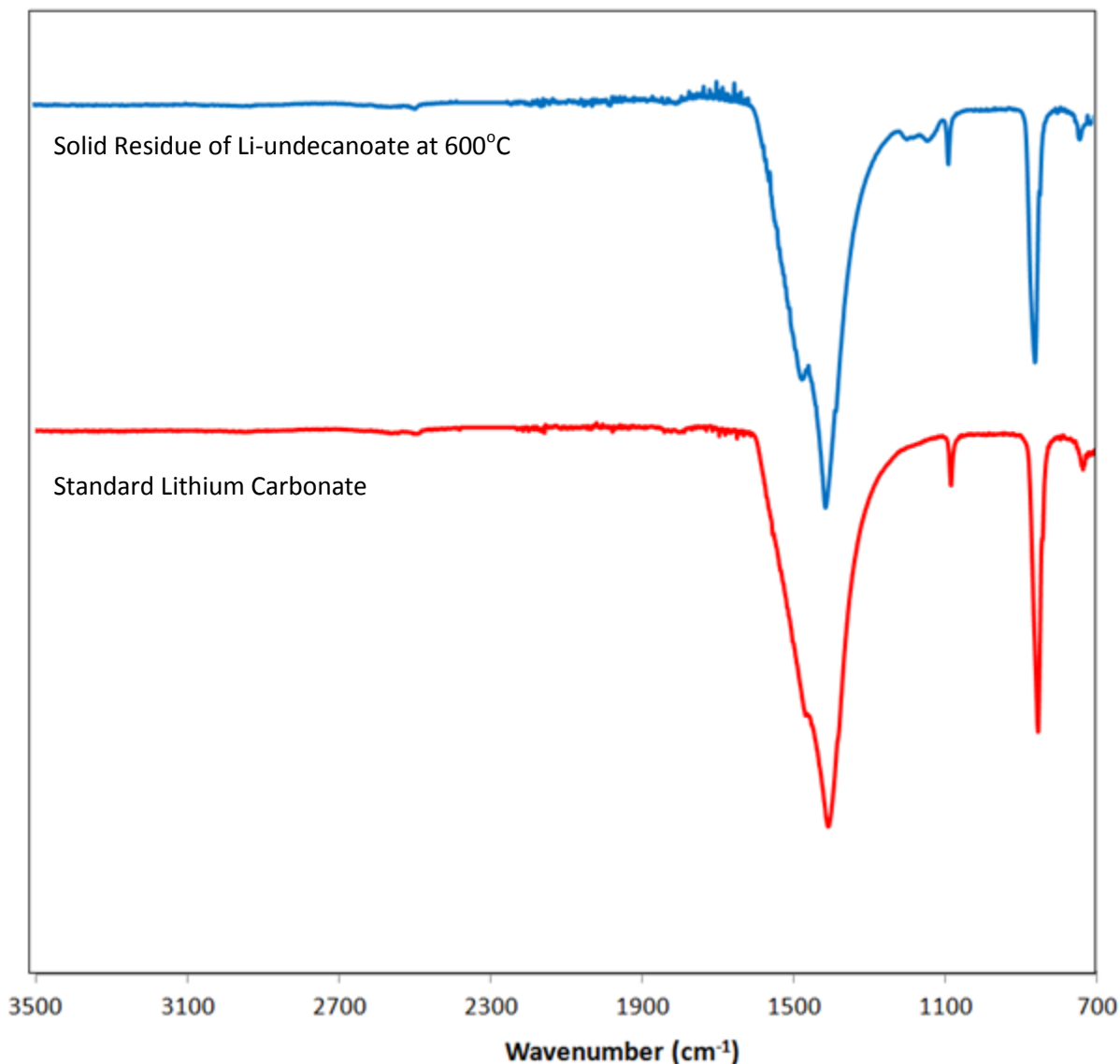


Figure 2-4 Infrared spectrum of the solid residue after thermal decomposition of lithium undecanoate and that of lithium carbonate showed for comparison. (as shown smaller image on the left hand side corner)

Figure 2-4 shows IR spectrum of the residue of Li-carboxylates at 600°C in comparison with IR spectrum of pure lithium carbonate. IR results confirmed that lithium carbonate is the final residue of Li-carboxylates when the samples were subjected to the final temperature of 600°C. Assuming that lithium carbonate was the final residue of Li-carboxylates at 600°C, theoretical mass loss was calculated and compared with the TGA total mass loss. The percentage difference was less than 7%.

$$\text{Theoretical mass loss} = 1 - M_{\text{lithium carbonate}} / (2 \times M_{\text{lithium carboxylate}})$$

### 2.3.4 Phase transitions by differential scanning calorimetry

DSC calorigrams of Li-carboxylates were presented in the supporting information document (Figures S38-S49). DSC-microscope and TGA analyses were used to assist with the assignment of the transitions. It was possible to unambiguously assign transitions for melting and decomposition (Figure 2-5). Phase transitions and their associated energies were reported in Table 2-6.

**Table 2-6 Phase transitions of the Li-carboxylates determined by DSC over the temperature range -30°C to the decomposition temperature.**

Li-carboxylates	Transitions <sup>a</sup>	Onset temperature (K)	Energy <sup>b</sup> (J/g)
Methanoate	s-s	508.6	-36.3
	s-l	545.4	-309.6
	d	662.0	529.0
Ethanoate	s-s	431	65.4
	s-l	556.3	-182.2
	d	<sup>c</sup> -	<sup>c</sup> -
Propanoate	s-s	530.6	-42.2
	s-l	604.2	-197.0
	d	<sup>c</sup> -	<sup>c</sup> -
Butanoate	s-l	590.0	-220.8
	d	780.1	-167.6
Pentanoate	s-s	323.5 <sup>d</sup>	-36.1
	s-l	574.3	-201.3
	d	728.5	-277.1
Hexanoate	s-l	560.4	-188.0
	d	723.9	-237.9
Heptanoate	s-s	316.6 <sup>d</sup>	-45.8
	s-l	547.6	-182.2
	d	721.8	-295.0
Octanoate	s-l	537.5	-159.6
	d	730.3	-299.2
Nonanoate	s-s	343.0 (349.0 <sup>d</sup> )	-48.9
	s-l	524.3	-156.1
	d	739.1	-322.3
Decanoate	s-s	309.7 <sup>d</sup>	-2.6

	s-l	517.0	-164.8
	d	740.7	-483.8
Undecanoate	s-s	364.6 <sup>d</sup>	-71.8
	s-l	508.7	-147.2
	d	709.9	-457.6
Dodecanoate	s-s	314.5 <sup>d</sup>	-2.8
	s-s	346.1 <sup>d</sup>	-33.7
	s-l	500.6	-137.5
	d	736.9	-311.1

<sup>a</sup> Transitions: s-s = solid-solid phase transition, s-l = solid-liquid phase transition (melting), d = decomposed

<sup>b</sup> Energy changes: endothermic values are negative, exothermic values are positive

<sup>c</sup> Onset of decomposition was ill-defined and could not be determined

<sup>d</sup> Solid-solid phase transitions were observed during the Cp measurement experiments

For some of the Li-carboxylates there were solid-solid phase transitions in addition to the solid-liquid phase transition. The solid-solid phase transitions were labeled reversible if the same but opposite transition could be observed upon cooling down to  $-30\text{ }^{\circ}\text{C}$ . When the same but opposite transition could not be observed on cooling to  $-30\text{ }^{\circ}\text{C}$ , the solid-solid transition was labeled as irreversible. It is likely that solid-solid transitions that were labeled as irreversible are indeed reversible and that the “irreversibility” is the result of sufficient metastability at temperatures down to  $-30\text{ }^{\circ}\text{C}$ ; therefore, the reverse solid-solid transition was not observed during analysis. No liquid-liquid phase transitions were observed for any of the Li-carboxylates.

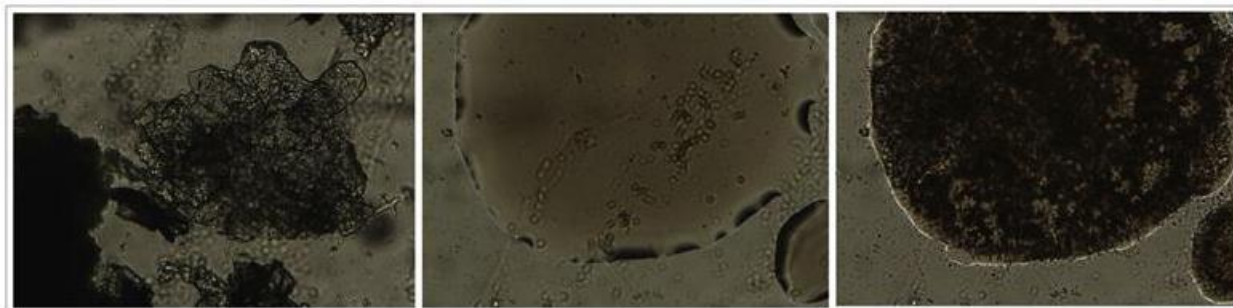


**Figure 2-5 Typical phase transitions of Li-carboxylates. From left to right: Li-Carboxylates at ambient temperature, at melting temperature, and at decomposition temperature.**

Decomposition temperatures of Li-carboxylates determined from DSC analysis were close to that of TGA analysis, i.e. within 5% difference with relatively same total % wt loss (Figure 2-6). The onset of decomposition temperatures of Li-ethanoate and Li-propanoate could not be analyzed from the DSC thermograms, as a result, no data was obtained to compare with those from TGA analysis. Thermal stability of Li-carboxylates increases with increasing carbon number in the aliphatic chain, clearly seen from Li-ethanoate to Li-butanoate and insignificant from Li-butanoate onwards.

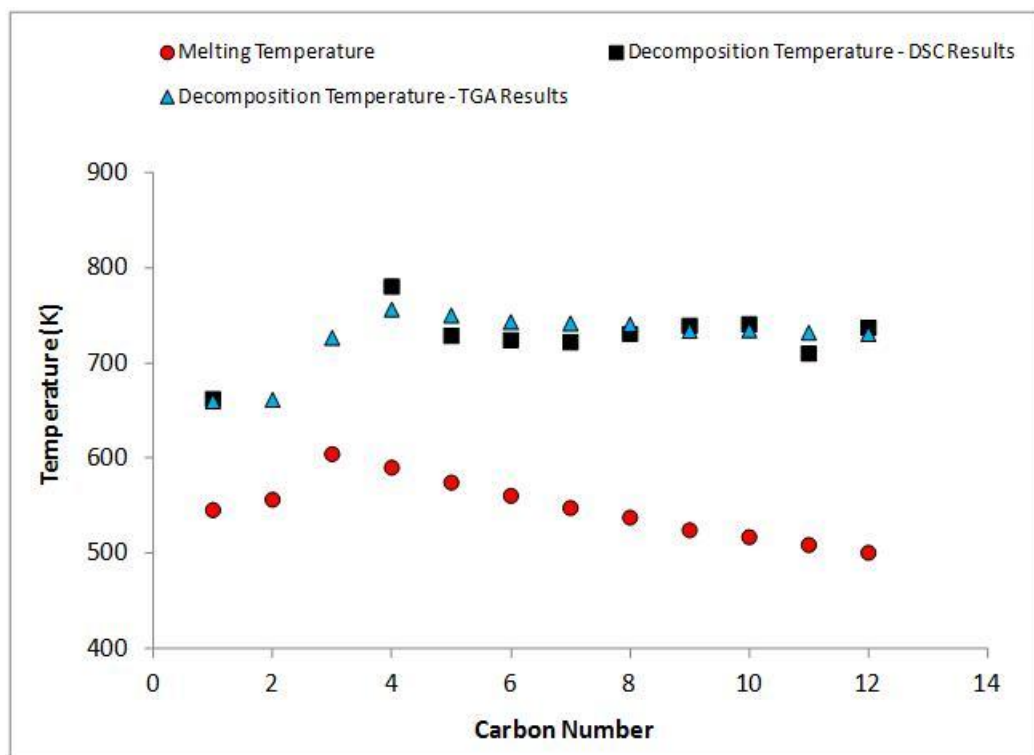


Figure 2-6 Onset temperatures of solid-to-liquid phase transition and decomposition of Li-carboxylates as reported by TGA and DSC analysis.

The melting temperatures increased from Li-C1 to Li-C3, then decreased smoothly from Li-C4 to Li-C12. The melting process of the aliphatic alkaline metal soap takes place in two major steps: the first corresponding to the melting of the aliphatic chains and the second to the melting of polar groups. In general, the melting point of the intermediate length aliphatic chains decreases with increasing chain length, starting from Li-propanoate. We can explain this by the fact that the polar force of the metallic ions and carboxylate group act as a cohesive force. The increasing chain length disrupts the compact structure and works against the cohesion forces<sup>34</sup>.

Figure 2-7 shows the enthalpy of phase transition (solid-to-liquid) of lithium carboxylates in comparison with the reported literature values of their corresponding alkanolic acids. There was no defined trend between enthalpy of phase transition of Li-carboxylates and carboxylic acids; hence the  $\text{Li}^+$  is not contributing a constant amount of energy to the  $\Delta H_{\text{melting}}$  compared to  $\text{H}^+$  for the carboxylic acids.

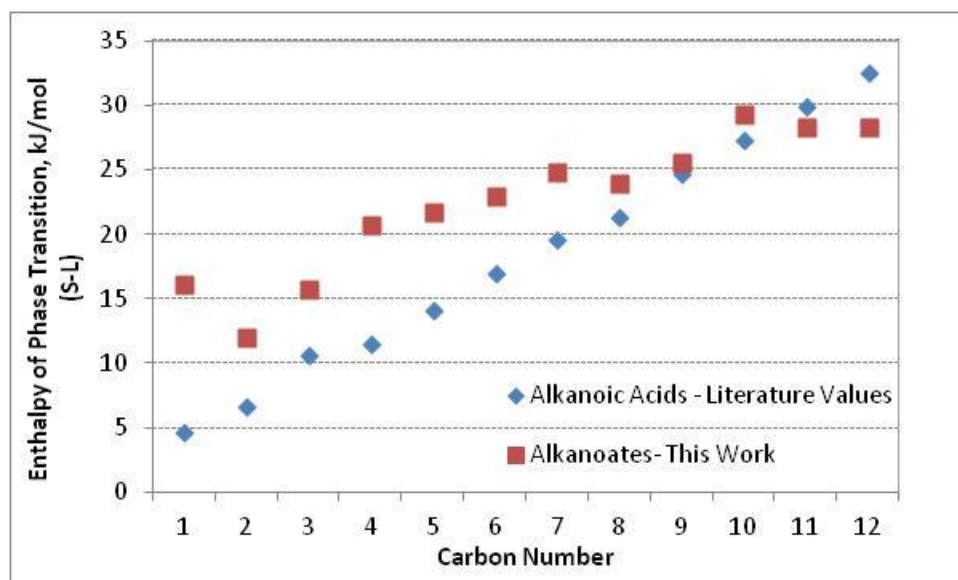


Figure 2-7 Enthalpy of Phase Transition (Solid-to-Liquid) of Lithium alkananoates and their corresponding acids. Enthalpy values of alkananoic acids were obtained from NIST<sup>35</sup>.

Phase transitions of Li-carboxylates agreed with the literature data, as shown in Table 2-7. Li-pentanoate, solid-to-solid phase transition ( $205.5 \pm 0.5$ ) is only detected if the sample is cooled at least until 173K and maintained at this temperature for 5 minutes<sup>24</sup>. The solid-to-solid transition was not detected in this study; perhaps it was due to the difference in our experimental procedure, of which the sample was cooled to 243.15K only. The solid-to-solid transition ( $325.2 \pm 0.7$ ) occurs in a very broad range of temperatures (250K-370K), similar observations from Li-pentanoate DSC thermogram, the transition was brought out during the heat capacity measurement.

A solid-to-solid phase transition was detected at  $495\text{K} \pm 1$ <sup>11</sup>. The same phase transition was also detected in this study at the same temperature, however was not reported as a true thermal event because the opposite transition could not be observed upon cooling down to 243.15K ( $-30^{\circ}\text{C}$ ).

Table 2-7 Comparison of the phase transitions of the Li-carboxylates reported in this study with that reported in literature

	Literature Value <sup>11</sup>		This Work	
	Transitions	T/K	Transitions	T/K
Li-methanoate	s-s	$495 \pm 1$	-	-
	s-l	$545 \pm 1$	s-l	$545.4 \pm 0.3$
Li-ethanoate	Literature Value <sup>11</sup>		This Work	
	Transitions	T/K	Transitions	T/K
	s-l	$558 \pm 1$	s-l	$556.3 \pm 0.3$
Li-Propanoate	Literature Value <sup>24</sup>		This Work	
	Transitions	T/K	Transitions	T/K
	s-s	$549.7 \pm 0.7$	s-s	$530.6 \pm 0.3$
	s-l	$606.4 \pm 0.5$	s-l	$604.15 \pm 0.3$
Li- Butanoate	Literature Value <sup>36</sup>		This Work	
	Transitions	T/K	Transitions	T/K

	s-l	591.0 ± 0.5	s-l	590.0 ± 0.3
Li-Pentanoate	Literature Value <sup>24</sup>		This Work	
	Transitions	T/K	Transitions	T/K
	s-s	205.5 ± 0.5	-	-
	s-s	325.2 ± 0.7	s-s	323.5 ± 0.3
	s-l	576.5 ± 0.3	s-l	574.3 ± 0.3
Li-Heptanoate	Literature Value <sup>12</sup>		This Work	
	Transitions	T/K	Transitions	T/K
	s-s	317.9 ± 0.8	s-s	319.8 ± 0.3
	s-l	550 ± 1	s-l	547.6 ± 0.3

### 2.3.5 Heat capacity by differential scanning calorimetry

The heat capacities of the Li-carboxylates were determined over the temperature range -30°C to 150 °C (243 to 423 K) by DSC. All heat capacity determinations were conducted in triplicate and the heat capacity versus temperature data are provided in the supporting information (Figures S50-S61). For some of the Li-carboxylates, the heat capacity measurements crossed solid-solid phase transitions (Table 2-6). A multivariate regression analysis was performed to fit all of the Cp vs. T for each compound to a typical correlation of  $C_p \text{ (J/g.K)} = A + B.T + C.T^2 + D.T^3$  with minimal error-of-fit, excluding temperature ranges where solid-to-solid phase transitions occurred (Table 2-8). No systematic trend was observed in the heat capacities from Li-methanoate to Li-dodecanoate at the same temperature.

**Table 2-8 Constant pressure heat capacity versus temperature correlations of the solid C<sub>1</sub>-C<sub>12</sub> Li-carboxylates in the temperature range -30 to +150 °C. Gaps in the temperature region covered indicate solid-solid phase transitions.**

Li-carboxylates	Valid range of T (K)	$C_p \text{ (J/g.K)} = A + B.T + C.T^2 + D.T^3$			
		A	B	C	D
Methanoate	249.7-416.3	-1.1506E+01	1.0364E-01	-2.7202E-04	2.6404E-07
Ethanoate	249.7-416.3	-7.4361E+00	6.6044E-02	-1.6421E-04	1.5692E-07
Propanoate	266.3-416.3	-2.0822E+00	1.9342E-02	-1.7931E-05	9.7550E-09
Butanoate	258.0-416.3	-6.8629E+00	6.2125E-02	-1.4871E-04	1.4453E-07
Pentanoate	249.7-316.3	-2.2187E+01	2.7078E-01	-1.0575E-03	1.4191E-06
Hexanoate	258.0-416.3	-8.0229E+00	7.2743E-02	-1.7497E-04	1.6873E-07
Heptanoate	249.7-309.2	-9.4570E+01	9.7725E-01	-3.3378E-03	3.8762E-06
	366.3-391.3	-1.7101E+02	1.4131E+00	-3.8287E-03	3.4833E-06
Octanoate	266.3-416.3	5.9084E+00	-5.2783E-02	1.9867E-04	-2.0715E-07
Nonanoate	264.7-333.2	-5.1648E+01	5.1275E-01	-1.6678E-03	1.8941E-06
	361.3-408.0	-3.7419E+01	2.9437E-01	-7.2211E-04	6.4102E-07
Decanoate	273.2-304.7	-3.7708E+00	2.7417E-02	-1.4090E-05	4.9520E-09
	319.2-393.2	-1.9975E+02	2.0951E+00	-7.3091E-03	8.6072E-06
Undecanoate	258.0-358.0	-2.5100E+01	2.5345E-01	-8.1787E-04	9.2741E-07
	383.0-416.3	2.7629E+02	-2.1070E+00	5.3910E-03	-4.5624E-06
Dodecanoate	249.7-308.0	-5.7585E+01	6.0576E-01	-2.0924E-03	2.4660E-06
	321.3-339.7	-2.3132E+02	2.1969E+00	-6.9294E-03	7.3435E-06
	358.0-408.0	-3.7761E+01	2.8599E-01	-6.8462E-04	5.7770E-07

Cp/R literature data was plotted against the calculated Cp/R data for Li-methanoate to Li-heptanoate (Figures S50-S61). The literature data was determined either by equilibrium adiabatic calorimetry or by differential scanning calorimetry. The calculated data however did not agree well with the literature data<sup>24 12 11 17</sup>. It is not likely to reach a conclusive discussion of the possible reasons for the difference because how the heat capacity measurements were conducted and how the values were calculated was not elaborated in the literature paper. The possibility of the impurity of lithium carboxylates samples were disregarded because the onset temperatures of phase transitions were all in well agreement with literature data. Even if there was a low concentration of impurities, it would have only a minor contribution to the overall heat capacity of the sample. The rate of temperature change employed in this study (10 °C/min) was the same as that of the reported literature, as was the procedure for DSC heat capacity measurement. The two main differences that were noted were in the sample weight used and the method of storage. It is recommended to employ a sample mass close to the mass of the sapphire standard (25 mg)<sup>27</sup>.

This was not possible due to the low bulk density of the Li-carboxylates and the mass (5-8 mg) was on the low side for heat capacity measurements. This is likely to be the main source of error in the present study. The preparation and storage of samples before heat capacity measurements, was also different. For example, in the study by Ferloni, et al.,**Error! Reference source not found.** the powdered samples were pressed into pellets, kept for 24 hours at 100 °C under vacuum and were then stored in a vacuum desiccator with P<sub>2</sub>O<sub>5</sub> for 15 days before being tightly sealed in crucibles and kept at 93 °C before analysis<sup>11</sup>.

## 2.4 Summaries

We reported on the synthesis, characterization and thermal behavior of lithium carboxylates. The products were pure enough for further thermal analysis. We were able to find literature data for phase transition for some shorter chain lithium n-alkanoates and the experimental data were in well agreement with those. Key observations from this study are:

- Clear spectroscopic evidence was presented that C<sub>3</sub>-C<sub>12</sub> Li-carboxylates exist in two different configurations and that the configurations persisted after melting. In both configurations, the equivalence of the C-O bonds was retained.
- Evidence for a more covalent character of the Li-O bond was found only for lithium methanoate, where the difference between the asymmetric and symmetric stretching of the carboxylate,  $\Delta\nu = \nu_{as}(\text{CO}_2^-) - \nu_s(\text{CO}_2^-)$ , was 220 cm<sup>-1</sup>. The C<sub>2</sub>-C<sub>12</sub> Li-carboxylates had  $\Delta\nu$ -values in the range 122-154 cm<sup>-1</sup>.
- Thermal decomposition of the C<sub>1</sub>-C<sub>2</sub> Li-carboxylates took place at 380-390 °C, whereas the thermal decomposition of C<sub>3</sub>-C<sub>12</sub> Li-carboxylates occurred in the range 450-485 °C.
- The Li-carboxylates decomposed to produce lithium carbonate (Li<sub>2</sub>CO<sub>3</sub>) as solid product and decomposition was consistent with ketonic decomposition reported in literature.

- Solid-solid phase transitions were found for all C<sub>1</sub>-C<sub>12</sub> Li-carboxylates in the temperature range studied, with the exception of lithium butanoate, hexanoate and octanoate.
- No liquid crystal phases were found for any of the C<sub>1</sub>-C<sub>12</sub> Li-carboxylates.
- The melting points of the C<sub>1</sub>-C<sub>2</sub> Li-carboxylates were 272 and 283 °C respectively. For the other Li-carboxylates, the melting points decreased monotonically from 331 °C for lithium propanoate, to 227 °C for lithium dodecanoate. The experimental values for melting point temperature and enthalpy of melting were consistent with literature.
- The constant pressure heat capacity (C<sub>p</sub>) of the solid C<sub>1</sub>-C<sub>12</sub> Li-carboxylates was experimentally determined by DSC over the temperature range -25 to +145 °C. However, for the C<sub>1</sub>-C<sub>7</sub> Li-carboxylates, where experimental data was available in literature, meaningful differences were noted.

### 3. Sodium C<sub>1</sub>-C<sub>12</sub>*n*-alkanoates: Thermal behavior from -30 to 600 °C

#### 3.1 Introduction

Sodium *n*-alkanoates (carboxylates) are the sodium salts of the corresponding linear carboxylic acids. The uses of alkali metal carboxylates and the reasons why their thermal properties are of interest were stated earlier. Additionally, the longer chains of Na-carboxylates have found uses as foaming agents and collectors in processing of many ores, including potash and phosphorite<sup>37</sup>. The shorter chains of Na-carboxylates are commonly encountered in anaerobic biomass pyrolysis, such as Na-ethanoate creating broad interests in the thermal decomposition these compounds<sup>38</sup>.

The ability of Na-carboxylates to form ionic liquid crystal (mesophases) was of the interest in this chapter, since Li-carboxylates did not form any mesophases. The thermotropic mesomorphism of alkali metalalkanoates was first described in 1910 by Daniel Vorländer, who noticed the double-melting, or mesophase, behavior of these compounds. Later work by other authors showed that the alkali metal alkanoates display a rich polymorphism with several phase transitions between the crystalline state and the isotropic liquid<sup>34</sup>. However, a wide spread of the reported phase transition temperatures is noticed, and this can partially be explained by the fact that some of the phase transitions are difficult to determine visually or by polarizing optical microscopy. Materials forming liquid crystalline phases (mesophases) have found wide applications in the manufacturing of displays, spatial light modulators, optical connectors and switches, molecular sensors and detectors, and in many other topics. Efforts have been directed to increase the mesophase range by lowering the melting point and increasing the clearing point (second melting point)<sup>34</sup>.

In this chapter we attempted a systematic thermal behavior study of nC<sub>1</sub>-nC<sub>12</sub> Na-carboxylates as well as a review and compare of previous studies in the same field.

#### 3.2 Experimental

##### 3.2.1 Materials

The high purity reference materials employed for temperature and enthalpy calibration of the differential scanning calorimeter were commercially obtained and used as received. These were: indium (Impag AG, supplied by Mettler-Toledo ME-119442, indium pills, 99.999%), tin (Alfa Aesar, #11013, 99.995% metal basis), lead (Alfa Aesar, #42928, 99.999% metal basis) and zinc (Impag AG supplied by Mettler-Toledo ME-119441, 99.999%) for the differential scanning calorimeter calibration; indium (supplied by Mettler-Toledo ME – 119442), zinc (supplied by Mettler-Toledo ME-119441), Aluminum (supplied by Mettler-Toledo ME-51119701) and Gold (supplied by Mettler-Toledo ME-51140816) for Thermogravimetric Analyzer Calibration.

Praxair's Ultra High Purity 5.0 nitrogen (99.999%) was used to maintain the inert atmospheric conditions during calorimetric runs.

The sodium carboxylates employed in this study were prepared from commercially obtained sodium carbonate (ACS reagent supplied by Sigma-Aldrich) and the linear carboxylic acids in the C<sub>1</sub>-C<sub>12</sub> range. Methanoic acid (99%), nonanoic acid (97%) and undecanoic acid (99%) were supplied by Acros Organics. Ethanoic acid (99.7%), propanoic acid (99.5%), butanoic acid (+99%), pentanoic acid (99%) and hexanoic acid (99%) were supplied by Aldrich. Heptanoic acid (+97%), octanoic acid (+99%), decanoic acid (96%) and dodecanoic acid (+99%) were supplied by Sigma.

The solvents that were used in the study were methanol (98%, Sigma-Aldrich), and ethanol (+99.8%, Fluka). Deionized water was prepared in the laboratory using a Millipore water purification system.

### **3.2.2 Analytical equipment and procedure**

The same analytical equipment and procedures were employed as for the study of the lithium carboxylates (Chapter 2 - Section 2.2.2)

### **3.2.3 Calibration**

The same temperature and caloric calibration was performed as for the study of the lithium carboxylates (Chapter 2 – Section 2.2.3)

### **3.2.4 Synthesis of sodium alkanoates**

The synthesis and purification of Na-carboxylates were based on the work of Franzosini et al<sup>16</sup>. Na-carboxylates were prepared by mixing sodium carbonate (in anhydrous methanol) with a slight excess (2% molar excess) of carboxylate acids<sup>14</sup>. The mixture was stirred for several hours without heating to allow sufficient time for the neutralization reaction to be complete, using a Heidolph MR Hei-Standard hot plate (heating power of 800W, maximum temperature of 300 °C, 30-1400 rpm at an accuracy of ± 1%). Solid Na-carboxylates were recovered by evaporation of the solvent and excess acid at 60 °C under reduced pressure at 9.6 kPa (absolute), using a HeidolphHei-VAP Precision with glassware set G3 rotary evaporator. The Na-carboxylates were purified by recrystallizing the products from a mixture of ethanol + methanol (1:1 by volume). The Na-carboxylates were further dried under vacuum at approximately 100 °C until they reached constant mass. The final products were finely ground before being used for thermal analysis.

## **3.3 Results& Discussions**

### **3.3.1 Infrared Spectroscopy**

Infrared spectroscopy was used primarily to confirm the success of the synthesis of the Na-carboxylates and provide information on structural changes that were observed during calorimetry. The IR spectra of the Na-carboxylates are provided in the supporting information (Figures S1-S12). In general, bands corresponding to aliphatic CH<sub>2</sub> and CH<sub>3</sub> stretching vibrations are observed below 3000cm<sup>-1</sup>. The difference between Na-methanoate and heavier carboxylates lies in the intensity of the aliphatic CH<sub>2</sub> and CH<sub>3</sub> stretching vibrations, the longer the aliphatic chain of the carboxylates is, the more intense it is. Methyl and methylene bending and rocking vibrations are measured between 500 and 1400cm<sup>-1</sup>. The C=O stretching vibration observed in the alkanolic acid around 1700cm<sup>-1</sup> disappears in the Na-carboxylates and is replaced by two new absorption bands. These bands correspond to the symmetric and asymmetric stretching vibrations of the carboxylate ion and listed in Table 3-1. The relative position of these two bands  $\Delta = \nu_{\text{asym}}(\text{COO}^-) - \nu_{\text{sym}}(\text{COO}^-)$  can be used to shed light on the type of carboxylate-to-metal complexation structure present in a given metal carboxylate<sup>29</sup>. Four metal-carboxylate configurations are possible (Figure 2-1). Ionic and bridging carboxylate structures cannot be distinguished from  $\Delta\nu$ , since the values for these two configurations overlap. Monodentate bonding, where the Na-O bond has covalent character, results in a much larger  $\Delta\nu$  than the ionic form, typically 200-300 cm<sup>-1</sup>. Conversely, bidentate bridging results in a much smaller  $\Delta\nu$  than the ionic form, typically <100 cm<sup>-1</sup>. Spectroscopic evidence for a more covalent character of the Na-O bond was found only for sodium methanoate, which has  $\Delta\nu = 217\text{-}227$  cm<sup>-1</sup> (Table 3-1). This was however not supported by the UV-Vis spectroscopy, all Na-carboxylates showed evidence of equivalent C-O bonds (Table 3-2). The C<sub>2</sub>-C<sub>12</sub> Na-carboxylates all have  $\Delta\nu$  values in the range typical of either ionic or bridging structures.

**Table 3-1. Strong carboxylate stretching vibrations in the IR spectra of the Na-carboxylates**

Na-carboxylates @ T <sub>ambient</sub>	Carboxylate stretching vibrations (cm <sup>-1</sup> )				$\Delta\nu$ (cm <sup>-1</sup> )
	IR, asymmetric		IR, symmetric		
Methanoate	1580		1353		227
Ethanoate	1566		1407		159
Propanoate	1557		1415		142
Butanoate	1557		1448	1409	148
Pentanoate	1556		1442	1418	138
Hexanoate	1559		1444	1414	145
Heptanoate	1557		1443	1418	139
Octanoate	1557		1444	1412	145
Nonanoate	1557		1444	1419	138
Decanoate	1557		1444	1424	133
Undecanoate	1558		1444	1419	139
Dodecanoate	1556		1444	1423	133
Na-carboxylates @ T <sub>melting</sub>	Carboxylate stretching vibrations (cm <sup>-1</sup> )				$\Delta\nu$ (cm <sup>-1</sup> )
	IR, asymmetric		IR, symmetric		
Methanoate	1571		1354		217
Ethanoate	1577	1558	1410		167
Propanoate	1576	1557	1436	1416	140-141
Butanoate	1576	1557	1436		140

Pentanoate	1576	1557	1439	1410	137-147
Hexanoate	1577	1555	1438		139
Heptanoate	1579	1555	1440	1405	139-150
Octanoate	1577	1555	1441		136
Nonanoate	1577	1555	1439	1404	138-151
Decanoate	1577	1556	1442	1403	135-153
Undecanoate	1578	1555	1444	1403	134-152
Dodecanoate		1557	1444	1422	135

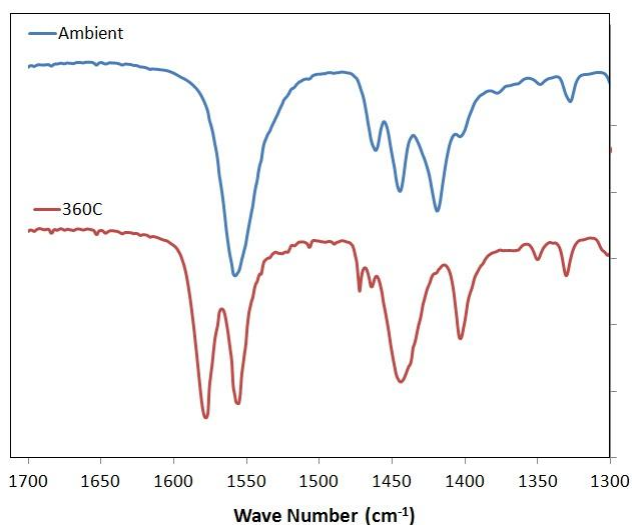


**Figure 3-1.** Example of IR spectrum where splitting of asymmetric stretching vibration of COO<sup>-</sup> was observed upon melting and splitting of symmetric stretching vibration of COO<sup>-</sup> was no longer observed upon melting.

For most Na-carboxylates, except Na-methanoate and Na-dodecanoate, splitting of asymmetric stretching vibration of carboxylate ion was observed upon melting, while splitting of symmetric stretching vibration of carboxylate ion was no longer observed upon melting (Figure 3-1). The presence of methyl deformation vibrations around 1450-1340 cm<sup>-1</sup> complicates the asymmetric and symmetric assignments of COO<sup>-</sup>. The splitting of the  $\nu_{as}(\text{CO}_2^-)$  and  $\nu_s(\text{CO}_2^-)$  absorptions could suggest that Na-carboxylates existed in two different configurations. The Raman spectra of the Na-carboxylates are provided in the supporting information (Figures S13-S24).

### 3.3.2. Ultraviolet-visible spectroscopy

The UV-Vis spectrum of carboxylate group is characterized mainly by a high intensity  $\pi \rightarrow \pi^*$  transition at around 200 nm. The UV-Vis spectra of the Na-carboxylates are provided in the supporting information (Figures S25-S36). The  $\pi \rightarrow \pi^*$  transitions are listed in Table 3-2.

**Table 3-2.** Carboxylate high intensity  $\pi \rightarrow \pi^*$  transitions in the UV-Vis spectra of the Na-carboxylates.

Na-Carboxylates	Carboxylate $\pi \rightarrow \pi^*$ transition (nm)
Methanoate	187
Ethanoate	189

Propanoate	188
Butanoate	188, 190
Pentanoate	187
Hexanoate	188
Heptanoate	188
Octanoate	188
Nonanoate	188
Decanoate	186
Undecanoate	189
Dodecanoate	188

### 3.3.3 Decomposition by thermogravimetric analysis

The decomposition temperature and total mass loss during decomposition was determined by TGA under inert atmosphere (Table 3-3). The TGA curves over the temperature range of 150 to 600 °C (423 to 873K) are provided in the supporting information (Figure S37). With the exception of Na-methanoate, the heavier Na-carboxylates were thermally stable to temperatures above 745K.

**Table 3-3. Onset temperature of decomposition and mass loss of Li-carboxylates determined by TGA, as well as the calculated mass loss assuming that the solid residue is Na<sub>2</sub>CO<sub>3</sub>.**

Na-carboxylates	Onset of decomposition (K)	TGA mass loss (%)	Calculated mass loss (%)
Methanoate	669.8	12.0	14.8 <sup>a</sup>
	839.9	21.0	22.1
Ethanoate	750.3	35.3	35.4
Propanoate	779.0	43.5	44.8
Butanoate	756.7	50.5	51.9
Pentanoate	753.5	58.7	57.3
Hexanoate	752.5	62.6	61.6
Heptanoate	750.5	64.9	65.2
Octanoate	750.1	68.2	68.1
Nonanoate	748.1	71.2	70.6
Decanoate	748.2	71.9	72.7
Undecanoate	747.2	74.8	74.6
Dodecanoate	746.5	74.5	76.2

<sup>a</sup> Calculated mass loss assuming that the intermediate product was Na<sub>2</sub>C<sub>2</sub>O<sub>4</sub>

It was anticipated based on literature that the solid material remaining after decomposition would be sodium carbonate (Na<sub>2</sub>CO<sub>3</sub>). The calculated mass loss for decomposition to yield Na<sub>2</sub>CO<sub>3</sub> corresponded well with the experimentally observed mass loss from TGA (Table 3-3). This was also confirmed by infrared analysis, which indicated that the solid residue after Na-carboxylate decomposition was indeed Na<sub>2</sub>CO<sub>3</sub> (Figure 3-2). The infrared spectra of the solid decomposition products from all of the C<sub>1</sub>-C<sub>12</sub> Na-carboxylates were the same, namely, that corresponding to Na<sub>2</sub>CO<sub>3</sub>.

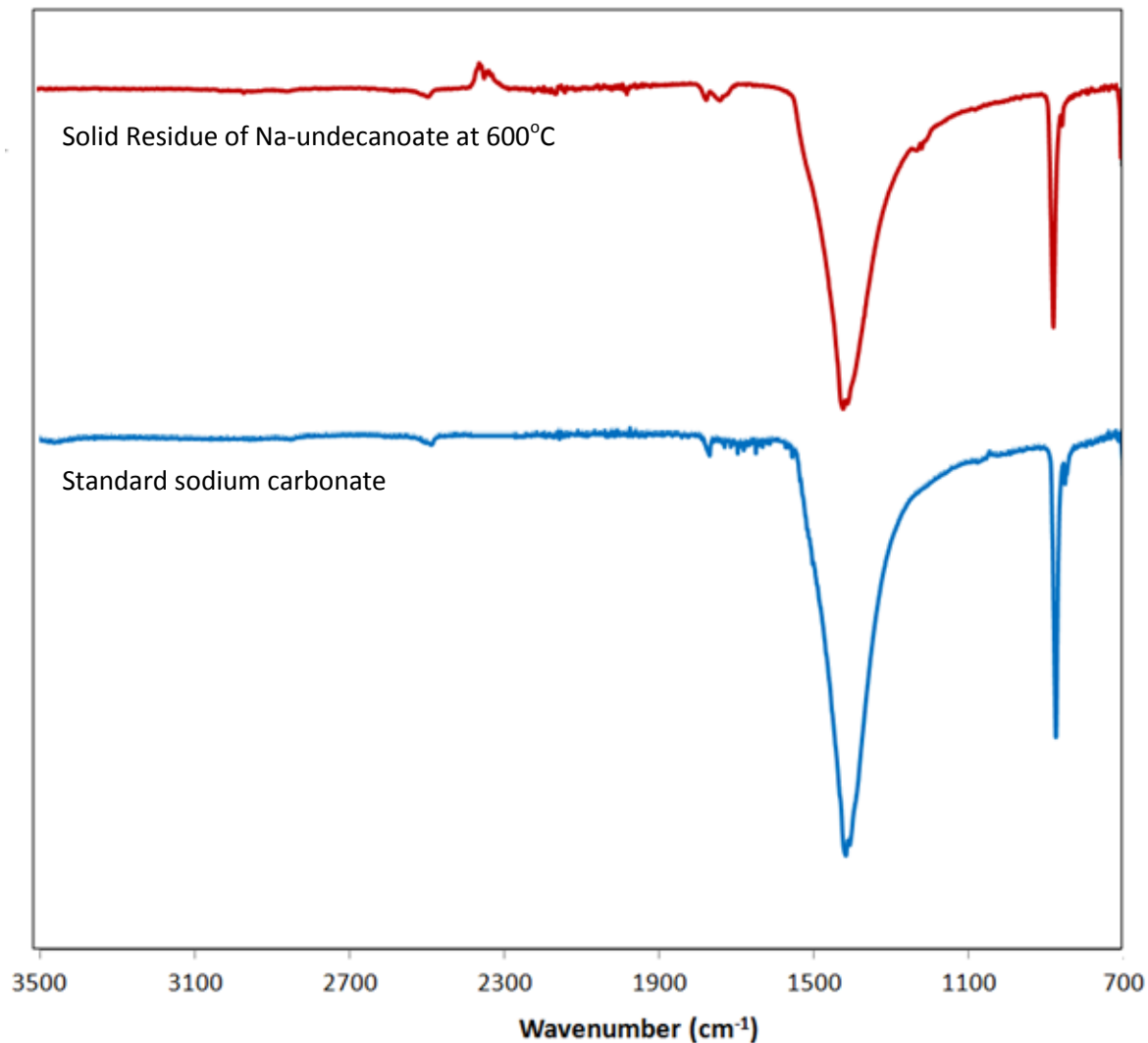
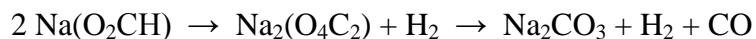


**Figure 3-2. Infrared spectrum of the solid residue after thermal decomposition of sodium undecanoate and that of sodium carbonate showed for comparison**

For all samples, mass loss occurred in a single event, except Na-methanoate. It is suggested that the Na-methanoate decompose to form the respective carbonate and oxalates in a first stage. The oxalate formed from this first stage decomposes further to carbonates and carbon monoxide. The formation of oxalate was not observed in the case of Li-methanoate.



Acetates and heavier carboxylates generally decompose via the formation of the metal carbonate and an organic component ketone. The metal carbonate decomposes further into carbon dioxide and the oxide of the metal. The temperature at which metal carbonate decomposes further depends on the electropositive nature of the metal. Alkaline metals are most electropositive of all because they have a single electron in their outer shell; as a result, carbonates of alkali metals are stable to the highest temperature. At the final temperature of 600°C in this work, it is expected metal carbonate is the final product rather than the oxide of the metal. The ketone is generally

oxidized by atmospheric oxygen to carbon dioxide and water at a temperature which is characteristic of a specific ketone.



### 3.3.4 Phase transitions by differential scanning calorimetry

DSC calorigrams of Na-carboxylates were presented in the supporting information document (Figures S38-S49). DSC-microscope and TGA analyses were made use to assist with the assignment of the transitions. Phase transitions and their associated energies were reported in Table 3-4.

**Table 3-4. Phase transitions of the Na-carboxylates determined by DSC over the temperature range  $-30^\circ\text{C}$  to the decomposition temperature.**

Na-carboxylates	Transitions <sup>a</sup>	Onset temperature (K)	Energy <sup>b</sup> (J/g)
Methanoate	s-l	530.6	-264.0
	d	841.0	-124.6
Ethanoate	s-l	601.0	-220.8
	d	c <sub>-</sub>	c <sub>-</sub>
Propanoate	s-s	469.8	-28.4
	s-s	494.2	-37.1
	s-l	561.8	-14.6
	d	791.4	-377.7
Butanoate	s-s	447.3	-15.6
	s-lc	509.0	-26.7
	lc-l	599.7	-20.4
	d	733.3	-533.7
Pentanoate	s-s	479.4	-8.5
	s-lc	501.7	-86.6
	lc-l	631.4	-15.7
	d	669.4	-440.6
Hexanoate	s-s	321.9 <sup>d</sup>	-7.66
	s-s	478.6	-12.9
	s-lc	504.9	-34.4
	lc-l	637.4	-11.9
	d	768.9	-457.9
Heptanoate	s-s	349.3 <sup>d</sup>	-10.44
	s-s	358.8	-23.0
	s-lc	512.5	-75.1
	lc-l	642.1	-9.6
	d	739.2	-458.2
Octanoate	s-s	383.8 (383.9 <sup>d</sup> )	-36.1
	s-lc	514.5	-50.1
	lc-l	636.7	-6.8
	d	747.2	-441.4
Nonanoate	s-s	412.8	51.4

	s-lc	515.6	-47.7
	lc-l	628.2	-6.0
	d	747.7	-492.7
Decanoate	s-s	409.5 <sup>d</sup>	-43.14
	s-s	414.7	-48.4
	s-lc	517.5	-43.0
	lc-l	623.8	-5.1
	d	760.4	-521.2
Undecanoate	s-s	421.5	-45.0
	s-s	453.6	-12.2
	s-lc	517.9	-37.1
	lc-l	615.2	-4.3
	d	756.6	-471.6
Dodecanoate	s-s	366.6 <sup>d</sup>	-23.04
	s-s	408.8 <sup>d</sup>	<sup>c</sup> -
	s-s	412.6	-43.0
	s-s	453.7	-16.9
	s-s	495.6	-4.7
	s-lc	520.7	-40.7
	lc-l	606.6	-4.2
	d	763.5	-522.5

<sup>a</sup> Transitions: s-s = solid-solid phase transition, s-l = solid-liquid phase transition (melting), s-lc = solid-liquid crystal phase transition, lc-l = liquid crystal-liquid phase transition, d = decomposed

<sup>b</sup> Energy changes: endothermic values are negative, exothermic values are positive

<sup>c</sup> Onset of decomposition was ill-defined and could not be determined

<sup>d</sup> Solid-solid phase transitions were observed during the Cp measurement experiments

For most of Na-carboxylates there were solid-solid phase transitions in addition to the solid-liquid phase transition. The solid-solid phase transitions were labeled reversible if the same but opposite transition could be observed upon cooling down to  $-30\text{ }^{\circ}\text{C}$ . When the same but opposite transition could not be observed on cooling to  $-30\text{ }^{\circ}\text{C}$ , the solid-solid transition was labeled as irreversible. It is likely that solid-solid transitions that were labeled as irreversible is indeed reversible and that the “irreversibility” is the result of sufficient metastability at temperatures down to  $-30\text{ }^{\circ}\text{C}$ ; therefore, the reverse solid-solid transition was not observed during analysis.

Successive stages of the melting process were observed for Na-butoanoate and onwards. The phase between the crystal solid phase and the isotropic liquid was considered to be a liquid-crystal phase. This is the state of matter that has the properties between solid crystal and common liquid. A liquid crystal phase can be detected using polarized optical microscopy, since liquid crystal phase exhibits its unique texture under this type of microscopy (Figure 3-3). The principle of the polarization of light is that light as wave oscillates in many orientations. A polarizer is a filter that only permits the light oriented in a specific direction with its polarizing direction to pass through. The two polarizers in a polarizing optical microscope are oriented at right angles to each other, hence the name; cross polar. The first polarizer is oriented in a vertical direction, so all planes of light are blocked leaving a single beam oscillating in the vertical direction. This incident beam passes through the sample, interacts with the specimen, and

continues to the second polarizer, called the analyzer. The analyzer can be oriented horizontally to the incident wave, so only light vibrating in this second direction can get through.<sup>39</sup> Since the light has already passed through the first vertical polarizer, there will be no horizontal vibrating light left over that can pass through the analyzer. The two polarizers are now crossed, and the viewer can only see darkness. The purpose of this arrangement is it allows the study of mineral characteristics.

The object of polarized light microscopy is to use plane-polarized light in this research is to analyze and identify birefringent structures. These are structures, such as liquid crystal phases, that have two different refractive indices at right angles to one another<sup>40</sup>. The liquid crystal molecules don't absorb much light; they refract it instead. Plane-polarized light only oscillates in one plane, and when this single incident beam passes through the liquid crystal a portion of it is twisted onto a different plane, producing two individual wave components in mutual perpendicular planes<sup>40</sup>. The velocities of these components are different and vary with the propagation direction through the specimen, caused by different refractive angles. As mentioned earlier, the source light has already passed through the first vertical polarizer, leaving a single beam vibrating in this same direction. When the second analyzer is used in the cross direction, only the light refracted by the liquid crystal into this same direction will pass to be seen by the viewer. Therefore, in cross polarized light a normal liquid will appear dark to a user, but a liquid crystal will twist a portion of the plane-polarized light so that the sample will be visible. The final result is a retardation of the incident beam, this is viewed at the end of the microscope as a spectrum of colors that has separated (out of phase) with the polarized beam<sup>41</sup>. The advantage of cross-polarized light microscopy is flexibility. Using only the bottom single polarizer a user can view the phase transitions of carboxylates. If the second polarizer, the analyzer, the user can find evidence of phase characteristics; proof of the existence of a liquid crystal phase.

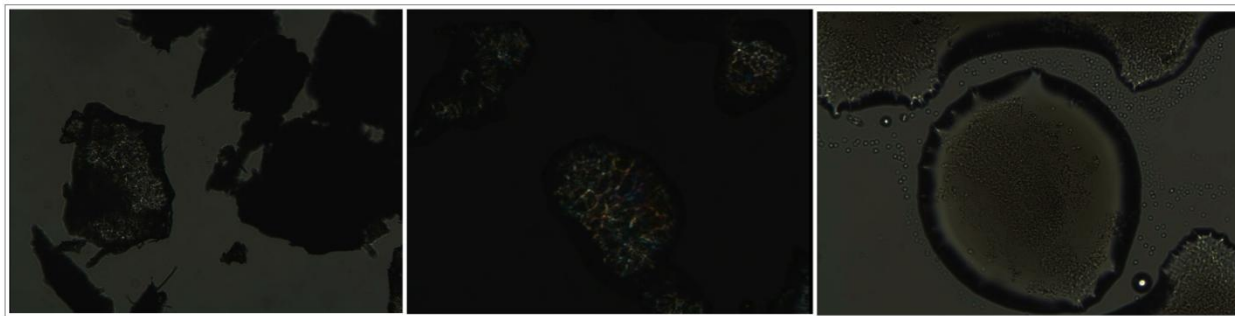


**Figure 3-3. Phase transitions of Na-octanoate. From left to right: the sample at solid phase, at liquid-crystalline phase, and at solid-liquid transition phase**

This phenomenon was not observed in the study of lithium carboxylates. The capabilities of metal alkanoates to form liquid crystalline phases (mesophases) are dictated by its cationic and anionic parameters and its crystal structure<sup>42</sup>. A rule of ionic mesogenicity can be expressed in terms of the following inequality<sup>42</sup>:

$$\frac{z_{anion} \cdot L_{anion}}{z_{cat} \cdot r_{cat}} > 3$$

at  $r_{\text{cat}} > 0.6 \text{ \AA}$

with  $r_{\text{cat}}$  = cation radius,  $L_{\text{anion}}$  = alkanooate anion length,  $z_{\text{anion}}$  = anion charge, and  $z_{\text{cat}}$  = cation charge.

The rule established evidences that a possibility of liquid-crystalline phase formation increases with increase in the alkanooate anion chain length and decreases with increase in the metal cation size and/or electrostatic charge. The metal alkanooates with such small radii of cations as  $\text{Li}^+$  do not form liquid-crystalline phase under any conditions ( $r_{\text{Li}^+} = 0.59 \text{ \AA}$ ). As a matter of fact, Li-carboxylates did not form liquid-crystalline phase meanwhile Na-carboxylates did from Na-butanoate and onwards. The second criterion of crystal structure mesogenicity is the necessity of having an infinite and continuous bridge metal-oxygen network to “sew” the alkanooate anions together into layers, and the layers into bilayers. It has been found in the coordination of metal cations in the alkanooate crystals are responsible for ionic mesogenicity. Every metal cation in the mesogenic crystals is coordinated by at least three alkanooate anions that play roles of bidentate and bridge ligands simultaneously. Two from these anions have to belong to just the same anionic layer, and the third anion has to belong to another layer. The bilayer ordering formed in this way is retained in the salt, creating the higher melting point of the metal alkanooate.

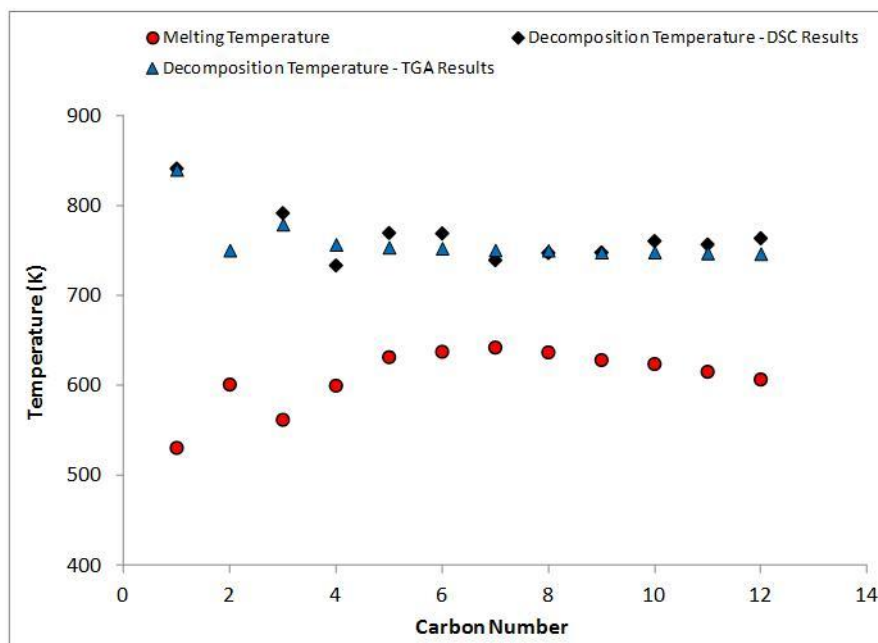


**Figure 3-4. Onset temperatures of solid-to-liquid (melting) and decomposition of Na-carboxylates as reported by TGA and DSC analysis.**

Decomposition temperatures of Na-carboxylates determined from DSC analysis were close to that of TGA analysis, i.e. within 5% difference with relatively same total % wt loss (Figure 3-4). The melting temperatures increased from Na-methanoate to Na-heptanoate (with the exception of Na-ethanoate) and decreased smoothly from Na-heptanoate onwards. The melting point of Na-carboxylates decreased with the increase in the aliphatic chain length, starting with Na-heptanoate, meanwhile same started with Li-propanoate.

Figure 3-5 shows the enthalpy of phase transition (solid-to-liquid) of sodium carboxylates in comparison with the reported literature values of their corresponding alkanolic acids. The  $\text{Na}^+$  is not contributing a constant amount of energy to the  $\Delta H_{\text{melting}}$  compared to  $\text{H}^+$  for the carboxylic acids.

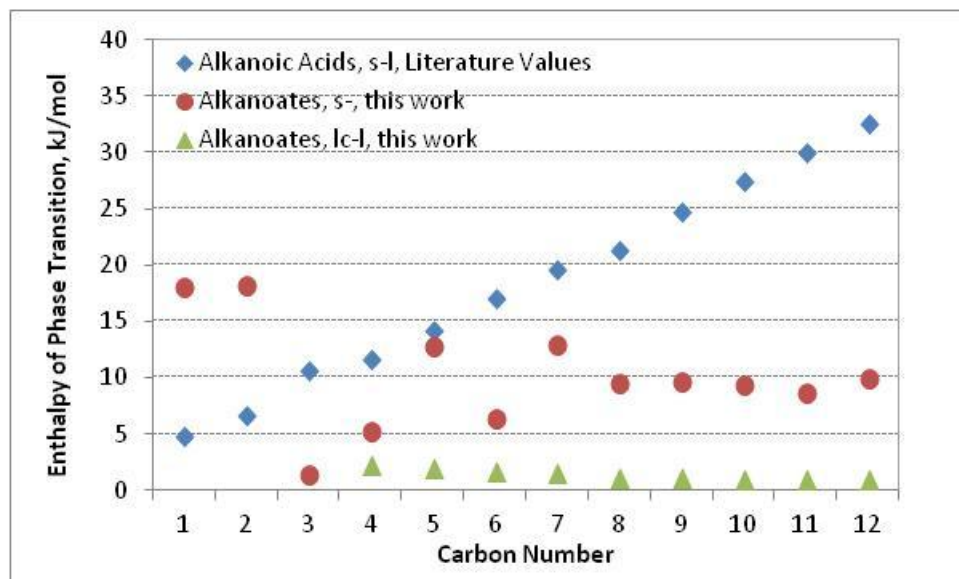


Figure 3-5. Enthalpies of Phase Transitions of Sodium alkanooates and their corresponding acids. Enthalpy values of alkanolic acids were obtained from NIST<sup>35</sup>.

Phase transitions of Na-carboxylates agreed with the literature data, as shown in Table 3-5

Table 3-5. Comparison of the phase transitions of the Na-carboxylates reported in this study with that reported in literature

Na-Methanoate	Literature Value <sup>14</sup>		This Work	
	Transitions	T/K	Transitions	T/K
	s-l	530.46	s-l	530.6 ± 0.3
Na-Propanoate	Literature Value <sup>16</sup>		This Work	
	Transitions	T/K	Transitions	T/K
	s-s	467 ± 1	s-s	469.8 ± 0.3
	s-s	491 ± 1	s-s	494.2 ± 0.3
s-l	561.88 ± 0.03	s-l	561.8 ± 0.3	

### 3.3.5 Heat capacity by differential scanning calorimetry

The heat capacities of the Na-carboxylates were determined over the temperature range -30°C to 150 °C (243 to 423 K) by DSC. All heat capacity determinations were conducted in triplicate and the heat capacity versus temperature data are provided in the supporting information (Figures S50-S61). For some of the Na-carboxylates, the heat capacity measurements crossed solid-solid phase transitions (Table 3-3). A multivariate regression analysis was performed to fit all of the  $C_p$  vs.  $T$  for each compound to a typical correlation of  $C_p$  (J/g.K) =  $A + B.T + C.T^2 + D.T^3$  with minimal error-of-fit, excluding temperature ranges where solid-to-solid phase transitions

occurred (Table 3-6). No systematic trend was observed in the heat capacities from Na-methanoate to Na-dodecanoate at the same temperature.

**Table 3-6. Constant pressure heat capacity versus temperature correlations of the solid C<sub>1</sub>-C<sub>12</sub> Na-carboxylates in the temperature range -30 to +150 °C. Gaps in the temperature region covered indicate solid-solid phase transitions.**

Na-Carboxylates	Valid Range of T (K)	C <sub>p</sub> = A + B.T + C.T <sup>2</sup> + D.T <sup>3</sup>			
		A	B	C	D
Methanoate	258.0-416.3	- 5.0926E+00	4.7461E-02	-1.1476E-04	1.1577E-07
Ethanoate	273.2-416.3	- 4.6559E+00	3.5663E-02	-4.9350E-05	4.9762E-08
Propanoate	249.7-416.3	- 5.6279E+00	5.4242E-02	-1.3951E-04	1.4257E-07
Butanoate	249.7-416.3	- 1.4092E+01	1.2234E-01	-3.1497E-04	3.0701E-07
Pentanoate	249.7-333.0	- 1.8370E+01	1.9081E-01	-6.2123E-04	6.9979E-07
Hexanoate	250.0-333.0	- 3.2406E+01	3.4216E-01	-1.1731E-03	1.3821E-06
Heptanoate	250.0-341.3	- 2.9972E+01	3.0655E-01	-1.0120E-03	1.1537E-06
Octanoate	250.0-341.3	- 2.0615E+01	2.1246E-01	-6.9241E-04	7.8936E-07
Nonanoate	250.0-366.3	3.0673E+00	-3.1115E-02	1.3011E-04	-1.2822E-07
Decanoate	250.0-374.7	- 8.0667E+00	6.5890E-02	-1.4733E-04	1.4875E-07
Undecanoate	249.7-383.0	- 3.1654E+01	3.1759E-01	-1.0211E-03	1.1277E-06
Dodecanoate	249.7-329.7	-2.5279E+01	-2.7248E-01	9.8803E-04	-1.1185E-06

C<sub>p</sub>/R literature data was plotted against the calculated C<sub>p</sub>/R data for Na-methanoate, Na-ethanoate and Na-propanoate (Figures S50-S52). The literature data was determined either by equilibrium adiabatic calorimetry or by differential scanning calorimetry. The calculated data however did not agree well with the literature data. It is not likely to reach a conclusive discussion of the possible reasons for the difference because how the heat capacity measurements were conducted and how the values were calculated was not elaborated in the literature paper. The possibility of the impurity of Na-carboxylates samples were disregarded because the onset temperatures of phase transitions were all in well agreement with literature data.

### 3.4 Summaries

The sodium C<sub>1</sub>-C<sub>12</sub> *n*-alkanoates (Na-carboxylates) were synthesized and studied over the temperature range -30 to +600 °C. Spectroscopic and thermal analyses are presented and compared to reported literature. Based on repeat measurements and calibration using standards, the onset temperatures of phase transitions were accurate to within 0.3 °C absolute and the energy changes associated with the phase transitions were accurate to within 3 % relative. Key observations from this study are:

- Evidence for a more covalent character of the Na-O bond was found only for sodium methanoate, where the difference between the asymmetric and symmetric stretching of the carboxylate,  $\Delta\nu = \nu_{as}(\text{CO}_2^-) - \nu_s(\text{CO}_2^-)$ , was 217-227 cm<sup>-1</sup>. The C<sub>2</sub>-C<sub>12</sub> Na-carboxylates had  $\Delta\nu$ -values in the range 109-167 cm<sup>-1</sup>.

- With the exception of Na-methanoate, the heavier Na-carboxylates were thermally stable to temperatures around 750K.
- Mass loss occurred in one single event upon heating, with the exception of Na-methanoate. All Na-carboxylates decomposed to produce sodium carbonate ( $\text{Na}_2\text{CO}_3$ ) as solid product and decomposition was consistent with ketonic decomposition reported in literature.
- Solid-solid phase transitions were found for all  $\text{C}_1\text{-C}_{12}$  Na-carboxylates in the temperature range studied, with the exception of sodium methanoate and ethanoate.
- Liquid crystal phases were found for  $\text{C}_4\text{-C}_{12}$  Na-carboxylates.
- The melting temperatures increased from Na-methanoate to Na-butanoate (with the exception of Na-ethanoate), remained almost constant from Na-butanoate to Na-heptanoate and decreased smoothly from Na-heptanoate onwards.
- The constant pressure heat capacity ( $C_p$ ) of the solid  $\text{C}_1\text{-C}_{12}$  Na-carboxylates was experimentally determined by DSC over the temperature range  $-30$  to  $+150$  °C. However, for the  $\text{C}_1\text{-C}_3$  Na-carboxylates, where experimental data was available in literature, meaningful differences were noted.

## 4. Potassium C<sub>1</sub>-C<sub>12</sub>*n*-alkanoates: Thermal behavior from -30 to 600 °C

### 4.1 Introduction

Potassium *n*-alkanoates (carboxylates) are the potassium salts of the corresponding linear carboxylic acids. The uses of alkali metal carboxylates and the reasons why their thermal properties are of interest were stated earlier. In addition, K-alkanoate soaps have found uses as a hydrotrope stabilizing agent in the creation of detergents, sanitizers, and other products. One specific example is the use of K-octanoate and K-decanoate for colloidal stabilization of ammonia preserved natural rubber latex, since they have the advantage of reducing the tendency to zinc-oxide thickening<sup>43</sup>. In this chapter we attempted a systematic thermal behavior study of nC<sub>1</sub>-C<sub>12</sub> K-carboxylates as well as a review and compare of previous studies in the same field.

### 4.2 Experimental

#### 4.2.1 Materials

The high purity reference materials employed for temperature and enthalpy calibration of the differential scanning calorimeter were commercially obtained and used as received. These were: indium (Impag AG, supplied by Mettler-Toledo ME-119442, indium pills, 99.999%), tin (Alfa Aesar, #11013, 99.995% metal basis), lead (Alfa Aesar, #42928, 99.999% metal basis) and zinc (Impag AG supplied by Mettler-Toledo ME-119441, 99.999%) for the differential scanning calorimeter calibration; indium (supplied by Mettler-Toledo ME – 119442), zinc (supplied by Mettler-Toledo ME-119441), Aluminum (supplied by Mettler-Toledo ME-51119701) and Gold (supplied by Mettler-Toledo ME-51140816) for Thermogravimetric Analyzer Calibration.

Praxair's Ultra High Purity 5.0 nitrogen (99.999%) was used to maintain the inert atmospheric conditions during calorimetric runs.

The potassium carboxylates employed in this study were prepared from commercially obtained potassium carbonate (Sigma-Aldrich) and the linear carboxylic acids in the C<sub>1</sub>-C<sub>12</sub> range. Methanoic acid (99%), nonanoic acid (97%) and undecanoic acid (99%) were supplied by Acros Organics. Ethanoic acid (99.7%), propanoic acid (99.5%), butanoic acid (+99%), pentanoic acid (99%) and hexanoic acid (99%) were supplied by Aldrich. Heptanoic acid (+97%), octanoic acid (+99%), decanoic acid (96%) and dodecanoic acid (+99%) were supplied by Sigma.

The solvents that were used in the study were methanol (98%) and 2-propanol (+99.5%) supplied by Sigma-Aldrich and Ethanol (+99.8%) supplied by Fluka. Deionized water was prepared in the laboratory using a Millipore water purification system.

#### 4.2.2 Analytical equipment and procedure

The same analytical equipment and procedures were employed as for the study of the lithium carboxylates (Chapter 2 - Section 2.2.2)

#### 4.2.3 Calibration

The same temperature and caloric calibration was performed as for the study of the lithium carboxylates (Chapter 2 – Section 2.2.3)

#### 4.2.4 Synthesis of potassium alkanoates

The synthesis and purification of K-carboxylates were based on the work of Franzosini et al<sup>15</sup>. K-carboxylates were prepared by mixing potassium carbonate (in anhydrous methanol) with a slight excess (2% molar excess) of carboxylic acids. The mixture was stirred for several hours without heating to allow sufficient time for the neutralization reaction to be complete, using a Heidolph MR Hei-Standard hot plate (heating power of 800W, maximum temperature of 300 °C, 30-1400 rpm at an accuracy of  $\pm 1\%$ ). Solid K-carboxylates were recovered by evaporation of the solvent and excess acid at 60 °C under reduced pressure at 9.6 kPa (absolute), using a HeidolphHei-VAP Precision with glassware set G3 rotary evaporator. The K-carboxylates were purified by recrystallizing the products from a mixture of 2-propanol + ethanol + methanol (4:2:1 by volume) and were further dried under vacuum at approximately 100 °C until they reached constant mass. The final products were finely ground before being used for thermal analysis.

### 4.3 Results & Discussions

#### 4.3.1 Infrared Spectroscopy

Infrared spectroscopy was used primarily to confirm the success of the synthesis of the K-carboxylates and provide information on structural changes that were observed during calorimetry. The IR spectra of the K-carboxylates are provided in the supporting information (Figures S1-S12). In general, bands corresponding to aliphatic CH<sub>2</sub> and CH<sub>3</sub> stretching vibrations are observed below 3000cm<sup>-1</sup>. The difference between K-methanoate and heavier carboxylates lies in the intensity of the aliphatic CH<sub>2</sub> and CH<sub>3</sub> stretching vibrations, the longer the aliphatic chain of the carboxylates is, the more intense it is. Methyl and methylene bending and rocking vibrations are measured between 500 and 1400cm<sup>-1</sup>. The C=O stretching vibration observed in the alkanolic acid around 1700cm<sup>-1</sup> disappears in the K-carboxylates and is replaced by two new absorption bands. These bands correspond to the symmetric and asymmetric stretching vibrations of the carboxylate ion and listed in Table 4-1. The relative position of these two bands  $\Delta = \nu_{\text{asym}}(\text{COO}^-) - \nu_{\text{sym}}(\text{COO}^-)$  can be used to shed light on the type of carboxylate-to-metal complexation structure present in a given metal carboxylate<sup>29</sup>. Four metal-carboxylate configurations are possible (Figure 2-1). Ionic and bridging carboxylate structures cannot be distinguished from  $\Delta\nu$ , since the values for these two configurations overlap. Monodentate bonding, where the K-O bond has covalent character, results in a much larger  $\Delta\nu$  than the ionic form, typically 200-300 cm<sup>-1</sup>. Conversely, bidentate bridging results in a much smaller  $\Delta\nu$  than

the ionic form, typically  $<100\text{ cm}^{-1}$ . Spectroscopic evidence for a more covalent character of the K-O bond was found only for potassium methanoate, which has  $\Delta\nu = 194\text{-}218\text{ cm}^{-1}$  (Table 4-1). The  $\text{C}_2\text{-C}_{12}$  K-carboxylates all have  $\Delta\nu$  values in the range typical of either ionic or bridging structures.

**Table 4-1. Strong carboxylate stretching vibrations in the IR spectra of the K-carboxylates**

K-carboxylates	Carboxylate stretching vibrations ( $\text{cm}^{-1}$ )			$\Delta\nu$ ( $\text{cm}^{-1}$ )
	IR, asymmetric	IR, symmetric		
Methanoate	1558	1364	1340	194-218
Ethanoate	1559	1395		164
Propanoate	1559	1410		149
Butanoate	1559	1402		157
Pentanoate	1561	1410		151
Hexanoate	1560	1404		156
Heptanoate	1559	1408		151
Octanoate	1561	1407		154
Nonanoate	1560	1410		150
Decanoate	1561	1411		150
Undecanoate	1558	1412		146
Dodecanoate	1557	1409		148

#### 4.3.2. Ultraviolet-visible spectroscopy

The UV-Vis spectrum of carboxylate group is characterized mainly by a high intensity  $\pi \rightarrow \pi^*$  transition at around 200 nm; the  $n \rightarrow \pi^*$  transition at longer wavelength is weak **Error! Reference source not found.** The UV-Vis spectra of the K-carboxylates are provided in the supporting information (Figures S13-S24). The  $\pi \rightarrow \pi^*$  transitions are listed in Table 4-2.

**Table 4-2. Carboxylate high intensity  $\pi \rightarrow \pi^*$  transitions in the UV-Vis spectra of the K-carboxylates.**

K-Carboxylates	Carboxylate $\pi \rightarrow \pi^*$ transition (nm)
Methanoate	187
Ethanoate	187
Propanoate	187
Butanoate	189, 187
Pentanoate	187
Hexanoate	188
Heptanoate	187
Octanoate	187
Nonanoate	187
Decanoate	187
Undecanoate	186
Dodecanoate	187

#### 4.3.3 Decomposition by thermogravimetric analysis

The decomposition temperature and total mass loss during decomposition was determined by TGA under inert atmosphere (Table 4-3). The TGA curves over the temperature range of 150 to 600 °C (423 to 873 K) are provided in the supporting information (Figure S37).

**Table 4-3. Onset temperature of decomposition and mass loss of K-carboxylates determined by TGA, as well as the calculated mass loss assuming that the solid residue is K<sub>2</sub>CO<sub>3</sub>.**

K-carboxylates	Onset of decomposition (K)	TGA mass loss (%)	Calculated mass loss (%)
Methanoate	857.8	17.0	17.9
Ethanoate	751.5	26.1	29.6
Propanoate	771.6	34.7	38.4
Butanoate	759.6	43.5	45.2
Pentanoate	758.2	50.8	50.7
Hexanoate	753.5	55.7	55.2
Heptanoate	752.0	57.7	58.9
Octanoate	755.2	58.3	62.1
Nonanoate	756.2	64.1	64.8
Decanoate	755.8	70.1	67.2
Undecanoate	757.1	68.0	69.2
Dodecanoate	754.0	69.0	71.1

Figure 4-1 shows IR spectrum of the residue of K-carboxylates at 600°C in comparison with IR spectrum of pure potassium carbonate. IR results confirmed that potassium carbonate is the final residue of K-carboxylates when the samples were subjected to the final temperature of 600°C. All potassium carboxylates decomposed in one single step to the final product potassium carbonate. The exception is K-methanoate. It is suggested that the K-methanoate decompose to form the respective carbonate and oxalates in a first stage. The oxalate formed from this first stage decomposes further to carbonates and carbon monoxide. The formation of oxalate did not occur in the cases of Li- and Cs-methanoates. Acetates and higher carboxylates generally decompose via the formation of the metal carbonate and an organic component ketone, both of which decompose according to their own characteristics. Calculated total mass loss keeping in mind that potassium carbonate was the final residue of K-carboxylates at 600°C were compared with the TGA total mass loss with percentage difference less than 7% (Table 4-3).

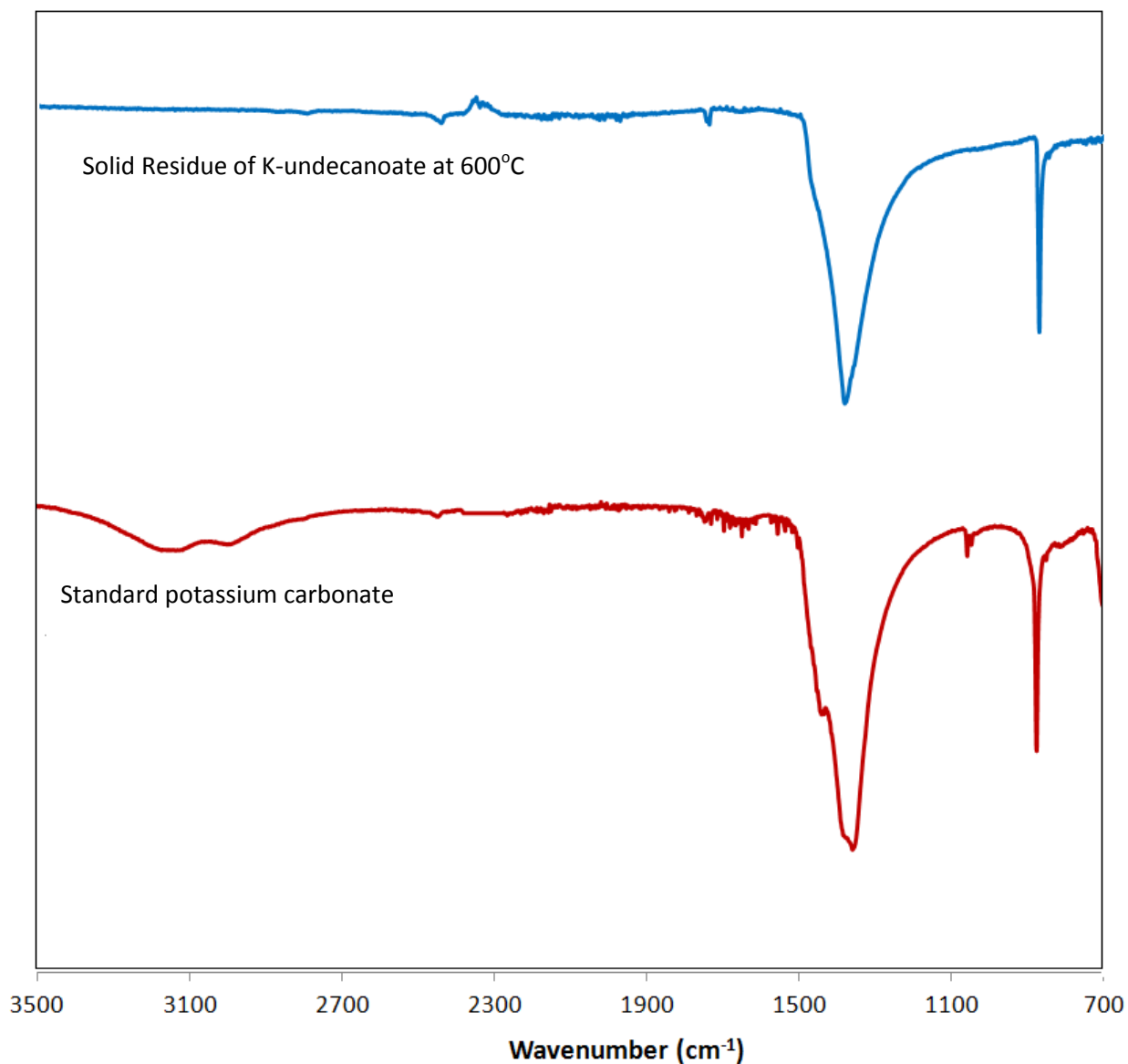


**Figure 4-1 Infrared spectrum of the solid residue after thermal decomposition of potassium undecanoate and that of potassium carbonate showed for comparison**

#### 4.3.4 Phase transitions by differential scanning calorimetry

DSC calorigrams of K-carboxylates were presented in the supporting information document (Figures S26-S37). DSC-microscope and TGA analyses were made use to assist with the assignment of the transitions. Phase transitions and their associated energies were reported in Table 4-4.

**Table 4-4. Phase transitions of the K-carboxylates determined by DSC over the temperature range  $-30^{\circ}\text{C}$  to the decomposition temperature.**

K-carboxylates	Transitions <sup>a</sup>	Onset temperature (K)	Energy <sup>b</sup> (J/g)
Methanoate	s-l	442.6	-134.2

	d	c <sub>-</sub>	c <sub>-</sub>
Ethanoate	s-s	331.7 <sup>d</sup>	-0.77
	s-l	578.7	-164.5
	d	784.7	-144.6
Propanoate	s-s	352.1 (353.4 <sup>d</sup> )	-15.6
	s-l	636.9	-182.3
	d	756.7	-555.3
Butanoate	s-s	181.6	-5.1
	s-s	563.3	-32.4
	s-lc	623.3	-84.1
	lc-l	667.0	-39.1
	d	750.4	-600.4
Pentanoate	s-s	397.7 <sup>d</sup>	-3.18
	s-s	589.1	-96.3
	s-l	697.9	-30.8
	d	739.5	-377.7
Hexanoate	s-s	577.6	-78.4
	s-l	712.6	-20.1
	d	737.7	-300.6
Heptanoate	s-s	320.9	-23.4
	s-s	333.7 <sup>d</sup>	-80.89
	s-s	566.5	-71.3
	s-l	716.8	-15.9
	d	738.3	-271.1
Octanoate	s-s	320.1	-15.6
	s-s	327.6 <sup>d</sup>	-61.2
	s-s	557.7	-72.1
	s-l	713.0	-10.8
	d	732.3	-345.6
Nonanoate	s-s	356.3	-44.9
	s-s	367.8 <sup>d</sup>	-78.3
	s-s	544.9	-74.4
	s-l	704.5	-9.5
	d	713.6	-370.9
Decanoate	s-s	334.0 <sup>d</sup>	-2.47
	s-s	346.4	-28.2
	s-s	349.5 <sup>d</sup>	-58.3
	s-s	383.2 <sup>d</sup>	-5.18
	s-s	546.6	-85.2
	s-l	691.5	-8.2
	d	745.3	-409.7
Undecanoate	s-s	353.3 (354.5 <sup>d</sup> )	-86.5
	s-s	542.5	-78.6
	s-l	680.8	-7.9
	d	717.0	-422.0

Dodecanoate	s-s	328.8 (328.1 <sup>d</sup> )	-49.5
	s-s	367.3 (365.1 <sup>d</sup> )	-1.92
	s-s	407.3 (405.3 <sup>d</sup> )	-13.1
	s-s	489.1	-18.4
	s-s	543.4	-50.1
	s-l	671.9	-5.9
	d	739.3	-467.3

<sup>a</sup> Transitions: s-s = solid-solid phase transition, s-l = solid-liquid phase transition (melting), s-lc = solid-liquid crystal phase transition, lc-l = liquid crystal-liquid phase transition, d = decomposed

<sup>b</sup> Energy changes: endothermic values are negative, exothermic values are positive

<sup>c</sup> Onset of decomposition was ill-defined and could not be determined

<sup>d</sup> Solid-solid phase transitions were observed during the Cp measurement experiments

For most of K-carboxylates there were solid-solid phase transitions in addition to the solid-liquid phase transition. K-butanoate is the shortest member of the K-carboxylates family which can exist as a mesomorphic liquid and the only in our study. Literature reported that K-hexanoate, like its earlier homolog potassium butanoate, exhibited a liquid crystalline phase at higher temperatures before finally clearing to the isotropic liquid (solid-to-liquid transition) as well <sup>18</sup>; however, this phenomenon was not observed. The capabilities of metal alkanates to form liquid crystalline phases (mesophases) are dictated by its cationic and anionic parameters and its crystal structure and explained in the previous chapter.

Decomposition followed immediately after clearing to isotropic liquid, making it difficult to evaluate the onset temperatures for decomposition. Decomposition temperatures of K-carboxylates determined from DSC analysis were close to that of TGA analysis, i.e. within 5% difference with relatively same total % wt loss (Figure 4-3).

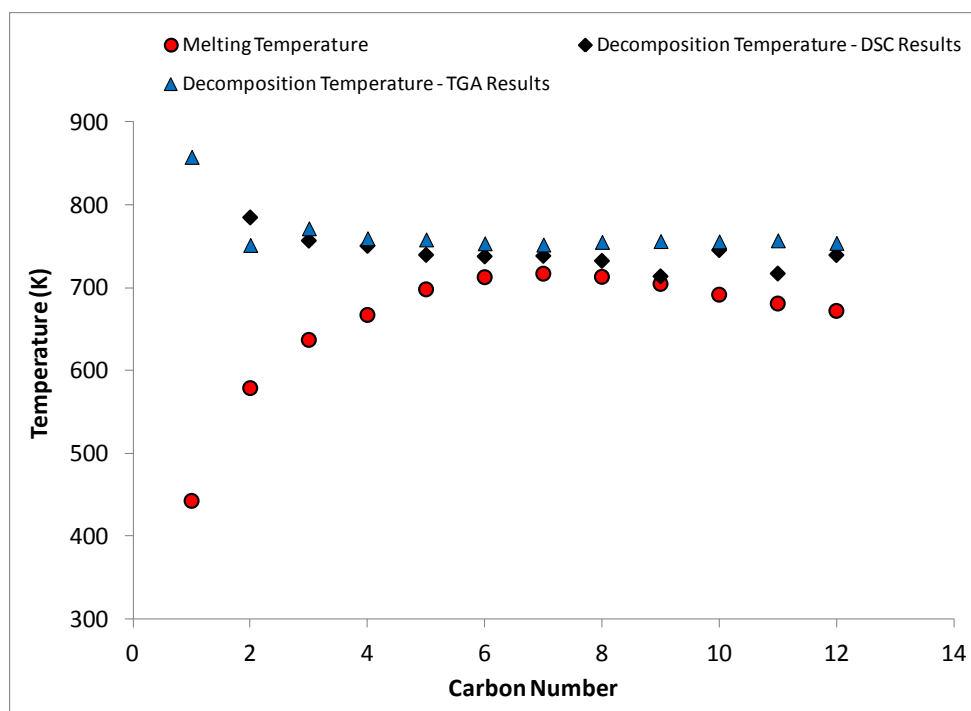


**Figure 4-2.** Onset temperatures of solid-to-liquid (melting) and decomposition of K-carboxylates as reported by TGA and DSC analysis.

Onset decomposition temperature of K-methanoate which was evaluated from the DSC results corresponded with the onset temperature of the first-stage of decomposition. The temperature as shown in Figure 4-2 was the onset temperature of the final stage of decomposition (which was also the second stage). It was also the highest decomposition temperature among the K-carboxylates in this study. The length of the aliphatic chain did not have much effect on the onset decomposition temperatures of K-carboxylates; in fact, they stayed almost constant from K-ethanoate onwards. The melting temperatures increased from K-methanoate to K-heptanoate and decreased smoothly from K-heptanoate onwards. The melting point of K-carboxylates decreased with the increase in the aliphatic chain length, starting with K-heptanoate, meanwhile same started with Li-propanoate.

Figure 4-3 shows the enthalpy of phase transition (solid-to-liquid) of K-carboxylates in comparison with the reported literature values of their corresponding alkanolic acids. The  $K^+$  is not contributing a constant amount of energy to the  $\Delta H_{\text{melting}}$  compared to  $H^+$  for the carboxylic acids.

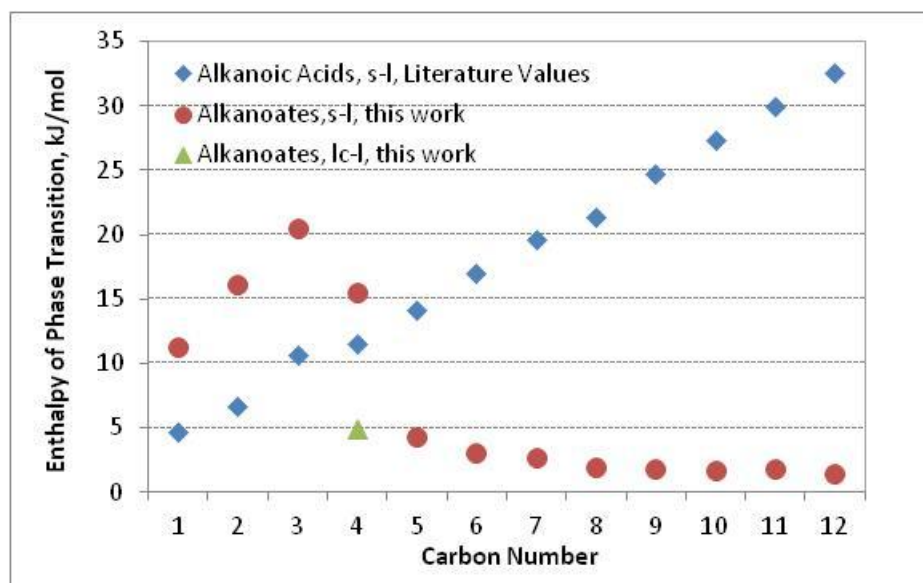


Figure 4-3. Enthalpies of Phase Transitions of Potassium alkananoates and their corresponding acids. Enthalpy values of alkananoic acids were obtained from NIST<sup>35</sup>.

Phase transitions of K-carboxylates agreed with the literature data, as shown in Table 4-5

A solid-to-solid phase transition ( $258 \pm 2\text{K}$ ) was detected when K-propanoate was cooled to about 30K below  $258\text{K}$ <sup>15</sup>. The solid-to-solid transition was not detected in this study; perhaps it is due to the difference in our experimental procedure, of which the sample was cooled to  $243.15\text{K}$  only.

Both of the solid state transformation are split into two component peaks for K-butanoate<sup>13</sup>. First solid-to-solid transition  $461.4\text{K} \pm 0.5\text{K}$  and  $467.2\text{K} \pm 0.5\text{K}$ , second solid-to-solid transition  $541\text{K} \pm 1\text{K}$ ,  $562.2\text{K} \pm 0.5\text{K}$ . No splitting was observed in this work. Only one solid-to-solid transition was observed.

Table 4-5. Comparison of the phase transitions of the K-carboxylates reported in this study with that reported in literature

Ethanoate	Literature Value <sup>35</sup>		This Work	
	Transition	T/K	Transition	T/K
	s-l	578.7	s-l	$578.7 \pm 0.3$
Propanoate	Literature Value <sup>15</sup>		This Work	
	Transition	T/K	Transition	T/K
	s-s	$258 \pm 2$		
	s-s	352.5	s-s	$352.1 \pm 0.3$
s-l	638.3	s-l	$636.9 \pm 0.3$	
Butanoate	Literature Value <sup>13</sup>		This work	
	Transition	T/K	Transition	T/K
	s-s	$461.4 \pm 0.5$		
	s-s	$467.2 \pm 0.5$		

	s-s	541 ± 1		
	s-s	562.2 ± 0.5	s-s	563.3 ± 0.3
	s-lc	626.1 ± 0.5	s-lc	623.3 ± 0.3
	lc-l	677.3 ± 0.5	lc-l	667.0 ± 0.3
Octanoate	Literature Value <sup>44</sup>		This work	
	Transition	T/K	Transition	T/K
	s-s	328.15	s-s	320.1 ± 0.3
Decanoate	Literature Value <sup>44</sup>		This work	
	Transition	T/K	Transition	T/K
	s-s	349.15	s-s	346.4 ± 0.3
Dodecanoate	Literature Value <sup>44</sup>		This work	
	Transition	T/K	Transition	T/K
	s-s	327.15	s-s	328.8 ± 0.3

#### 4.3.5 Heat capacity by differential scanning calorimetry

The heat capacities of the K-carboxylates were determined over the temperature range -30°C to 150 °C (243 to 423 K) by DSC. All heat capacity determinations were conducted in triplicate and the heat capacity versus temperature data are provided in the supporting information (Figures S38-S49). For some of the K-carboxylates, the heat capacity measurements crossed solid-solid phase transitions (Table 4-3). A multivariate regression analysis was performed to fit all of the Cp vs. T for each compound to a typical correlation of  $C_p \text{ (J/g.K)} = A + B.T + C.T^2 + D.T^3$  with minimal error-of-fit, excluding temperature ranges where solid-to-solid phase transitions occurred (Table 4-6). No systematic trend was observed in the heat capacities from K-methanoate to K-dodecanoate at the same temperature. Splitting was observed for K-heptanoate, nonanoate, decanoate.

**Table 4-6. Constant pressure heat capacity versus temperature correlations of the solid C<sub>1</sub>-C<sub>12</sub> K-carboxylates in the temperature range -30 to +150 °C. Gaps in the temperature region covered indicate solid-solid phase transitions.**

K-Carboxylates	Valid Range of T (K)	$C_p \text{ (J/g.K)} = A + B.T + C.T^2 + D.T^3$			
		A	B	C	D
Methanoate	253.0-399.7	- 3.4336E+00	3.5674E-02	-9.5190E-05	9.7702E-08
Ethanoate	249.7-323.0	- 3.8621E+01	3.8555E-01	-1.2564E-03	1.4023E-06
	339.7-416.3	-3.2161E+01	2.7239E-01	-7.4146E-04	7.0021E-07
Propanoate	249.7-346.3	- 3.7529E+01	3.7268E-01	-1.2038E-03	1.3352E-06
	373.0-416.3	7.0994E+00	-3.8302E-02	8.4639E-05	-3.5250E-08
Butanoate	258.0-416.3	- 1.1054E+00	1.3856E-02	-2.2472E-05	2.5371E-08
Pentanoate	249.7-326.0	- 4.2763E+01	4.2754E-01	-1.3990E-03	1.5726E-06
	333.0-396.3	-9.3247E+00	6.4396E-02	-1.1486E-04	8.4287E-08
Hexanoate	271.3-406.3	9.8223E-01	3.7978E-03	-9.4807E-06	3.6669E-08
Heptanoate	251.3-328.0	- 3.7069E+01	3.6862E-01	-1.1923E-03	1.3484E-06
	373.0-416.3	2.0530E+02	-1.5645E+00	4.0132E-03	-3.3942E-06
Octanoate	249.7-321.2	- 4.2973E+01	4.3765E-01	-1.4577E-03	1.6694E-06

	339.7-394.7	-9.5283E+01	7.9528E-01	-2.1740E-03	2.0094E-06
Nonanoate	249.7-358.0	-1.9495E+01	1.8190E-01	-5.3342E-04	5.6378E-07
Decanoate	291.3-332.2	- 8.4060E+01	8.5405E-01	-2.8444E-03	3.1890E-06
Undecanoate	249.7-336.3	- 4.4886E+01	4.4664E-01	- 1.4534E-03	1.6361E-06
	366.3-406.3	-6.0783E+02	4.8329E+00	-1.2778E-02	1.1311E-05
Dodecanoate	249.7-316.3	- 6.9064E+01	7.1221E-01	-2.4215E-03	2.8036E-06
	349.3-358.2	- 2.3714E+02	2.1291E+00	-6.3380E-03	6.3445E-06
	340.2-346.3	6.0192E+03	-5.2529E+01	1.5283E-01	-1.4814E-04
	372.2-403.0	-1.9074E+03	1.4989E+01	-3.9243E-02	3.4307E-05

Cp/R literature data was plotted against the calculated Cp/R data for K-ethanoate, K-propanoate, K-butanoate and K-hexanoate (Figures S38-S49). The literature data was determined either by equilibrium adiabatic calorimetry or by differential scanning calorimetry. The calculated data however did not agree well with the literature data. It is not likely to reach a conclusive discussion of the possible reasons for the difference because how the heat capacity measurements were conducted and how the values were calculated was not elaborated in the literature paper. The Cp measurements obtained from adiabatic calorimetry did not agree with the Cp measurement obtained from the differential scanning calorimeter for the K-hexanoate in the literature. The possibility of the impurity of K-carboxylates samples were disregarded because the onset temperatures of phase transitions were all in agreement with literature data.

#### 4.4 Summaries

The potassium C<sub>1</sub>-C<sub>12</sub> *n*-alkanoates (K-carboxylates) were synthesized and studied over the temperature range -30 to +600 °C. Spectroscopic and thermal analyses are presented and compared to reported literature. Based on repeat measurements and calibration using standards, the onset temperatures of phase transitions were accurate to within 0.3 °C absolute and the energy changes associated with the phase transitions were accurate to within 3 % relative. Key observations from this study are:

- Evidence for a more covalent character of the K-O bond was found only for potassium methanoate, where the difference between the asymmetric and symmetric stretching of the carboxylate,  $\Delta\nu = \nu_{as}(\text{CO}_2^-) - \nu_s(\text{CO}_2^-)$ , was 194-218cm<sup>-1</sup>. The C<sub>2</sub>-C<sub>12</sub> K-carboxylates had  $\Delta\nu$ -values in the range 146-164 cm<sup>-1</sup>.
- The melting temperatures increased from K-methanoate to K-heptanoate and decreased smoothly from K-heptanoate onwards. The length of the aliphatic chain did not have much effect on the onset decomposition temperatures of K-carboxylates; in fact, the difference is insignificant from K-ethanoate onwards.
- Mass loss occurred in one single event upon heating, with the exception of K-methanoate. All K-carboxylates decomposed to produce potassium carbonate (K<sub>2</sub>CO<sub>3</sub>) as solid product and decomposition was consistent with ketonic decomposition reported in literature.

- Solid-solid phase transitions were found for all C<sub>1</sub>-C<sub>12</sub> K-carboxylates in the temperature range studied, with the exception of potassium methanoate.
- Liquid crystalline formation (mesophases) was observed for K-butanoate only.
- The constant pressure heat capacity (C<sub>p</sub>) of the solid C<sub>1</sub>-C<sub>12</sub> K-carboxylates was experimentally determined by DSC over the temperature range -30 to +150 °C. However, for the C<sub>2</sub>, C<sub>3</sub>, C<sub>4</sub> and C<sub>6</sub> K-carboxylates, where experimental data was available in literature, meaningful differences were noted.

## 5. Rubidium C<sub>1</sub>-C<sub>12</sub>*n*-alkanoates: Thermal behavior from -30 to 600 °C

### 5.1 Introduction

Rubidium *n*-alkanoates (carboxylates) are the rubidium salts of the corresponding linear carboxylic acids. The uses of alkali metal carboxylates and the reasons why their thermal properties are of interest were stated earlier. In this chapter we attempted a systematic thermal behavior study of nC<sub>1</sub>-nC<sub>12</sub> Rb-carboxylates as well as a review and compare of previous studies in the same field.

### 5.2 Experimental

#### 5.2.1 Materials

The high purity reference materials employed for temperature and enthalpy calibration of the differential scanning calorimeter were commercially obtained and used as received. These were: indium (Impag AG, supplied by Mettler-Toledo ME-119442, indium pills, 99.999%), tin (Alfa Aesar, #11013, 99.995% metal basis), lead (Alfa Aesar, #42928, 99.999% metal basis) and zinc (Impag AG supplied by Mettler-Toledo ME-119441, 99.999%) for the differential scanning calorimeter calibration; indium (supplied by Mettler-Toledo ME – 119442), zinc (supplied by Mettler-Toledo ME-119441), Aluminum (supplied by Mettler-Toledo ME-51119701) and Gold (supplied by Mettler-Toledo ME-51140816) for Thermogravimetric Analyzer Calibration.

Praxair's Ultra High Purity 5.0 nitrogen (99.999%) was used to maintain the inert atmospheric conditions during calorimetric runs.

The rubidium carboxylates employed in this study were prepared from commercially obtained rubidium carbonate (99% Aldrich) and the linear carboxylic acids in the C<sub>1</sub>-C<sub>12</sub> range. Methanoic acid (99%), nonanoic acid (97%) and undecanoic acid (99%) were supplied by Acros Organics. Ethanoic acid (99.7%), propanoic acid (99.5%), butanoic acid (+99%), pentanoic acid (99%) and hexanoic acid (99%) were supplied by Aldrich. Heptanoic acid (+97%), octanoic acid (+99%), decanoic acid (96%) and dodecanoic acid (+99%) were supplied by Sigma.

The solvents that were used in the study were ethanol (puriss.p.a., ACS reagent, absolute alcohol, without additive, A15 o<sup>1</sup>, ≥99.8%) supplied by Fluka, n-butanol (+99.9%, FCC) and n-heptane (anhydrous 99%) supplied by Sigma-Aldrich.

#### 5.2.2 Analytical equipment and procedure

The same analytical equipment and procedures were employed as for the study of the lithium carboxylates (Chapter 2 - Section 2.2.2)

### 5.2.3 Calibration

The same temperature and caloric calibration was performed as for the study of the lithium carboxylates (Chapter 2 – Section 2.2.3)

### 5.2.4 Synthesis of rubidium alkanoates

The synthesis and purification of Rb-carboxylates were based on the work of Martinez Casado et al<sup>36</sup>. Rb-carboxylates were prepared by the chemical reaction between rubidium carbonate (in anhydrous ethanol) and a slight excess amount of carboxylic acids (2% molar excess). The mixture was stirred for several hours without heating to allow sufficient time for the neutralization reaction to be complete, using a Heidolph MR Hei-Standard hot plate (heating power of 800W, maximum temperature of 300 °C, 30-1400 rpm at an accuracy of  $\pm 1\%$ ). Solid Rb-carboxylates were recovered by evaporation of the solvent and excess acid at 60 °C under reduced pressure at 9.6 kPa (absolute), using a HeidolphHei-VAP Precision with glassware set G3 rotary evaporator. The recrystallization was carried out in n-butanol, washed with n-heptane and then vacuum dried at approximately 100 °C until they reached constant mass. The final products were finely ground before being used for thermal analysis.

## 5.3 Results & Discussions

### 5.3.1 Infrared Spectroscopy

Infrared spectroscopy was used primarily to confirm the success of the synthesis of the Rb-carboxylates and provide information on structural changes that were observed during calorimetry. The IR spectra of the Rb-carboxylates are provided in the supporting information (Figures S1-S12). In general, bands corresponding to aliphatic CH<sub>2</sub> and CH<sub>3</sub> stretching vibrations are observed below 3000cm<sup>-1</sup>. The difference between Rb-methanoate and heavier carboxylates lies in the intensity of the aliphatic CH<sub>2</sub> and CH<sub>3</sub> stretching vibrations, the longer the aliphatic chain of the carboxylates is, the more intense it is. Methyl and methylene bending and rocking vibrations are measured between 500 and 1400cm<sup>-1</sup>. The C=O stretching vibration observed in the alkanoic acid around 1700cm<sup>-1</sup> disappears in the Rb-carboxylates and is replaced by two new absorption bands. These bands correspond to the symmetric and asymmetric stretching vibrations of the carboxylate ion and listed in Table 5-1. The relative position of these two bands  $\Delta = \nu_{\text{asym}}(\text{COO}^-) - \nu_{\text{sym}}(\text{COO}^-)$  can be used to shed light on the type of carboxylate-to-metal complexation structure present in a given metal carboxylate<sup>29</sup>. Four metal-carboxylate configurations are possible (Figure 2-1). Ionic and bridging carboxylate structures cannot be distinguished from  $\Delta\nu$ , since the values for these two configurations overlap. Monodentate bonding, where the Rb-O bond has covalent character, results in a much larger  $\Delta\nu$  than the ionic form, typically 200-300 cm<sup>-1</sup>. Conversely, bidentate bridging results in a much smaller  $\Delta\nu$  than the ionic form, typically <100 cm<sup>-1</sup>. Spectroscopic evidence for a more covalent character of the Rb-O bond was found only for rubidium methanoate, which has  $\Delta\nu = 200-223$  cm<sup>-1</sup> (Table 5-1). The C<sub>2</sub>-C<sub>12</sub> Rb-carboxylates all have  $\Delta\nu$  values in the range typical of either ionic or bridging structures.

**Table 5-1. Strong carboxylate stretching vibrations in the IR spectra of the Rb-carboxylates**

Rb-carboxylates	Carboxylate stretching vibrations (cm <sup>-1</sup> )		$\Delta\nu$ (cm <sup>-1</sup> )
	IR, asymmetric	IR, symmetric	
Methanoate	1561	1361, 1338	200-223
Ethanoate	1554	1391	163
Propanoate	1559	1395, 1361	164-198
Butanoate	1557	1397	160
Pentanoate	1560	1401	159
Hexanoate	1560	1400	160
Heptanoate	1559	1404	155
Octanoate	1560	1401	159
Nonanoate	1559	1405	154
Decanoate	1558	1407	151
Undecanoate	1558	1409	149
Dodecanoate	1553	1394	159

### 5.3.2. Ultraviolet-visible spectroscopy

The UV-Vis spectrum of the carboxylate group is characterized mainly by a high intensity  $\pi \rightarrow \pi^*$  transition at around 200 nm; the  $n \rightarrow \pi^*$  transition at longer wavelength is weak. The UV-Vis spectra of the Rb-carboxylates are provided in the supporting information (Figures S13-S24). The  $\pi \rightarrow \pi^*$  transitions are listed in Table 5-2.

**Table 5-2. Carboxylate high intensity  $\pi \rightarrow \pi^*$  transitions in the UV-Vis spectra of the Rb-carboxylates.**

Rb-Carboxylates	Carboxylate $\pi \rightarrow \pi^*$ transition (nm)
Methanoate	188
Ethanoate	189
Propanoate	187
Butanoate	188
Pentanoate	187
Hexanoate	188
Heptanoate	187
Octanoate	187
Nonanoate	187
Decanoate	187
Undecanoate	187
Dodecanoate	187

### 5.3.3 Decomposition by thermogravimetric analysis

The decomposition temperature and total mass loss during decomposition was determined by TGA under inert atmosphere (Table 5-3). The TGA curves over the temperature range of 150 to 600 °C (423 to 873 K) are provided in the supporting information (Figure S37).

**Table 5-3. Onset temperature of decomposition and mass loss of Rb-carboxylates determined by TGA, as well as the calculated mass loss assuming that the solid residue is  $\text{Rb}_2\text{CO}_3$ .**

Rb-carboxylates	Onset of decomposition (K)	TGA mass loss (%)	Calculated mass loss (%)
Methanoate	834.9	10.8	11.5
Ethanoate	758.6	20.5	20.1
Propanoate	766.3	25.4	27.2
Butanoate	757.0	35.4	33.1
Pentanoate	756.0	37.2	38.1
Hexanoate	758.8	42.2	42.4
Heptanoate	752.9	46.8	46.2
Octanoate	752.2	50.1	49.5
Nonanoate	754.3	53.5	52.4
Decanoate	753.7	53.6	55.0
Undecanoate	752.4	55.8	57.4
Dodecanoate	753.4	57.6	59.5

Figure 5-1 shows IR spectrum of the residue of Rb-carboxylates at 600°C in comparison with IR spectrum of pure rubidium carbonate. IR results confirmed that rubidium carbonate is the final residue of Rb-carboxylates when the samples were subjected to the final temperature of 600°C. All rubidium carboxylates decomposed in one step to the final product sodium carbonate. The exception is Rb-methanoate, It is suggested that the Rb-methanoate decompose to form the respective carbonate and oxalates in a first stage. The oxalate formed from this first stage decomposes further to carbonates and carbon monoxide. The formation of oxalate did not occur in the cases of lithium and cesium methanoates. Acetates and higher carboxylates generally decompose via the formation of the metal carbonate and an organic component ketone, both of which decompose according to their own characteristics. Calculated total mass loss keeping in mind that rubidium carbonate was the final residue of Rb-carboxylates at 600°C were compared with the TGA total mass loss with percentage difference less than 7%.

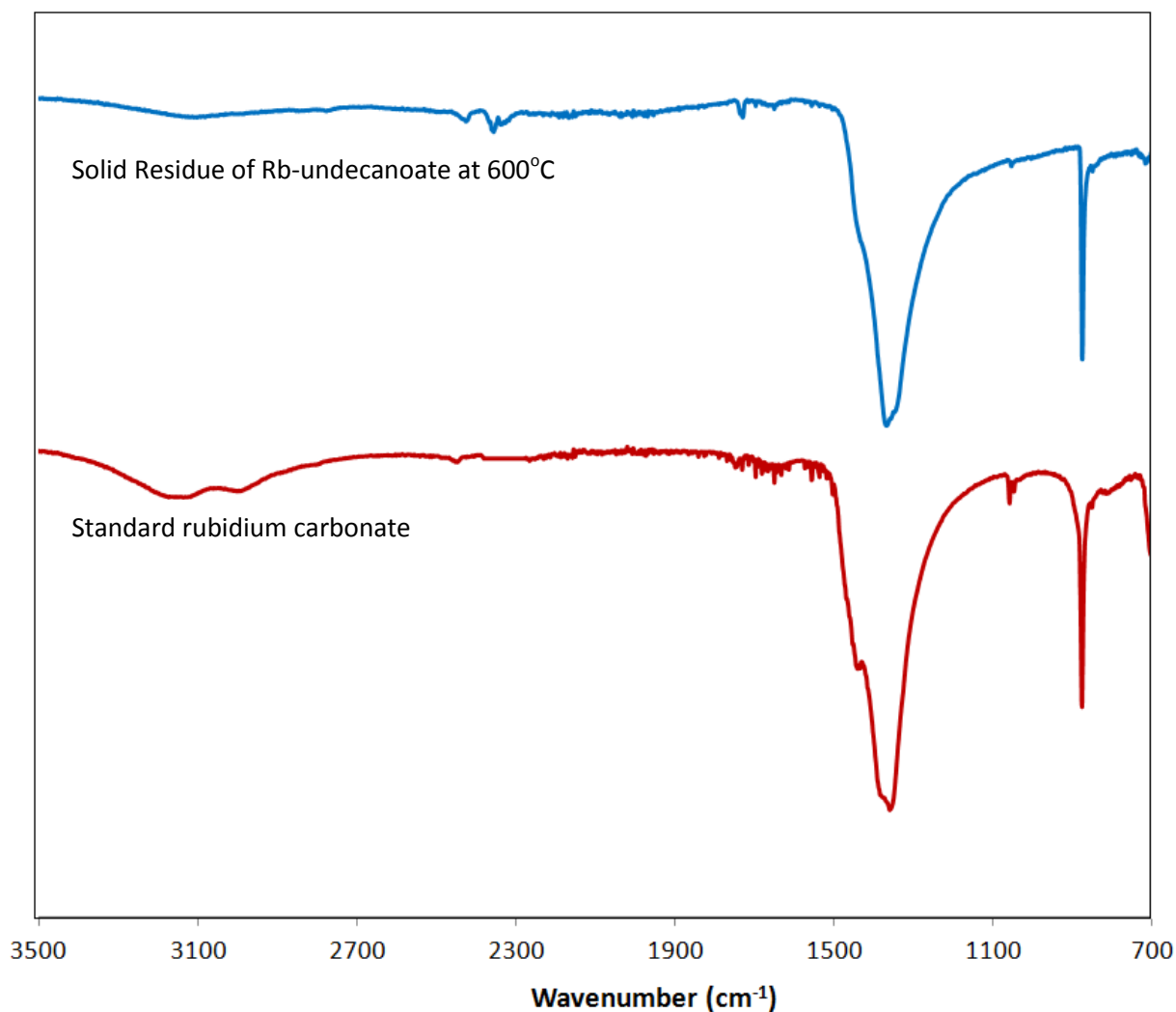


**Figure 5-1. Infrared spectrum of the solid residue after thermal decomposition of rubidium undecanoate and that of rubidium carbonate showed for comparison**

### 5.3.4 Phase transitions by differential scanning calorimetry

DSC calorigrams of Rb-carboxylates were presented in the supporting information document (Figures S26-S37). DSC-microscope and TGA analyses were made use to assist with the assignment of the transitions. Phase transitions and their associated energies were reported in Table 5-4.

**Table 5-4. Phase transitions of the Rb-carboxylates determined by DSC over the temperature range  $-30^{\circ}\text{C}$  to the decomposition temperature.**

Rb-carboxylates	Transitions <sup>a</sup>	Onset temperature (K)	Energy <sup>b</sup> (J/g)
Methanoate	s-s	366.2 <sup>d</sup>	-2.0
	s-l	445.4	-98.0

	d	c <sub>-</sub>	c <sub>-</sub>
Ethanoate	s-s	498.6	-14.8
	s-l	515.3	-76.0
	d	756.	-169.7
Propanoate	s-s	325.6 (325.8 <sup>d</sup> )	-10.3
	s-s	565.9	-16.4
	s-l	624.0	-83.3
	d	759.5	-403.0
Butanoate	s-s	350.0 <sup>d</sup>	-5.69
	s-s	465.3	-14.0
	s-l	651.3	-83.6
	d	738.8	-462.6
Pentanoate	s-s	260.4 (256.7 <sup>d</sup> )	-16.5
	s-s	328.2 <sup>d</sup>	-1.50
	s-s	494.8	-23.4
	s-lc	636.4	-53.5
	lc-l	682.8	-26.9
	d	737.5	-403.6
Hexanoate	s-s	309.4 <sup>d</sup>	-3.27
	s-s	505.3	-12.3
	s-lc	614.6	-38.8
	lc-l	700.7	-19.0
	d	734.1	-330.1
Heptanoate	s-s	302.8	-10.7
	s-s	322.5 <sup>d</sup>	-59.7
	s-s	403.6 <sup>d</sup>	-2.03
	s-s	509.4	-9.9
	s-lc	606.2	-32.7
	lc-l	710.5	-14.3
	d	735.0	-250.7
Octanoate	s-s	281.2 <sup>d</sup>	-8.89
	s-s	293.0	-12.7
	s-s	300.9 <sup>d</sup>	-35.1
	s-s	336.2 <sup>d</sup>	-6.78
	s-s	412.0 <sup>d</sup>	-14.4
	s-s	508.0	-8.6
	s-lc	594.7	-34.7
	lc-l	712.8	-12.1
	d	737.2	-254.1
Nonanoate	s-s	325.6	-31.6
	s-s	339.0 <sup>d</sup>	-72.3
	s-s	340.0 <sup>d</sup>	-5.47
	s-s	510.0	-7.0
	s-lc	579.3	-37.7
	lc-l	706.2	-9.8

	d	727.6	-332.6
Decanoate	s-s	310.6	-88.1
	s-s	314.1 <sup>d</sup>	-71.9
	s-s	506.3	-11.7
	s-lc	565.0	-115.5
	lc-l	698.2	-23.9
	d	748.3	-1108.3
Undecanoate	s-s	337.2	-62.0
	s-s	350.3 <sup>d</sup>	-94.9
	s-lc	559.7	-46.0
	lc-l	689.7	-7.1
	s-s	741.0	-435.9
Dodecanoate	s-s	332.4 (335.0 <sup>d</sup> )	-55.3
	s-s	365.4 <sup>d</sup>	-10.3
	s-lc	515.1	-9.3
	lc-lc	556.6	-33.5
	lc-l	682.2	-5.9
	D	740.1	-413.1

<sup>a</sup> Transitions: s-s = solid-solid phase transition, s-l = solid-liquid phase transition (melting), s-lc= solid-liquid crystal phase transition, lc-l = liquid crystal-liquid phase transition, d = decomposed

<sup>b</sup> Energy changes: endothermic values are negative, exothermic values are positive

<sup>c</sup> Onset of decomposition was ill-defined and could not be determined

<sup>d</sup> Solid-solid phase transitions were observed during the Cp measurement experiments

For most of Rb-carboxylates, there were solid-solid phase transitions in addition to the solid-liquid phase transition. Liquid crystal formation was observed for Rb-pentanoate and onwards. The capabilities of metal alkanates to form liquid crystalline phases (mesophases) are dictated by its cationic and anionic parameters and its crystal structure and explained in the previous chapter. Decomposition followed immediately after clearing to isotropic liquid, making it difficult to evaluate the onset temperatures for decomposition. Decomposition temperatures of Rb-carboxylates determined from DSC analysis were close to that of TGA analysis, i.e. within 5% difference with relatively same total % wt loss (Figure 5-2). Onset decomposition temperature of Rb-methanoate which was evaluated from the DSC results corresponded with the onset temperature of the first-stage of decomposition. The temperature as shown in Figure 5-2 was the onset temperature of the final stage of decomposition (which was also the second stage). It was also the highest decomposition temperature among the Rb-carboxylates in this study. The length of the aliphatic chain did not have much effect on the onset decomposition temperatures of Rb-carboxylates; in fact, the difference is negligible from Rb-ethanoate onwards.

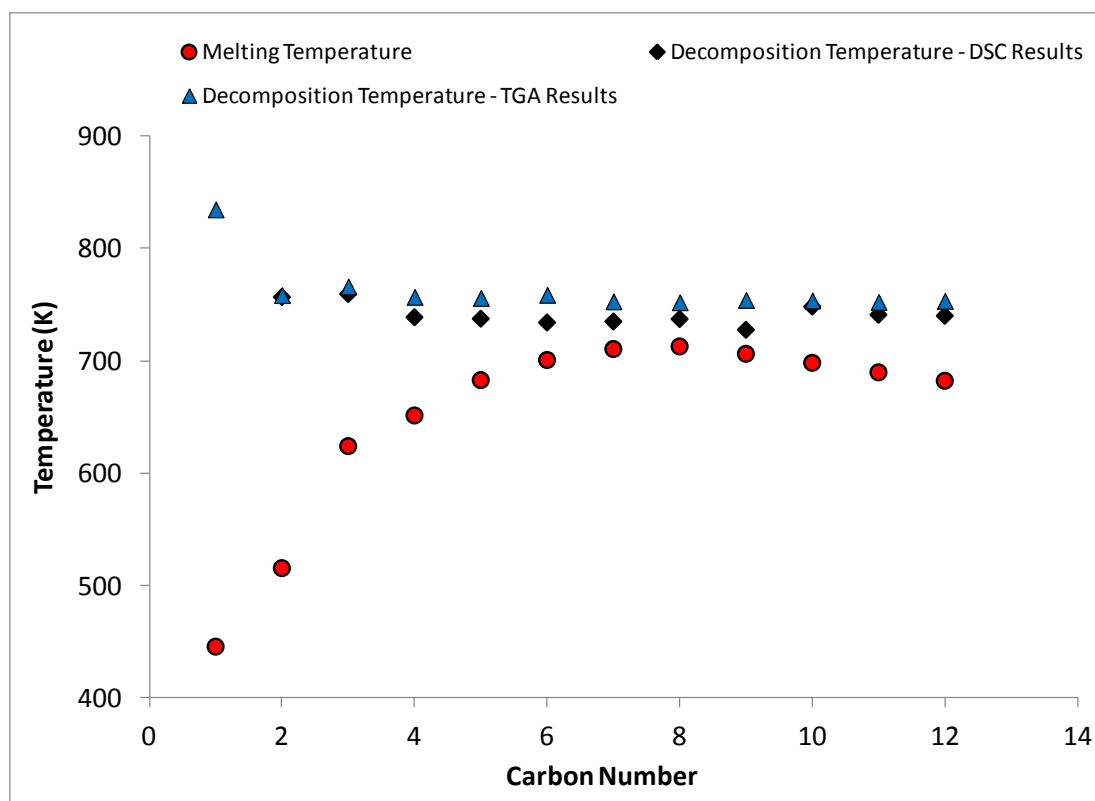


**Figure 5-2. Onset temperatures of solid-to-liquid (melting) and decomposition of Rb-carboxylates as reported by TGA and DSC analysis.**

The melting temperatures increased from Rb-methanoate to Rb-octanoate and decreased gradually from Rb-octanoate onwards. The melting point of Rb-carboxylates decreased with the increase in the aliphatic chain length, starting with Rb-octanoate, meanwhile same started with Li-propanoate.

Figure 5-3 shows the enthalpy of phase transition (solid-to-liquid) of Rb-carboxylates in comparison with the reported literature values of their corresponding alkanolic acids. The  $\text{Cs}^+$  is not contributing a constant amount of energy to the  $\Delta H_{\text{melting}}$  compared to  $\text{H}^+$  for the carboxylic acids.

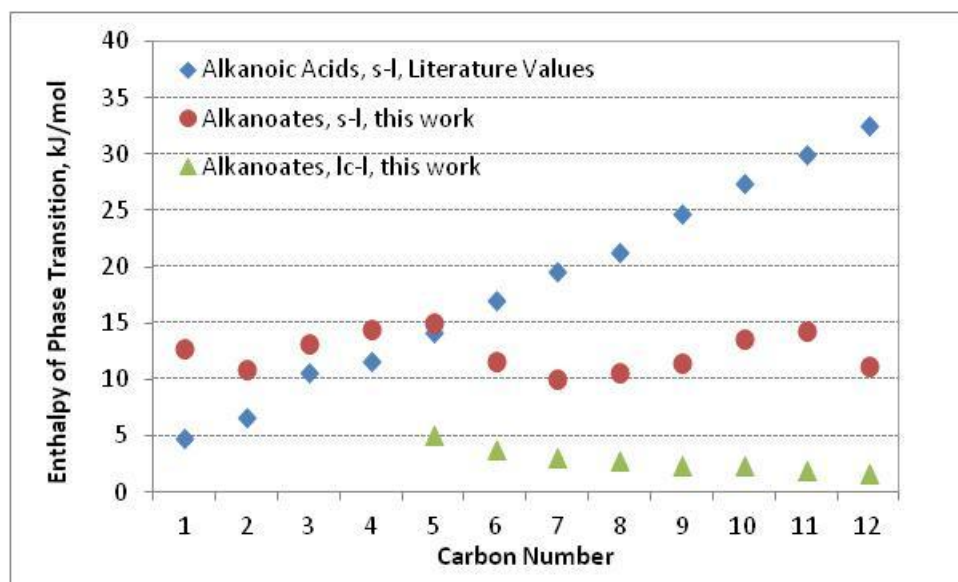


Figure 5-3. Enthalpies of Phase Transitions of Rubidium alkananoates and their corresponding acids. Enthalpy values of alkananoic acids were obtained from NIST<sup>35</sup>.

Phase transitions of Rb-carboxylates agreed with the literature data, as shown in Table 5-5

Table 5-5. Comparison of the phase transitions of the Rb-carboxylates reported in this study with that reported in literature

	Literature Value <sup>35</sup>		This Work	
	Transitions	T/K	Transition	T/K
Rb-propanoate	s-s	317	s-s	325.6 ± 0.3
	s-s	564.3	s-s	565.9 ± 0.3
	s-l	623.1	s-l	624.0 ± 0.3
Rb-butoanoate	Literature Value <sup>35</sup>		This Work	
	Transitions	T/K	Transition	T/K
	s-s	191	s-s	-
	s-s	346	s-s	353 ± 0.3
	s-s	466	s-s	465.3 ± 0.3
s-l	652	s-l	651.3 ± 0.3	

### 5.3.5 Heat capacity by differential scanning calorimetry

The heat capacities of the Rb-carboxylates were determined over the temperature range -30°C to 150 °C (243 to 423 K) by DSC. All heat capacity determinations were conducted in triplicate and the heat capacity versus temperature data are provided in the supporting information (Figures S38-S49). For some of the Rb-carboxylates, the heat capacity measurements crossed solid-solid phase transitions (Table 5-4). A multivariate regression analysis was performed to fit all of the  $C_p$  vs.  $T$  for each compound to a typical correlation of  $C_p$  (J/g.K) =  $A + B.T + C.T^2 + D.T^3$  with minimal error-of-fit, excluding temperature ranges where solid-to-solid phase transitions occurred (Table 5-6). No systematic trend was observed in the heat capacities from Rb-methanoate to Rb-dodecanoate at the same temperature. Splitting was observed Rb-

heptanoate, decanoate and undecanoate. No heat capacity values for Cp for Rb-carboxylates were found to be compared with our experimental values.

**Table 5-6. Constant pressure heat capacity versus temperature correlations of the solid C<sub>1</sub>-C<sub>12</sub> Rb-carboxylates in the temperature range -30 to +150 °C. Gaps in the temperature region covered indicate solid-solid phase transitions.**

Rb-carboxylates	Valid Range of T (K)	Cp (J/g.K) = A + B.T + C.T <sup>2</sup> + D.T <sup>3</sup>			
		A	B	C	D
Methanoate	273.2-364.2	-5.9858E+00	5.3844E-02	-1.4258E-04	1.4117E-07
	378.0-408.0	-3.0471E+00	3.5926E-02	-1.1136E-04	1.2974E-07
Ethanoate	273.2-408.0	-4.4174E+00	4.0280E-02	-1.0237E-04	1.0349E-07
Propanoate	273.2-320.5	-3.0414E+01	3.1975E-01	-1.1016E-03	1.3011E-06
	332.2-408.0	-1.8931E+01	1.6255E-01	-4.4025E-04	4.1438E-07
Butanoate	273.2-338.8	-5.8715E+00	5.8365E-02	-1.6931E-04	1.8020E-07
	362.2-408.0	-3.8477E+01	3.0877E-01	-8.0381E-04	7.0966E-07
Pentanoate	273.2-327.2	-1.2359E+01	1.2469E-01	-3.9356E-04	4.4054E-07
	338.0-408.0	-1.8097E+01	1.6390E-01	-4.5730E-04	4.3333E-07
Hexanoate	273.2-338.0	4.4156E+00	-2.8984E-02	8.0183E-05	-5.1648E-08
	353.0-399.7	1.8310E+01	-1.4115E-01	3.8521E-04	-3.3508E-07
Heptanoate	273.2-318.0	-2.4754E+01	2.5320E-01	-8.4218E-04	9.7129E-07
	376.3-408.0	-2.5930E+03	2.0093E+01	-5.1867E-02	4.4641E-05
Octanoate	313.8-324.7	1.2101E+03	-1.1194E+01	3.4533E-02	-3.5476E-05
	366.3-408.0	-2.4537E+02	1.9385E+00	-5.0752E-03	4.4420E-06
Nonanoate	273.2-313.8	- 6.3123E+01	6.4763E-01	-2.1987E-03	2.5329E-06
	358.0-389.7	5.0879E+01	-3.7787E-01	9.5858E-04	-7.8607E-07
Decanoate	273.2-308.0	- 8.2172E+01	8.6677E-01	-3.0260E-03	3.5641E-06
	367.2-403.0	- 2.1466E+02	1.7044E+00	-4.4794E-03	3.9416E-06
Undecanoate	273.2-343.8	- 3.4138E+00	4.2369E-02	-1.4156E-04	2.1514E-07
	368.0-408.0	2.7669E+01	-1.9288E-01	4.8081E-04	-3.6629E-07
Dodecanoate	273.2-328.0	- 2.3480E+01	2.3950E-01	-7.8855E-04	9.1226E-07
	345.5-360.5	- 7.0050E+02	5.9637E+00	-1.6890E-02	1.5978E-05
	374.7-393.0	4.1465E+02	-3.1996E+00	8.2626E-03	-7.0890E-06

## 5.4 Summaries

The rubidium C<sub>1</sub>-C<sub>12</sub> *n*-alkanoates (Rb-carboxylates) were synthesized and studied over the temperature range -30 to +600 °C. Spectroscopic and thermal analyses are presented and compared to reported literature. Based on repeat measurements and calibration using standards, the onset temperatures of phase transitions were accurate to within 0.3 °C absolute and the energy changes associated with the phase transitions were accurate to within 3 % relative. Key observations from this study are:

- Evidence for a more covalent character of the Rb-O bond was found only for rubidium methanoate, where the difference between the asymmetric and symmetric stretching of the carboxylate,  $\Delta\nu = \nu_{as}(\text{CO}_2^-) - \nu_s(\text{CO}_2^-)$ , was 231 cm<sup>-1</sup>. The C<sub>2</sub>-C<sub>12</sub> Rb-carboxylates had  $\Delta\nu$ -values in the range 149-164 cm<sup>-1</sup>.

- The melting temperatures increased from Rb-methanoate to Rb-octanoate and decreased gradually from Rb-octanoate onwards. The length of the aliphatic chain did not have much effect on the onset decomposition temperatures of Rb-carboxylates; in fact, the difference is insignificant from Rb-ethanoate onwards.
- Mass loss occurred in one single event upon heating with the exception of Rb-methanoate. All Rb-carboxylates decomposed to produce rubidium carbonate ( $\text{Rb}_2\text{CO}_3$ ) as solid product and decomposition was consistent with ketonic decomposition reported in literature.
- Solid-solid phase transitions were found for all  $\text{C}_1\text{-C}_{12}$  Rb-carboxylates in the temperature range studied
- Liquid crystalline formation (mesophases) was observed for Rb-pentanoate and onwards
- The constant pressure heat capacity ( $C_p$ ) of the solid  $\text{C}_1\text{-C}_{12}$  Rb-carboxylates was experimentally determined by DSC over the temperature range  $-30$  to  $+150$  °C.

## 6. Cesium C<sub>1</sub>-C<sub>12</sub>*n*-alkanoates: Thermal behavior from -30 to 600 °C

### 6.1 Introduction

Cesium *n*-alkanoates (carboxylates) are the cesium salts of the corresponding linear carboxylic acids. The uses of alkali metal carboxylates and the reasons why their thermal properties are of interest were stated earlier. The application of cesium alkanoates has attracted attention, as the nucleophilicity and large ion size of the cesium make it ideal for nucleophilic substitutions with little racemisation of responsive compounds<sup>45</sup>. The short chain cesium soaps, such as cesium ethanoate, are used to catalyze the synthesis of Merrifield resin, which are then used extensively in polypeptide production<sup>45</sup>. In this chapter, we attempted a systematic thermal behavior study of nC<sub>1</sub>-C<sub>12</sub> Cs-carboxylates as well as a review and compare of previous studies in the same field.

### 6.2 Experimental

#### 6.2.1 Materials

The high purity reference materials employed for temperature and enthalpy calibration of the differential scanning calorimeter were commercially obtained and used as received. These were: indium (Impag AG, supplied by Mettler-Toledo ME-119442, indium pills, 99.999%), tin (Alfa Aesar, #11013, 99.995% metal basis), lead (Alfa Aesar, #42928, 99.999% metal basis) and zinc (Impag AG supplied by Mettler-Toledo ME-119441, 99.999%) for the differential scanning calorimeter calibration; indium (supplied by Mettler-Toledo ME – 119442), zinc (supplied by Mettler-Toledo ME-119441), Aluminum (supplied by Mettler-Toledo ME-51119701) and Gold (supplied by Mettler-Toledo ME-51140816) for Thermogravimetric Analyzer Calibration.

Praxair's Ultra High Purity 5.0 nitrogen (99.999%) was used to maintain the inert atmospheric conditions during calorimetric runs.

The cesium carboxylates employed in this study were prepared from commercially obtained cesium carbonate (ReagentPlus® 99% Aldrich) and the linear carboxylic acids in the C<sub>1</sub>-C<sub>12</sub> range. Methanoic acid (99%), nonanoic acid (97%) and undecanoic acid (99%) were supplied by Acros Organics. Ethanoic acid (99.7%), propanoic acid (99.5%), butanoic acid (+99%), pentanoic acid (99%) and hexanoic acid (99%) were supplied by Aldrich. Heptanoic acid (+97%), octanoic acid (+99%), decanoic acid (96%) and dodecanoic acid (+99%) were supplied by Sigma.

The solvents that were used in the study were methanol (98%, Sigma-Aldrich), and ethanol (+99.8%, Fluka).

#### 6.2.2 Analytical equipment and procedure

The same analytical equipment and procedures were employed as for the study of the lithium carboxylates (Chapter 2 - Section 2.2.2)

### 6.2.3 Calibration

The same temperature and caloric calibration was performed as for the study of the lithium carboxylates (Chapter 2 – Section 2.2.3)

### 6.2.4 Synthesis of cesium alkanoates

The synthesis and purification of Cs-carboxylates were based on the work of Mirnaya et al<sup>46</sup>. Cs-carboxylates were prepared by mixing cesium carbonate (in anhydrous methanol) with a slight excess (2% molar excess) of carboxylic acids. The mixture was stirred for several hours without heating to allow sufficient time for the neutralization reaction to be complete, using a Heidolph MR Hei-Standard hot plate (heating power of 800W, maximum temperature of 300 °C, 30-1400 rpm at an accuracy of  $\pm 1\%$ ). Solid Cs-carboxylates were recovered by evaporation of the solvent and excess acid at 60 °C under reduced pressure at 9.6 kPa (absolute), using a HeidolphHei-VAP Precision with glassware set G3 rotary evaporator. The Cs-carboxylates were purified by recrystallizing the products from ethanol, were washed with acetone and further dried under vacuum at approximately 100 °C until they reached constant mass. The final products were finely ground before being used for thermal analysis.

## 6.3 Results& Discussions

### 6.3.1 Infrared Spectroscopy

Infrared spectroscopy was used primarily to confirm the success of the synthesis of the Cs-carboxylates and provide information on structural changes that were observed during calorimetry. The IR spectra of the Cs-carboxylates are provided in the supporting information (Figures S1-S12). In general, bands corresponding to aliphatic CH<sub>2</sub> and CH<sub>3</sub> stretching vibrations are observed below 3000cm<sup>-1</sup>. The difference between Cs-methanoate and heavier carboxylates lies in the intensity of the aliphatic CH<sub>2</sub> and CH<sub>3</sub> stretching vibrations, the longer the aliphatic chain of the carboxylates is, the more intense it is. Methyl and methylene bending and rocking vibrations are measured between 500 and 1400cm<sup>-1</sup>. The C=O stretching vibration observed in the alkanolic acid around 1700cm<sup>-1</sup> disappears in the Cs-carboxylates and is replaced by two new absorption bands. These bands correspond to the symmetric and asymmetric stretching vibrations of the carboxylate ion and listed in Table 6-1. The relative position of these two bands  $\Delta = \nu_{\text{asym}}(\text{COO}^-) - \nu_{\text{sym}}(\text{COO}^-)$  can be used to shed light on the type of carboxylate-to-metal complexation structure present in a given metal carboxylate<sup>29</sup>. Four metal-carboxylate configurations are possible (Figure 2-1). Ionic and bridging carboxylate structures cannot be distinguished from  $\Delta\nu$ , since the values for these two configurations overlap. Monodentate bonding, where the Cs-O bond has covalent character, results in a much larger  $\Delta\nu$  than the ionic form, typically 200-300 cm<sup>-1</sup>. Conversely, bidentate bridging results in a much smaller  $\Delta\nu$  than the ionic form, typically <100 cm<sup>-1</sup>. Spectroscopic evidence for a more covalent character of the

Cs-O bond was found only for cesium methanoate, which has  $\Delta\nu = 231 \text{ cm}^{-1}$  (Table 6-1). The  $\text{C}_2\text{-C}_{12}$  Cs-carboxylates all have  $\Delta\nu$  values in the range typical of either ionic or bridging structures.

**Table 6-1. Strong carboxylate stretching vibrations in the IR spectra of the Cs-carboxylates**

Cs-carboxylates	Carboxylate stretching vibrations ( $\text{cm}^{-1}$ )		$\Delta\nu$ ( $\text{cm}^{-1}$ )
	IR, asymmetric	IR, symmetric	
Methanoate	1569	1338	231
Ethanoate	1560	1390	170
Propanoate	1557	1388	169
Butanoate	1554	1391	163
Pentanoate	1556	1391	165
Hexanoate	1551	1395	156
Heptanoate	1551	1396	155
Octanoate	1551	1399	152
Nonanoate	1551	1399	152
Decanoate	1551	1399	152
Undecanoate	1554	1401	150
Dodecanoate	1551	1401	150

### 6.3.2. Ultraviolet-visible spectroscopy

The UV-Vis spectrum of the carboxylate group is characterized mainly by a high intensity  $\pi \rightarrow \pi^*$  transition at around 200 nm; the  $n \rightarrow \pi^*$  transition at longer wavelength is weak. The UV-Vis spectra of the Cs-carboxylates are provided in the supporting information (Figures S13-S24). The  $\pi \rightarrow \pi^*$  transitions are listed in Table 6-2.

**Table 6-2. Carboxylate high intensity  $\pi \rightarrow \pi^*$  transitions in the UV-Vis spectra of the Cs-carboxylates.**

Cs-Carboxylates	Carboxylate $\pi \rightarrow \pi^*$ transition (nm)
Methanoate	188
Ethanoate	188
Propanoate	188, 186
Butanoate	187
Pentanoate	186
Hexanoate	188
Heptanoate	186
Octanoate	187
Nonanoate	187
Decanoate	187
Undecanoate	186
Dodecanoate	187

### 6.3.3 Decomposition by thermogravimetric analysis

The decomposition temperature and total mass loss during decomposition was determined by TGA under inert atmosphere (Table 6-3). The TGA curves over the temperature range of 150 to 600 °C (423 to 873 K) are provided in the supporting information (Figure S25).

**Table 6-3. Onset temperature of decomposition and mass loss of Cs-carboxylates determined by TGA, as well as the calculated mass loss assuming that the solid residue is Cs<sub>2</sub>CO<sub>3</sub>.**

Cs-carboxylates	Onset of decomposition (K)	TGA mass loss (%)	Calculated mass loss (%)
Methanoate	709.6	12.7	8.4
Ethanoate	746.8	15.3	15.1
Propanoate	763.7	19.8	20.9
Butanoate	737.4	29.9	26.0
Pentanoate	740.0	28.3	30.4
Hexanoate	750.9	34.9	34.3
Heptanoate	749.0	36.0	37.8
Octanoate	747.3	40.6	41.0
Nonanoate	748.5	44.2	43.9
Decanoate	747.1	46.0	46.4
Undecanoate	746.7	48.6	48.8
Dodecanoate	747.0	50.0	51.0

Acetates and heavier carboxylates generally decompose via the formation of the metal carbonate and an organic component ketone, with the exception of lithium formate. The metal carbonate decomposes further into carbon dioxide and the oxide of the metal. The temperature at which metal carbonate decomposes further depends on the electropositive nature of the metal. Alkaline metals are most electropositive of all because they have a single electron in their outer shell; as a result, carbonates of alkali metals are stable to the highest temperature. At the final temperature of 600°C in this work, it is expected metal carbonate is the final product rather than the oxide of the metal. The ketone is generally oxidized by atmospheric oxygen to carbon dioxide and water at a temperature which is characteristic of a specific ketone.

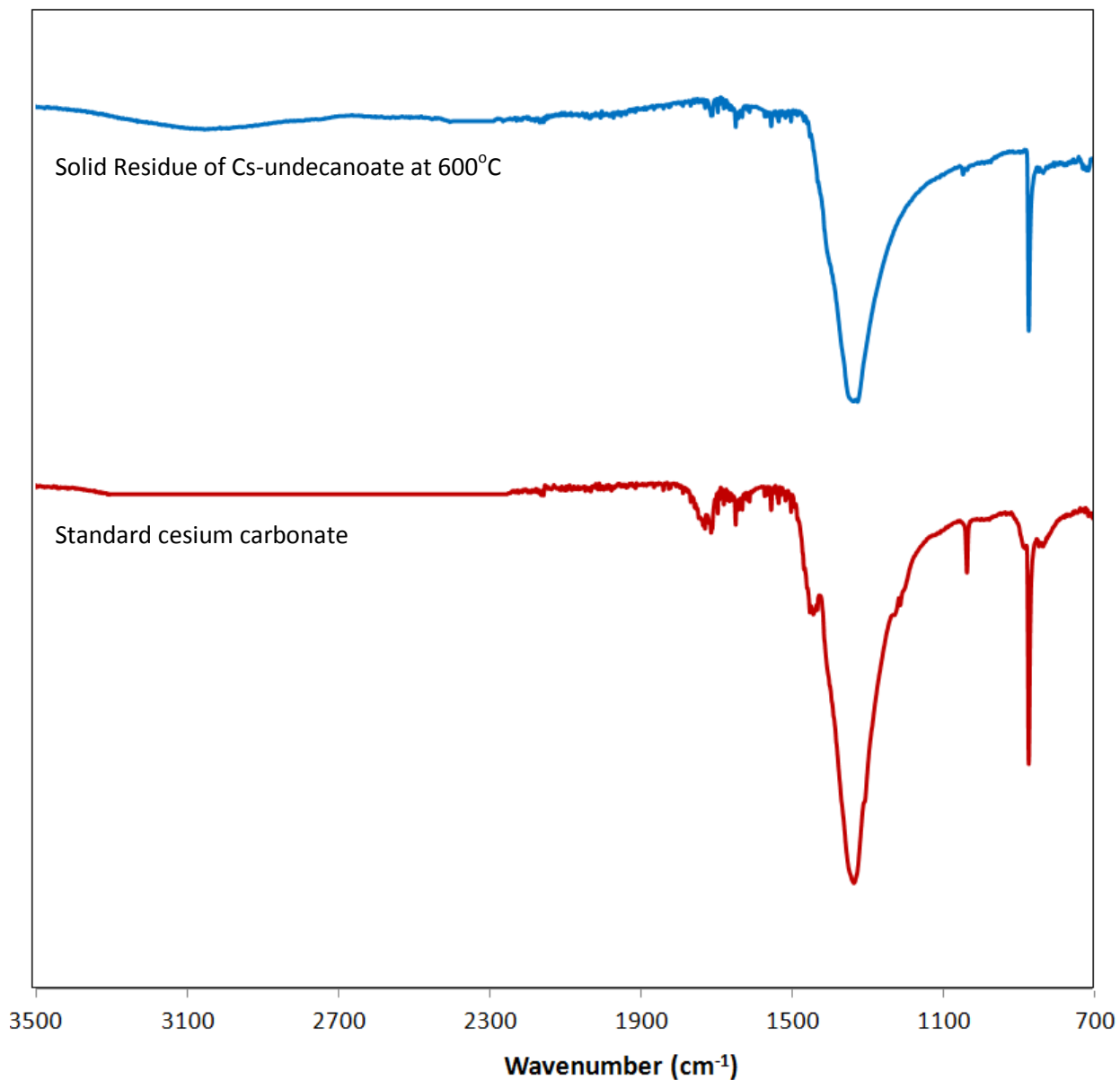


**Figure 6-1. Infrared spectrum of the solid residue after thermal decomposition of cesium undecanoate and that of cesium carbonate showed for comparison.**

Figure 6-1 shows IR spectrum of the residue of Cs-carboxylates at 600°C in comparison with IR spectrum of pure cesium carbonate. IR results confirmed that potassium carbonate is the final residue of Cs-carboxylates when the samples were subjected to the final temperature of 600°C. Calculated total mass loss keeping in mind that cesium carbonate was the final residue of Cs-carboxylates at 600°C were compared with the TGA total mass loss with percentage difference less than 7%. The decomposition of formates however follows a different course than other carboxylates. It consists of the formation of either ( $\text{H}_2 + \text{CO} + \text{M}_2\text{CO}_3$ ) or/and ( $\text{H}_2 + \text{M}_2\text{C}_2\text{O}_4$ ) (which will decompose further to form carbonate and carbon dioxide). It is likely that cesium formate decomposed directly to form cesium carbonate in this study, since only one stage of decomposition was observed from TGA results.

### 6.3.4 Phase transitions by differential scanning calorimetry

DSC calorigrams of Cs-carboxylates were presented in the supporting information document (Figures S26-S37). DSC-microscope and TGA analyses were made use to assist with the assignment of the transitions. Phase transitions and their associated energies were reported in Table 6-4.

**Table 6-4. Phase transitions of the Cs-carboxylates determined by DSC over the temperature range  $-30^{\circ}\text{C}$  to the decomposition temperature.**

Cs-carboxylates	Transitions <sup>a</sup>	Onset temperature (K)	Energy <sup>b</sup> (J/g)
Methanoate	s-s	298.4 <sup>c</sup>	-25.1
	s-s	315.9	-25.7
	s-s	340.1 <sup>c</sup>	-17.5
	s-l	535.1	-36.7
	d	718.6	-103.3
Ethanoate	s-l	466.0	-72.6
	d	764.7	-151.3
Propanoate	s-s	325.6 (325.9 <sup>c</sup> )	-7.2
	s-s	420.2 (414.8 <sup>c</sup> )	-9.0
	s-l	583.2	-58.8
	d	759.3	-406.6
Butanoate	s-s	279.9 <sup>c</sup>	-8.12
	s-lc	344.8 (344.8 <sup>c</sup> )	-6.1
	lc-l	628.3	-60.5
	d	746.6	-433.9
Pentanoate	s-s	304.8	-13.3
	s-s	370.1 <sup>c</sup>	-14.77
	s-l	643.0	-63.2
	d	745.0	-405.3
Hexanoate	s-s	384.5 (387.0 <sup>c</sup> )	-8.5
	s-s	412.6 <sup>c</sup>	-0.51
	s-lc	629.9	-40
	lc-l	664.2	-18.0
	d	740.0	-426.3
Heptanoate	s-s	272.2	-16.7
	s-s	286.4 <sup>c</sup>	-26.2
	s-s	362.0 <sup>c</sup>	-0.49
	s-s	379.8 <sup>c</sup>	-6.0
	s-s	383.9	-7.5
	s-s	616.9	-35.3
	s-l	683.3	-16.6
	d	728.9	-384.1
Octanoate	s-s	261.0	-8.0
	s-s	283.2 <sup>c</sup>	-20.7

	s-s	372.3 <sup>c</sup>	-6.63
	s-s	378.3	-6.0
	s-s	605.6	-33.4
	s-l	686.9	-13.5
	d	771.8	-368.4
Nonanoate	s-s	262.6 <sup>c</sup>	-11.95
	s-s	294.4	-15.4
	s-s	310.5 <sup>c</sup>	-29.6
	s-s	378.6	-5.1
	s-s	381.0 <sup>c</sup>	-0.17
	s-s	596.5	-30.6
	s-l	684.4	-10.8
	d	726.7	-347.0
Decanoate	s-s	285.0	-11.1
	s-s	298.7 <sup>c</sup>	-26.5
	s-s	372.3 <sup>c</sup>	-5.91
	s-s	376.7	-4.9
	s-s	588.9	-31.3
	s-l	680.9	-9.0
	d	725.1	-374.5
Undecanoate	s-s	312.1	-26.2
	s-s	319.0 <sup>c</sup>	-62.2
	s-s	377.0 (375.8 <sup>c</sup> )	-5.3
	s-s	580.4	-37.4
	s-l	679.2	-8.3
	d	723.6	-411.2
Dodecanoate	s-s	313.6 (313.2 <sup>c</sup> )	-30.2
	s-s	378.0 (375.6 <sup>c</sup> )	-4.6
	s-s	572.5	-36.2
	s-l	672.9	-6.3
	d	734.1	-389.1

<sup>a</sup> Transitions: s-s = solid-solid phase transition, s-l = solid-liquid phase transition (melting), s-lc = solid-liquid crystal phase transition, lc-l = liquid crystal-liquid phase transition, d = decomposed

<sup>b</sup> Energy changes: endothermic values are negative, exothermic values are positive

<sup>c</sup> Solid-solid phase transitions were observed during the Cp measurement experiments

For most of Cs-carboxylates there were solid-solid phase transitions in addition to the solid-liquid phase transition. Liquid crystal formation was observed for Cs-butanoate and hexanoate. The capabilities of metal alkanates to form liquid crystalline phases (mesophases) are dictated by its cationic and anionic parameters and its crystal structure and explained in the previous chapter. Decomposition followed immediately after clearing to isotropic liquid, making it difficult to evaluate the onset temperatures for decomposition. Decomposition temperatures of Cs-carboxylates determined from DSC analysis were close to that of TGA analysis, i.e. within 5% difference with relatively same total % wt loss (Figure 6-2). The length of the aliphatic chain did not have much effect on the onset decomposition temperatures of Cs-carboxylates; in fact, the difference is negligible.

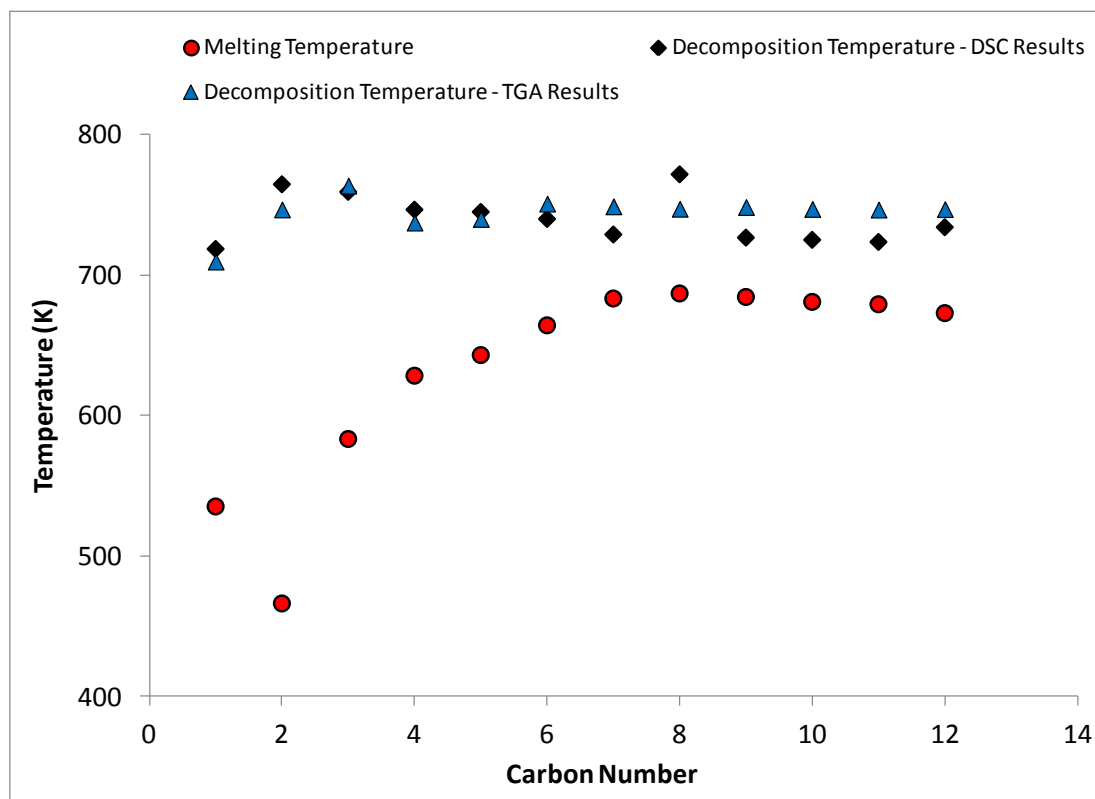


**Figure 6-2. Onset temperatures of solid-to-liquid (melting) and decomposition of Cs-carboxylates as reported by TGA and DSC analysis.**

The melting temperatures increased from Cs-methanoate to Cs-octanoate (with the exception of Cs-ethanoate) and decreased gradually from Cs-octanoate onwards. The melting point of Cs-carboxylates decreased with the increase in the aliphatic chain length, starting with Cs-octanoate, meanwhile same started with Li-propanoate.

Figure 6-3 shows the enthalpy of phase transition (solid-to-liquid) of Cs-carboxylates in comparison with the reported literature values of their corresponding aliphatic acids. The  $\text{Cs}^+$  is not contributing a constant amount of energy to the  $\Delta H_{\text{melting}}$  compared to  $\text{H}^+$  for the carboxylic acids.

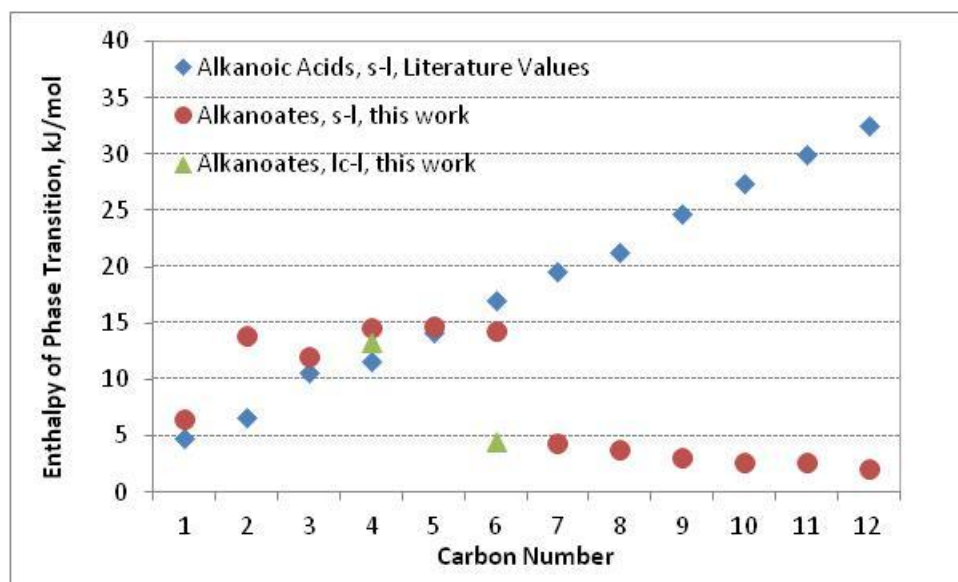


Figure 6-3. Enthalpies of Phase Transitions of Cesium alkanoates and their corresponding acids. Enthalpy values of alkanolic acids were obtained from NIST<sup>35</sup>.

Phase transitions of Cs-carboxylates agreed with the literature data, as shown in Table 6-5

Table 6-5. Comparison of the phase transitions of the Cs-carboxylates reported in this study with that reported in literature

	Literature Value <sup>35</sup>		This Work	
	Transitions	T/K	Transition	T/K
Propanoate	s-s	314	s-s	325.6 ± 0.3
	s-s	419	s-s	420.2 ± 0.3
	s-l	580	s-l	583.2 ± 0.3
Butanoate	Literature Value <sup>35</sup>		This Work	
	Transitions	T/K	Transition	T/K
	s-s	263	s-s	269.8 ± 0.3
	s-s	344	s-s	344.8 ± 0.3 (348.7 ± 0.3)
s-l	628	s-l	628.3 ± 0.3	

### 6.3.5 Heat capacity by differential scanning calorimetry

The heat capacities of the Cs-carboxylates were determined over the temperature range -30°C to 150 °C (243 to 423 K) by DSC. All heat capacity determinations were conducted in triplicate and the heat capacity versus temperature data are provided in the supporting information (Figures S38-S49). For some of the Cs-carboxylates, the heat capacity measurements crossed solid-solid phase transitions (Table 6-4). A multivariate regression analysis was performed to fit all of the Cp vs. T for each compound to a typical correlation of  $C_p \text{ (J/g.K)} = A + B.T + C.T^2 + D.T^3$  with minimal error-of-fit, excluding temperature ranges where solid-to-solid phase transitions occurred (Table 6-6). No systematic trend was observed in the heat capacities from

Cs-methanoate to Cs-dodecanoate at the same temperature. Splitting was observed Cs-heptanoate, decanoate, undecanoate, dodecanoate. No heat capacity values for Cp for Cs-carboxylates were found to be compared with our experimental values.

**Table 6-6. Constant pressure heat capacity versus temperature correlations of the solid C<sub>1</sub>-C<sub>12</sub> Cs-carboxylates in the temperature range -30 to +150 °C. Gaps in the temperature region covered indicate solid-solid phase transitions.**

Cs-Carboxylates	Valid Range of T (K)	Cp (J/g.K) = A + B.T + C.T <sup>2</sup> + D.T <sup>3</sup>			
		A	B	C	D
Methanoate	359.7-414.7	-7.6052E+01	5.9839E-01	-1.5548E-03	1.3528E-06
Ethanoate	249.7-416.3	-1.7813E+00	1.9988E-02	-4.4651E-05	3.7486E-08
Propanoate	286.3-319.7	-3.3161E+00	4.0880E-02	-1.4608E-04	1.8949E-07
	356.3-416.3	-5.9913E+01	4.8032E-01	-1.2683E-03	1.1233E-06
Butanoate	278.0-339.7	-2.2019E+01	2.1900E-01	-7.0433E-04	7.7588E-07
	361.3-393.2	-5.4290E+01	4.3552E-01	-1.1436E-03	1.0131E-06
Pentanoate	253.0-341.3	-2.4103E+00	2.833E-02	-8.7104E-05	1.0054E-07
	386.3-408.0	1.0158E+02	-7.6087E-01	1.9165E-03	-1.6033E-06
Hexanoate	258.0-378.0	4.3314E-02	6.0409E-03	-1.8238E-05	3.6186E-08
Heptanoate	299.2-359.7	-8.8149E+00	8.8413E-02	-2.6733E-04	2.8934E-07
Octanoate	298.2-367.2	-6.8386E+00	7.0988E-02	-2.1623E-04	2.4010E-07
	383.2-408.0	1.0231E+02	-7.5045E-01	1.8552E-03	-1.5131E-06
Nonanoate	349.7-374.7	-5.5486E+02	4.6460E+00	-1.2943E-02	1.2029E-05
	274.7-300	-9.2971E+01	9.8726E-01	-3.4652E-03	4.0768E-06
Decanoate	313.0-369.7	-2.5850E+01	2.4814E-01	-7.5751E-04	7.8854E-07
	383.0-416.3	9.4427E+01	-6.9941E-01	1.7478E-03	-1.4366E-06
Undecanoate	333.0-373.0	-5.3627E+01	4.8706E-01	-1.4374E-03	1.4347E-06
	383.0-416.3	-8.5814E+00	7.4619E-02	-1.8365E-04	1.6837E-07
Dodecanoate	338.0-351.3	-1.3026E+02	1.1864E+00	-3.5654E-03	3.5817E-06
	356.3-366.3	-7.6236E+02	6.3441E+00	-1.7575E-02	1.6247E-05
	386.3-408.0	-1.7643E+02	1.3372E+00	-3.3571E-03	2.8238E-06

## 6.4 Summaries

The cesium C<sub>1</sub>-C<sub>12</sub> *n*-alkanoates (Cs-carboxylates) were synthesized and studied over the temperature range -30 to +600 °C. Spectroscopic and thermal analyses are presented and compared to reported literature. Based on repeat measurements and calibration using standards, the onset temperatures of phase transitions were accurate to within 0.3 °C absolute and the energy changes associated with the phase transitions were accurate to within 3 % relative. Key observations from this study are:

- Evidence for a more covalent character of the Cs-O bond was found only for cesium methanoate, where the difference between the asymmetric and symmetric stretching of the carboxylate,  $\Delta\nu = \nu_{as}(\text{CO}_2^-) - \nu_s(\text{CO}_2^-)$ , was 231cm<sup>-1</sup>. The C<sub>2</sub>-C<sub>12</sub> Cs-carboxylates had  $\Delta\nu$ -values in the range 150-170 cm<sup>-1</sup>.

- The melting temperatures increased from Cs-methanoate to Cs-octanoate (with the exception of Cs-ethanoate) and decreased gradually from Cs-octanoate onwards. The length of the aliphatic chain did not have much effect on the onset decomposition temperatures of Cs-carboxylates.
- Mass loss occurred in one single event. All Cs-carboxylates decomposed to produce cesium carbonate ( $\text{Cs}_2\text{CO}_3$ ) as solid product and decomposition was consistent with ketonic decomposition reported in literature.
- Solid-solid phase transitions were found for all  $\text{C}_1\text{-C}_{12}$  Cs-carboxylates in the temperature range studied, with the exception of cesium ethanoate.
- Liquid crystalline formation (mesophases) was observed for Cs-butanoate and hexanoate only.
- The constant pressure heat capacity ( $C_p$ ) of the solid  $\text{C}_1\text{-C}_{12}$  Cs-carboxylates was experimentally determined by DSC over the temperature range  $-30$  to  $+150$  °C.

## 7. Conclusions and Recommendations

The success of the synthesis and purification of Group I (Li, Na, K, Cs and Rb) carboxylates have been confirmed by the infrared spectroscopy. The C=O stretching vibration observed in the alkanolic acid around  $1700\text{cm}^{-1}$  disappears in the carboxylates and is replaced by two new absorption bands. These bands correspond to the carboxylate group's characteristic asymmetrical  $\nu_{\text{as}}(\text{CO}_2^-)$ , and symmetrical  $\nu_{\text{s}}(\text{CO}_2^-)$ , stretching bands at around  $1600\text{-}1550\text{ cm}^{-1}$  and around  $1400\text{ cm}^{-1}$ . The products were pure enough based on the FTIR analysis for further thermal analysis.

DSC and TGA were employed primarily to study the thermal behavior of carboxylates. The carboxylates exist in a number of polymorphic forms and as a result these tend to undergo several transitions prior to melting. Liquid crystalline phase was observed for some carboxylates. Li-carboxylates did not form liquid crystalline phase. Na-carboxylates formed liquid crystalline phase from C<sub>4</sub> Li-carboxylates onwards, C<sub>4</sub> K-carboxylates onwards, Cs-butanoate and Cs-hexanoate, and C<sub>5</sub> Rb-carboxylates onwards.

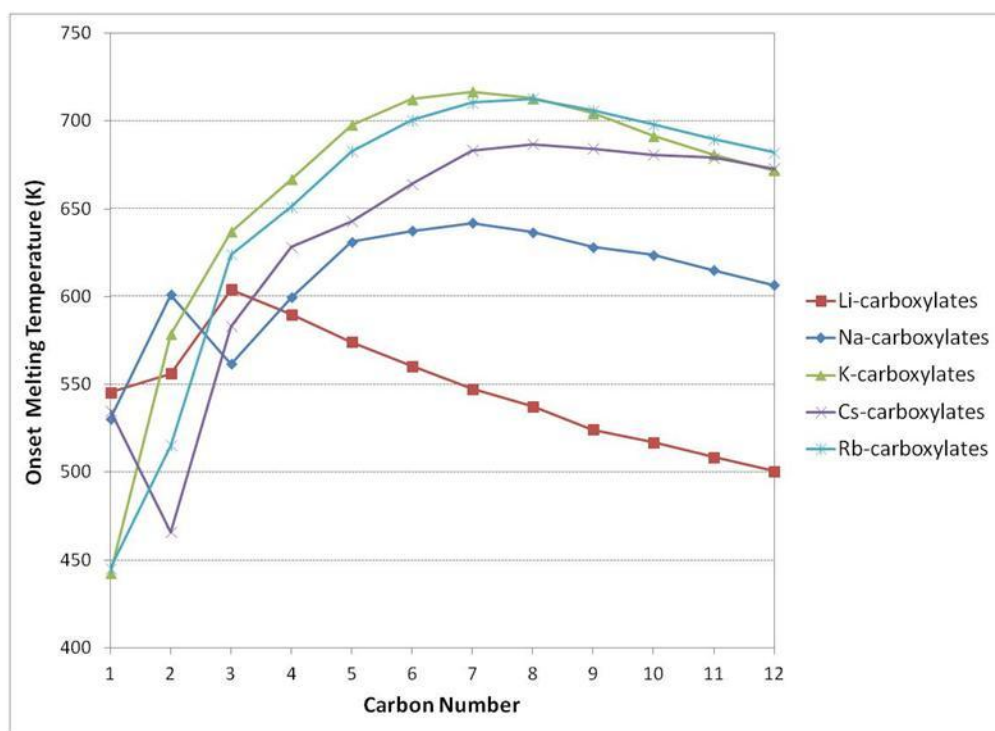


Figure 7-1. Comparison of onset melting temperatures

Onset melting temperatures of carboxylates increased first and then decreased gradually with the length of the aliphatic chain length, as seen in Na, K, Cs, Rb-carboxylates and more dramatically as seen in Li-carboxylates. It was noted that Li-carboxylates which did not form a liquid crystal phase had a much lower onset melting temperatures compared with other carboxylates. In order

to understand and explain the trend of the alkali metal carboxylates, it would require a detailed look at the crystal structure of each carboxylates, which is not within the scope of this work.

Thermal analyses of carboxylates indicate that their decomposition temperatures were in the range, Li (659.6K-756.1K), Na (746.5K-839.8K), K (751.5K-857.8K), Rb (752.2K-834.9K) and Cs (709.6K-763.7K) under inert atmosphere. Lithium and cesium methanoate have the lowest onset decomposition temperatures. Note that one single stage of decomposition was observed for lithium and cesium carboxylates, while two stages for others.

The decomposition of the C<sub>2</sub>-C<sub>12</sub> carboxylates takes place via the ketonization reaction, to yield the symmetric ketone and carbonate as products



The formation of M<sub>2</sub>CO<sub>3</sub> as solid decomposition product was confirmed by comparing the calculated and observed mass loss on decomposition and by infrared analysis of the solid residue. Further decomposition of the carbonate into the oxide and CO<sub>2</sub> was not observed at the final temperature of 600°C. The decomposition of methanoate also produced M<sub>2</sub>CO<sub>3</sub> as solid residue, but the other decomposition product/s was not determined, but is reportedly H<sub>2</sub> and CO

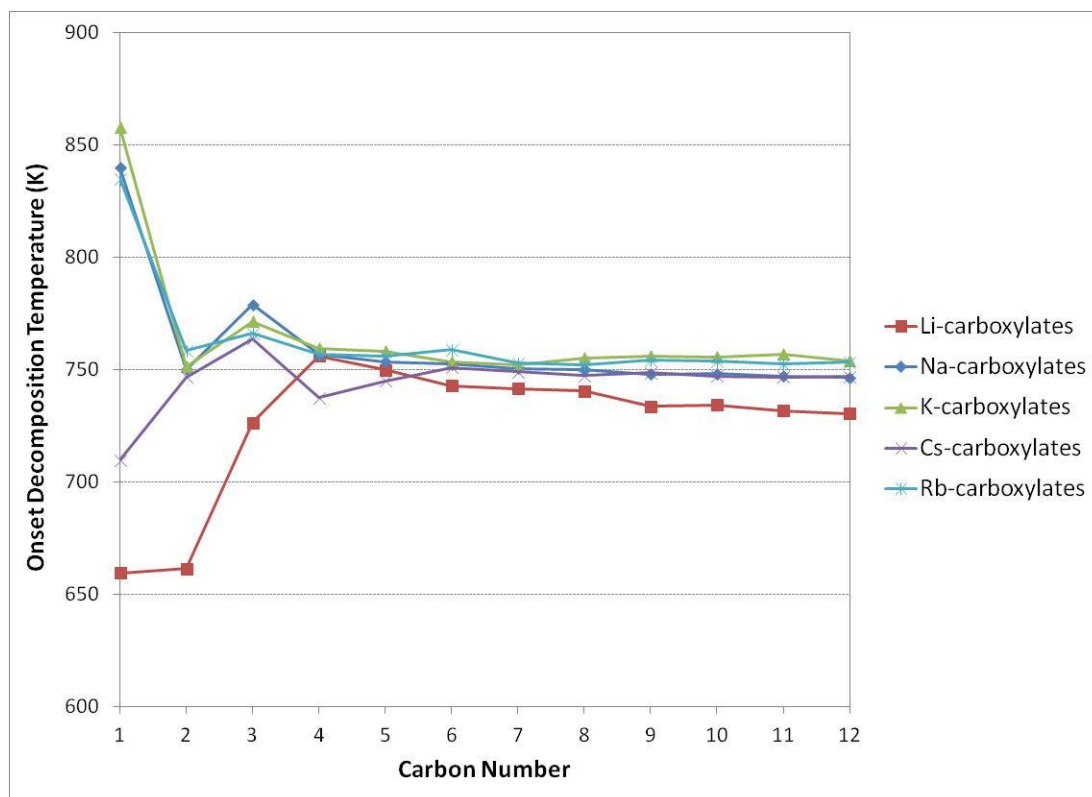
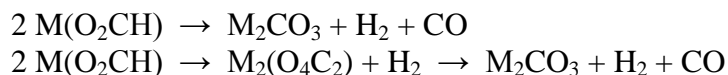


Figure 7-2. Comparison of onset decomposition temperature of the carboxylates

Our study concluded that the carboxylates were stable at temperatures below 700K. The decomposition temperatures of the carboxylates are therefore higher than the operating temperature in the reactor of the current FT process (423-573K)<sup>1</sup>. Failure of the carboxylates to decompose would result in plugging and pressure drop problems in downstream equipment of the FT process as mentioned earlier. It is however impractical to operate at temperatures higher than the decomposition temperatures of the carboxylates due to the excessive gas production<sup>1</sup>.

Even though we did not reach a conclusive solution for this carboxylates problem, it is important to point out that the formation of carboxylates was also accountable for production failure. For example, the failure of the Oryx GTL facility to reach production capacity was mainly ascribed to catalyst attrition, but metal leaching was also partially responsible<sup>47</sup>. Furthermore one initial objective was achieved, which was the compilation of engineering data for operation and design purposes.

Based on the results of our study, we have the following recommendations:

- The heat capacity measurements in this work did not agree well with that in literature, where available. This discrepancy raised two concerns, whether the carboxylates were truly pure enough for further thermal analysis or a different approach for the experimental procedure and calculations should be adopted. Further analysis should be conducted in addition to FTIR analysis to confirm that the carboxylates were pure enough for further thermal analysis, such as elemental analysis. In elemental analysis, the carbon (C-) and hydrogen (H-) contents of the products are determined using standard combustion technique (ISCW). The difference between the expected C- and H- values and the actual C- and H- values would be an indication of impurity. Cp measurements should also be performed on organic compounds such as benzoic acid to validate the experimental procedure and calculations.
- We were able to collect solid residue products of the carboxylates and analyzed the products with FTIR. Ketone - a product of decomposition process, which was present in the vapor phase, could not be verified. It is necessary to combine the mass spectroscopy (MS) with the TGA technique in order to collect and analyze vapor products simultaneously.
- All thermal analyses were conducted under inert environment at atmospheric pressure. It is of interest to investigate the thermal behavior of carboxylates in a reactive environment (atmosphere) and/or elevated pressures.

## References

1. de Klerk, A., *Fischer-Tropsch Refining*. Wiley-VCH, Weinheim: July 2011.
2. Klerk, A. d., Hydroprocessing peculiarities of Fischer-Tropsch syncrude. *Catalysis Today* **2008**, *130*, 439-445.
3. Furimsky, A. d. K. a. E., *Catalysis in the Refining of Fischer-Tropsch Syncrude*. 1st ed.; Royal Society of Chemistry: 2010.
4. De Klerk, A. Fischer-Tropsch refining. Doctoral Thesis, University of Pretoria, 2008-04-11.
5. Bartoo, R., Removing acid gas by the Benfield Process. *Chem. Eng. Prog.* **1984**, *80*, 35-39.
6. Turner, M., Smith, C.P., Controls on soap scale formation, including naphthenate soaps, drivers and mitigation. In *7th International Symposium on Oilfield Scale*, Aberdeen U.K., 2005.
7. Gallup, D. L. S., P. C.; Chipponeri, J.; Abuyazid, A.; Mulyono,; D., Formation and Mitigation of "Metallic Soap" Sludge, Serang, Indonesia Field. *Society of Petroleum Engineers* **2002**.
8. Turner, M. S., P. C., Experiences in Handling Production Fluids that Form Metallic Soaps/Naphthenate Scales,. In *Produced Water Society 12th Annual Produced Water Seminar*, Houston TX, 2002.
9. Gallup, D. L. S., J., Soap Sludges: Aggravating Factors and Mitigation Measures. In *Society of Petroleum Engineers*, 2004.
10. Curiale, D. L. G. a. J. A., Characterization of Sodium Emulsion Soaps Formed from Production Fluids of Kutei Basin, Indonesia. *Energy & Fuels* **2007**, *21*, 1741-1759.
11. Ferloni, P.; Kenesey, C.; Westrum Jr, E. F., Thermodynamics of alkali alkanoates X. Heat capacities and thermodynamic properties of lithium methanoate and lithium ethanoate at temperatures from  $\approx 5$  K to 580 K. *The Journal of Chemical Thermodynamics* **1994**, *26* (12), 1349-1363.
12. Franzosini, P.; Ngeyi, S. P.; Westrum Jr, E. F., Thermophysics of metal alkanoates VI. Heat capacities and thermodynamic properties of lithium n-pentanoate and n-heptanoate. *The Journal of Chemical Thermodynamics* **1986**, *18* (12), 1169-1181.
13. Franzosini, P.; Ngeyi, S. P.; Westrum Jr, E. F., Thermophysics of metal alkanoates VII. Heat capacities and thermodynamic properties of potassium n-butanoate. *The Journal of Chemical Thermodynamics* **1987**, *19* (2), 113-123.
14. Franzosini, P.; Plautz, W. A.; Westrum Jr, E. F., Thermophysics of metal alkanoates I. Heat capacities and thermodynamic properties of sodium methanoate and ethanoate. *The Journal of Chemical Thermodynamics* **1983**, *15* (5), 445-456.
15. Franzosini, P.; Westrum Jr, E. F., Thermophysics of metal alkanoates III. Heat capacities and thermodynamic properties of lithium and potassium propanoates. *The Journal of Chemical Thermodynamics* **1984**, *16* (1), 81-90.
16. Franzosini, P.; Westrum Jr, E. F.; Plautz, W. A., Thermophysics of metal alkanoates II. Heat capacities and thermodynamic properties of sodium propanoate. *The Journal of Chemical Thermodynamics* **1983**, *15* (7), 609-618.
17. Ngeyi, S. P.; Westrum Jr, E. F.; Franzosini, P., Thermophysics of metal alkanoates V. Heat capacities and thermodynamic properties of lithium n-butanoate and n-hexanoate. *The Journal of Chemical Thermodynamics* **1986**, *18* (7), 609-618.

18. Stanley P. Ngeyi, I. M., Bruce H. Justice, and Edgar F. Westrum, Jr, Thermophysics of metal alkanoates. Heat capacities and thermodynamic properties of potassium n-hexanoate from temperatures from 6 K to 600 K. VIII. *J. Chem. Thermodynamics* **2001**, *33*, 423-431.
19. R.C. Mehrota, R. B., *Metal carboxylates*. Academic Press: London, 1983.
20. Adolfsson, E.; Carlsson, G.; Grindborg, J.-E.; Gustafsson, H.; Lund, E.; Tedgren, Å., Response of Lithium Formate EPR Dosimeters at Photon Energies Relevant to Brachytherapy. In *World Congress on Medical Physics and Biomedical Engineering, September 7 - 12, 2009, Munich, Germany*, Dössel, O.; Schlegel, W., Eds. Springer Berlin Heidelberg: 2009; Vol. 25/1, pp 236-239.
21. Brody, J. R.; Kern, S. E., History and principles of conductive media for standard DNA electrophoresis. *Anal Biochem* **2004**, *333* (1), 1-13.
22. Markley, K. S., Salts of Fatty Acids. In *Fatty Acids. Their chemistry, properties, production, and uses.*, 2 ed.; Markley, K. S., Ed. Interscience Publisher, Inc.: New York, 1961; Vol. 2, pp 715-756.
23. Levy, J., Utilization of fatty acids in metallic soaps and greases. In *Fatty acids and their industrial applications*, Pattison, S. E., Ed. New York, 1968; pp 209-220.
24. Martínez Casado, F. J.; Riesco, M. R.; García Pérez, M. V.; Redondo, M. I.; López-Andrés, S.; Rodríguez Cheda, J. A., Structural and Thermodynamic Study on Short Metal Alkanoates: Lithium Propanoate and Pentanoate. *The Journal of Physical Chemistry B* **2009**, *113* (39), 12896-12902.
25. G.W.H. Höhne, W. F. H., H.-J. Flammersheim, *Differential scanning calorimetry*. 2 ed.; Springer: Berlin, 2003.
26. Höhne G., H. W. a. F. H. J., *Differential Scanning Calorimetry*. Springer-Verlag, Berlin Heidelberg: 1996.
27. *ASTM. E 1269 – 01 Standard test method for determining specific heat capacity by differential scanning calorimetry*. West Conshohocken: PA, 2001.
28. Szymanski, H. A., *A systematic approach to the interpretation of infrared spectra*. 2 ed.; Hertillon Press, Cambridge Springs: PA, 1971.
29. Nakamoto, K., *Infrared and Raman spectra of inorganic and coordination compounds*. 3rd ed.; Wiley: New York, 1978.
30. R.M. Silverstein, G. C. B., T.C. Morrill, *Spectrometric identification of organic compounds*. 4th ed.; Wiley: New York, 1981.
31. N.B. C., L.H. Daly, S.E. Wiberley, *Introduction to infrared and Raman spectroscopy*. 3rd ed.; Academic Press: San Diego, CA, 1990.
32. Frost, R. L.; Kloprogge, J. T., Raman spectroscopy of the acetates of sodium, potassium and magnesium at liquid nitrogen temperature. *Journal of Molecular Structure* **2000**, *526* (1–3), 131-141.
33. H.H Jaffé, M. O., *Theory and application of ultraviolet spectroscopy*. Wiley: New York, 1962.
34. Binnemans, K., Ionic Liquid Crystals. *Chem. Rev.* **2005**, *105*, 4148-4204.
35. <http://webbook.nist.gov/>.
36. Martínez Casado, F.; Ramos Riesco, M.; Cheda, J., Rubidium and lithium butanoates binary phase diagram. *Journal of Thermal Analysis and Calorimetry* **2007**, *87* (1), 73-77.
37. I. I. Goncharik, F. F. M., A. I. Voitenko, and T. P. Kulikova, Foaming and Stabilizing Activity of Binary Solutions of Sodium Carboxylates of Different Chain Length. *Russian Journal of Applied Chemistry* **2006**, *79*, 470-474.
38. Michael P. Landoll, M. T. H., Kinetics study of thermal decomposition of sodium carboxylate salts. *Biomass and Bioenergy* **October 2012**, *45*, 195–202.
39. Xiang, C. B., A., The Analysis of Liquid Crystal Phases using Polarized Optical Microscopy. **May 17, 2011**.
40. [http://www.jic.ac.uk/microscopy/more/T5\\_3.htm](http://www.jic.ac.uk/microscopy/more/T5_3.htm) (accessed 1/2013).

41. Basic of polarizing microscopy. Olympus.
42. Robin D. Rogers, K. R. S., Sergei Volkov, *Green Industrial Applications of Ionic Liquids*. Springer: 2003.
43. Blackley, D. C., *Polymer Latices*. 2nd ed.; 1997.
44. Lomer, T., The unit-cell dimensions of potassium soaps. *Acta Crystallographica* **1952**, 5 (1), 11-14.
45. R.M.Kellogg, *Section 8.4.3, Science of Synthesis* 2006.
46. T. A. Mirnaya, G. G. Y., and S. V. Volkov, PHASE STATES OF BINARY SYSTEMS OF SODIUM, POTASSIUM AND CESIUM PROPIONATES. *Theoretical and Experimental Chemistry* **1994**, 30.
47. Petroleum Economist. **2008**.

## Supporting Information

The complete set of spectra, calorigrams and derived properties for the C1-C12 carboxylates are presented: Infrared spectra (Figures S1-S12), Raman spectra (Figures S13-S24), UV-Vis spectra (Figures S25-S36), TGA analysis (Figure S37), DSC calorigrams (Figures S38-S49) and isobaric heat capacity ( $C_p$ ) versus temperature curves (Figures S50-S61).

## **Lithium C<sub>1</sub>-C<sub>12</sub> *n*-alkanoates: Thermal behavior from –30 to 600 °C**

The primary aim of the investigation was to study thermal behaviour. The spectroscopic data was employed to support the thermal investigation. The reasoning behind the collection of the spectroscopic data was as follows:

- (a) Infrared (IR) spectroscopy is sensitive for the detection of carbonyl and carboxylate compounds. It could therefore be used to confirm synthesis of the lithium carboxylates, as well as provide an indication of purity. Synthesis was performed with a 2 % molar excess of carboxylic acid and if the acid was not completely removed during purification, it would be visible on the infrared spectrum.
- (b) IR spectroscopy was also employed to determine whether chemical changes took place during calorimetry. Once a thermal event was observed, a sample was run to a temperature just above the temperature of the observed thermal event and the IR spectrum of the sample thus treated was collected and compared with the starting material.
- (c) IR, Raman and Ultraviolet-Visible (UV-Vis) spectra were collected in the hope of finding explanations for differences in thermal behaviour, and in the hope that additional information about the nature of the lithium carboxylates can be deduced.

## IR Spectra

### Lithium methanoate (formate)

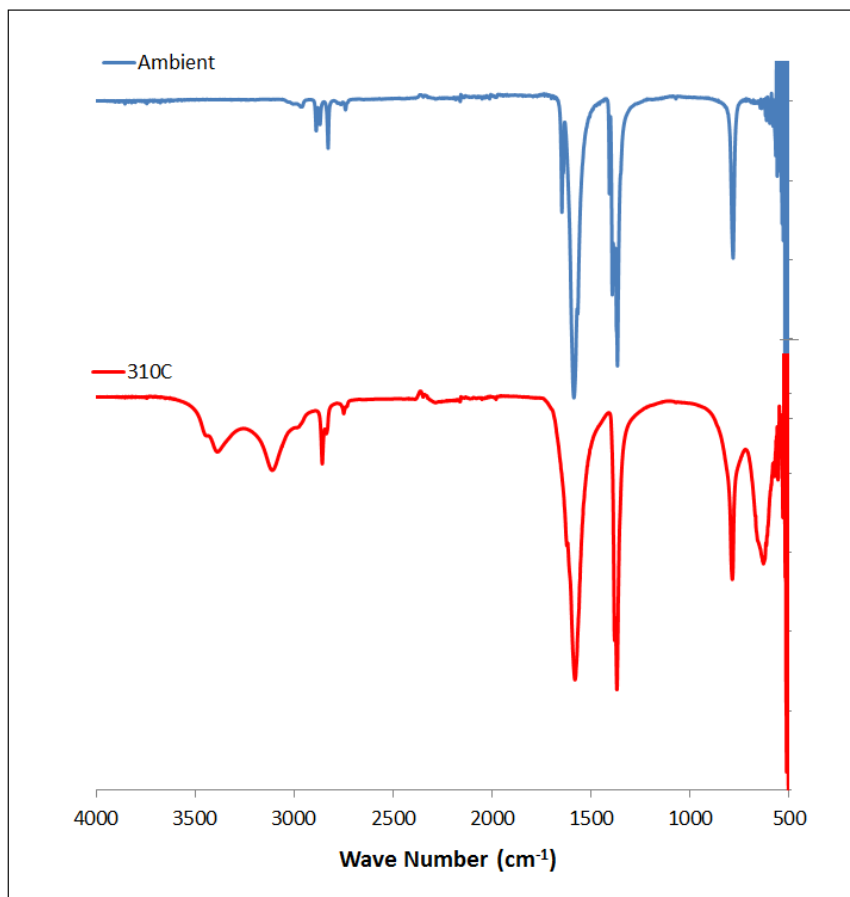


Figure S 1. IR spectrum of lithium methanoate before and after melting

## Lithium ethanoate (acetate)

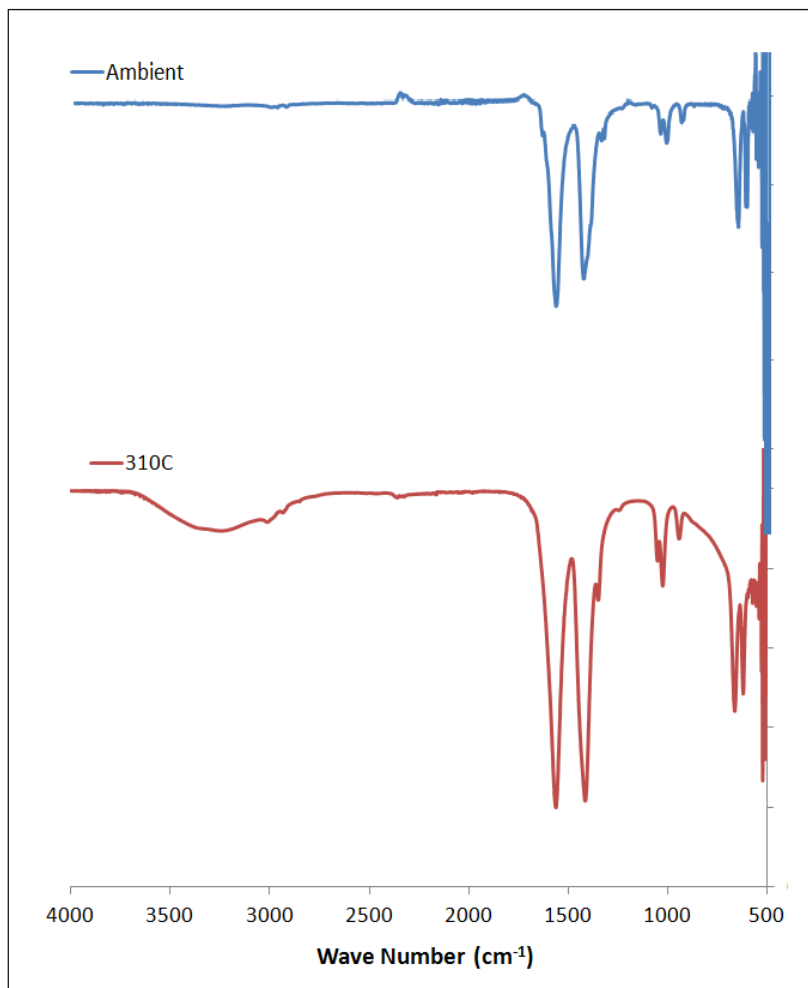


Figure S 2. IR spectrum of lithium ethanoate before and after melting.

## Lithium propanoate

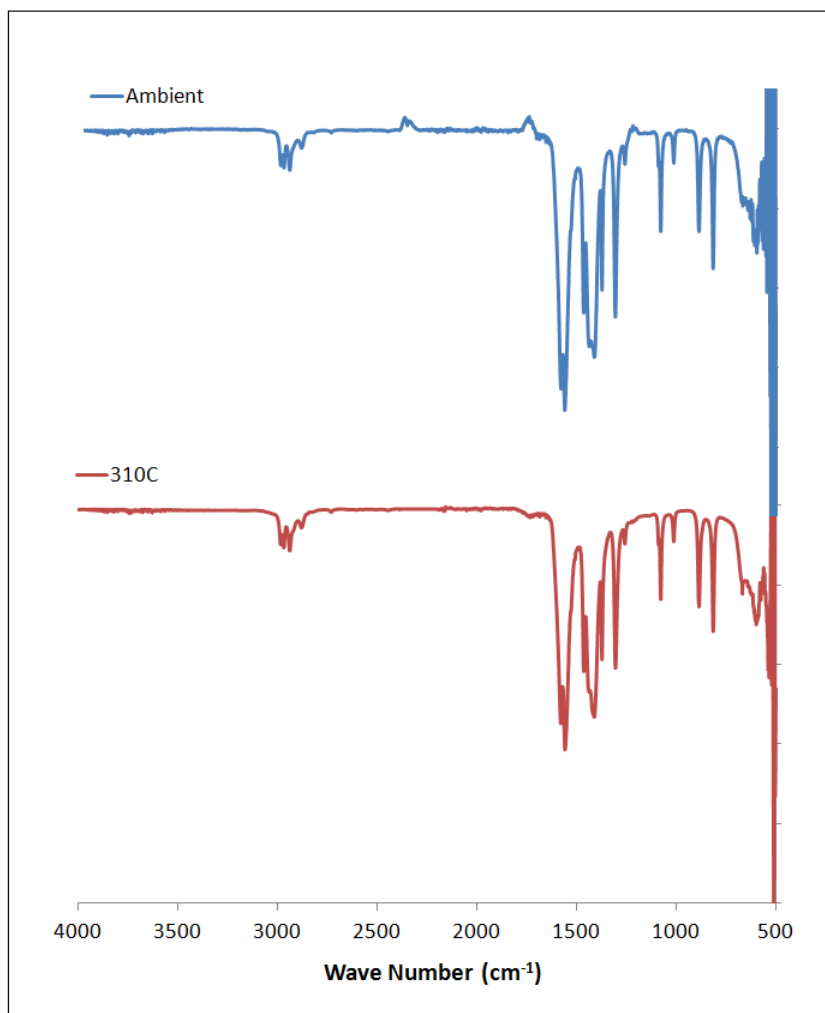


Figure S 3. IR spectrum of lithium propanoate before and after melting.

## Lithium butanoate (butyrate)

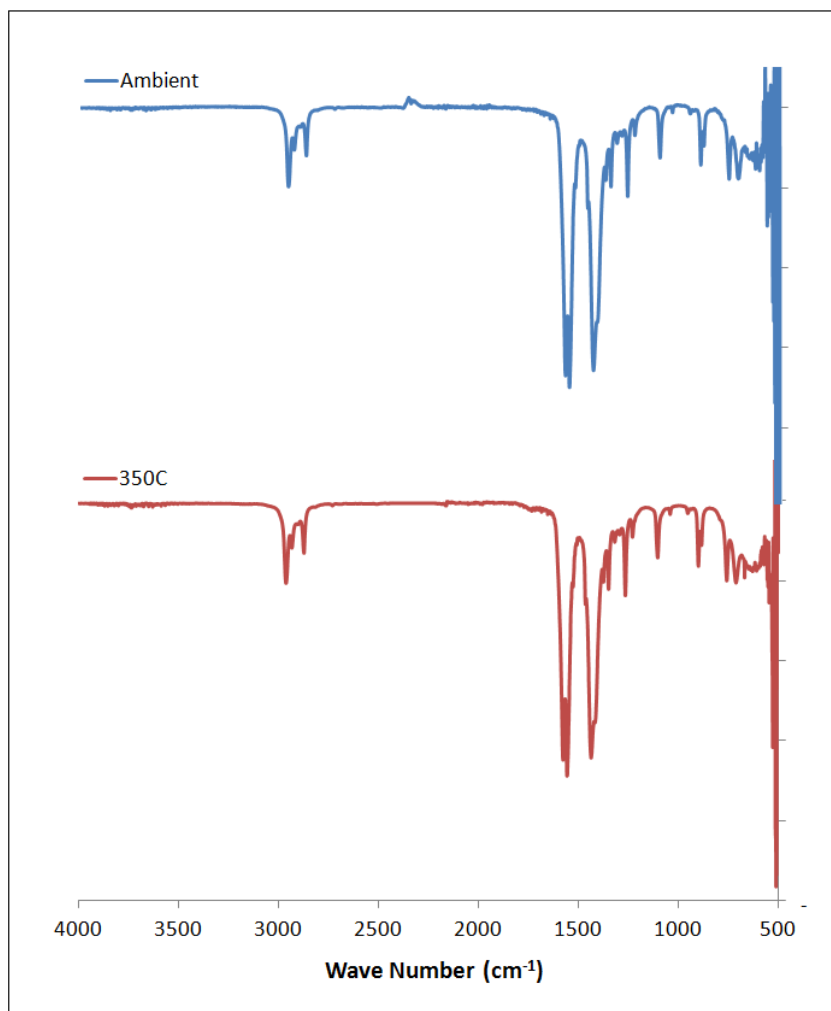


Figure S 4. IR spectrum of lithium butanoate before and after melting.

## Lithium pentanoate (valerate)

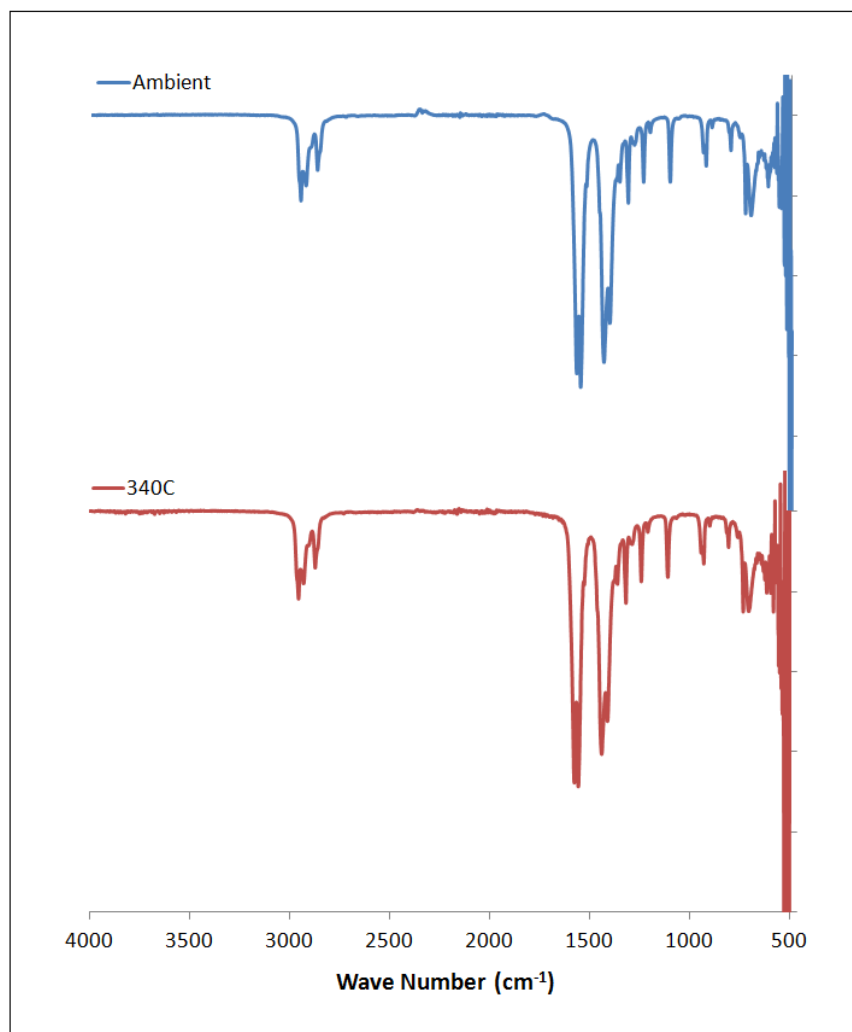


Figure S 5. IR spectrum of lithium pentanoate before and after melting.

## Lithium hexanoate (caproate)

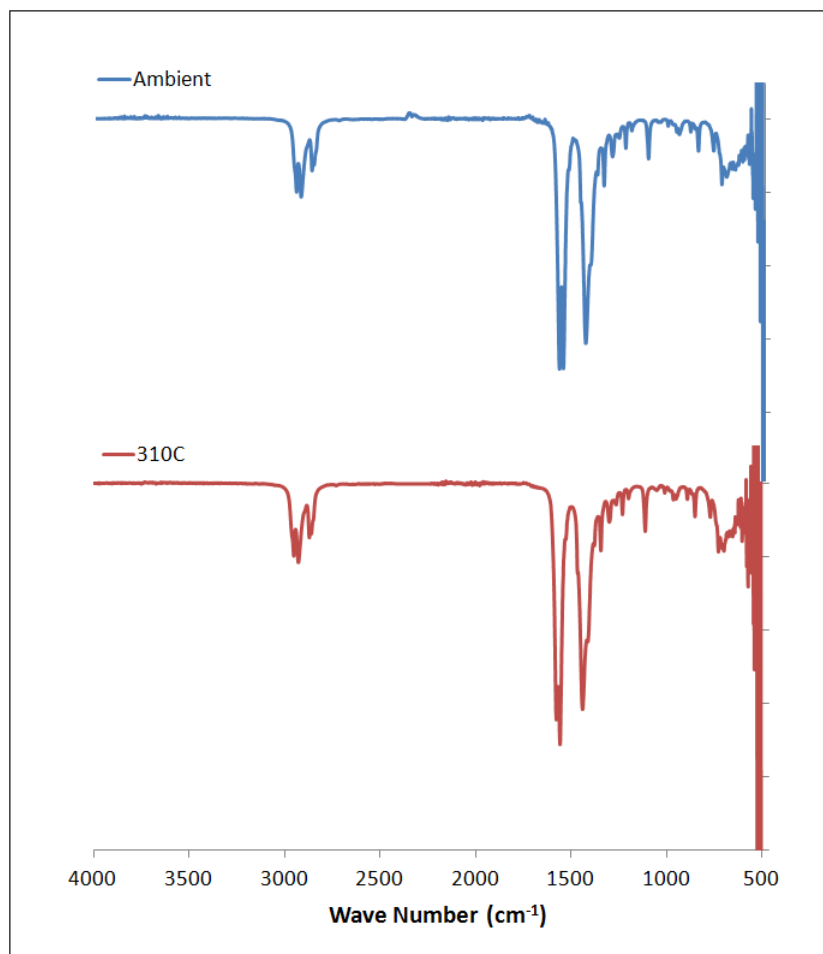


Figure S 6. IR spectrum of lithium hexanoate before and after melting.

## Lithium heptanoate

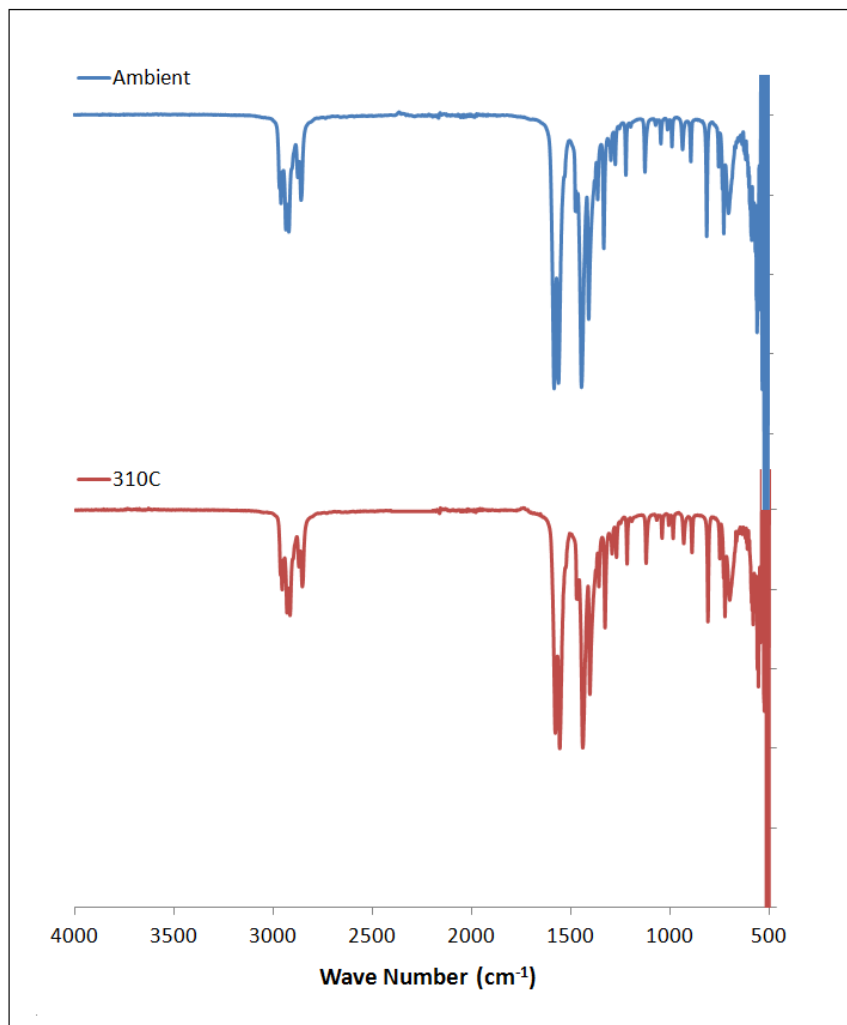


Figure S 7. IR spectrum of lithium heptanoate before and after melting.

## Lithium octanoate (caprylate)

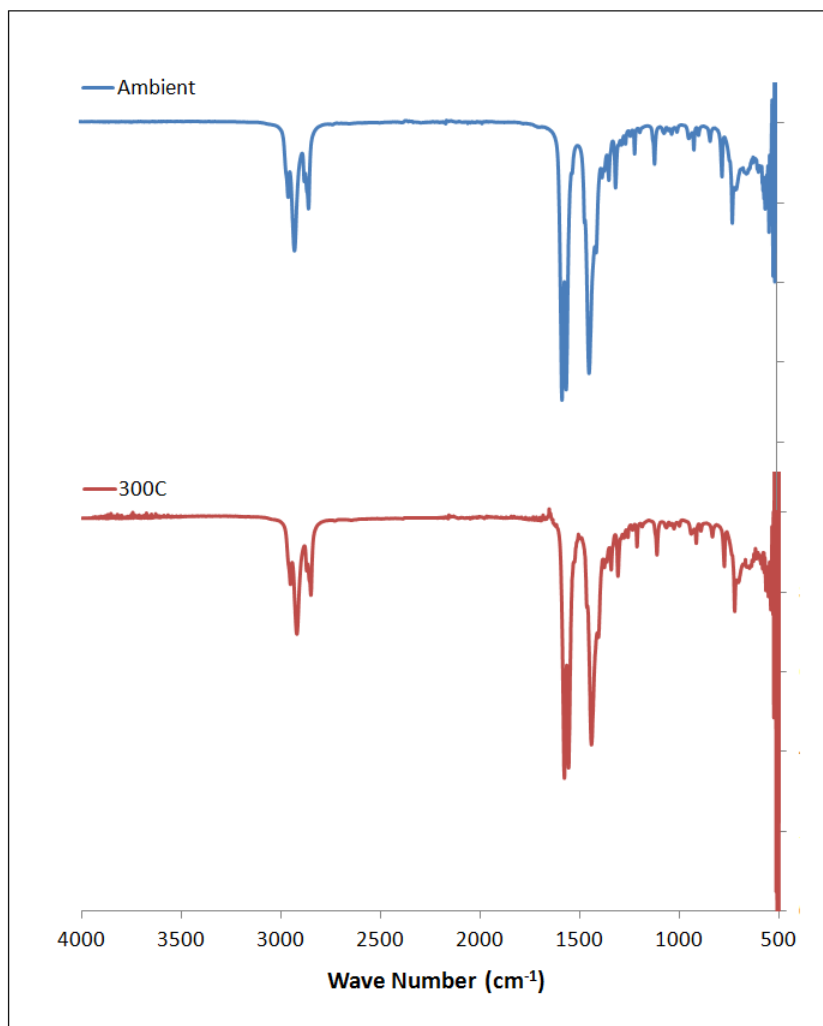
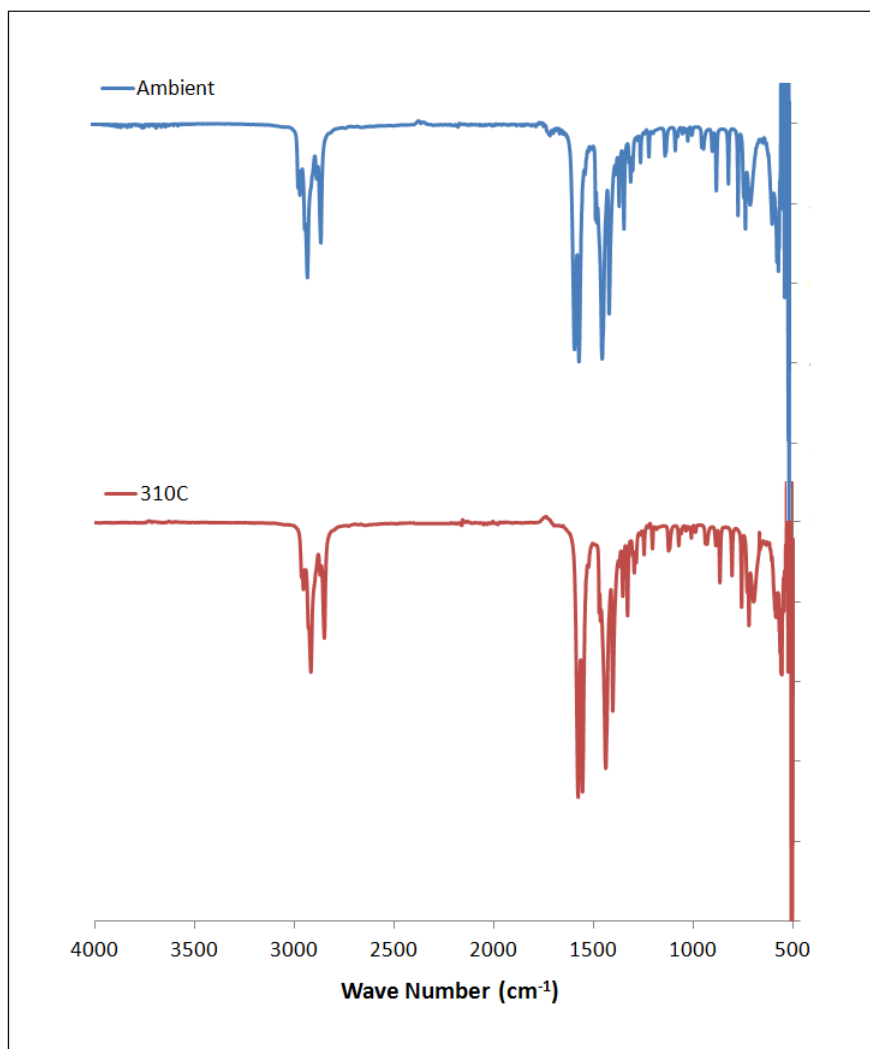


Figure S 8. IR spectrum of lithium octanoate before and after melting.

## Lithium nonanoate (pelargonate)



**Figure S 9. IR spectrum of lithium nonanoate before and after melting.**

## Lithium decanoate (caprate)

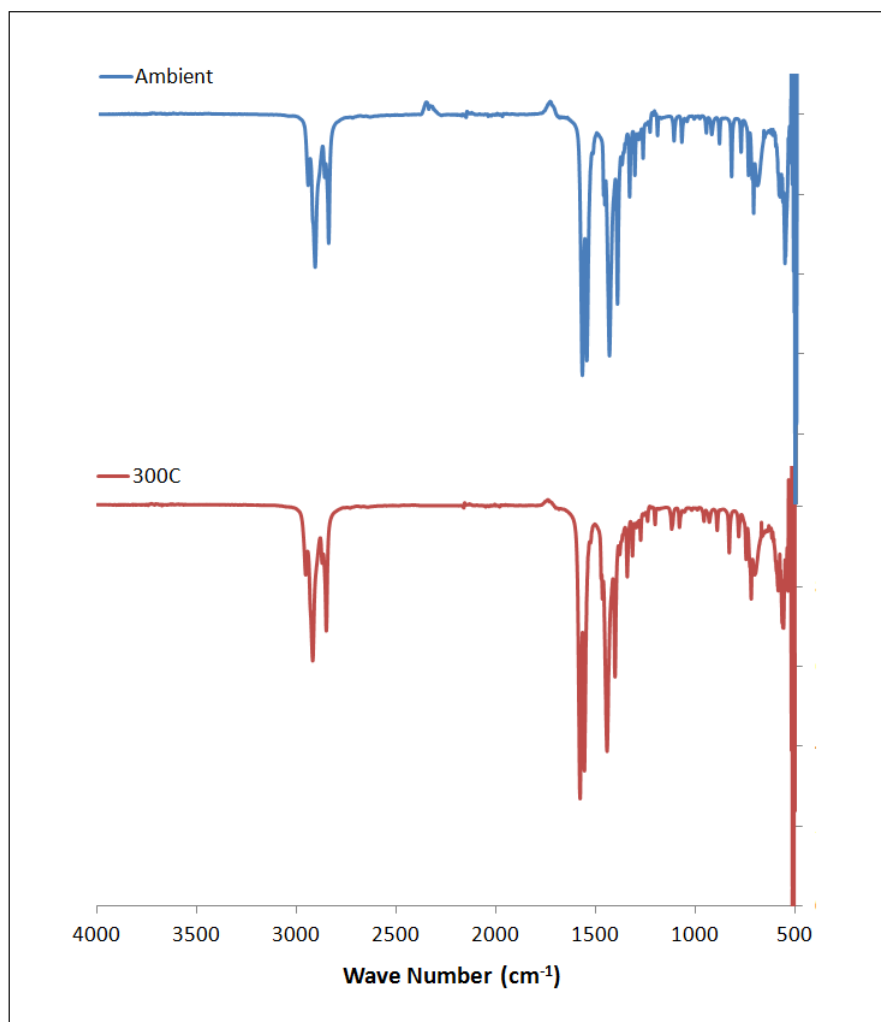


Figure S 10. IR spectrum of lithium decanoate before and after melting.

## Lithium undecanoate

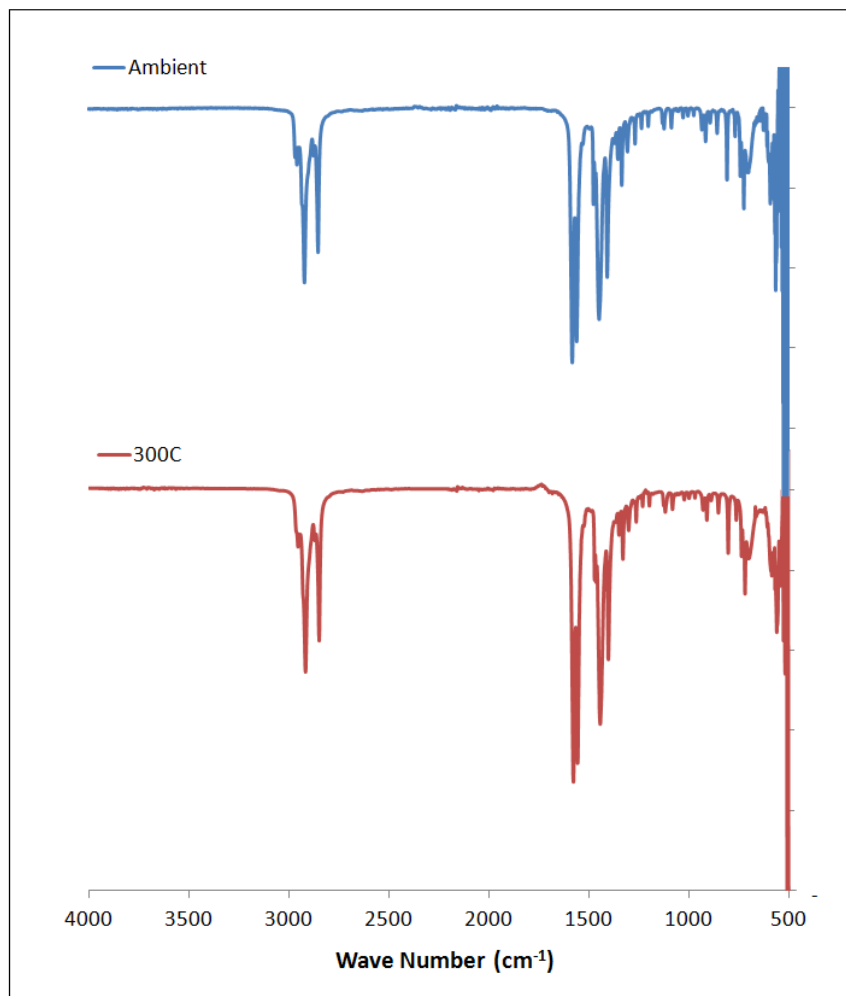


Figure S 11. IR spectrum of lithium undecanoate before and after melting.

## Lithium dodecanoate (laurate)

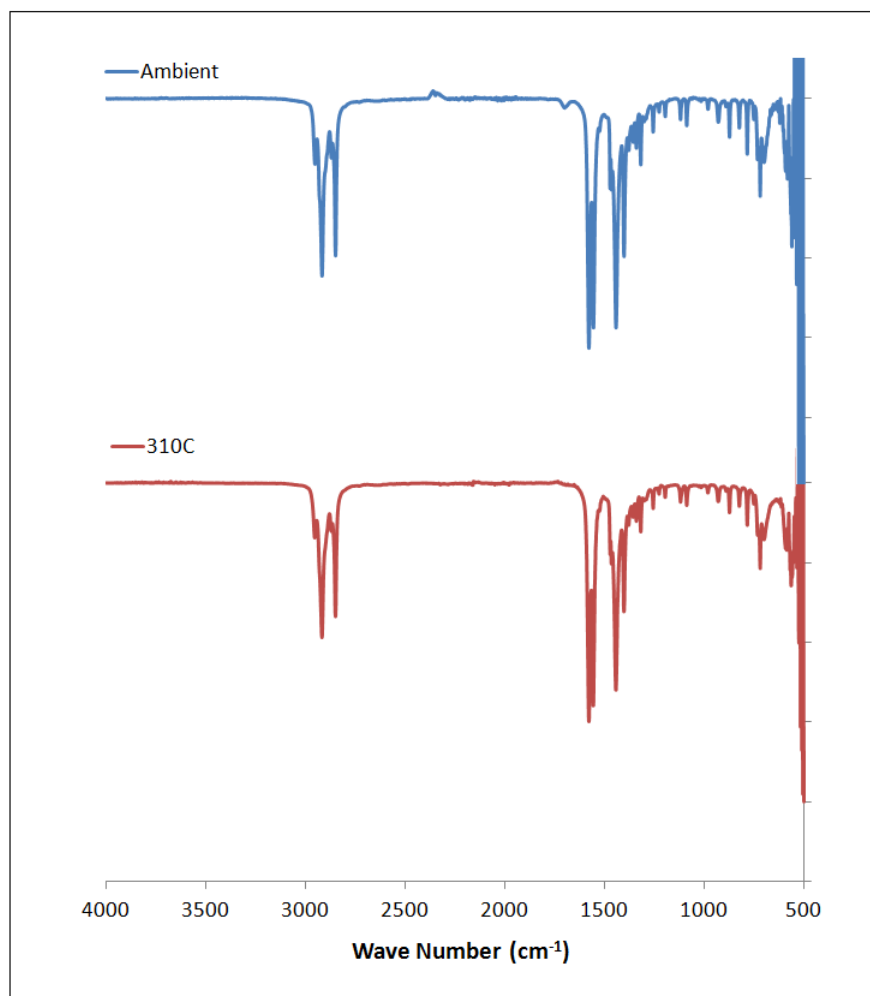


Figure S 12. IR spectrum of lithium dodecanoate before and after melting.

## Raman Spectra

### Lithium methanoate (formate)

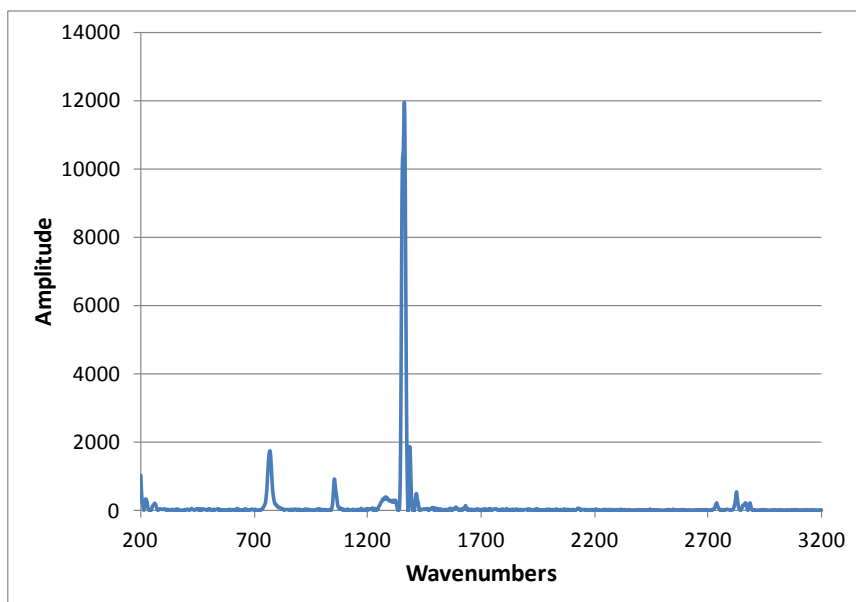


Figure S 13. Raman spectrum of lithium methanoate

### Lithium Ethanoate (acetate)

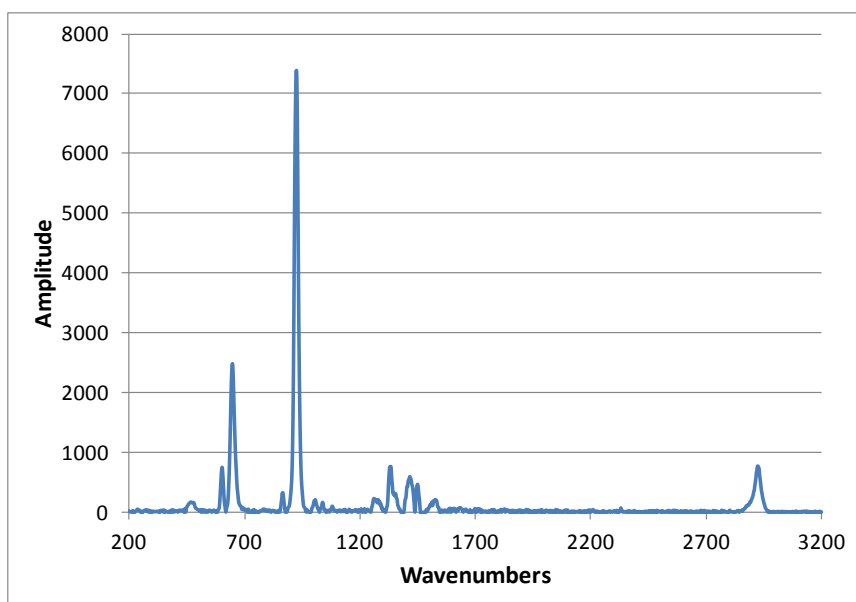


Figure S 14. Raman spectrum of lithium ethanoate

## Lithium Propanoate

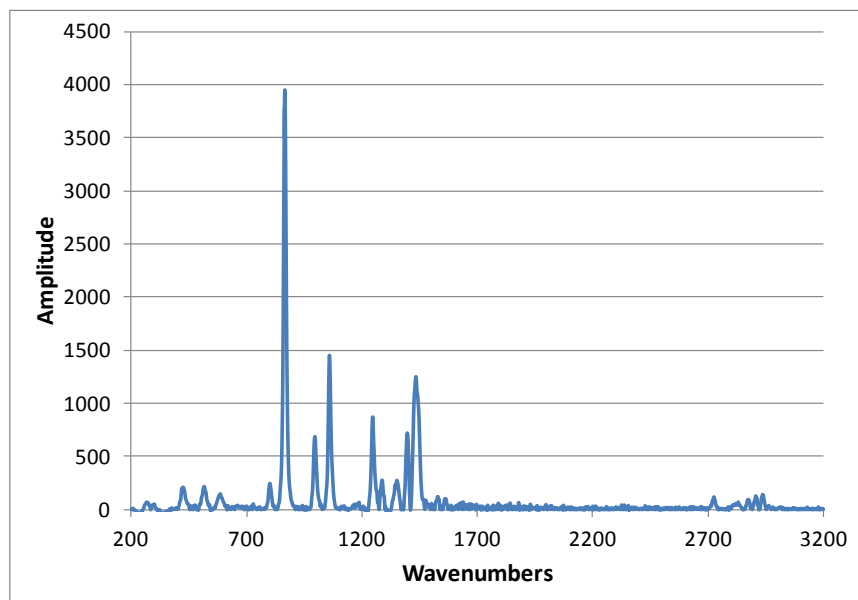


Figure S 15. Raman spectrum of lithium propanoate

## Lithium Butanoate (butyrate)

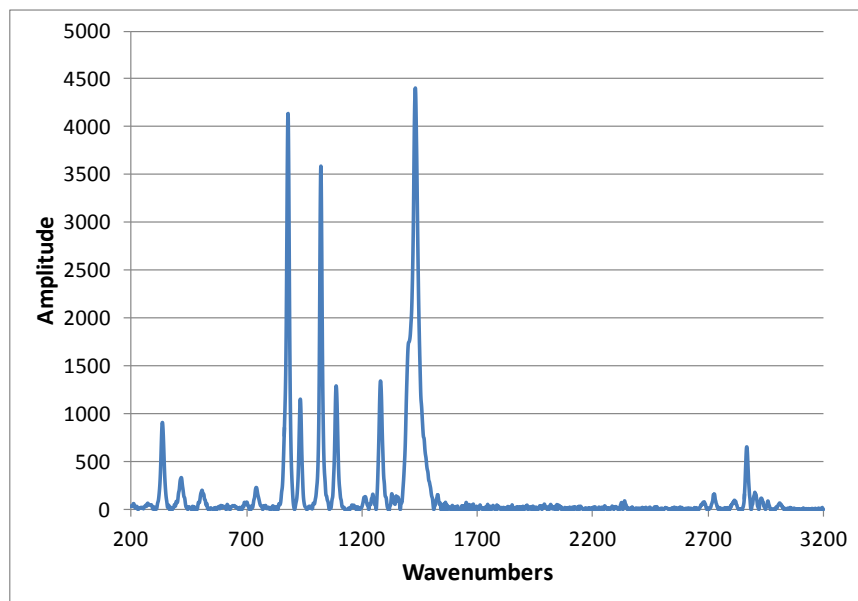


Figure S 16. Raman spectrum of lithium butanoate

### Lithium Pentanoate (valerate)

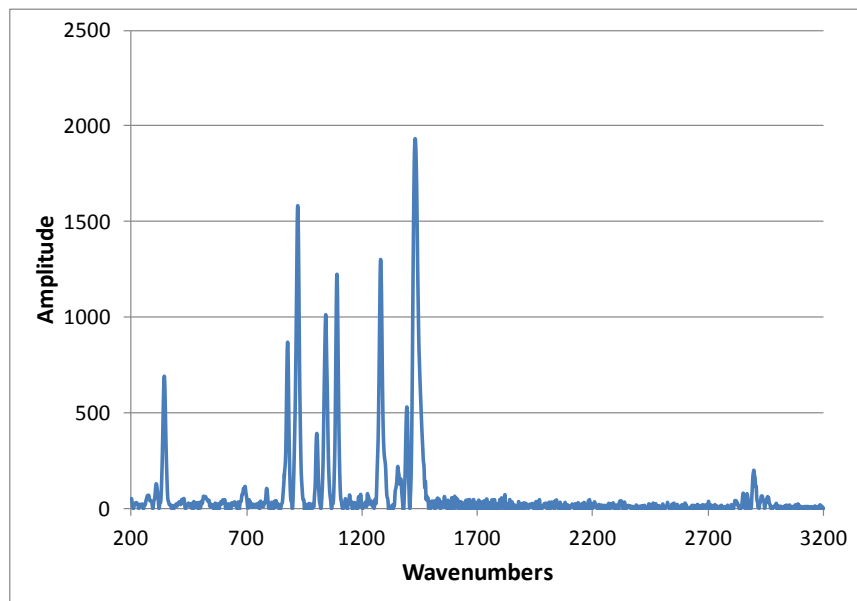


Figure S 17. Raman spectrum of lithium pentanoate

### Lithium Hexanoate (caproate)

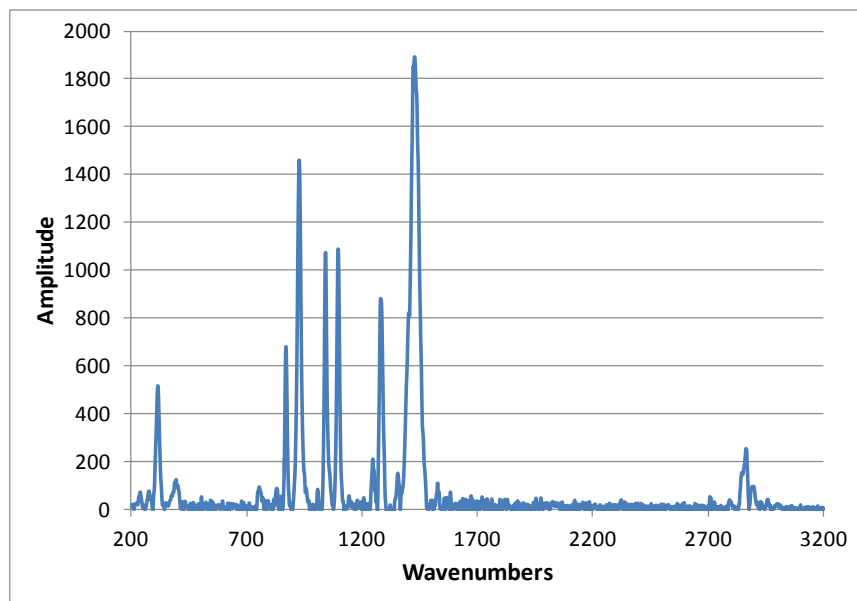


Figure S 18. Raman spectrum of lithium hexanoate

## Lithium Heptanoate

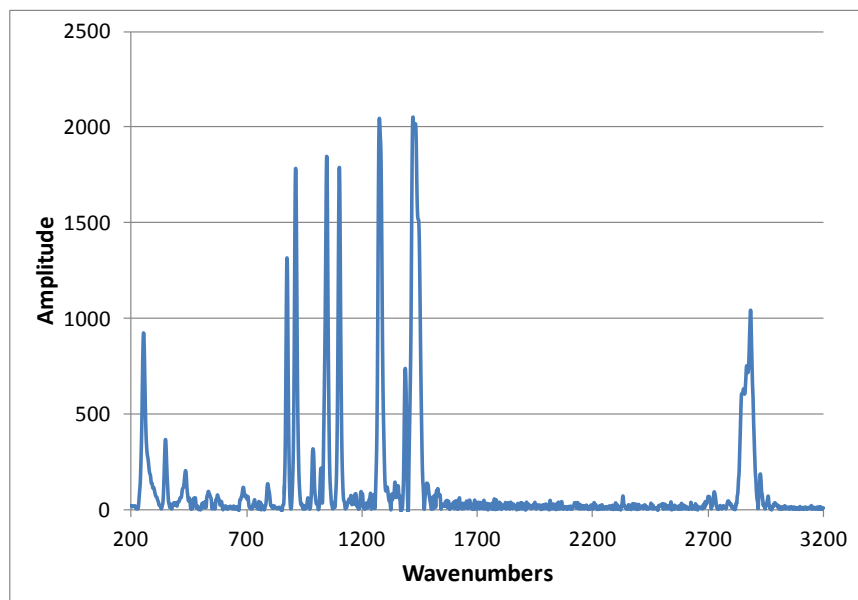


Figure S 19. Raman spectrum of lithium heptanoate

## Lithium Octanoate (caprylate)

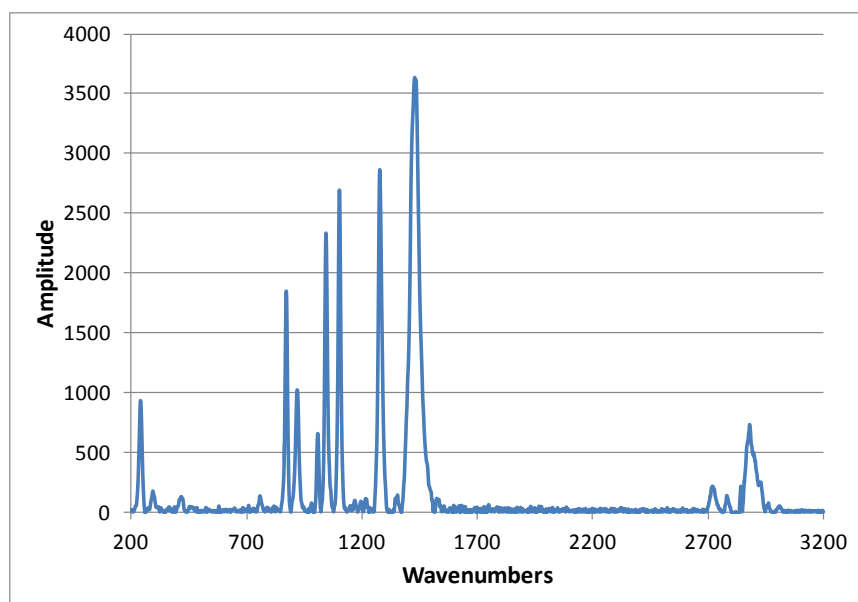


Figure S 20. Raman spectrum of lithium octanoate

### Lithium Nonanoate (pelargonate)

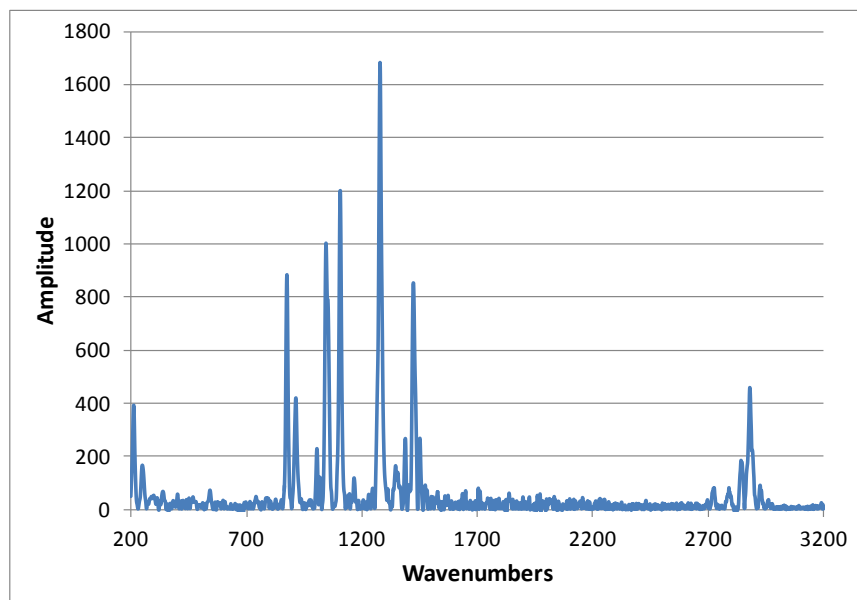


Figure S 21. Raman spectrum of lithium nonanoate

### Lithium Decanoate (caprate)

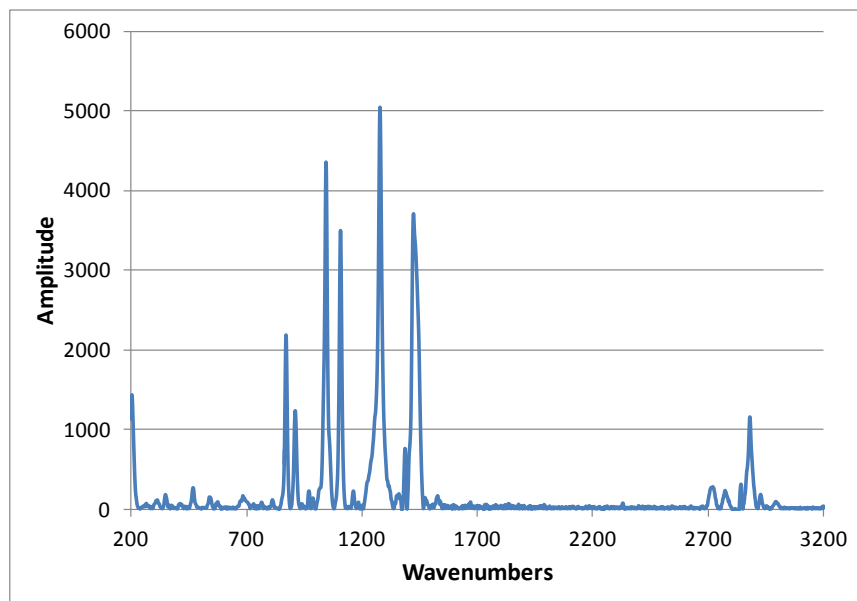


Figure S 22. Raman spectrum of lithium decanoate

## Lithium Undecanoate

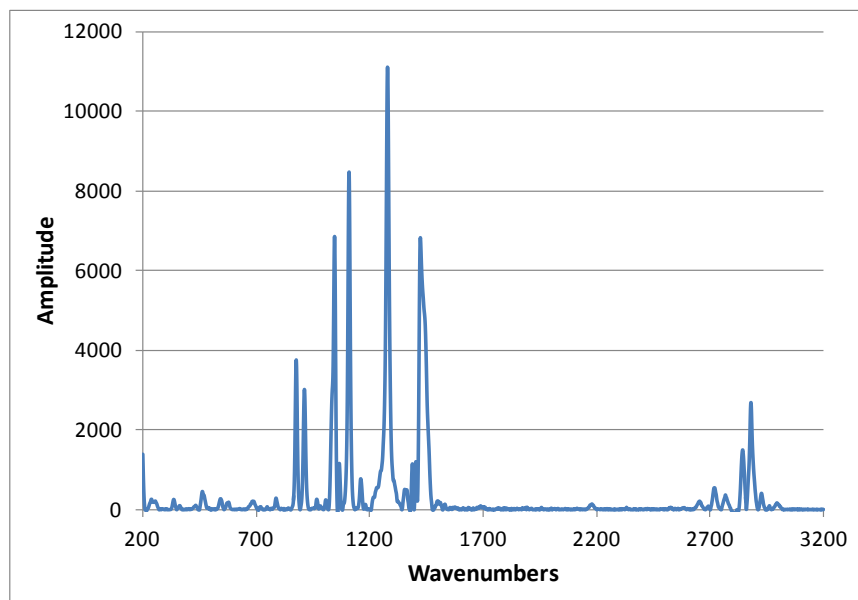


Figure S 23. Raman spectrum of lithium undecanoate

## Lithium Dodecanoate (laurate)

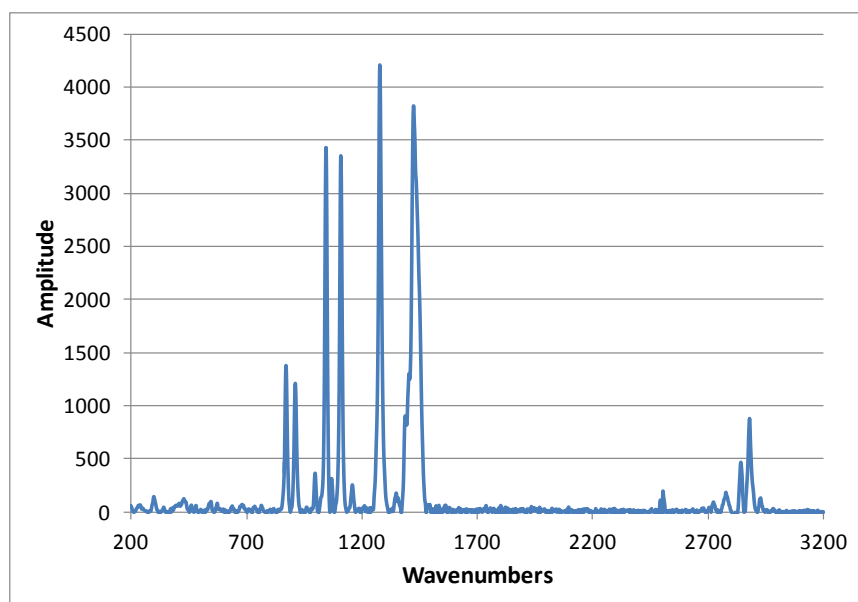


Figure S 24. Raman spectra of lithium dodecanoate

## UV-Vis Spectra

### Lithium Methanoate

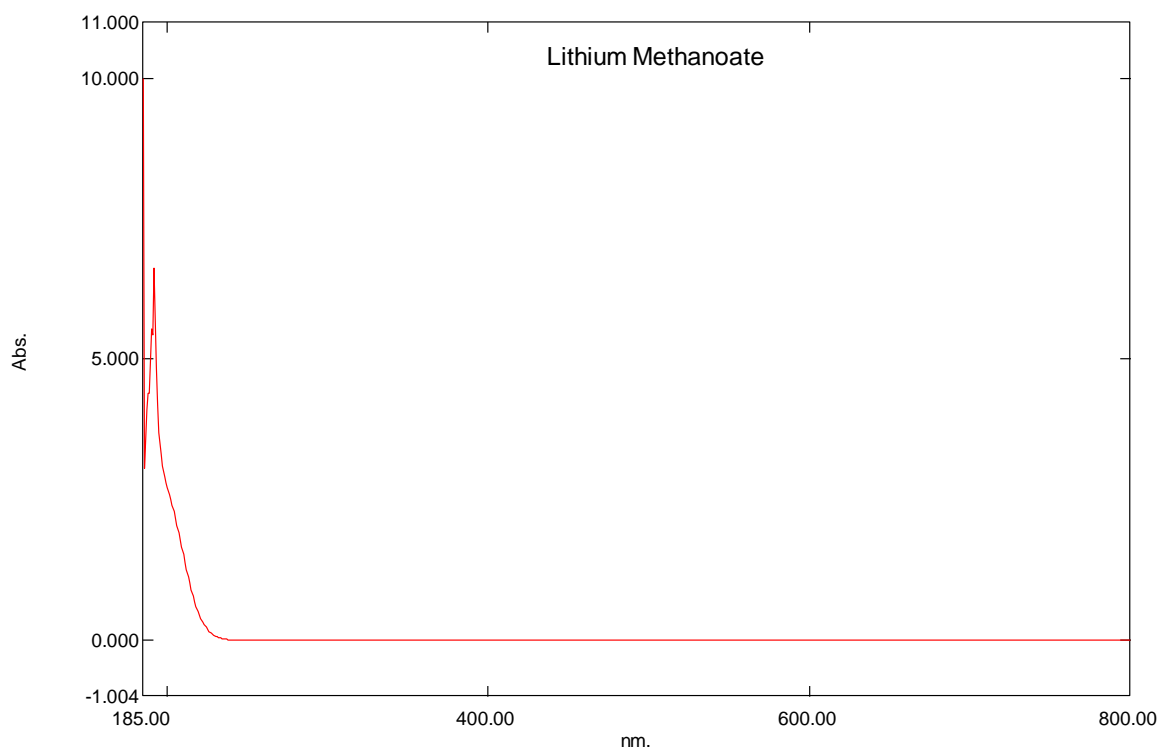


Figure S 25. UV-Vis spectrum of lithium methanoate

## Lithium Ethanoate

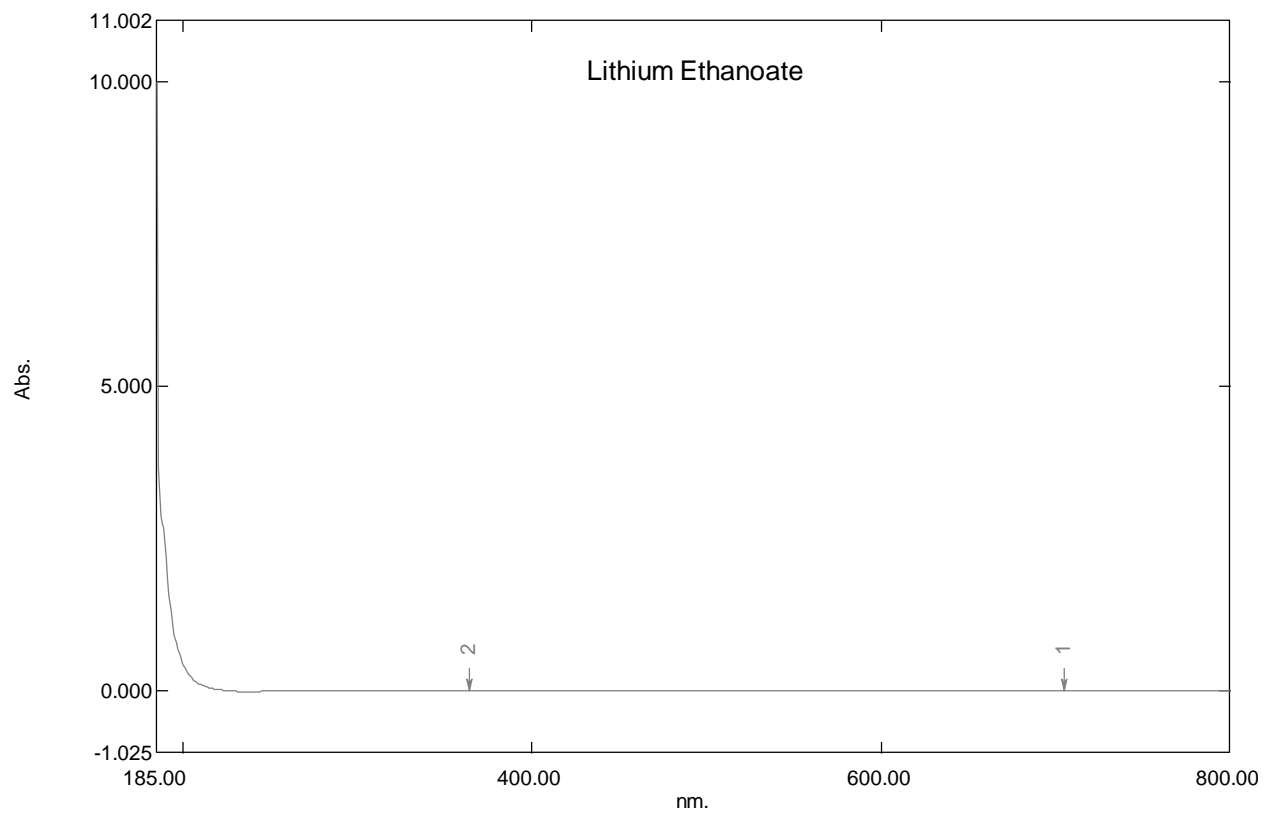


Figure S 26. UV-Vis spectrum of lithium ethanoate

## Lithium Propanoate

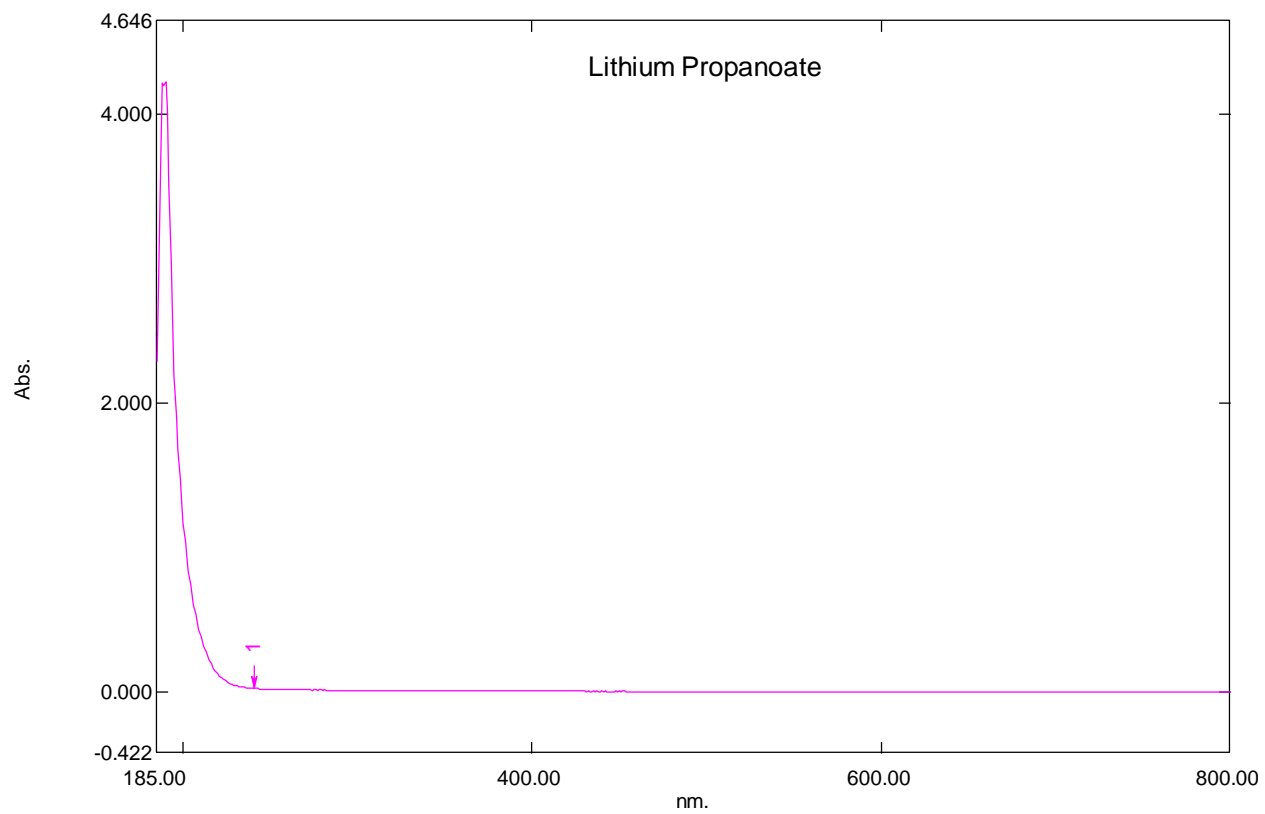


Figure S 27. UV-Vis spectrum of lithium propanoate

# Lithium Butanoate (butyrate)

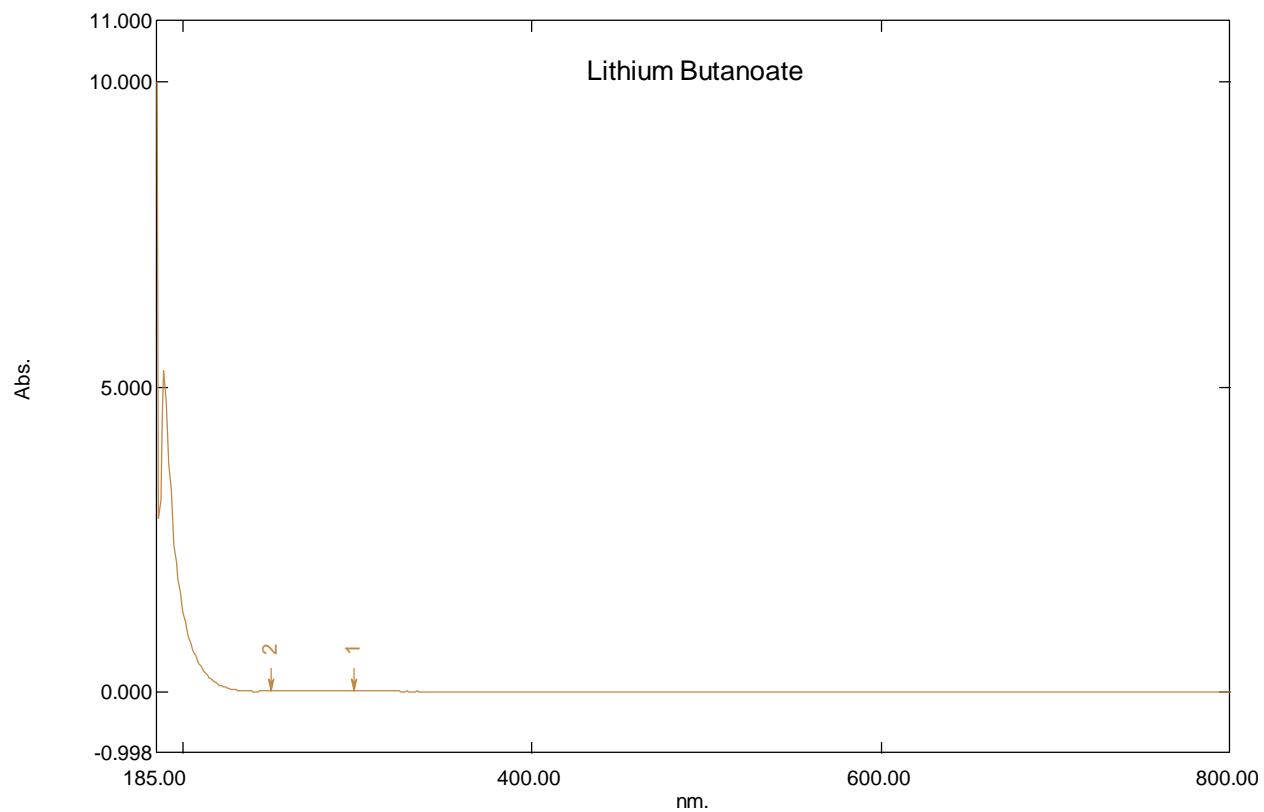


Figure S 28. UV-Vis spectrum of lithium butanoate

### Lithium Pentanoate (valerate)

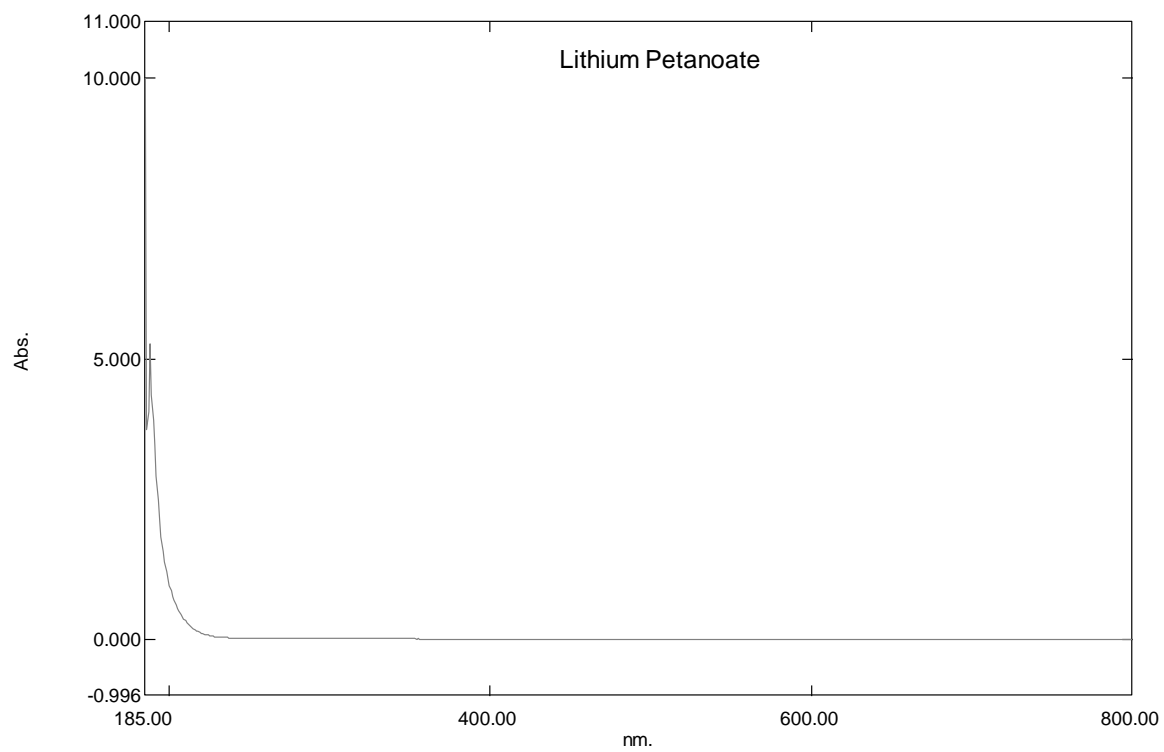


Figure S 29. UV-Vis spectrum of lithium pentanoate

# Lithium Hexanoate (caproate)

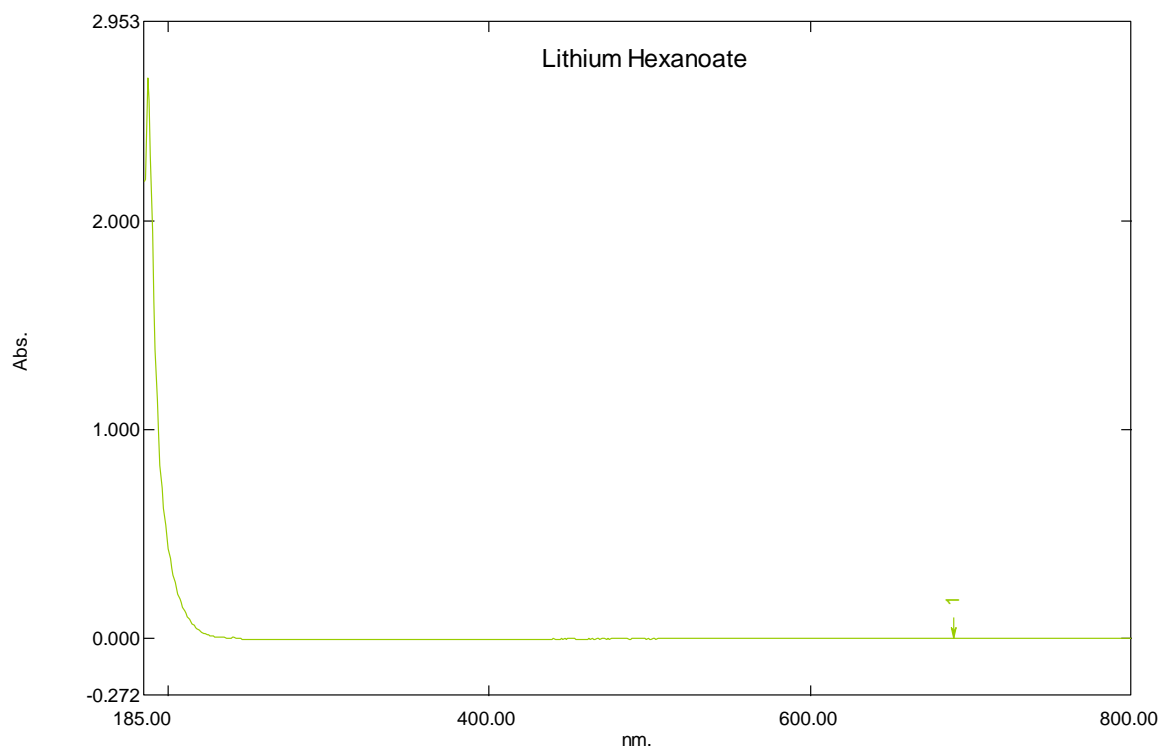


Figure S 30. UV-Vis of lithium hexanoate

## Lithium Heptanoate

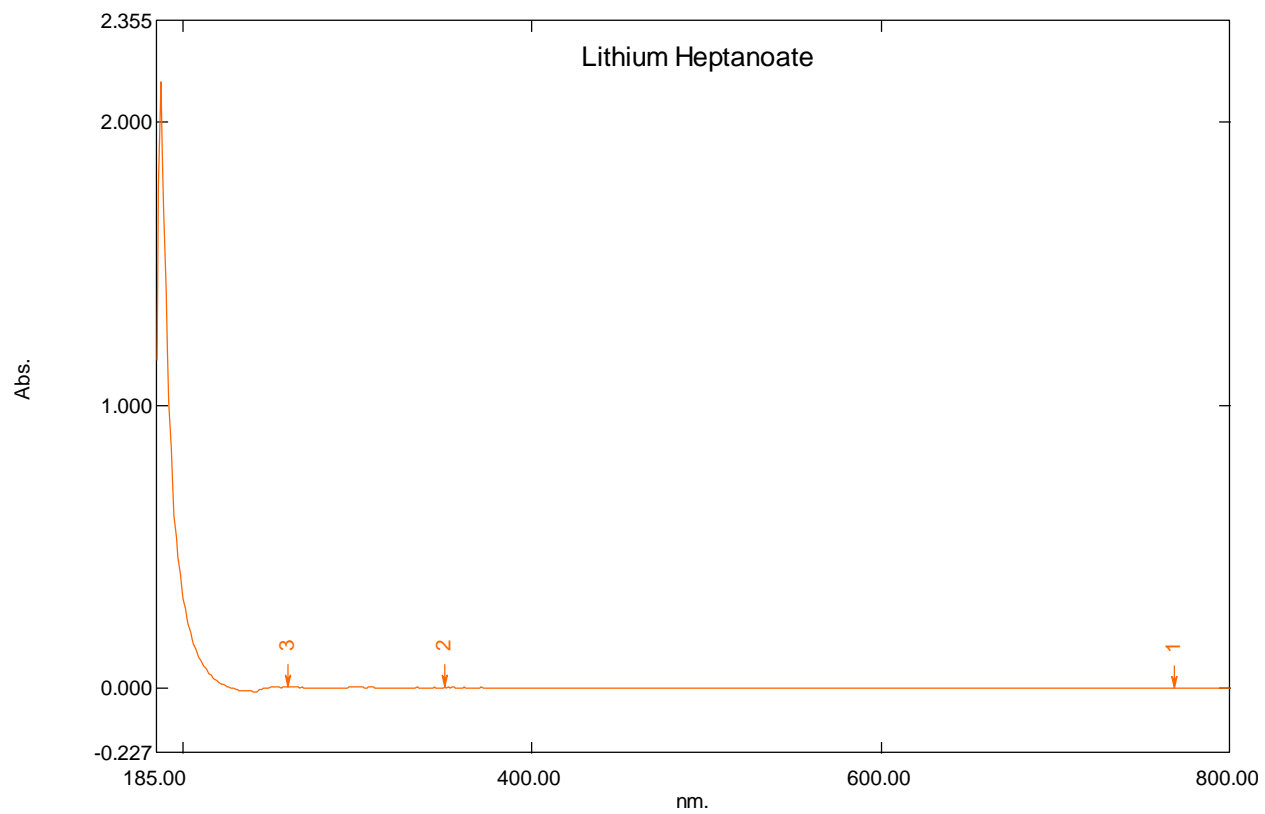


Figure S 31. UV-Vis spectrum of lithium heptanoate

## Lithium Octanoate (caprylate)

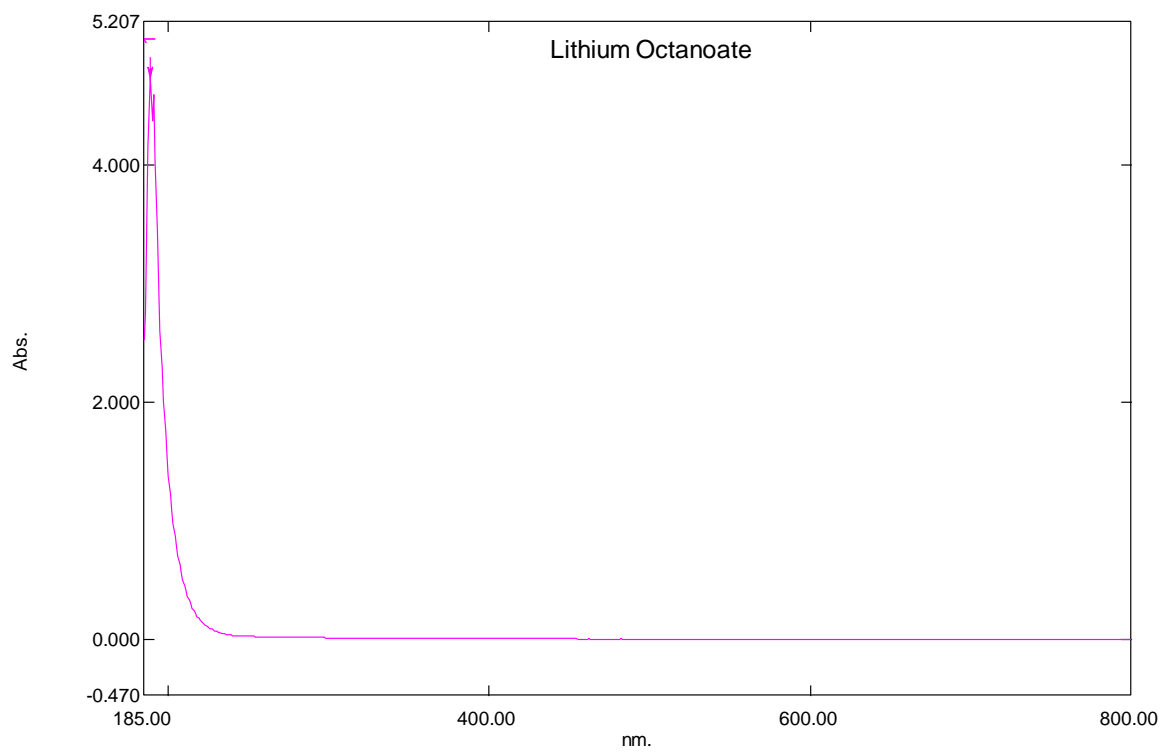


Figure S 32. UV-Vis of lithium octanoate

## Lithium Nonanoate (pelargonate)

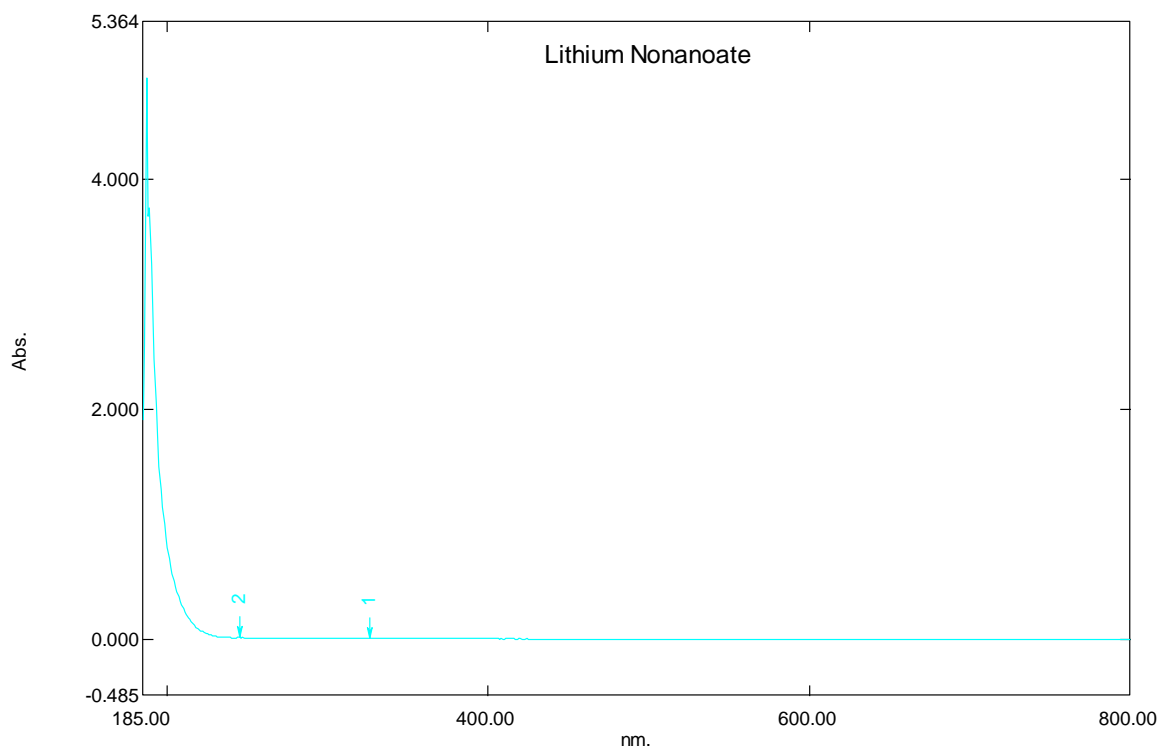


Figure S 33. UV-Vis of lithium nonanoate

# Lithium Decanoate (caprate)

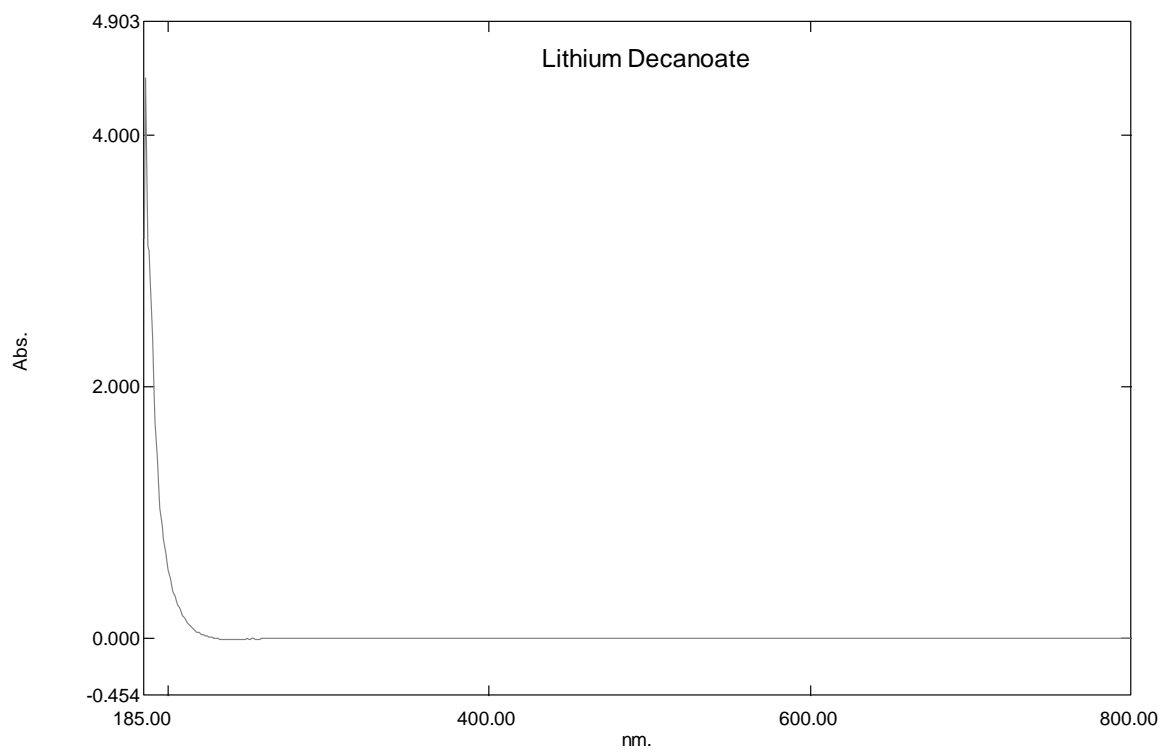


Figure S 34. UV-Vis of lithium decanoate

## Lithium Undecanoate

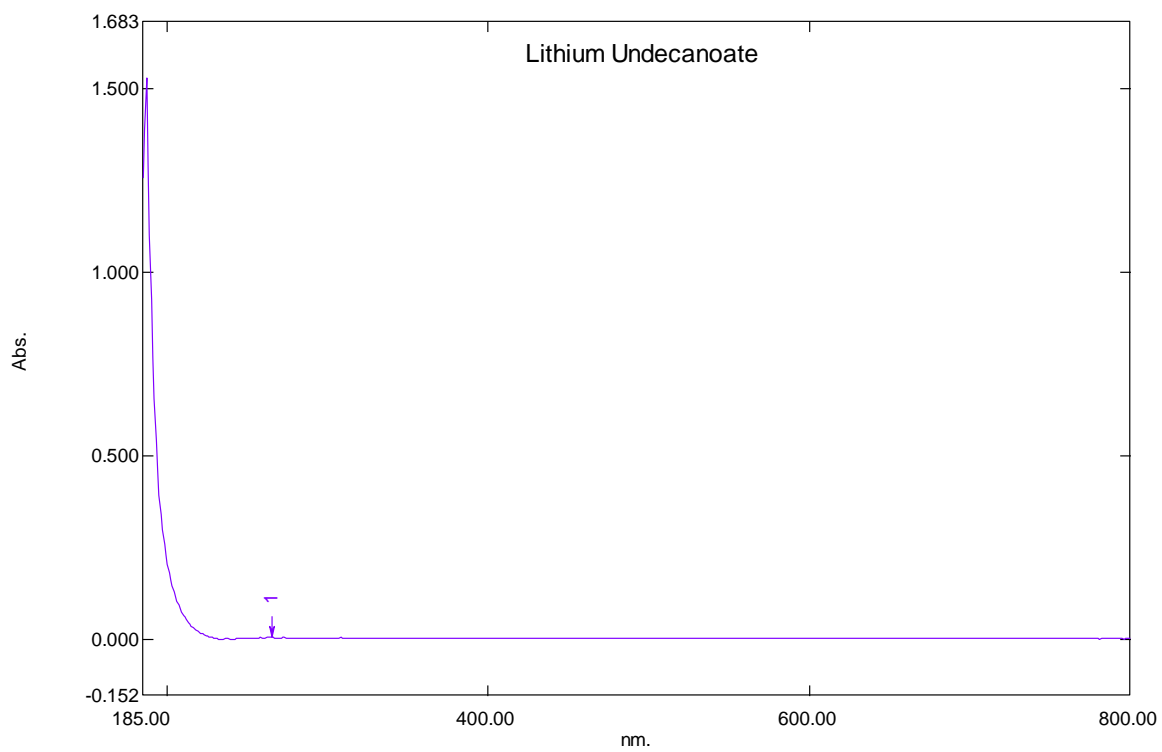


Figure S 35. UV-Vis of lithium undecanoate

## Lithium Dodecanoate (laurate)

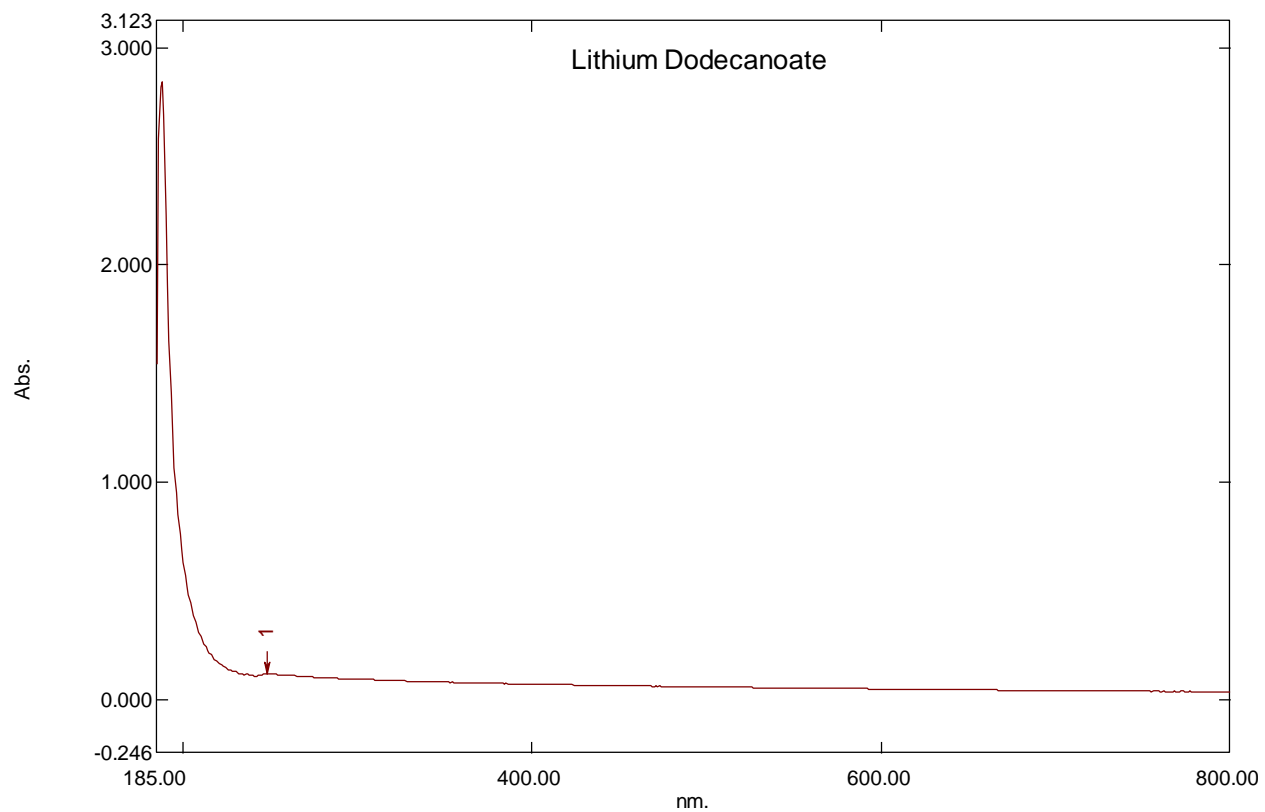


Figure S 36. UV-Vis of lithium dodecanoate

## TGA Results

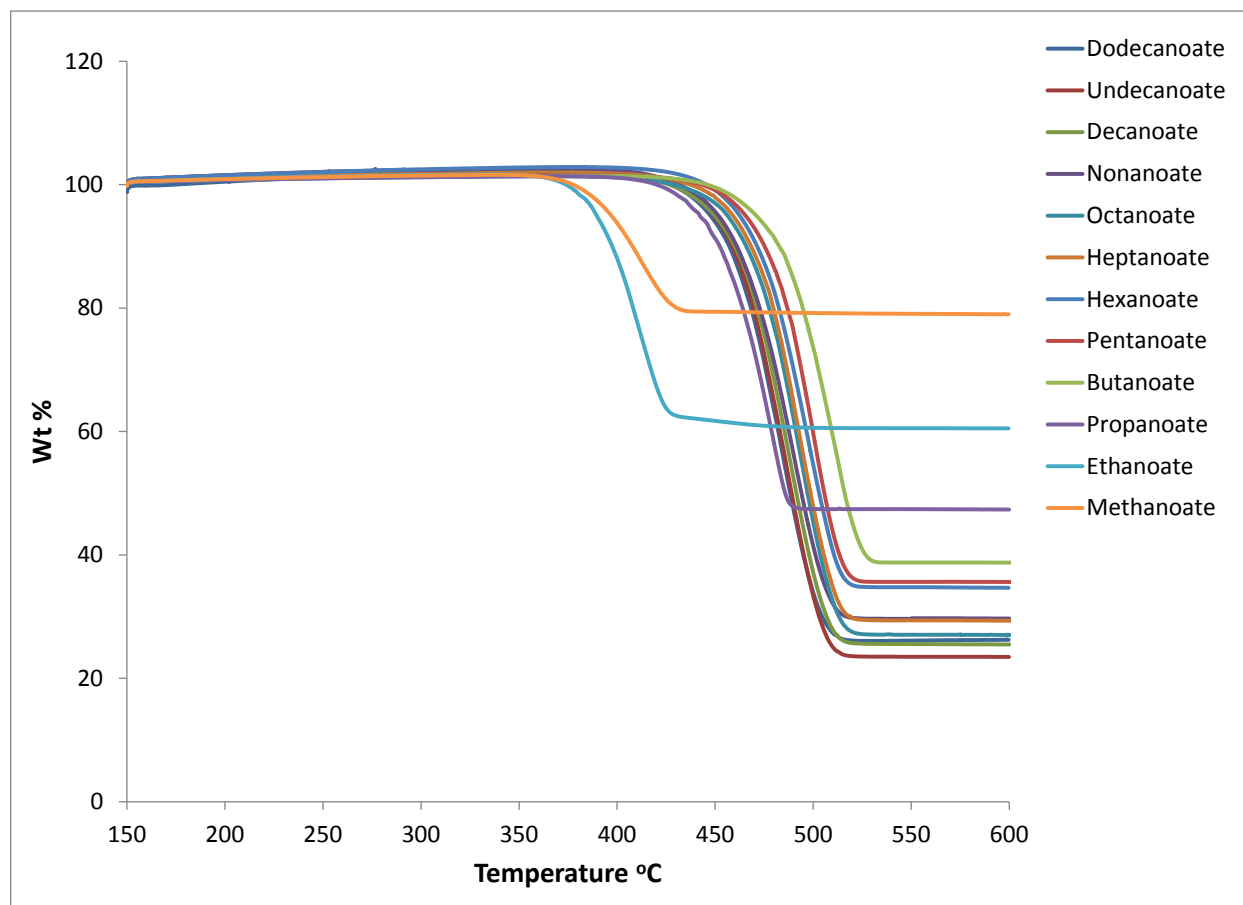


Figure S 37. TGA profile of Li-carboxylates

## Calorigrams of Li-Carboxylates determined by the Differential Scanning Calorimeter (DSC)

### Lithium Methanoate

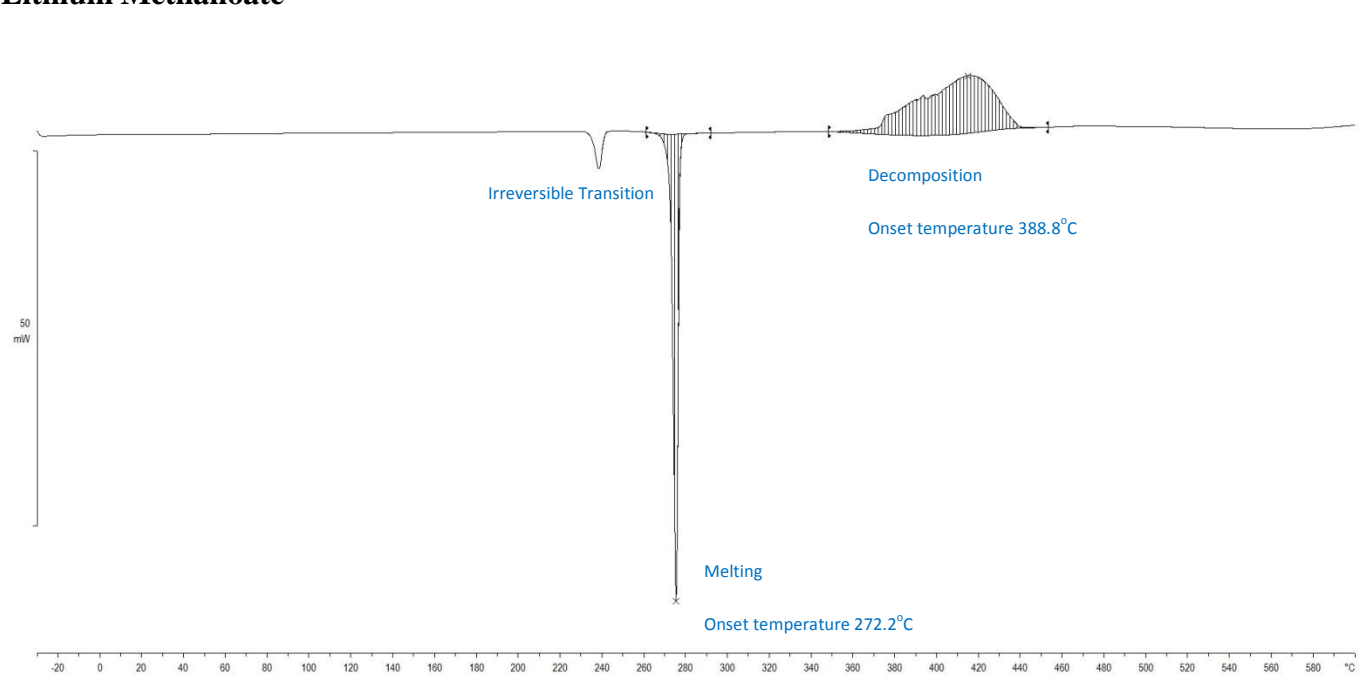


Figure S 38. Calorigram of Lithium Methanoate determined by the DSC over the range of -30-600°C at 10°C·min<sup>-1</sup> heating rate and 100mL·min<sup>-1</sup> nitrogen flow.

### Lithium Ethanoate

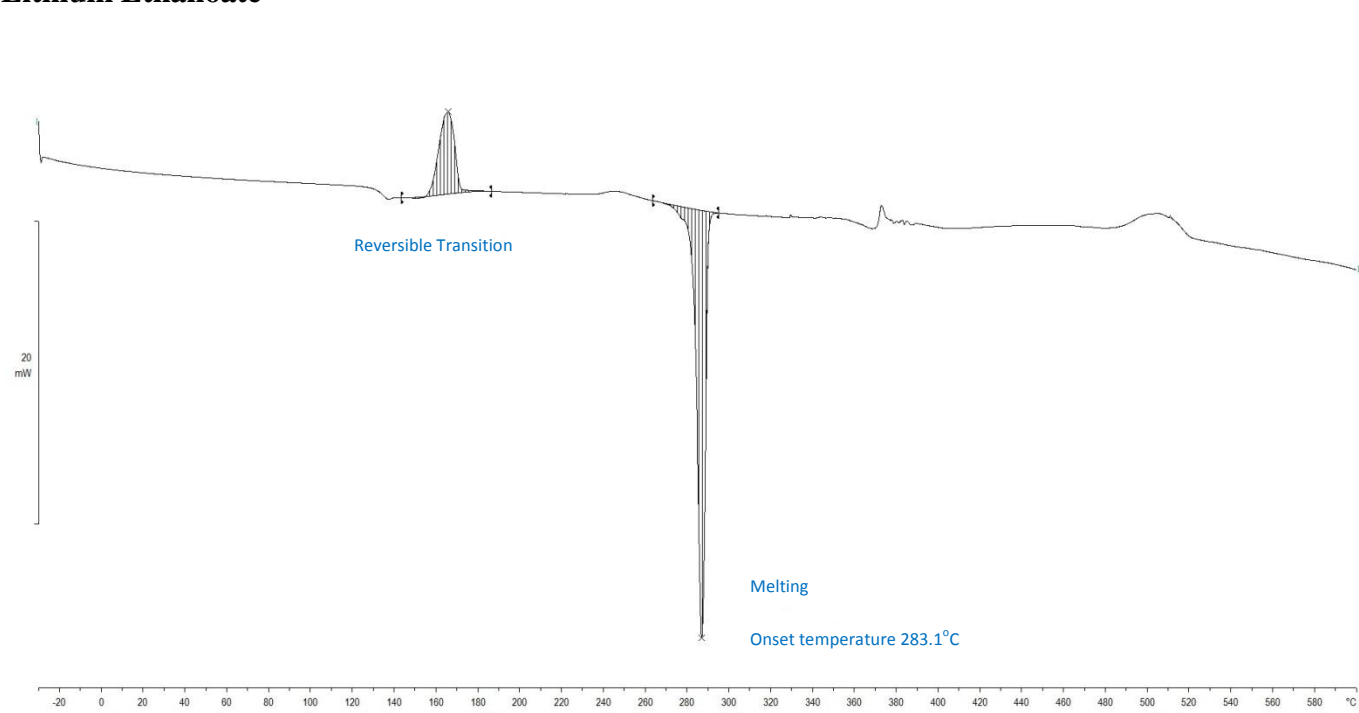


Figure S 39. Calorigram of Lithium Ethanoate determined by the DSC over the range of -30-600°C at 10°C·min<sup>-1</sup> heating rate and 100mL·min<sup>-1</sup> nitrogen flow.

## Lithium Propanoate

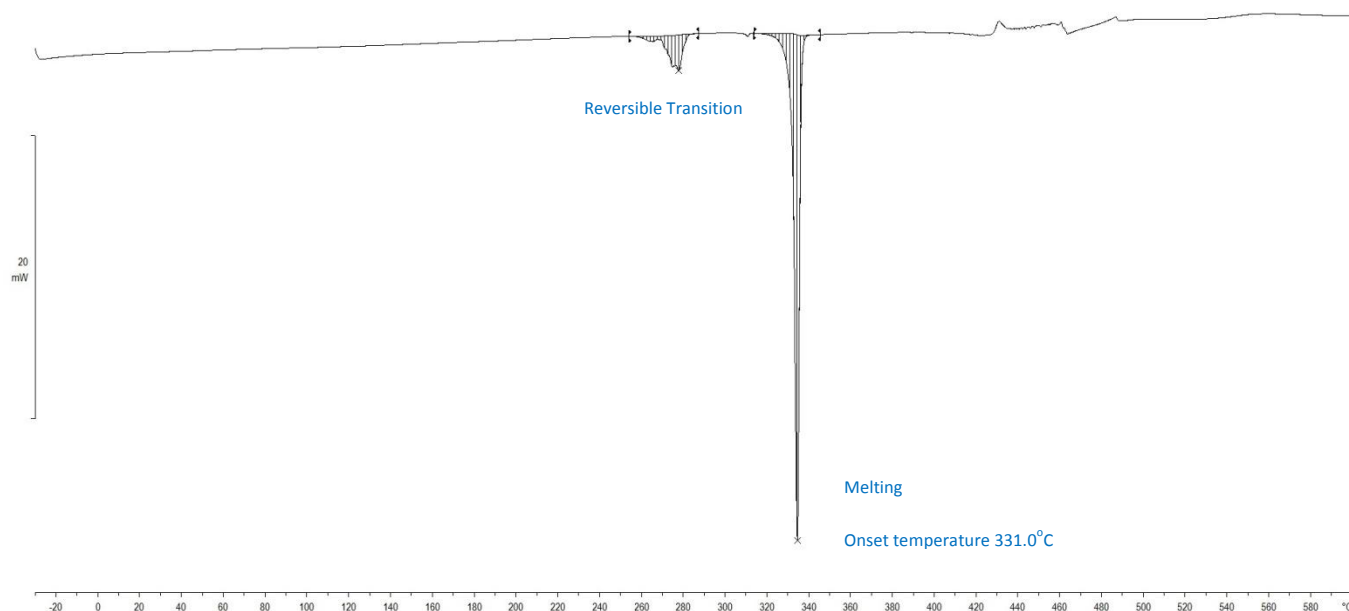


Figure S 40. Calorigram of Lithium Propanoate determined by the DSC over the range of -30-600°C at 10°C·min<sup>-1</sup> heating rate and 100mL·min<sup>-1</sup> nitrogen flow.

## Lithium Butanoate (butyrate)

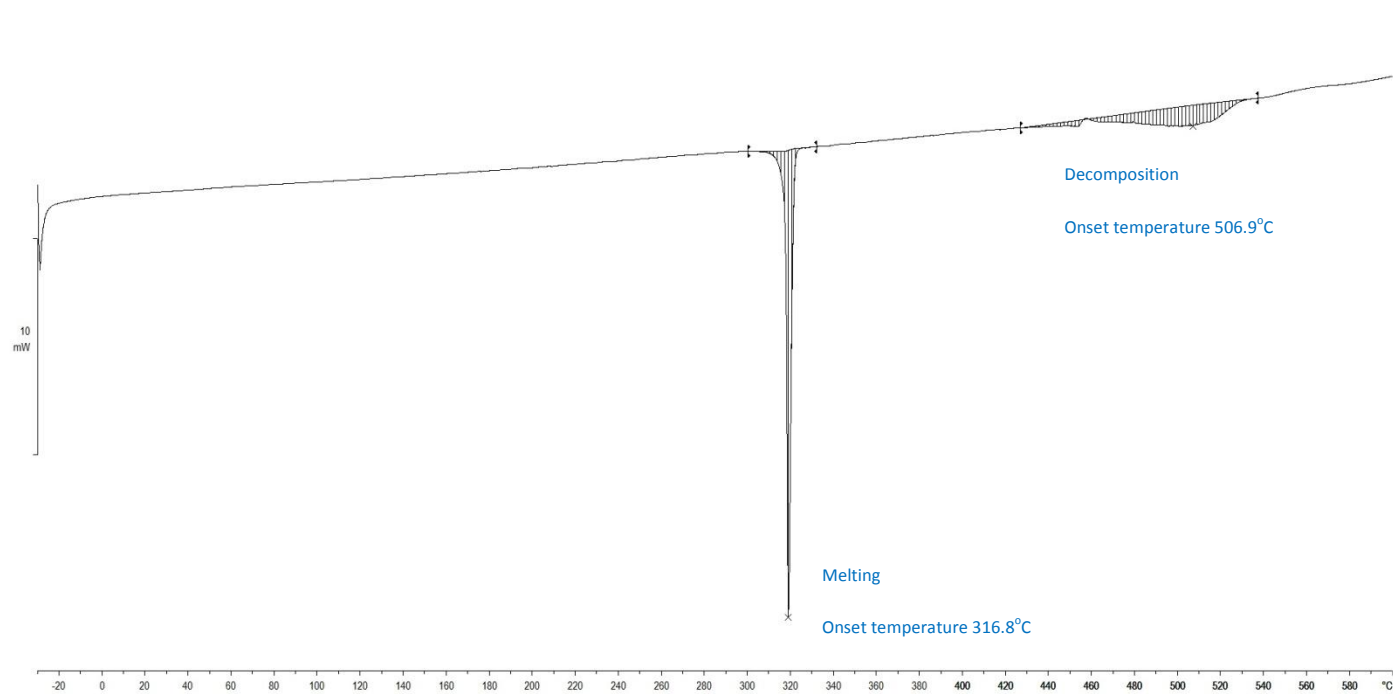


Figure S 41. Calorigram of Lithium Butanoate determined by the DSC over the range of -30-600°C at 10°C·min<sup>-1</sup> heating rate and 100mL·min<sup>-1</sup> nitrogen flow.

### Lithium Pentanoate (valerate)

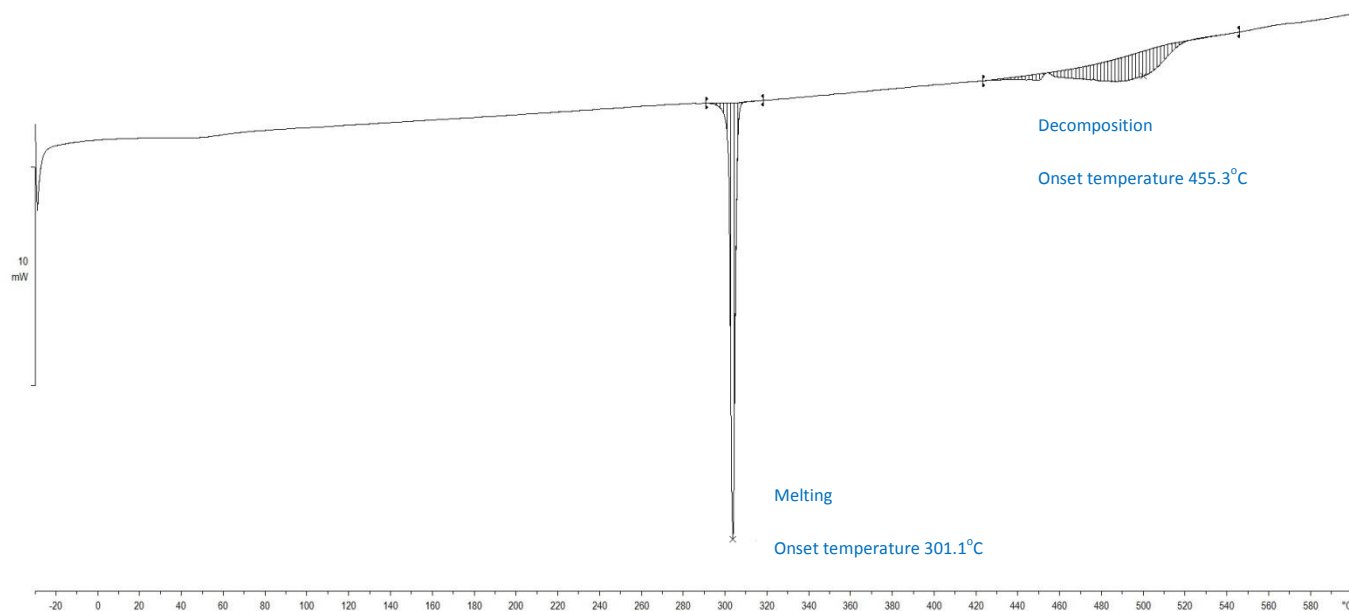


Figure S 42. Calorigram of Lithium Pentanoate determined by the DSC over the range of -30-600°C at 10°C·min<sup>-1</sup> heating rate and 100mL·min<sup>-1</sup> nitrogen flow.

### Lithium Hexanoate (caproate)

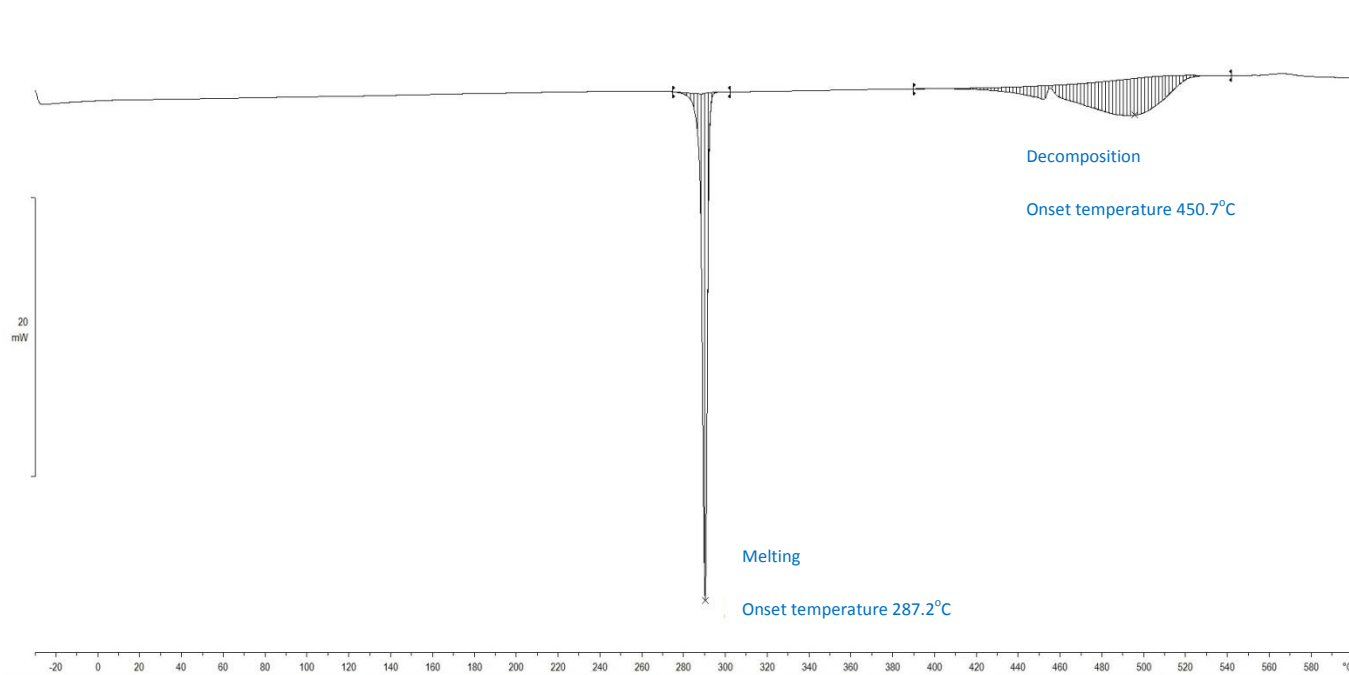


Figure S 43. Calorigram of Lithium Hexanoate determined by the DSC over the range of -30-600°C at 10°C·min<sup>-1</sup> heating rate and 100mL·min<sup>-1</sup> nitrogen flow.

## Lithium Heptanoate

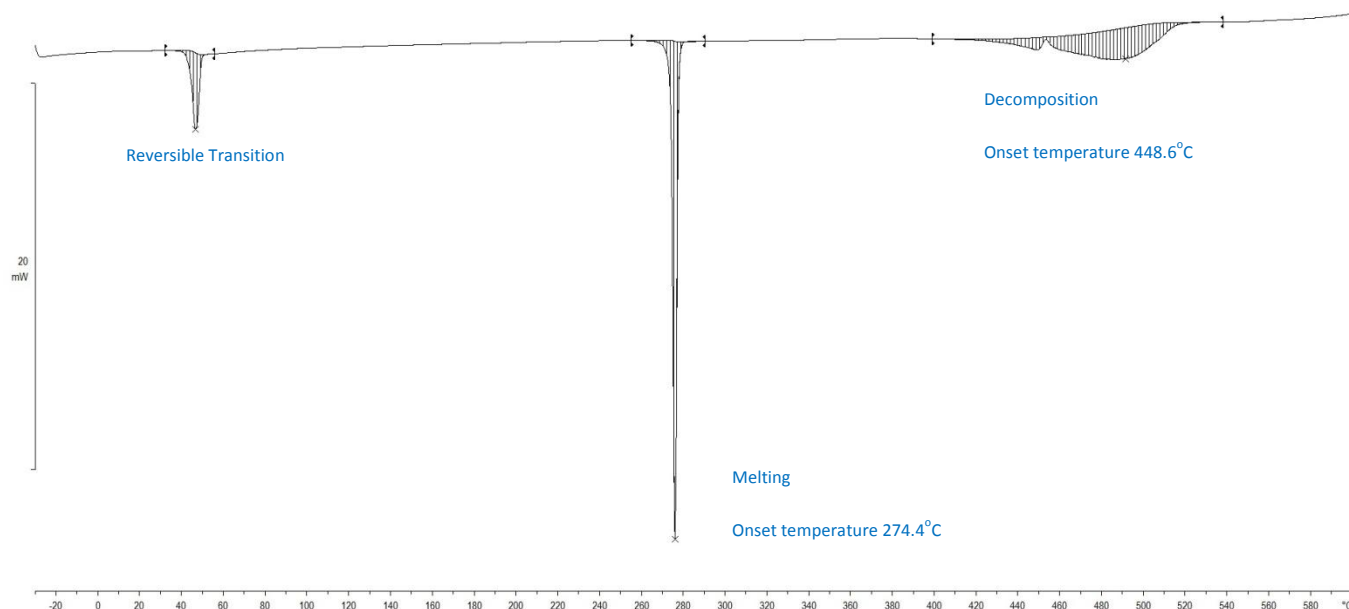


Figure S 44. Calorigram of Lithium Heptanoate determined by the DSC over the range of -30-600°C at 10°C·min<sup>-1</sup> heating rate and 100mL·min<sup>-1</sup> nitrogen flow.

## Lithium Octanoate (caprylate)

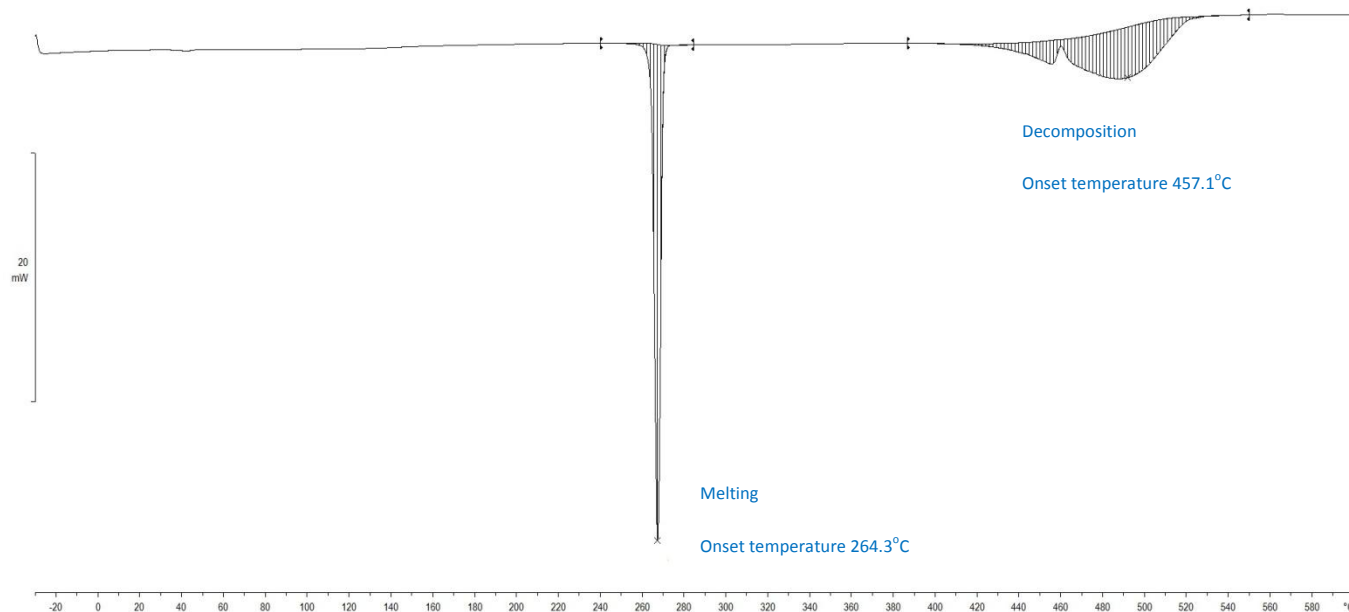


Figure S 45. Calorigram of Lithium Octanoate determined by the DSC over the range of -30-600°C at 10°C·min<sup>-1</sup> heating rate and 100mL·min<sup>-1</sup> nitrogen flow.

### Lithium Nonanoate (pelargonate)

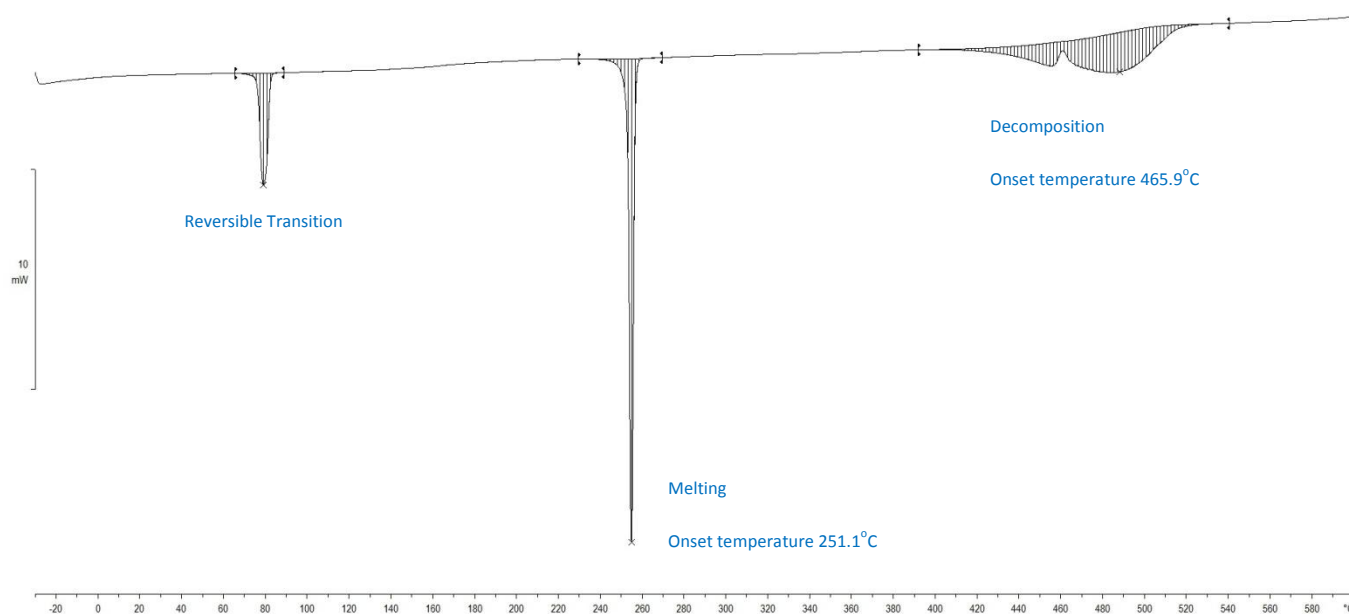


Figure S 46. Calorigram of Lithium Nonanoate determined by the DSC over the range of -30-600°C at 10°C·min<sup>-1</sup> heating rate and 100mL·min<sup>-1</sup> nitrogen flow.

### Lithium Decanoate (caprate)

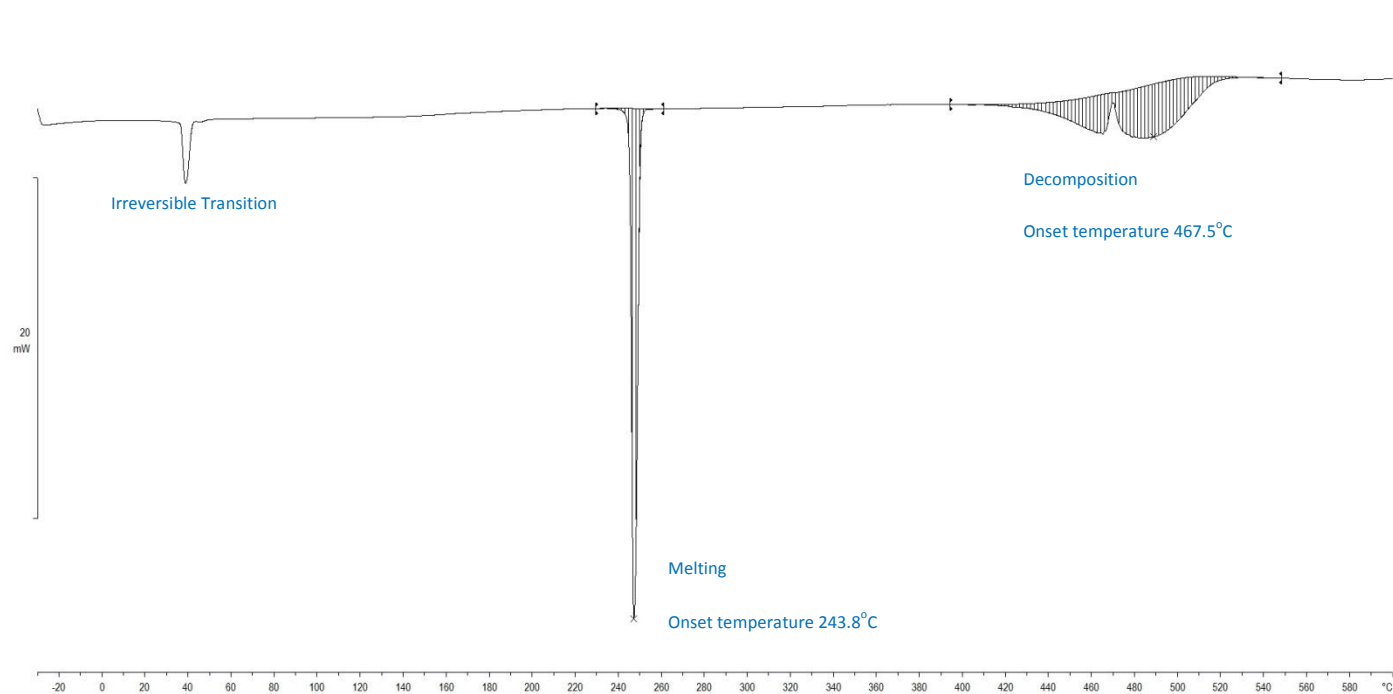


Figure S 47. Calorigram of Lithium Decanoate determined by the DSC over the range of -30-600°C at 10°C·min<sup>-1</sup> heating rate and 100mL·min<sup>-1</sup> nitrogen flow.

## Lithium Undecanoate

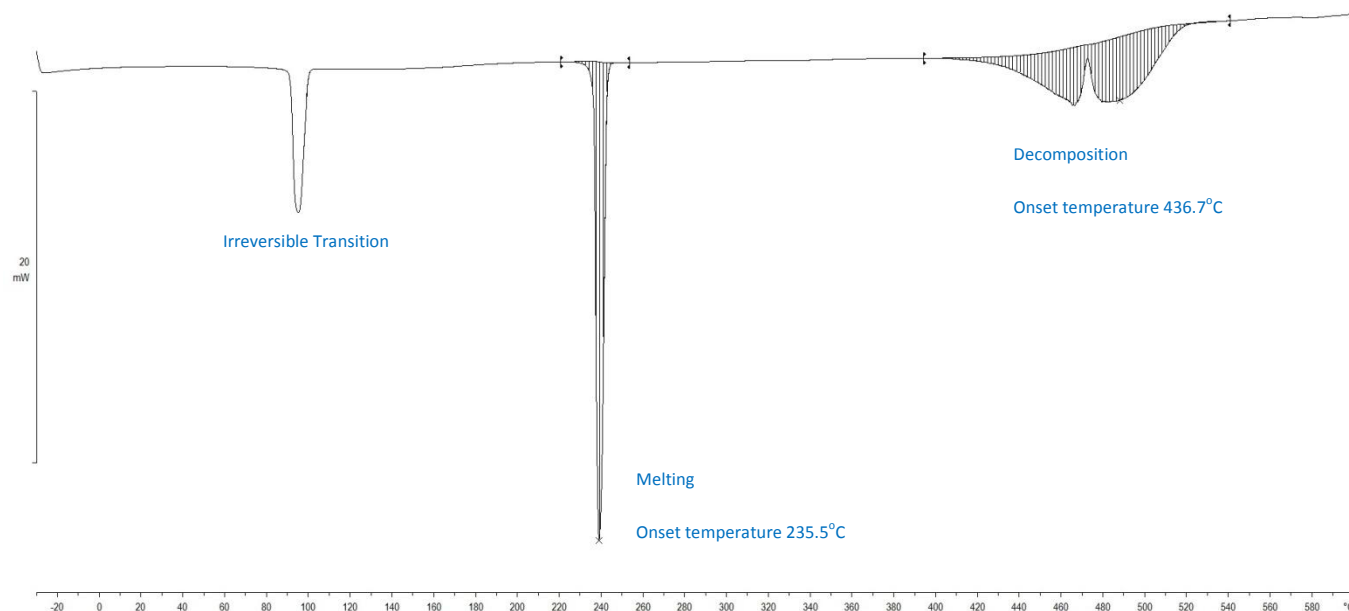


Figure S 48. Calorigram of Lithium Undecanoate determined by the DSC over the range of -30-600°C at 10°C min<sup>-1</sup> heating rate and 100mL min<sup>-1</sup> nitrogen flow.

## Lithium Dodecanoate (laurate)

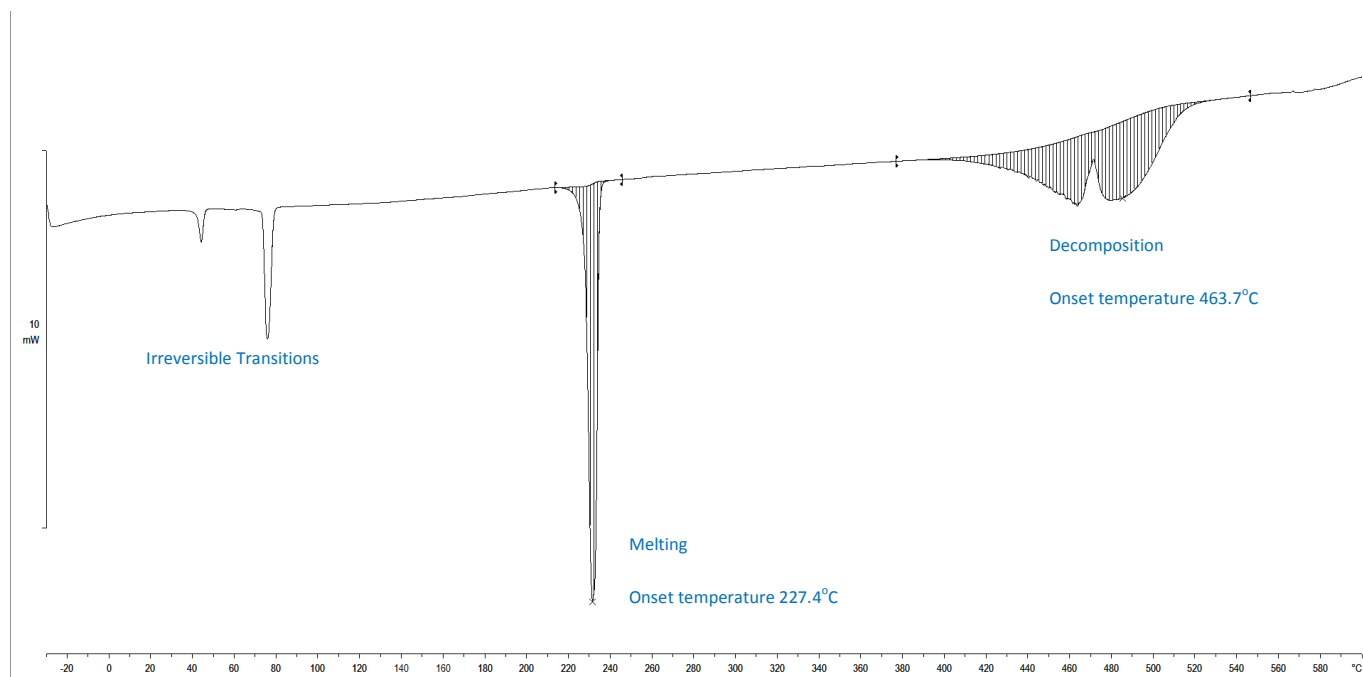


Figure S 49. Calorigram of Lithium Dodecanoate determined by the DSC over the range of -30-600°C at 10°C min<sup>-1</sup> heating rate and 100mL min<sup>-1</sup> nitrogen flow.

## Heat Capacity

### Lithium Methanoate

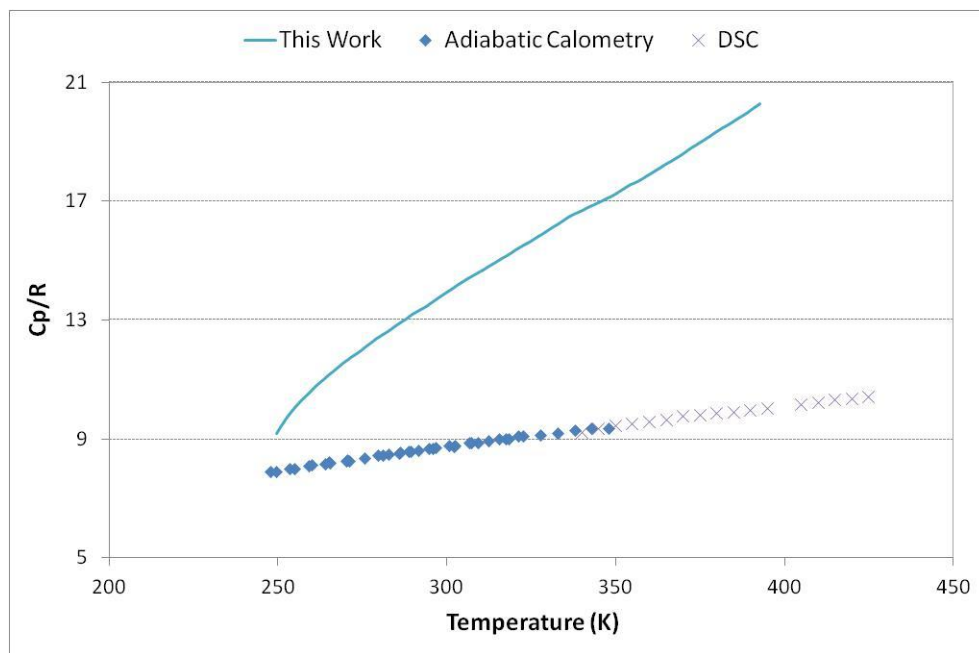


Figure S 50. Experimental molar heat capacities for Li-methanoate ( $R = 8.31451 \text{ JK}^{-1}\text{mol}^{-1}$ )

### Lithium Ethanoate

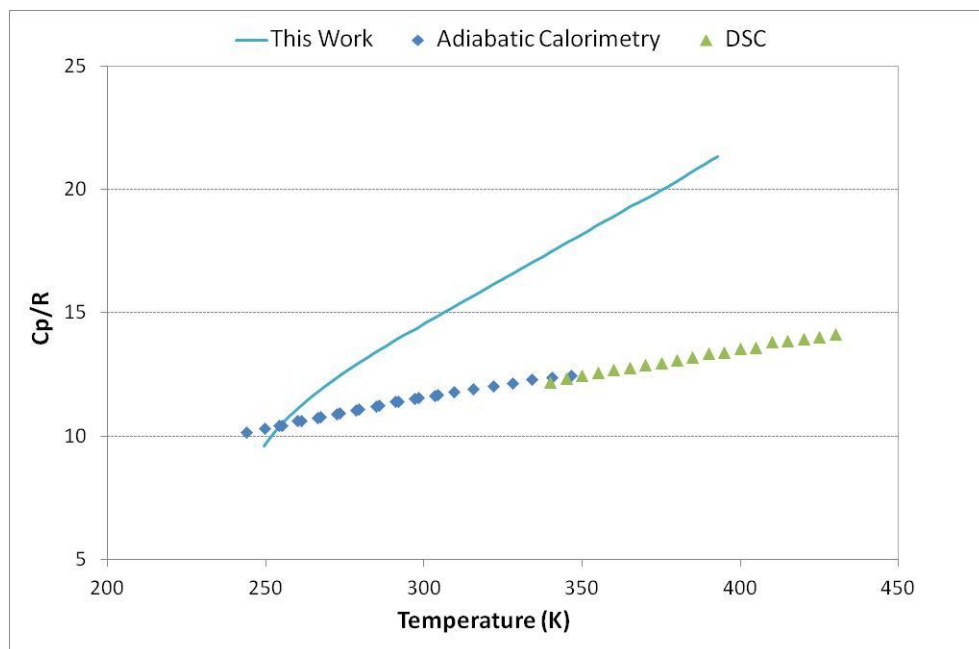


Figure S 51. Experimental molar heat capacities for Li-ethanoate ( $R = 8.31451 \text{ JK}^{-1}\text{mol}^{-1}$ )

## Lithium Propanoate

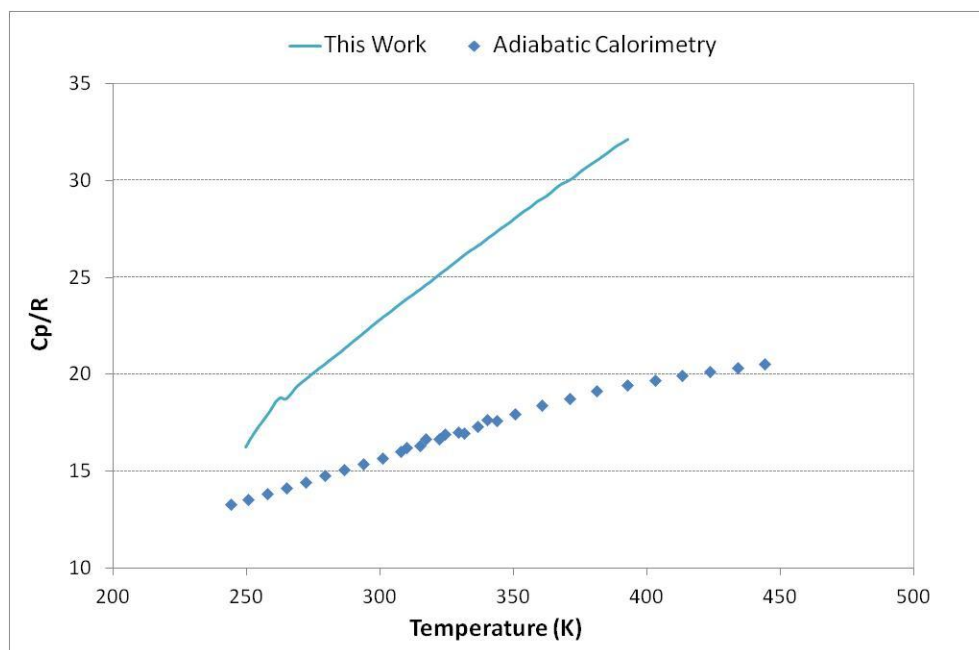


Figure S 52. Experimental molar heat capacities for Li-propanoate ( $R = 8.31451 \text{ JK}^{-1} \text{ mol}^{-1}$ )

## Lithium Butanoate (butyrate)

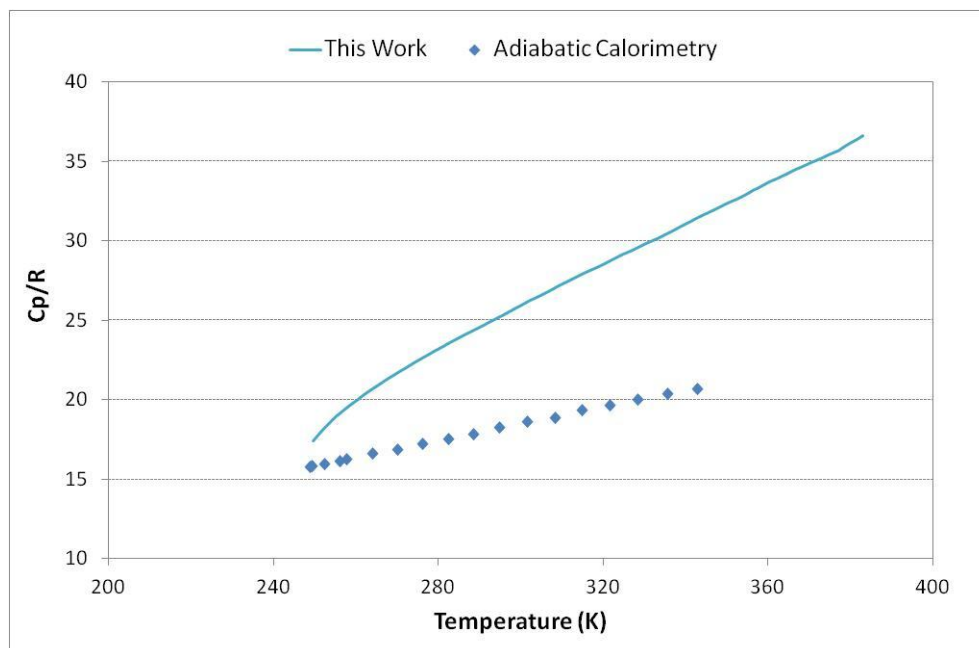


Figure S 53. Experimental molar heat capacities for Li-butanoate ( $R = 8.31451 \text{ JK}^{-1} \text{ mol}^{-1}$ )

### Lithium Pentanoate (valerate)

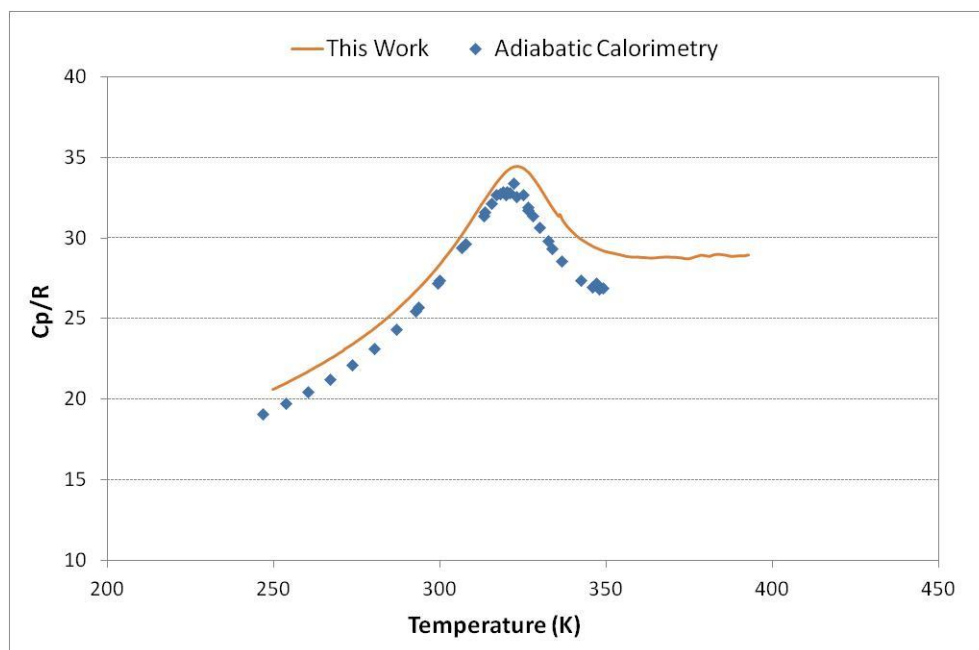


Figure S 54. Experimental molar heat capacities for Li-pentanoate ( $R = 8.31451 \text{ JK}^{-1} \text{ mol}^{-1}$ )

### Lithium Hexanoate (caproate)

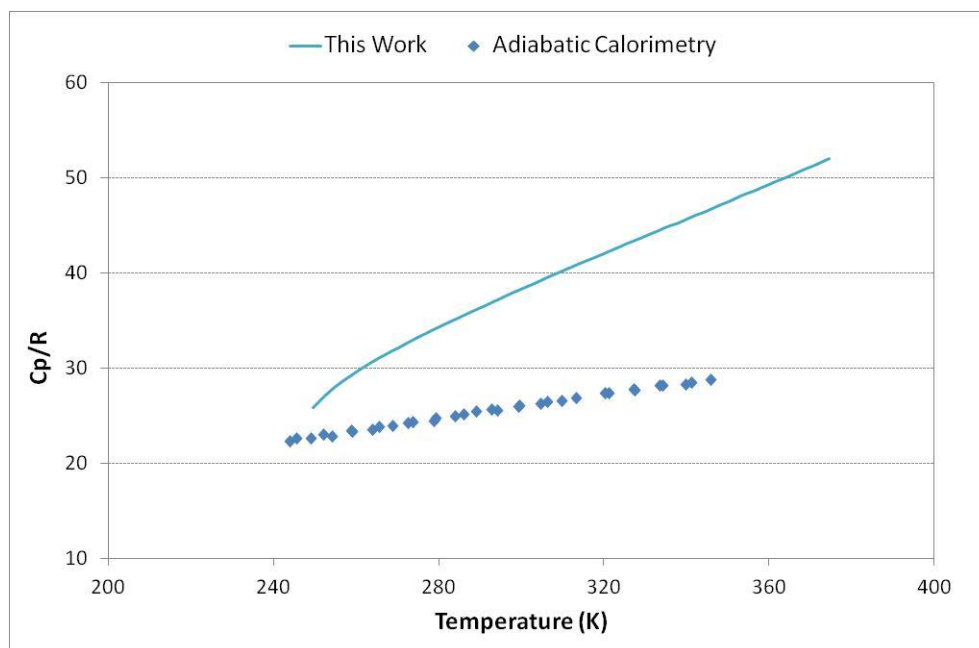


Figure S 55. Experimental molar heat capacities for Li-hexanoate ( $R = 8.31451 \text{ JK}^{-1} \text{ mol}^{-1}$ )

## Lithium Heptanoate

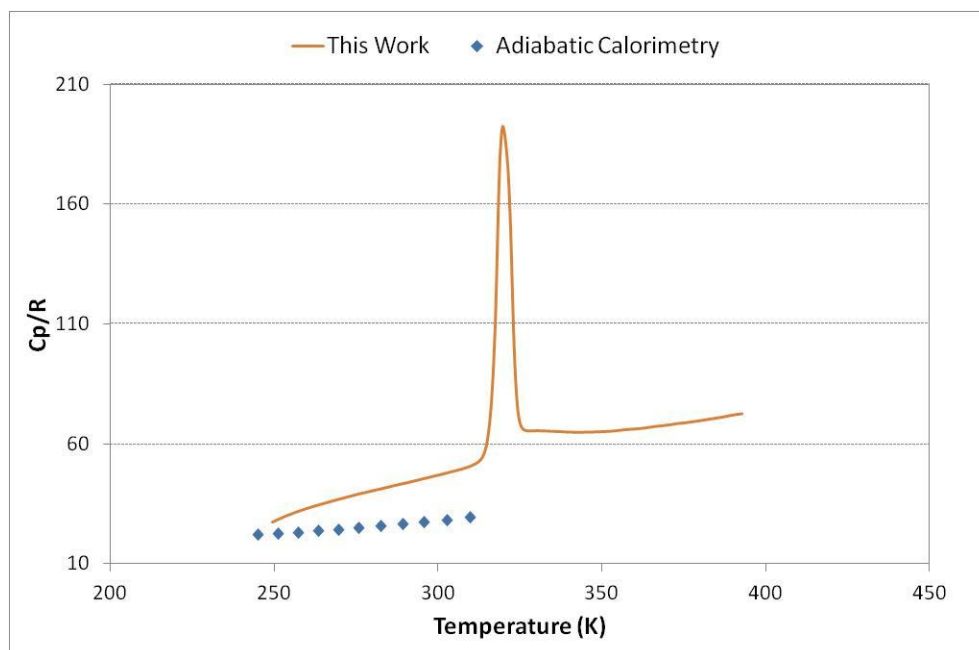


Figure S 56. Experimental molar heat capacities for Li-heptanoate ( $R = 8.31451 \text{ JK}^{-1}\text{mol}^{-1}$ )

## Lithium Octanoate (caprylate)

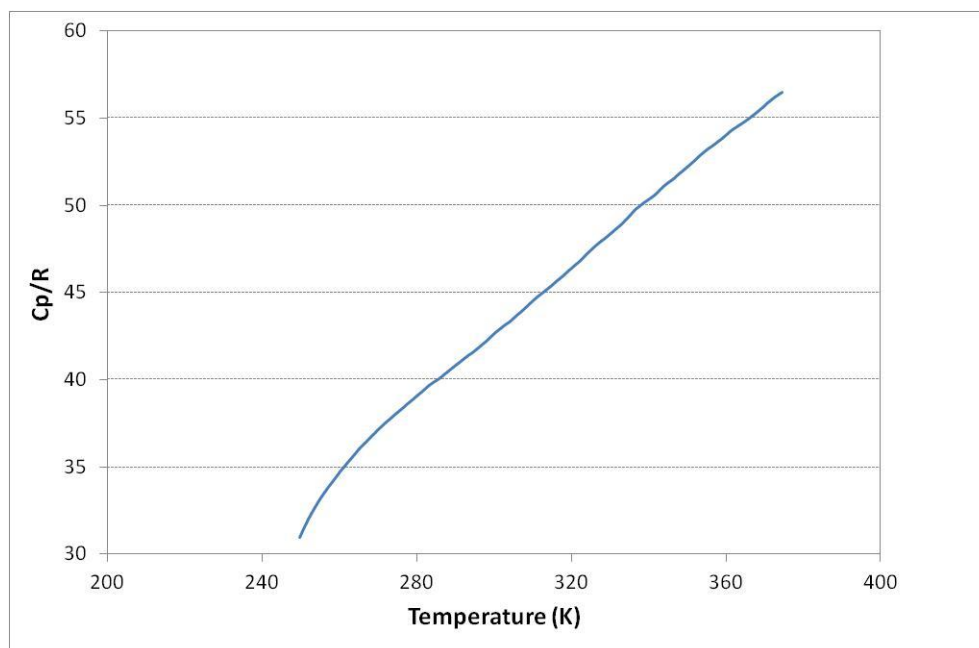


Figure S 57. Experimental molar heat capacities for Li-octanoate ( $R = 8.31451 \text{ JK}^{-1}\text{mol}^{-1}$ )

### Lithium Nonanoate (pelargonate)

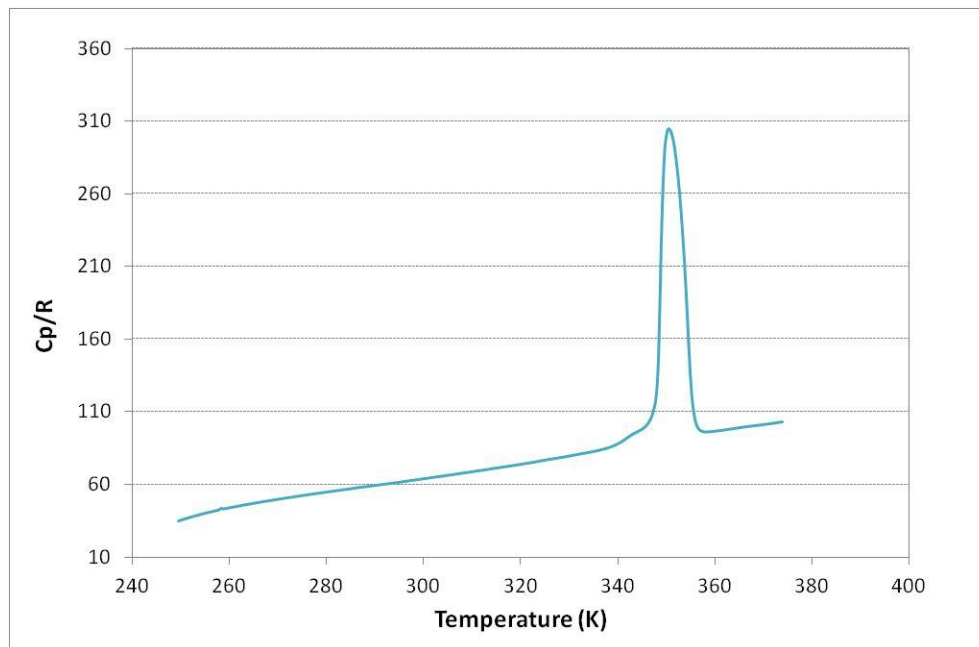


Figure S 58. Experimental molar heat capacities for Li-nonanoate ( $R = 8.31451 \text{ JK}^{-1}\text{mol}^{-1}$ )

### Lithium Decanoate (caprate)

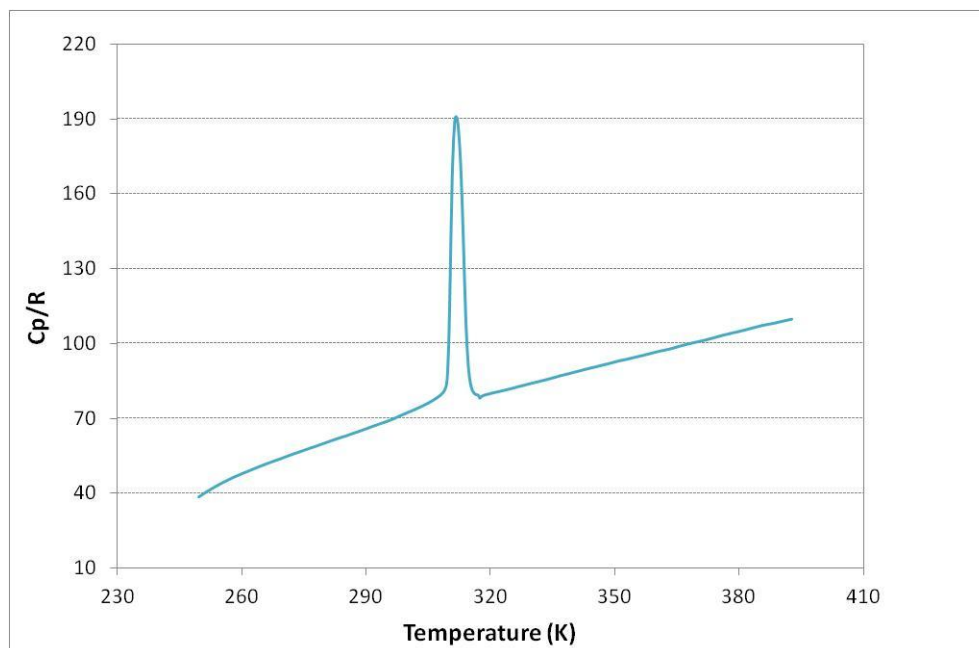


Figure S 59. Experimental molar heat capacities for Li-decanoate ( $R = 8.31451 \text{ JK}^{-1}\text{mol}^{-1}$ )

## Lithium Undecanoate

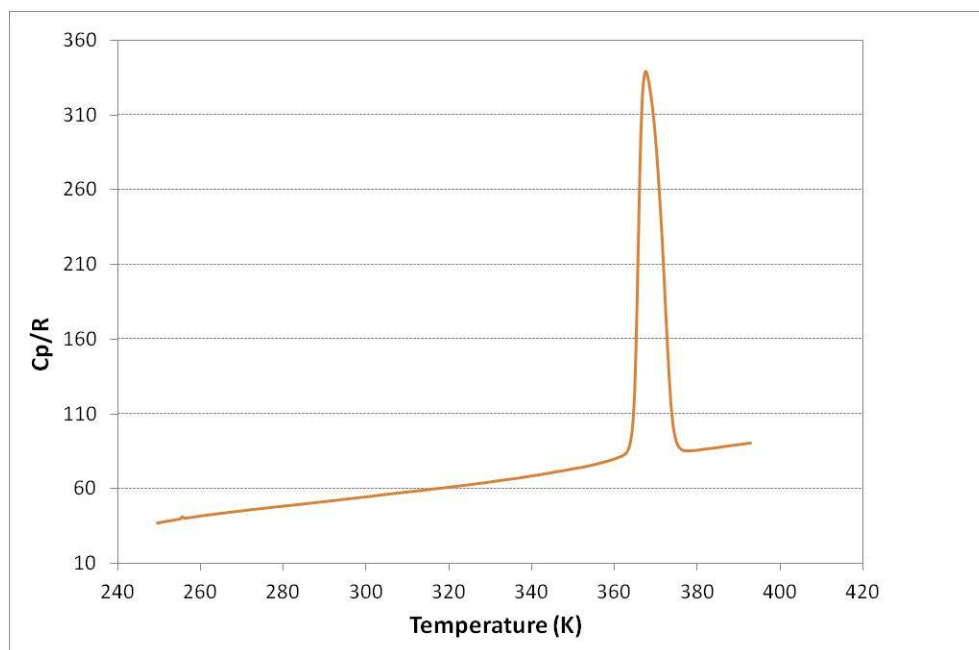


Figure S 60. Experimental molar heat capacities for Li-undecanoate ( $R = 8.31451 \text{ JK}^{-1} \text{ mol}^{-1}$ )

## Lithium Dodecanoate (laurate)

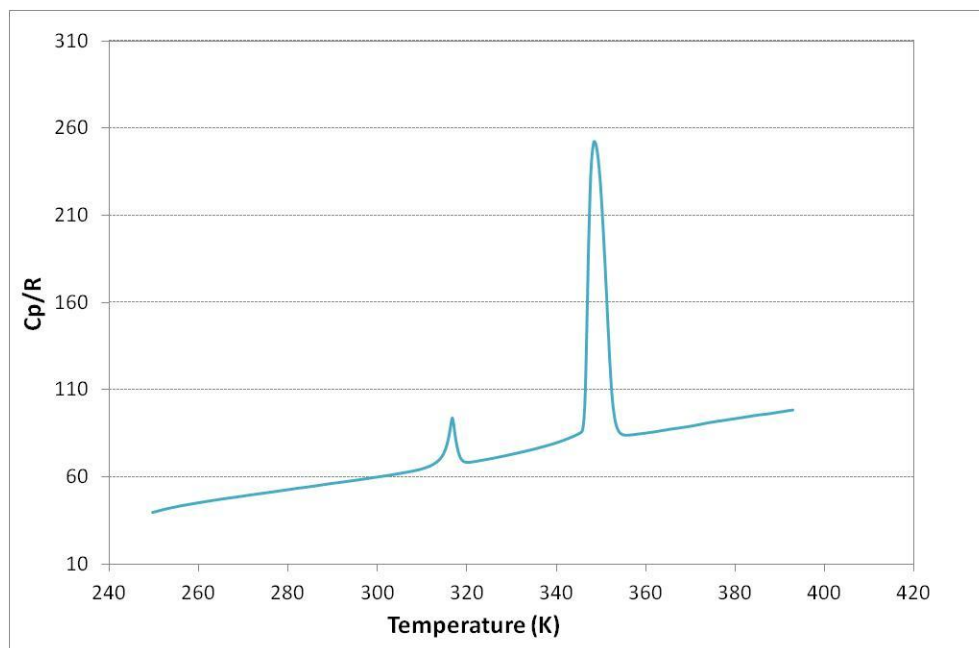


Figure S 61. Experimental molar heat capacities for Li-dodecanoate ( $R = 8.31451 \text{ JK}^{-1} \text{ mol}^{-1}$ )

## **Sodium C<sub>1</sub>-C<sub>12</sub> *n*-alkanoates: Thermal behavior from –30 to 600 °C**

The primary aim of the investigation was to study thermal behaviour. The spectroscopic data was employed to support the thermal investigation. The reasoning behind the collection of the spectroscopic data was as follows:

- (a) Infrared (IR) spectroscopy is sensitive for the detection of carbonyl and carboxylate compounds. It could therefore be used to confirm synthesis of the sodium carboxylates, as well as provide an indication of purity. Synthesis was performed with a 2 % molar excess of carboxylic acid and if the acid was not completely removed during purification, it would be visible on the infrared spectrum.
- (b) IR spectroscopy was also employed to determine whether chemical changes took place during calorimetry. Once a thermal event was observed, a sample was run to a temperature just above the temperature of the observed thermal event and the IR spectrum of the sample thus treated was collected and compared with the starting material.
- (c) IR, Raman and Ultraviolet-Visible (UV-Vis) spectra were collected in the hope of finding explanations for differences in thermal behaviour, and in the hope that additional information about the nature of the sodium carboxylates can be deduced.

## IR Spectra

### Sodium methanoate (formate)

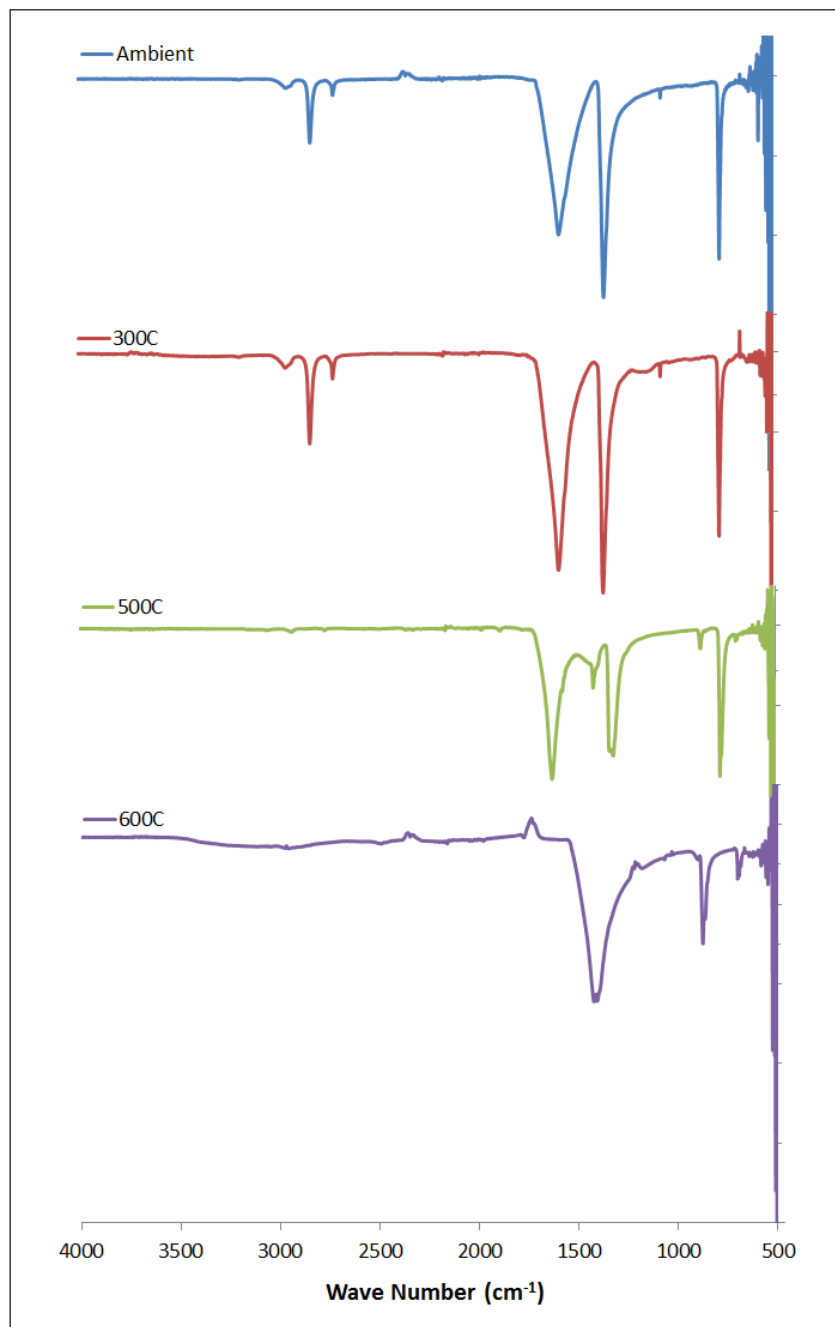


Figure S 62. IR spectrum of sodium methanoate before and after melting

## Sodium ethanoate (acetate)

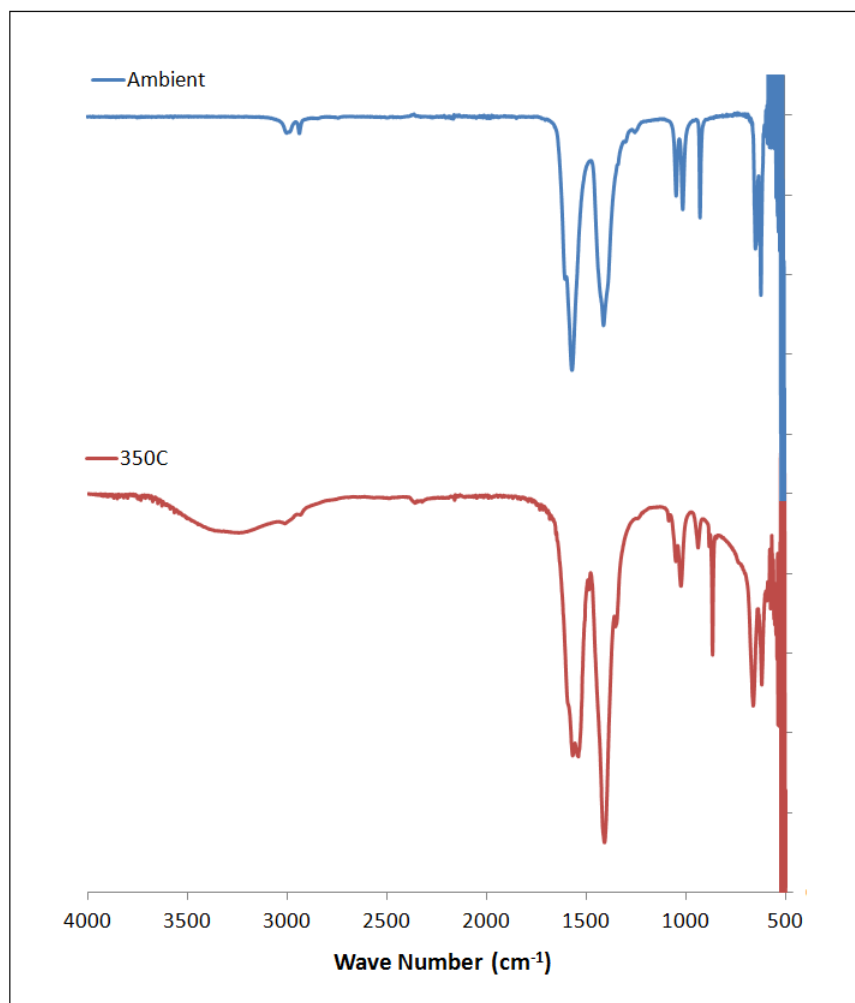


Figure S 63. IR spectrum of sodium ethanoate before and after melting.

## Sodium propanoate

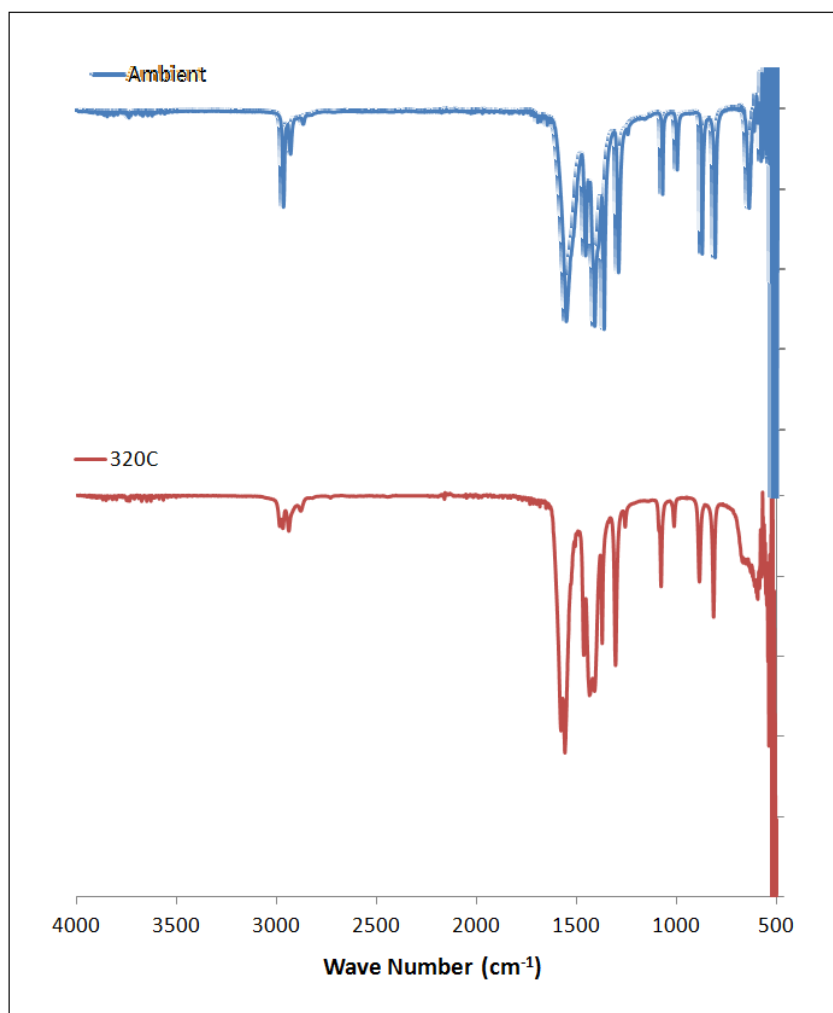
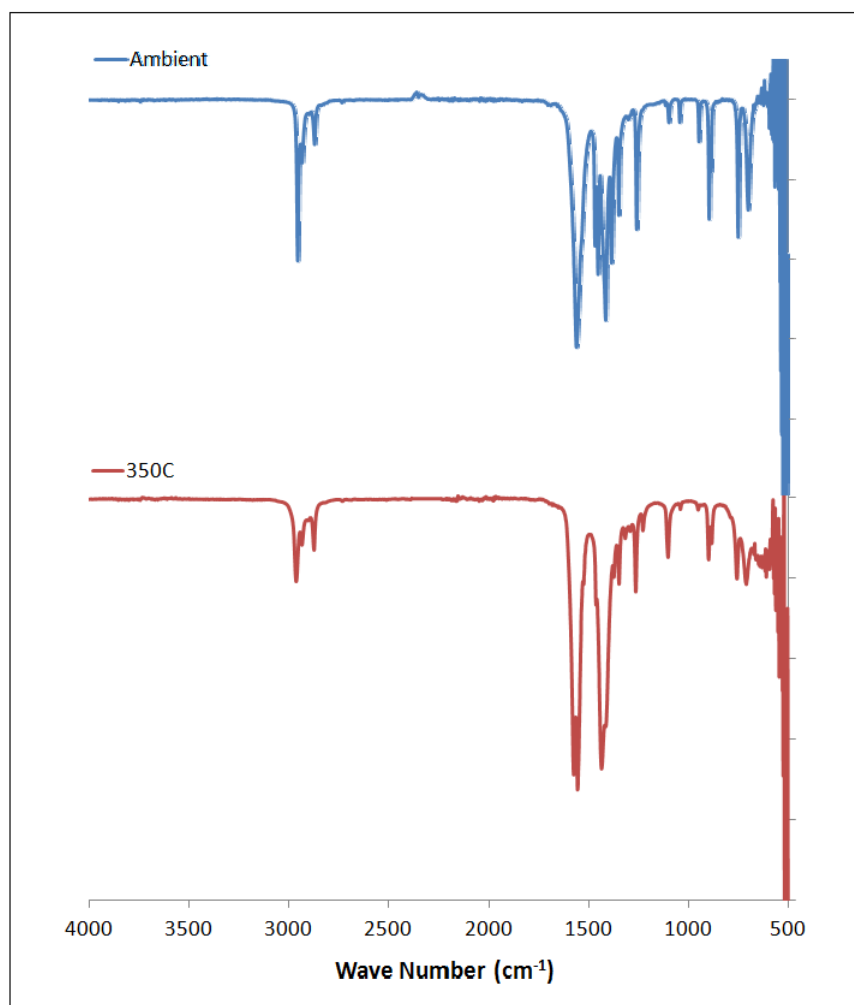


Figure S 64. IR spectrum of sodium propanoate before and after melting.

**Sodium butanoate (butyrate)**



**Figure S 65. IR spectrum of sodium butanoate before and after melting.**

## Sodium pentanoate (valerate)

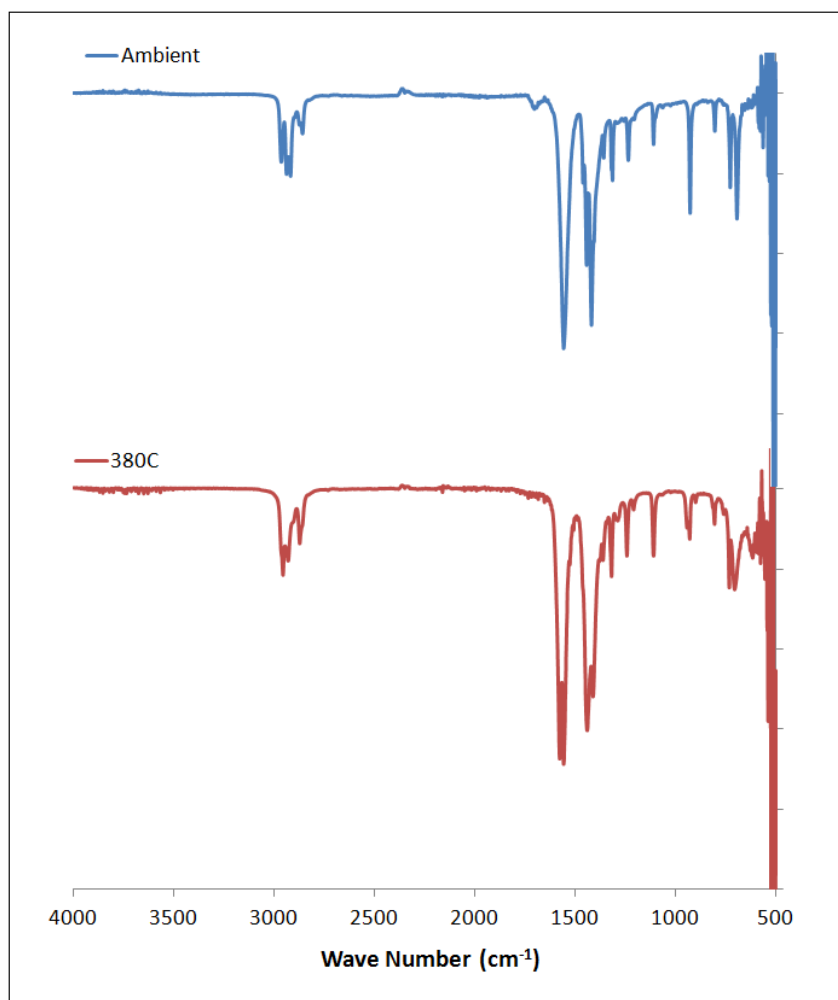


Figure S 66. IR spectrum of sodium pentanoate before and after melting.

## Sodium hexanoate (caproate)

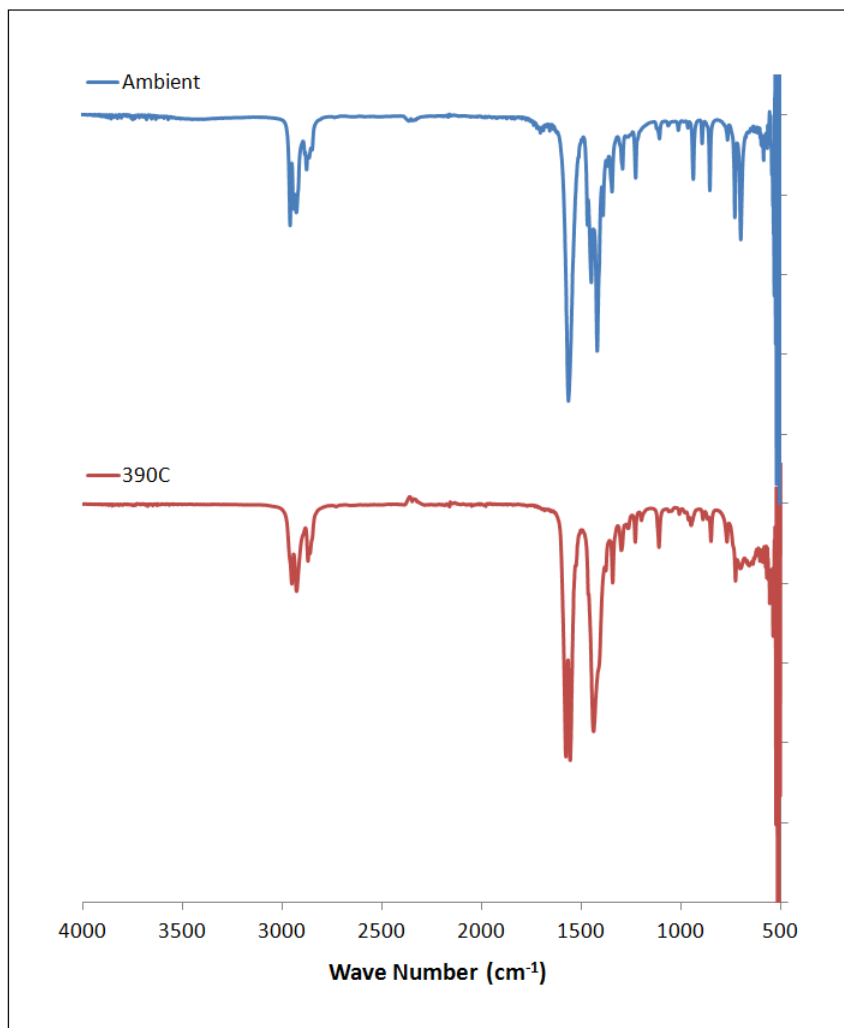


Figure S 67. IR spectrum of sodium hexanoate before and after melting.

## Sodium heptanoate

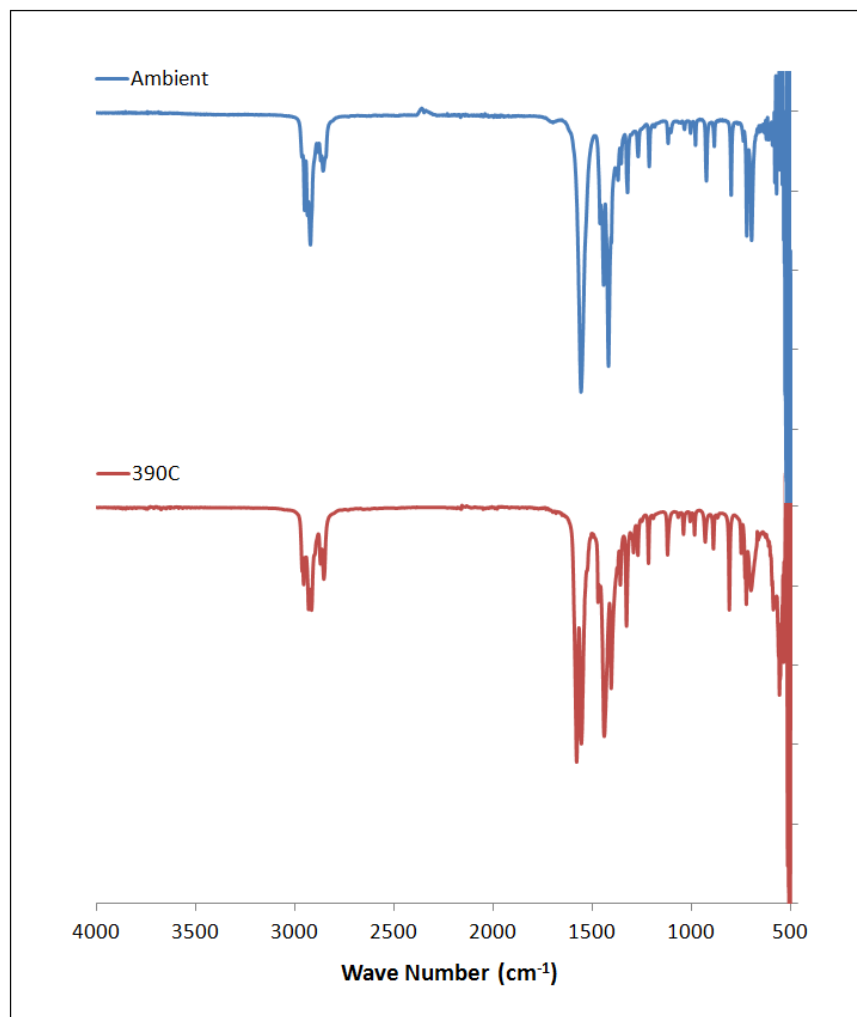


Figure S 68. IR spectrum of sodium heptanoate before and after melting.

## Sodium octanoate (caprylate)

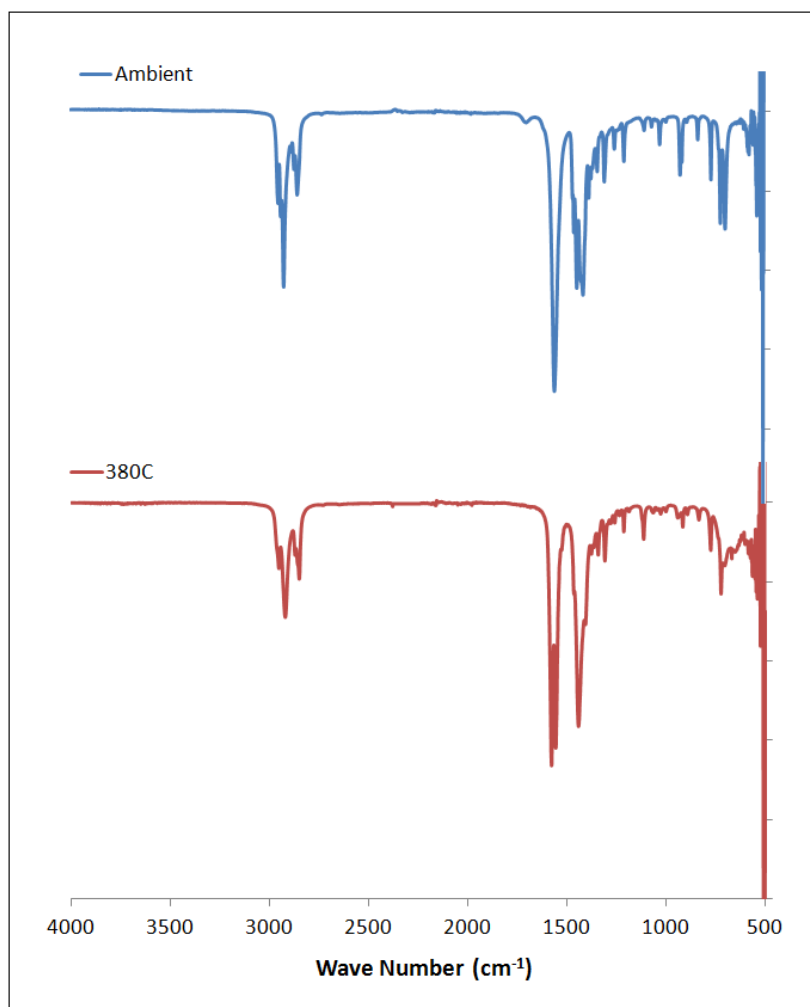


Figure S 69. IR spectrum of sodium octanoate before and after melting.

## Sodium nonanoate (pelargonate)

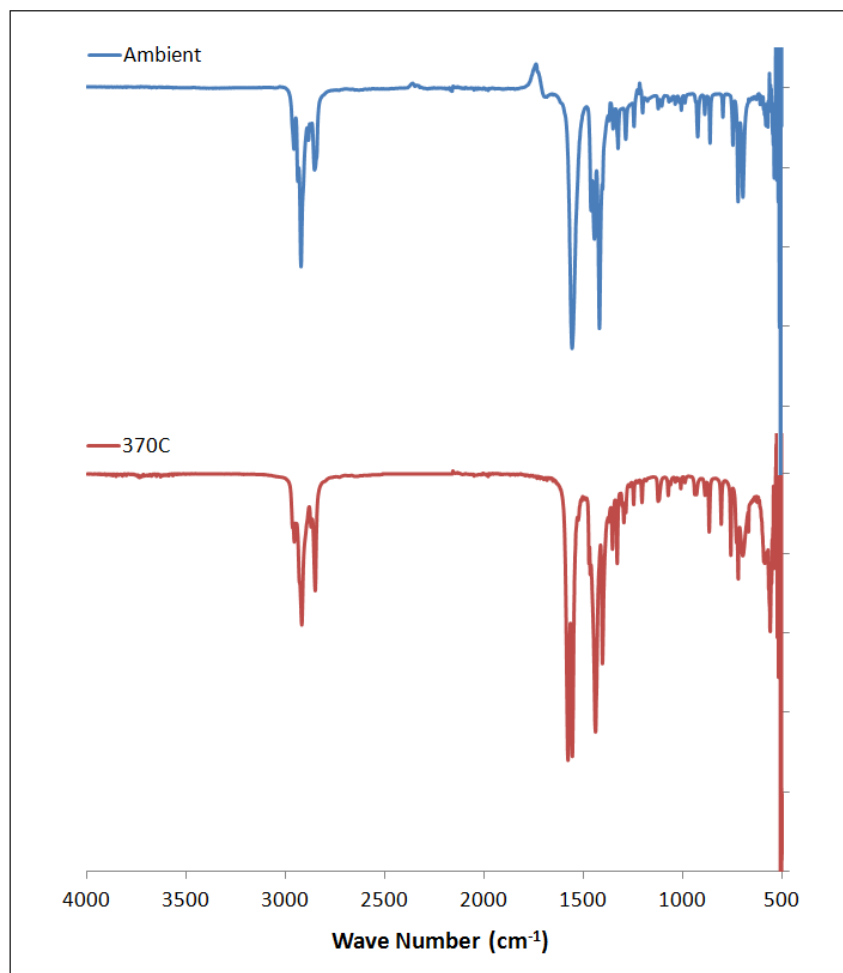


Figure S 70. IR spectrum of sodium nonanoate before and after melting.

## Sodium decanoate (caprate)

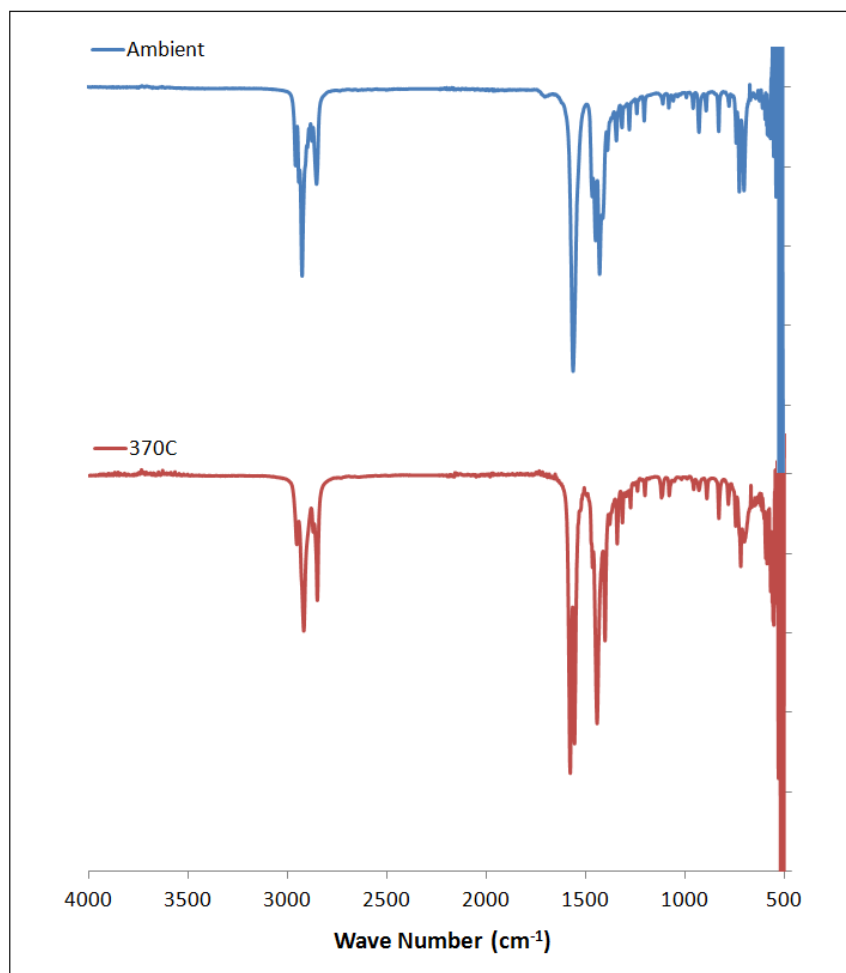


Figure S 71. IR spectrum of sodium decanoate before and after melting.

## Sodium undecanoate

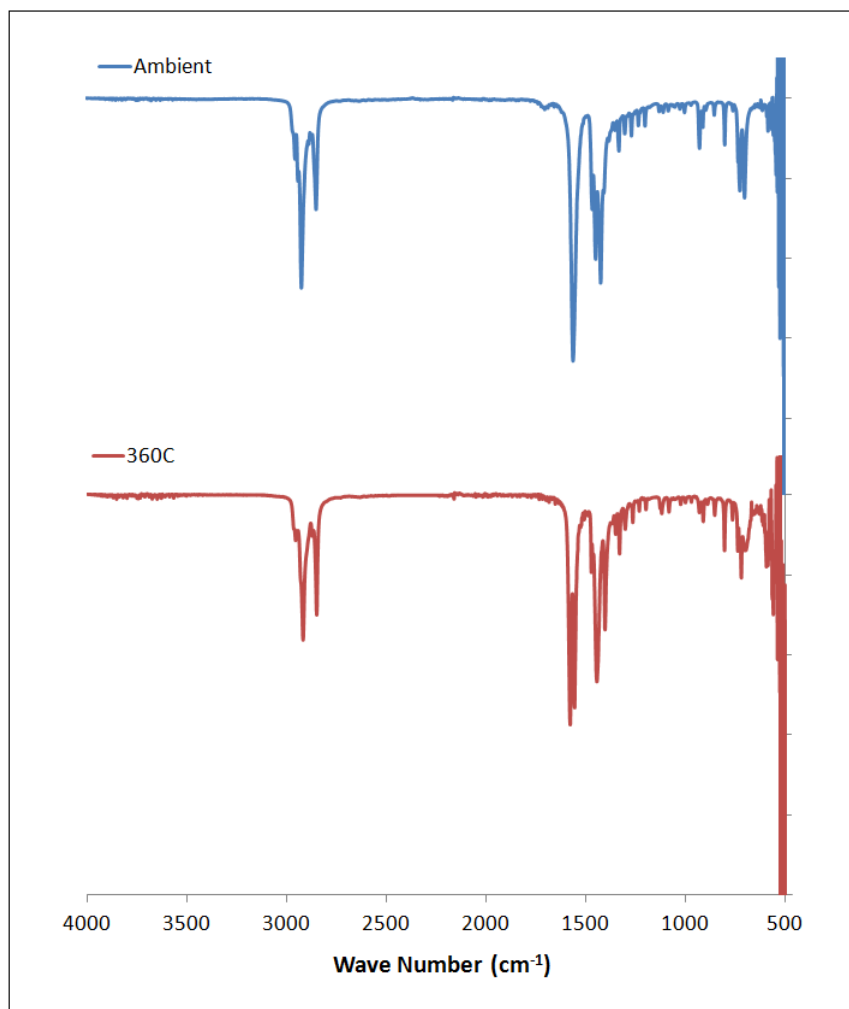


Figure S 72. IR spectrum of sodium undecanoate before and after melting.

## Sodium dodecanoate (laurate)

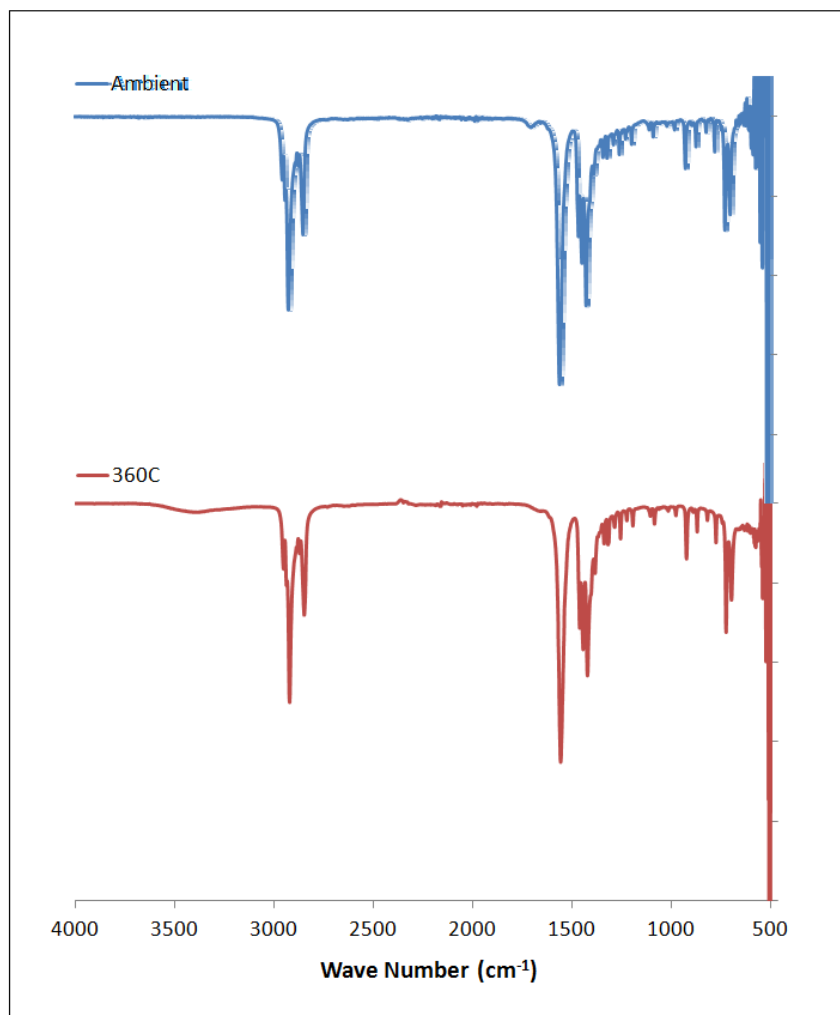


Figure S 73. IR spectrum of sodium dodecanoate before and after melting.

## Raman Spectra

### Sodium methanoate (formate)

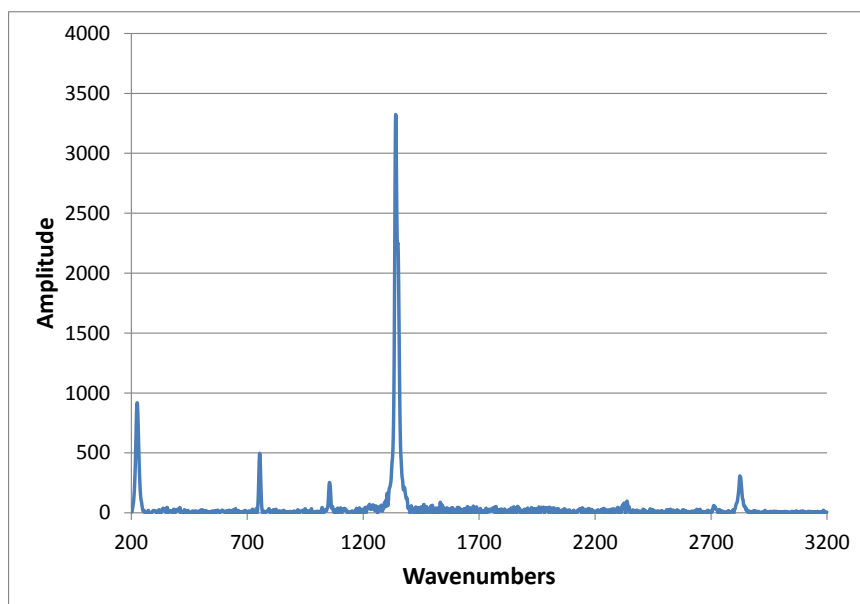


Figure S 74. Raman spectrum of sodium methanoate

### Sodium Ethanoate (acetate)

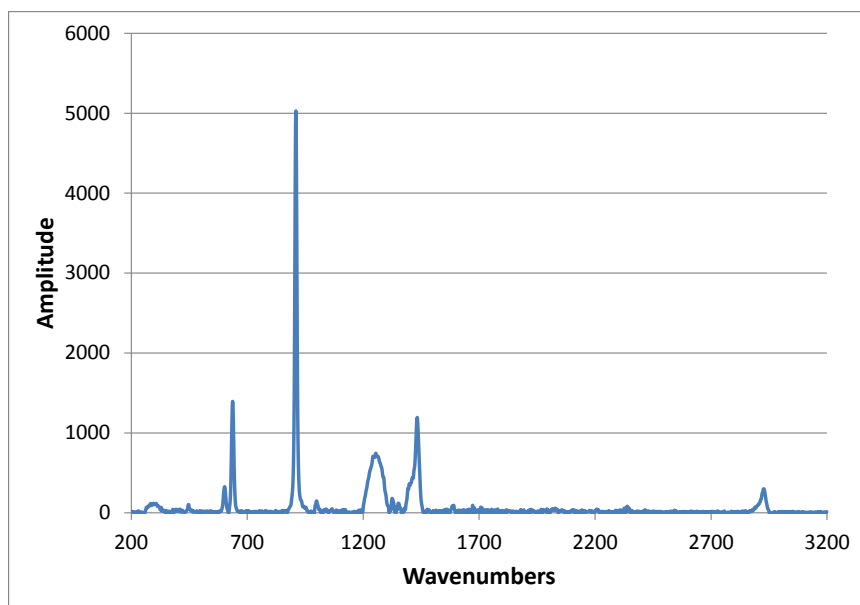


Figure S 75. Raman spectrum of sodium ethanoate

## Sodium Propanoate

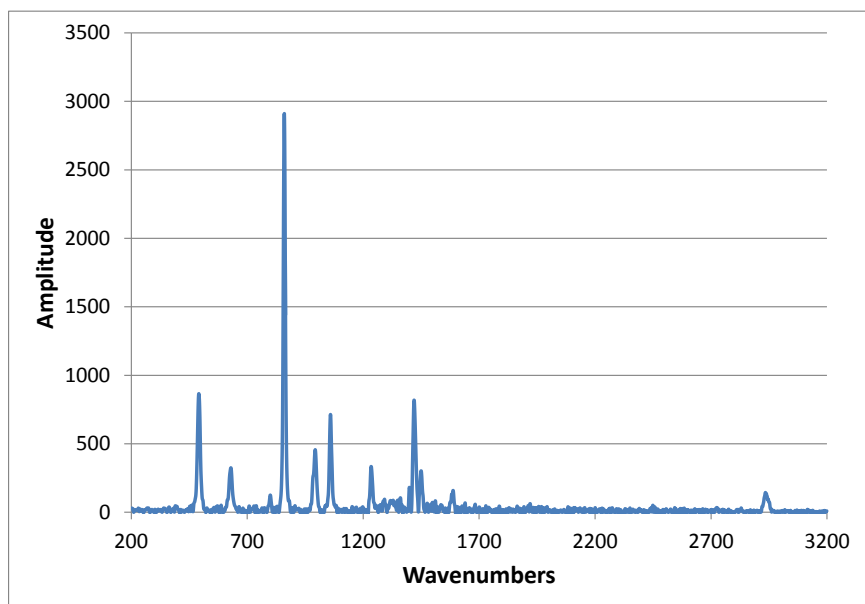


Figure S 76. Raman spectrum of sodium propanoate

## Sodium Butanoate (butyrate)

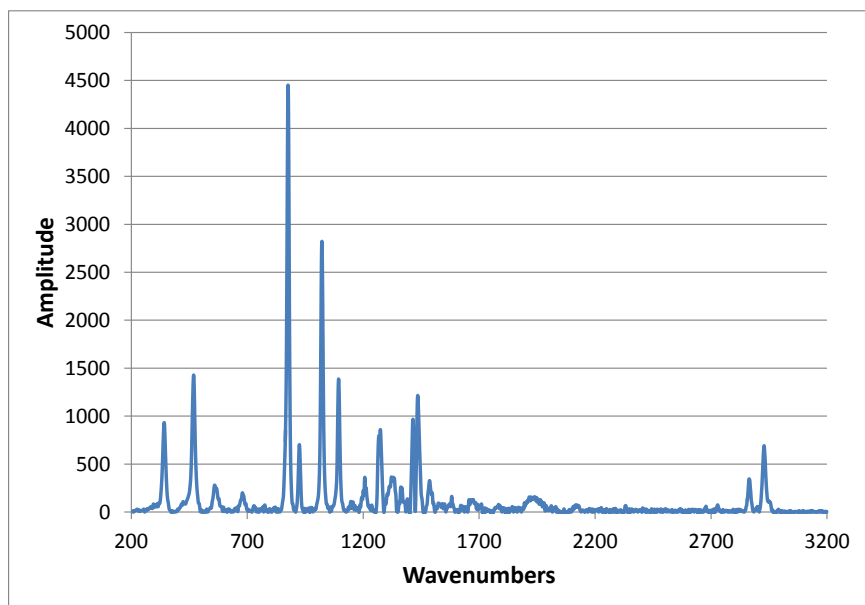


Figure S 77. Raman spectrum of sodium butanoate

### Sodium Pentanoate (valerate)

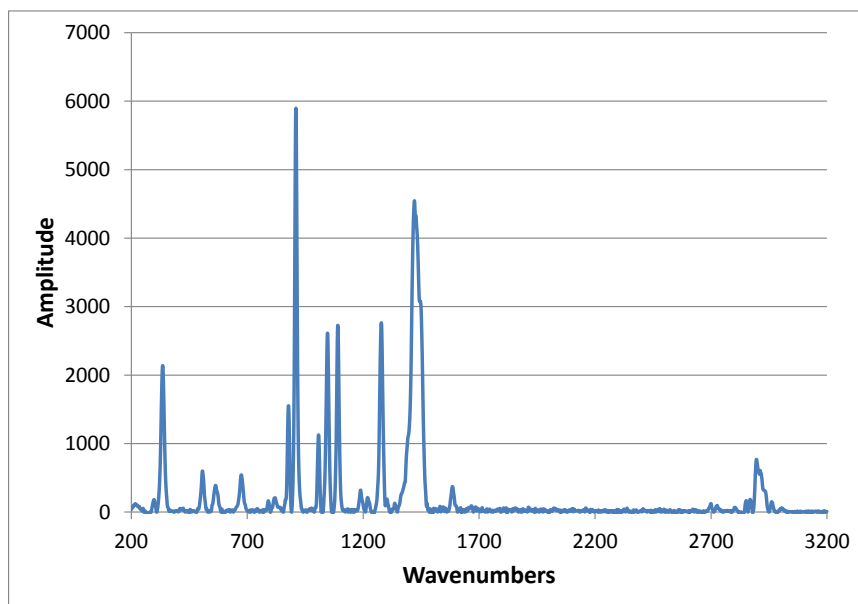


Figure S 78. Raman spectrum of sodium pentanoate

### Sodium Hexanoate (caproate)

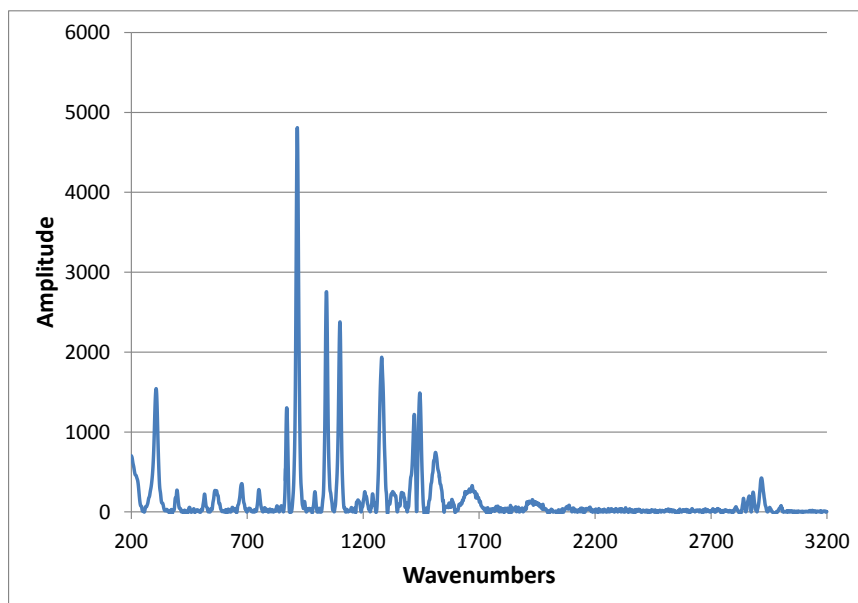


Figure S 79. Raman spectrum of sodium hexanoate

## Sodium Heptanoate

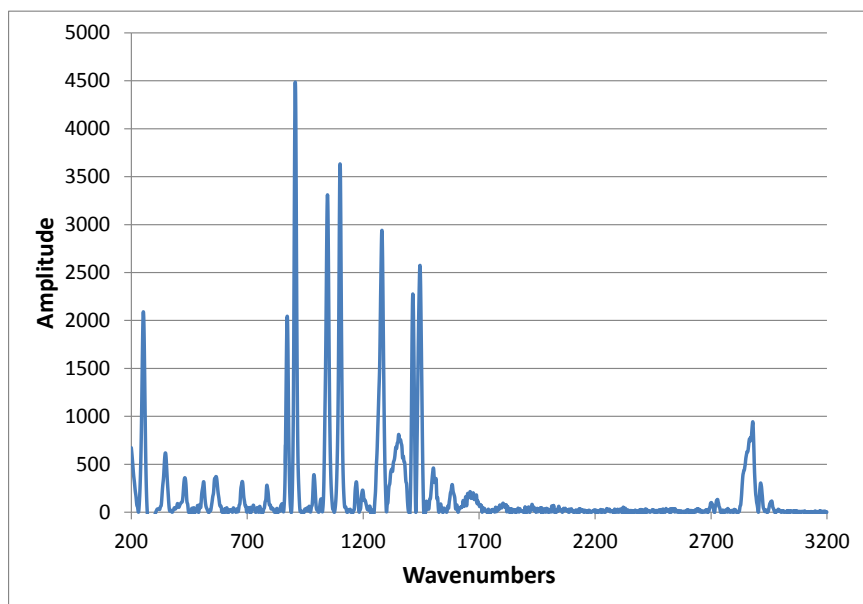


Figure S 80. Raman spectrum of sodium heptanoate

## Sodium Octanoate (caprylate)

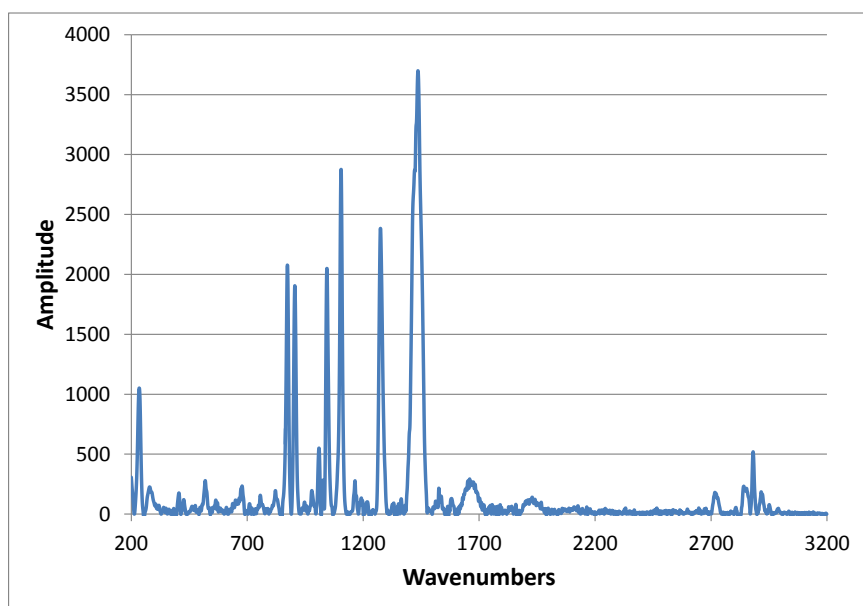


Figure S 81. Raman spectrum of sodium octanoate

### Sodium Nonanoate (pelargonate)

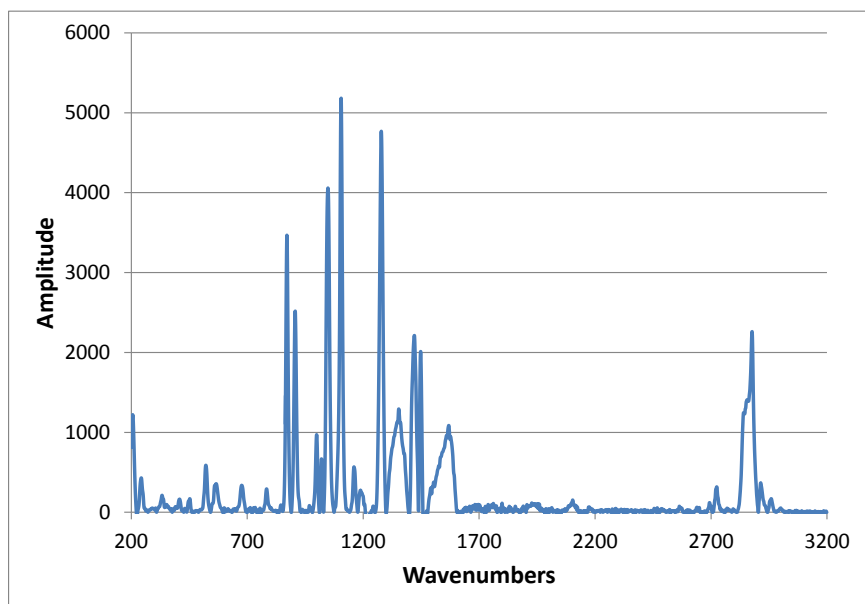


Figure S 82. Raman spectrum of sodium nonanoate

### Sodium Decanoate (caprate)

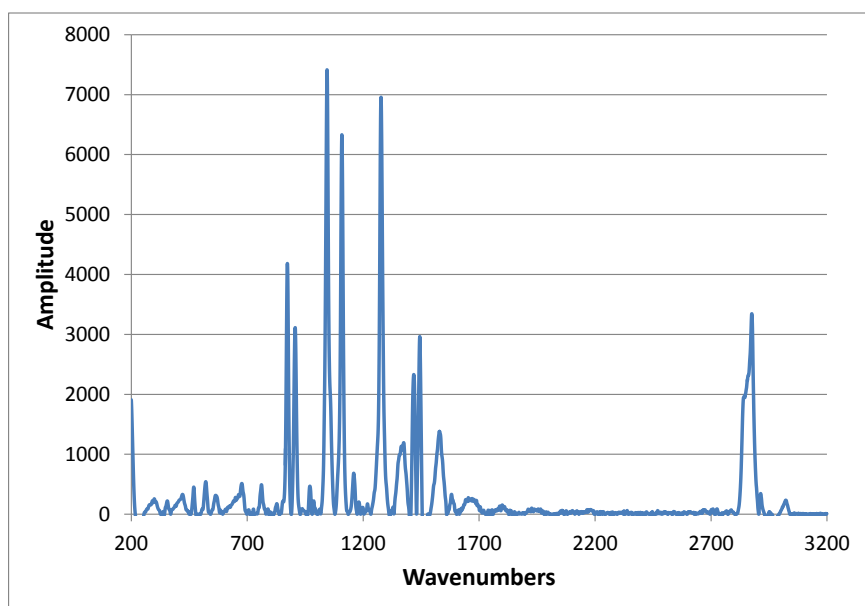


Figure S 83. Raman spectrum of sodium decanoate

## Sodium Undecanoate

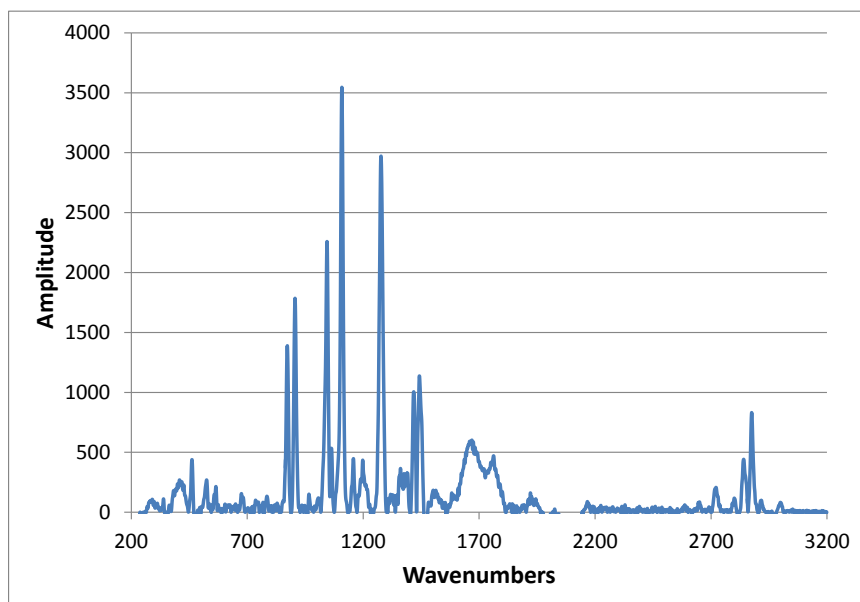


Figure S 84. Raman spectrum of sodium undecanoate

## Sodium Dodecanoate (laurate)

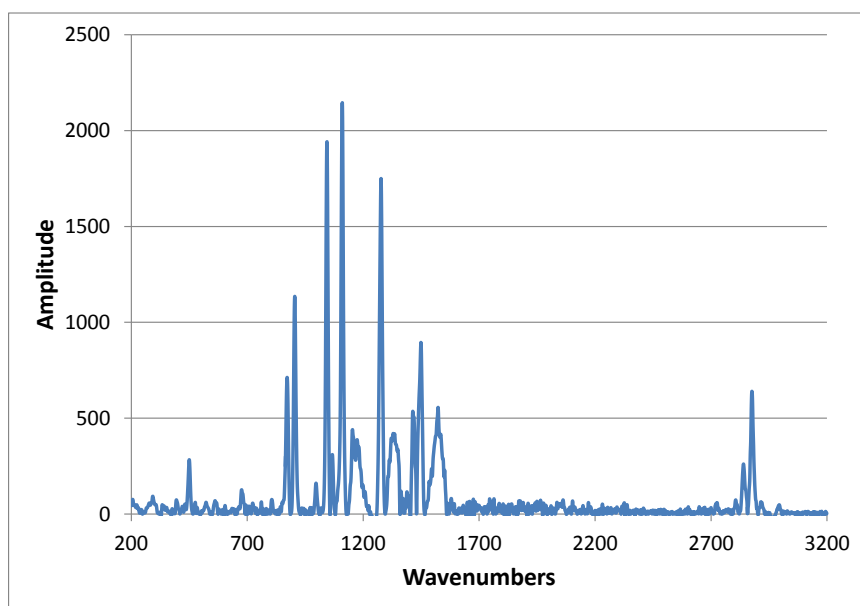


Figure S 85. Raman spectra of sodium dodecanoate

## UV-Vis Spectra

### Sodium Methanoate

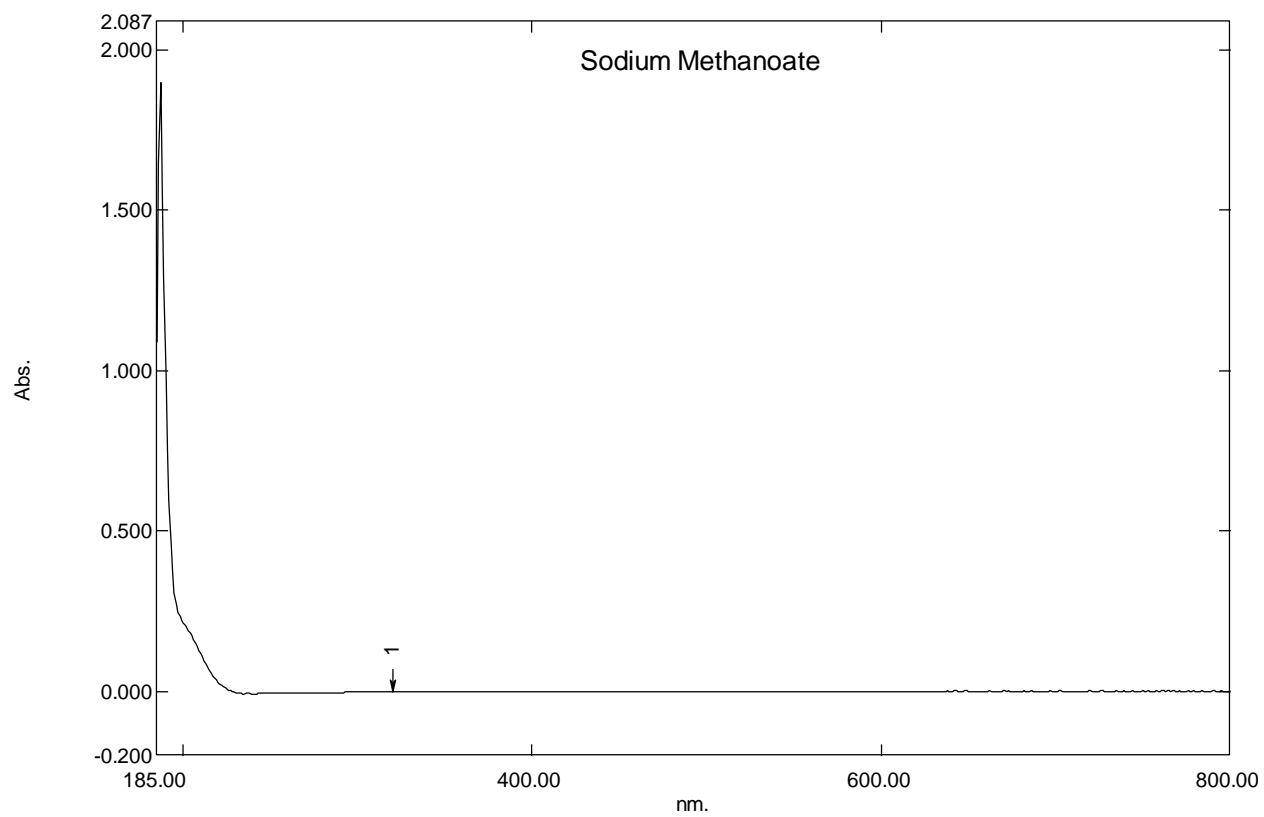


Figure S 86. UV-Vis spectrum of sodium methanoate

## Sodium Ethanoate

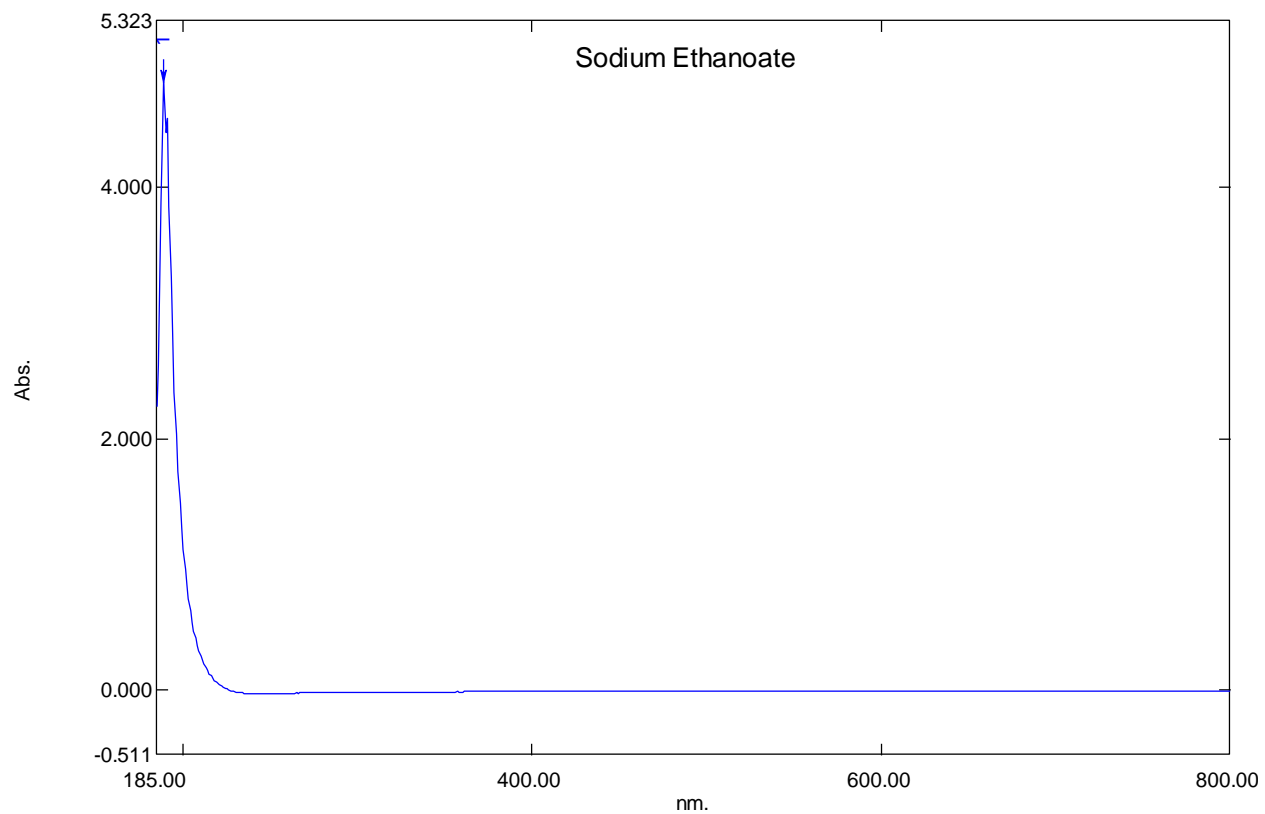


Figure S 87. UV-Vis spectrum of sodium ethanoate

## Sodium Propanoate

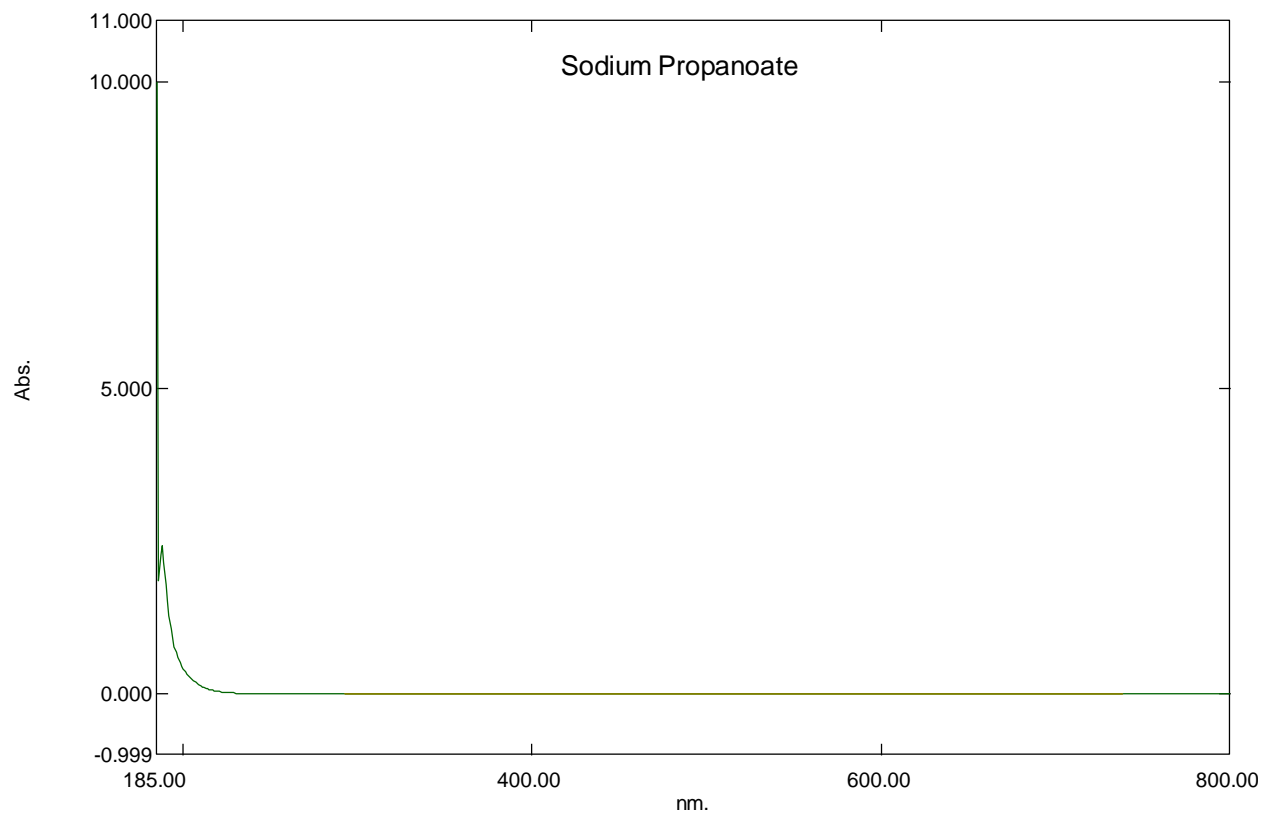


Figure S 88. UV-Vis spectrum of sodium propanoate

### Sodium Butanoate (butyrate)

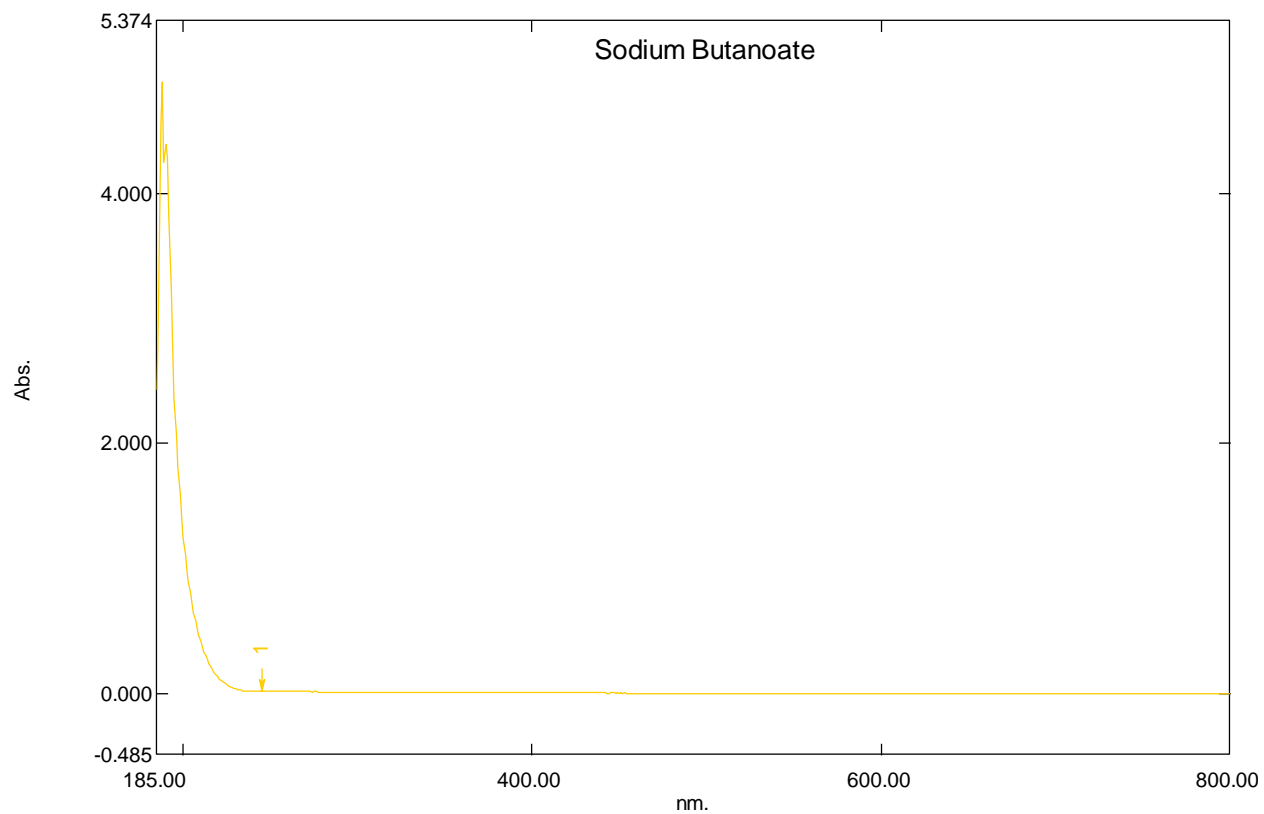


Figure S 89. UV-Vis spectrum of sodium butanoate

### Sodium Pentanoate (valerate)

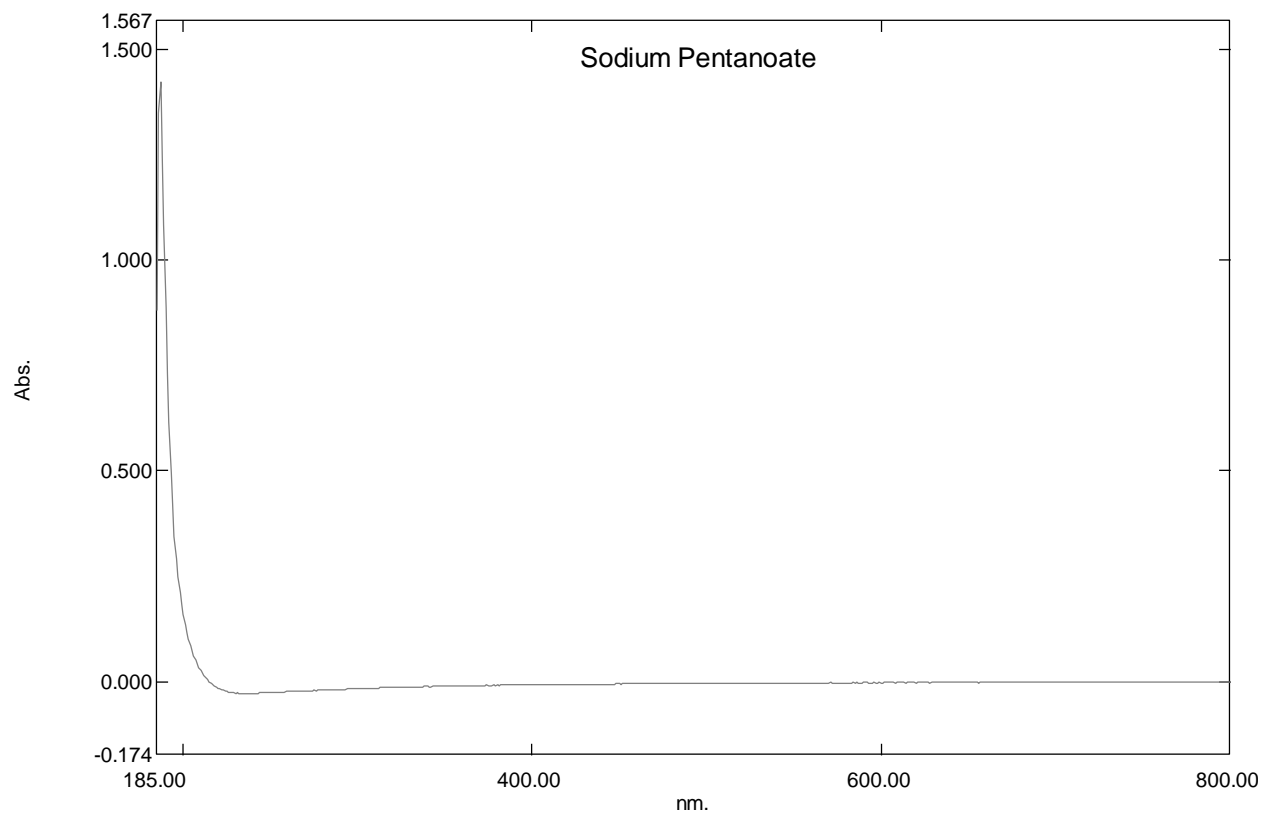


Figure S 90. UV-Vis spectrum of sodium pentanoate

## Sodium Hexanoate (caproate)

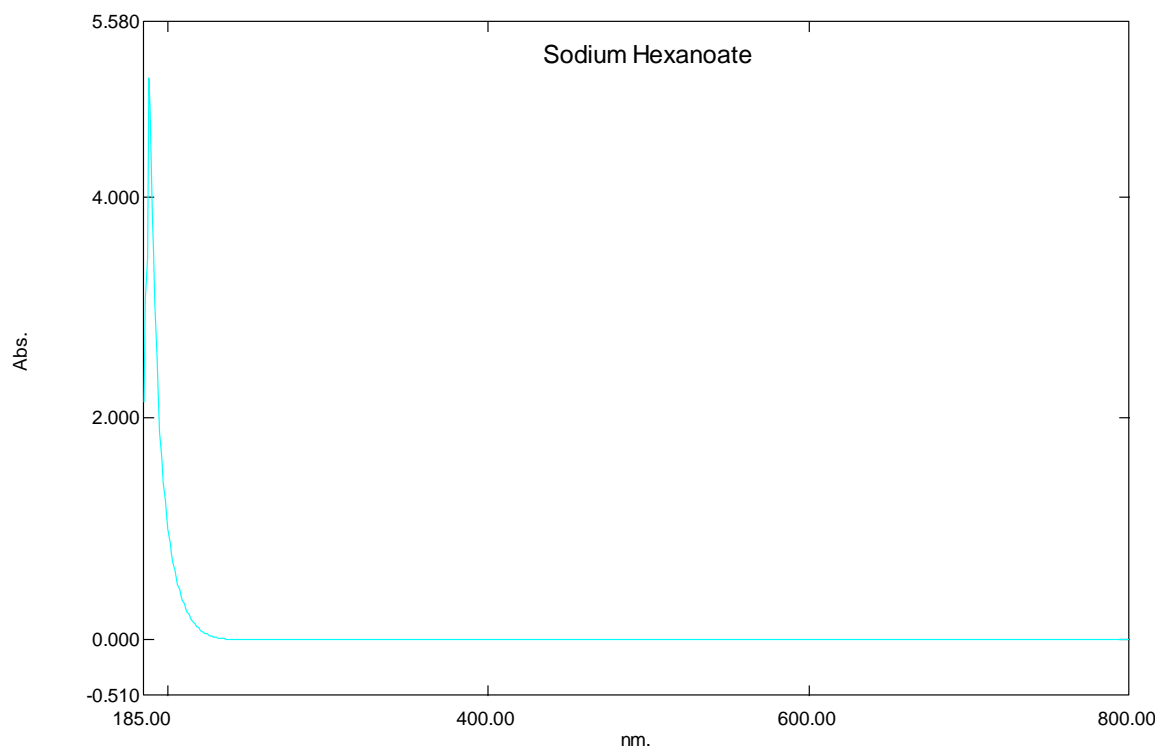


Figure S 91. UV-Vis of sodium hexanoate

## Sodium Heptanoate

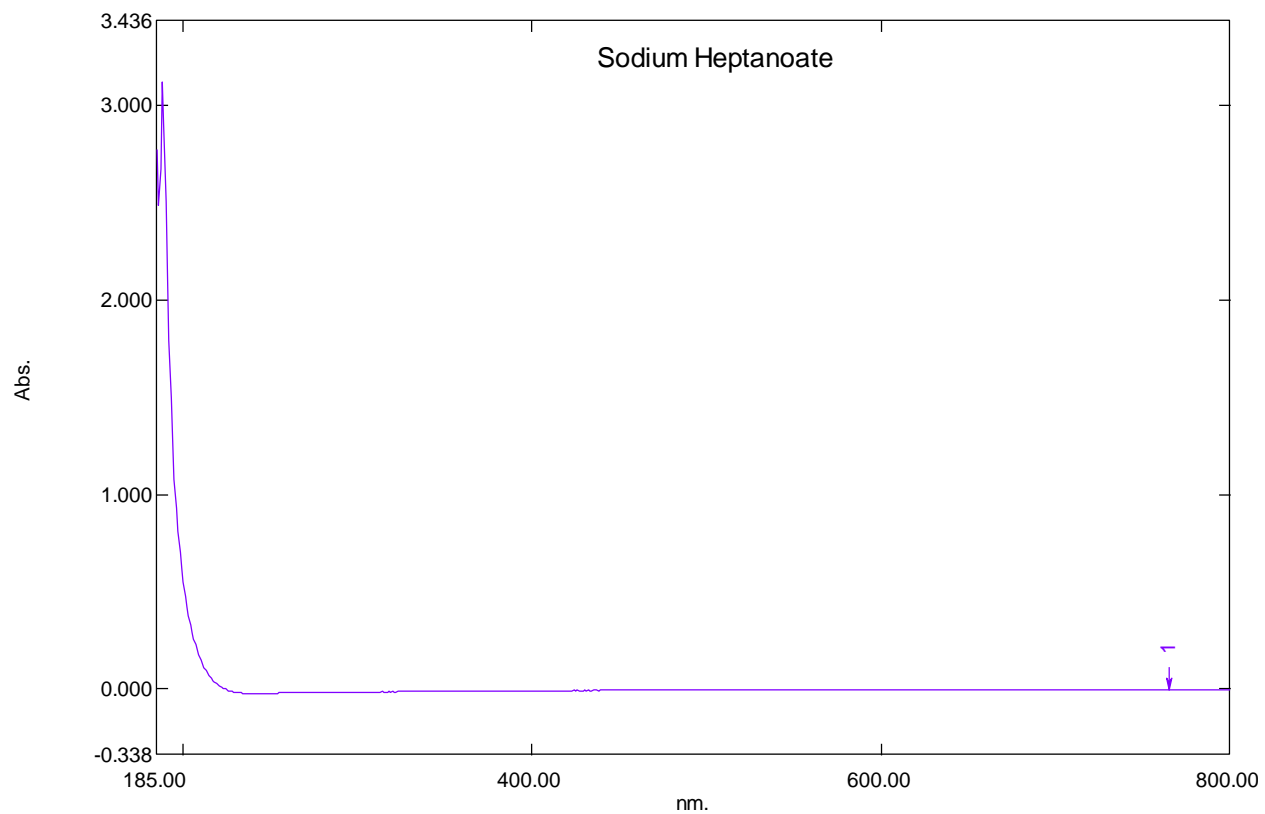


Figure S 92. UV-Vis spectrum of sodium heptanoate

### Sodium Octanoate (caprylate)

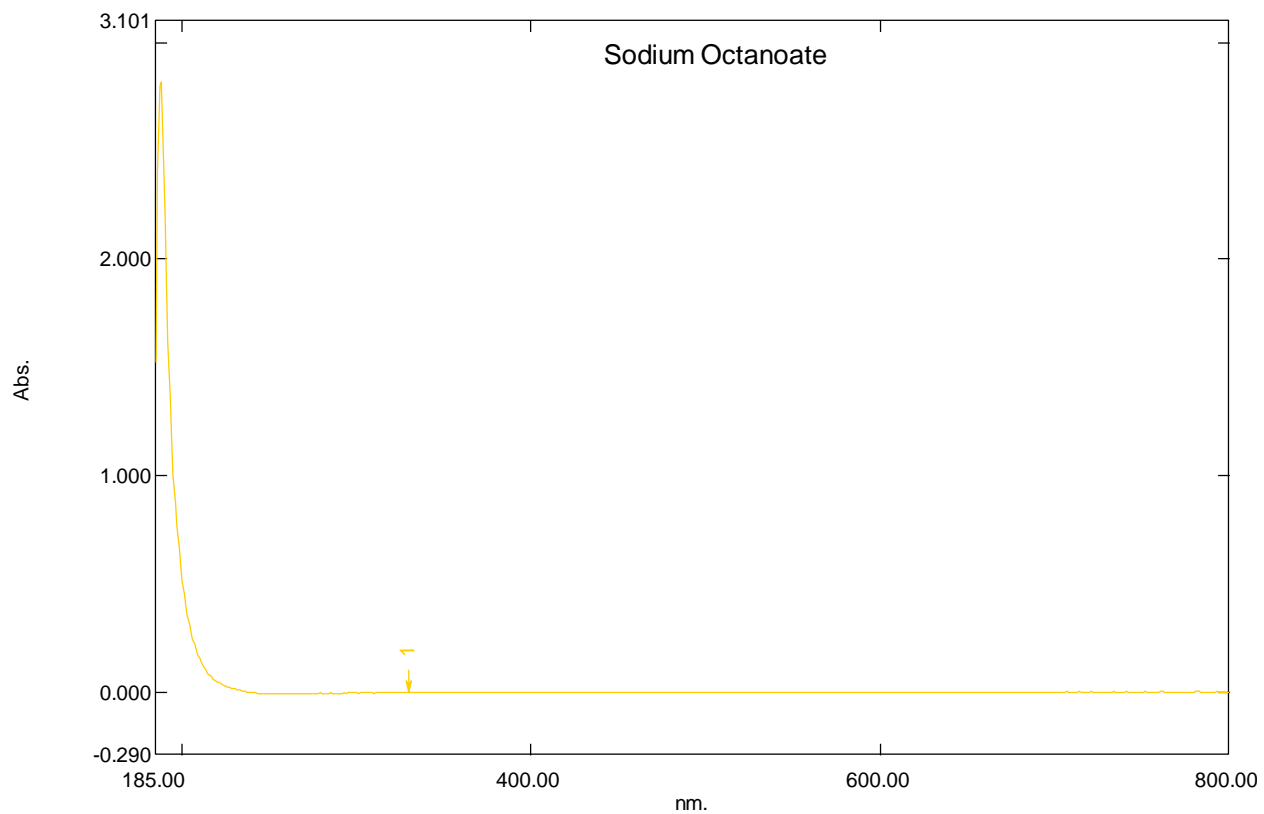


Figure S 93. UV-Vis of sodium octanoate

## Sodium Nonanoate (pelargonate)

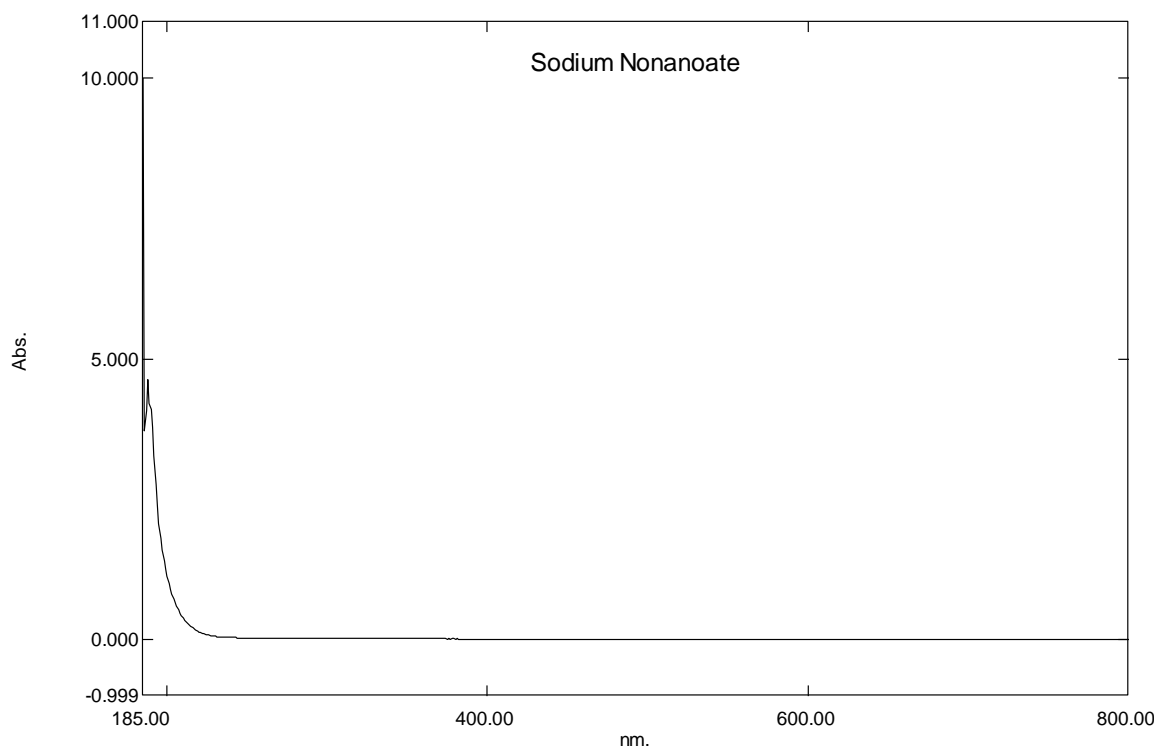


Figure S 94. UV-Vis of sodium nonanoate

### Sodium Decanoate (caprate)

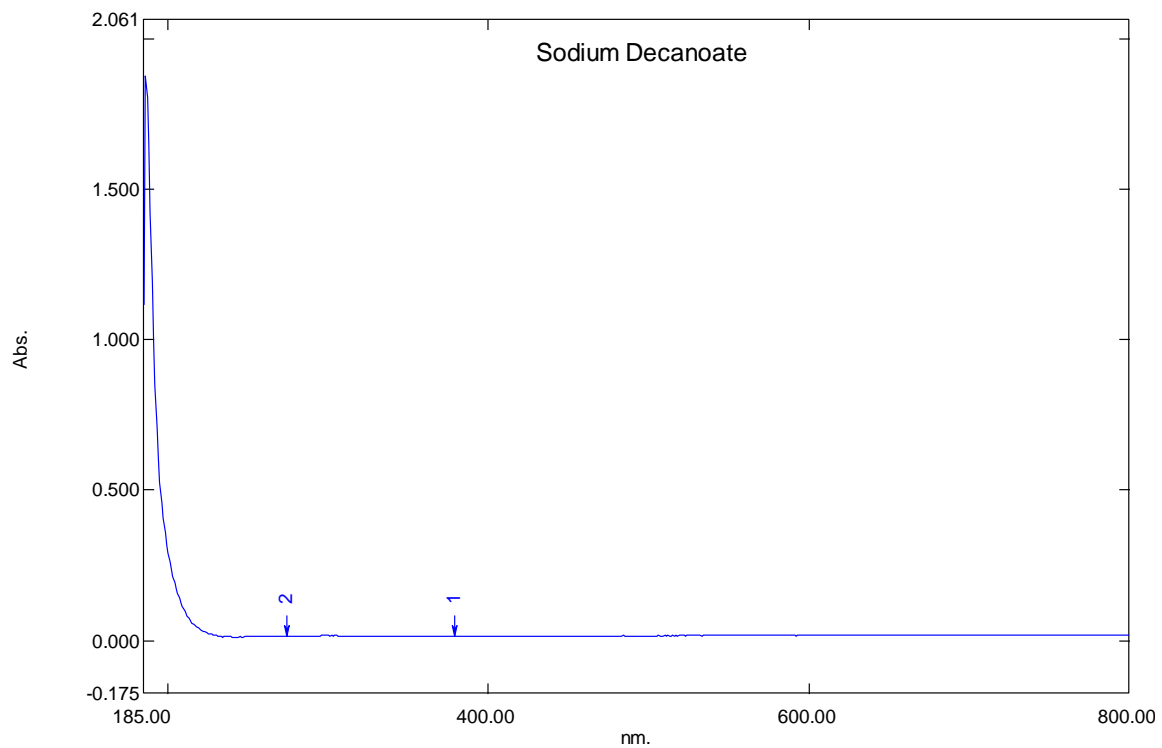


Figure S 95. UV-Vis of sodium decanoate

## Sodium Undecanoate

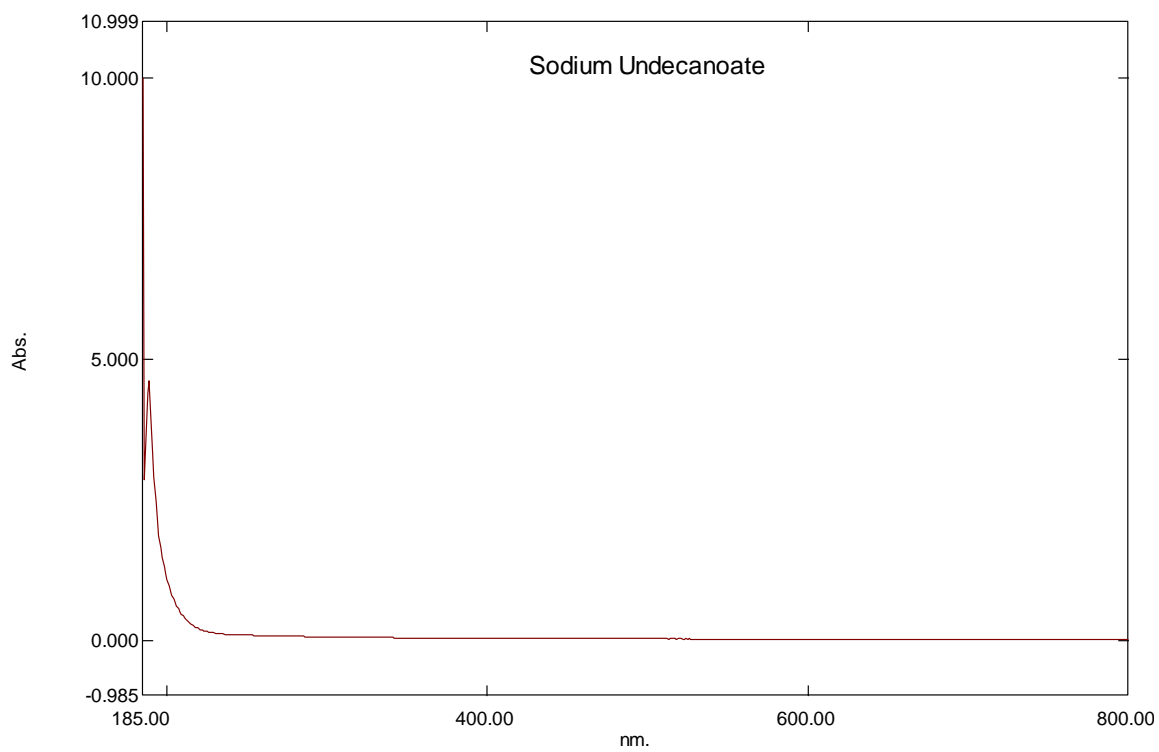


Figure S 96. UV-Vis of sodium undecanoate

# Sodium Dodecanoate (laurate)

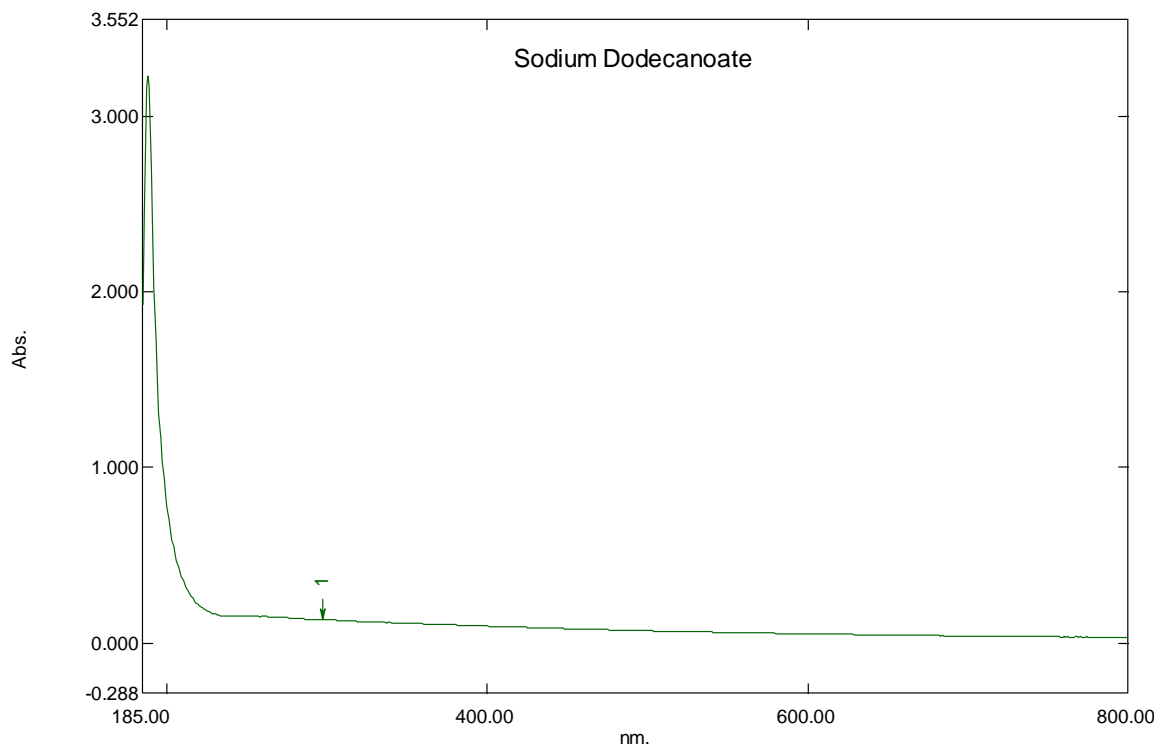


Figure S 97. UV-Vis of sodium dodecanoate

## TGA Results

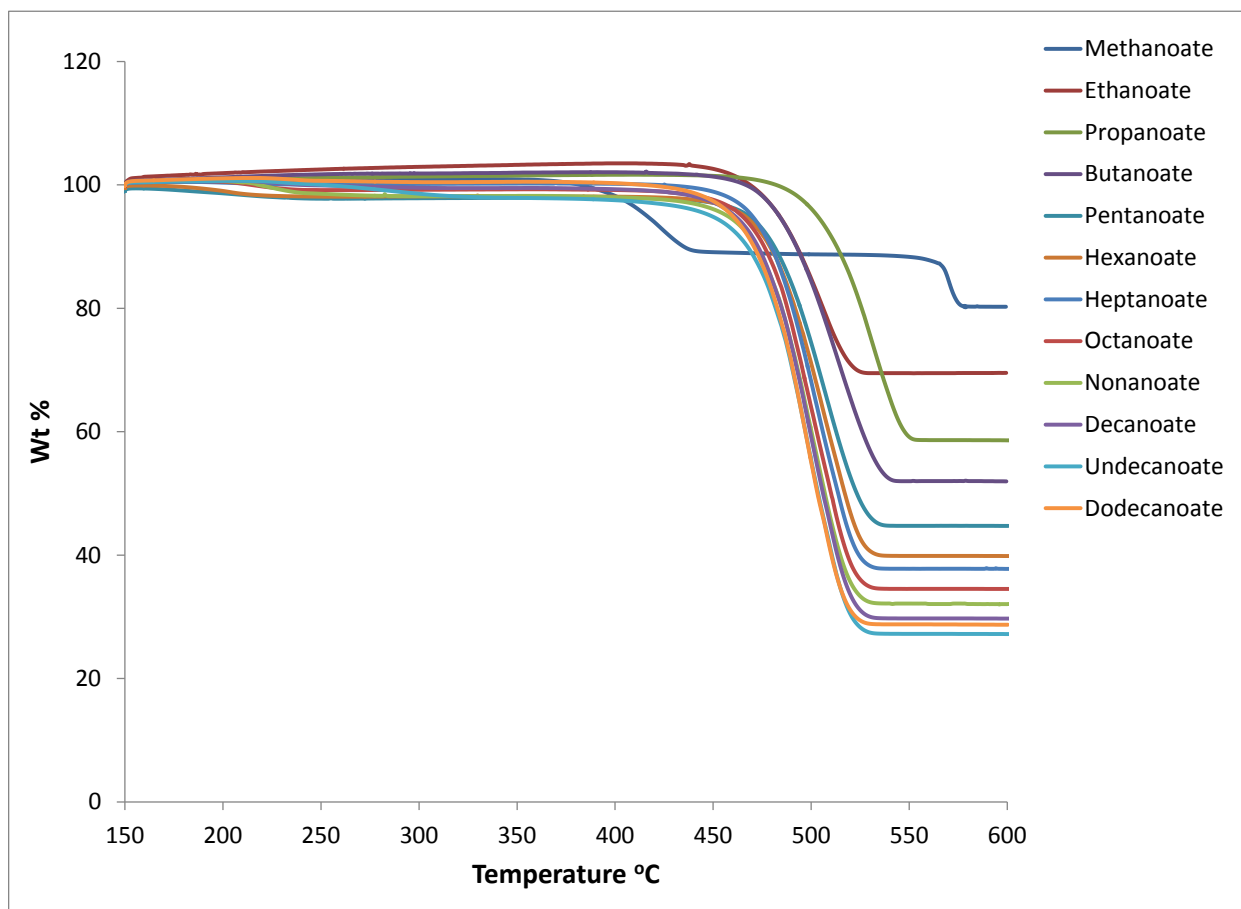


Figure S 98. TGA profile of Na-carboxylates

## Calorigrams of Na-Carboxylates determined by the Differential Scanning Calorimeter (DSC)

### Sodium Methanoate

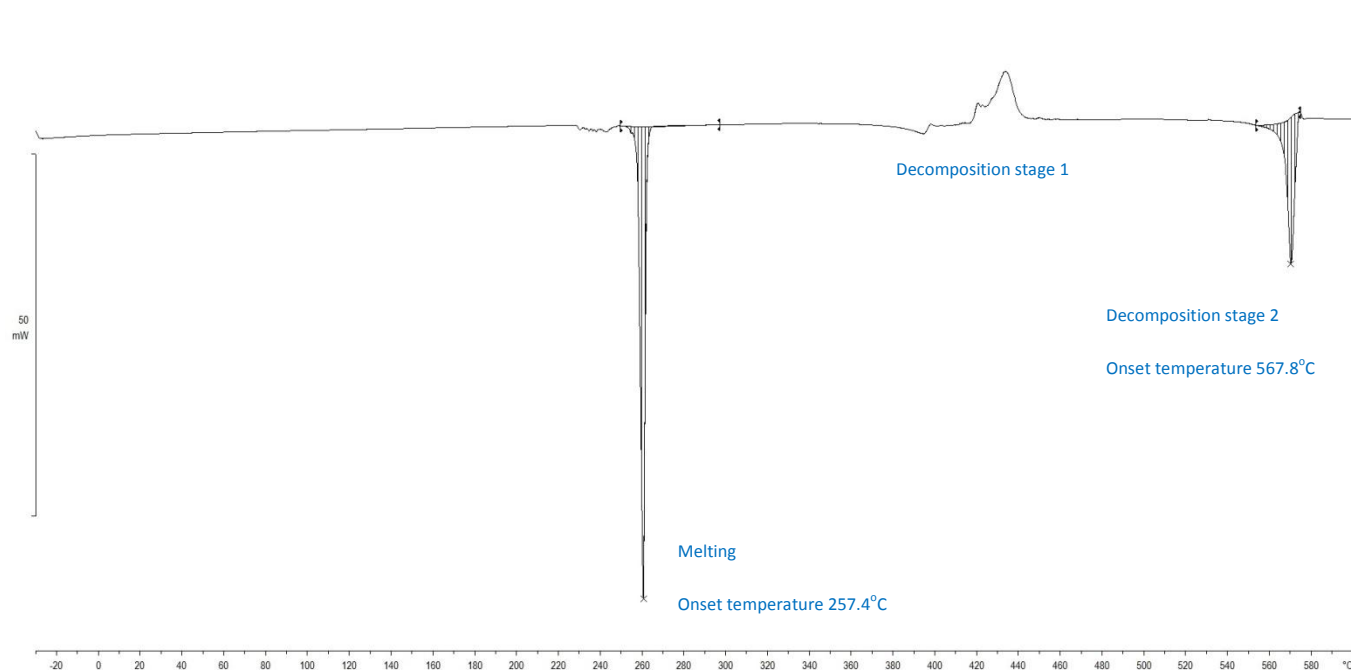


Figure S 99. Calorigram of Sodium Methanoate determined by the DSC over the range of -30-600°C at 10°C·min<sup>-1</sup> heating rate and 100mL·min<sup>-1</sup> nitrogen flow.

### Sodium Ethanoate

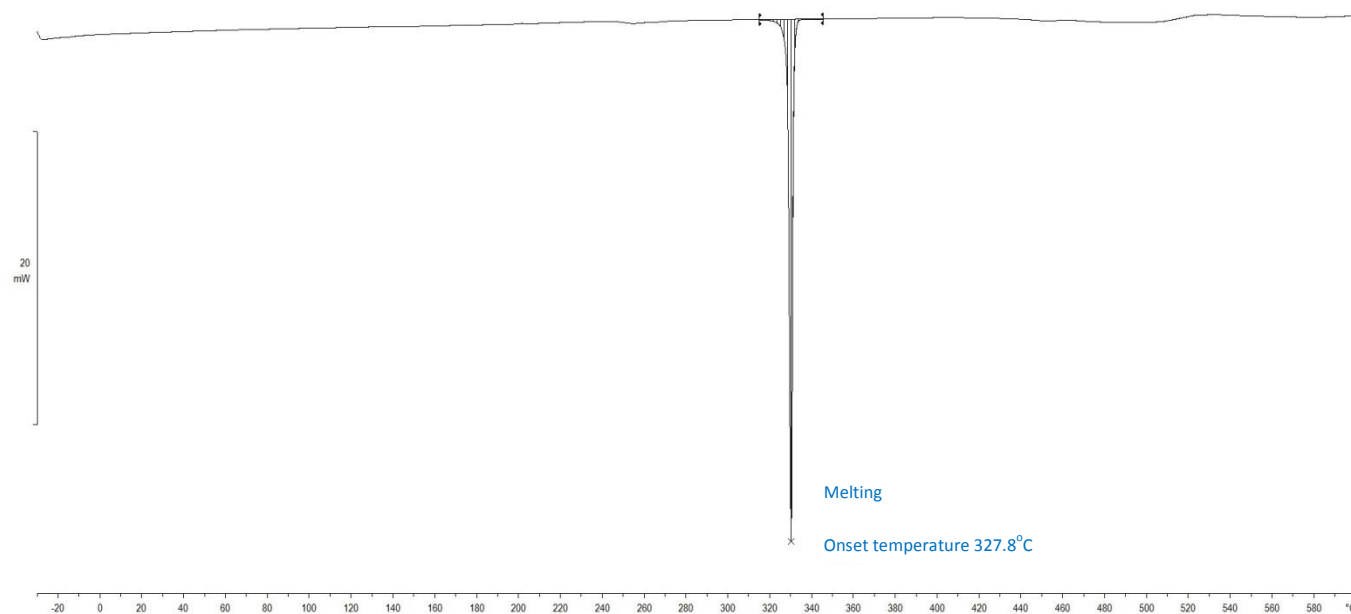


Figure S 100. Calorigram of Sodium Ethanoate determined by the DSC over the range of -30-600°C at 10°C·min<sup>-1</sup> heating rate and 100mL·min<sup>-1</sup> nitrogen flow.

## Sodium Propanoate

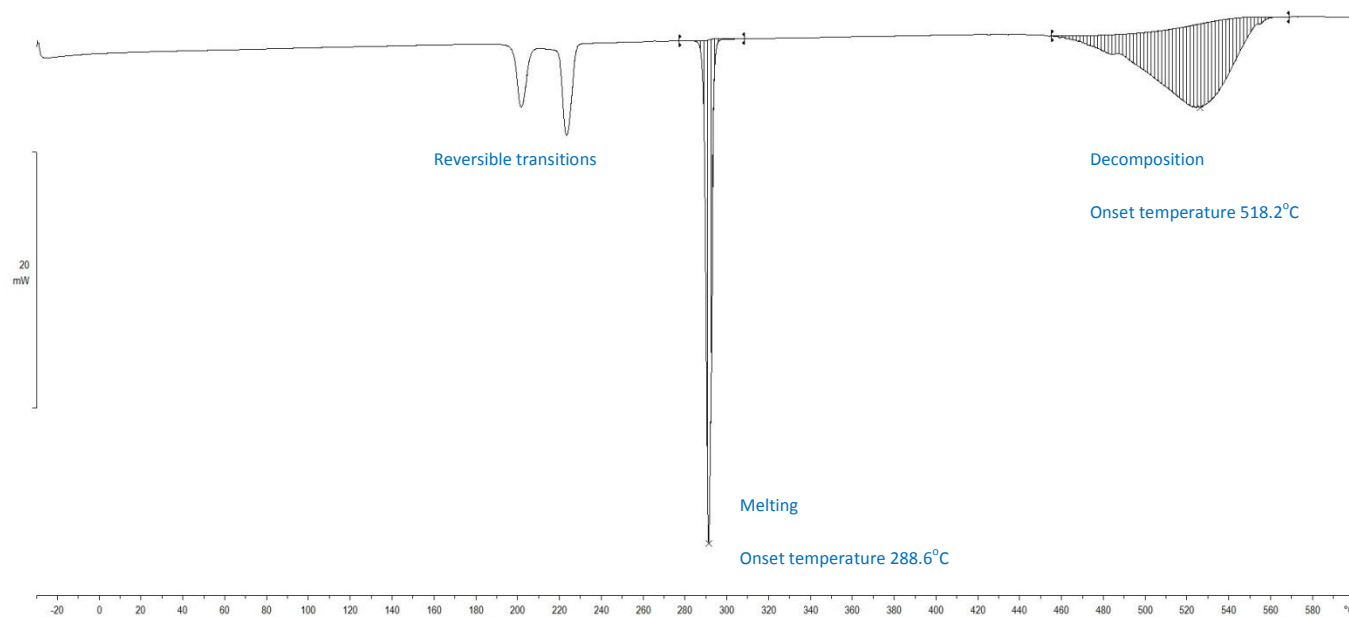


Figure S 101. Calorigram of Sodium Propanoate determined by the DSC over the range of -30-600°C at 10°C·min<sup>-1</sup> heating rate and 100mL·min<sup>-1</sup> nitrogen flow.

## Sodium Butanoate (butyrate)

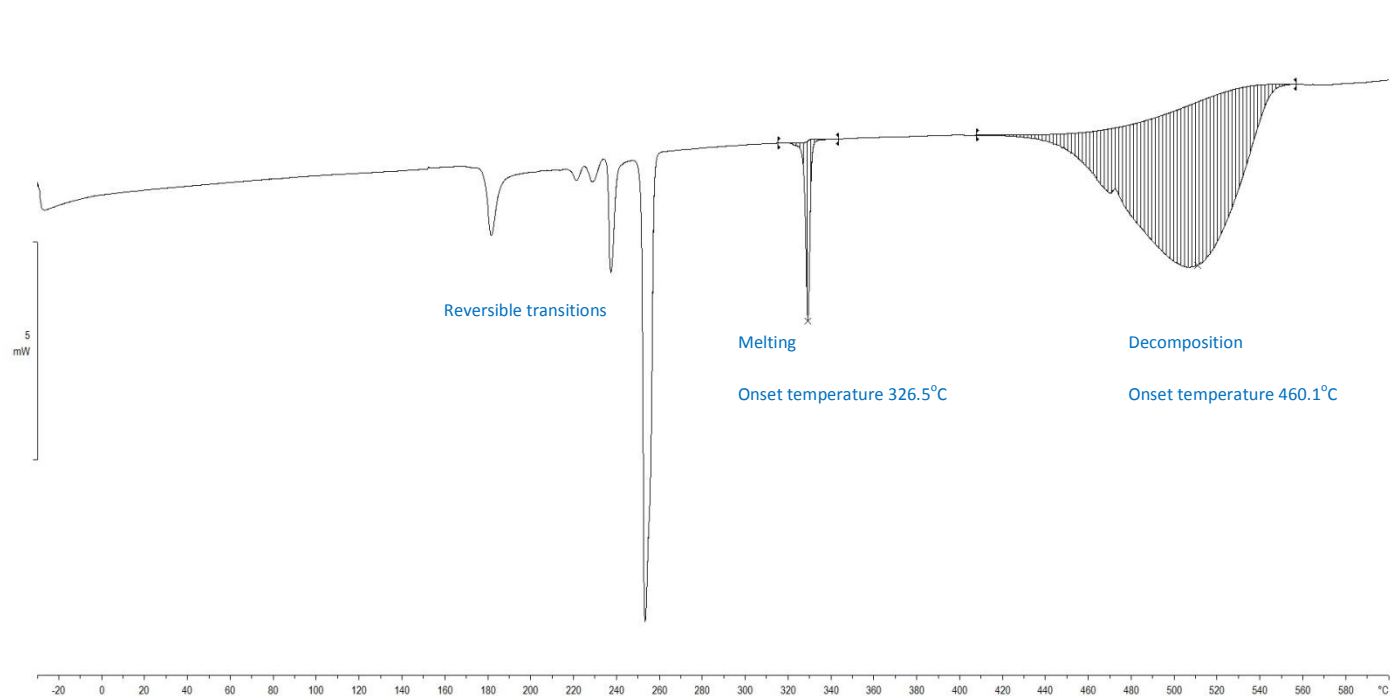


Figure S 102. Calorigram of Sodium Butanoate determined by the DSC over the range of -30-600°C at 10°C·min<sup>-1</sup> heating rate and 100mL·min<sup>-1</sup> nitrogen flow.

### Sodium Pentanoate (valerate)

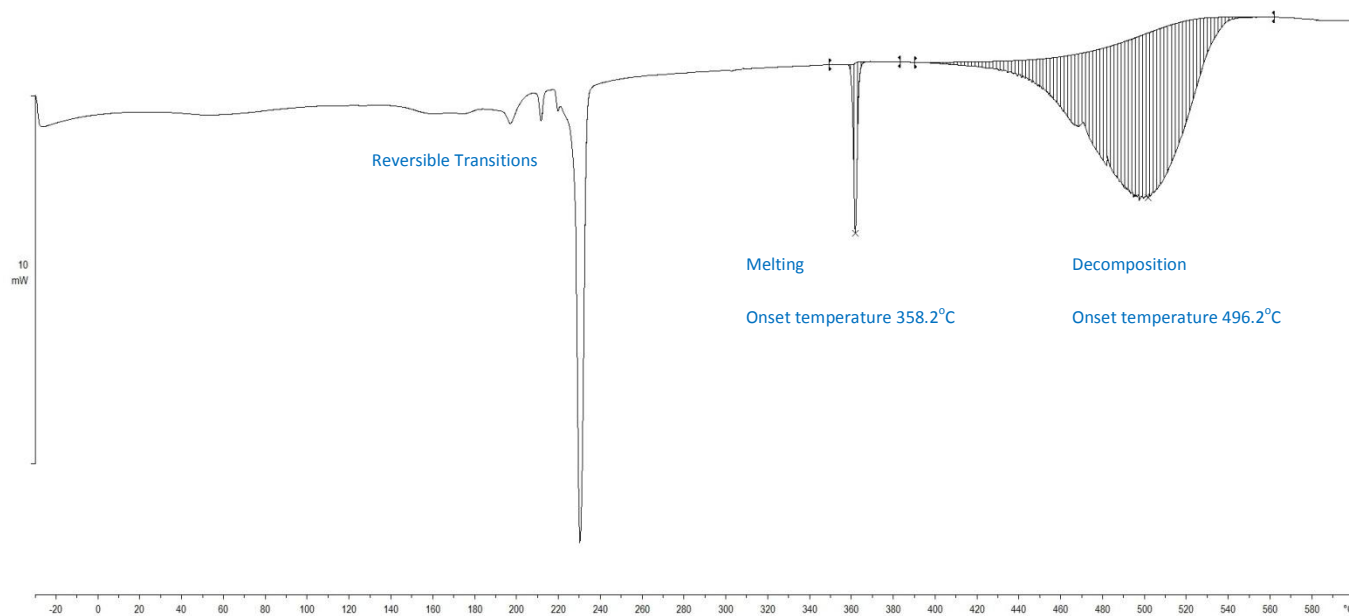


Figure S 103. Calorigram of Sodium Pentanoate determined by the DSC over the range of -30-600°C at 10°C·min<sup>-1</sup> heating rate and 100mL·min<sup>-1</sup> nitrogen flow.

### Sodium Hexanoate (caproate)

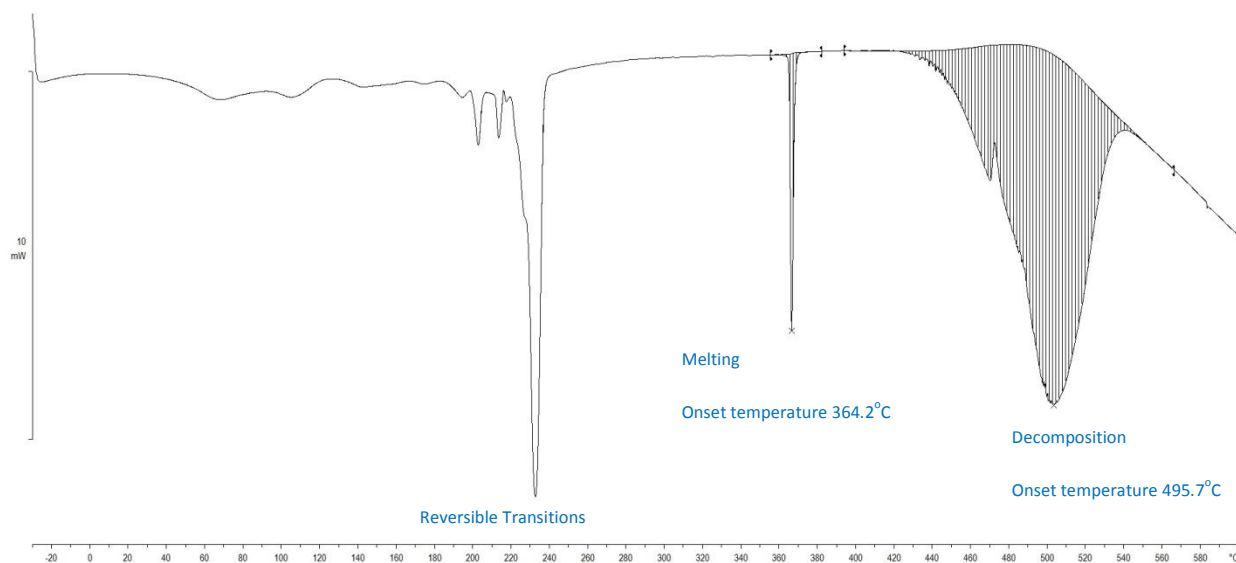


Figure S 104. Calorigram of Sodium Hexanoate determined by the DSC over the range of -30-600°C at 10°C·min<sup>-1</sup> heating rate and 100mL·min<sup>-1</sup> nitrogen flow.

## Sodium Heptanoate

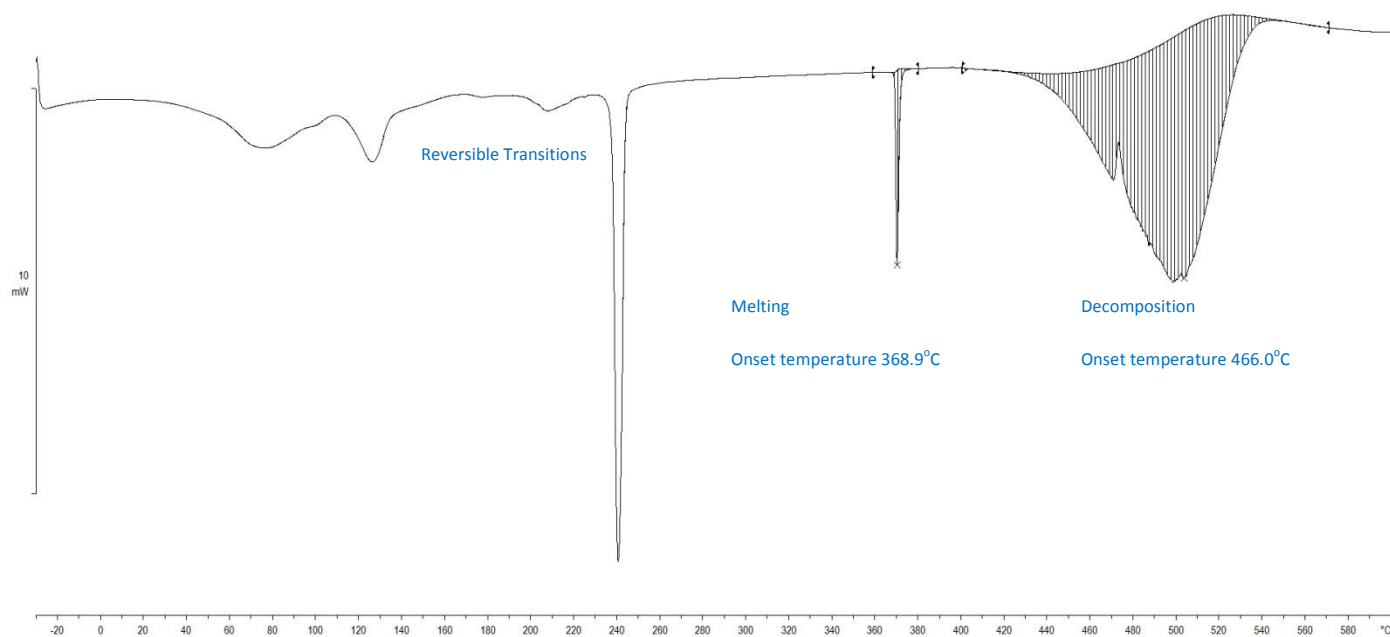


Figure S 105. Calorigram of Sodium Heptanoate determined by the DSC over the range of -30-600°C at 10°C min<sup>-1</sup> heating rate and 100mL min<sup>-1</sup> nitrogen flow.

## Sodium Octanoate (caprylate)

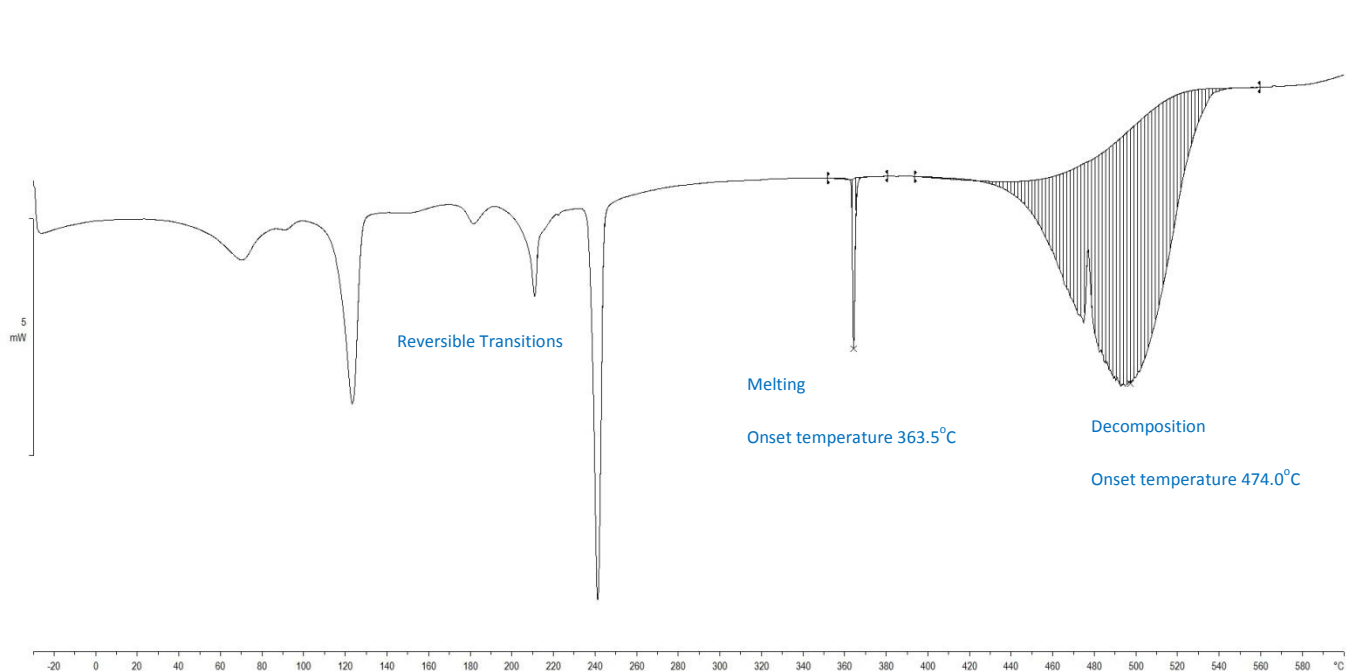


Figure S 106. Calorigram of Sodium Octanoate determined by the DSC over the range of -30-600°C at 10°C min<sup>-1</sup> heating rate and 100mL min<sup>-1</sup> nitrogen flow.

### Sodium Nonanoate (pelargonate)

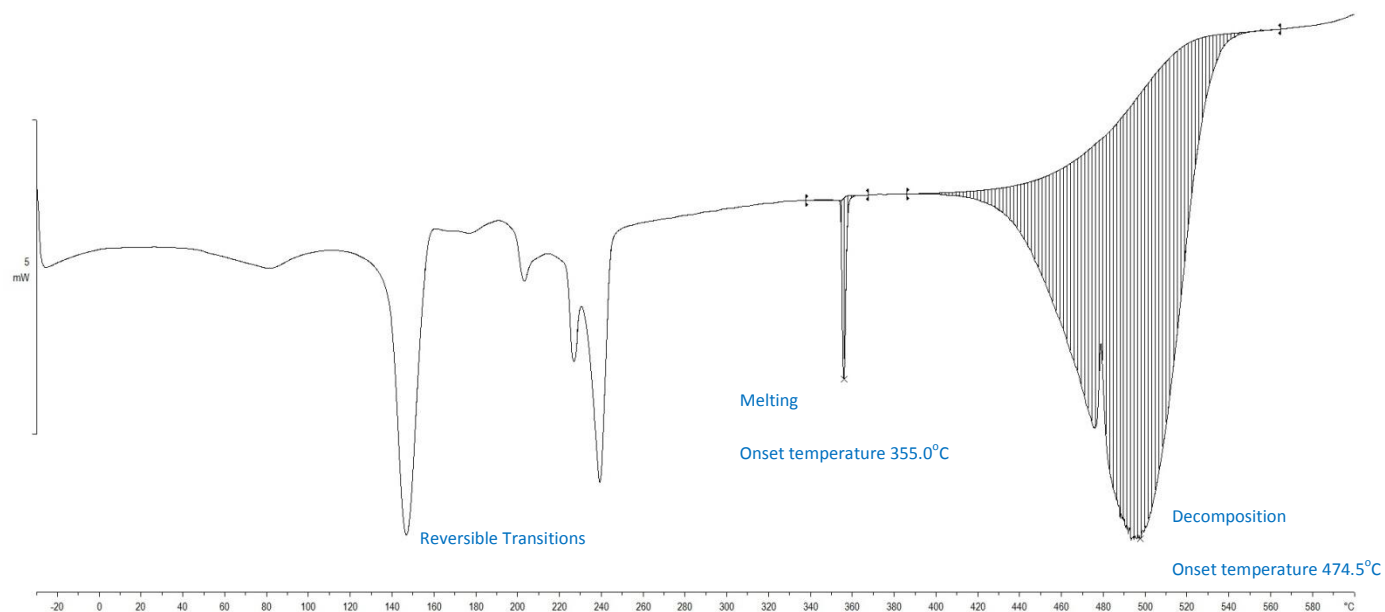


Figure S 107. Calorigram of Sodium Nonanoate determined by the DSC over the range of -30-600°C at 10°C·min<sup>-1</sup> heating rate and 100mL·min<sup>-1</sup> nitrogen flow.

### Sodium Decanoate (caprate)

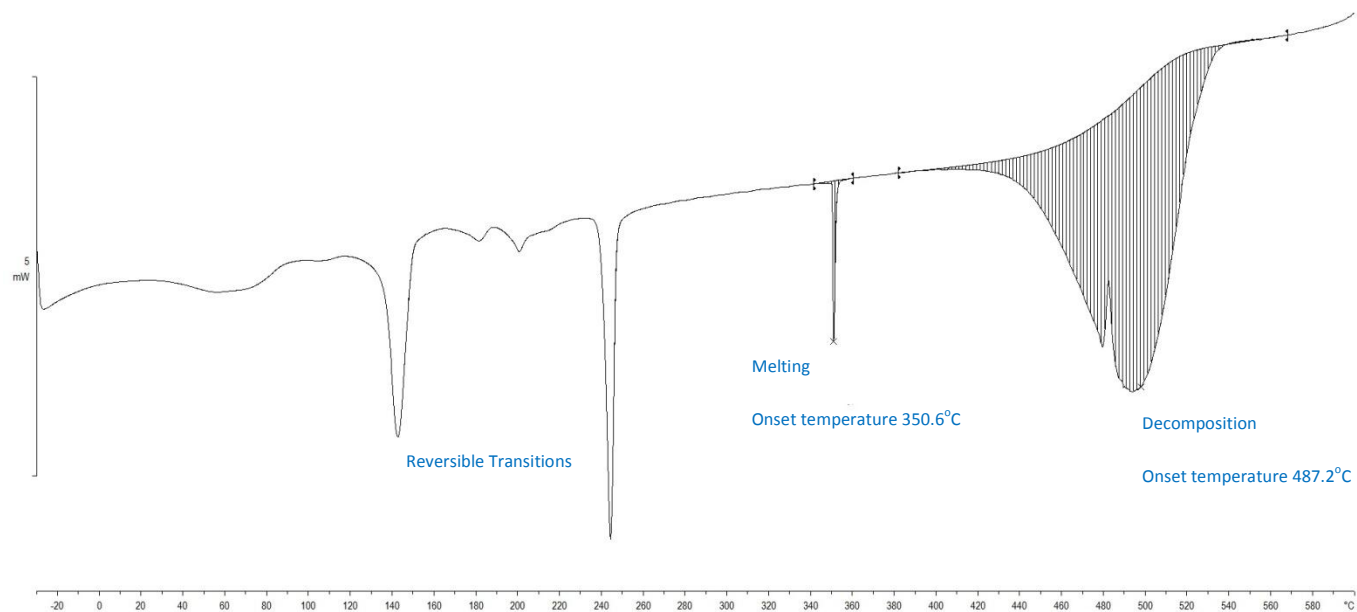


Figure S 108. Calorigram of Sodium Decanoate determined by the DSC over the range of -30-600°C at 10°C·min<sup>-1</sup> heating rate and 100mL·min<sup>-1</sup> nitrogen flow.

## Sodium Undecanoate

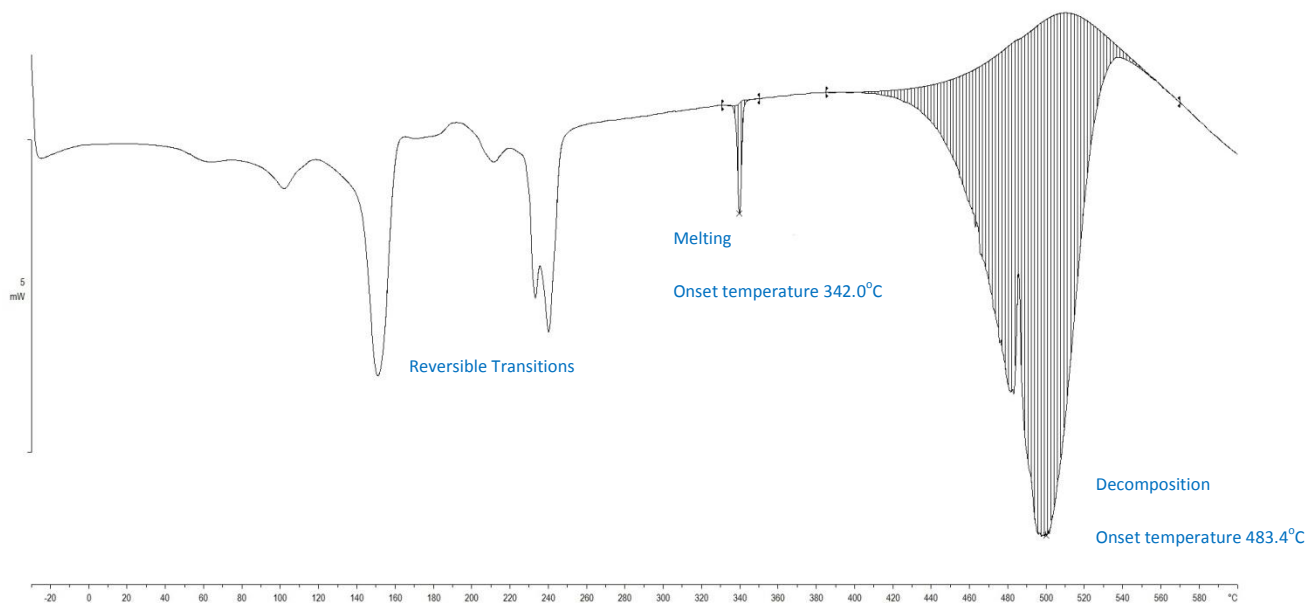


Figure S 109. Calorigram of Sodium Undecanoate determined by the DSC over the range of -30-600°C at 10°C min<sup>-1</sup> heating rate and 100mL min<sup>-1</sup> nitrogen flow.

## Sodium Dodecanoate (laurate)

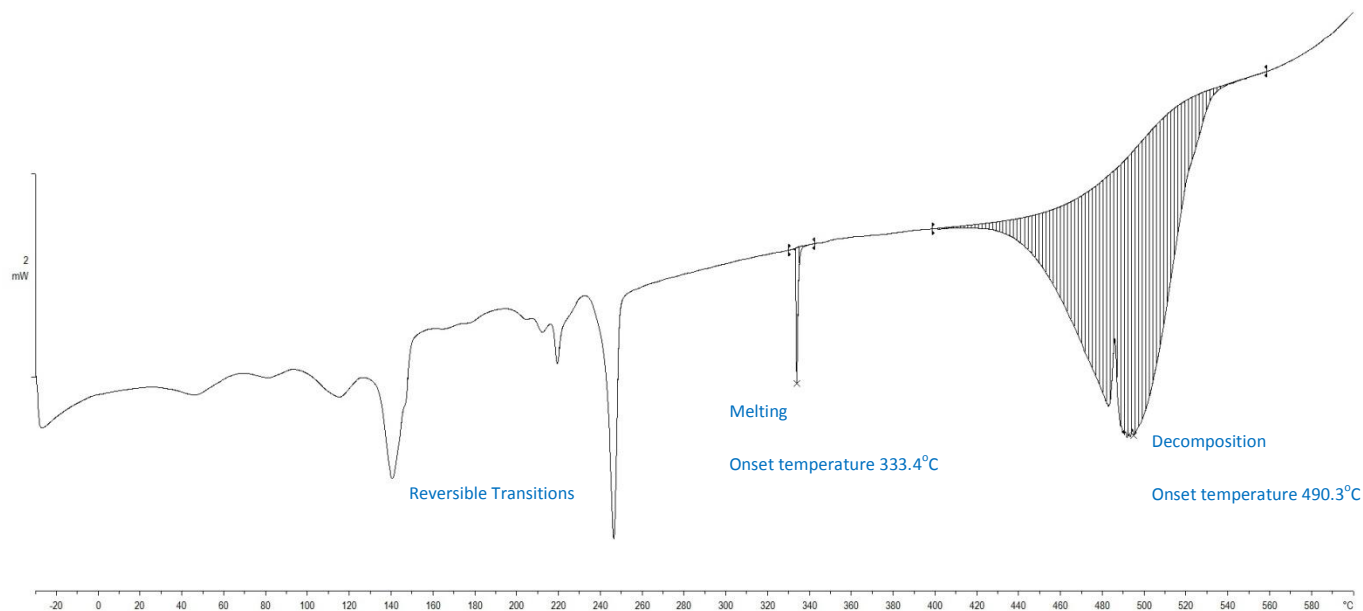


Figure S 110. Calorigram of Sodium Dodecanoate determined by the DSC over the range of -30-600°C at 10°C min<sup>-1</sup> heating rate and 100mL min<sup>-1</sup> nitrogen flow.

## Heat Capacity

### Sodium Methanoate

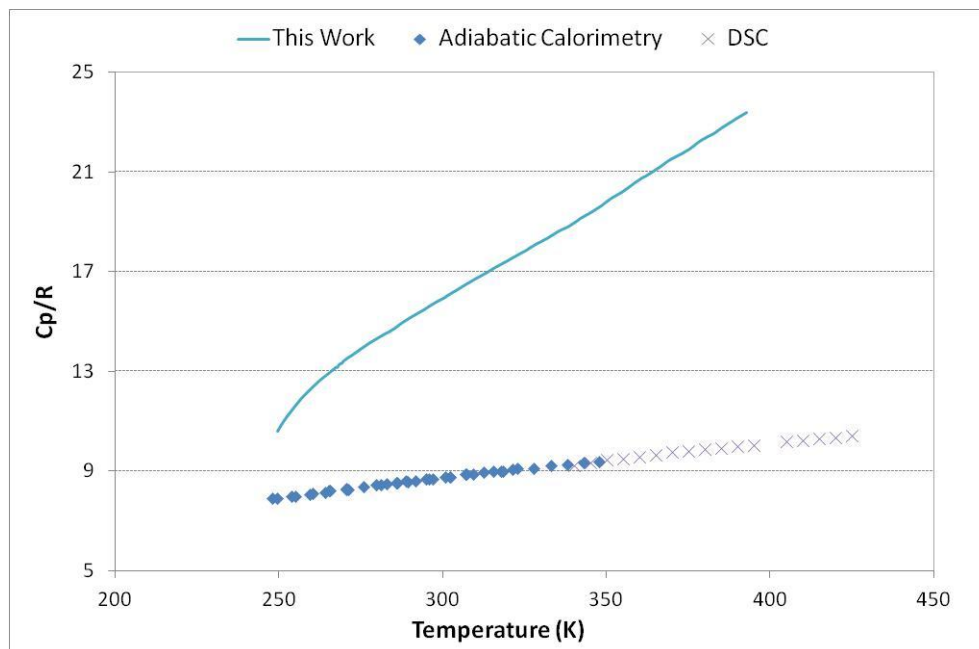


Figure S 111. Experimental molar heat capacities for Na-methanoate ( $R = 8.31451 \text{ JK}^{-1}\text{mol}^{-1}$ )

### Sodium Ethanoate

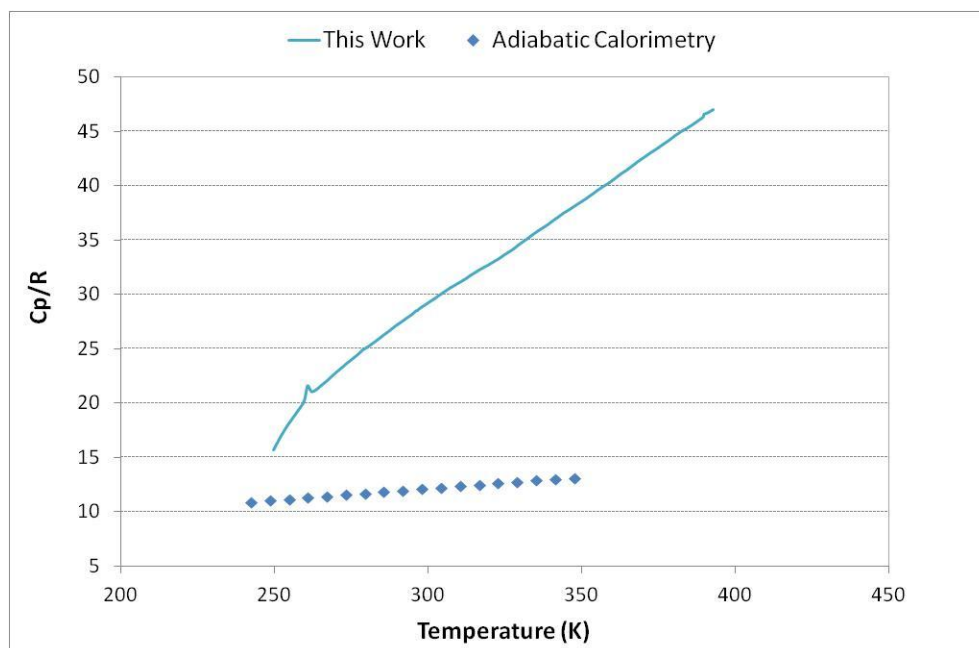


Figure S 112. Experimental molar heat capacities for Na-ethanoate ( $R = 8.31451 \text{ JK}^{-1}\text{mol}^{-1}$ )

## Sodium Propanoate

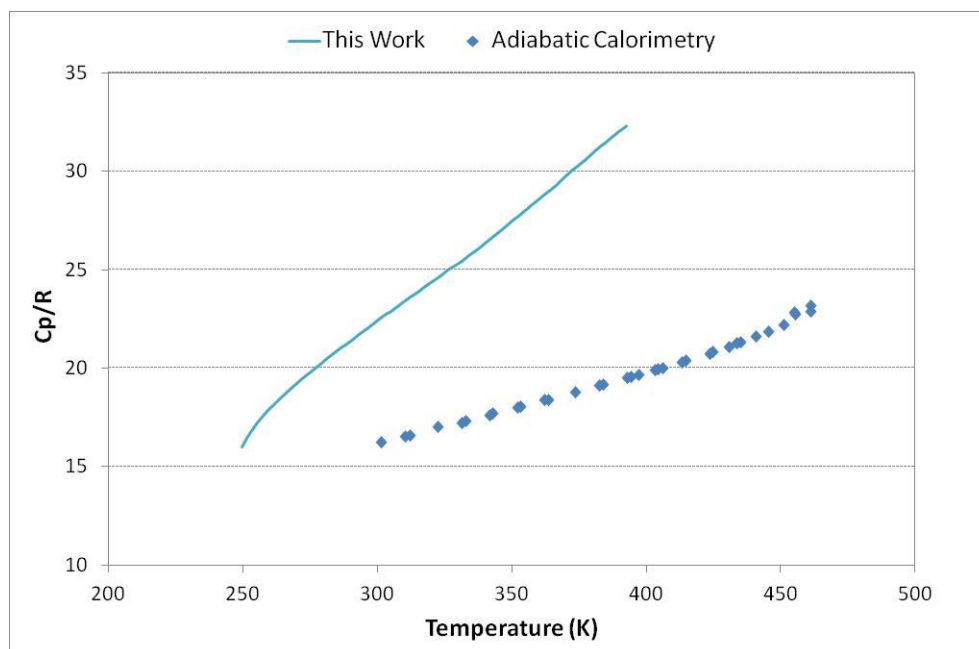


Figure S 113. Experimental molar heat capacities for Na-propanoate ( $R = 8.31451 \text{ JK}^{-1}\text{mol}^{-1}$ )

## Sodium Butanoate (butyrate)

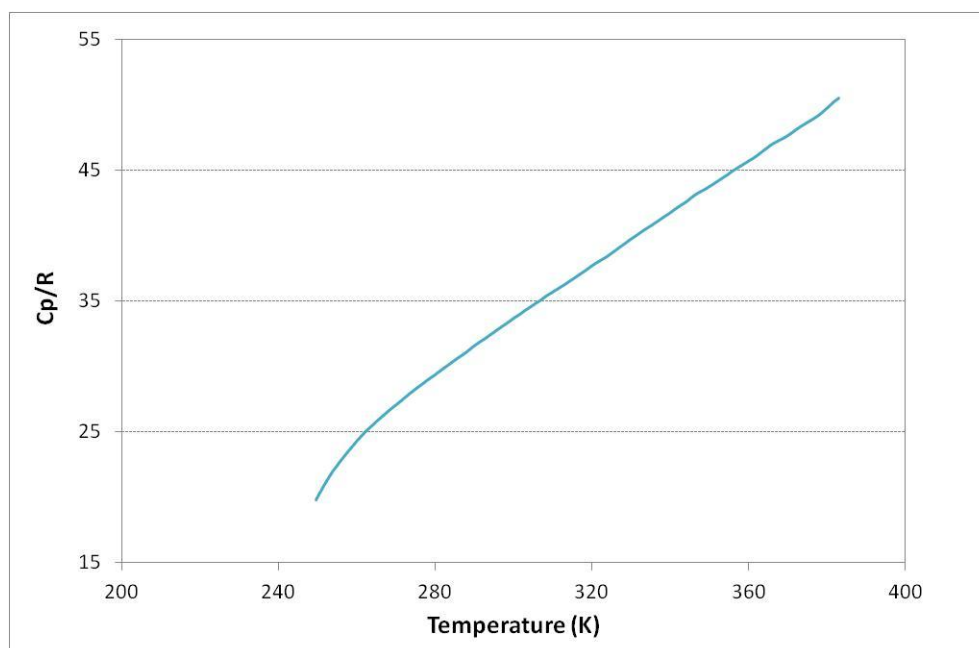


Figure S 114. Experimental molar heat capacities for Na-butanoate ( $R = 8.31451 \text{ JK}^{-1}\text{mol}^{-1}$ )

### Sodium Pentanoate (valerate)

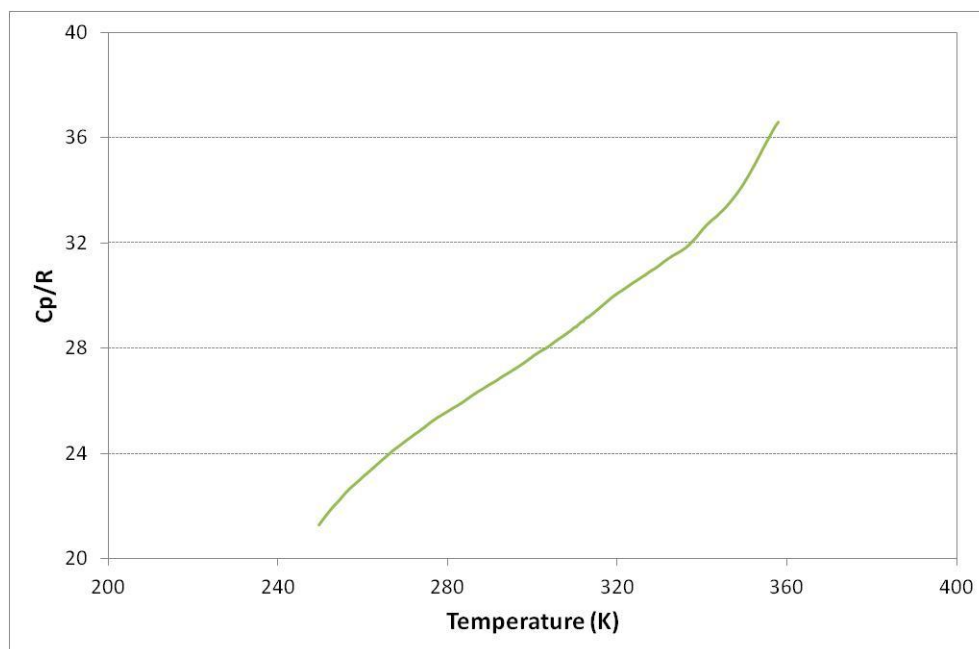


Figure S 115. Experimental molar heat capacities for Na-pentanoate ( $R = 8.31451 \text{ JK}^{-1}\text{mol}^{-1}$ )

### Sodium Hexanoate (caproate)

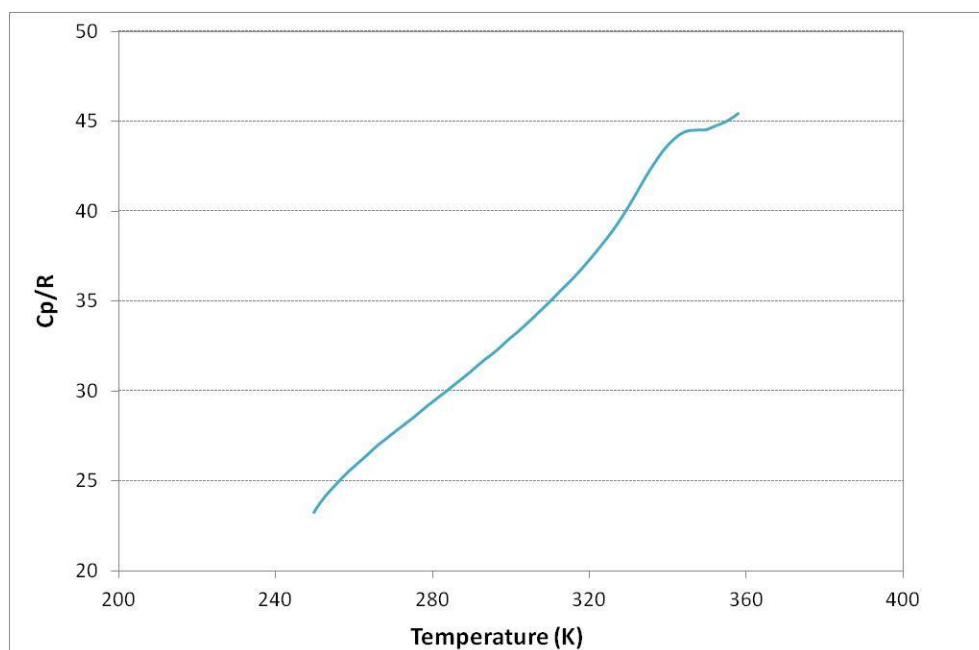


Figure S 116. Experimental molar heat capacities for Na-hexanoate ( $R = 8.31451 \text{ JK}^{-1}\text{mol}^{-1}$ )

## Sodium Heptanoate

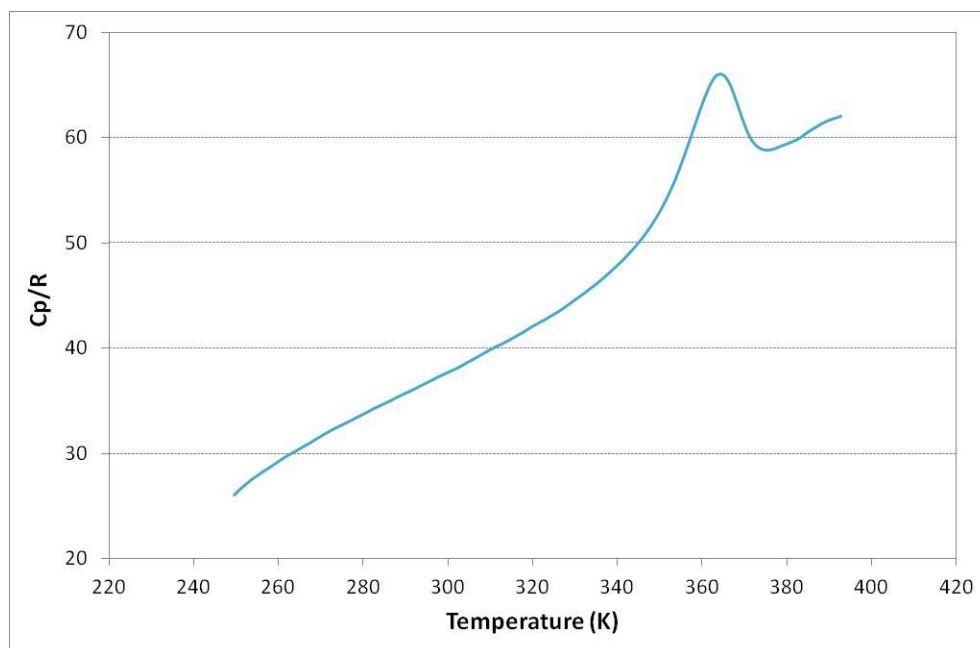


Figure S 117. Experimental molar heat capacities for Na-heptanoate ( $R = 8.31451 \text{ JK}^{-1} \text{ mol}^{-1}$ )

## Sodium Octanoate (caprylate)

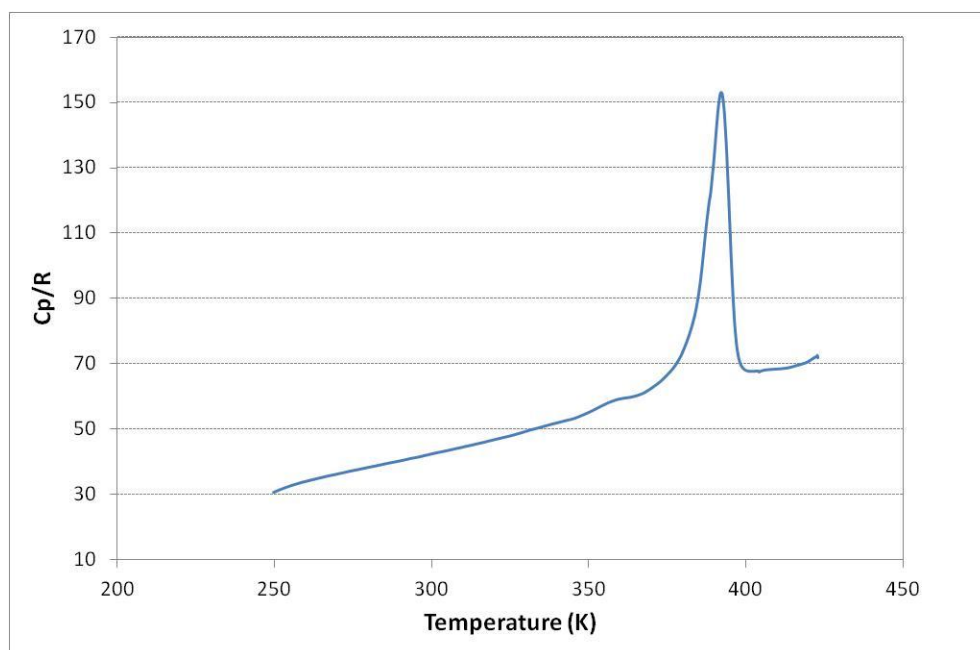


Figure S 118. Experimental molar heat capacities for Na-octanoate ( $R = 8.31451 \text{ JK}^{-1} \text{ mol}^{-1}$ )

### Sodium Nonanoate (pelargonate)

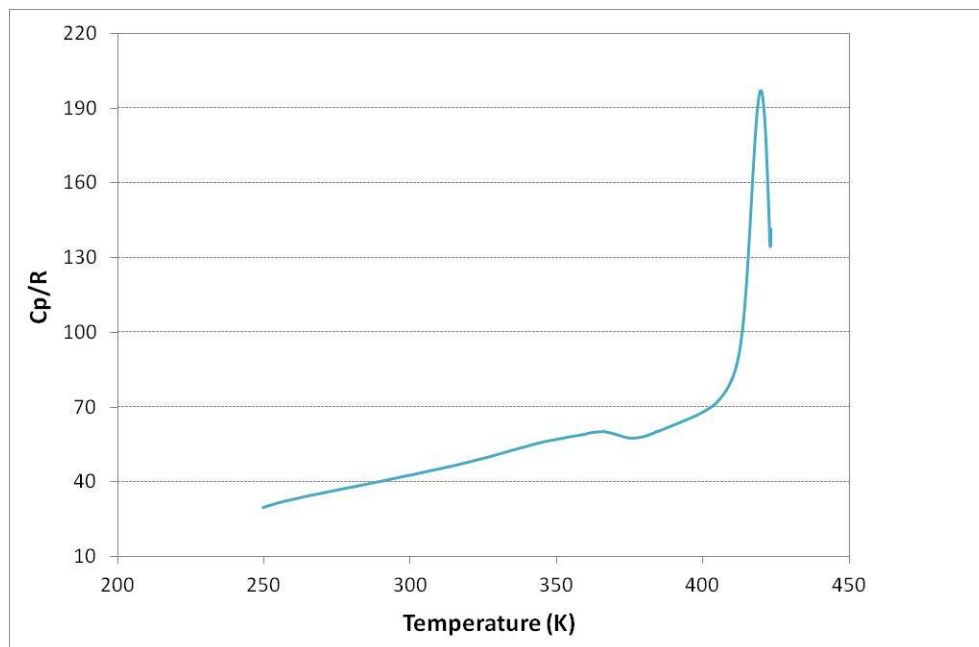


Figure S 119. Experimental molar heat capacities for Na-nonanoate ( $R = 8.31451 \text{ JK}^{-1}\text{mol}^{-1}$ )

### Sodium Decanoate (caprate)

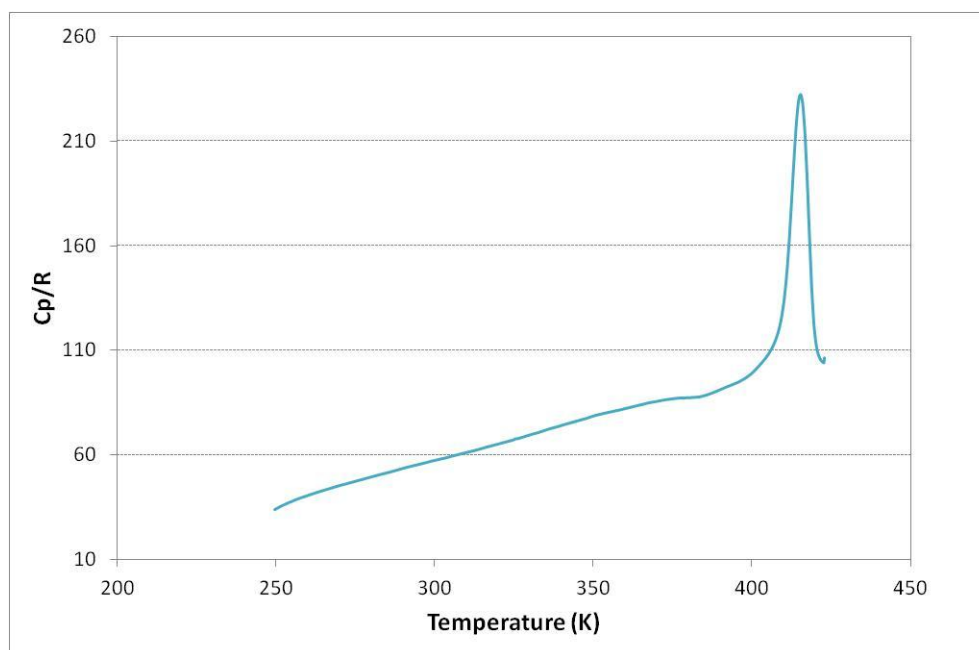


Figure S 120. Experimental molar heat capacities for Na-decanoate ( $R = 8.31451 \text{ JK}^{-1}\text{mol}^{-1}$ )

## Sodium Undecanoate

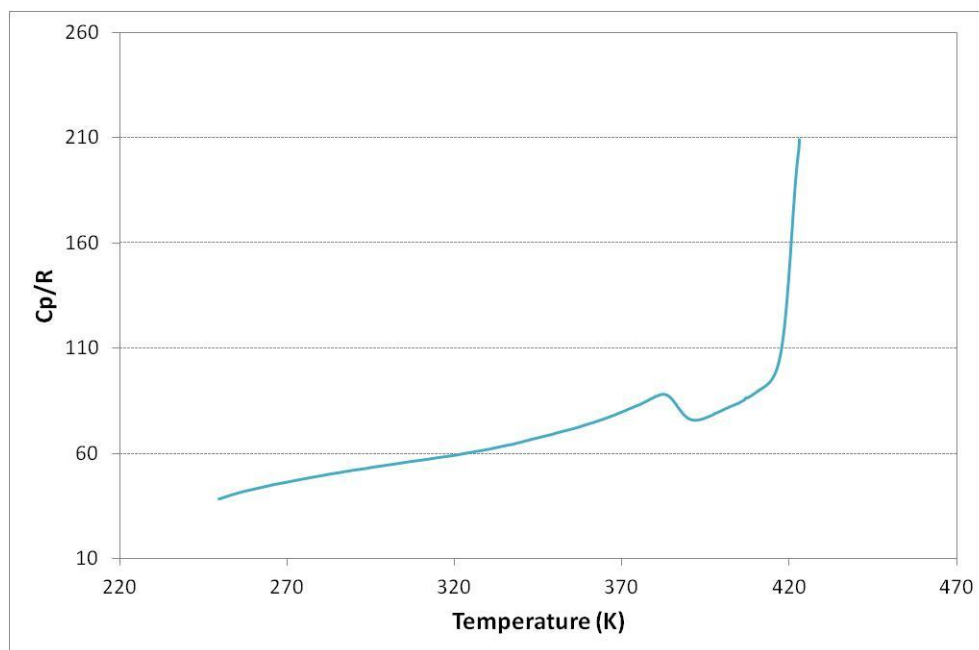


Figure S 121. Experimental molar heat capacities for Na-undecanoate ( $R = 8.31451 \text{ JK}^{-1} \text{ mol}^{-1}$ )

## Sodium Dodecanoate (laurate)

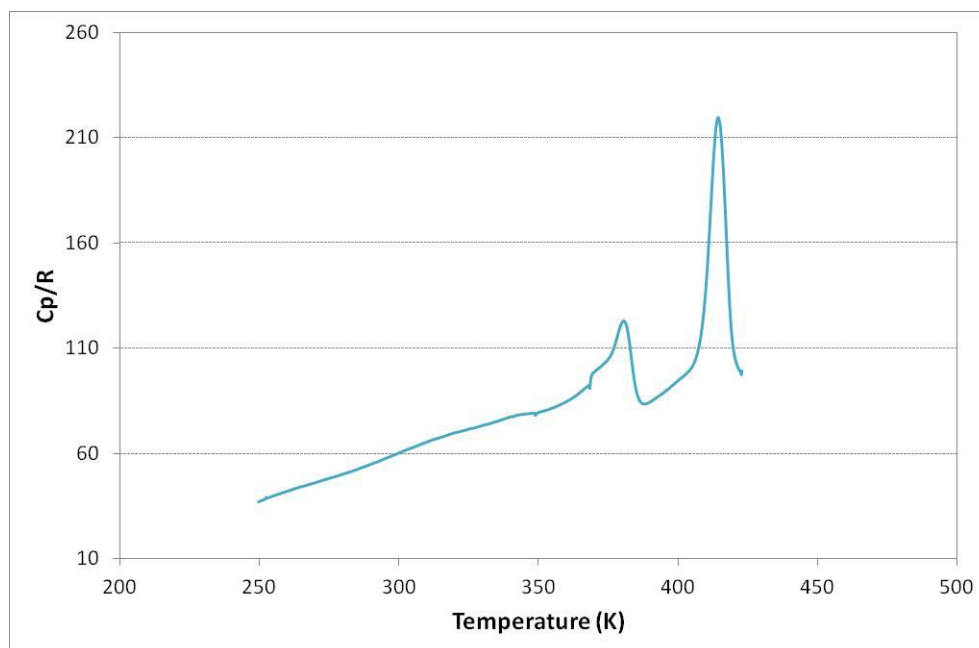


Figure S 122. Experimental molar heat capacities for Na-dodecanoate ( $R = 8.31451 \text{ JK}^{-1} \text{ mol}^{-1}$ )

## Potassium C<sub>1</sub>-C<sub>12</sub> *n*-alkanoates: Thermal behavior from –30 to 600 °C

The primary aim of the investigation was to study thermal behaviour. The spectroscopic data was employed to support the thermal investigation. The reasoning behind the collection of the spectroscopic data was as follows:

- (a) Infrared (IR) spectroscopy is sensitive for the detection of carbonyl and carboxylate compounds. It could therefore be used to confirm synthesis of the potassium carboxylates, as well as provide an indication of purity. Synthesis was performed with a 2 % molar excess of carboxylic acid and if the acid was not completely removed during purification, it would be visible on the infrared spectrum.
- (b) IR spectroscopy was also employed to determine whether chemical changes took place during calorimetry. Once a thermal event was observed, a sample was run to a temperature just above the temperature of the observed thermal event and the IR spectrum of the sample thus treated was collected and compared with the starting material.
- (c) IR and Ultraviolet-Visible (UV-Vis) spectra were collected in the hope of finding explanations for differences in thermal behaviour, and in the hope that additional information about the nature of the potassium carboxylates can be deduced.

## IR Spectra

### Potassium methanoate (formate)

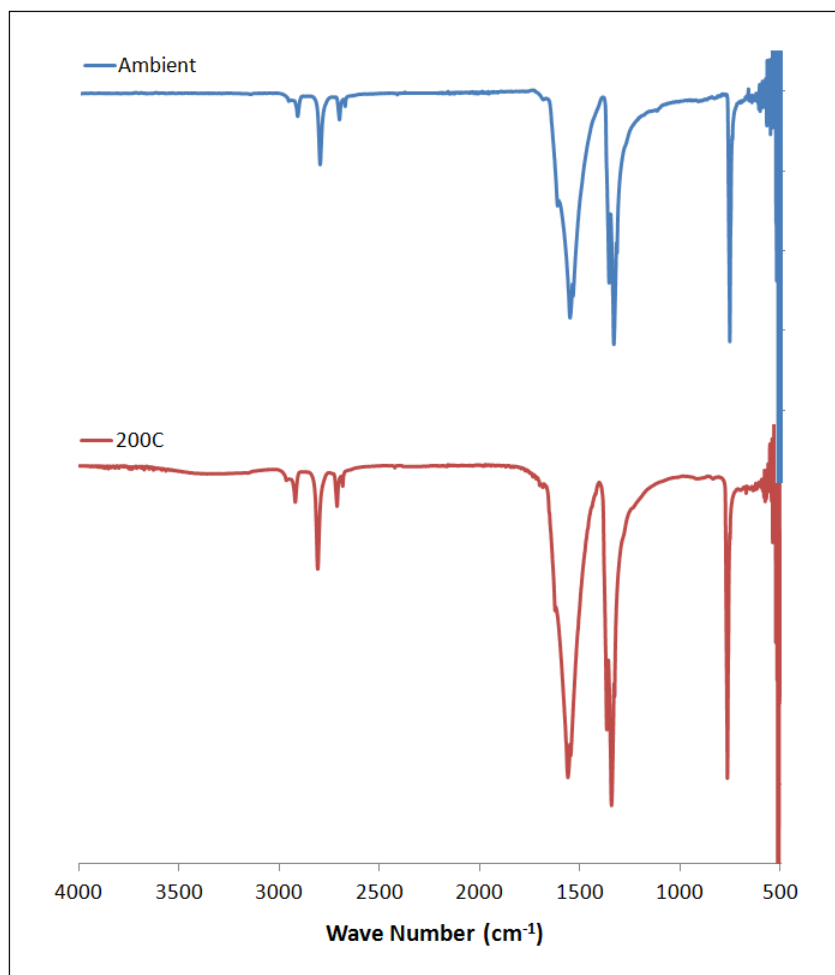
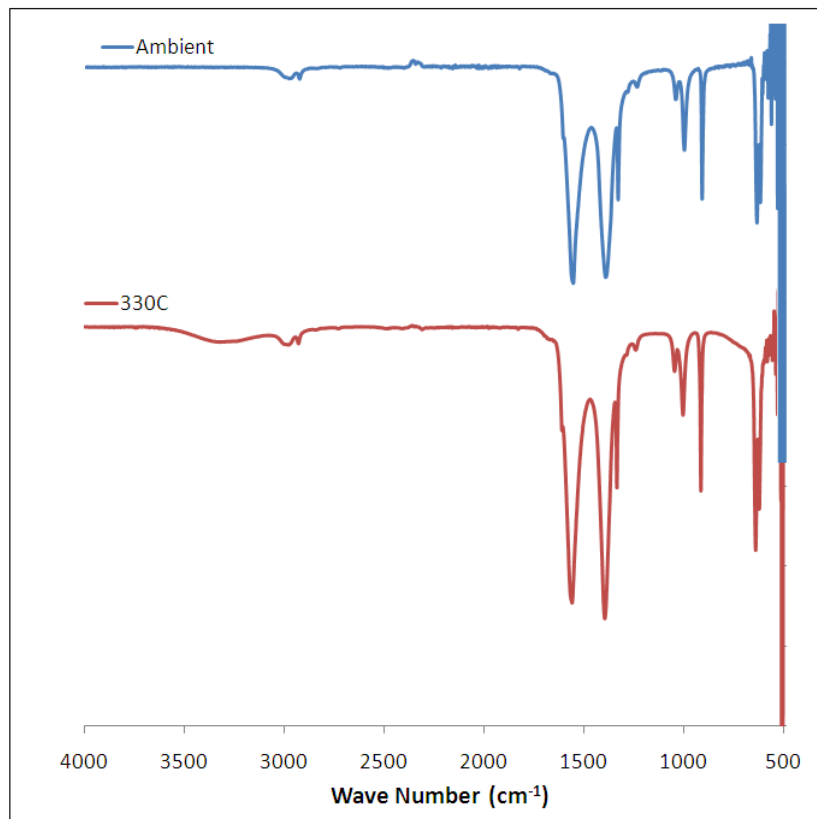


Figure S 123. IR spectrum of potassium methanoate before and after melting

**Potassium ethanoate (acetate)**



**Figure S 124. IR spectrum of potassium ethanoate before and after melting.**

## Potassium propanoate

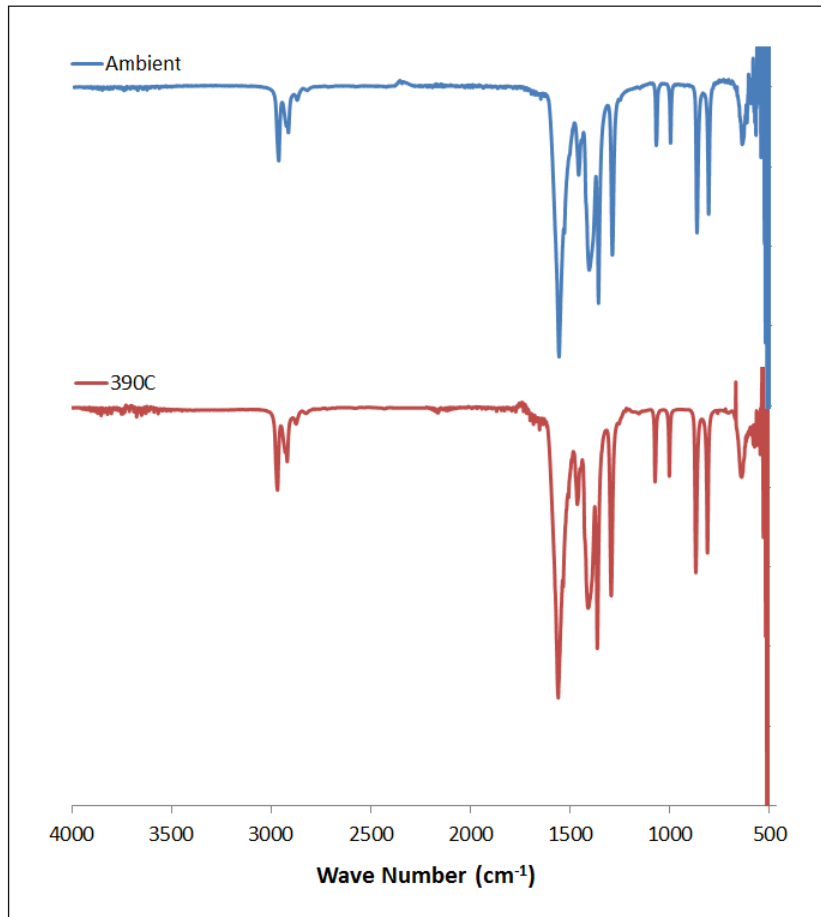
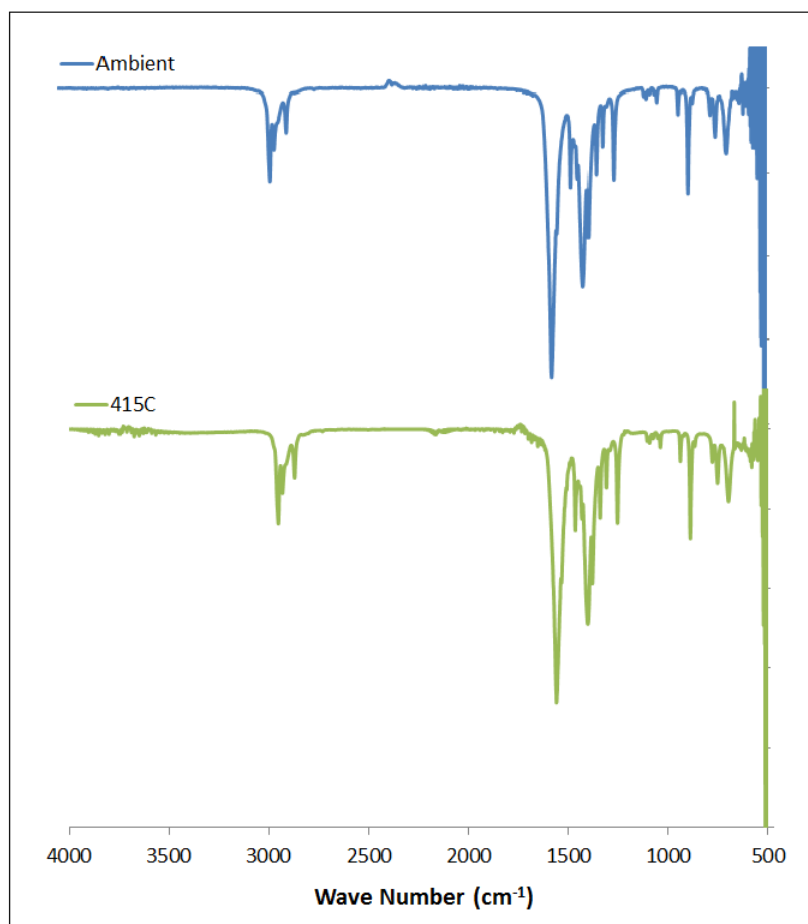


Figure S 125. IR spectrum of potassium propanoate before and after melting.

**Potassium butanoate (butyrate)**



**Figure S 126. IR spectrum of potassium butanoate before and after melting.**

**Potassium pentanoate (valerate)**

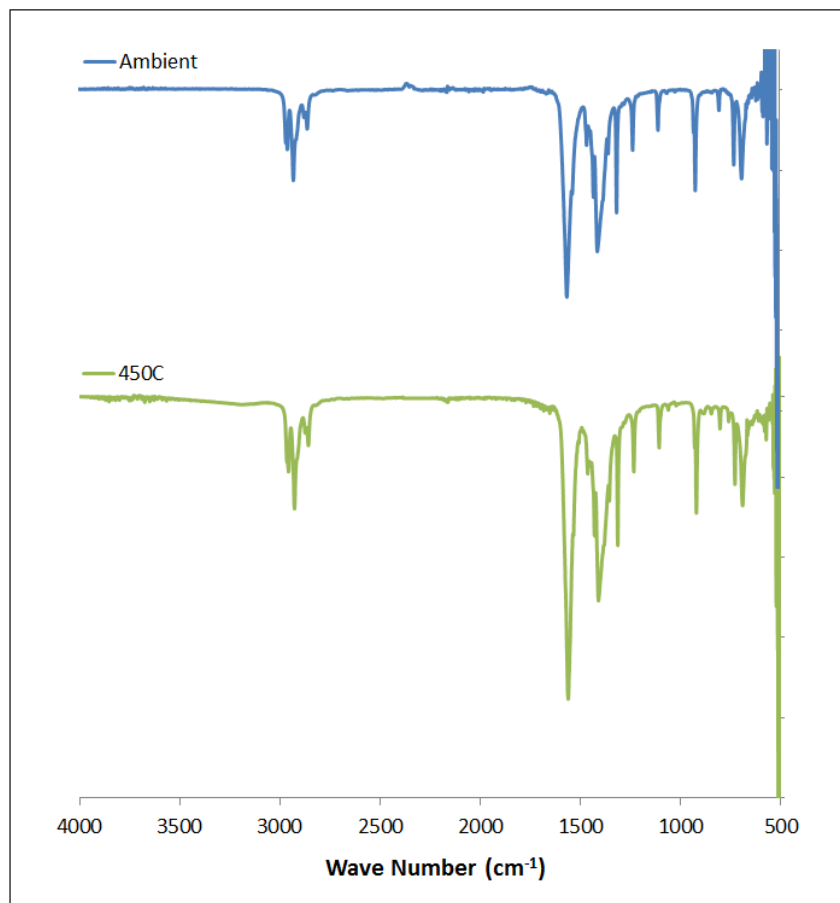


**Figure S 127. IR spectrum of potassium pentanoate before and after melting.**

## Potassium hexanoate (caproate)

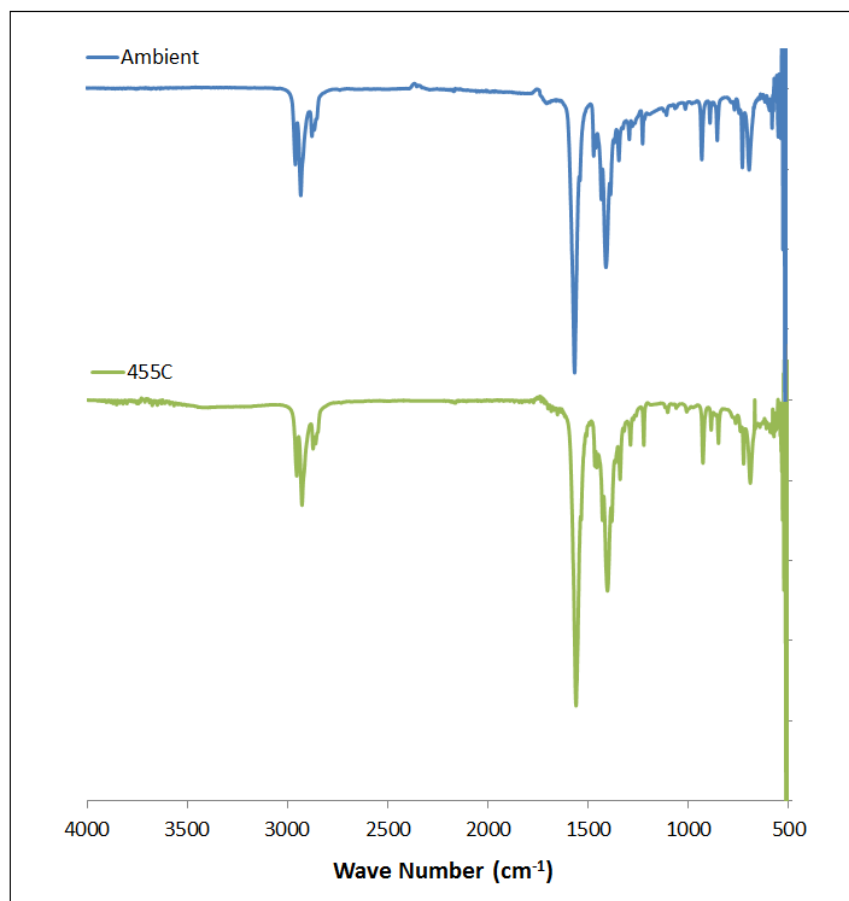


Figure S 128. IR spectrum of potassium hexanoate before and after melting.

## Potassium heptanoate

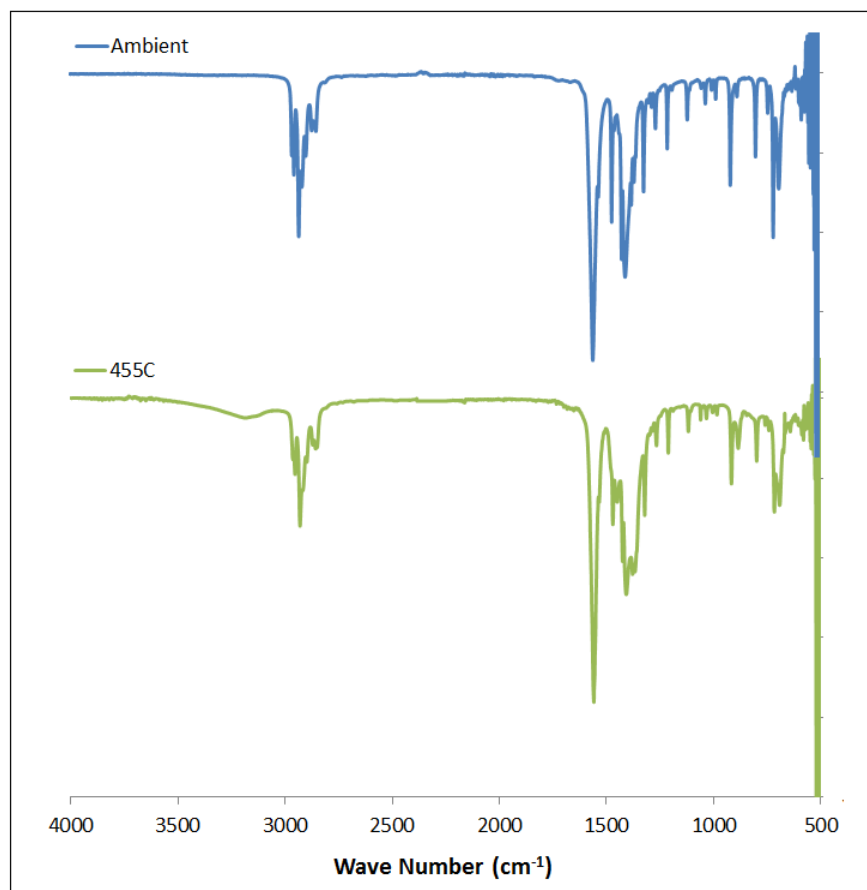


Figure S 129. IR spectrum of potassium heptanoate before and after melting.

## Potassium octanoate (caprylate)

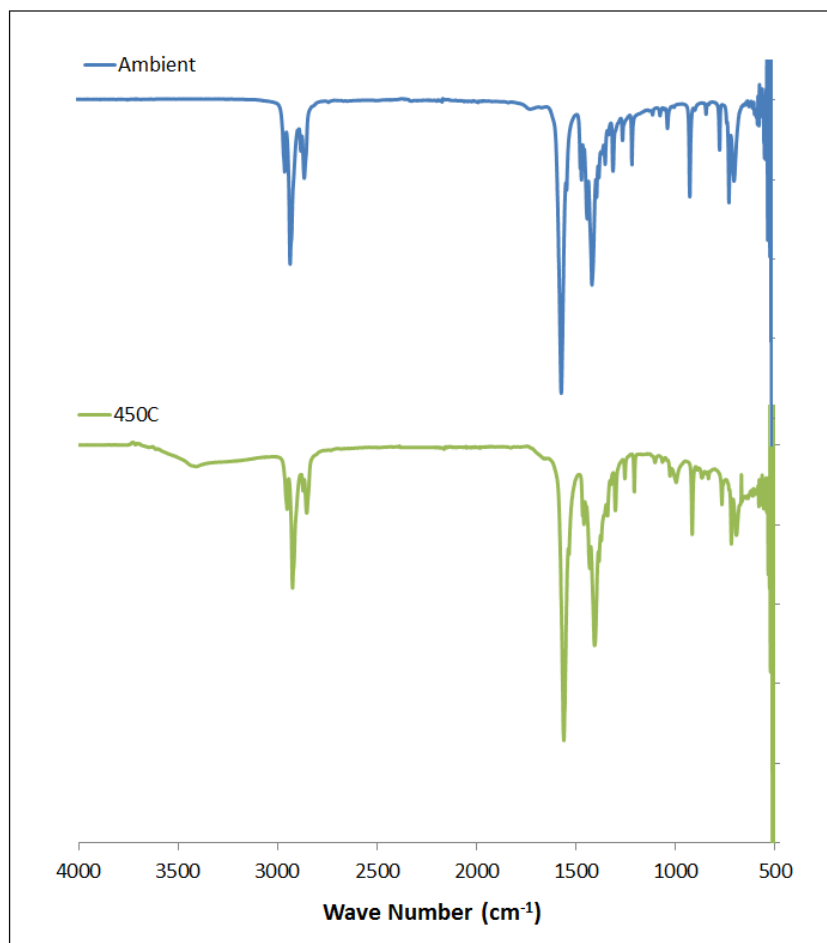


Figure S 130. IR spectrum of potassium octanoate before and after melting.

## Potassium nonanoate (pelargonate)

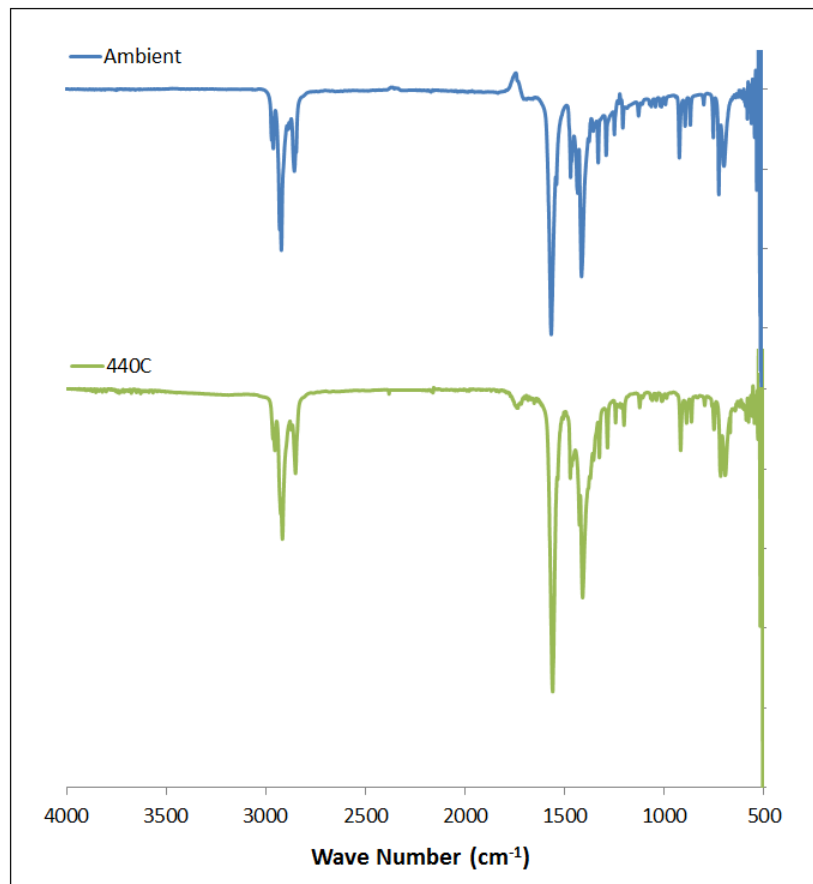


Figure S 131. IR spectrum of potassium nonanoate before and after melting.

## Potassium decanoate (caprate)

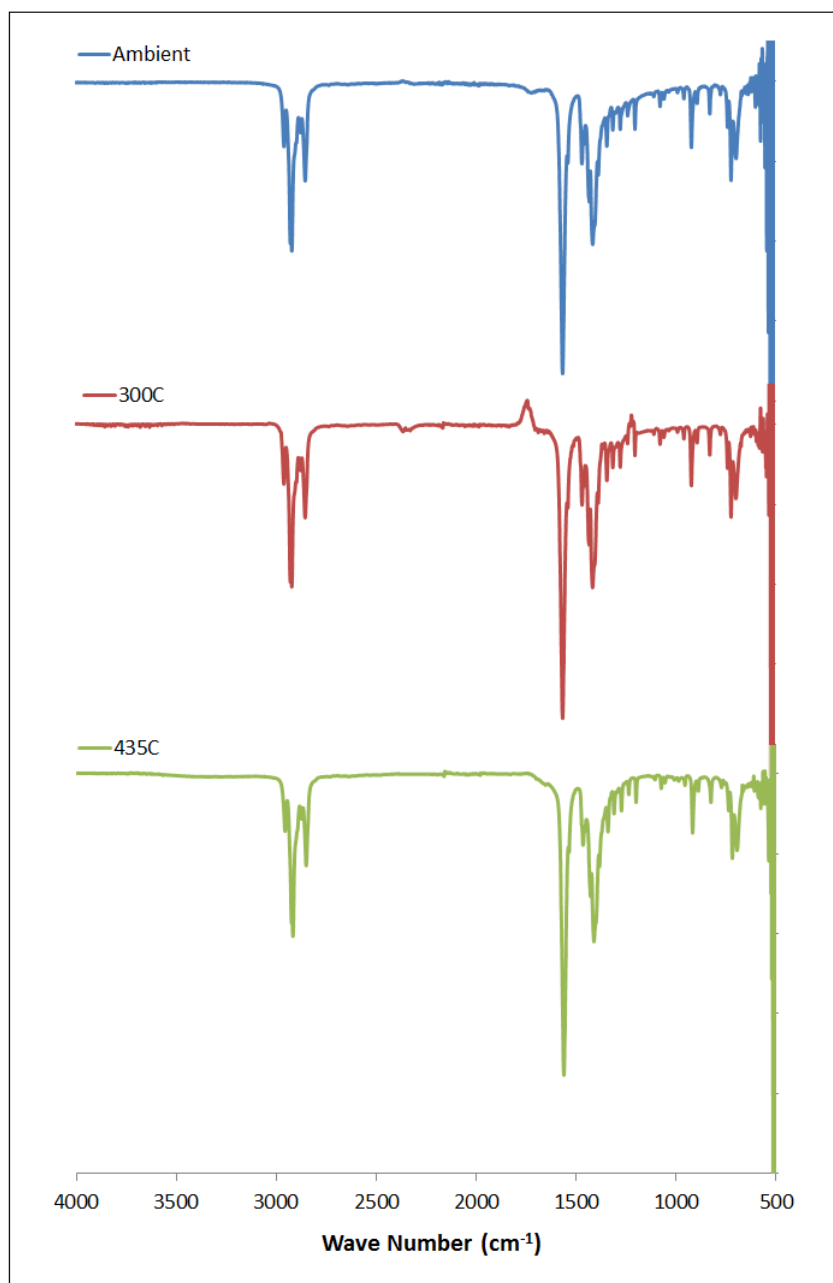


Figure S 132. IR spectrum of potassium decanoate before and after melting.

## Potassium undecanoate

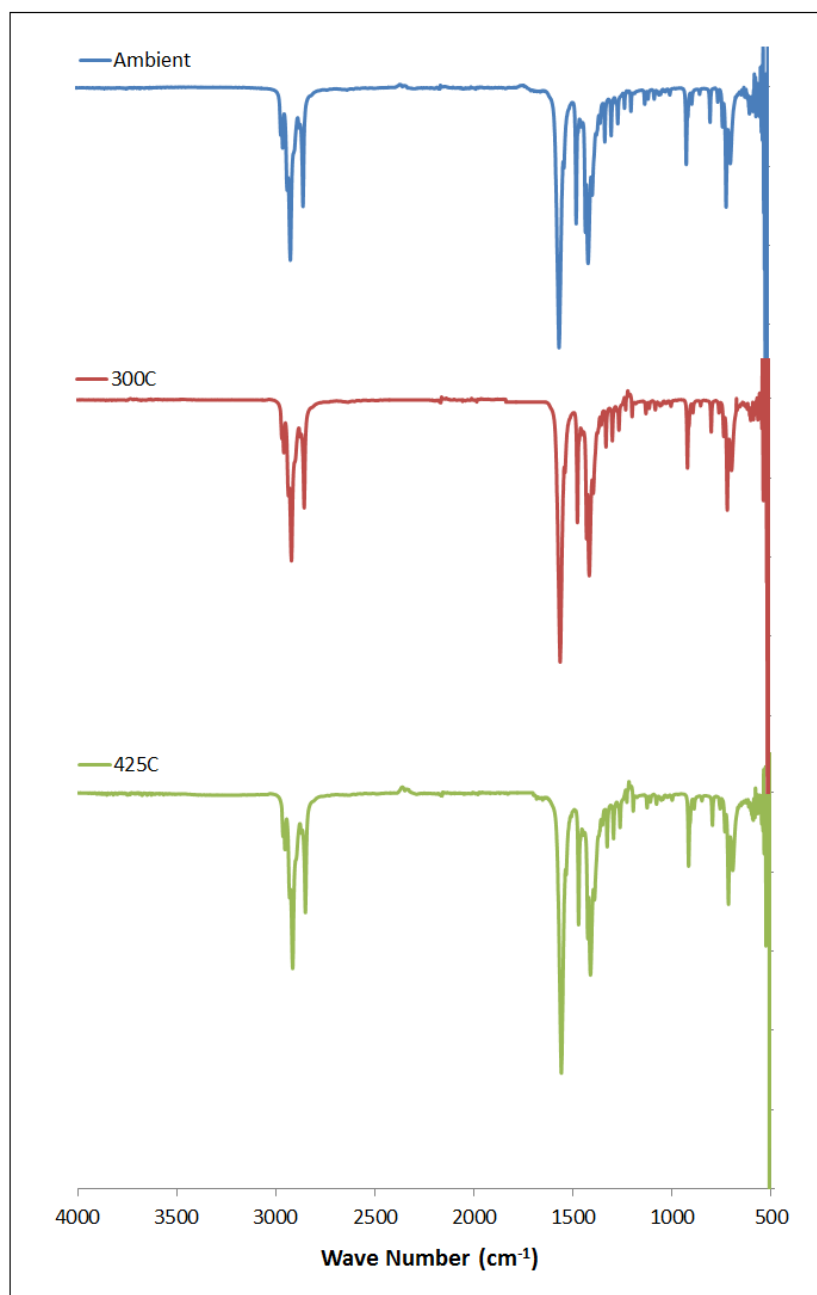


Figure S 133. IR spectrum of potassium undecanoate before and after melting.

## Potassium dodecanoate (laurate)

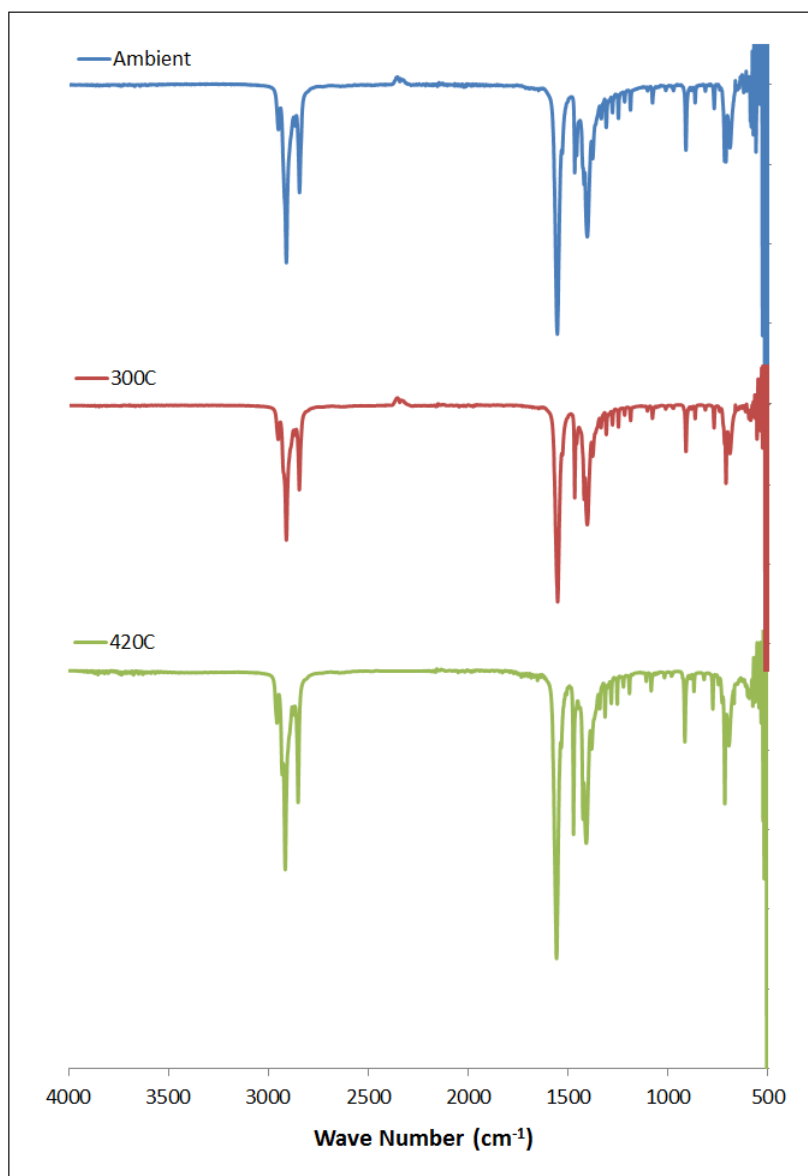


Figure S 134. IR spectrum of potassium dodecanoate before and after melting.

## UV-Vis Spectra

### Potassium Methanoate

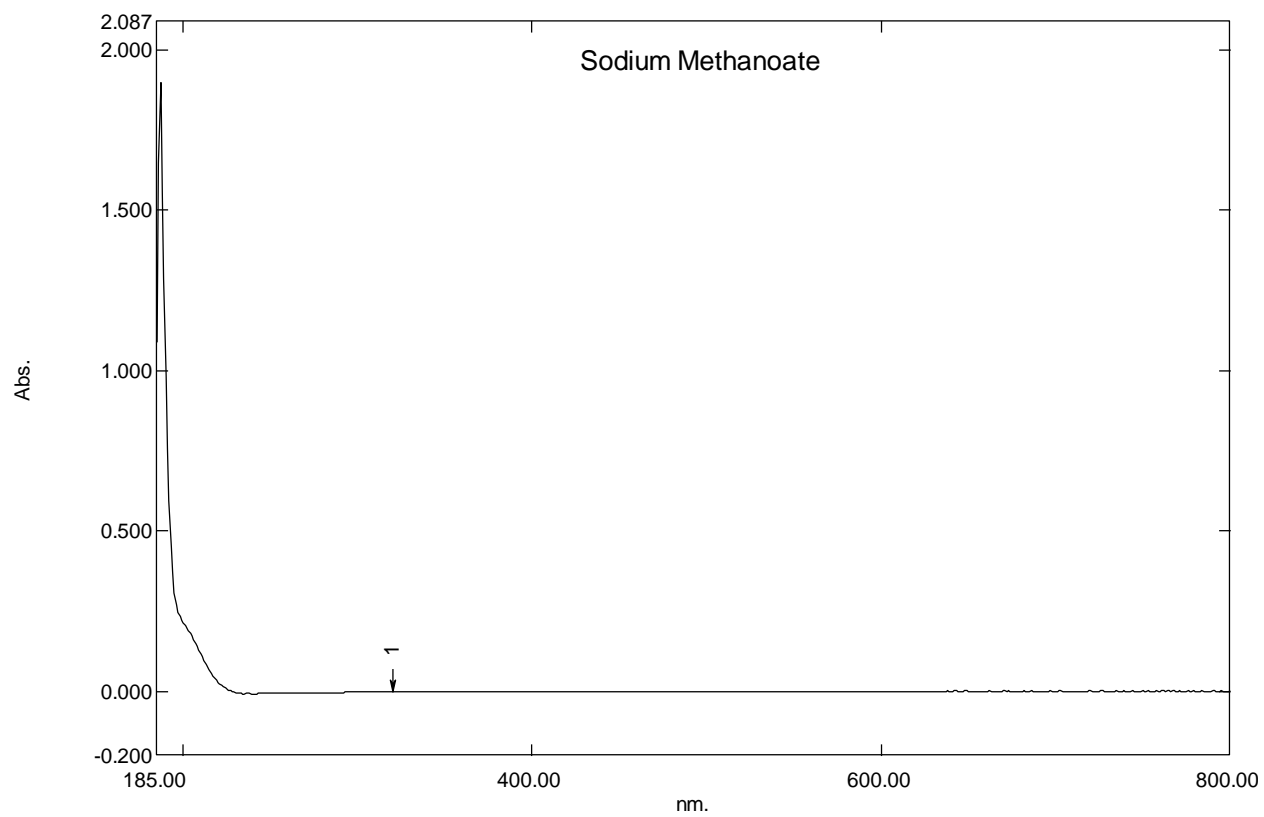


Figure S 135. UV-Vis spectrum of potassium methanoate

# Potassium Ethanoate

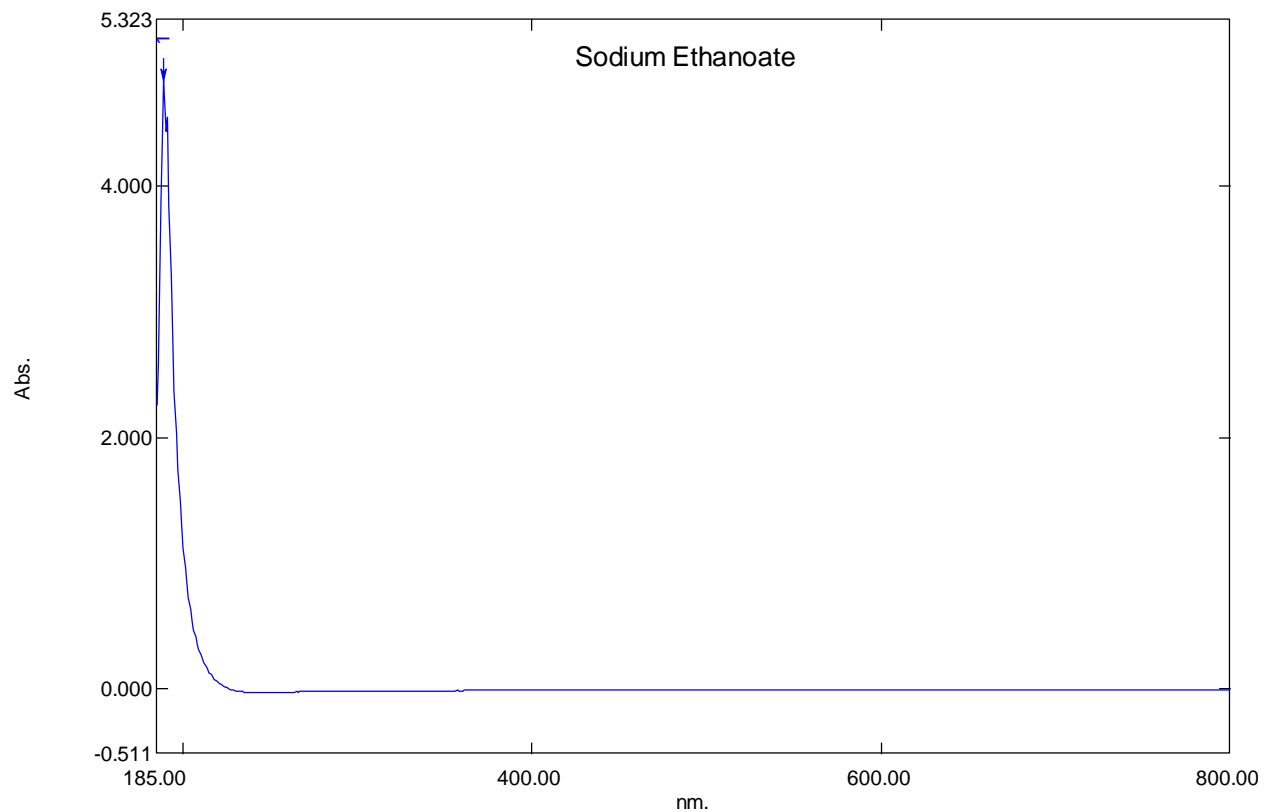


Figure S 136. UV-Vis spectrum of potassium ethanoate

# Potassium Propanoate

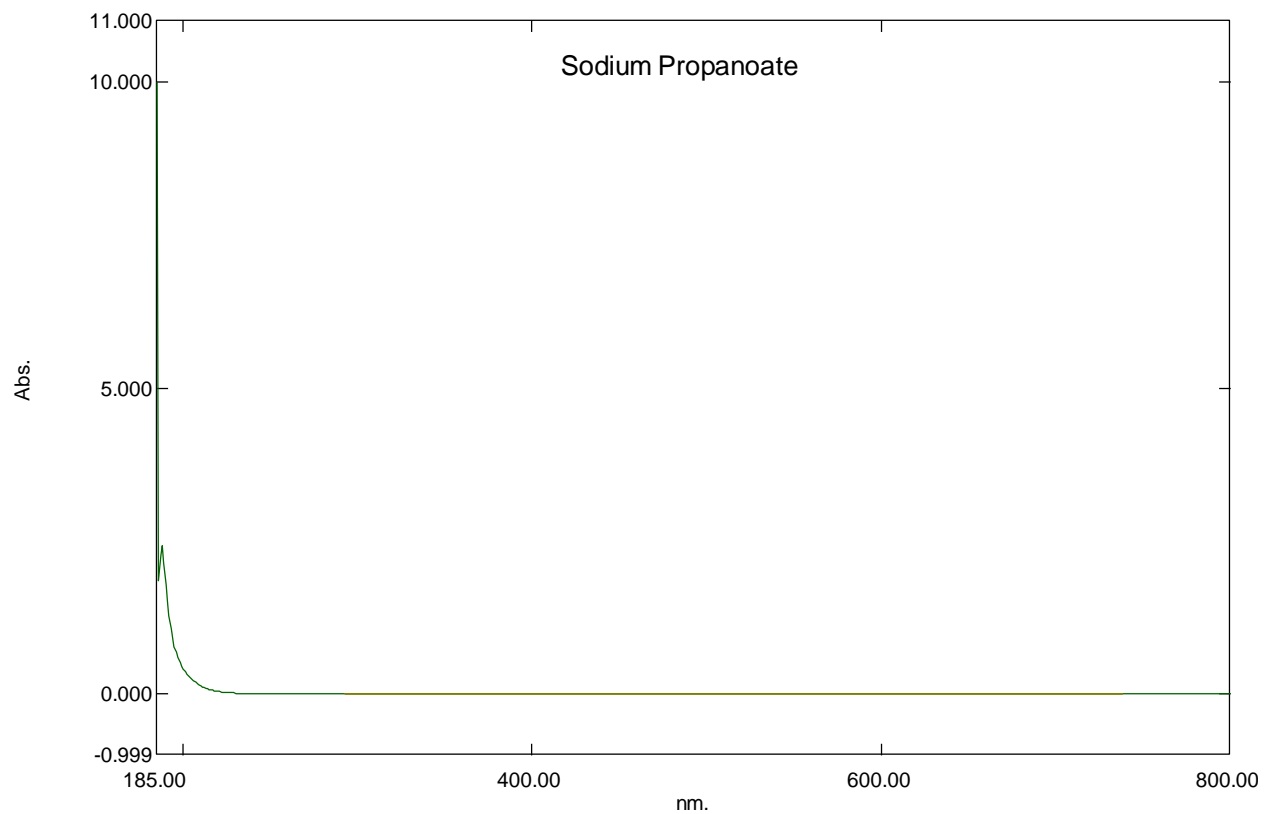
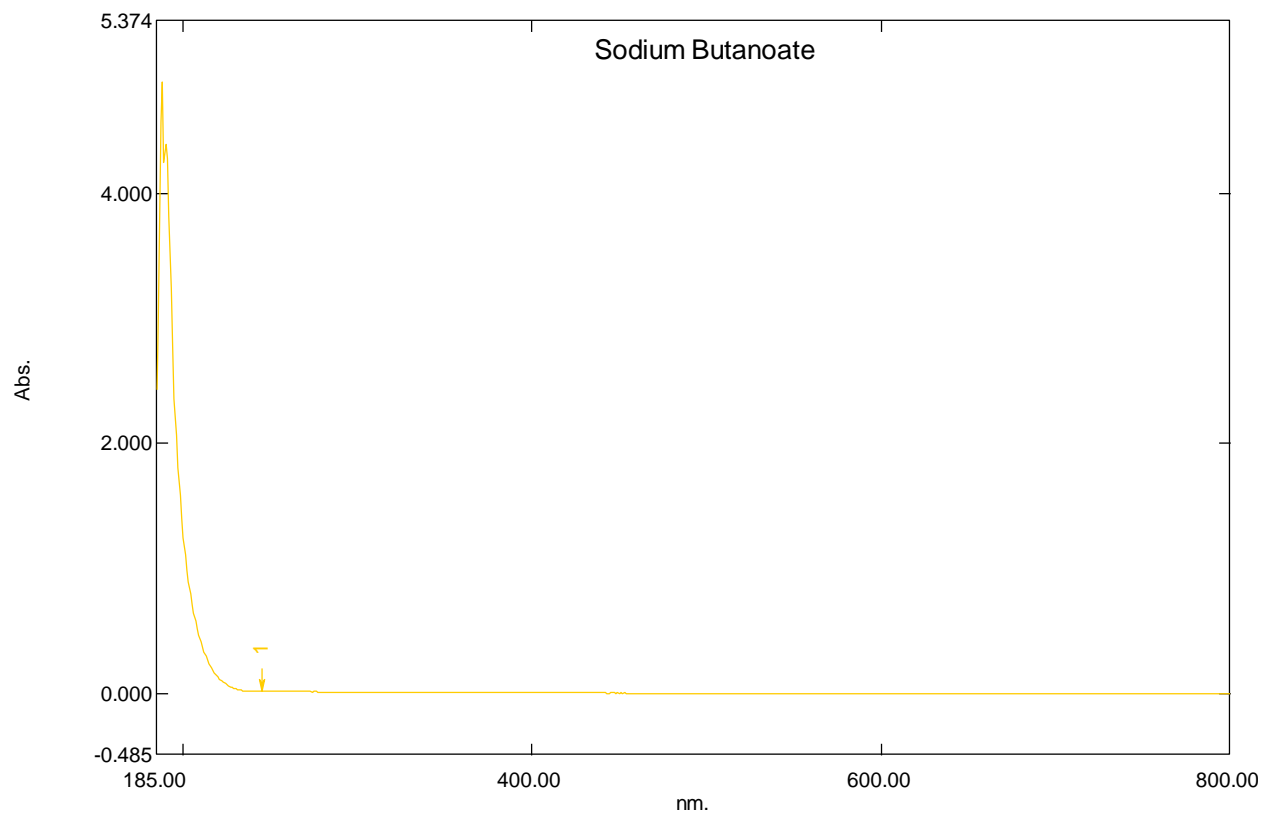


Figure S 137. UV-Vis spectrum of potassium propanoate

**Potassium Butanoate (butyrate)**



**Figure S 138. UV-Vis spectrum of potassium butanoate**

**Potassium Pentanoate (valerate)**

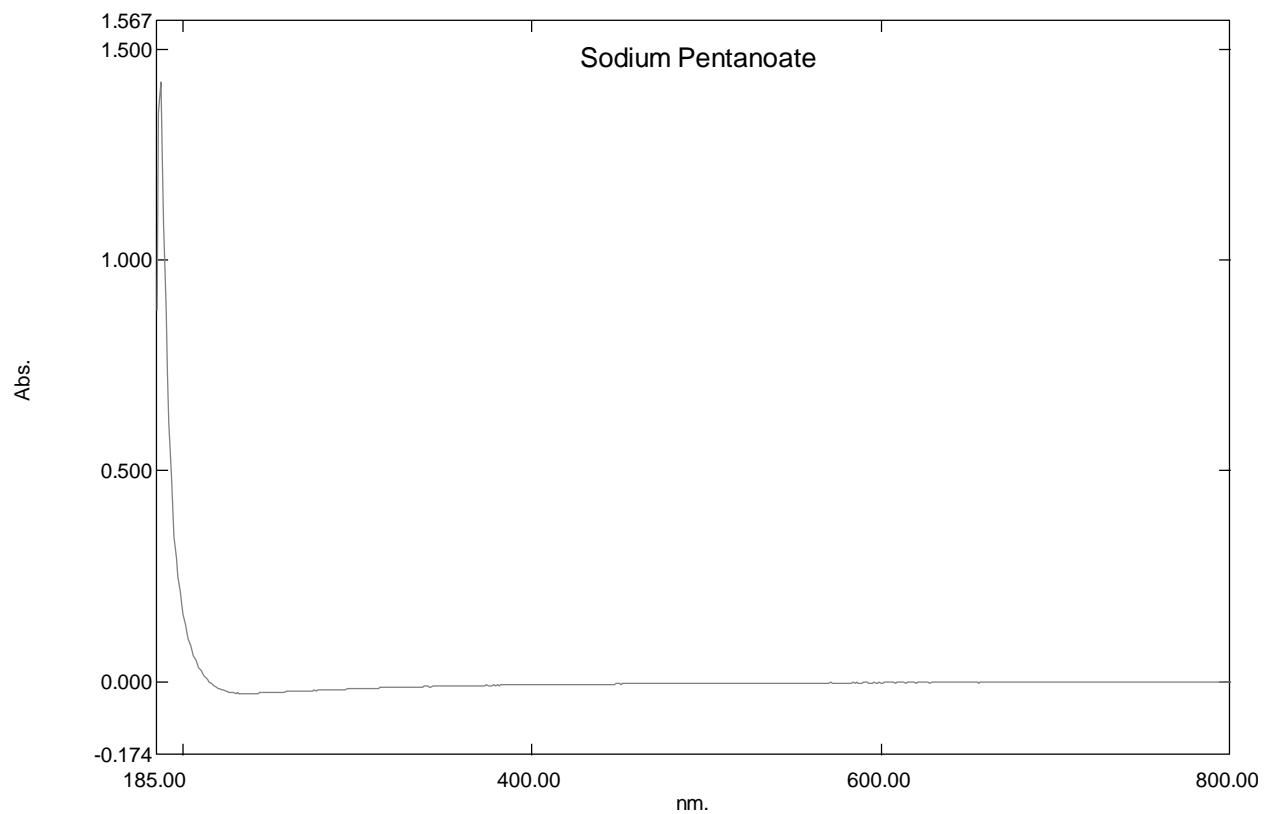


**Figure S 139. UV-Vis spectrum of potassium pentanoate**

## Potassium Hexanoate (caproate)

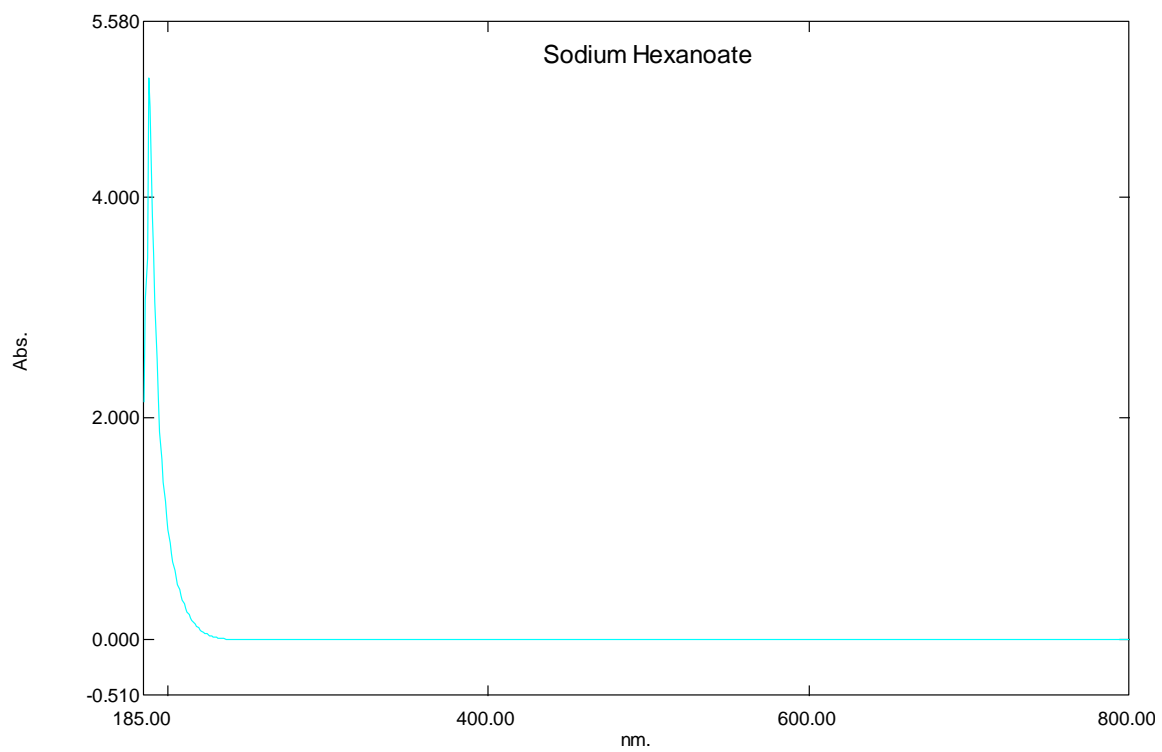


Figure S 140. UV-Vis of potassium hexanoate

# Potassium Heptanoate

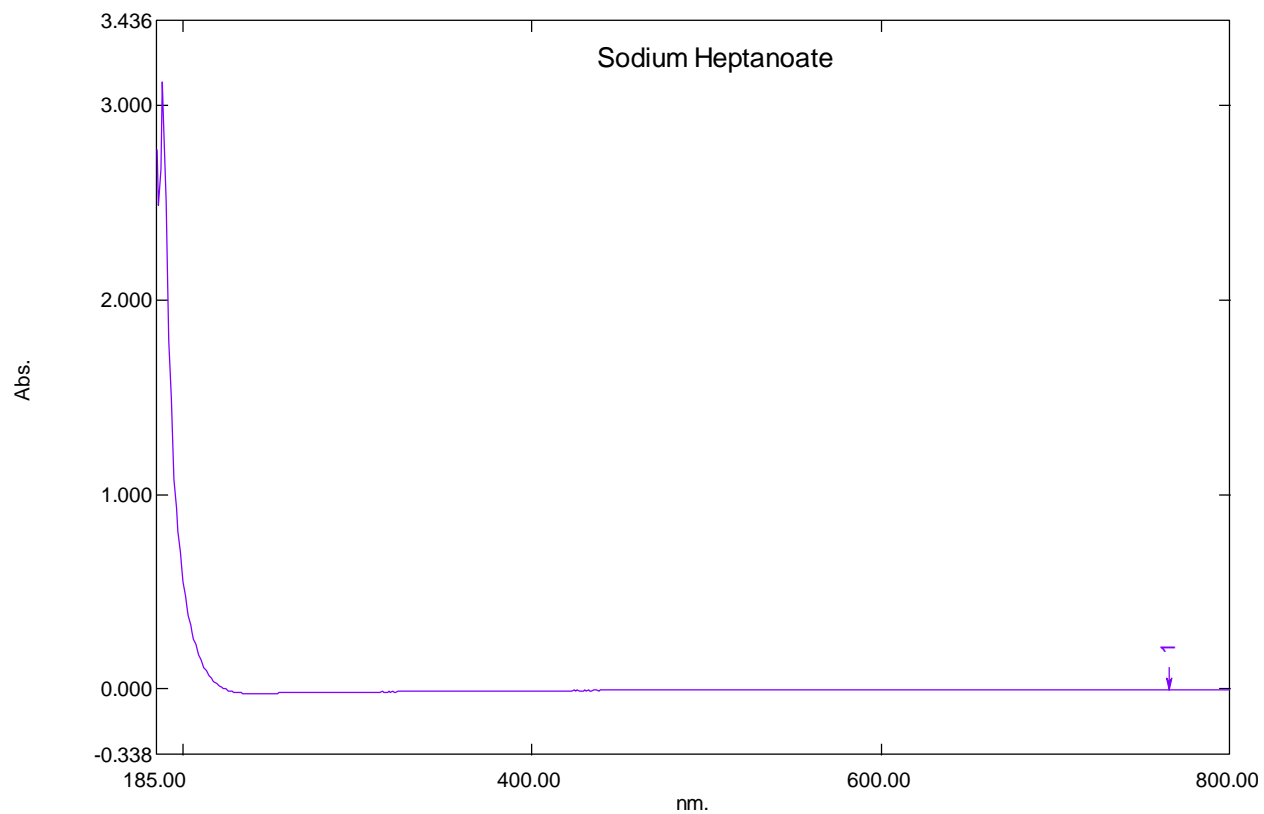


Figure S 141. UV-Vis spectrum of potassium heptanoate

# Potassium Octanoate (caprylate)

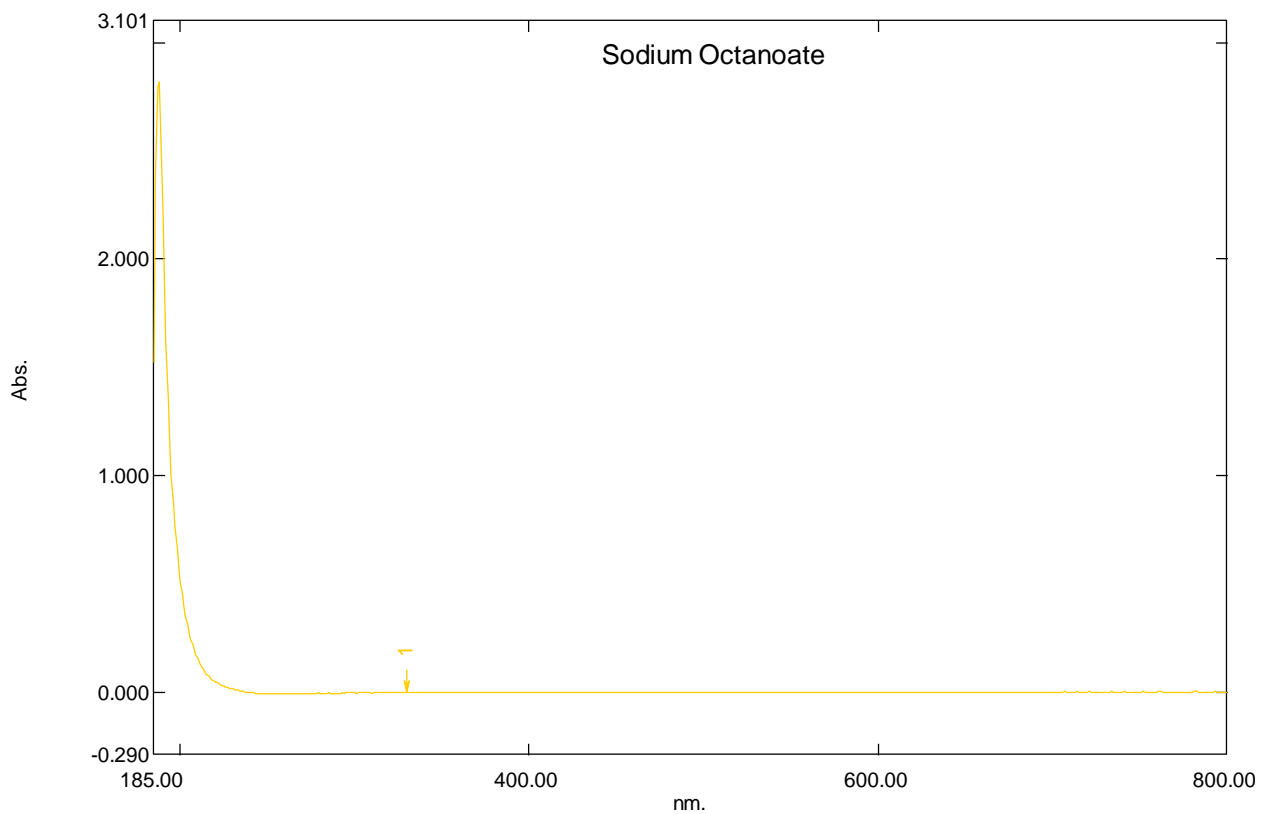
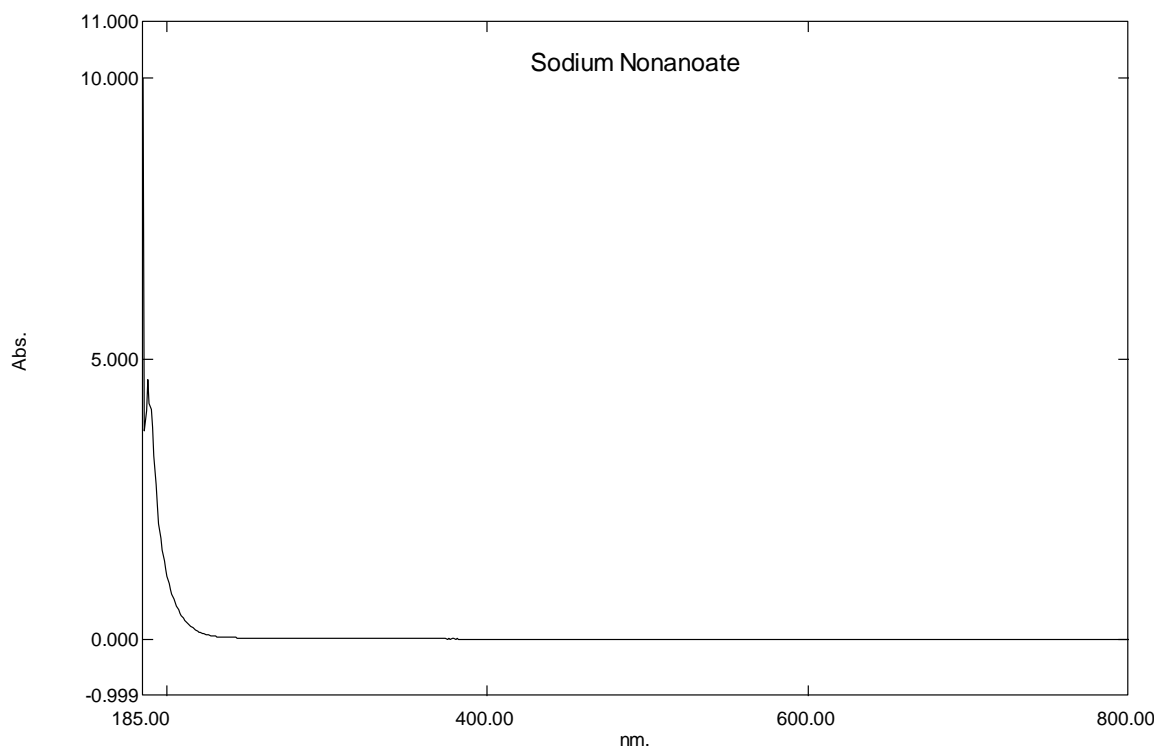


Figure S 142. UV-Vis of potassium octanoate

**Potassium Nonanoate (pelargonate)**



**Figure S 143. UV-Vis of potassium nonanoate**

# Potassium Decanoate (caprate)

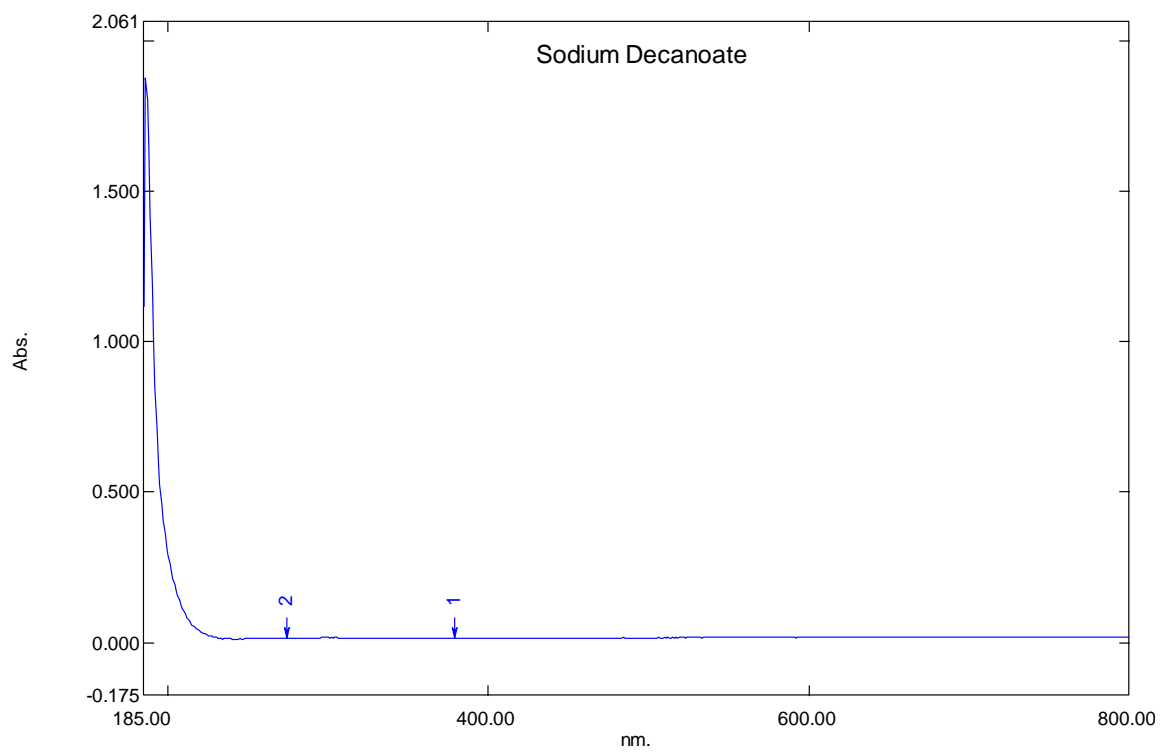


Figure S 144. UV-Vis of potassium decanoate

# Potassium Undecanoate

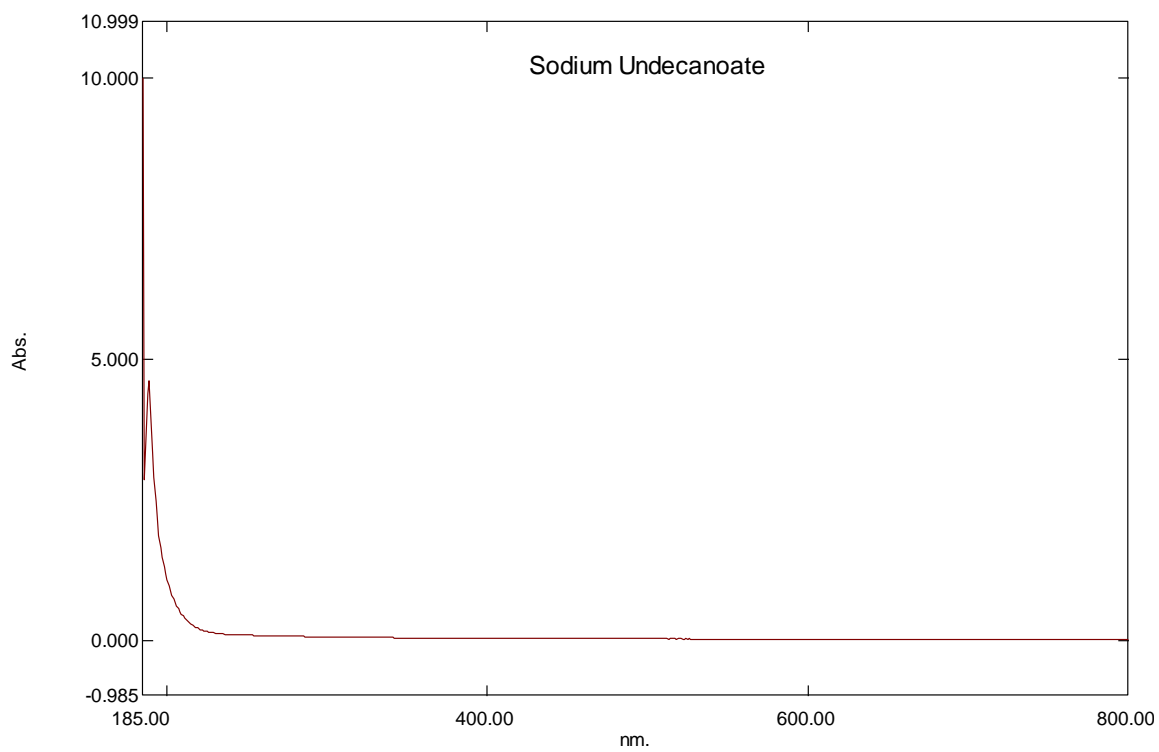


Figure S 145. UV-Vis of potassium undecanoate

# Potassium Dodecanoate (laurate)

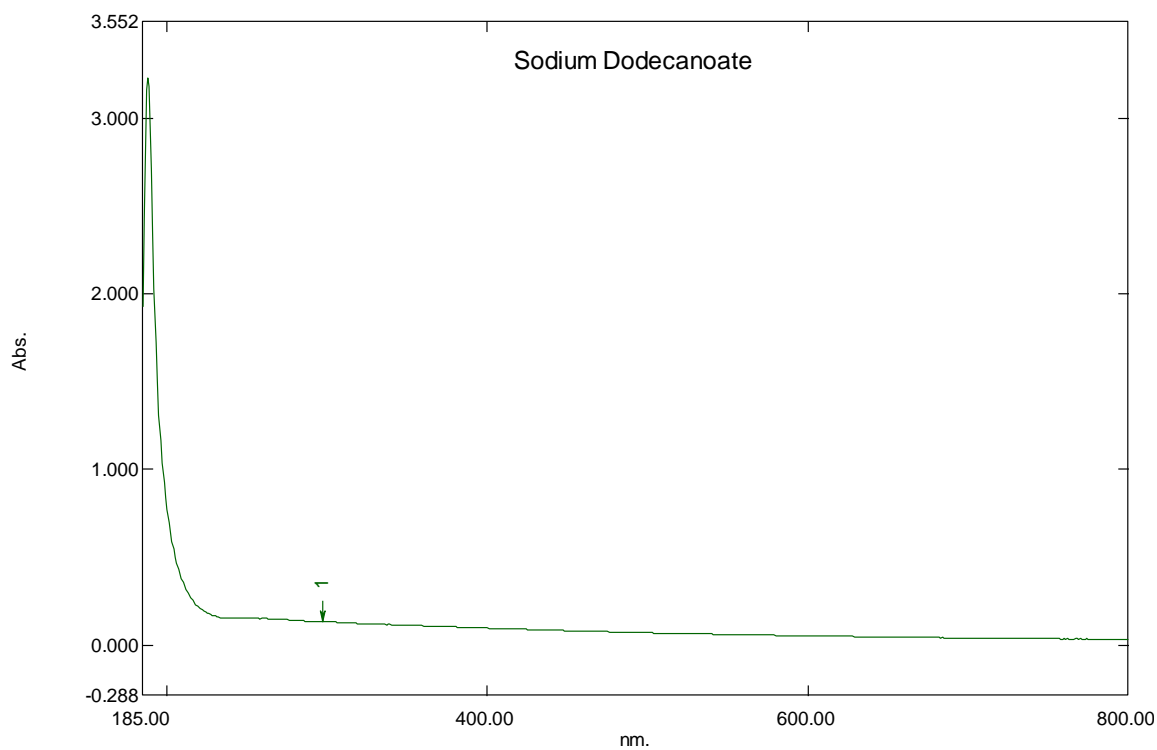


Figure S 146. UV-Vis of potassium dodecanoate

## TGA Results

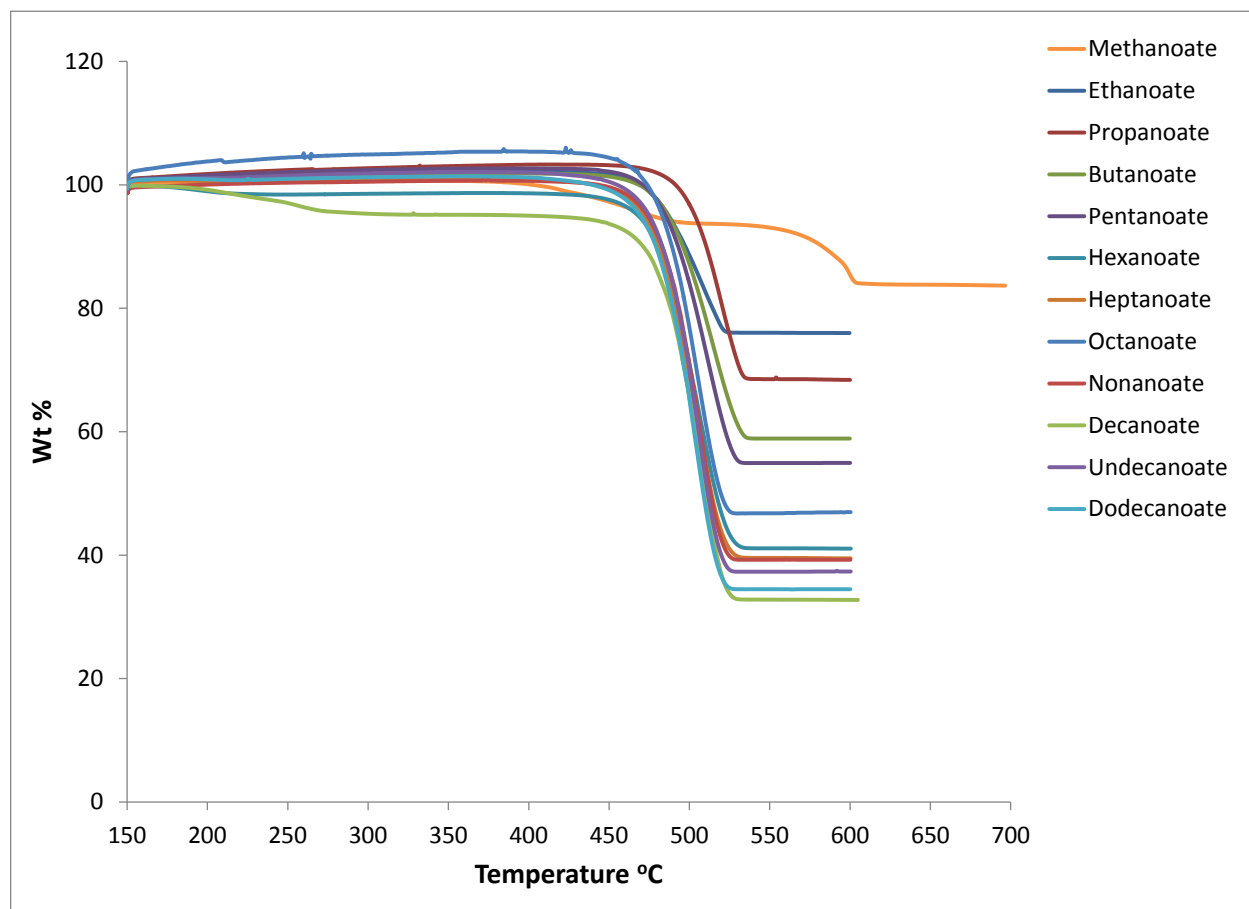


Figure S 147. TGA profile of K-carboxylates

## Calorigrams of K-Carboxylates determined by the Differential Scanning Calorimeter (DSC)

### Potassium Methanoate

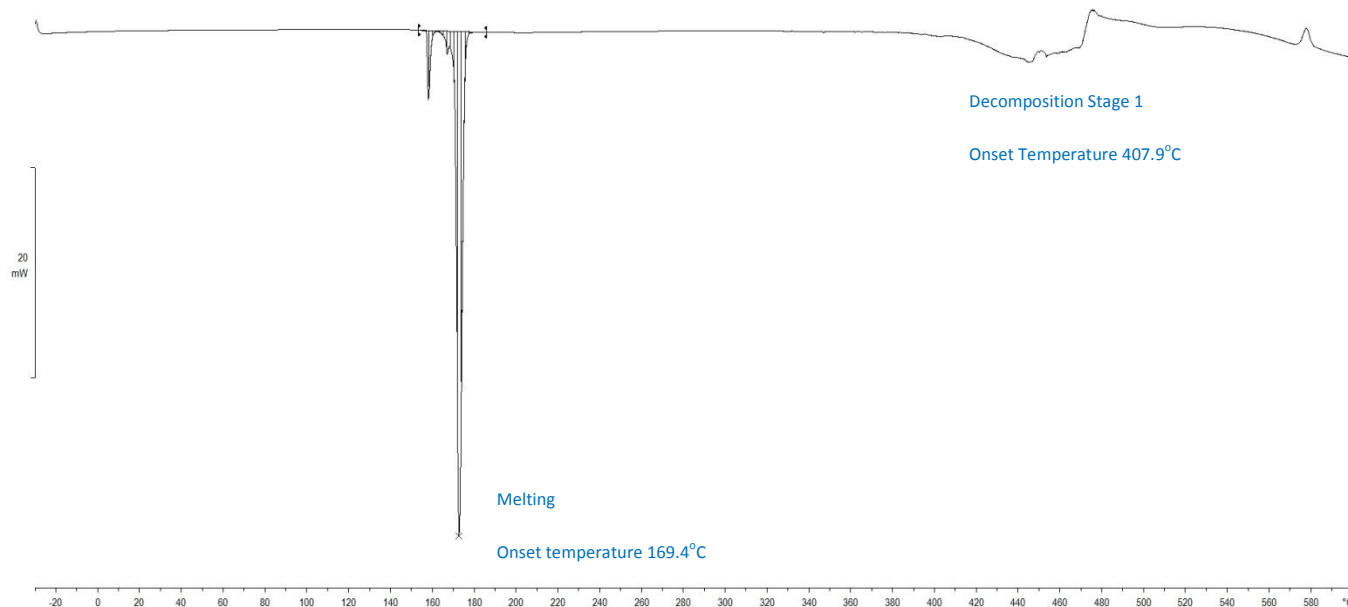


Figure S 148. Calorigram of Potassium Methanoate determined by the DSC over the range of -30-600°C at 10°C min<sup>-1</sup> heating rate and 100mL min<sup>-1</sup> nitrogen flow.

### Potassium Ethanoate

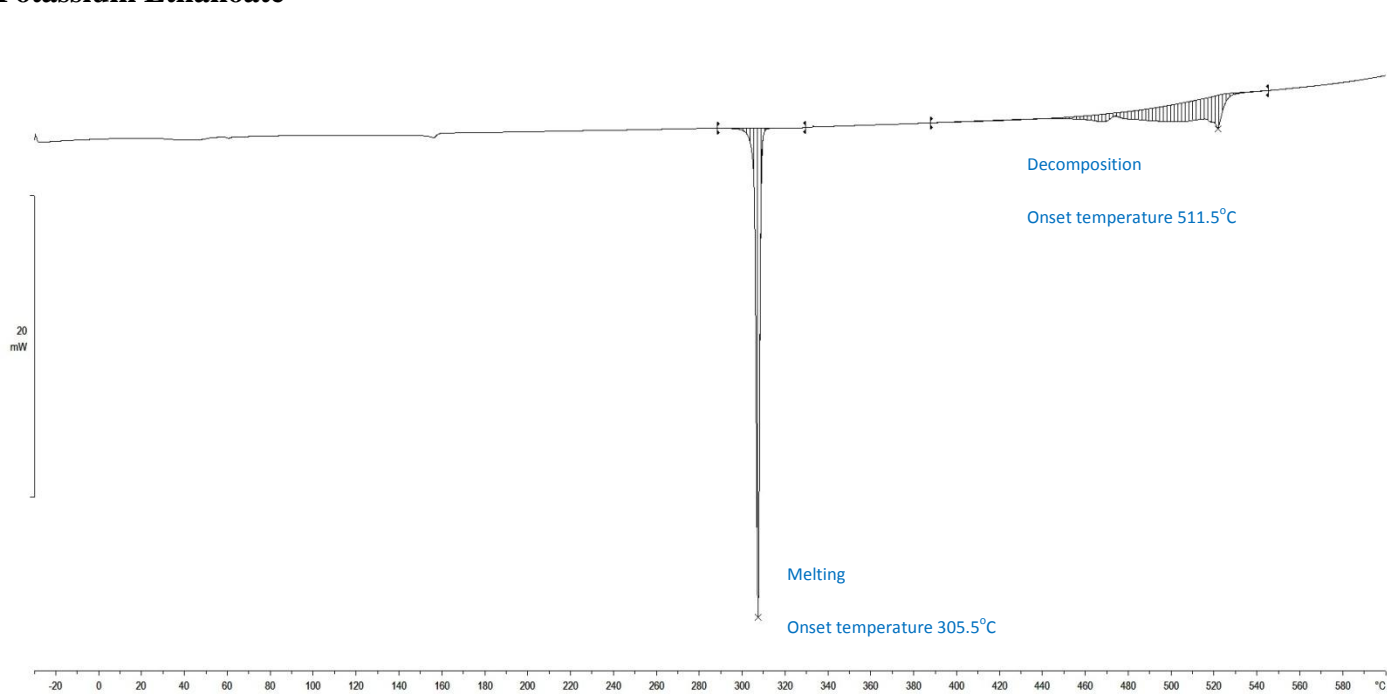


Figure S 149. Calorigram of Potassium Ethanoate determined by the DSC over the range of -30-600°C at 10°C min<sup>-1</sup> heating rate and 100mL min<sup>-1</sup> nitrogen flow.

## Potassium Propanoate

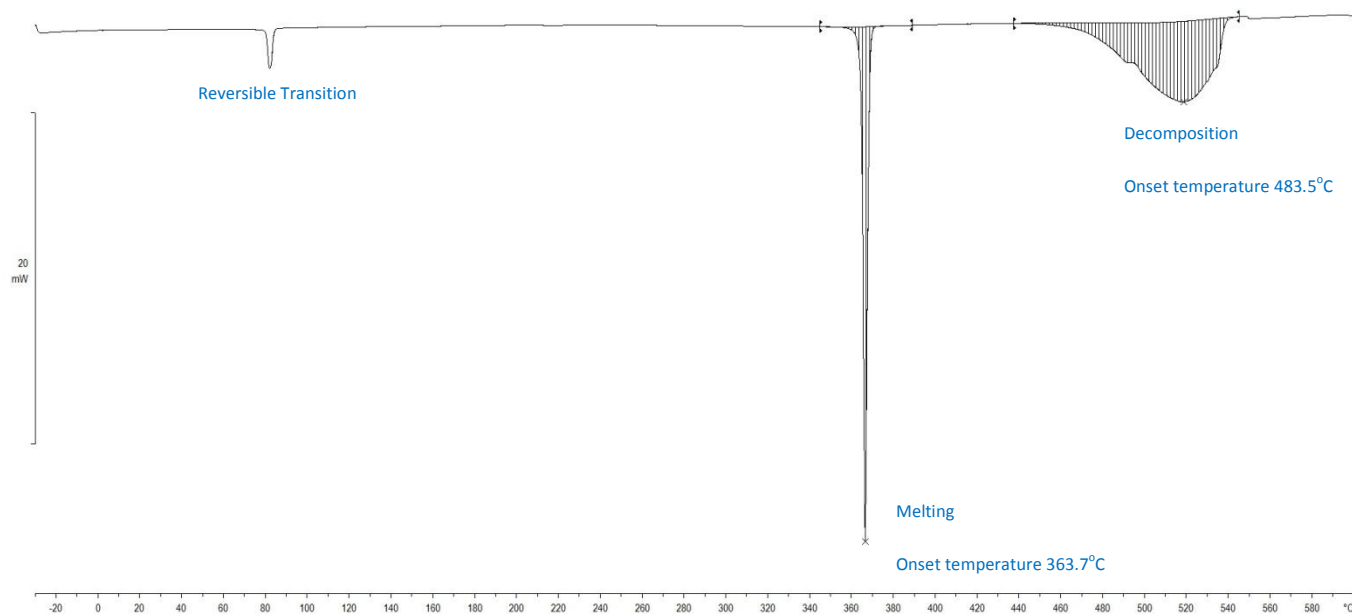


Figure S 150. Calorigram of Potassium Propanoate determined by the DSC over the range of -30-600°C at 10°C min<sup>-1</sup> heating rate and 100mL min<sup>-1</sup> nitrogen flow.

## Potassium Butanoate (butyrate)

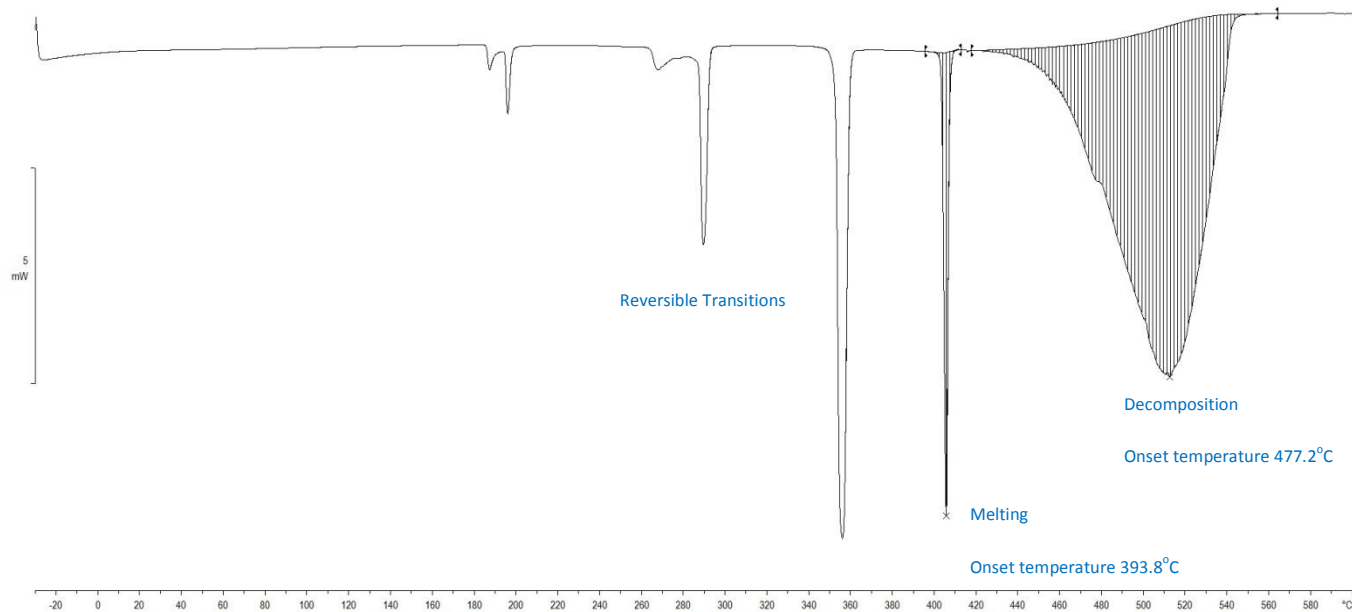


Figure S 151. Calorigram of Potassium Butanoate determined by the DSC over the range of -30-600°C at 10°C min<sup>-1</sup> heating rate and 100mL min<sup>-1</sup> nitrogen flow.

### Potassium Pentanoate (valerate)

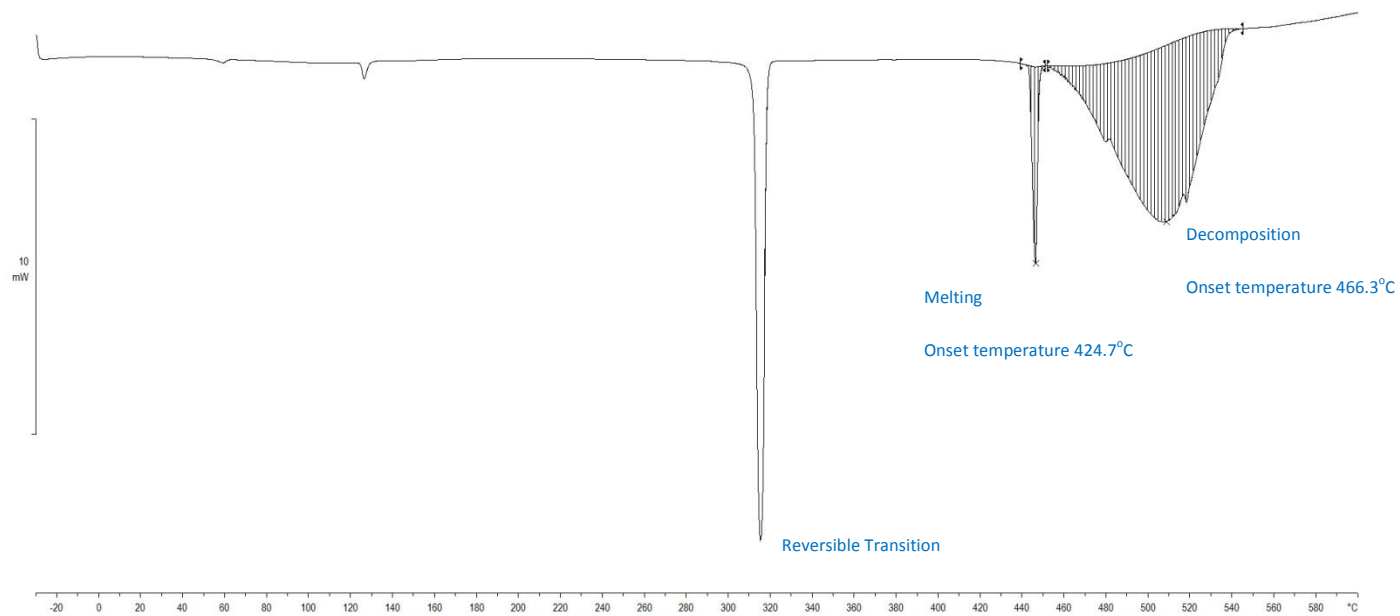


Figure S 152. Calorigram of Potassium Pentanoate determined by the DSC over the range of -30-600°C at 10°C·min<sup>-1</sup> heating rate and 100mL·min<sup>-1</sup> nitrogen flow.

### Potassium Hexanoate (caproate)

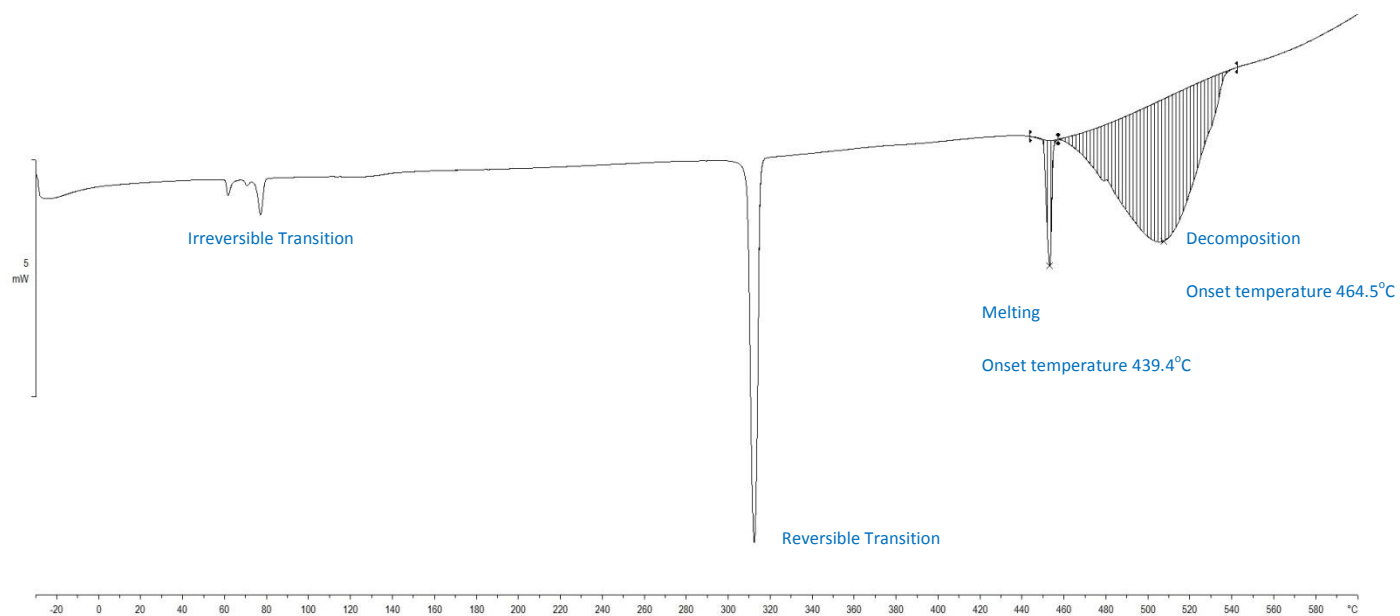


Figure S 153. Calorigram of Potassium Hexanoate determined by the DSC over the range of -30-600°C at 10°C·min<sup>-1</sup> heating rate and 100mL·min<sup>-1</sup> nitrogen flow.

## Potassium Heptanoate

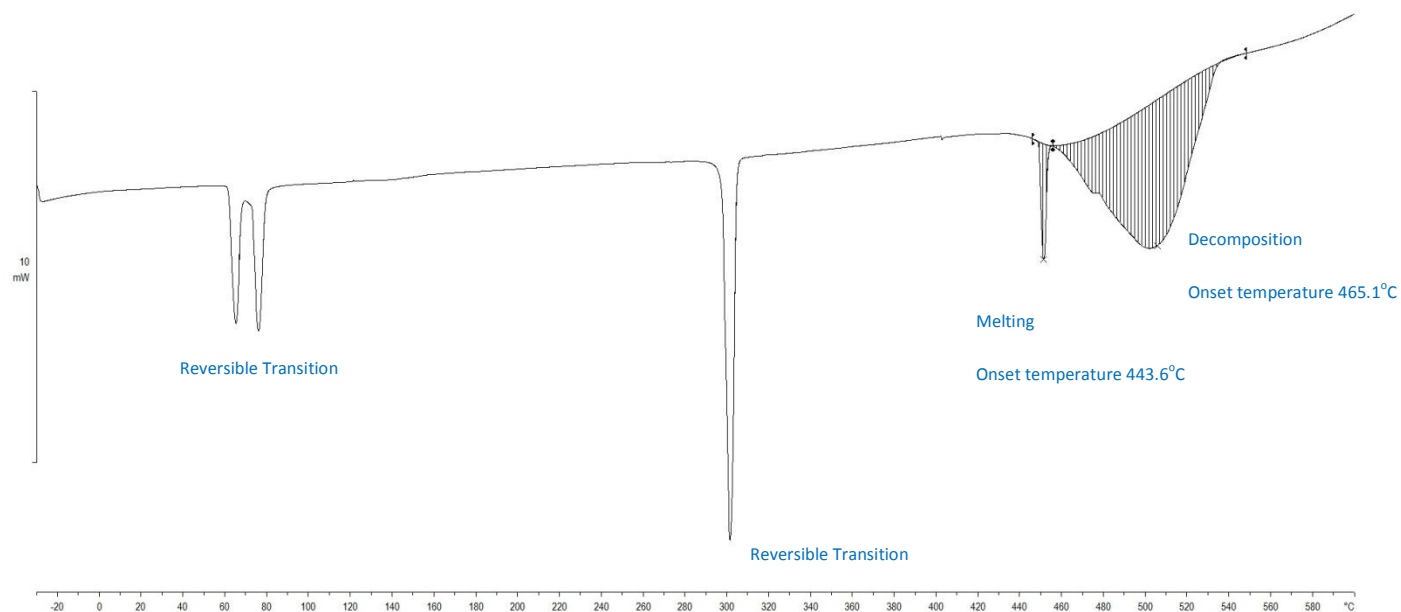


Figure S 154. Calorigram of Potassium Heptanoate determined by the DSC over the range of -30-600°C at 10°C·min<sup>-1</sup> heating rate and 100mL·min<sup>-1</sup> nitrogen flow.

## Potassium Octanoate (caprylate)

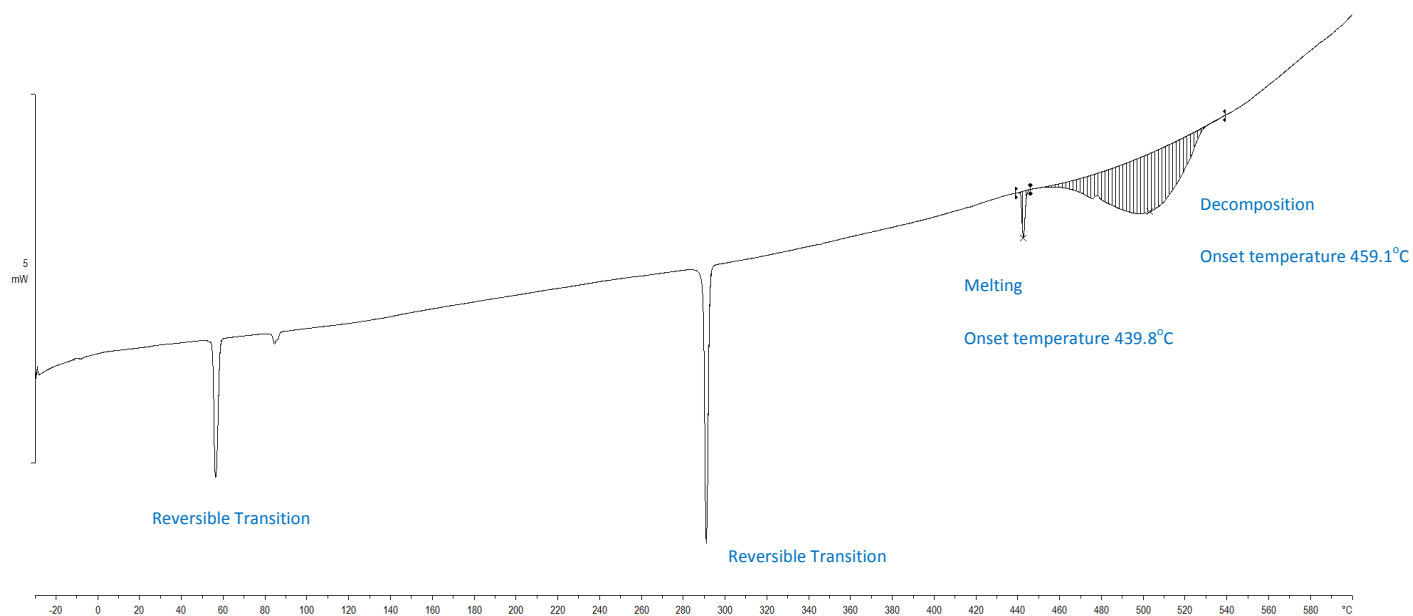


Figure S 155. Calorigram of Potassium Octanoate determined by the DSC over the range of -30-600°C at 10°C·min<sup>-1</sup> heating rate and 100mL·min<sup>-1</sup> nitrogen flow.

### Potassium Nonanoate (pelargonate)

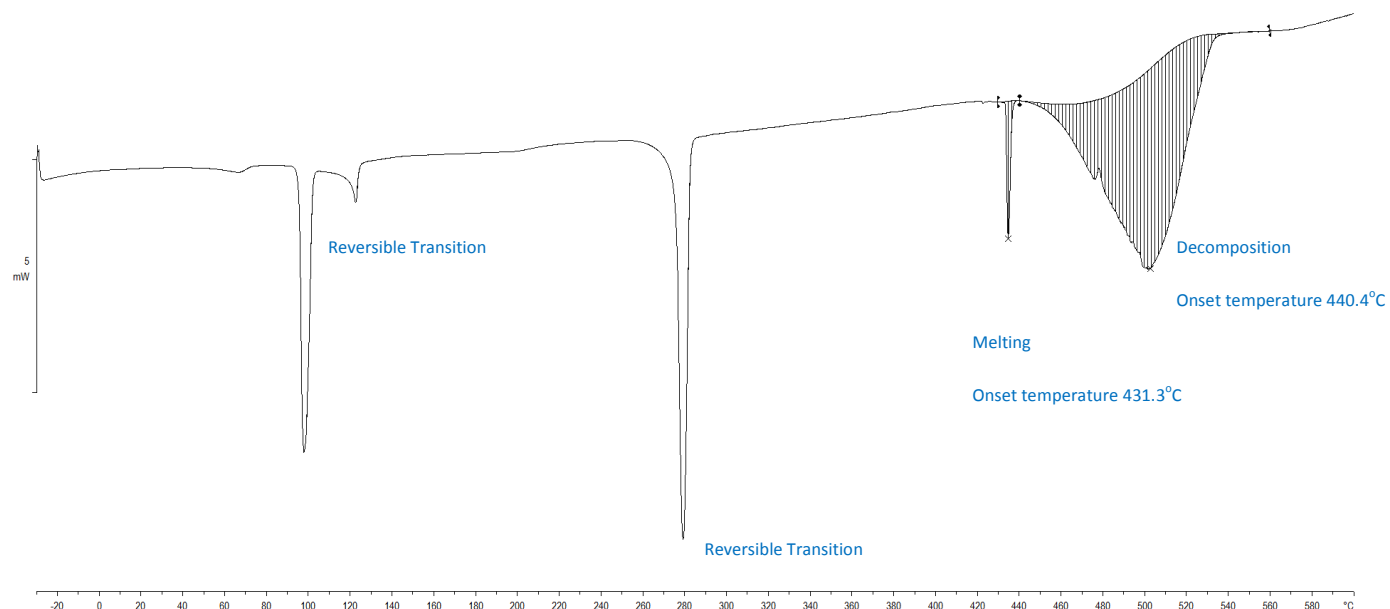


Figure S 156. Calorigram of Potassium Nonanoate determined by the DSC over the range of -30-600°C at 10°C·min<sup>-1</sup> heating rate and 100mL·min<sup>-1</sup> nitrogen flow.

### Potassium Decanoate (caprate)

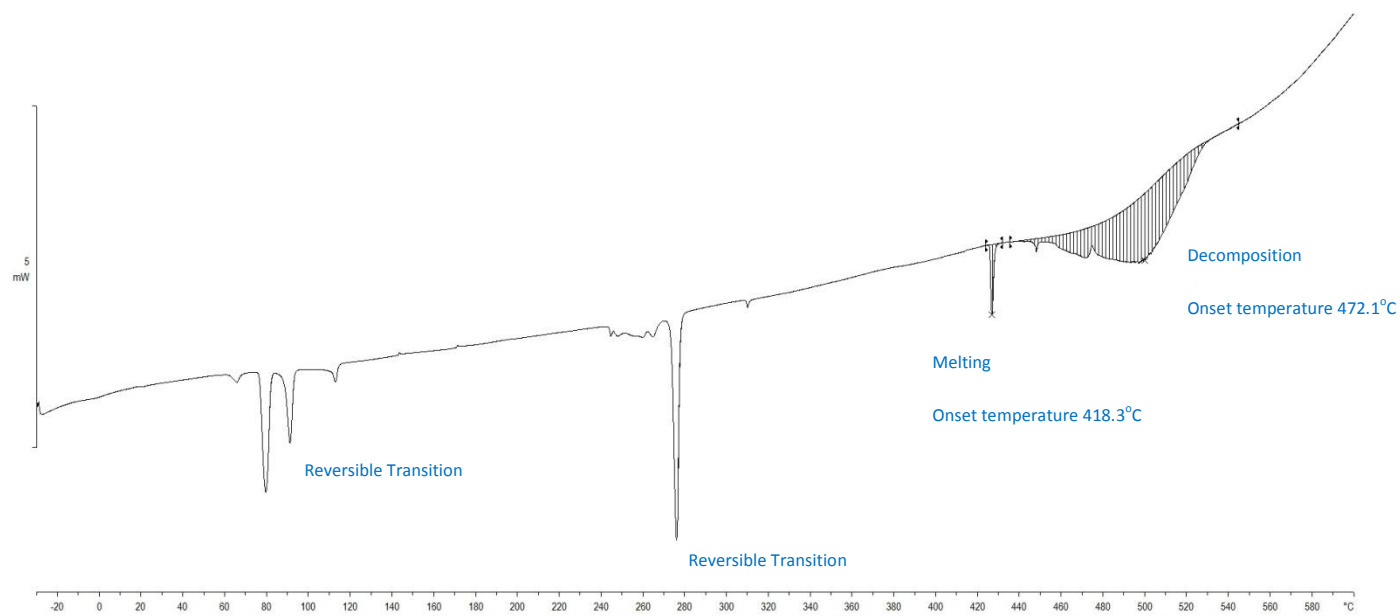


Figure S 157. Calorigram of Potassium Decanoate determined by the DSC over the range of -30-600°C at 10°C·min<sup>-1</sup> heating rate and 100mL·min<sup>-1</sup> nitrogen flow.

## Potassium Undecanoate

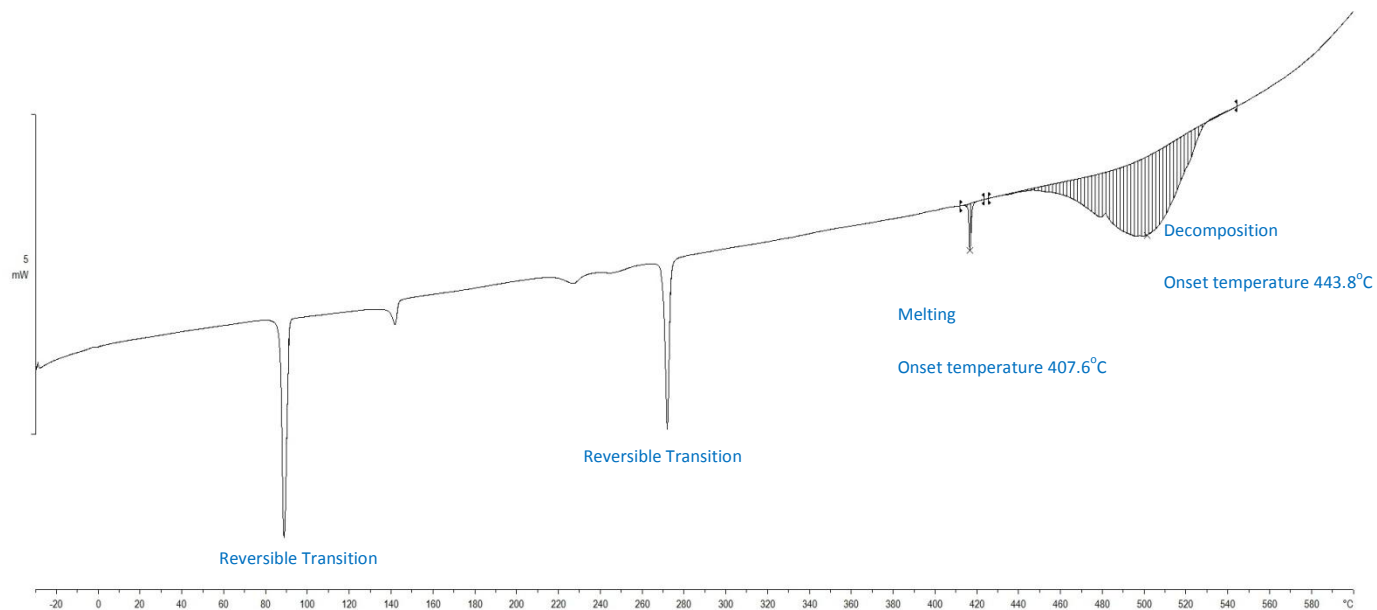


Figure S 158. Calorigram of Potassium Undecanoate determined by the DSC over the range of -30-600°C at 10°C·min<sup>-1</sup> heating rate and 100mL·min<sup>-1</sup> nitrogen flow.

## Potassium Dodecanoate (laurate)

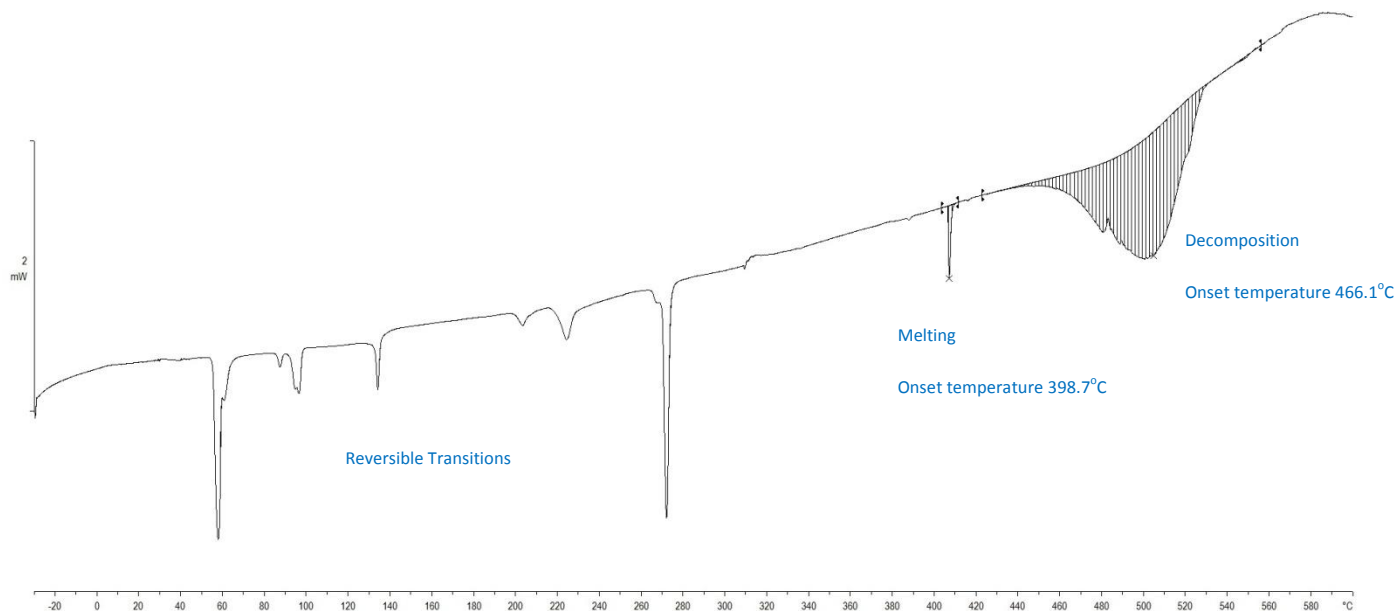


Figure S 159. Calorigram of Potassium Dodecanoate determined by the DSC over the range of -30-600°C at 10°C·min<sup>-1</sup> heating rate and 100mL·min<sup>-1</sup> nitrogen flow.

## Heat Capacity

### Potassium Methanoate

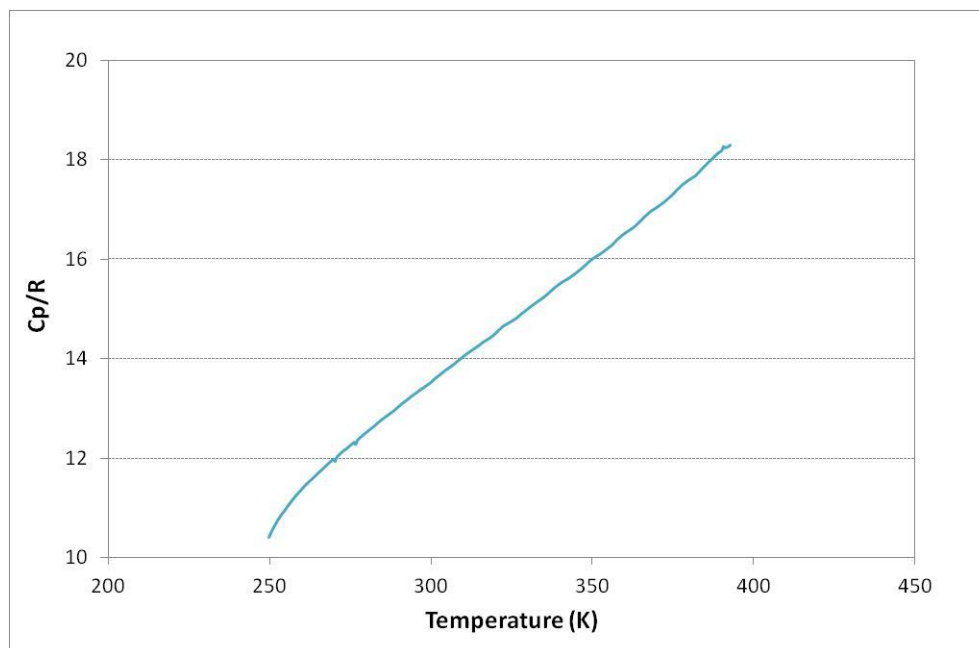


Figure S 160. Experimental molar heat capacities for K-methanoate ( $R = 8.31451 \text{ JK}^{-1}\text{mol}^{-1}$ )

### Potassium Ethanoate

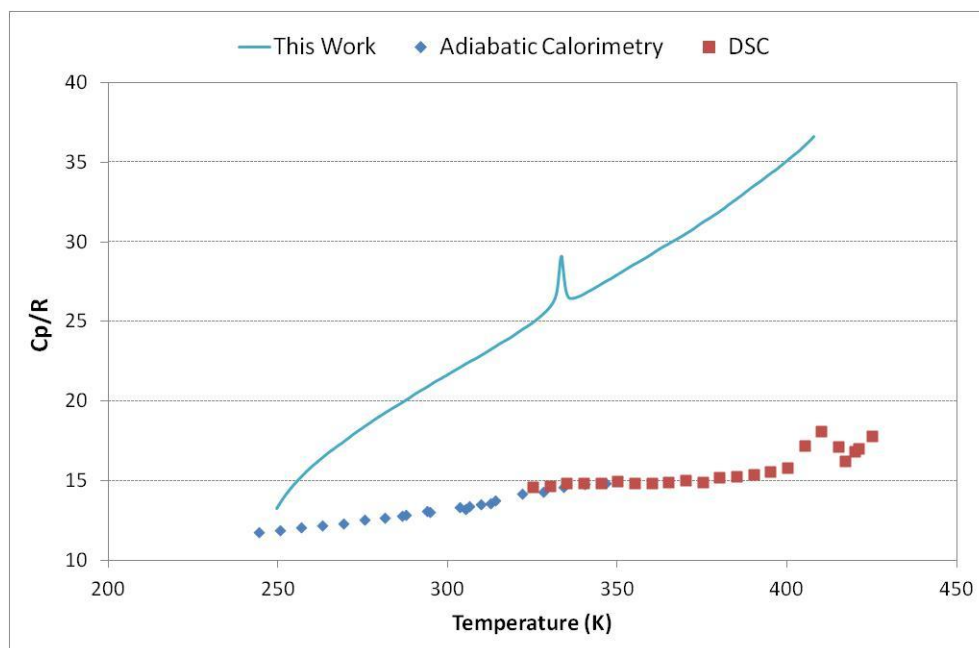


Figure S 161. Experimental molar heat capacities for K-ethanoate ( $R = 8.31451 \text{ JK}^{-1}\text{mol}^{-1}$ )

## Potassium Propanoate

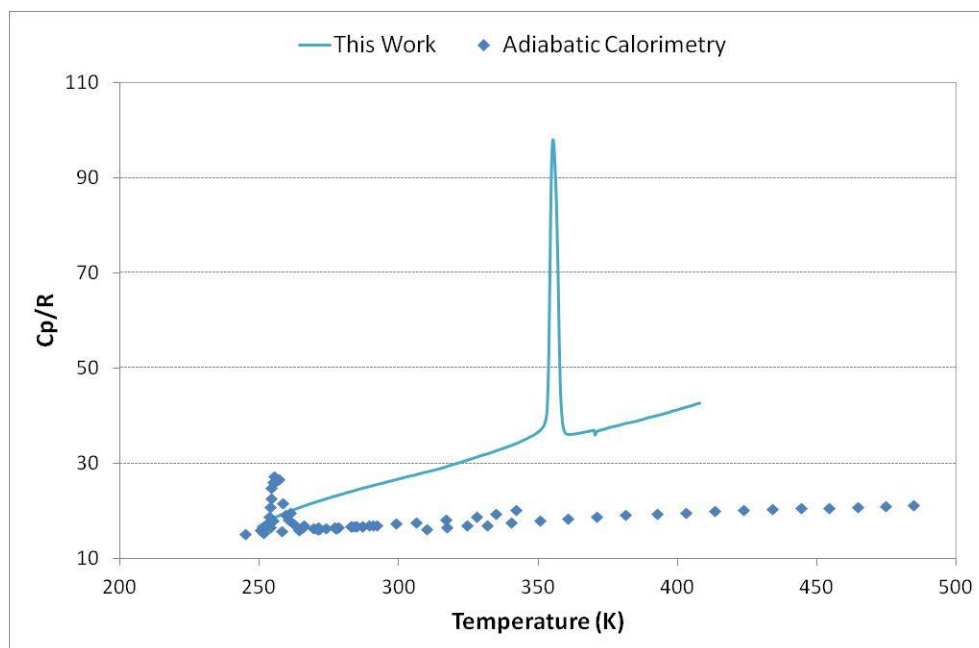


Figure S 162. Experimental molar heat capacities for K-propanoate ( $R = 8.31451 \text{ JK}^{-1}\text{mol}^{-1}$ )

## Potassium Butanoate

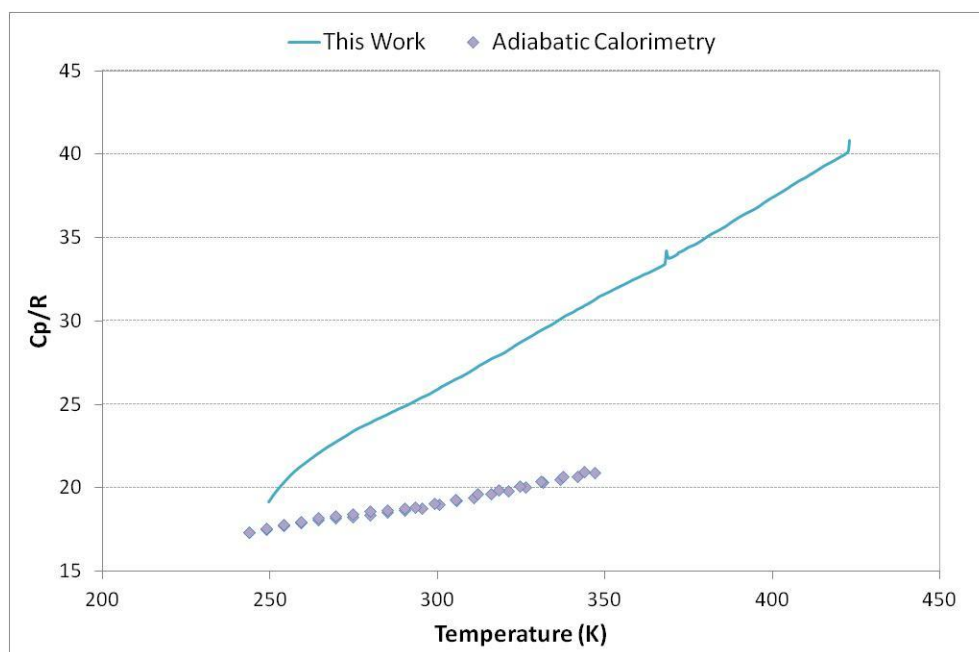


Figure S 163. Experimental molar heat capacities for K-butanoate ( $R = 8.31451 \text{ JK}^{-1}\text{mol}^{-1}$ )

### Potassium Pentanoate (valerate)

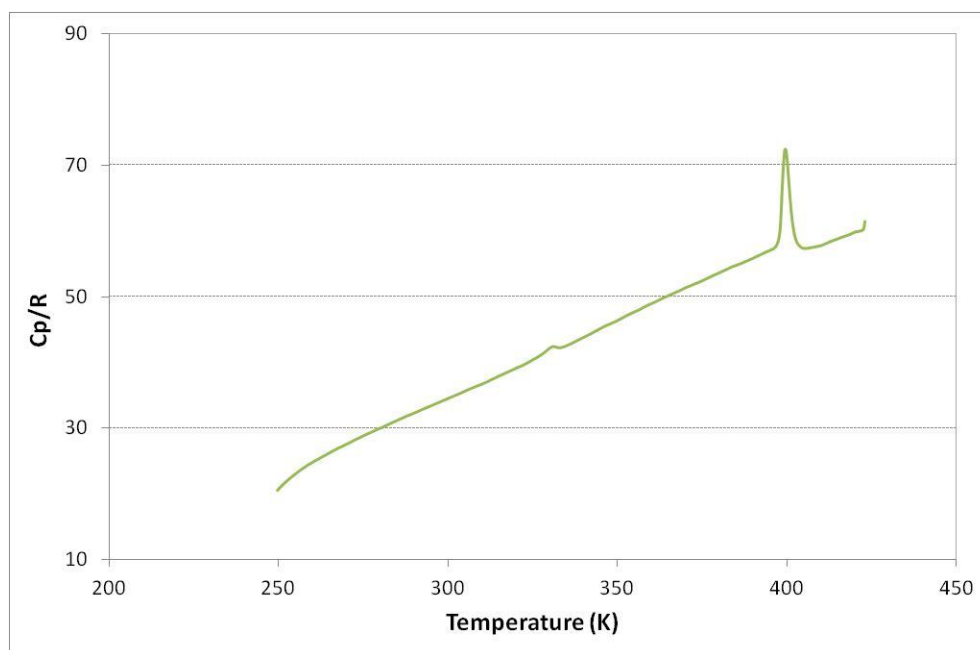


Figure S 164. Experimental molar heat capacities for K-pentanoate ( $R = 8.31451 \text{ JK}^{-1}\text{mol}^{-1}$ )

### Potassium Hexanoate (caproate)

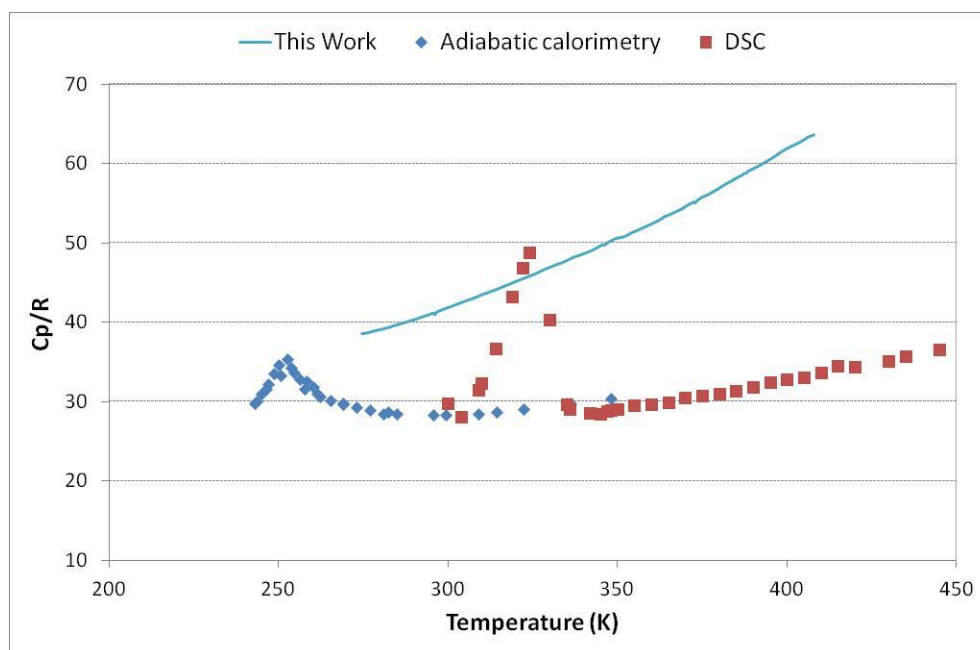


Figure S 165. Experimental molar heat capacities for K-hexanoate ( $R = 8.31451 \text{ JK}^{-1}\text{mol}^{-1}$ )

## Potassium Heptanoate

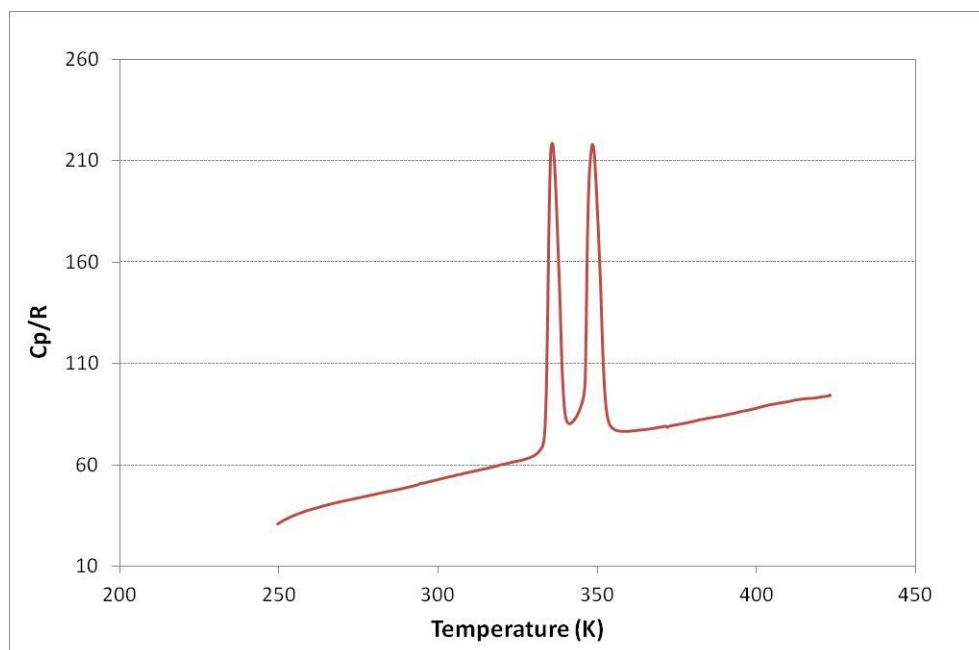


Figure S 166. Experimental molar heat capacities for K-heptanoate ( $R = 8.31451 \text{ JK}^{-1}\text{mol}^{-1}$ )

## Potassium Octanoate (caprylate)

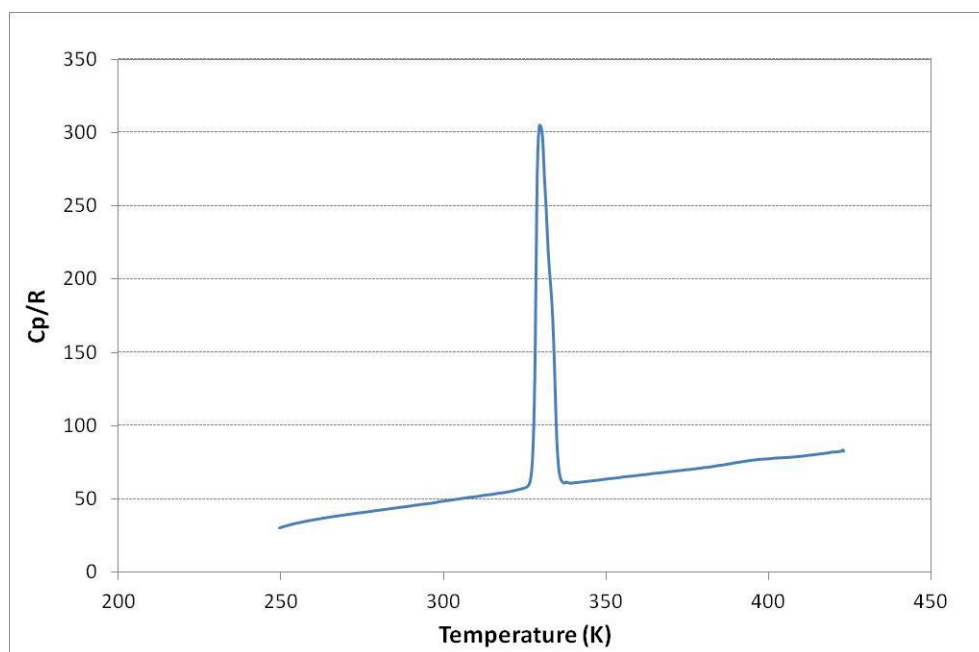


Figure S 167. Experimental molar heat capacities for K-octanoate ( $R = 8.31451 \text{ JK}^{-1}\text{mol}^{-1}$ )

### Potassium Nonanoate (pelargonate)

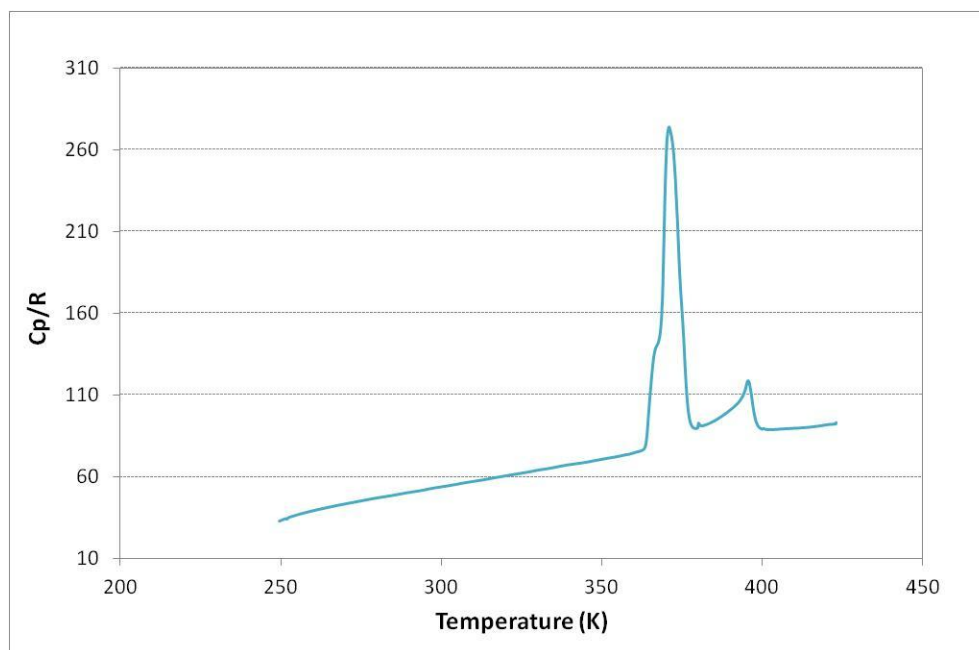


Figure S 168. Experimental molar heat capacities for K-nonanoate ( $R = 8.31451 \text{ JK}^{-1}\text{mol}^{-1}$ )

### Potassium Decanoate (caprate)

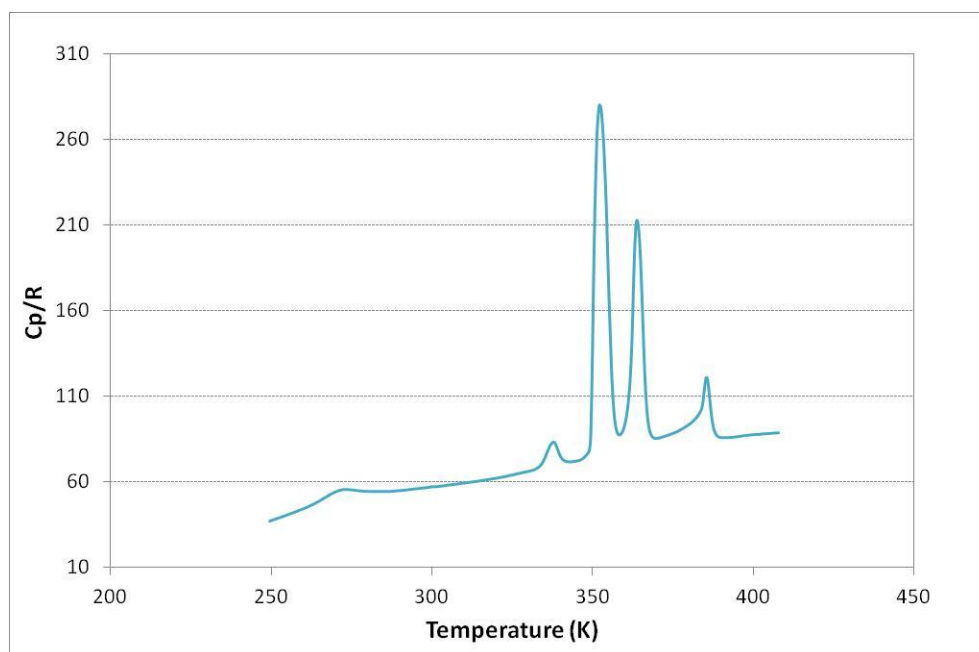


Figure S 169. Experimental molar heat capacities for K-decanoate ( $R = 8.31451 \text{ JK}^{-1}\text{mol}^{-1}$ )

## Potassium Undecanoate

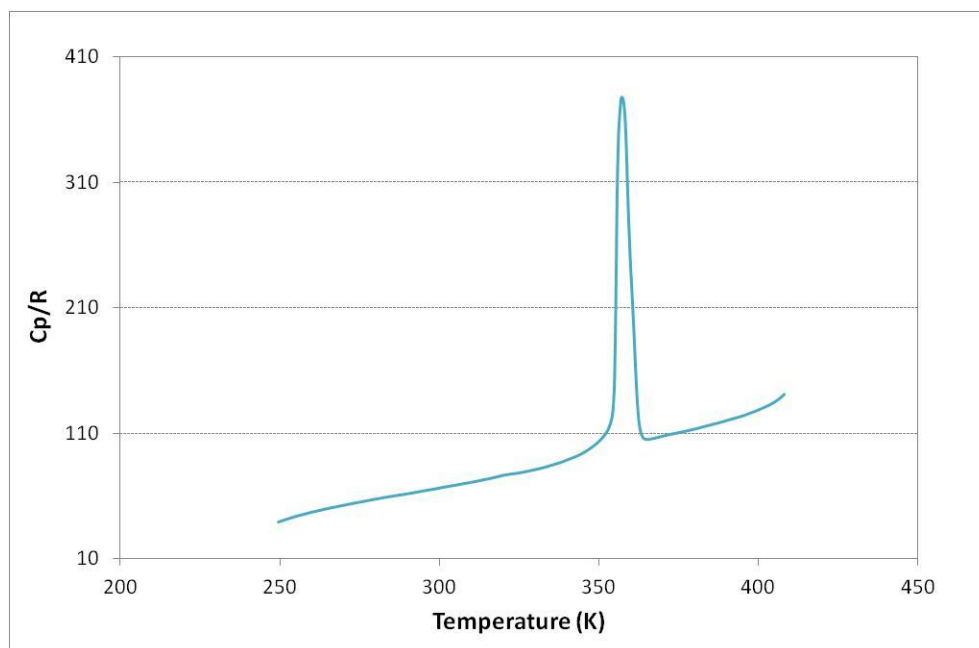


Figure S 170. Experimental molar heat capacities for K-undecanoate ( $R = 8.31451 \text{ JK}^{-1} \text{ mol}^{-1}$ )

## Potassium Dodecanoate (laurate)

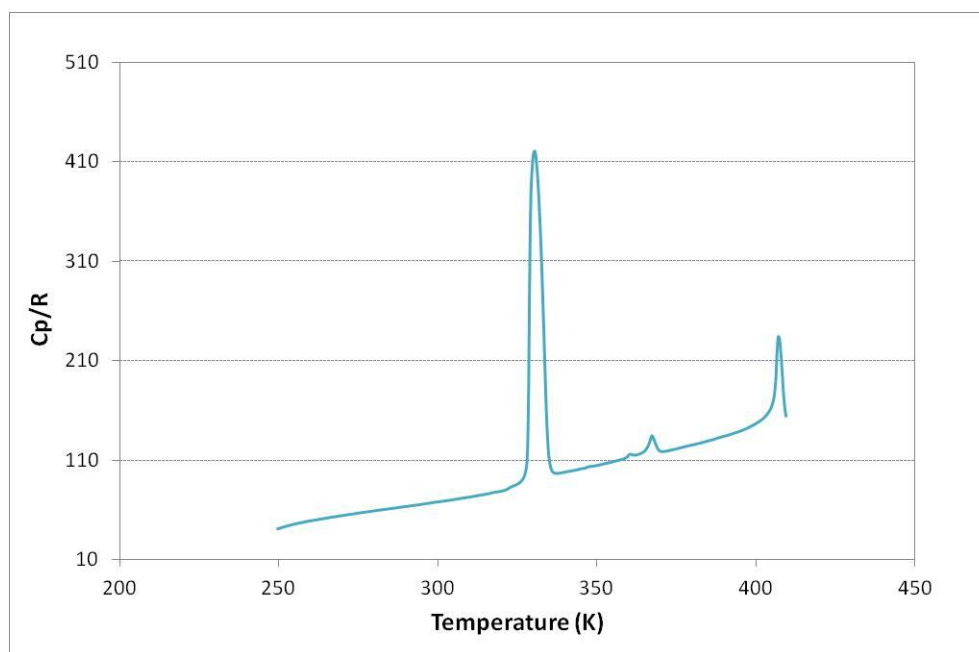


Figure S 171. Experimental molar heat capacities for K-dodecanoate ( $R = 8.31451 \text{ JK}^{-1} \text{ mol}^{-1}$ )

## **Rubidium C<sub>1</sub>-C<sub>12</sub> *n*-alkanoates: Thermal behavior from –30 to 600 °C**

The primary aim of the investigation was to study thermal behaviour. The spectroscopic data was employed to support the thermal investigation. The reasoning behind the collection of the spectroscopic data was as follows:

- (a) Infrared (IR) spectroscopy is sensitive for the detection of carbonyl and carboxylate compounds. It could therefore be used to confirm synthesis of the rubidium carboxylates, as well as provide an indication of purity. Synthesis was performed with a 2% molar excess of carboxylic acid and if the acid was not completely removed during purification, it would be visible on the infrared spectrum.
- (b) IR spectroscopy was also employed to determine whether chemical changes took place during calorimetry. Once a thermal event was observed, a sample was run to a temperature just above the temperature of the observed thermal event and the IR spectrum of the sample thus treated was collected and compared with the starting material.
- (c) IR, Raman and Ultraviolet-Visible (UV-Vis) spectra were collected in the hope of finding explanations for differences in thermal behaviour, and in the hope that additional information about the nature of the rubidium carboxylates can be deduced.

## IR Spectra

### Rubidium methanoate (formate)

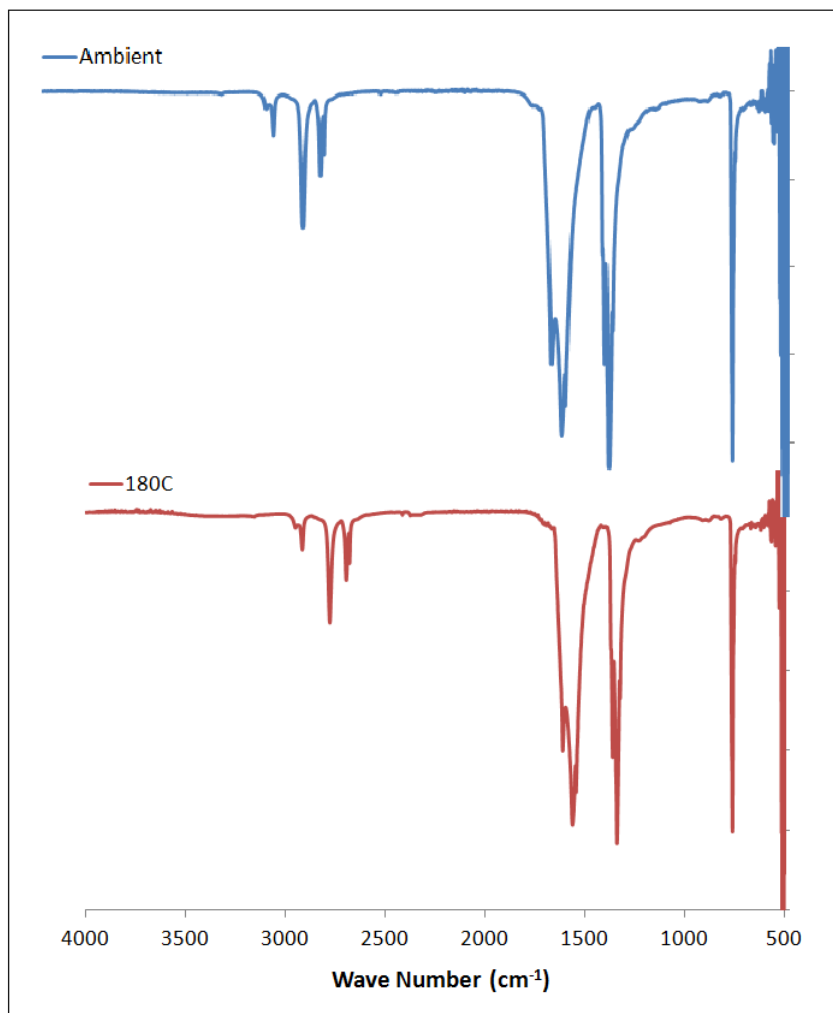


Figure S 172. IR spectrum of rubidium methanoate before and after melting

## Rubidium ethanoate (acetate)

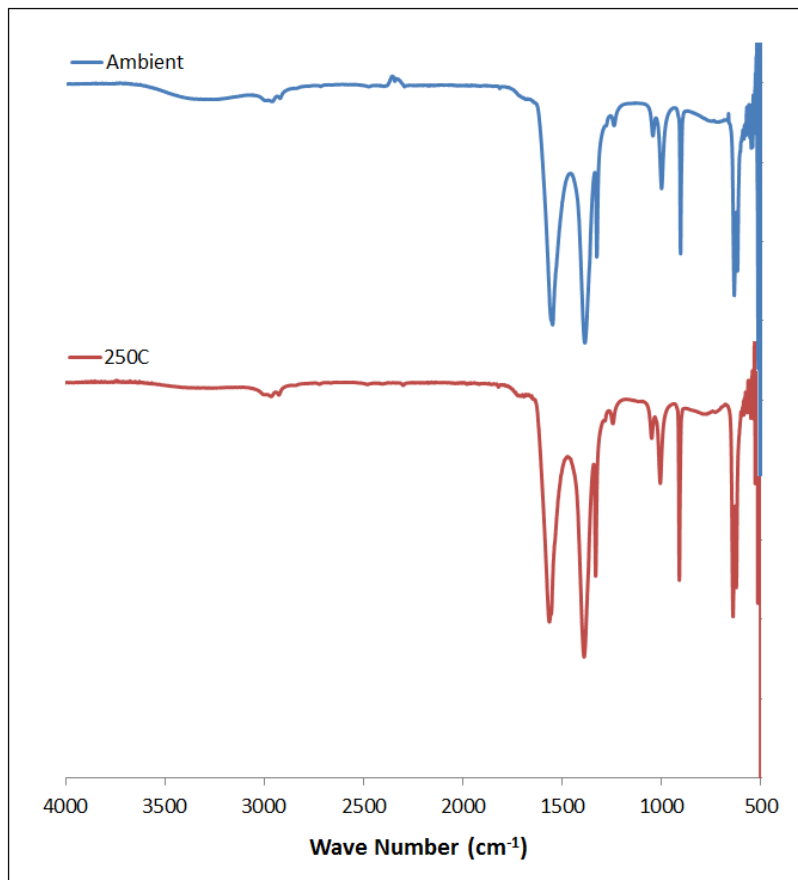


Figure S 173. IR spectrum of rubidium ethanoate before and after melting.

## Rubidium propanoate

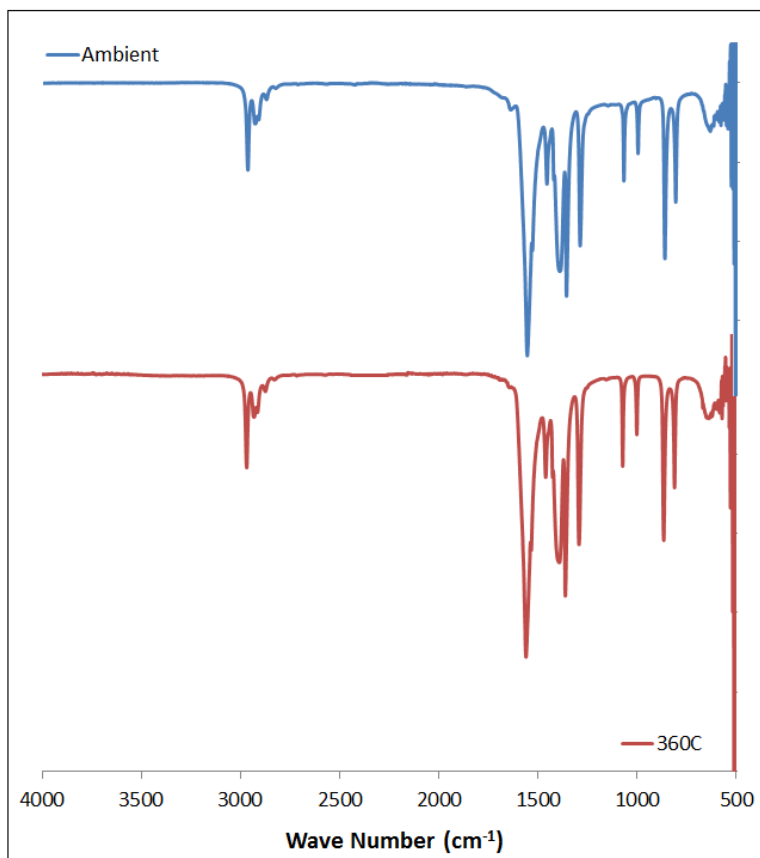


Figure S 174. IR spectrum of rubidium propanoate before and after melting.

## Rubidium butanoate (butyrate)

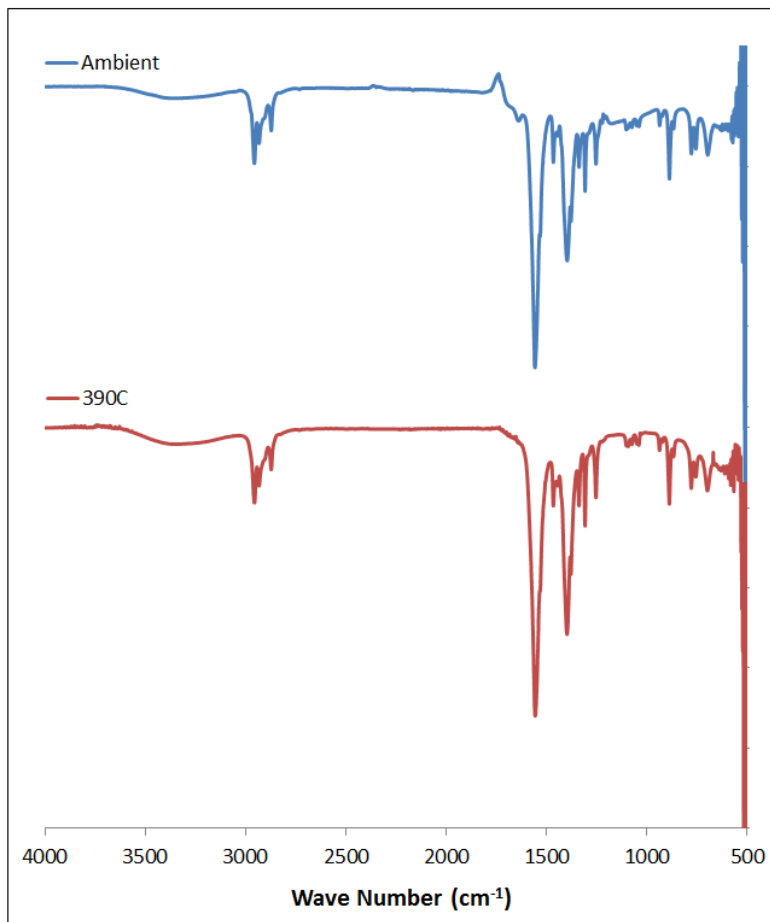


Figure S 175. IR spectrum of rubidium butanoate before and after melting.

## Rubidium pentanoate (valerate)

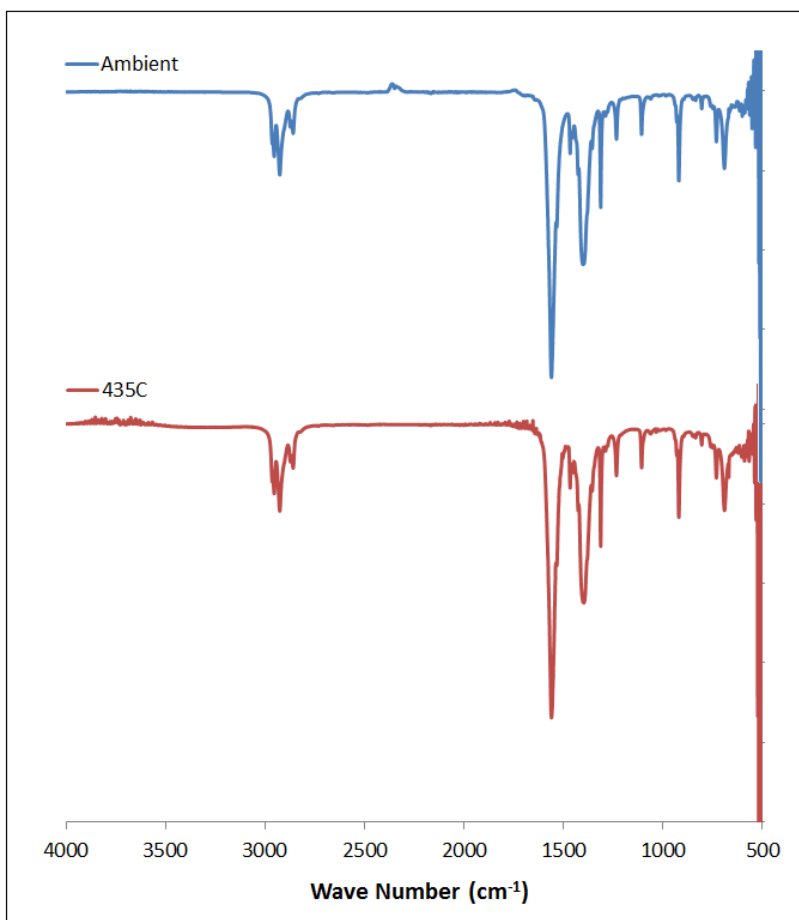


Figure S 176. IR spectrum of rubidium pentanoate before and after melting.

## Rubidium hexanoate (caproate)

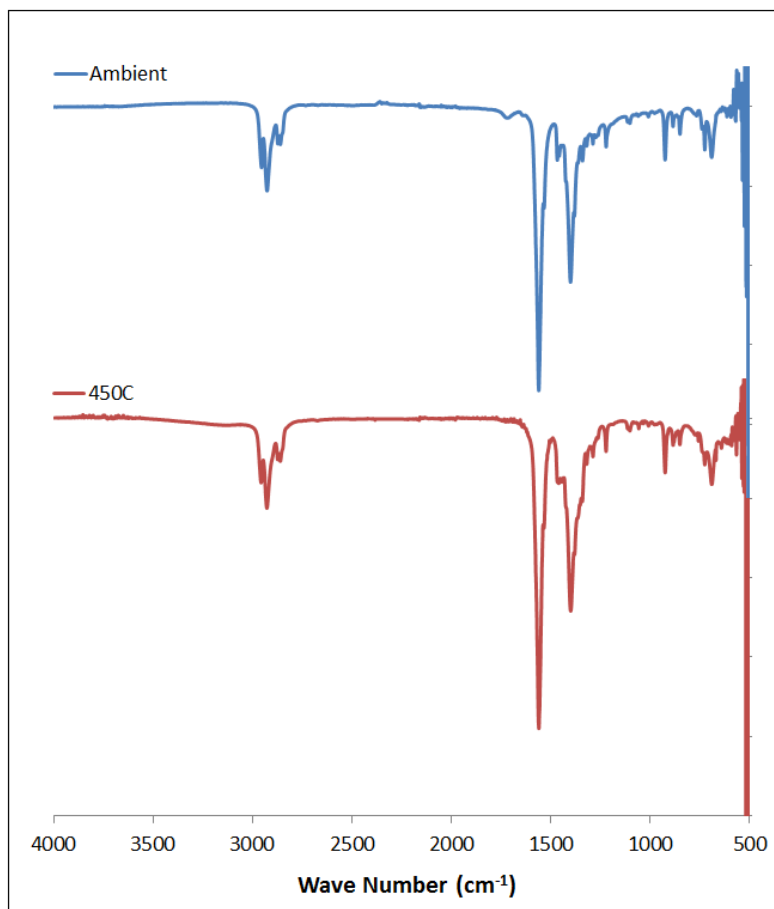


Figure S 177. IR spectrum of rubidium hexanoate before and after melting.

## Rubidium heptanoate

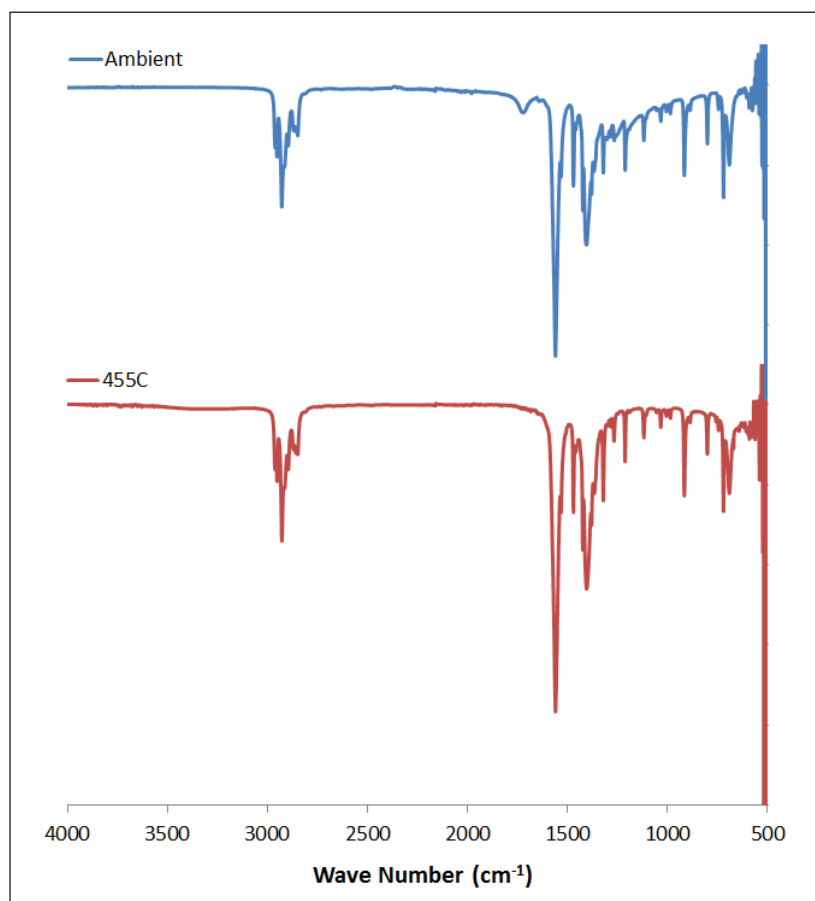


Figure S 178. IR spectrum of rubidium heptanoate before and after melting.

## Rubidium octanoate (caprylate)

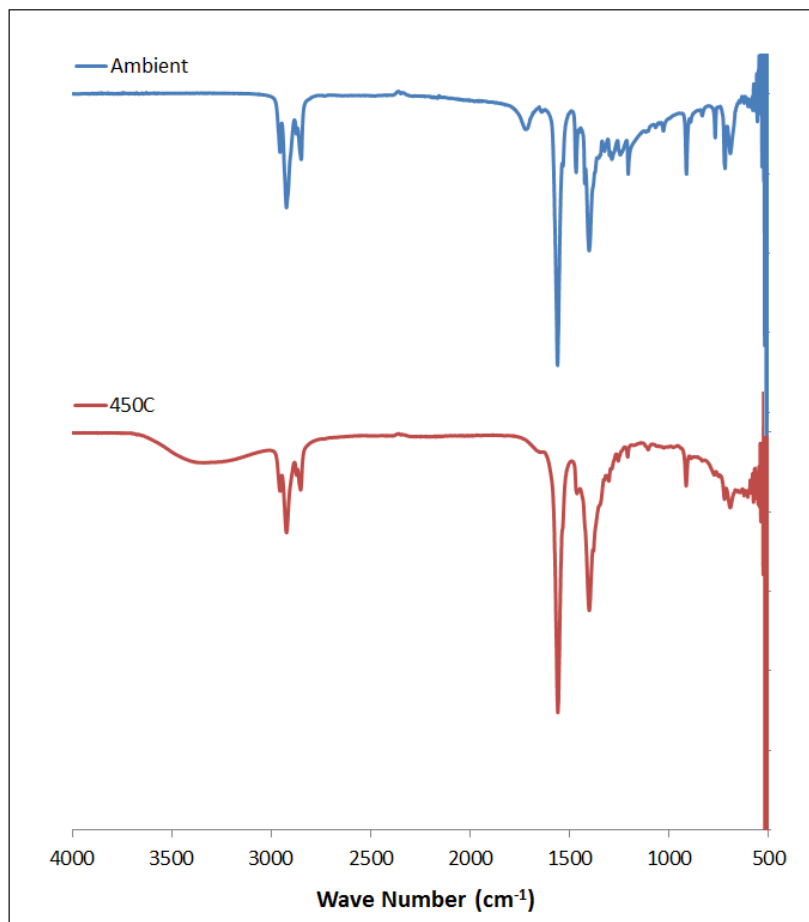


Figure S 179. IR spectrum of rubidium octanoate before and after melting.

## Rubidium nonanoate (pelargonate)

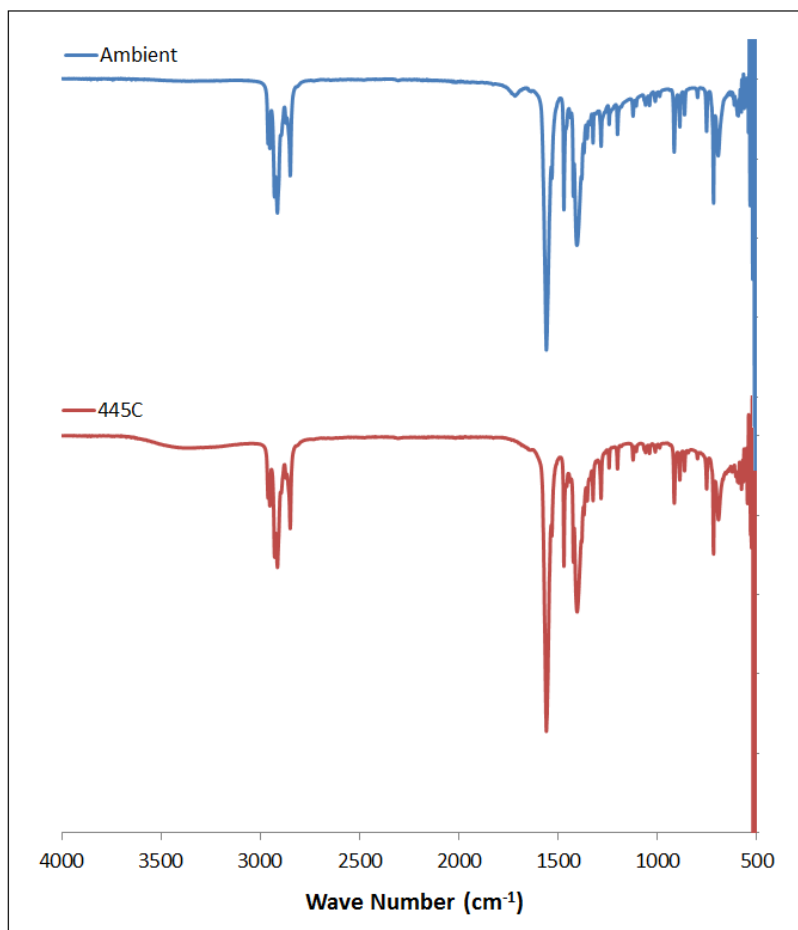


Figure S 180. IR spectrum of cesium nonanoate before and after melting.

## Rubidium decanoate (caprate)

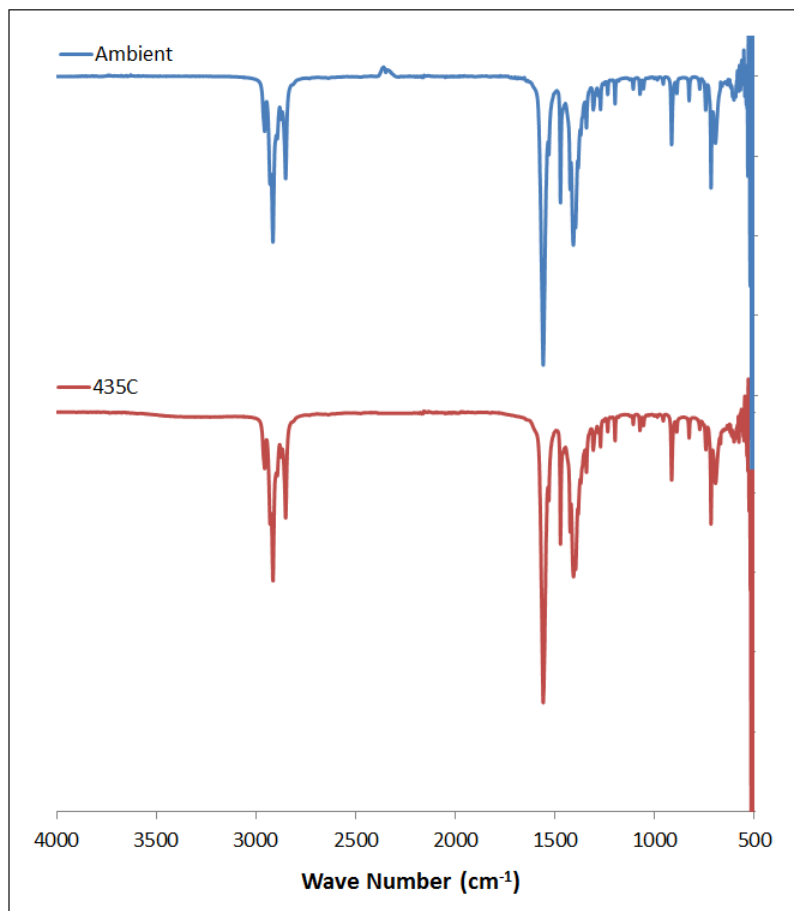


Figure S 181. IR spectrum of rubidium decanoate before and after melting.

## Rubidium undecanoate

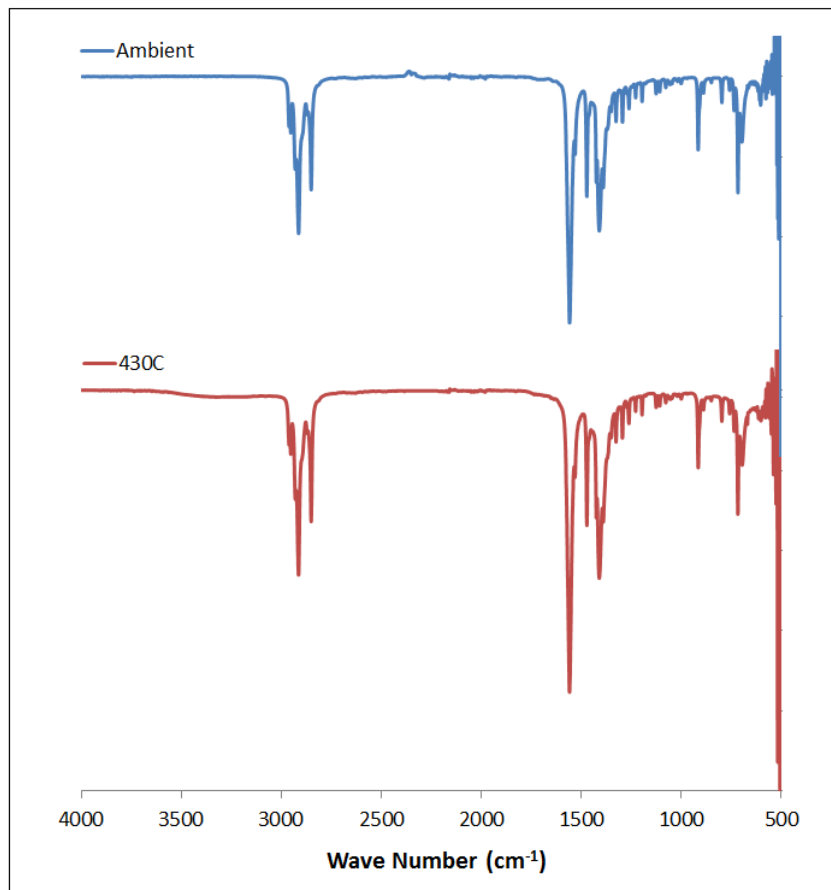


Figure S 182. IR spectrum of rubidium undecanoate before and after melting.

## Rubidium dodecanoate (laurate)

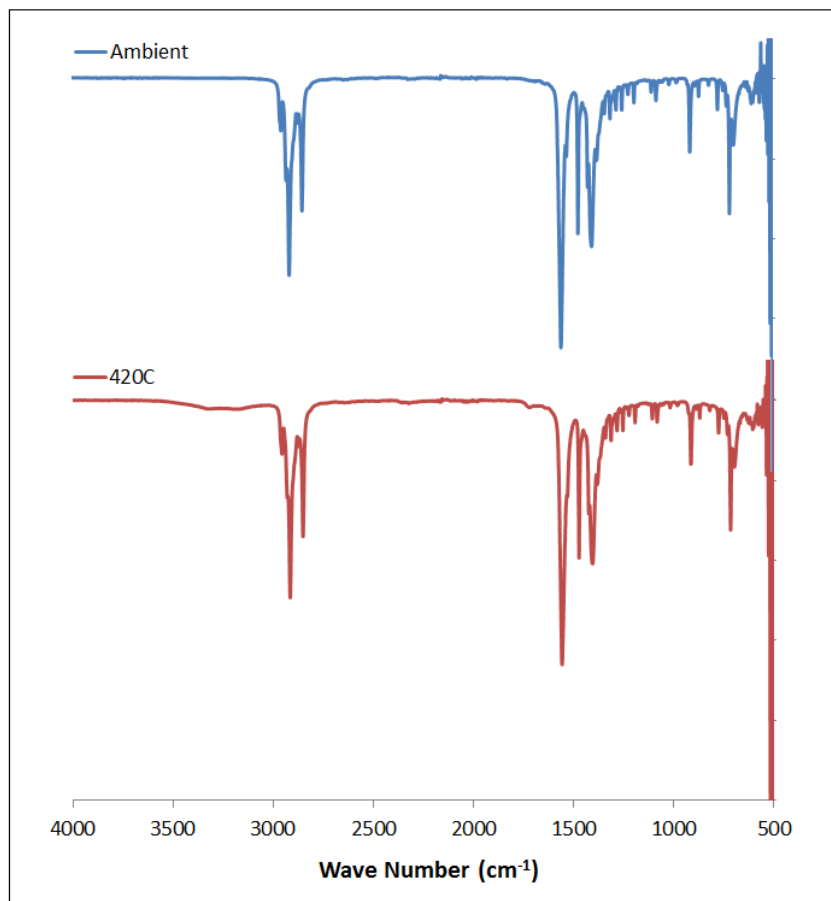


Figure S 183. IR spectrum of rubidium dodecanoate before and after melting.

## UV-Vis Spectra

### Rubidium Methanoate

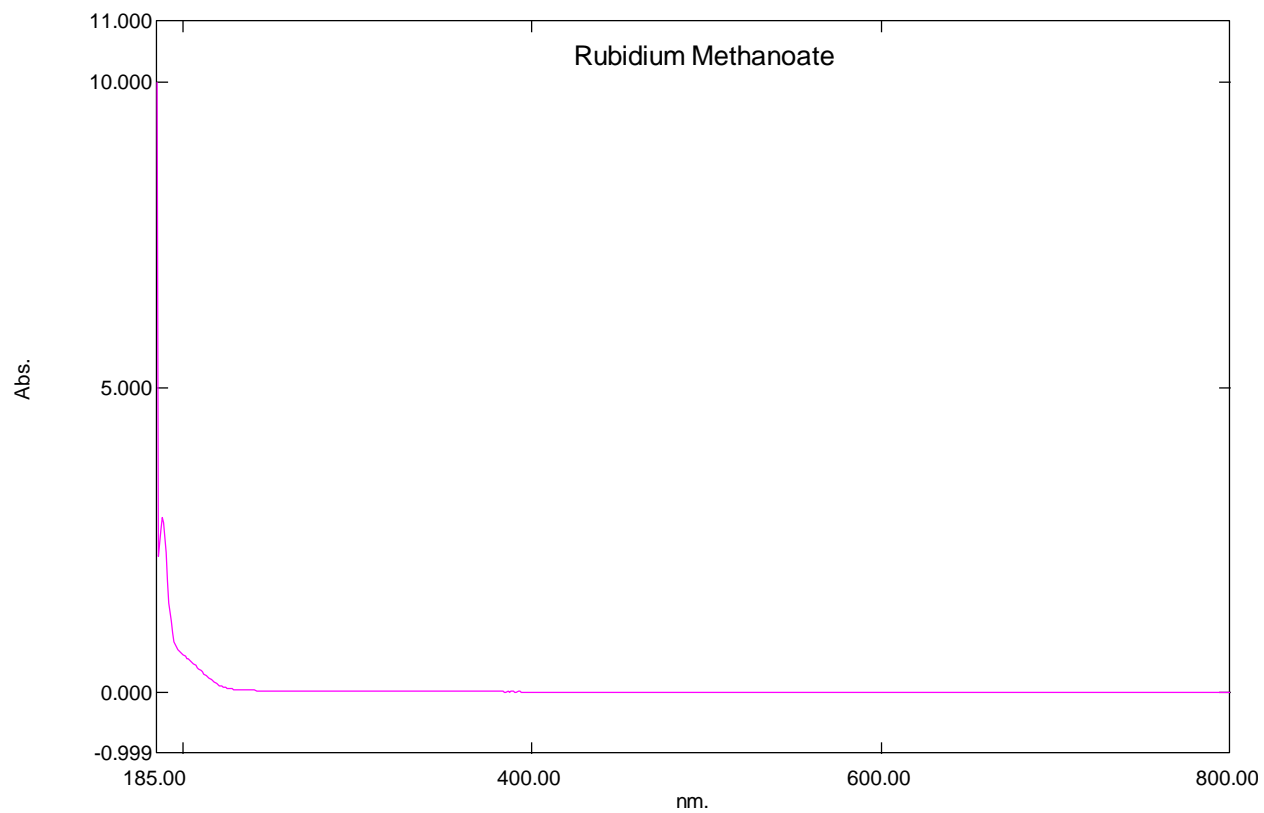
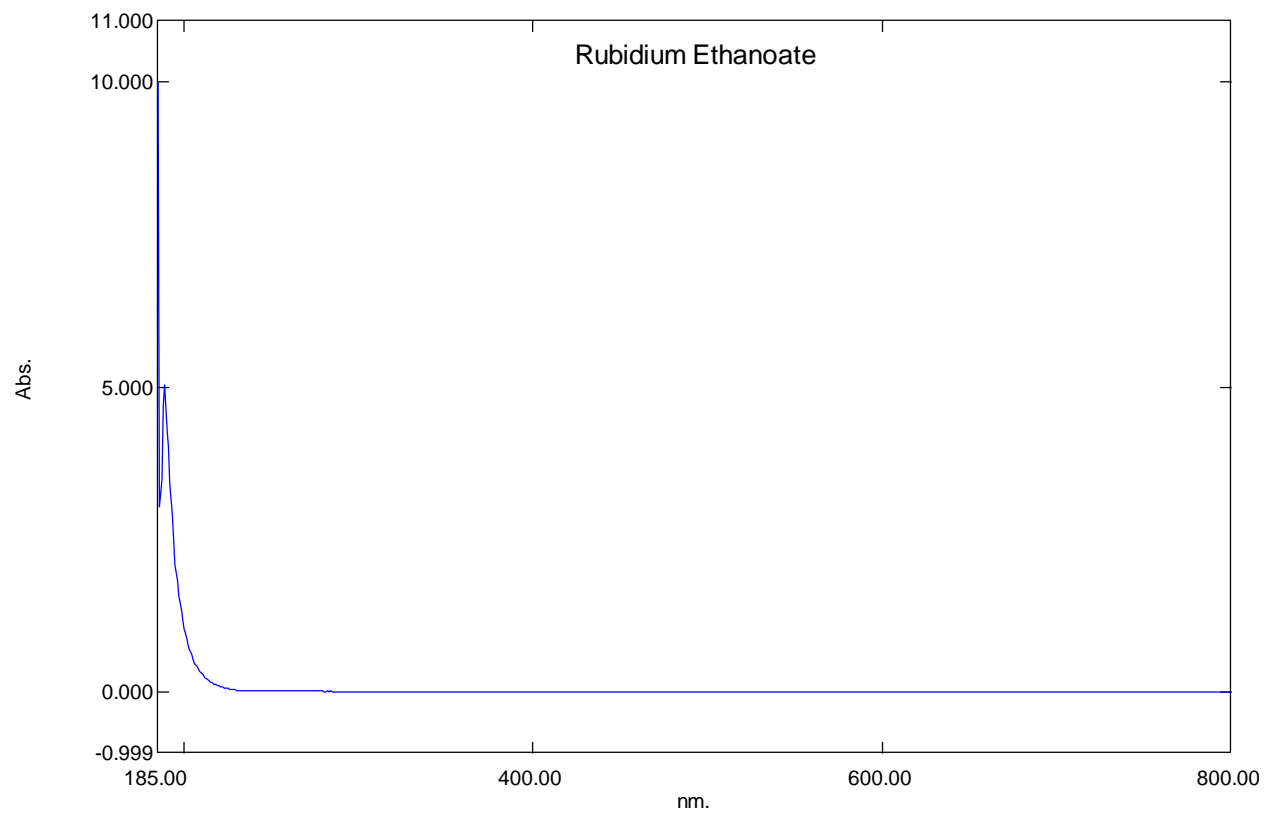


Figure S 184. UV-Vis spectrum of rubidium methanoate

## Rubidium Ethanoate



**Figure S 185. UV-Vis spectrum of rubidium ethanoate**

## Rubidium Propanoate

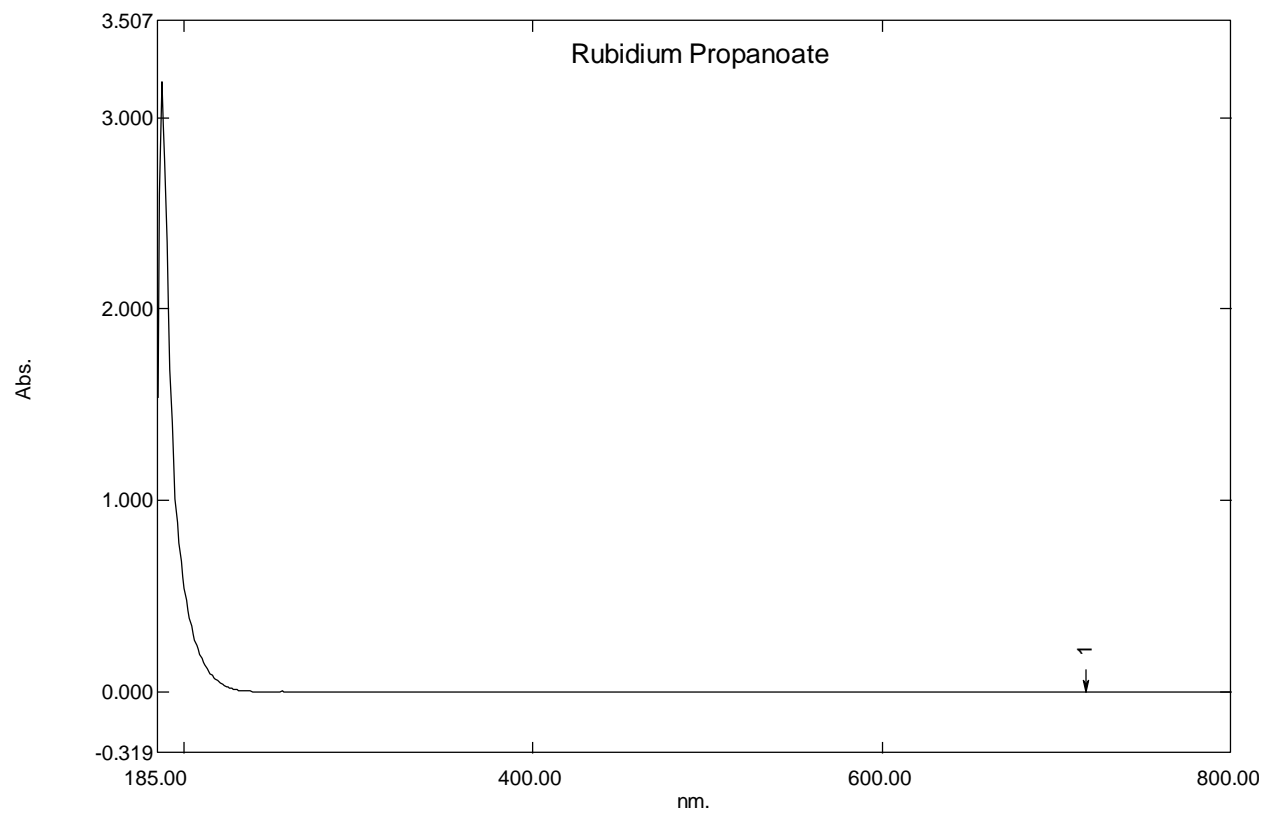
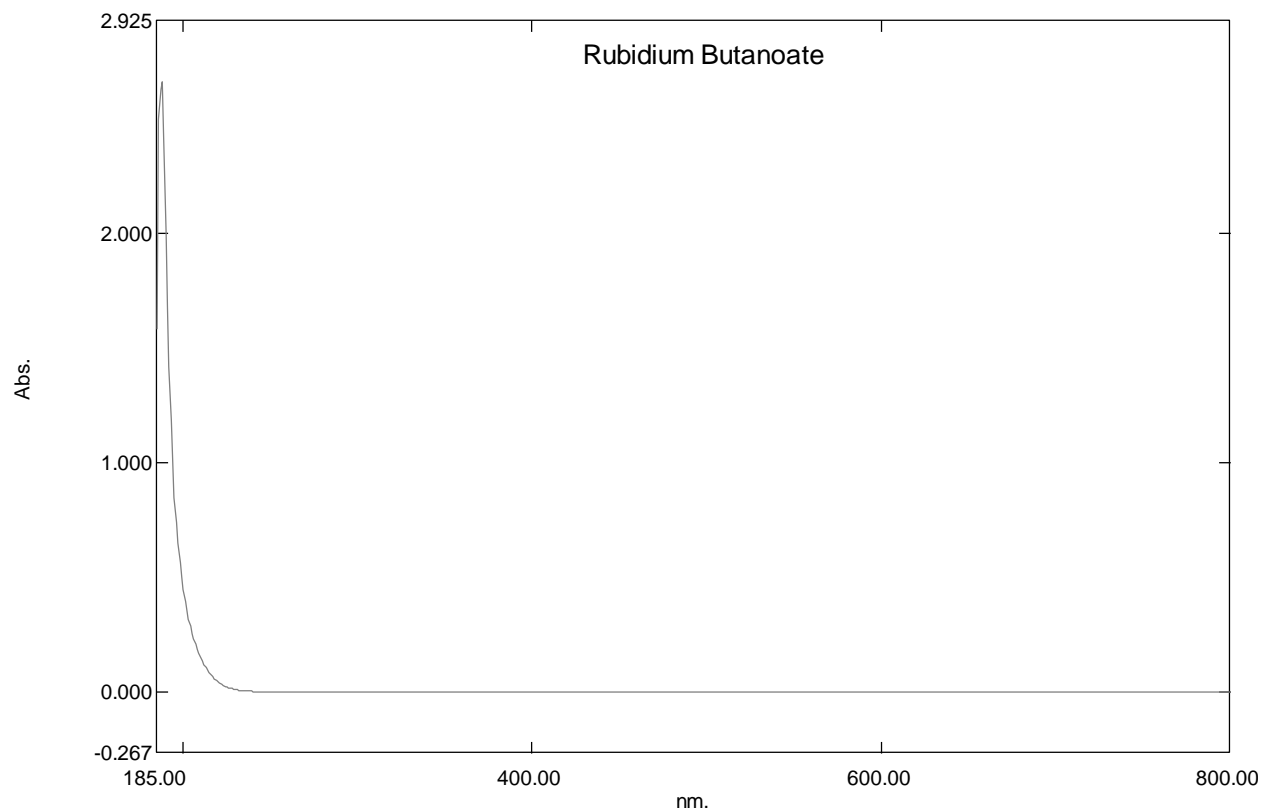


Figure S 186. UV-Vis spectrum of rubidium propanoate

**Rubidium Butanoate (butyrate)**



**Figure S 187. UV-Vis spectrum of rubidium butanoate**

### Rubidium Pentanoate (valerate)

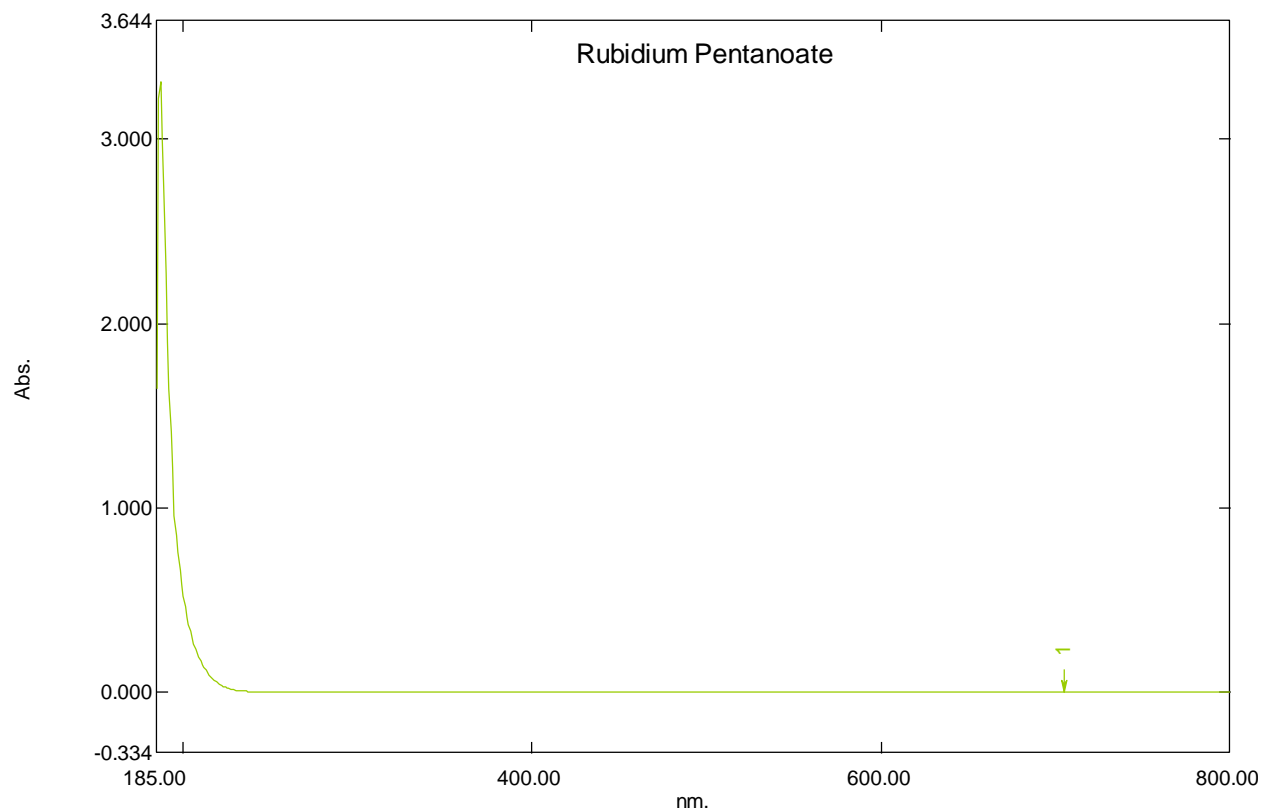


Figure S 188. UV-Vis spectrum of rubidium pentanoate

## Rubidium Hexanoate (caproate)

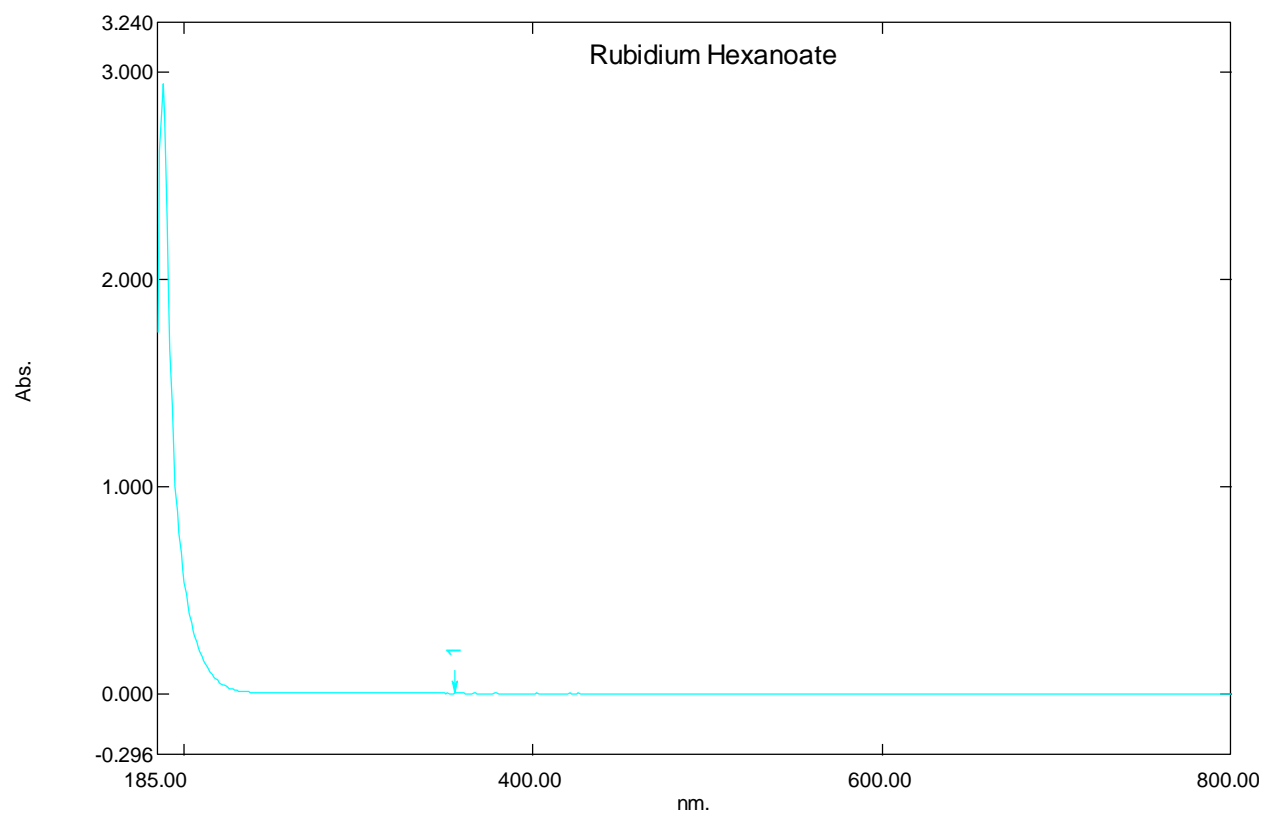


Figure S 189. UV-Vis of rubidium hexanoate

## Rubidium Heptanoate

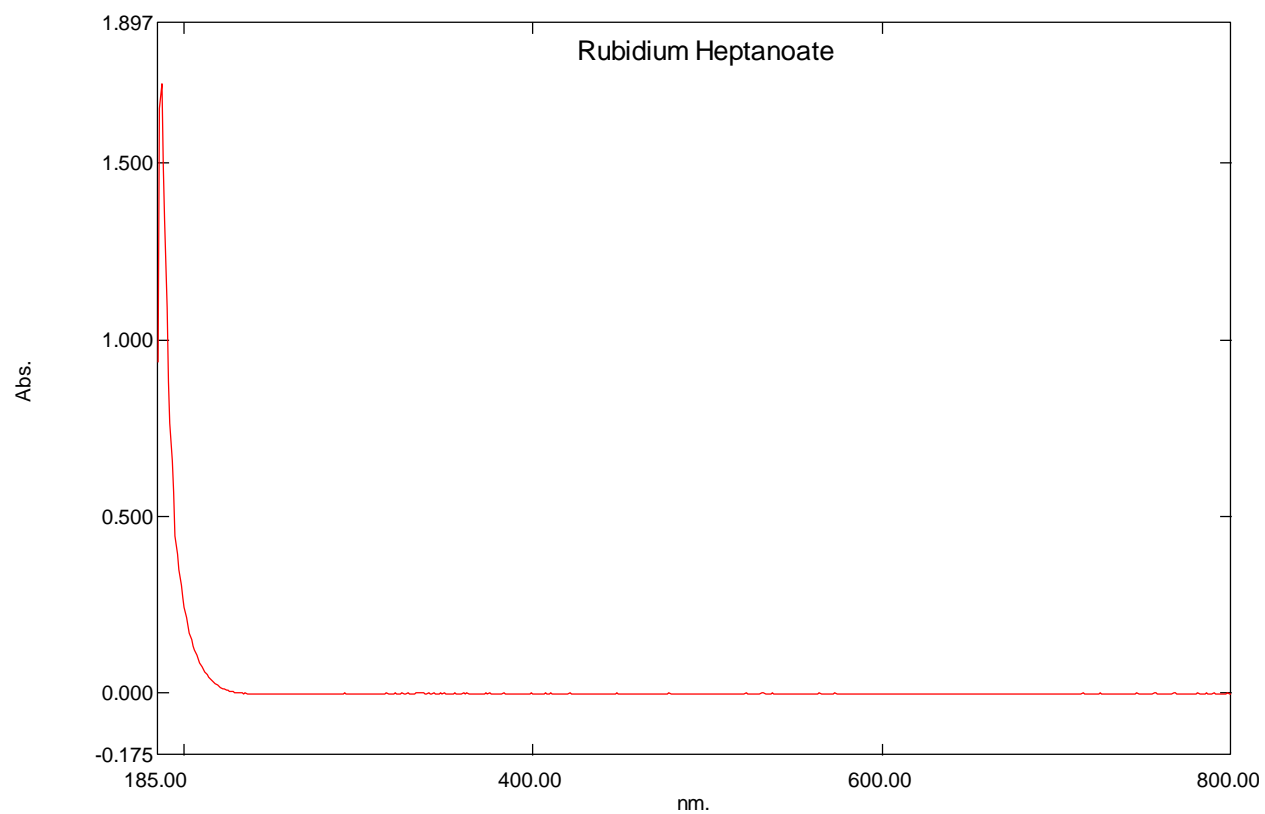


Figure S 190. UV-Vis spectrum of rubidium heptanoate

## Rubidium Octanoate (caprylate)

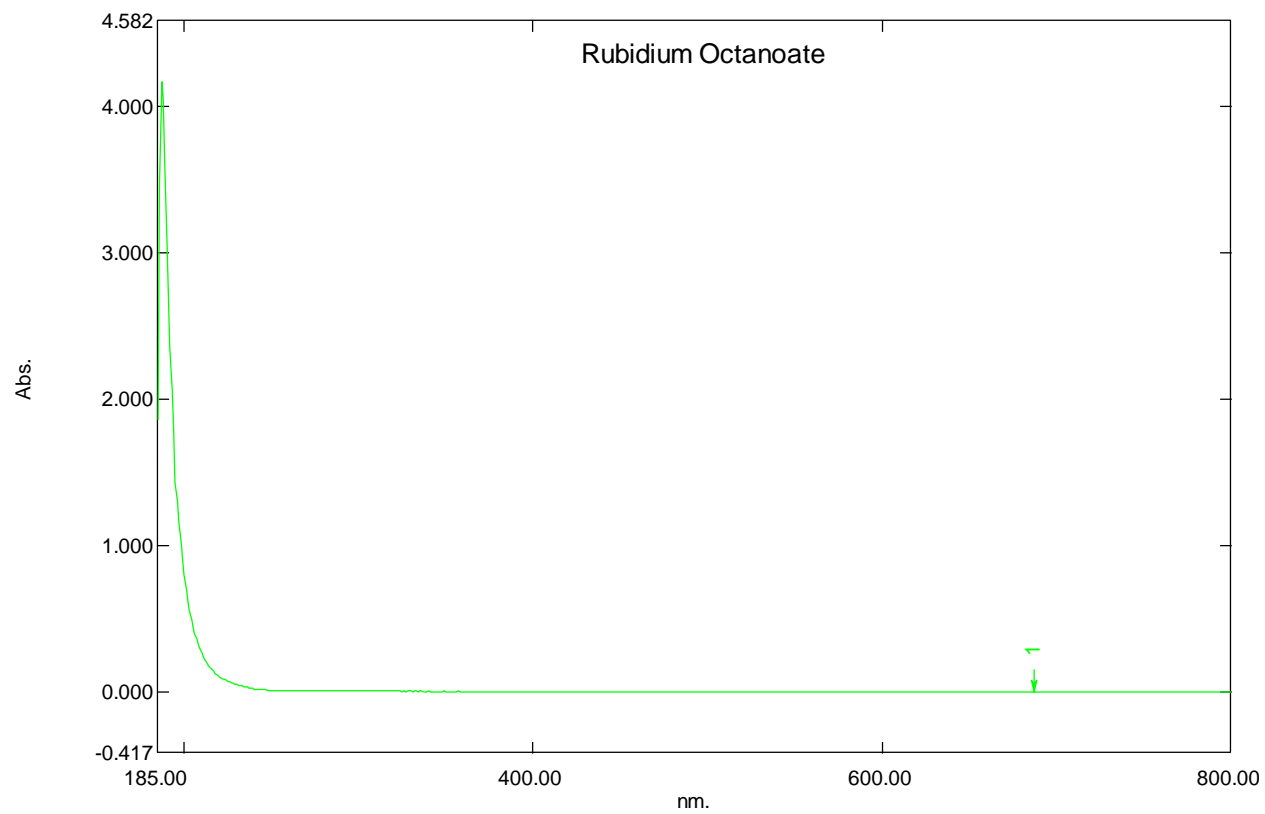


Figure S 191. UV-Vis of rubidium octanoate

## Rubidium Nonanoate (pelargonate)

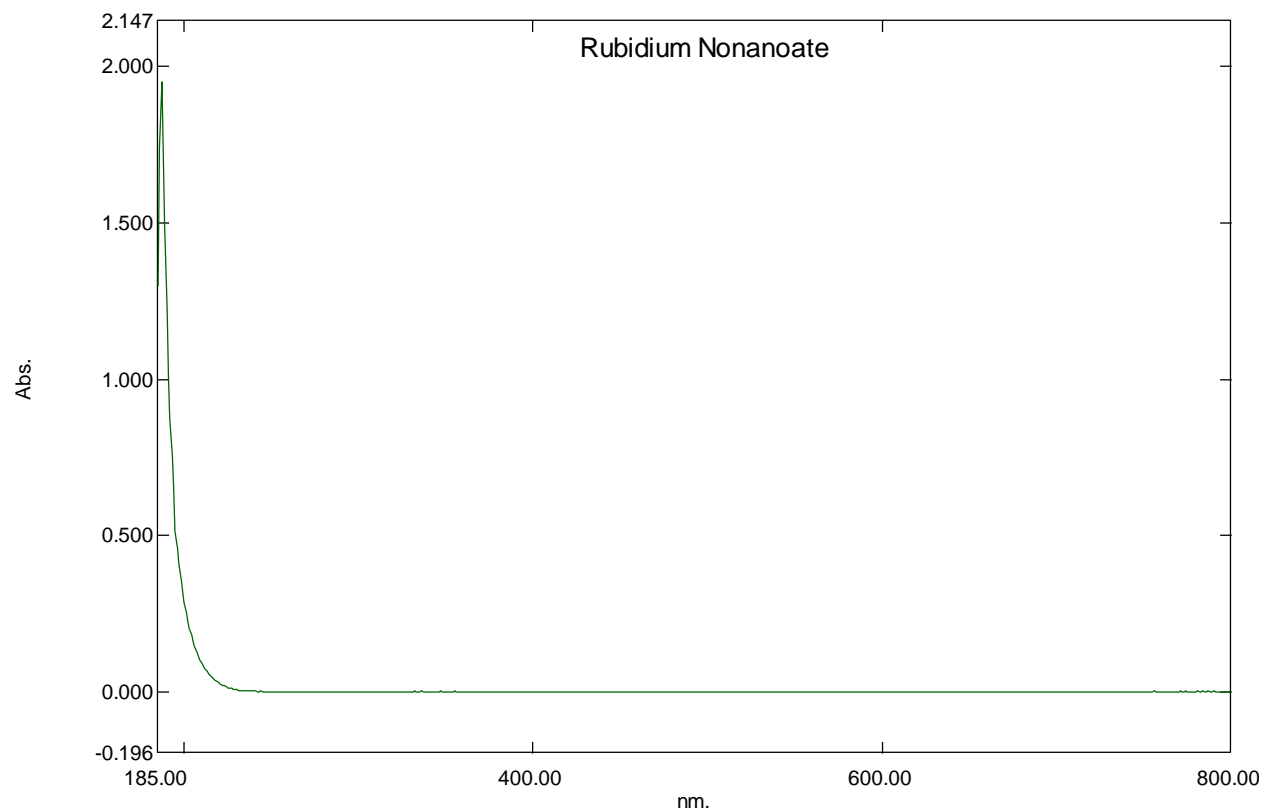


Figure S 192. UV-Vis of rubidium nonanoate

## Rubidium Decanoate (caprate)

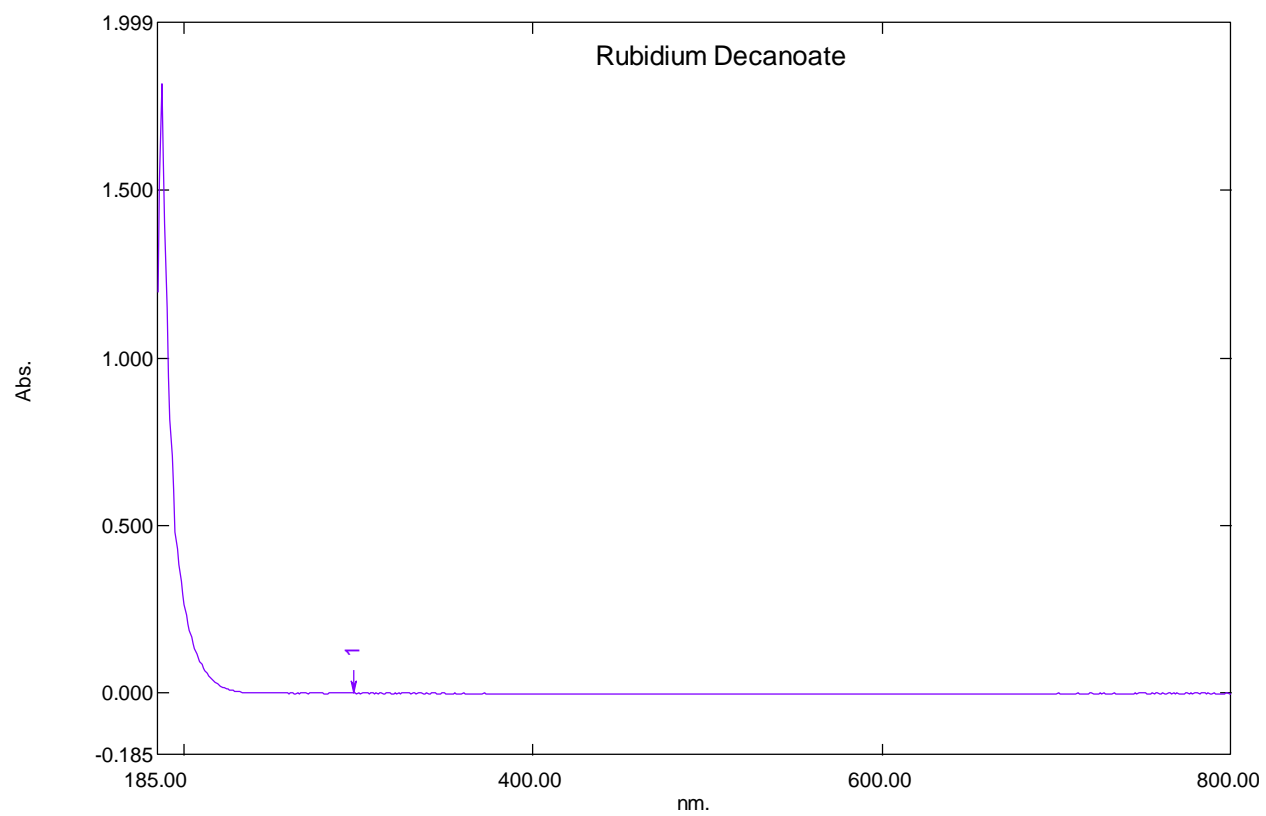


Figure S 193. UV-Vis of rubidium decanoate

## Rubidium Undecanoate

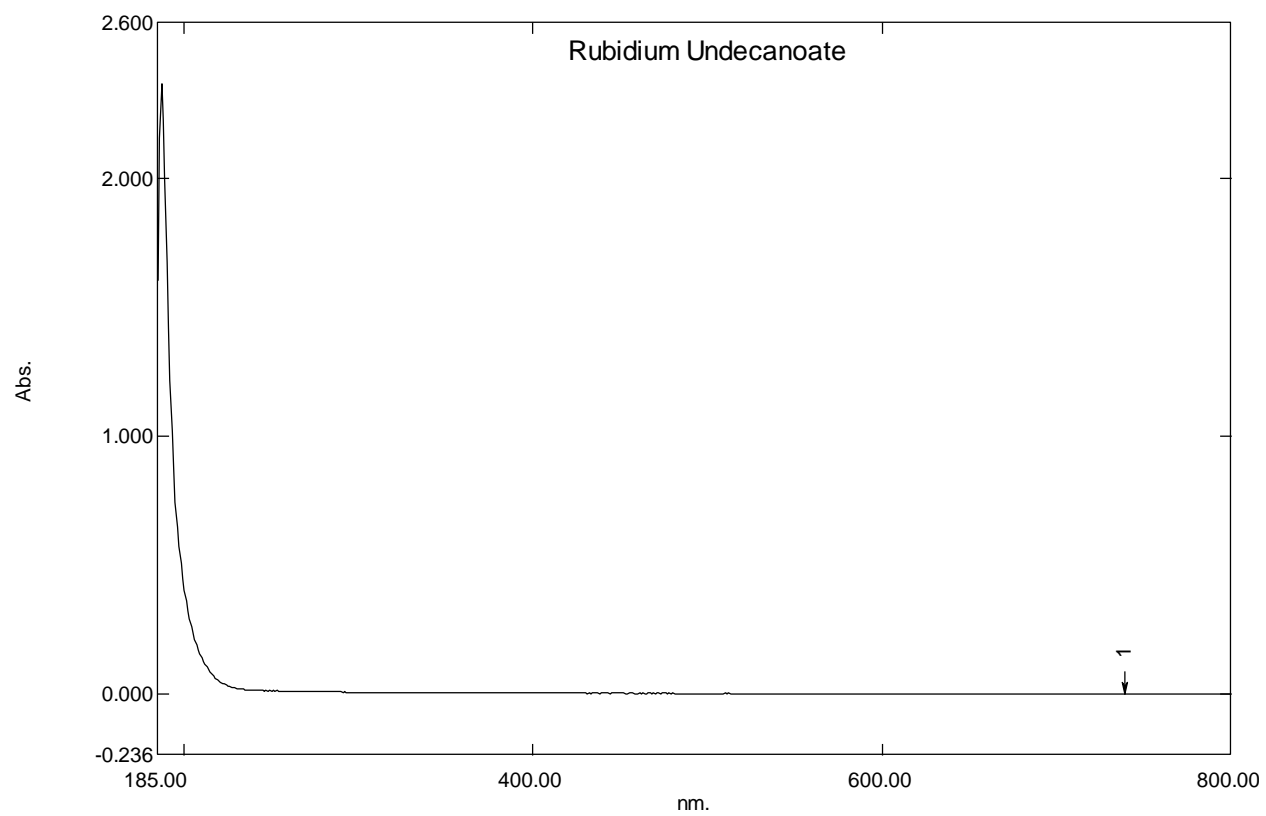


Figure S 194. UV-Vis of rubidium undecanoate

### Rubidium Dodecanoate (laurate)

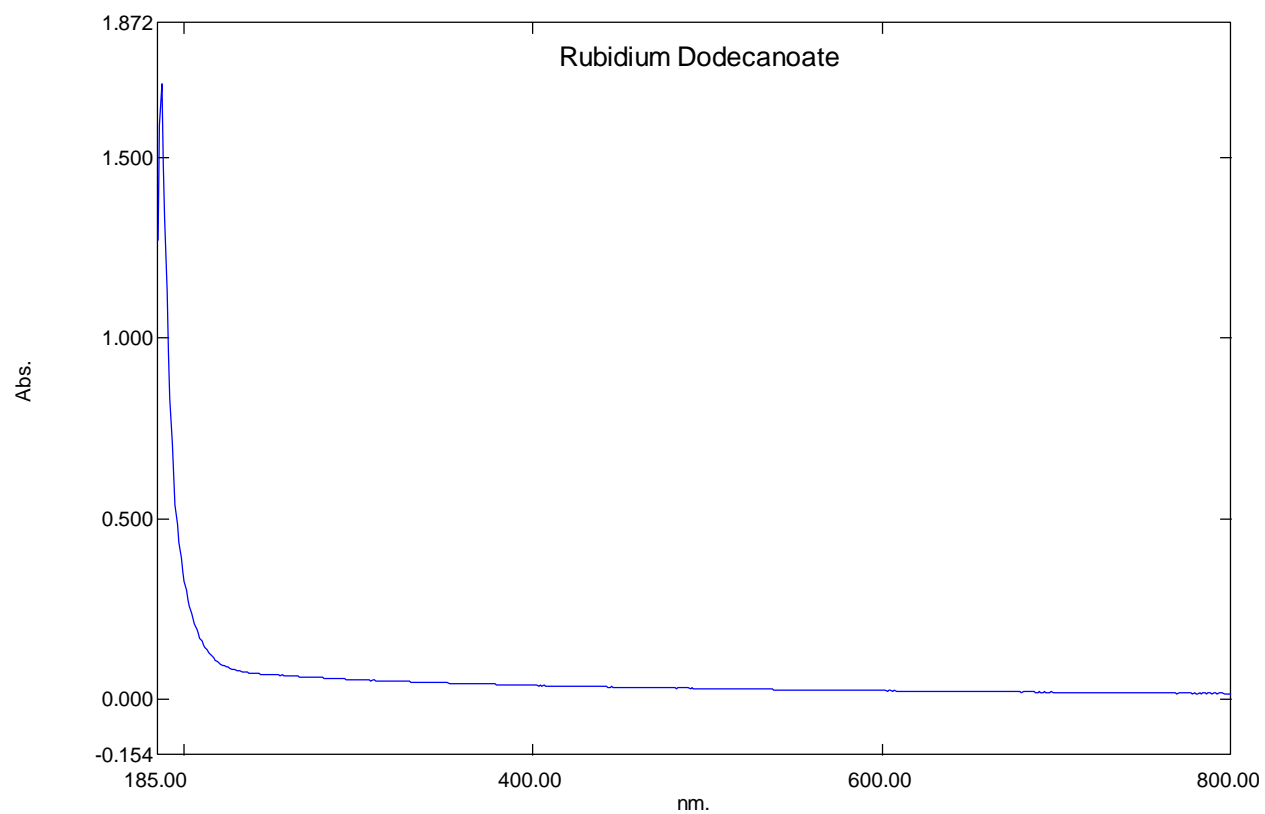


Figure S 195. UV-Vis of rubidium dodecanoate

## TGA Results

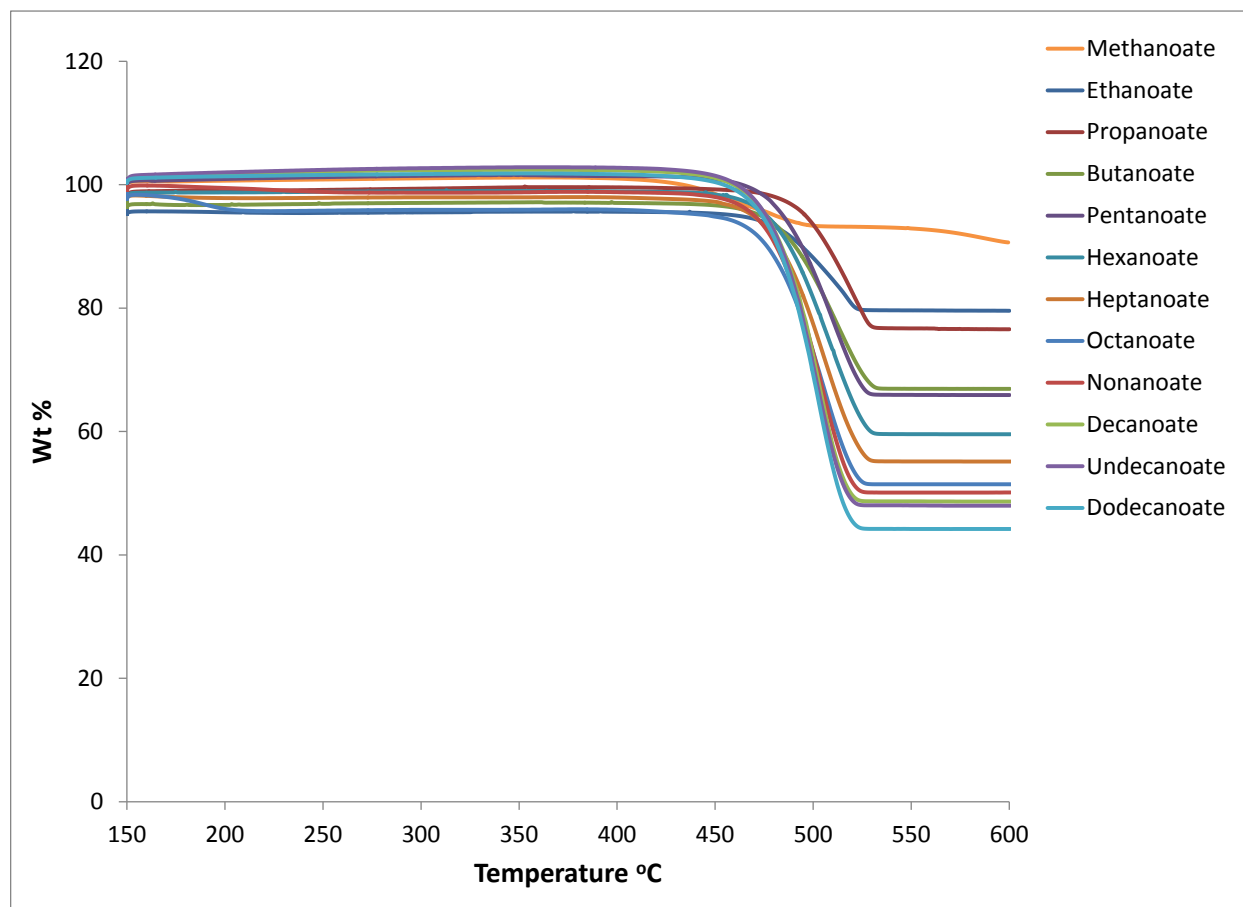


Figure S 196. TGA profile of Rb-carboxylates

## Calorigrams of Rb-Carboxylates determined by the Differential Scanning Calorimeter (DSC)

### Rubidium Methanoate

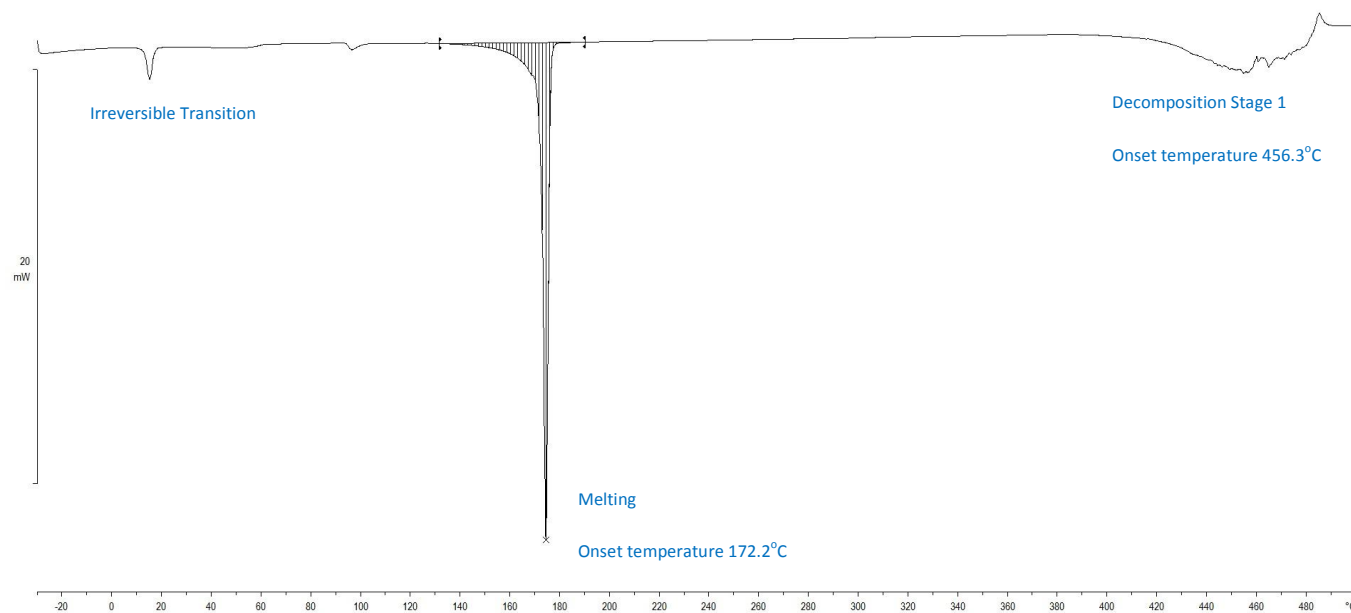


Figure S 197. Calorigram of Rubidium Methanoate determined by the DSC over the range of -30-600°C at 10°C·min<sup>-1</sup> heating rate and 100mL·min<sup>-1</sup> nitrogen flow.

### Rubidium Ethanoate

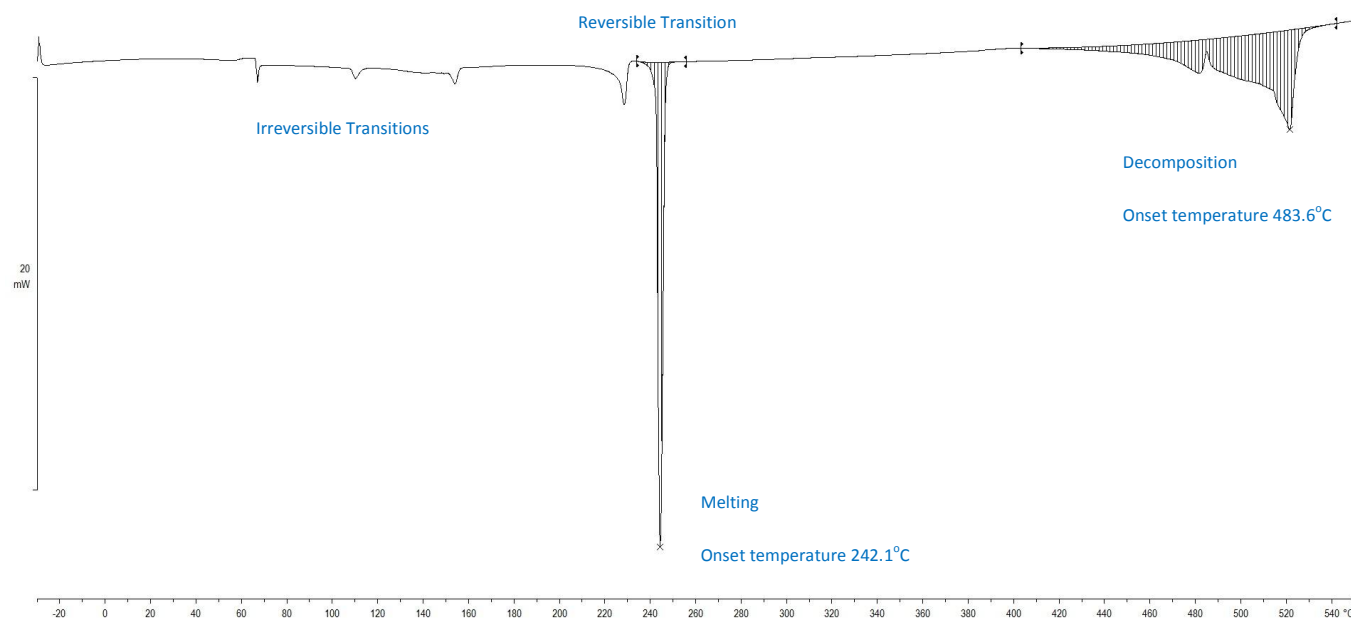


Figure S 198. Calorigram of Rubidium Ethanoate determined by the DSC over the range of -30-600°C at 10°C·min<sup>-1</sup> heating rate and 100mL·min<sup>-1</sup> nitrogen flow.

## Rubidium Propanoate

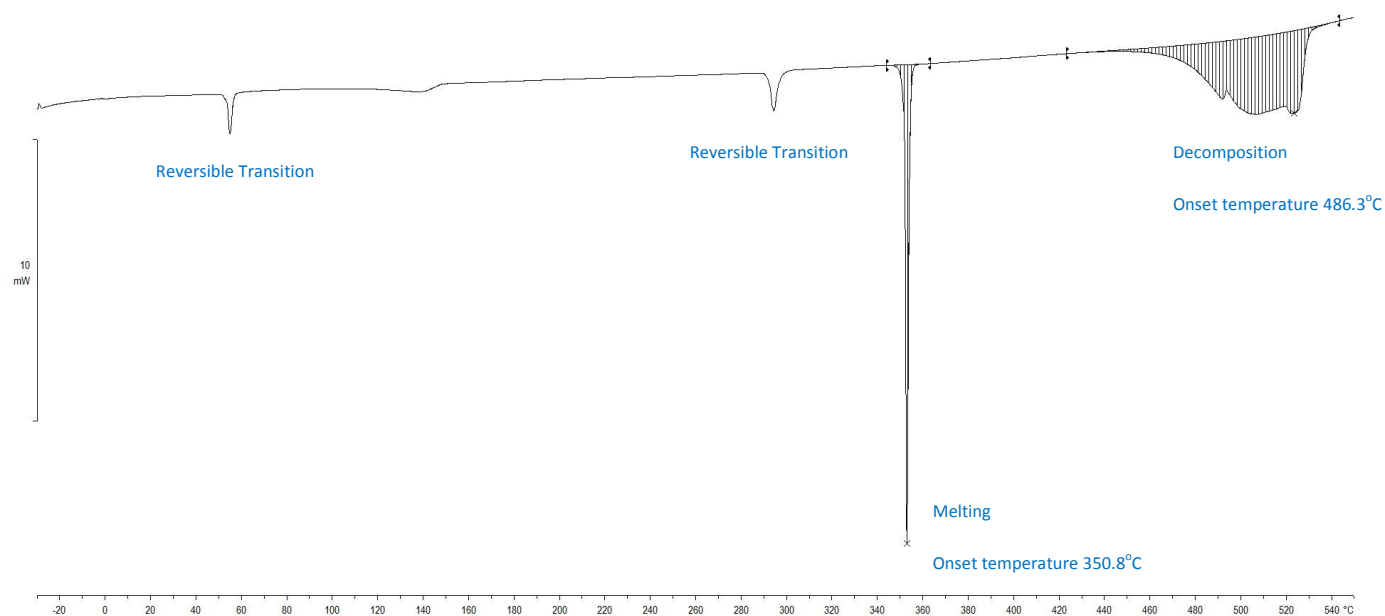


Figure S 199. Calorigram of Rubidium Propanoate determined by the DSC over the range of -30-600°C at 10°C·min<sup>-1</sup> heating rate and 100mL·min<sup>-1</sup> nitrogen flow.

## Rubidium Butanoate (butyrate)

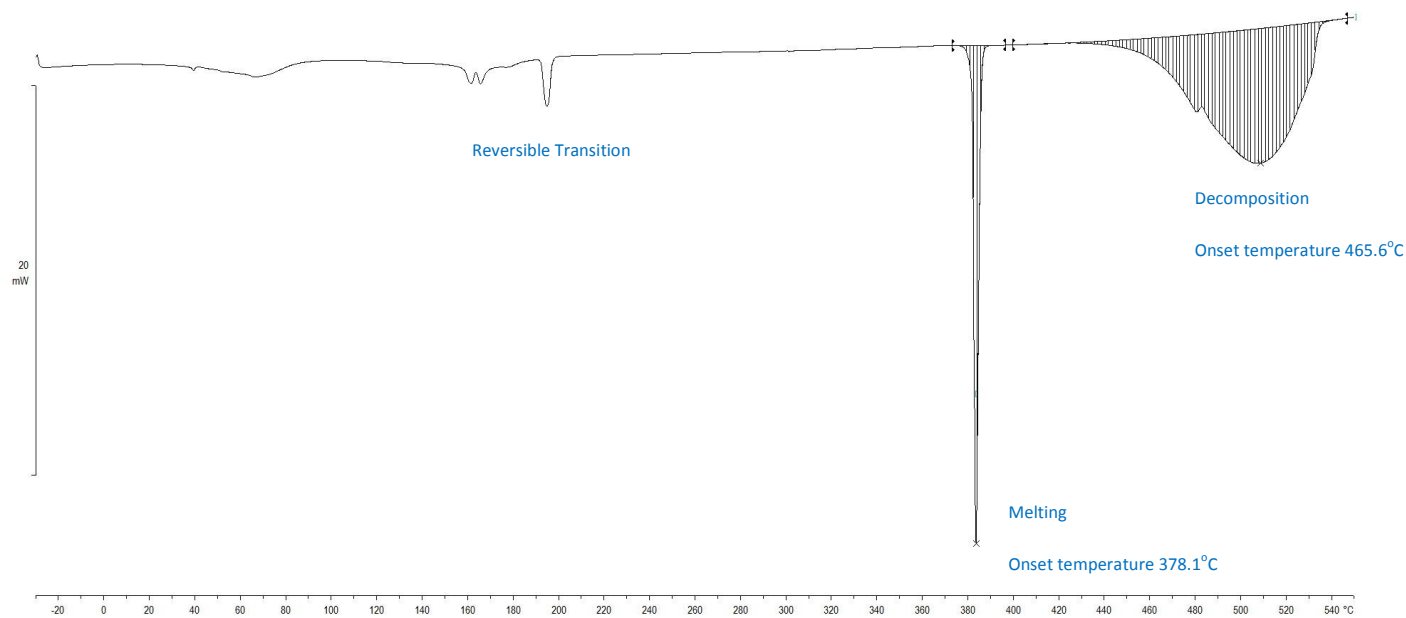


Figure S 200. Calorigram of Rubidium Butanoate determined by the DSC over the range of -30-600°C at 10°C·min<sup>-1</sup> heating rate and 100mL·min<sup>-1</sup> nitrogen flow.

### Rubidium Pentanoate (valerate)

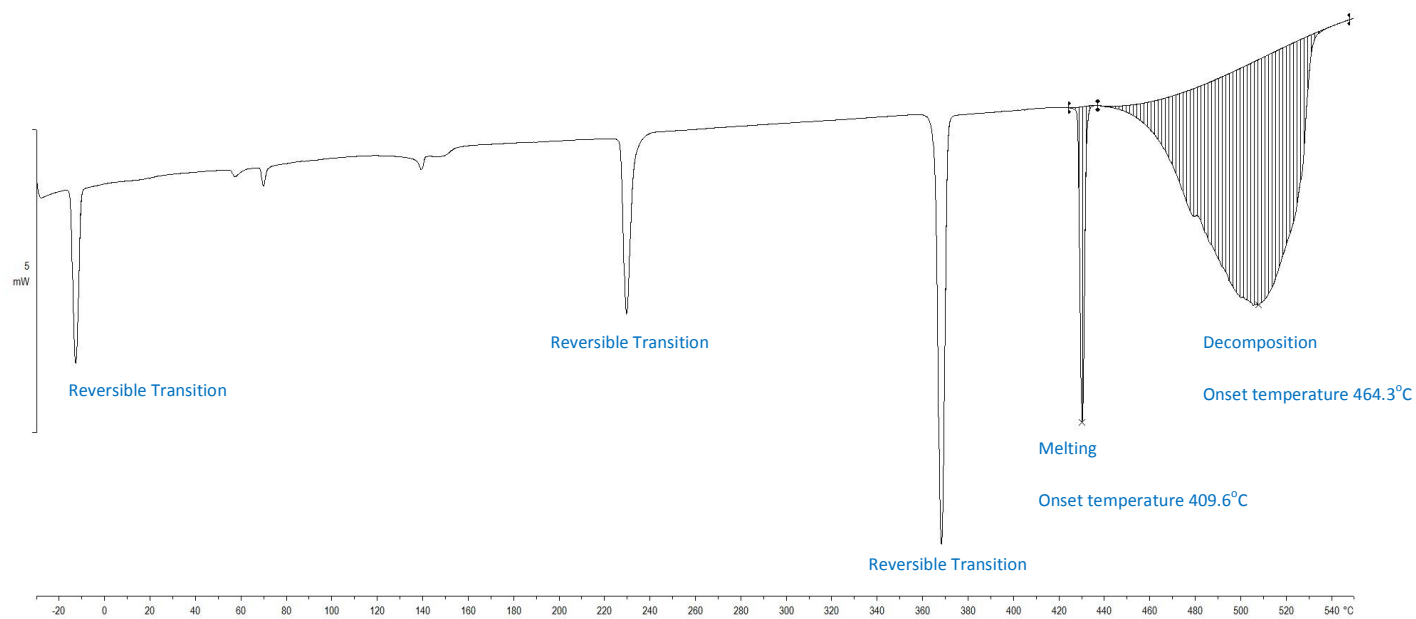


Figure S 201. Calorigram of Rubidium Pentanoate determined by the DSC over the range of -30-600°C at 10°C·min<sup>-1</sup> heating rate and 100mL·min<sup>-1</sup> nitrogen flow.

### Rubidium Hexanoate (caproate)

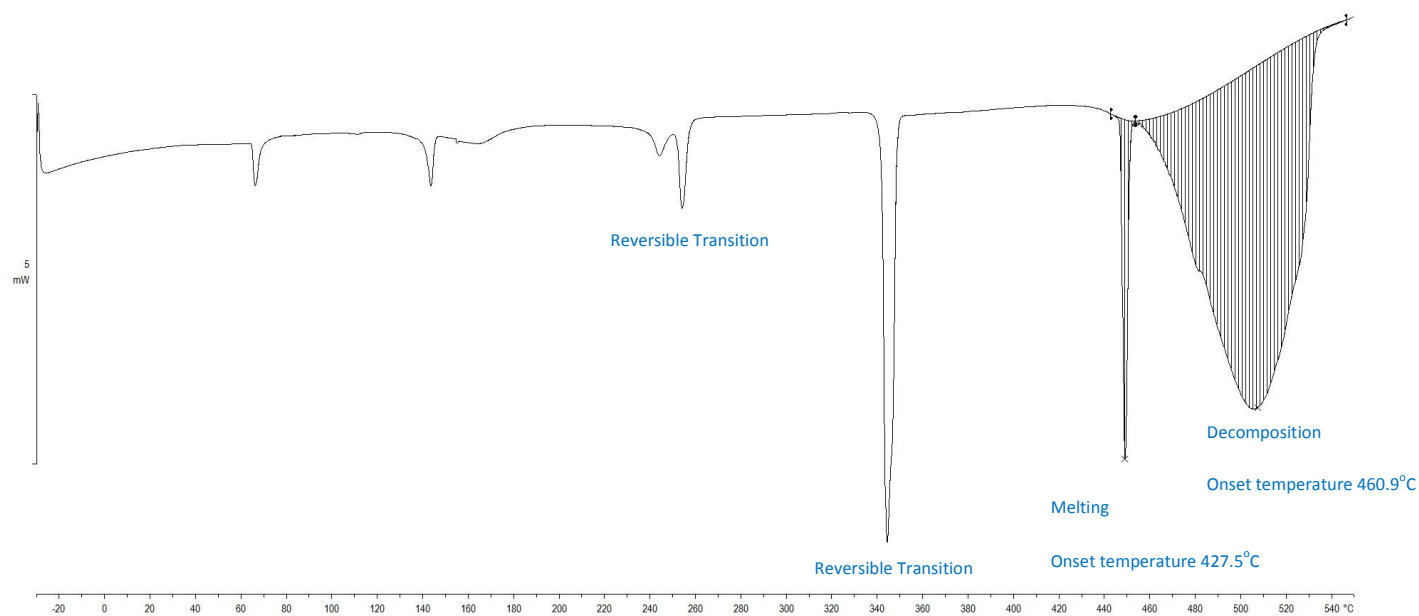


Figure S 202. Calorigram of Rubidium Hexanoate determined by the DSC over the range of -30-600°C at 10°C·min<sup>-1</sup> heating rate and 100mL·min<sup>-1</sup> nitrogen flow.

## Rubidium Heptanoate

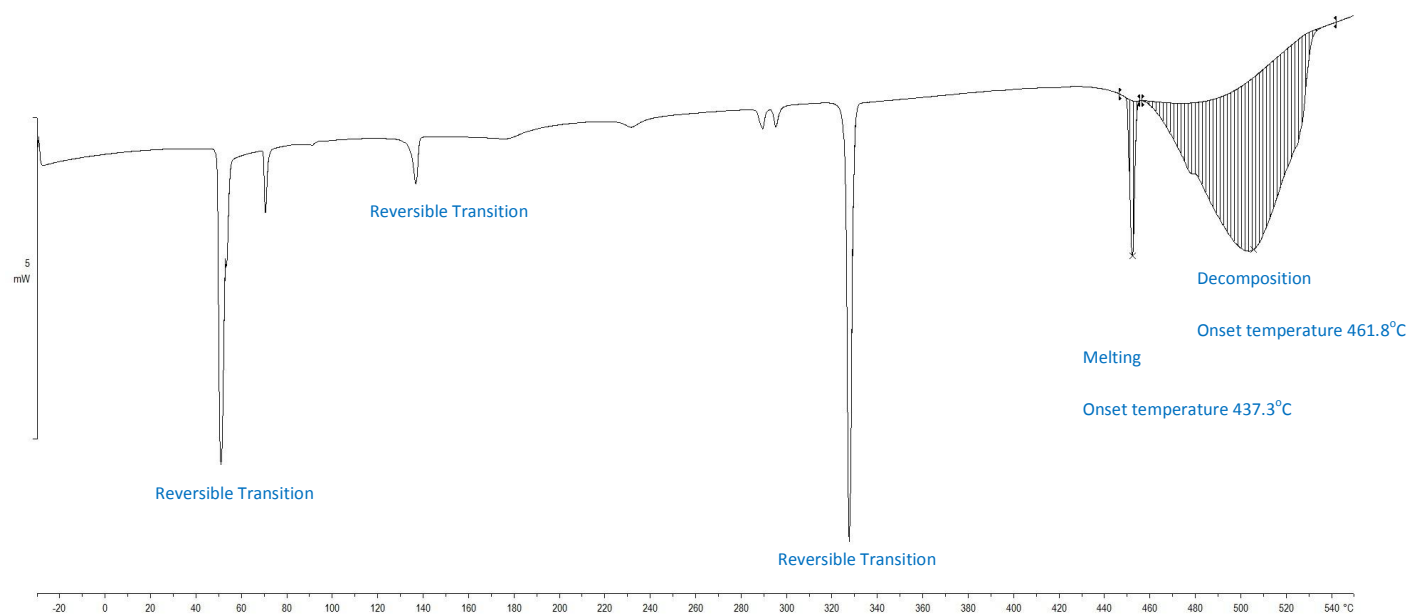


Figure S 203. Calorigram of Rubidium Heptanoate determined by the DSC over the range of -30-600°C at 10°C·min<sup>-1</sup> heating rate and 100mL·min<sup>-1</sup> nitrogen flow.

## Rubidium Octanoate (caprylate)

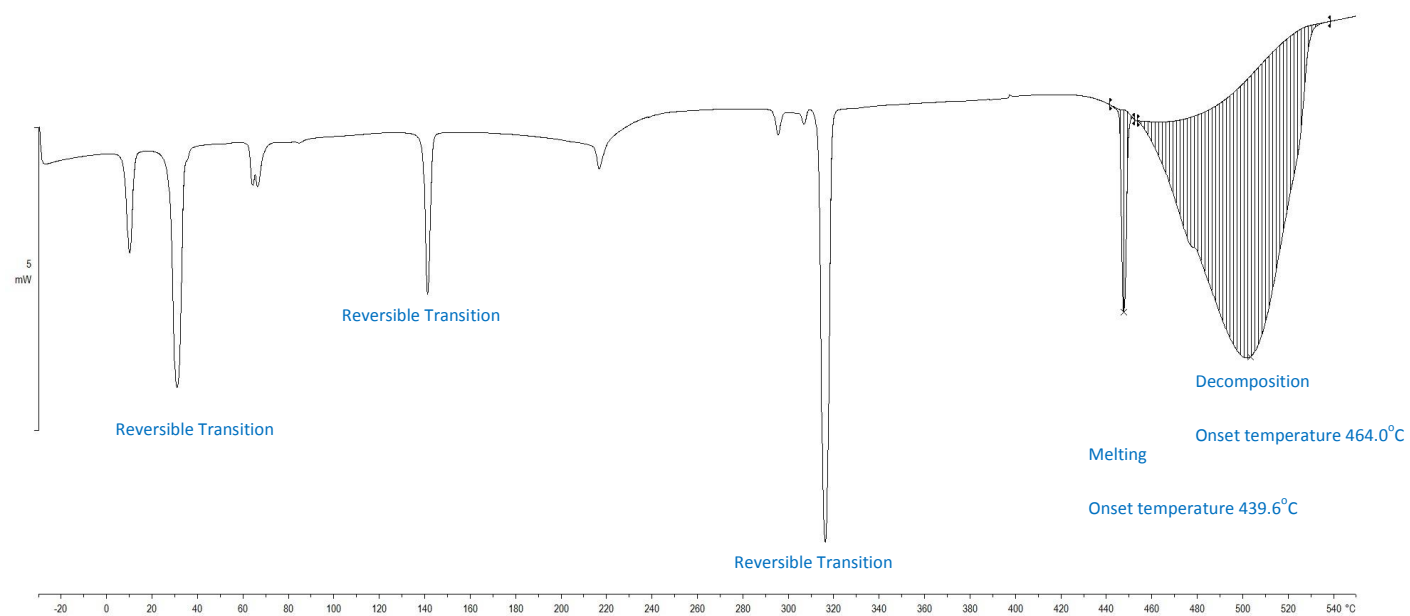


Figure S 204. Calorigram of Rubidium Octanoate determined by the DSC over the range of -30-600°C at 10°C·min<sup>-1</sup> heating rate and 100mL·min<sup>-1</sup> nitrogen flow.

## Rubidium Nonanoate (pelargonate)

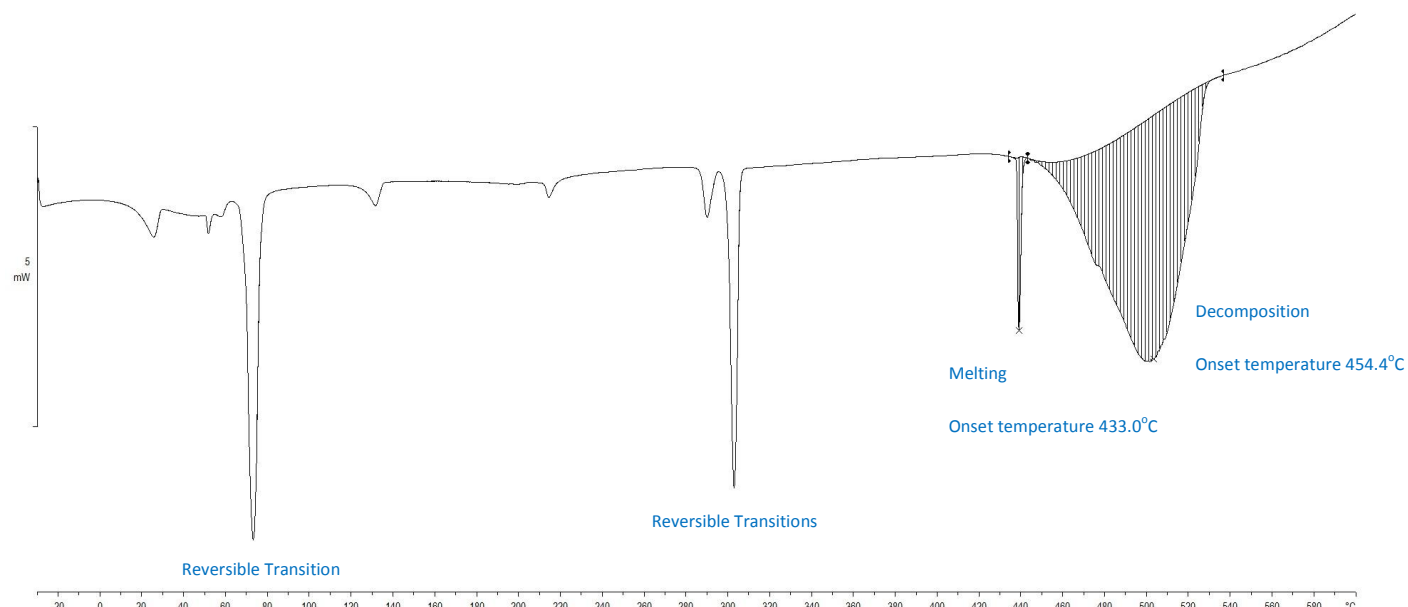


Figure S 205. Calorigram of Rubidium Nonanoate determined by the DSC over the range of -30-600°C at 10°C·min<sup>-1</sup> heating rate and 100mL·min<sup>-1</sup> nitrogen flow.

## Rubidium Decanoate (caprate)

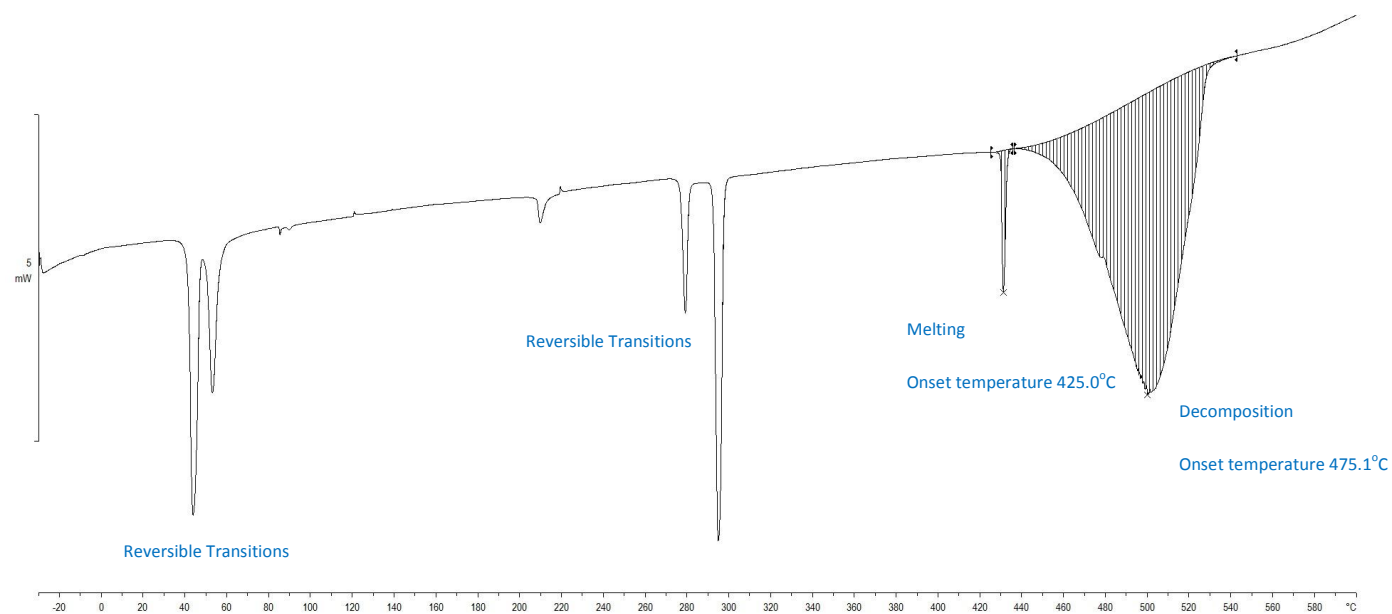


Figure S 206. Calorigram of Rubidium Decanoate determined by the DSC over the range of -30-600°C at 10°C·min<sup>-1</sup> heating rate and 100mL·min<sup>-1</sup> nitrogen flow.

## Rubidium Undecanoate

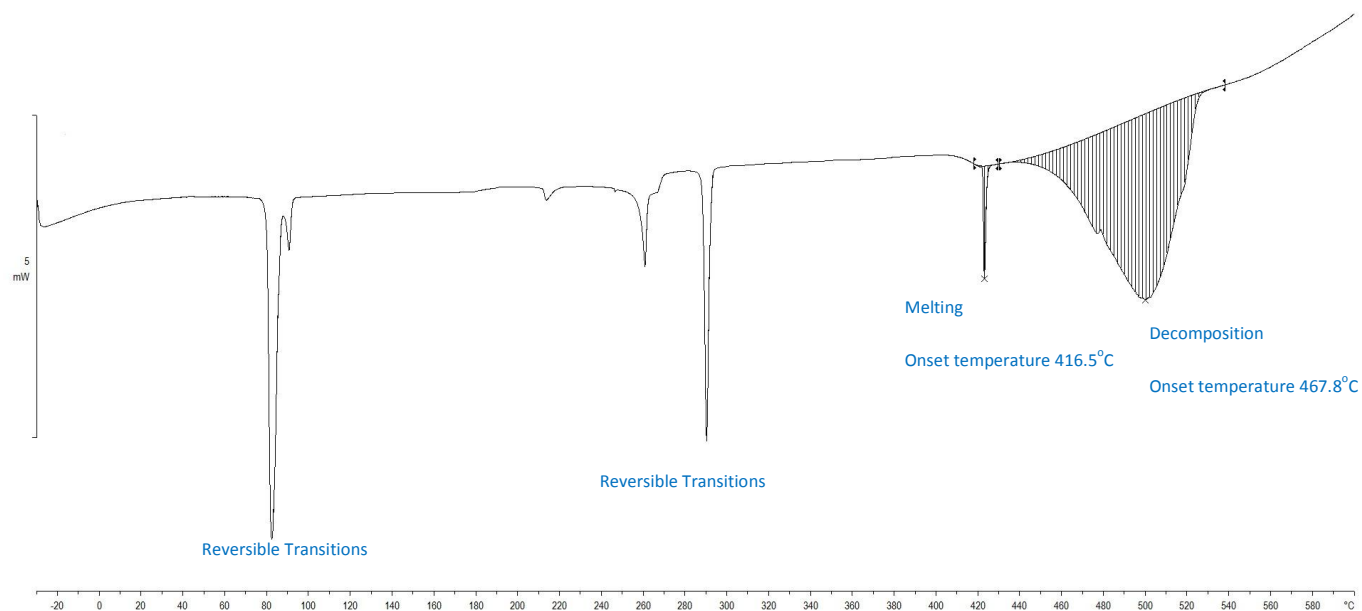


Figure S 207. Calorigram of Rubidium Undecanoate determined by the DSC over the range of -30-600°C at 10°C·min<sup>-1</sup> heating rate and 100mL·min<sup>-1</sup> nitrogen flow.

## Rubidium Dodecanoate (laurate)

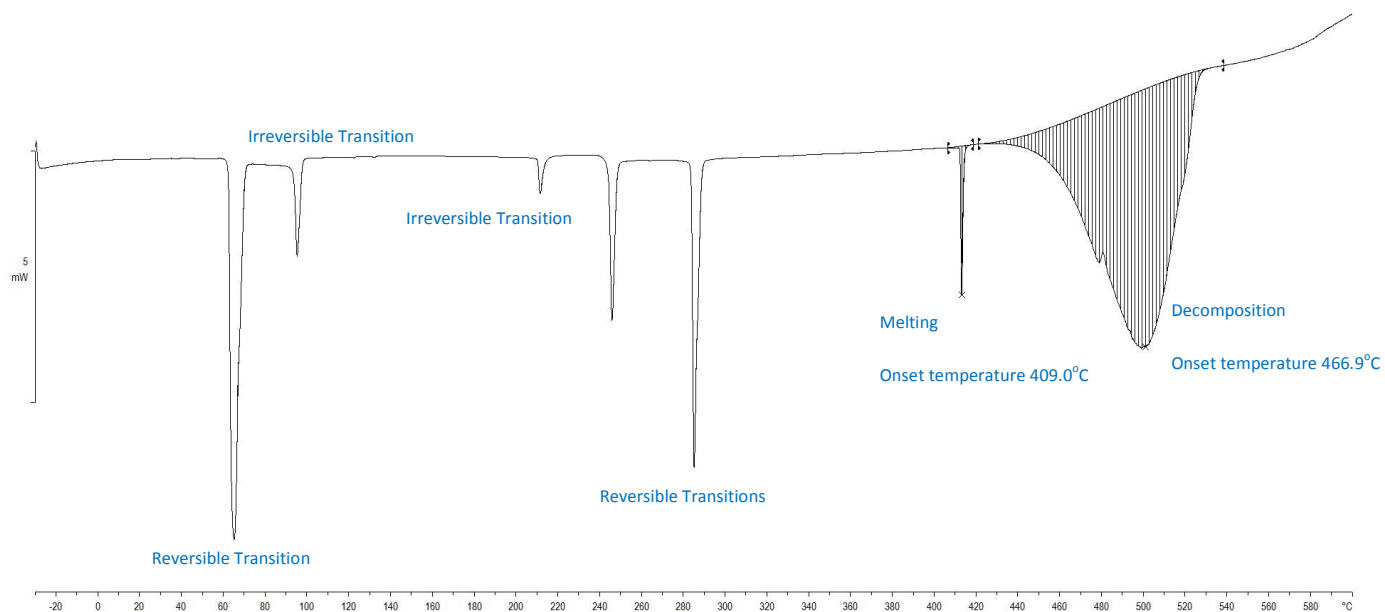


Figure S 208. Calorigram of Rubidium Dodecanoate determined by the DSC over the range of -30-600°C at 10°C·min<sup>-1</sup> heating rate and 100mL·min<sup>-1</sup> nitrogen flow.

## Heat Capacity

### Rubidium Methanoate

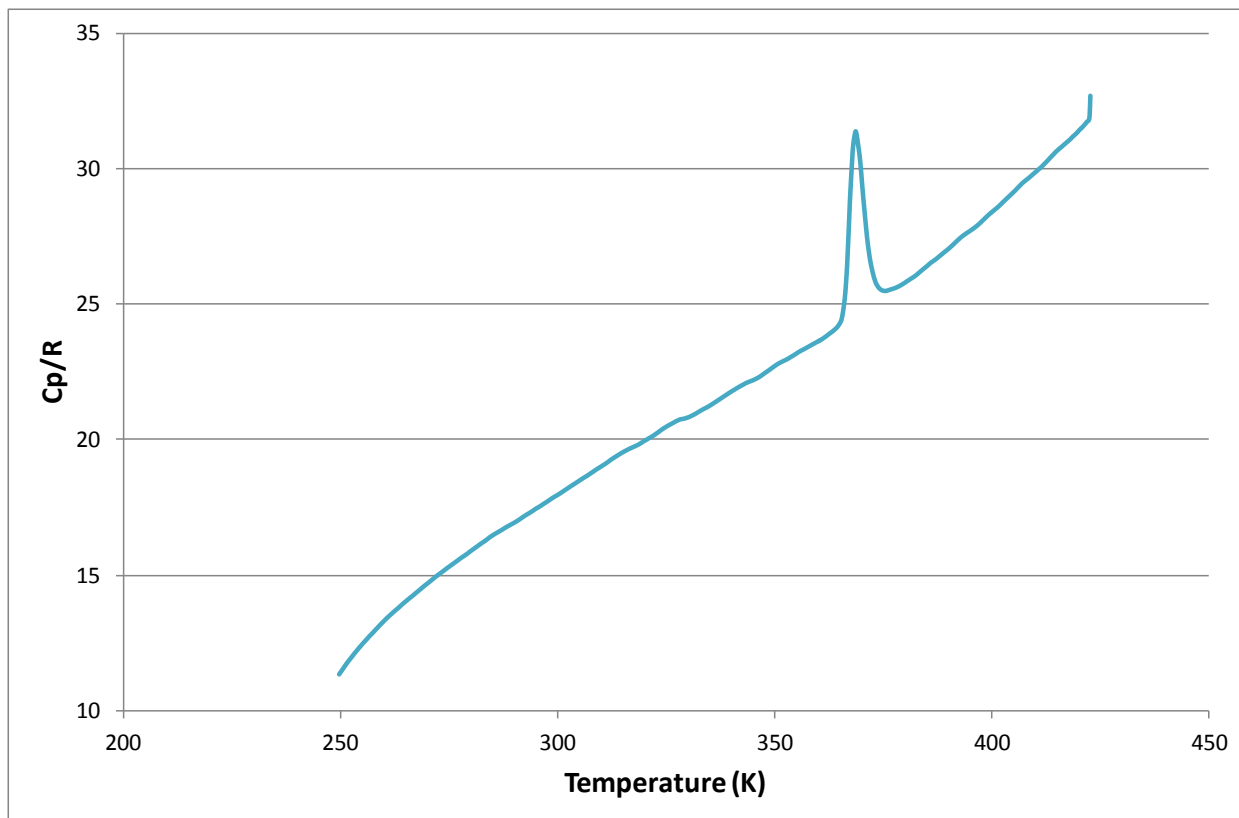


Figure S 209. Experimental molar heat capacities for Rb-methanoate ( $R = 8.31451 \text{ JK}^{-1}\text{mol}^{-1}$ )

## Rubidium Ethanoate

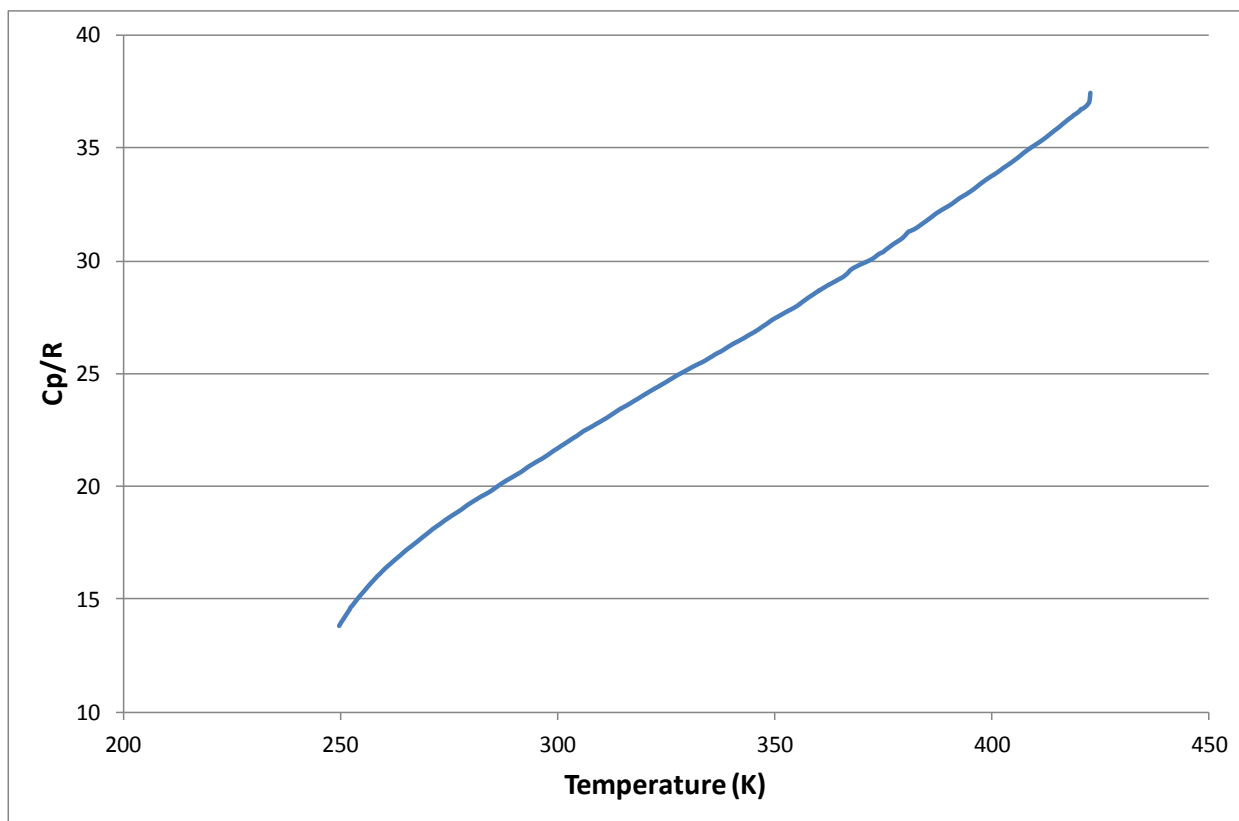


Figure S 210. Experimental molar heat capacities for Rb-ethanoate ( $R = 8.31451 \text{ JK}^{-1}\text{mol}^{-1}$ )

## Rubidium Propanoate

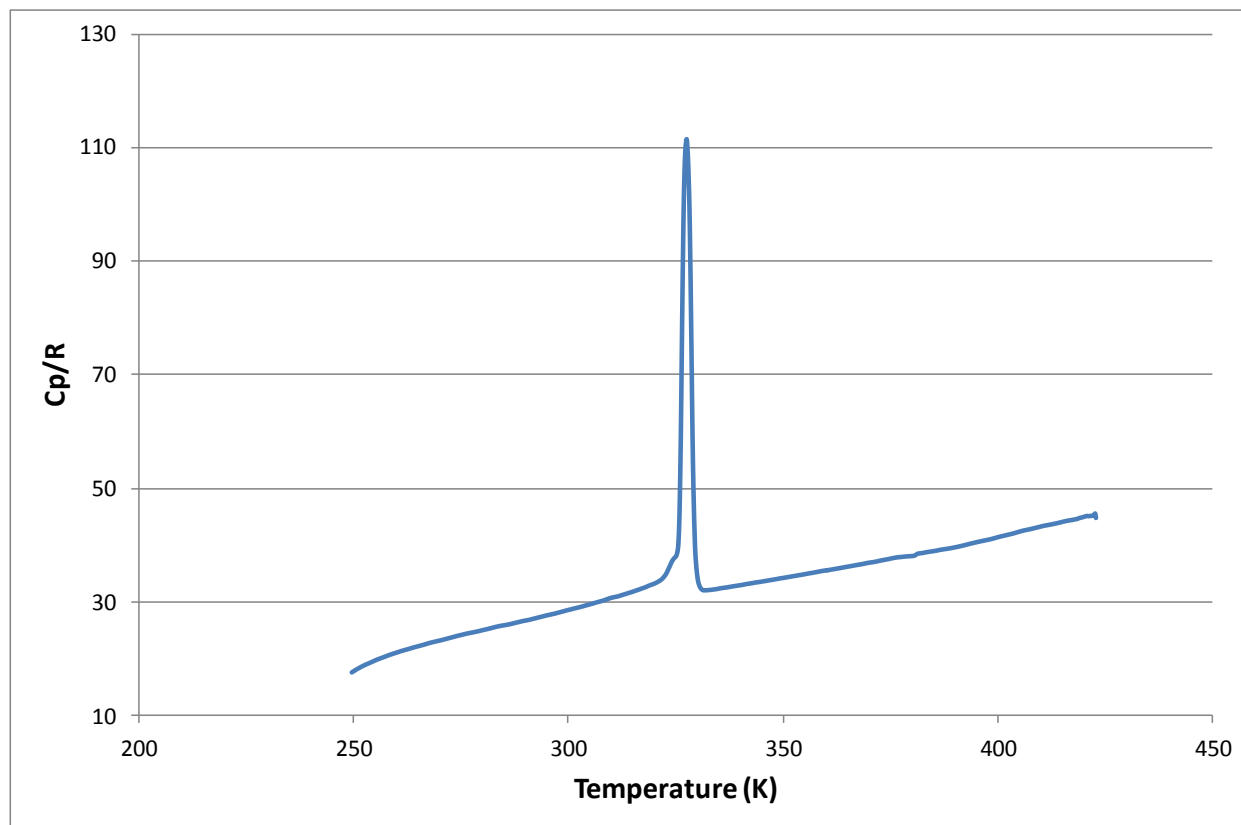


Figure S 211. Experimental molar heat capacities for Rb-propanoate ( $R = 8.31451 \text{ JK}^{-1}\text{mol}^{-1}$ )

## Rubidium Butanoate

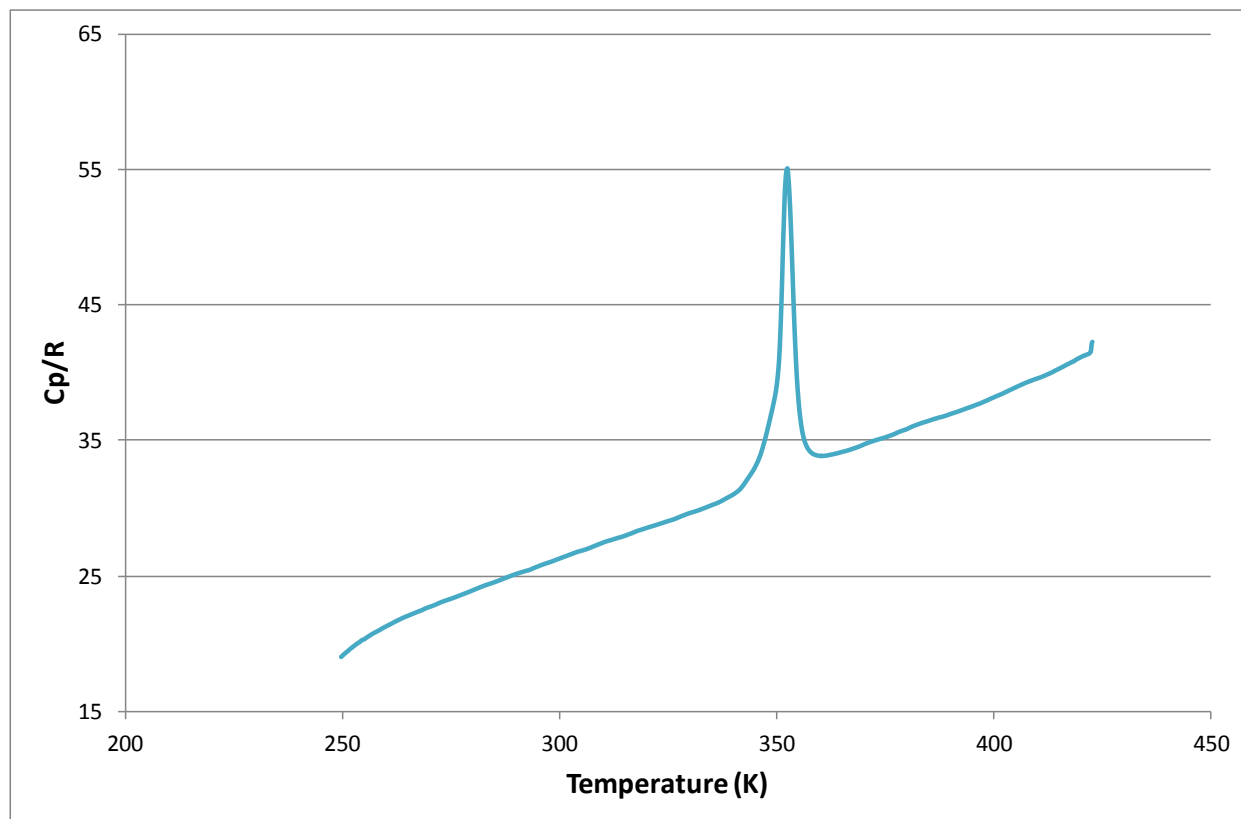


Figure S 212. Experimental molar heat capacities for Rb-butanoate ( $R = 8.31451 \text{ JK}^{-1}\text{mol}^{-1}$ )

### Rubidium Pentanoate (valerate)

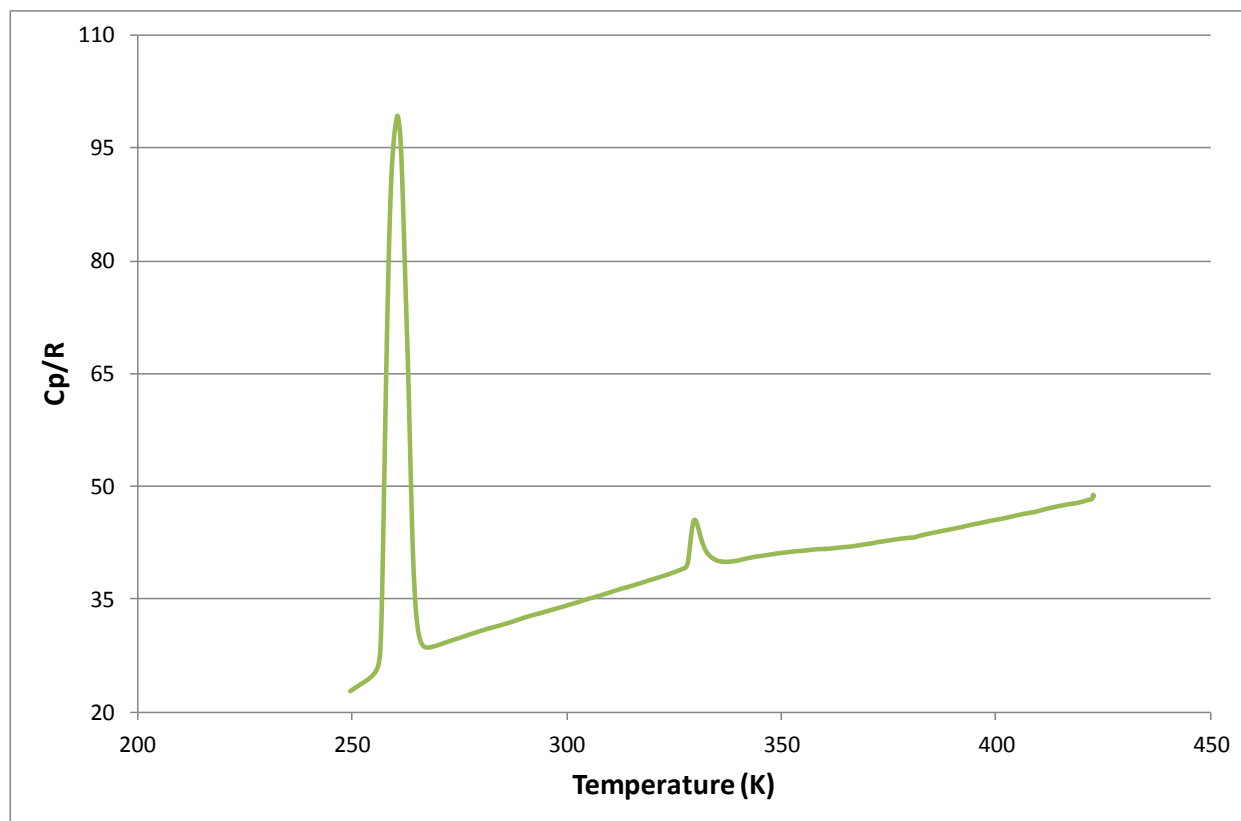


Figure S 213. Experimental molar heat capacities for Rb-pentanoate ( $R = 8.31451 \text{ JK}^{-1}\text{mol}^{-1}$ )

## Rubidium Hexanoate (caproate)

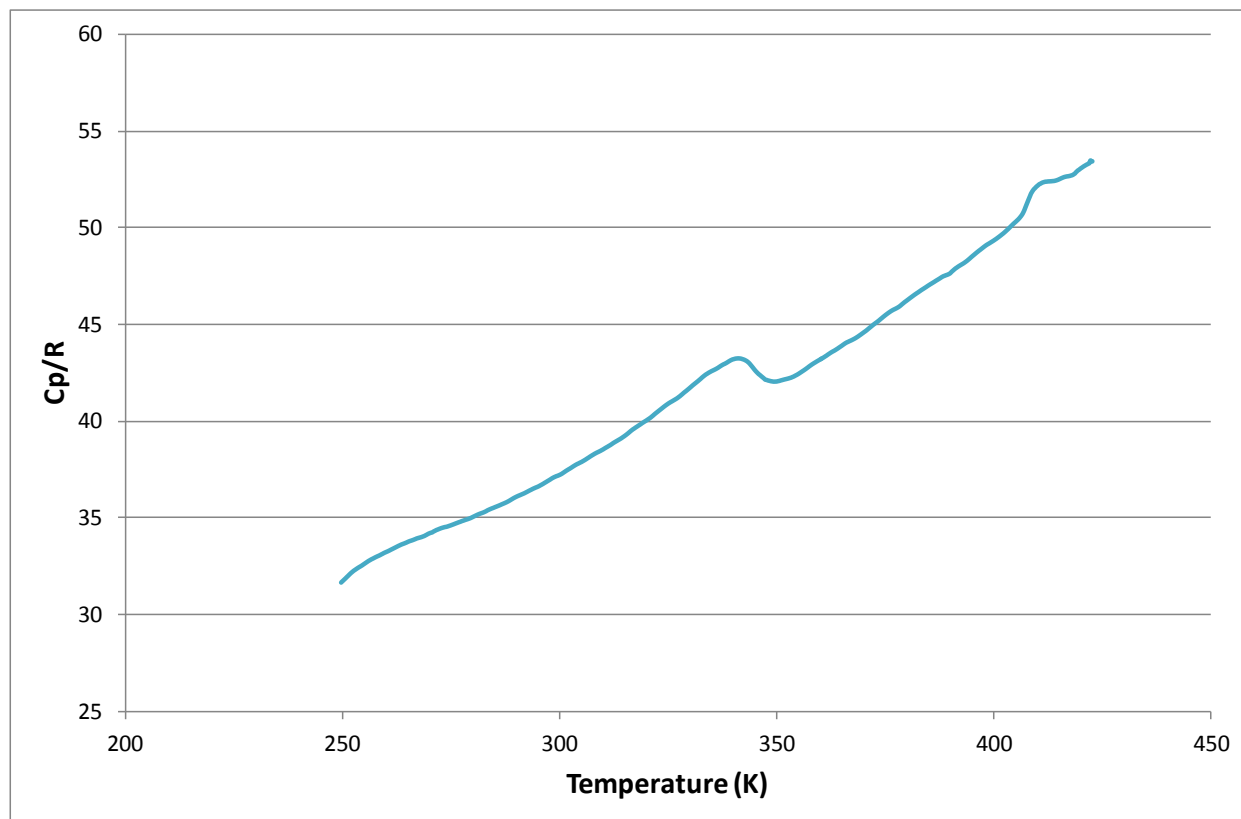


Figure S 214. Experimental molar heat capacities for Rb-hexanoate ( $R = 8.31451 \text{ JK}^{-1}\text{mol}^{-1}$ )

## Rubidium Heptanoate

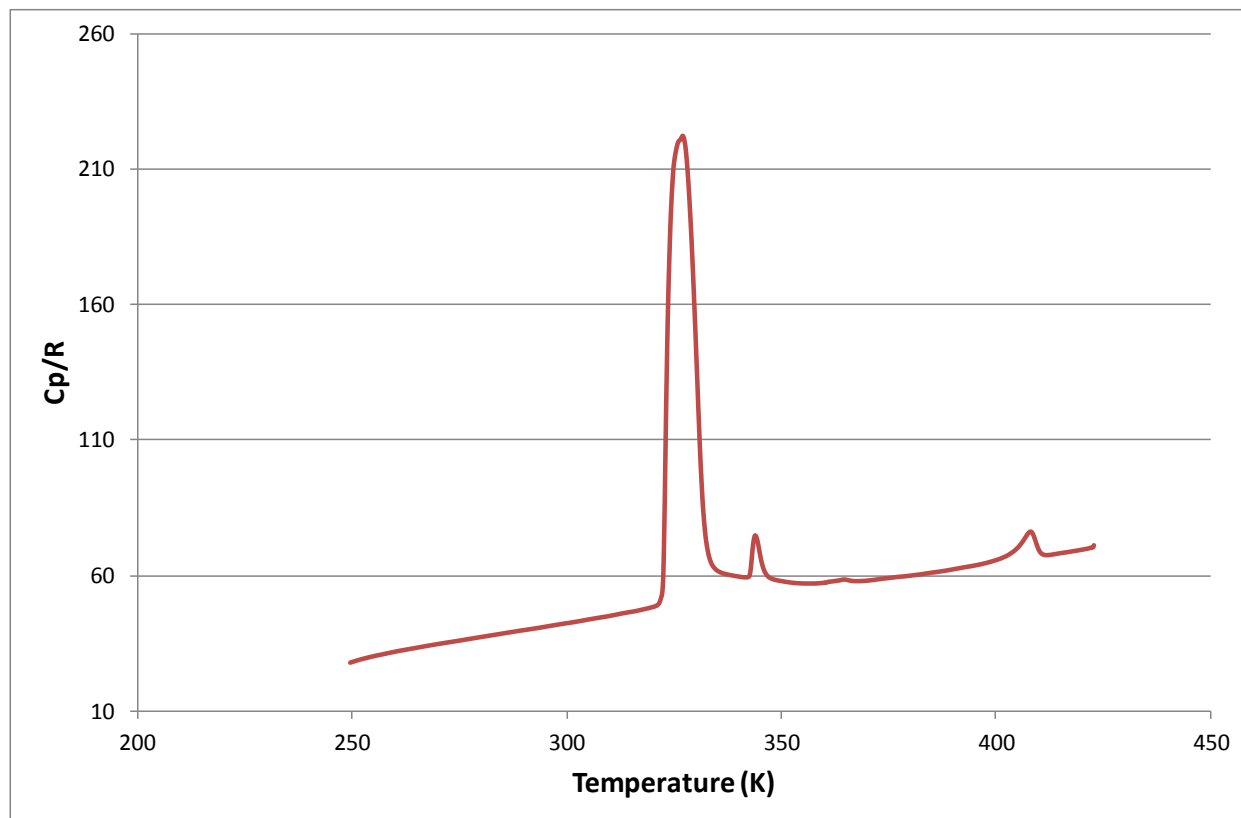


Figure S 215. Experimental molar heat capacities for Rb-heptanoate ( $R = 8.31451 \text{ JK}^{-1} \text{ mol}^{-1}$ )

## Rubidium Octanoate (caprylate)

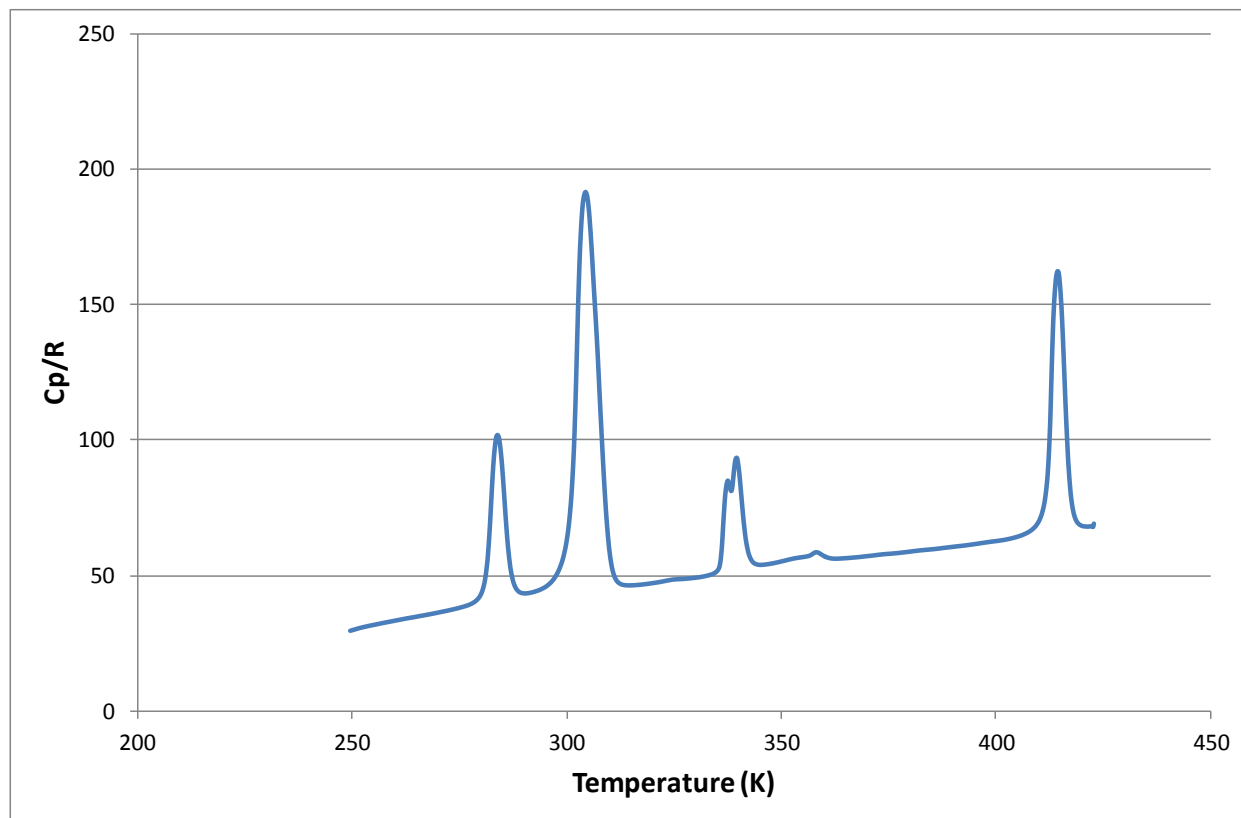


Figure S 216. Experimental molar heat capacities for Rb-octanoate ( $R = 8.31451 \text{ JK}^{-1} \text{ mol}^{-1}$ )

## Rubidium Nonanoate (pelargonate)

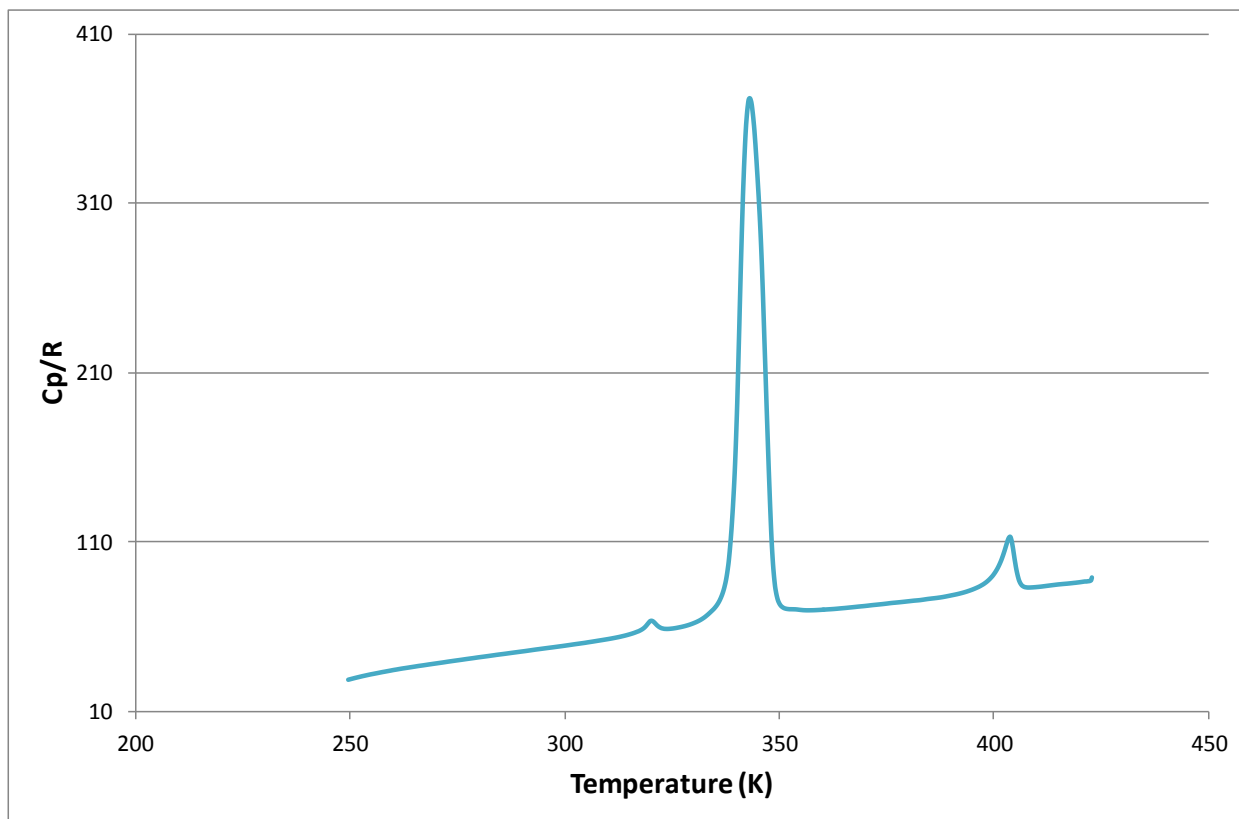


Figure S 217. Experimental molar heat capacities for Rb-nonanoate ( $R = 8.31451 \text{ JK}^{-1}\text{mol}^{-1}$ )

## Rubidium Decanoate (caprate)

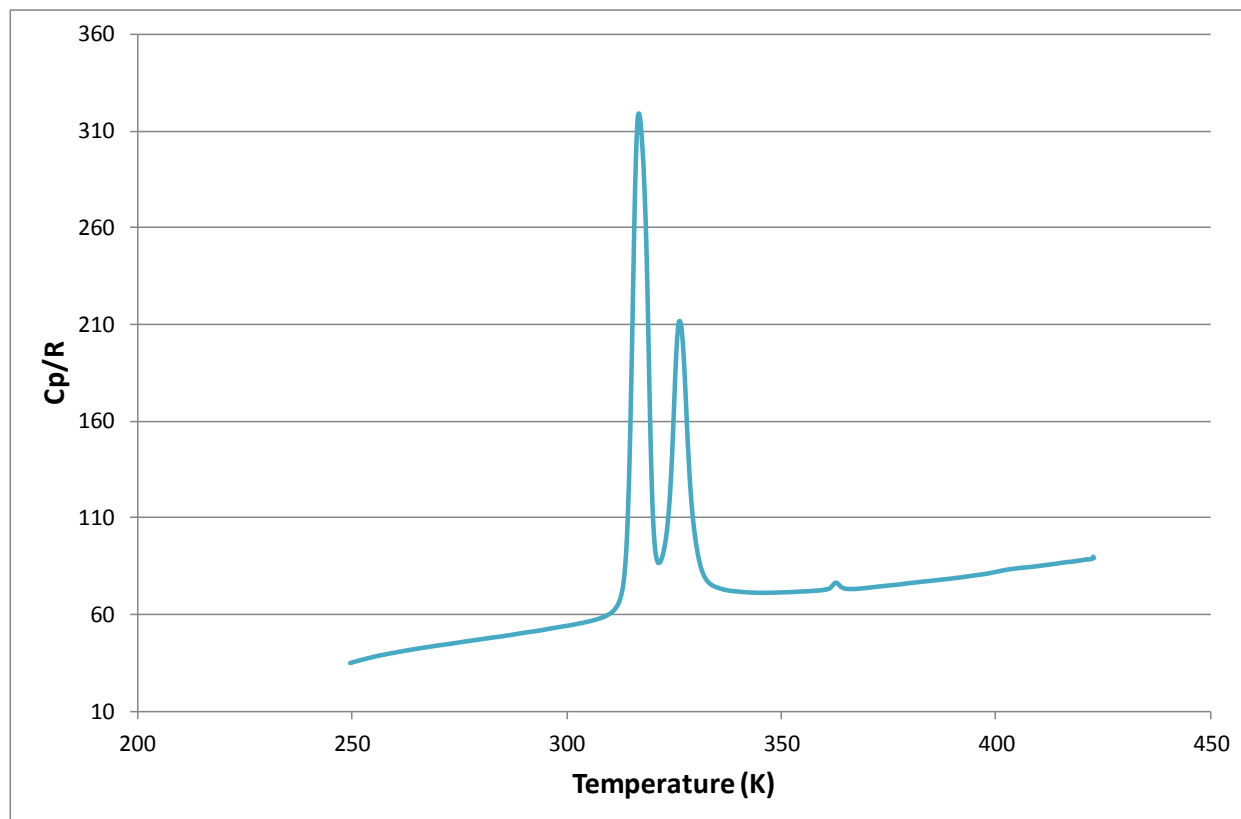


Figure S 218. Experimental molar heat capacities for Rb-decanoate ( $R = 8.31451 \text{ JK}^{-1}\text{mol}^{-1}$ )

## Rubidium Undecanoate

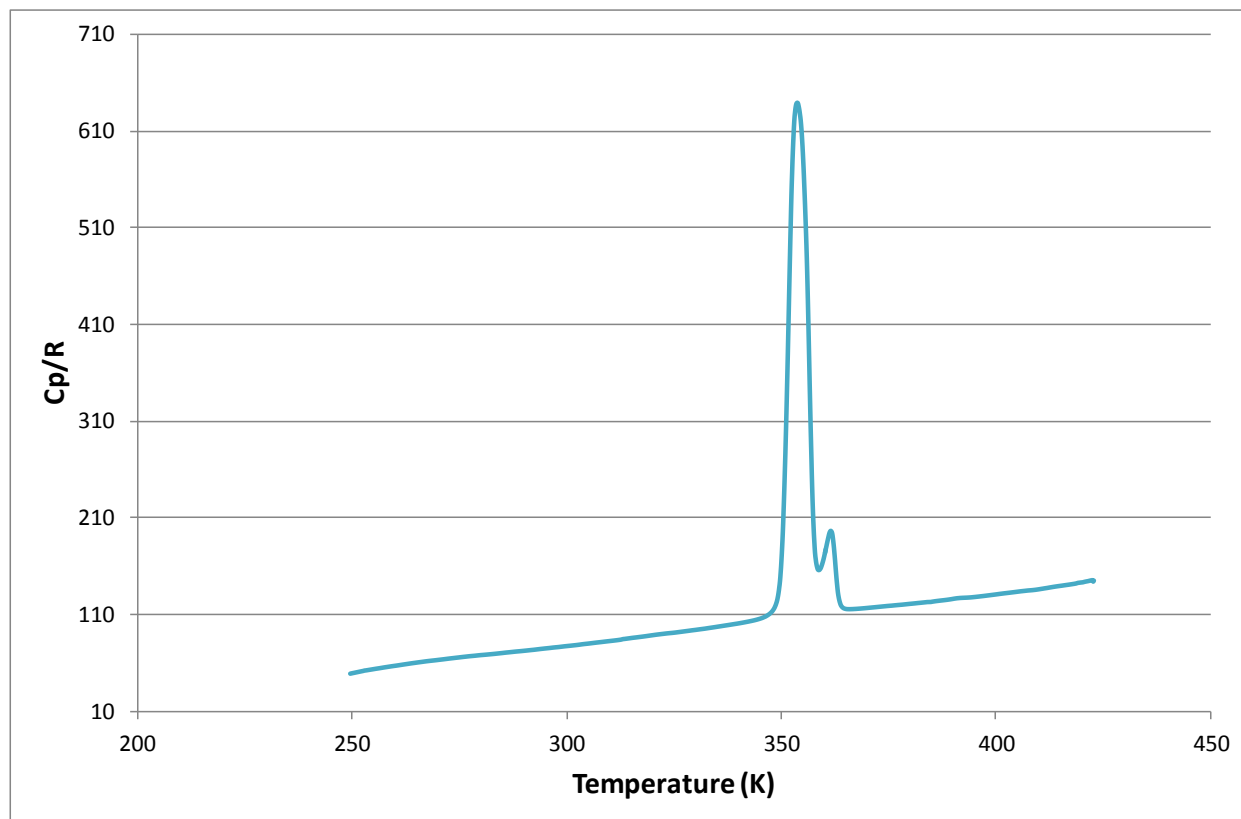


Figure S 219. Experimental molar heat capacities for Rb-undecanoate ( $R = 8.31451 \text{ JK}^{-1}\text{mol}^{-1}$ )

## Rubidium Dodecanoate (laurate)

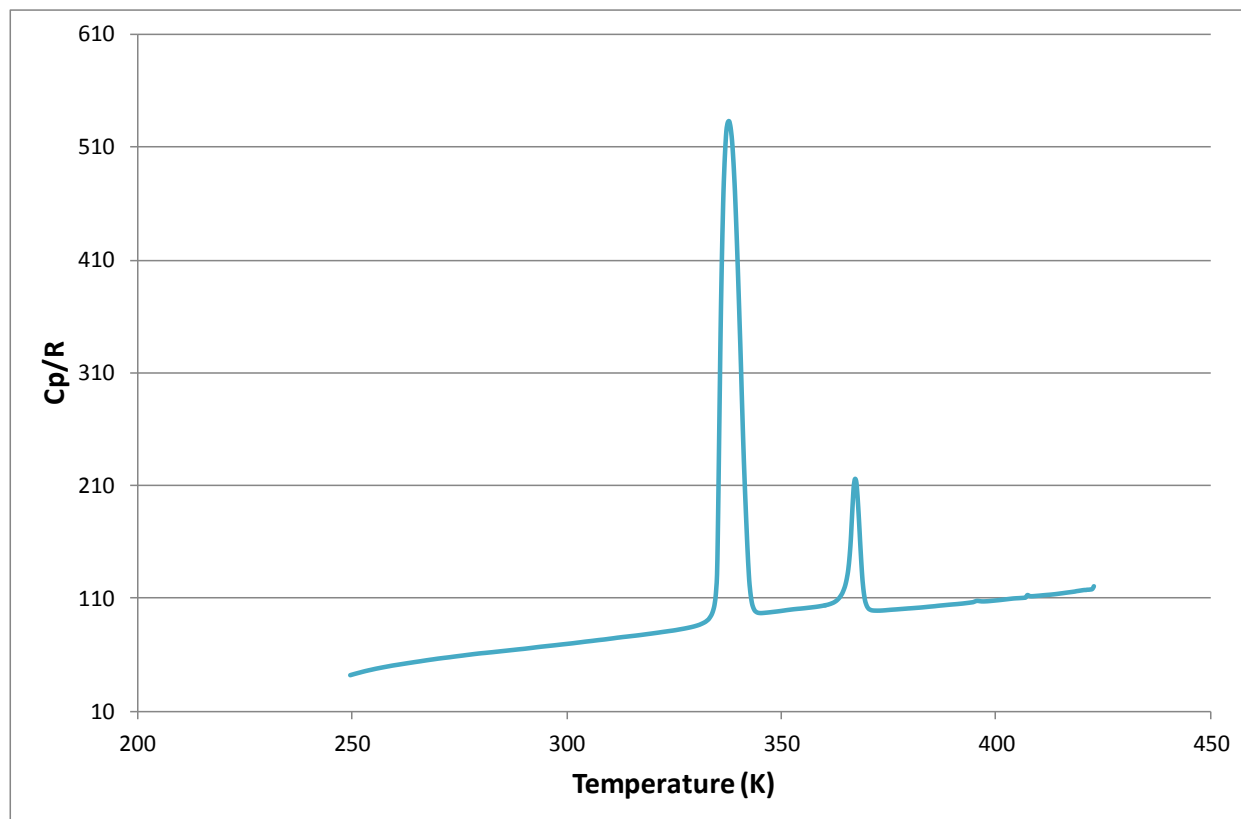


Figure S 220. Experimental molar heat capacities for Rb-dodecanoate ( $R = 8.31451 \text{ JK}^{-1}\text{mol}^{-1}$ )

## Cesium C<sub>1</sub>-C<sub>12</sub> *n*-alkanoates: Thermal behavior from –30 to 600 °C

The primary aim of the investigation was to study thermal behaviour. The spectroscopic data was employed to support the thermal investigation. The reasoning behind the collection of the spectroscopic data was as follows:

- (a) Infrared (IR) spectroscopy is sensitive for the detection of carbonyl and carboxylate compounds. It could therefore be used to confirm synthesis of the cesium carboxylates, as well as provide an indication of purity. Synthesis was performed with a 2 % molar excess of carboxylic acid and if the acid was not completely removed during purification, it would be visible on the infrared spectrum.
- (b) IR spectroscopy was also employed to determine whether chemical changes took place during calorimetry. Once a thermal event was observed, a sample was run to a temperature just above the temperature of the observed thermal event and the IR spectrum of the sample thus treated was collected and compared with the starting material.
- (c) IR, Raman and Ultraviolet-Visible (UV-Vis) spectra were collected in the hope of finding explanations for differences in thermal behaviour, and in the hope that additional information about the nature of the cesium carboxylates can be deduced.

## IR Spectra

### Cesium methanoate (formate)

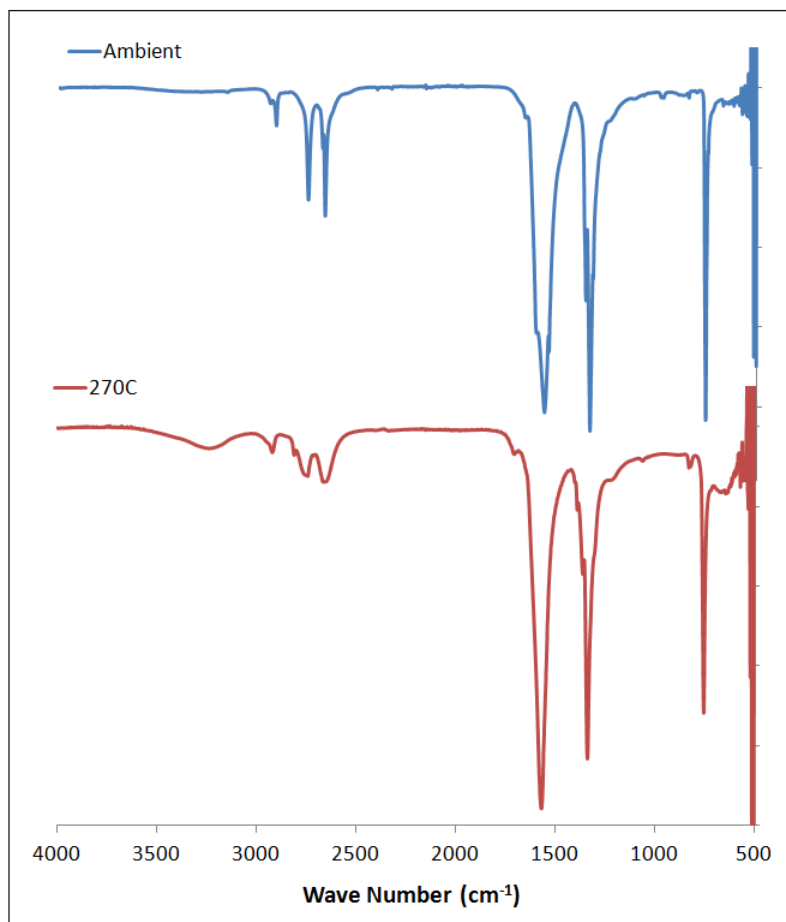
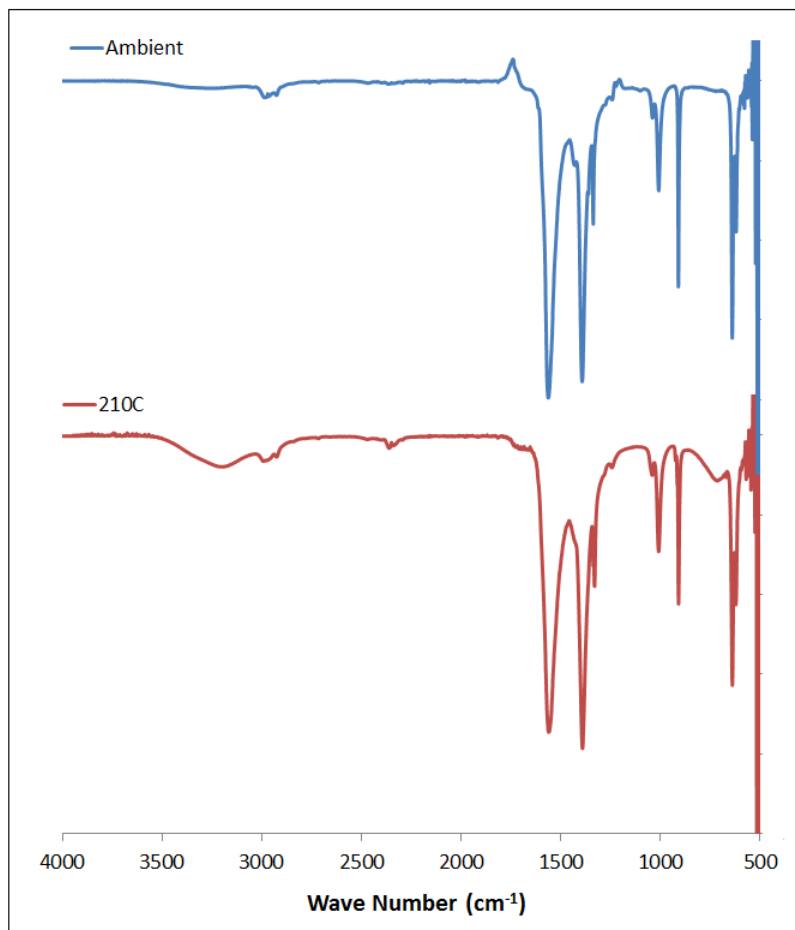


Figure S 221. IR spectrum of cesium methanoate before and after melting

**Cesium ethanoate (acetate)**



**Figure S 222. IR spectrum of cesium ethanoate before and after melting.**

## Cesium propanoate

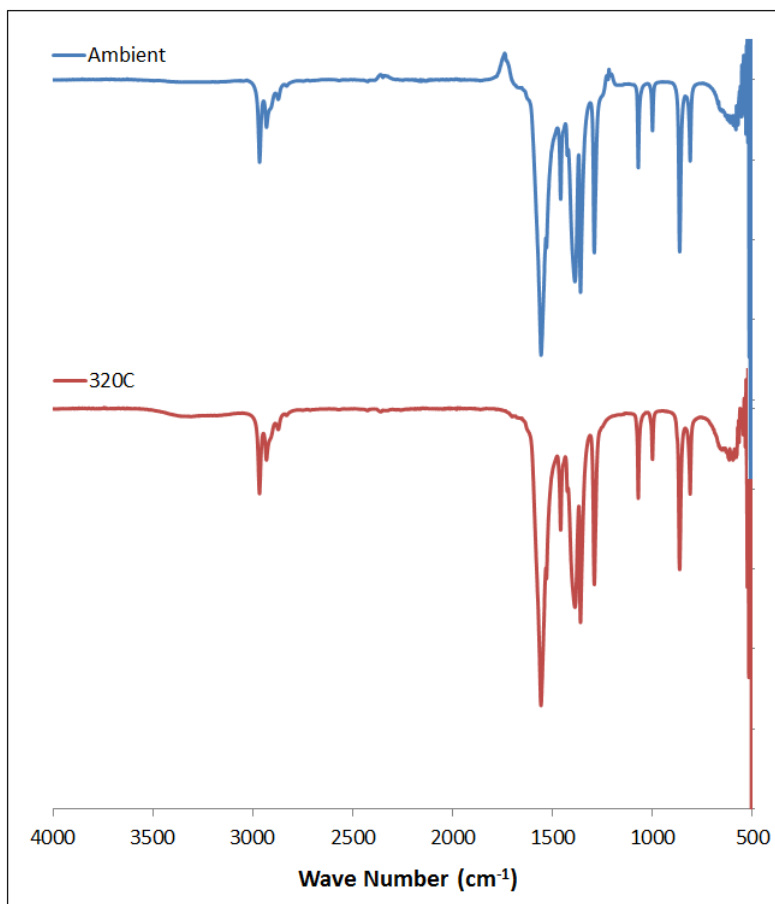


Figure S 223. IR spectrum of cesium propanoate before and after melting.

## Cesium butanoate (butyrate)

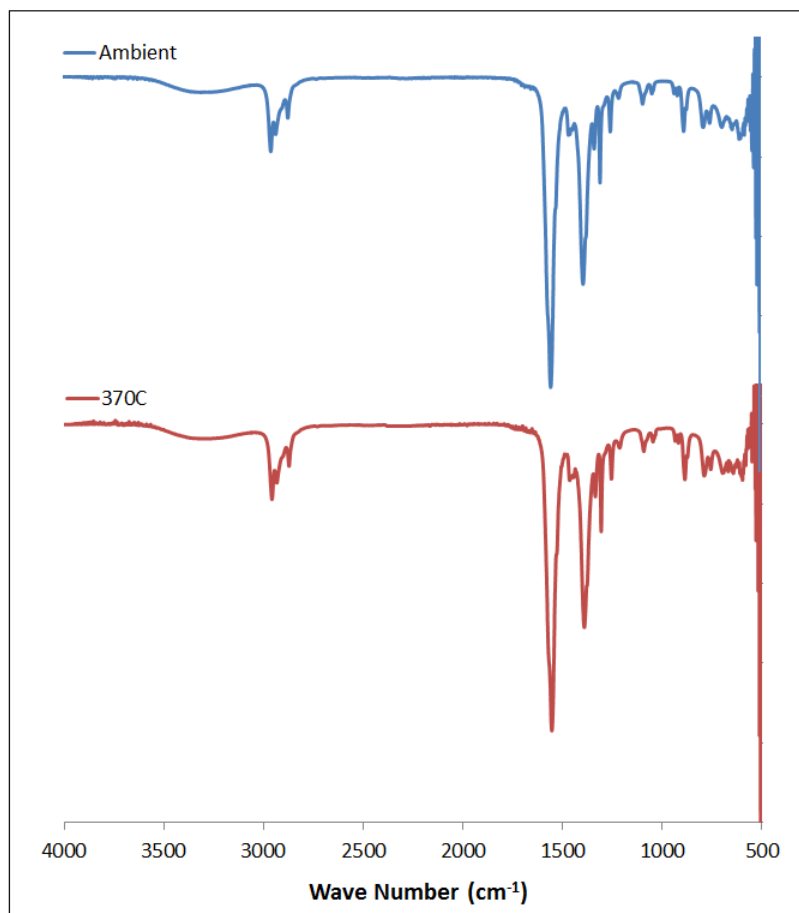


Figure S 224. IR spectrum of cesium butanoate before and after melting.

## Cesium pentanoate (valerate)

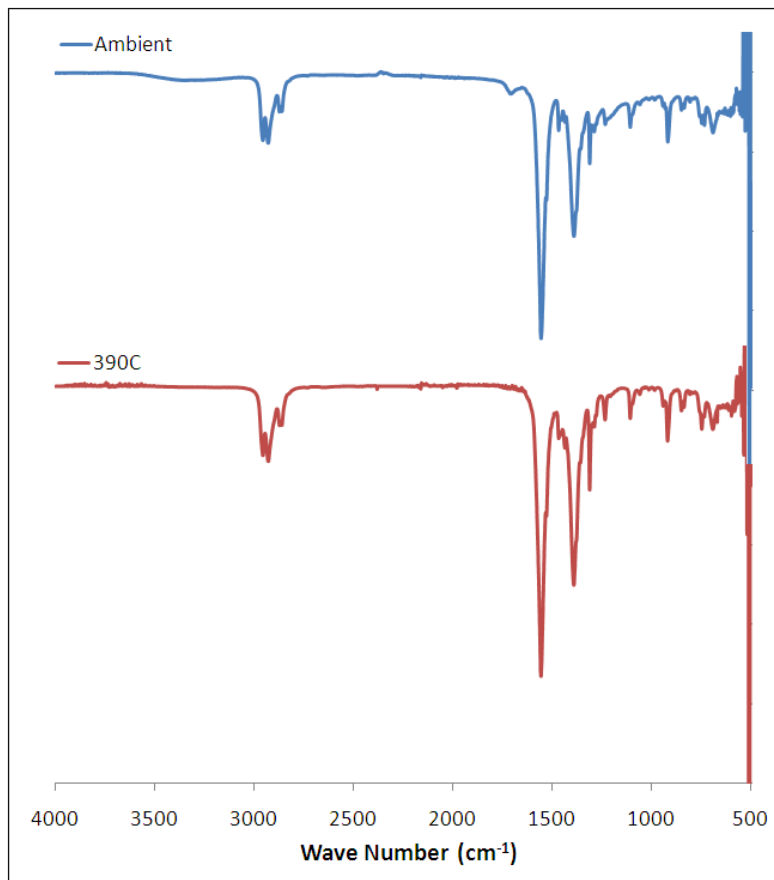
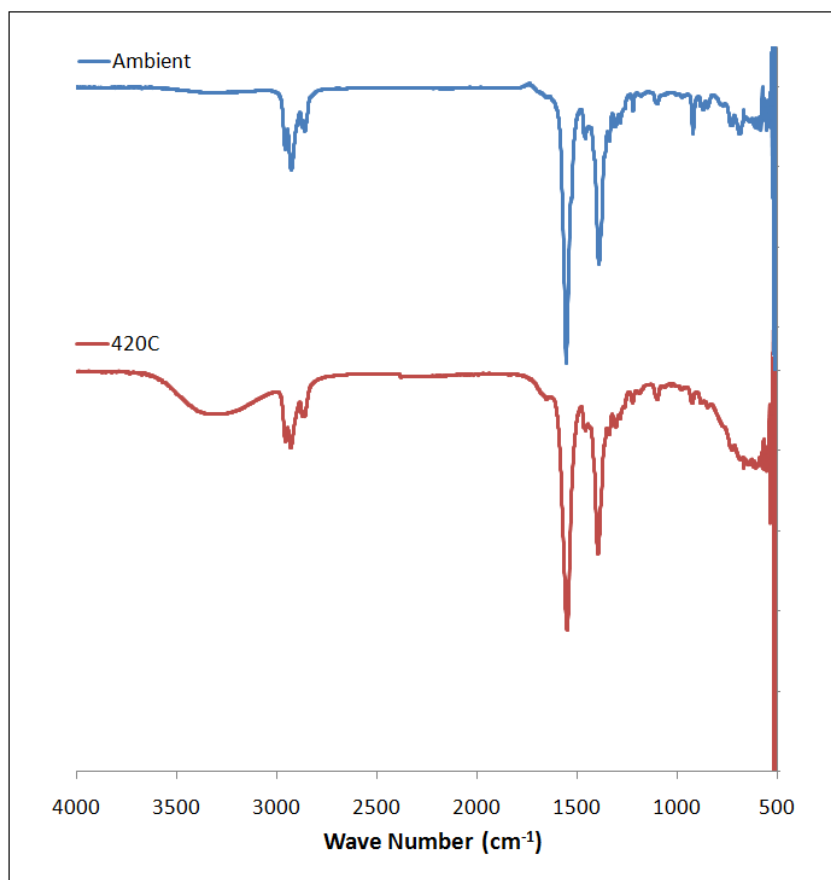


Figure S 225. IR spectrum of cesium pentanoate before and after melting.

**Cesium hexanoate (caproate)**



**Figure S 226. IR spectrum of cesium hexanoate before and after melting.**

## Cesium heptanoate

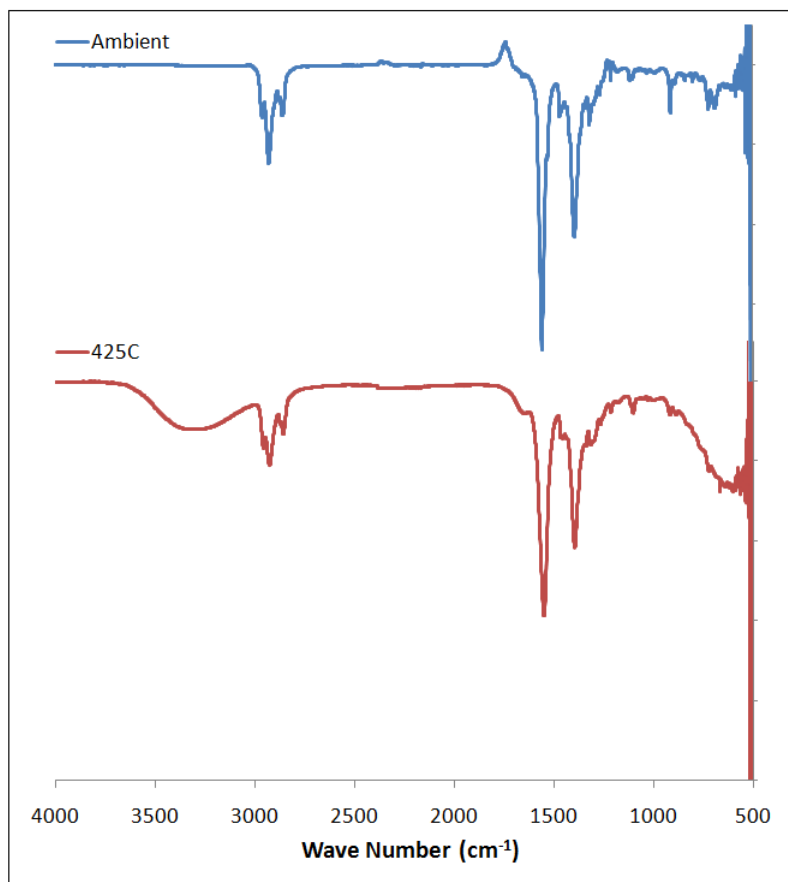


Figure S 227. IR spectrum of cesium heptanoate before and after melting.

## Cesium octanoate (caprylate)

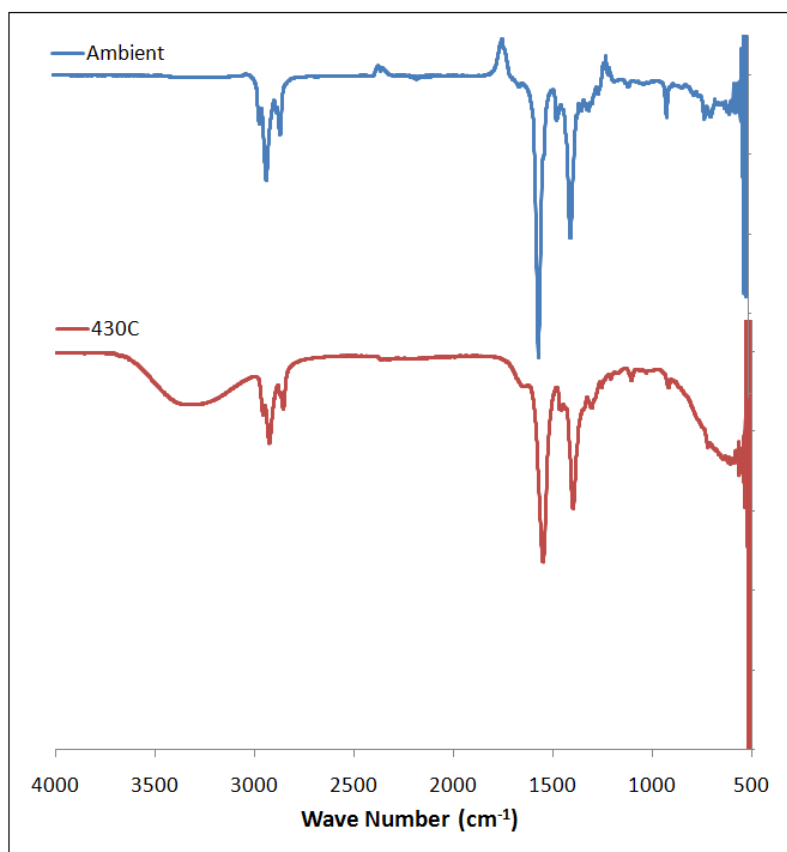


Figure S 228. IR spectrum of cesium octanoate before and after melting.

## Cesium nonanoate (pelargonate)

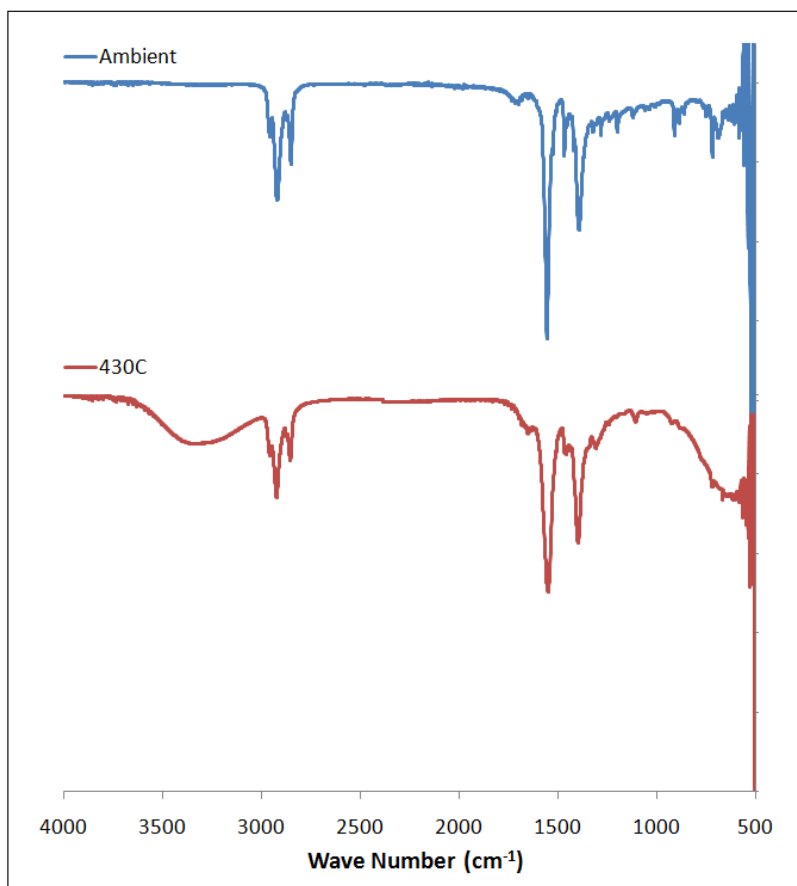


Figure S 229. IR spectrum of cesium nonanoate before and after melting.

## Cesium decanoate (caprate)

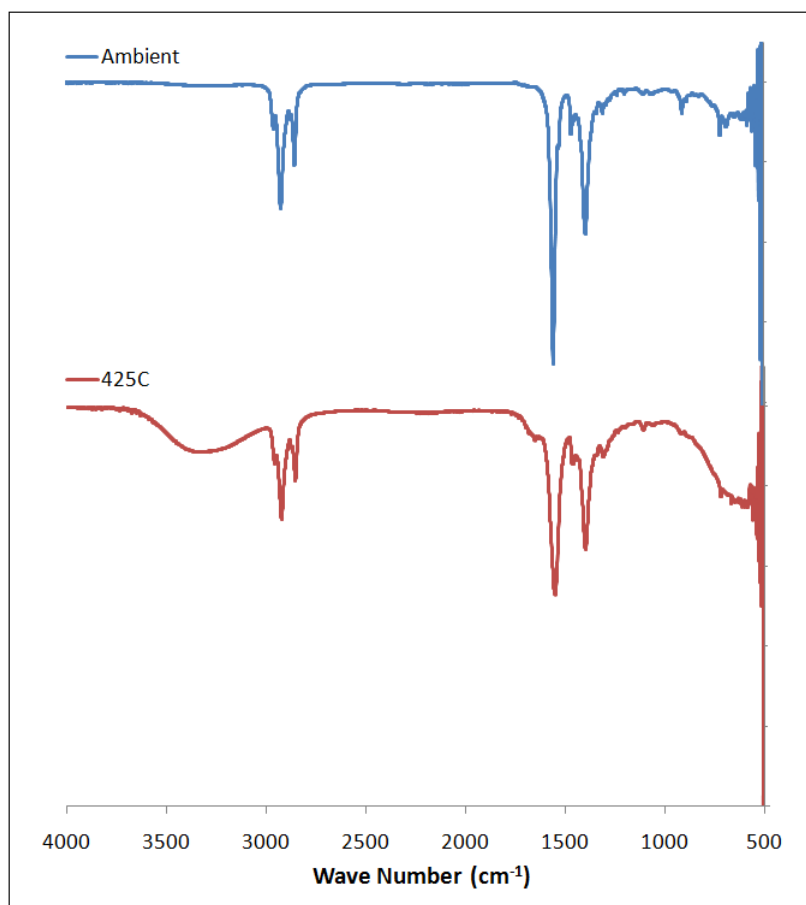


Figure S 230. IR spectrum of cesium decanoate before and after melting.

## Cesium undecanoate

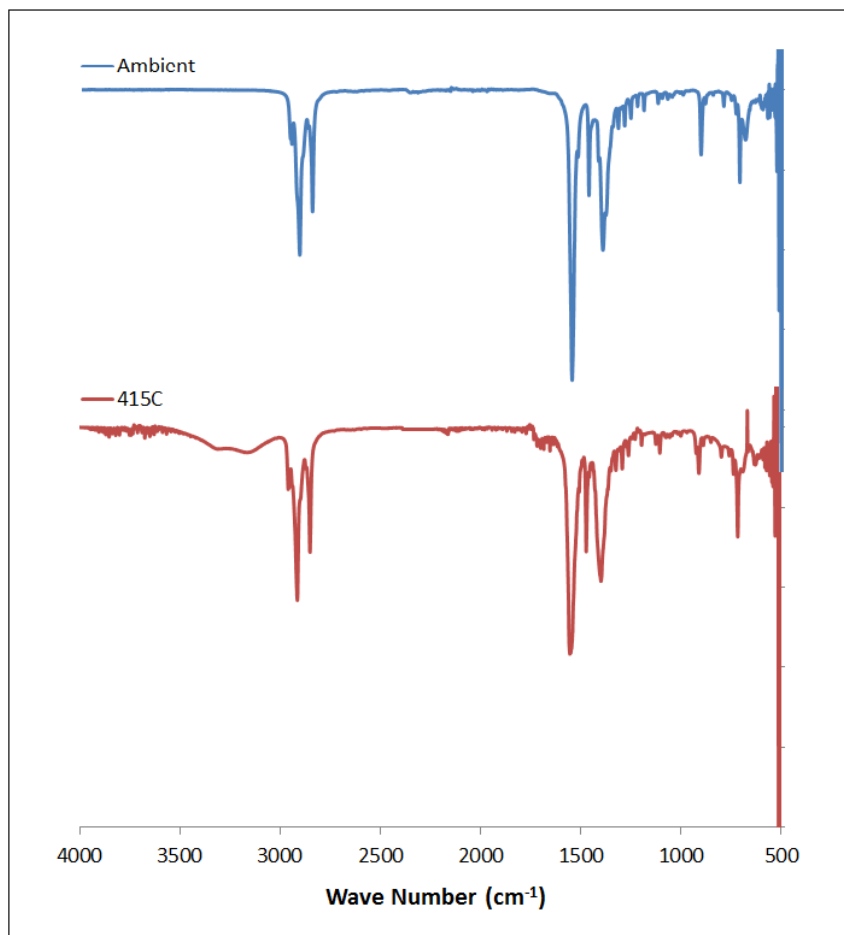


Figure S 231. IR spectrum of cesium undecanoate before and after melting.

## Cesium dodecanoate (laurate)

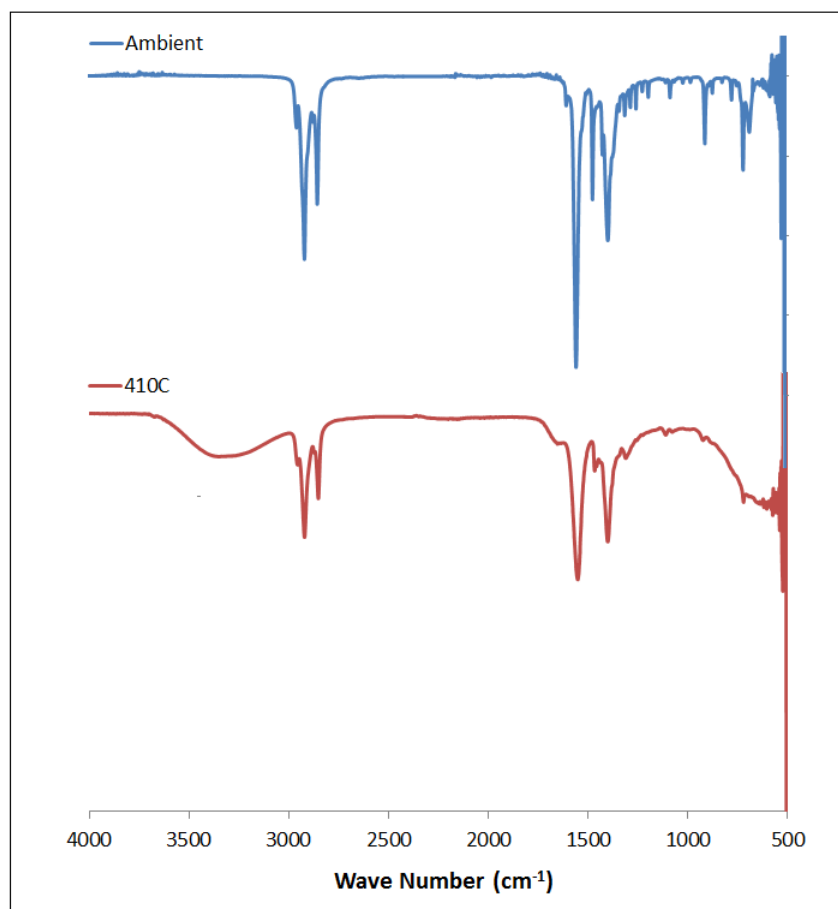


Figure S 232. IR spectrum of cesium dodecanoate before and after melting.

## UV-Vis Spectra

### Cesium Methanoate

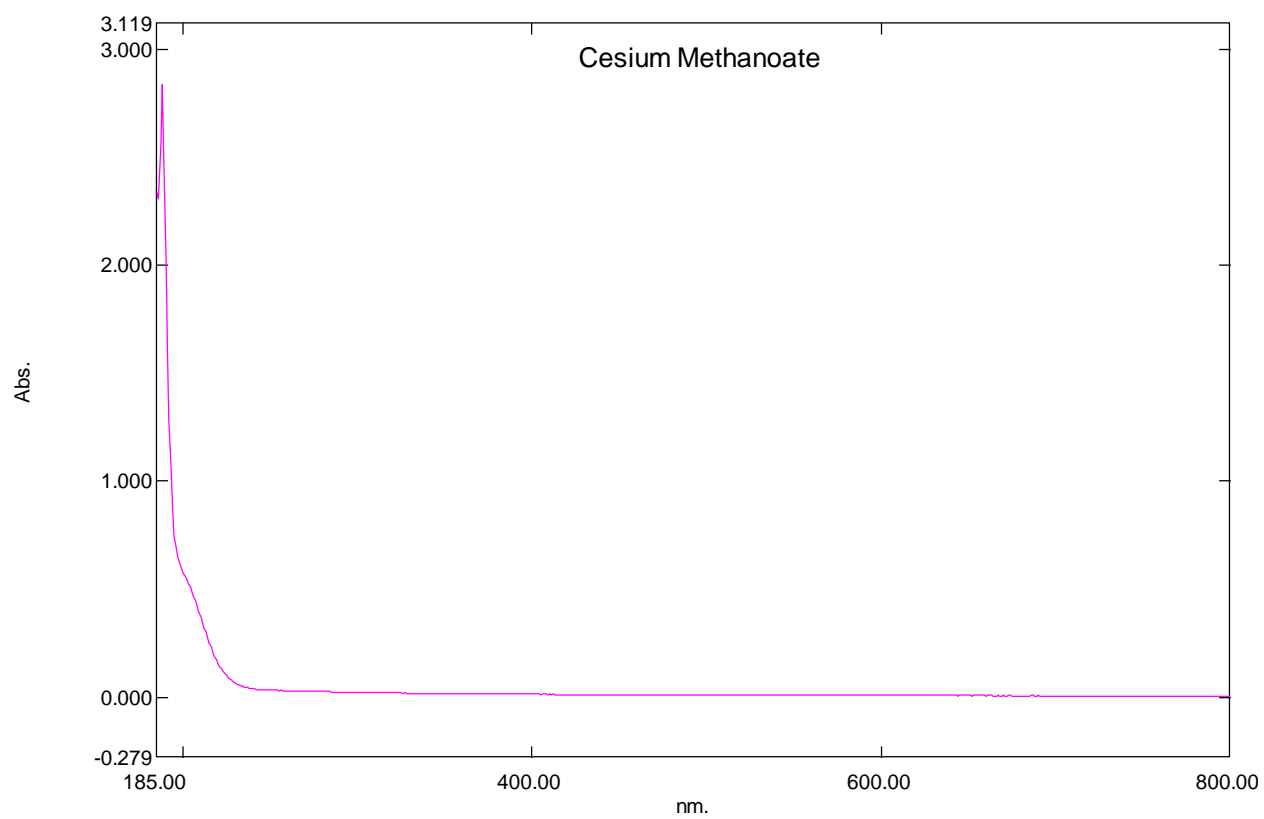


Figure S 233. UV-Vis spectrum of cesium methanoate

## Cesium Ethanoate

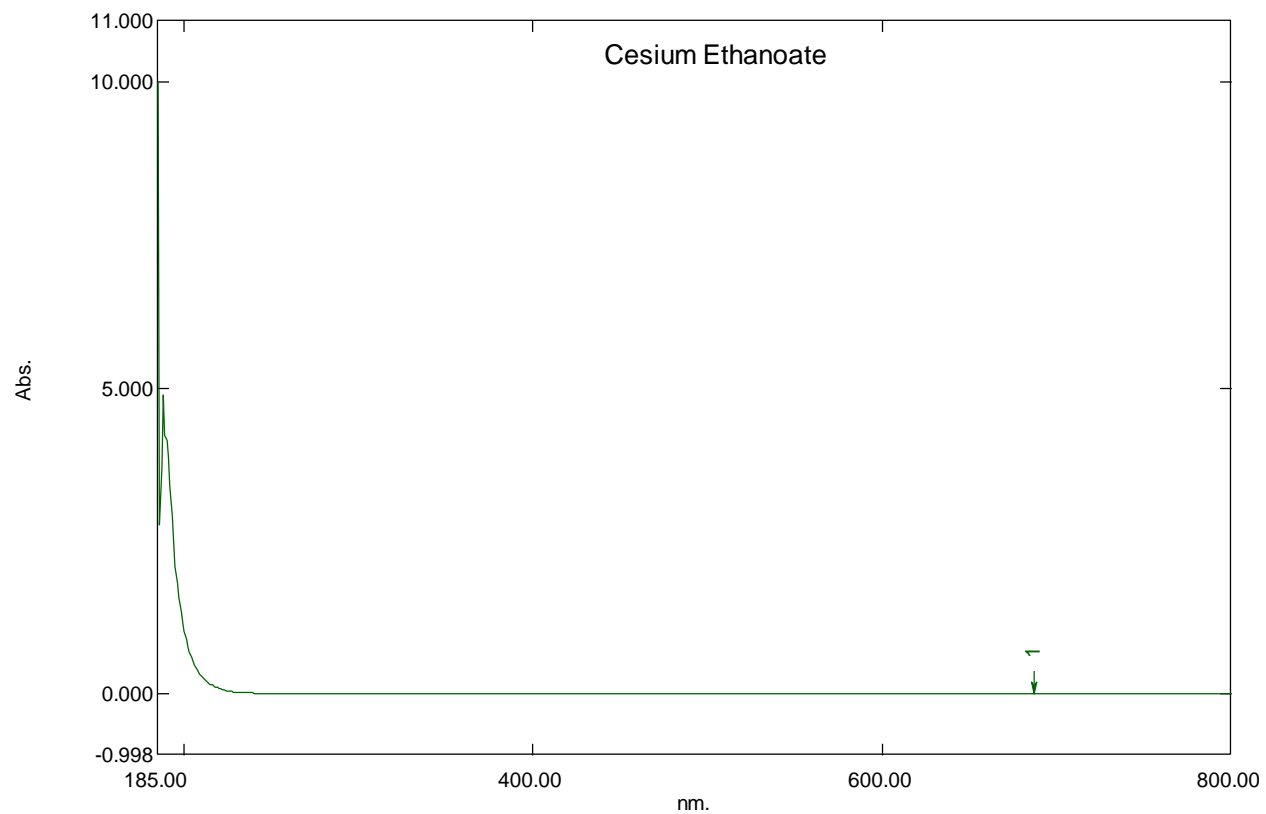


Figure S 234. UV-Vis spectrum of cesium ethanoate

## Cesium Propanoate

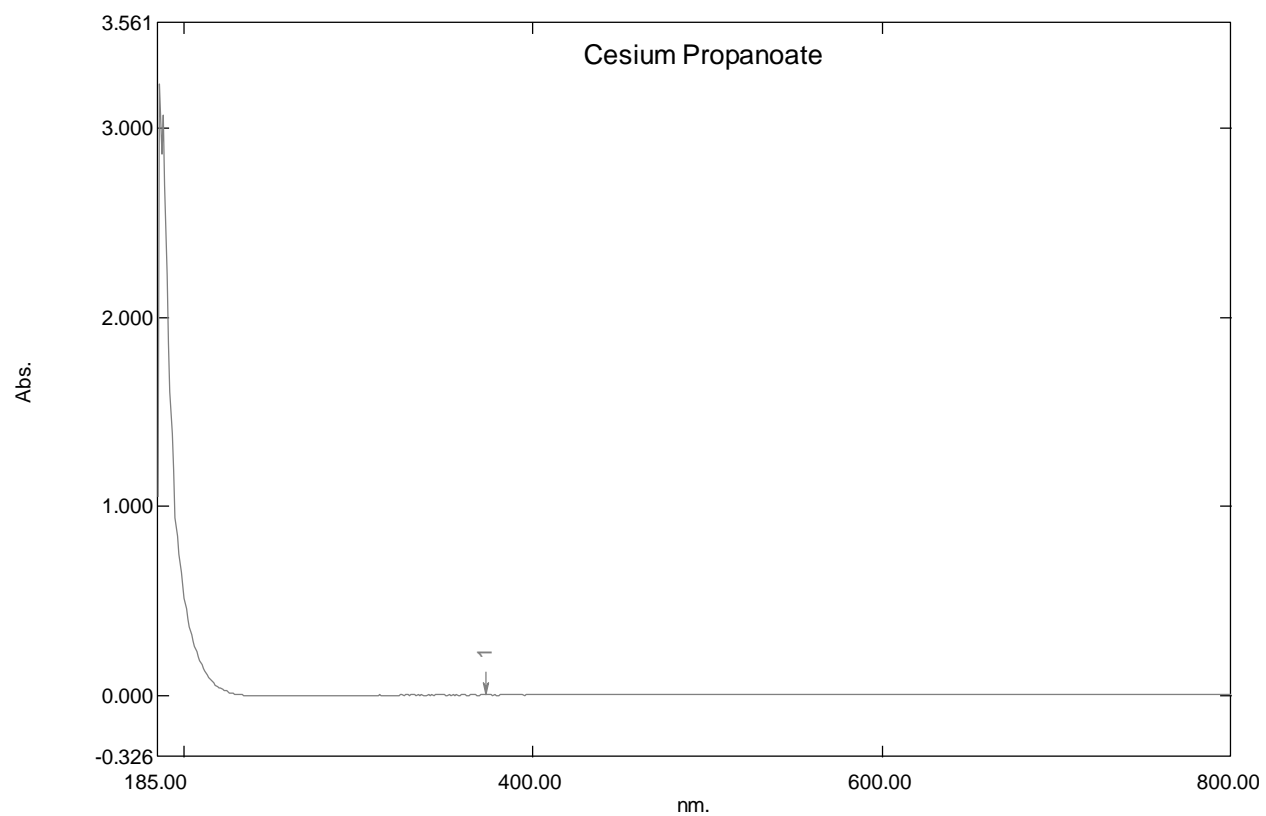


Figure S 235. UV-Vis spectrum of cesium propanoate

### Cesium Butanoate (butyrate)

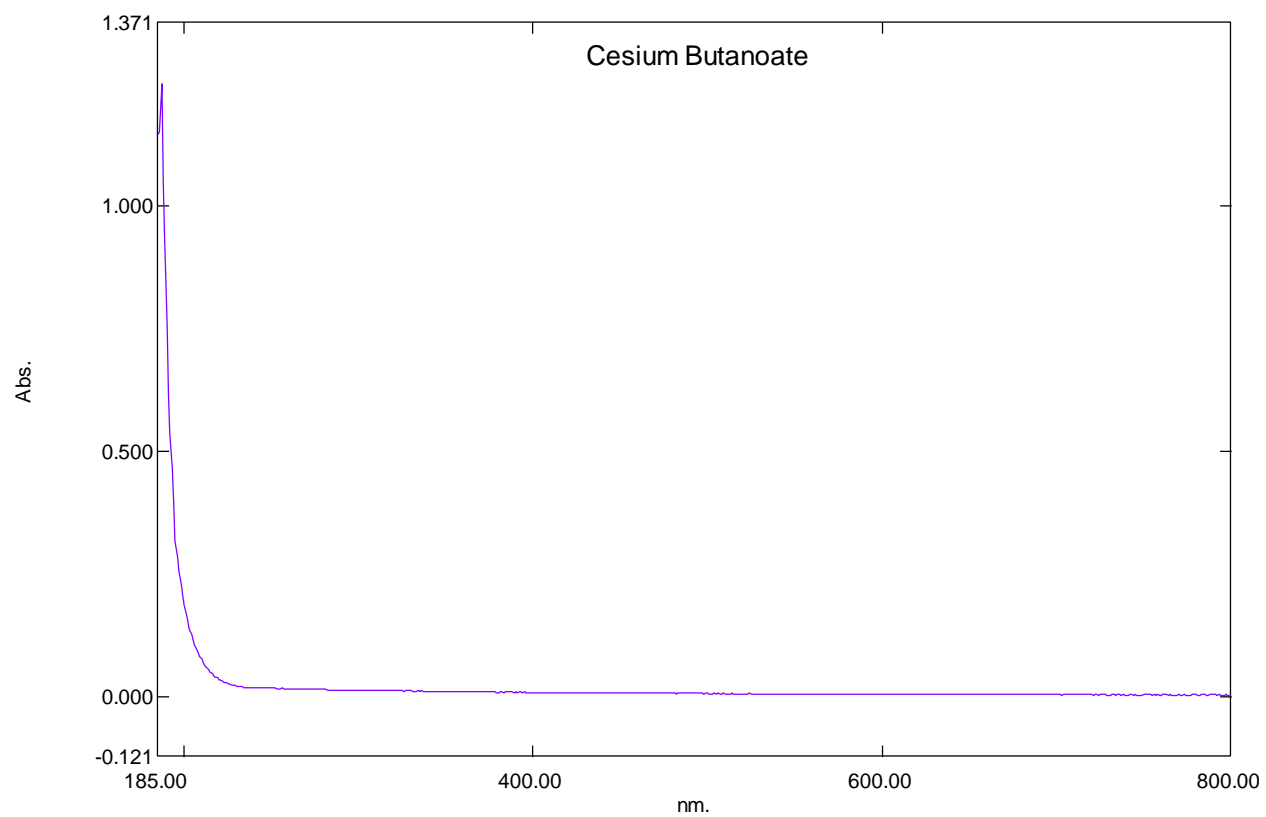


Figure S 236. UV-Vis spectrum of cesium butanoate

### Cesium Pentanoate (valerate)

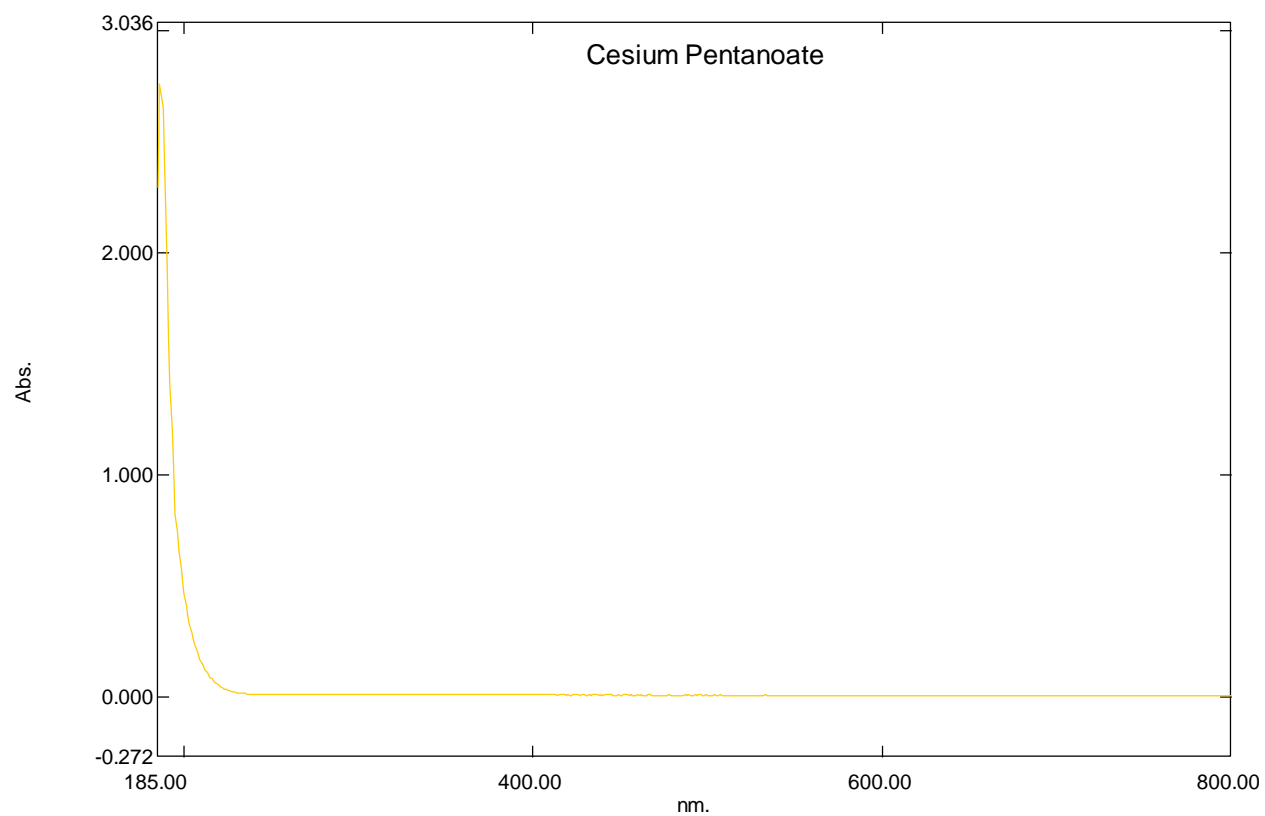


Figure S 237. UV-Vis spectrum of cesium pentanoate

## Cesium Hexanoate (caproate)

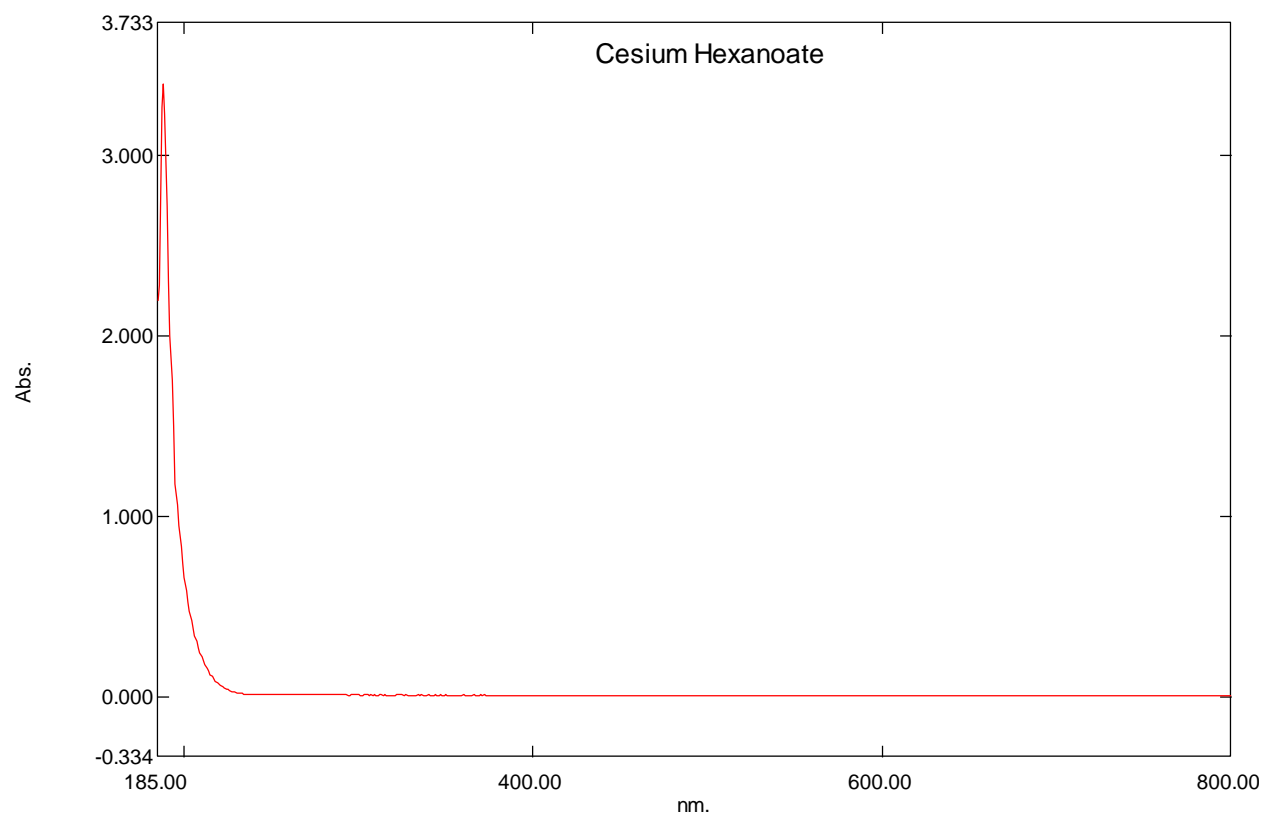


Figure S 238. UV-Vis of cesium hexanoate

## Cesium Heptanoate

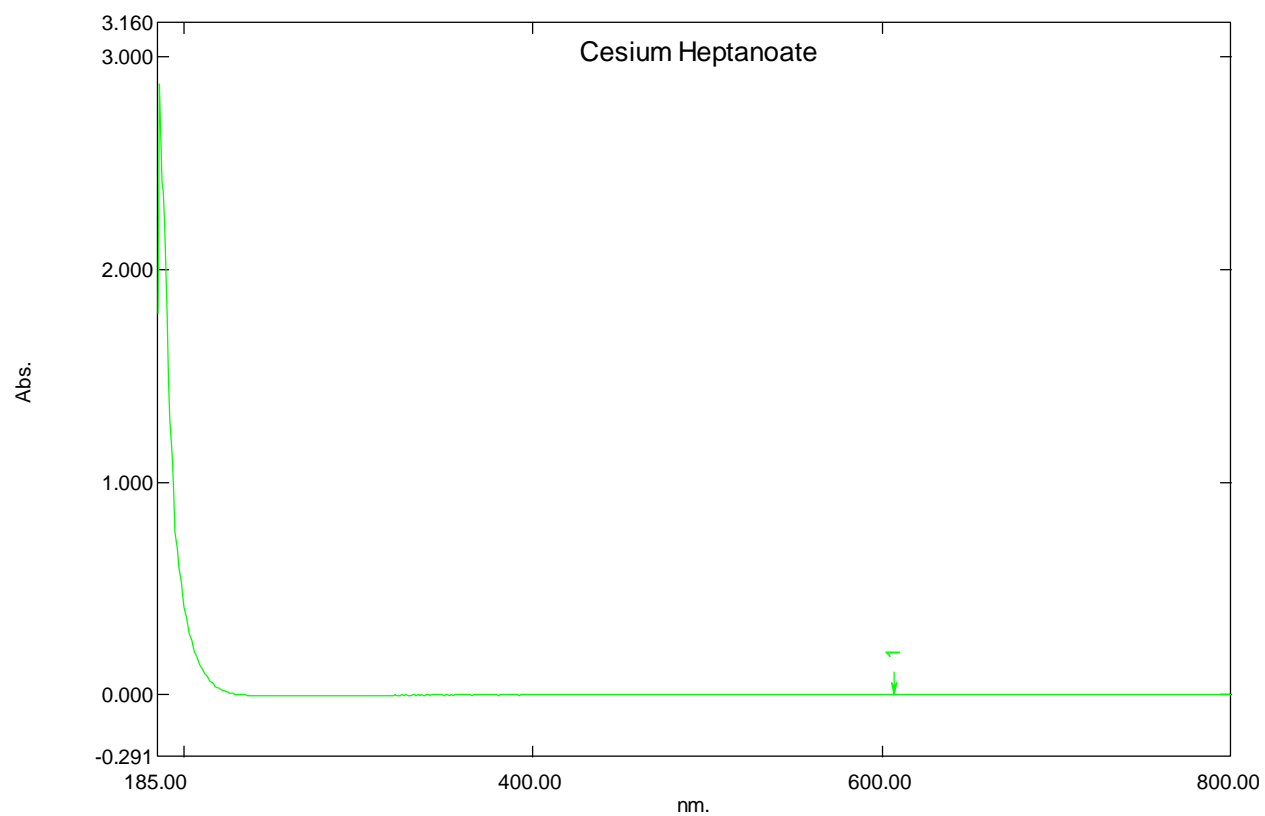


Figure S 239. UV-Vis spectrum of cesium heptanoate

### Cesium Octanoate (caprylate)

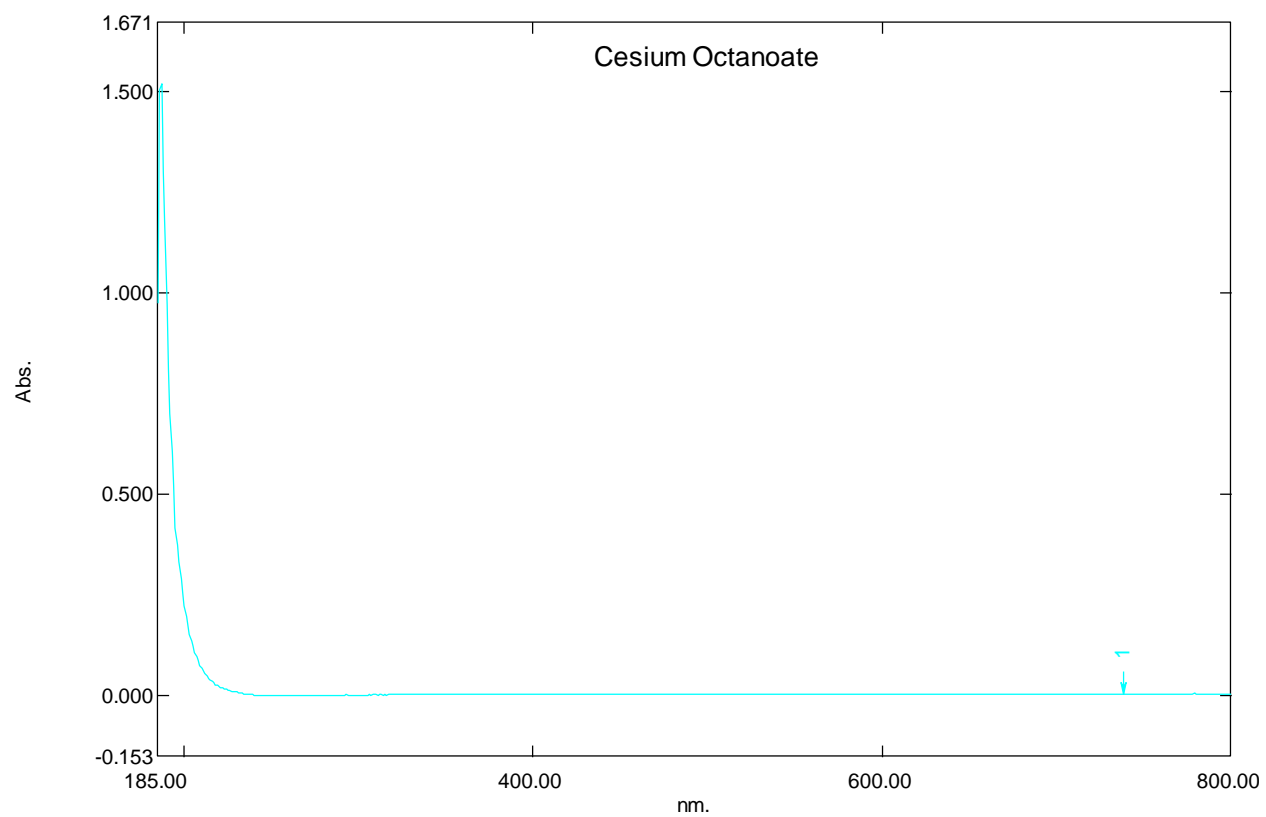


Figure S 240. UV-Vis of cesium octanoate

### Cesium Nonanoate (pelargonate)

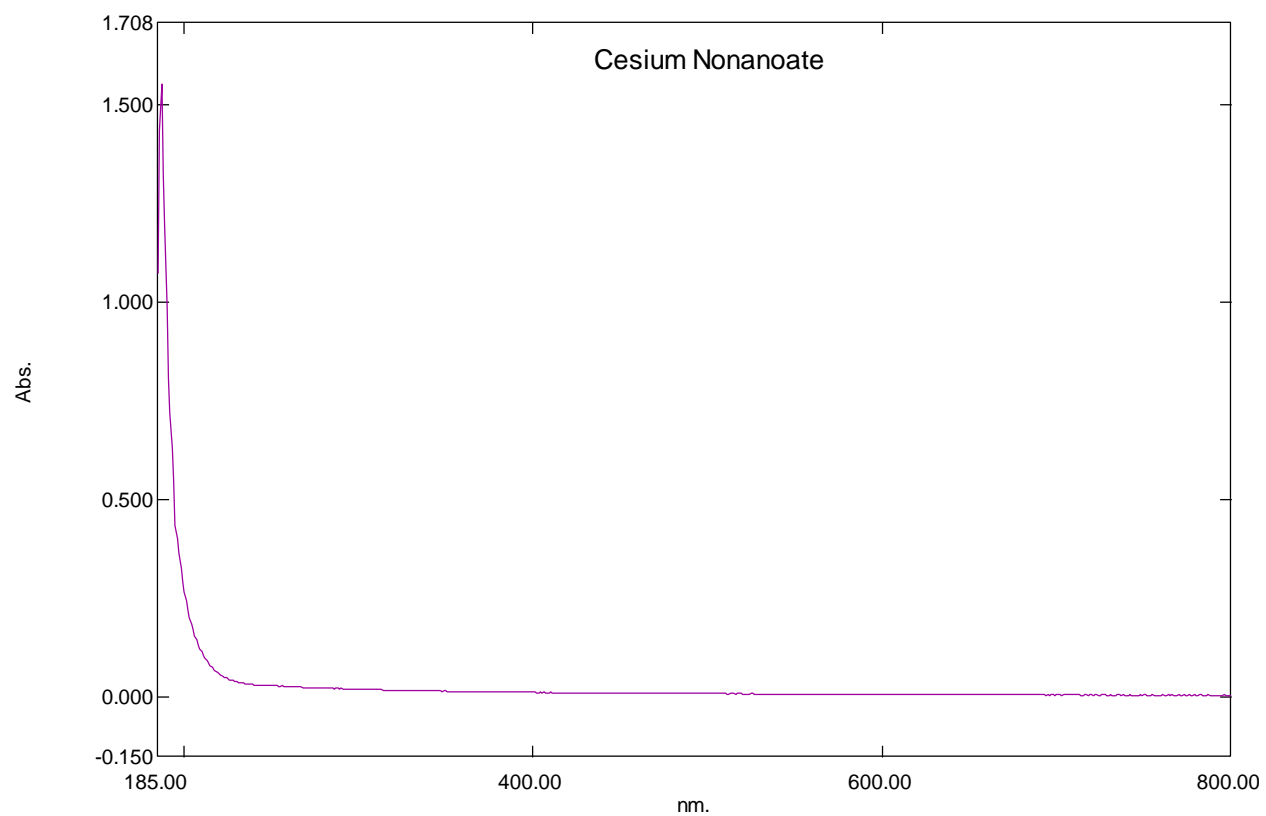


Figure S 241. UV-Vis of cesium nonanoate

### Cesium Decanoate (caprate)

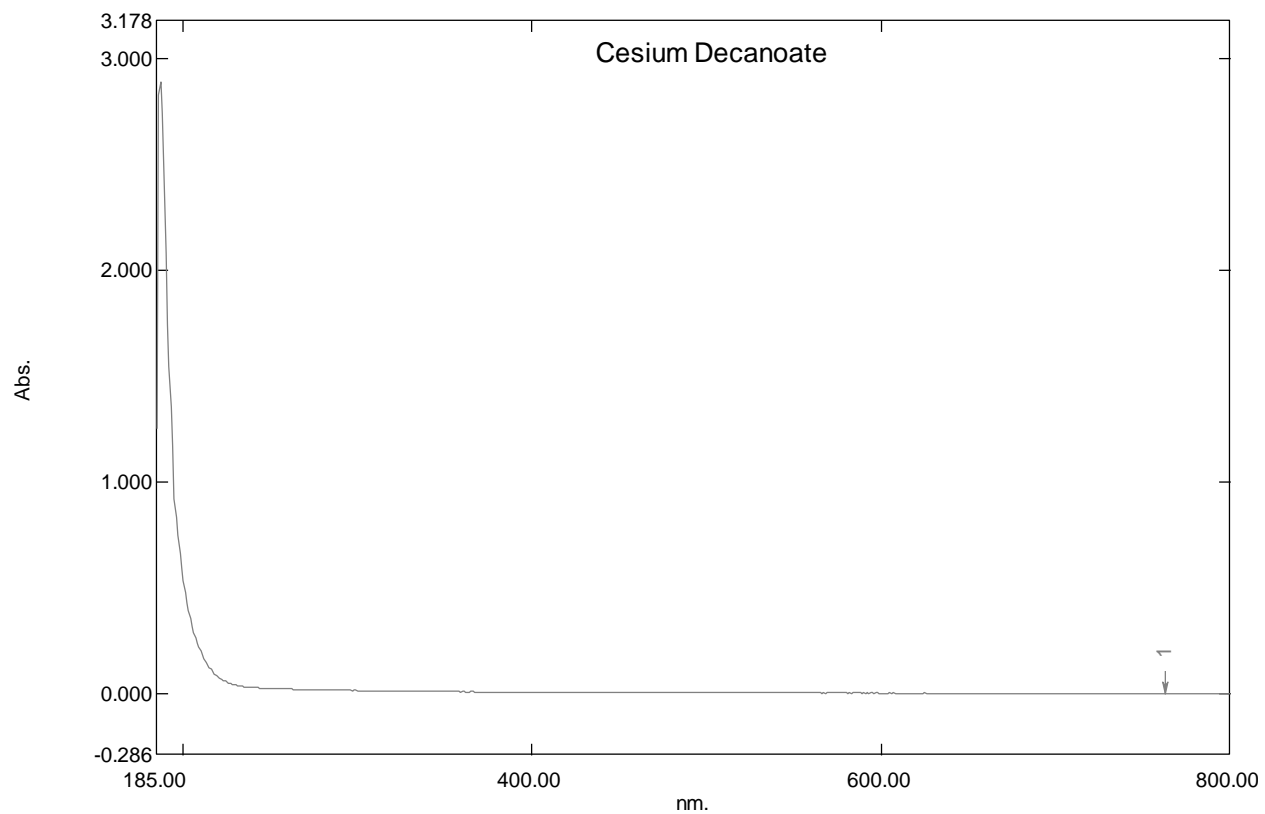


Figure S 242. UV-Vis of cesium decanoate

# Cesium Undecanoate

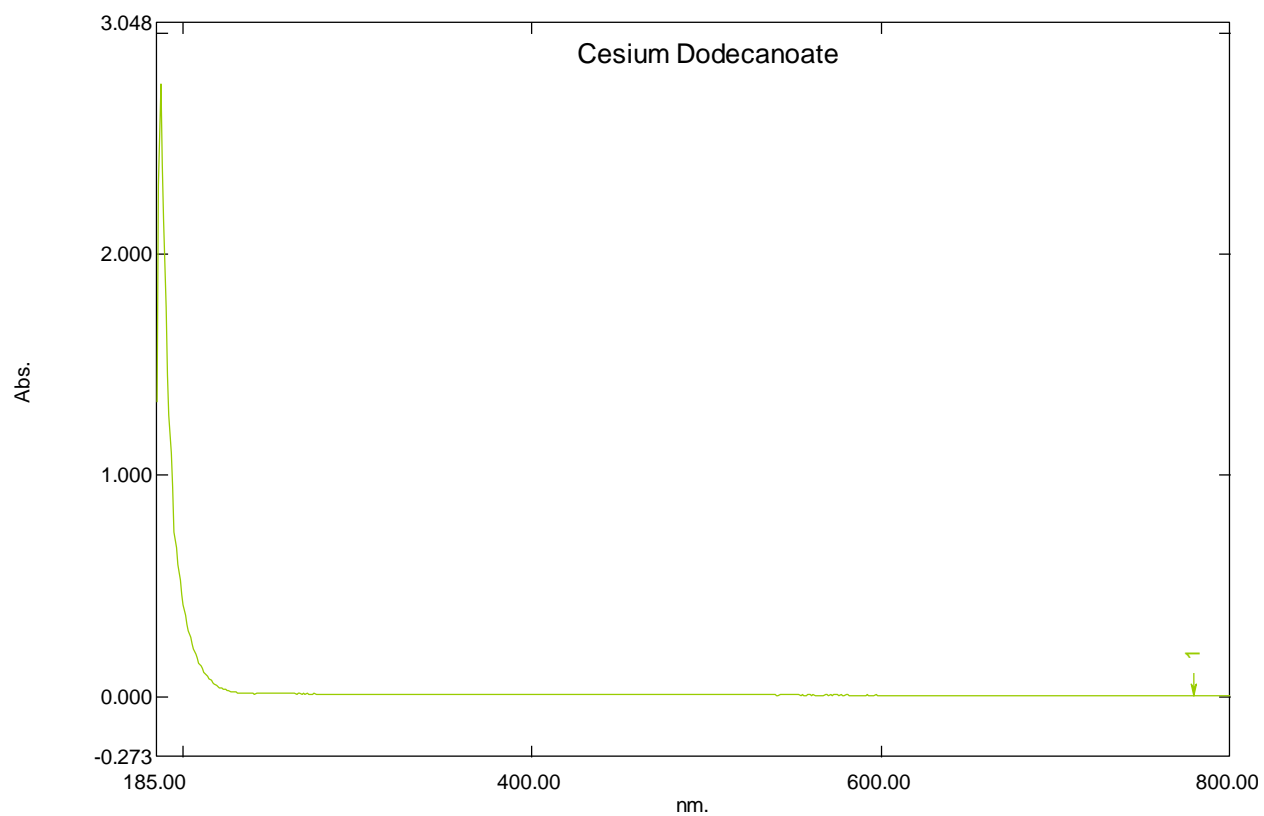


Figure S 243. UV-Vis of cesium undecanoate

### Cesium Dodecanoate (laurate)

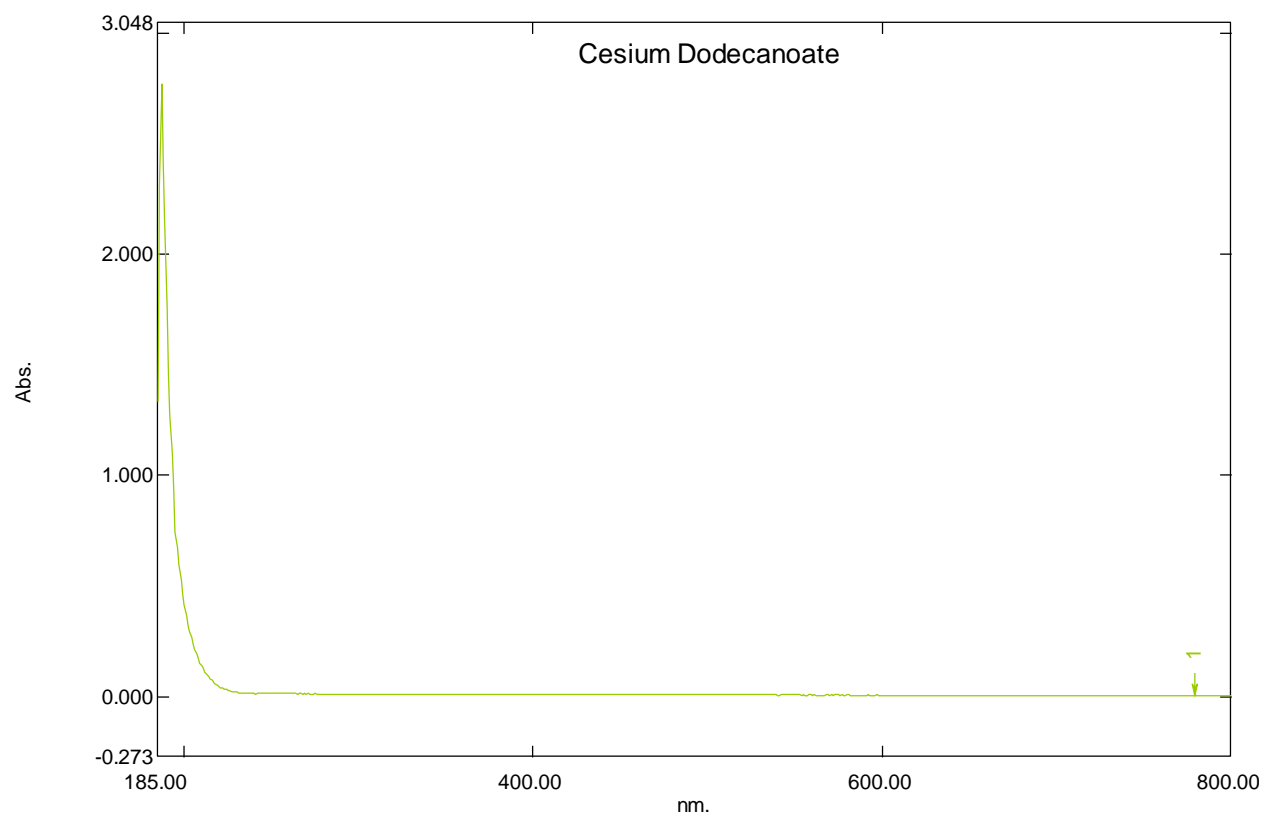


Figure S 244. UV-Vis of cesium dodecanoate

## TGA Results

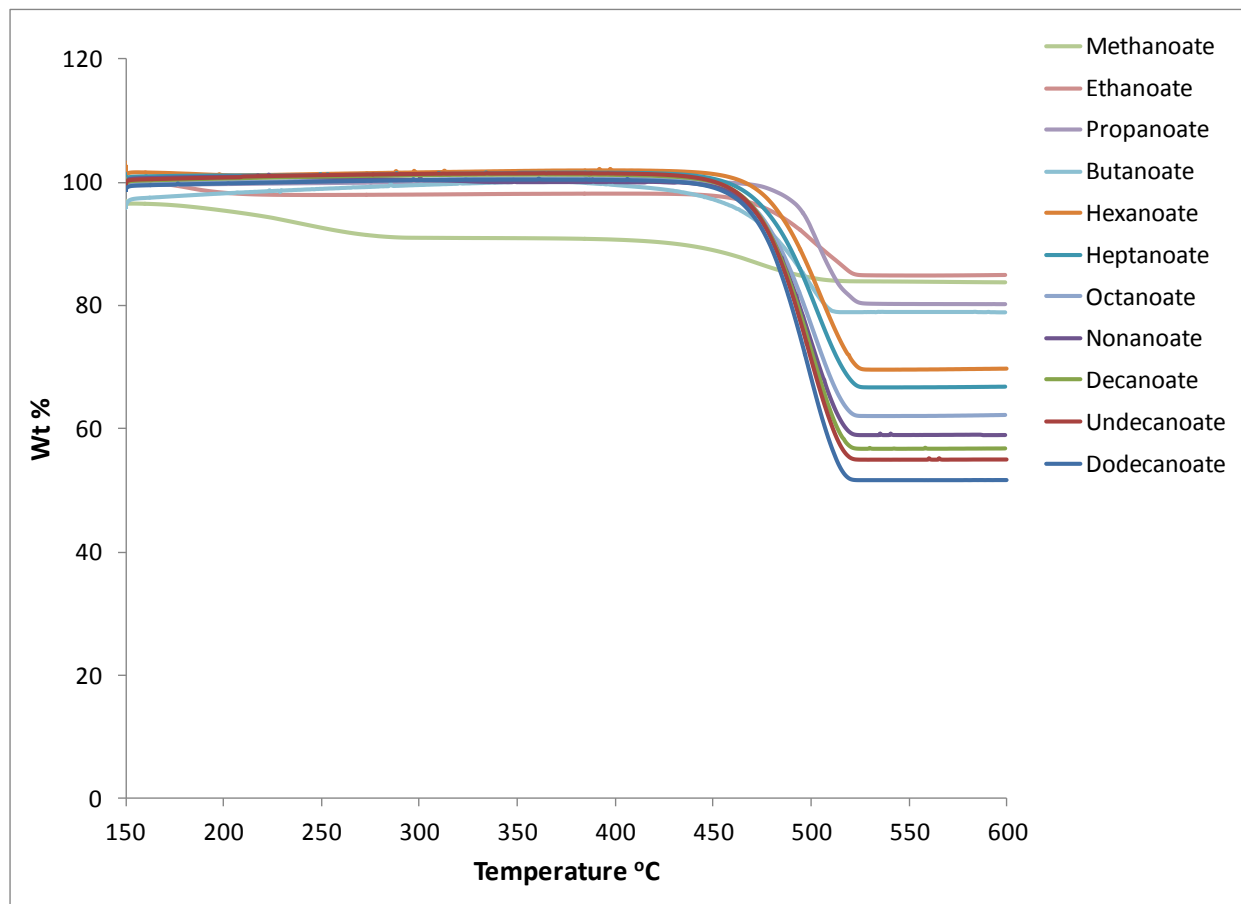


Figure S 245. TGA profile of Cs-carboxylates

## Calorigrams of Cs-Carboxylates determined by the Differential Scanning Calorimeter (DSC)

### Cesium Methanoate

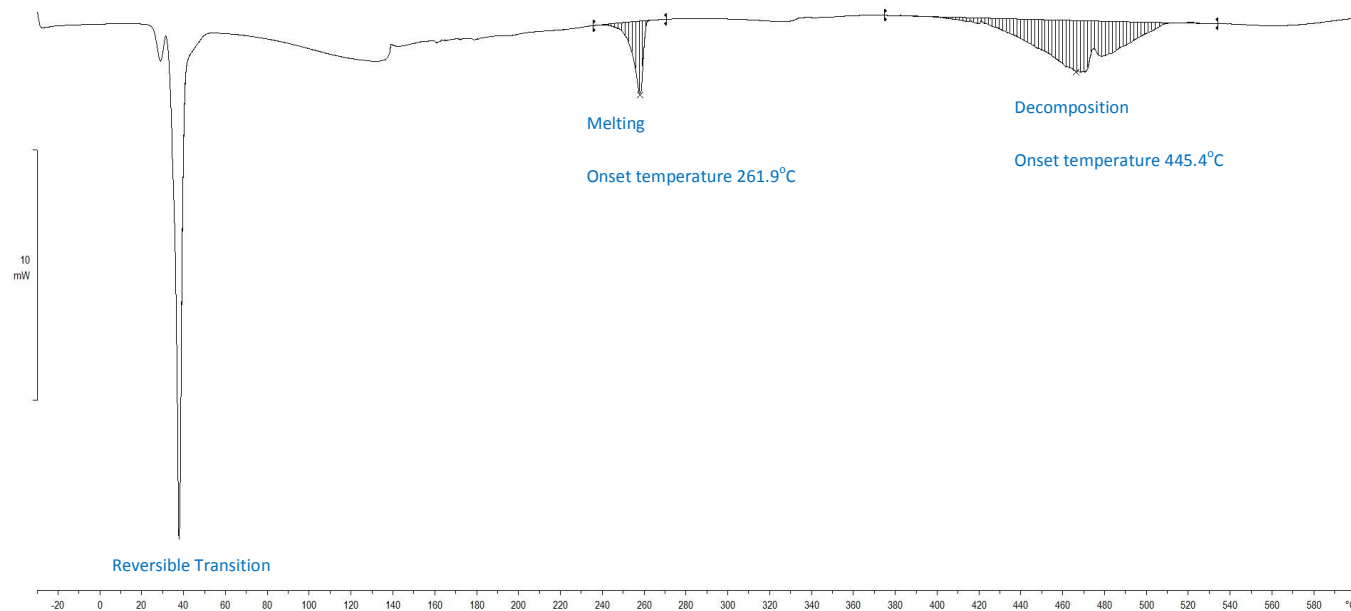


Figure S 246. Calorigram of Cesium Methanoate determined by the DSC over the range of -30-600°C at 10°C·min<sup>-1</sup> heating rate and 100mL·min<sup>-1</sup> nitrogen flow.

### Cesium Ethanoate

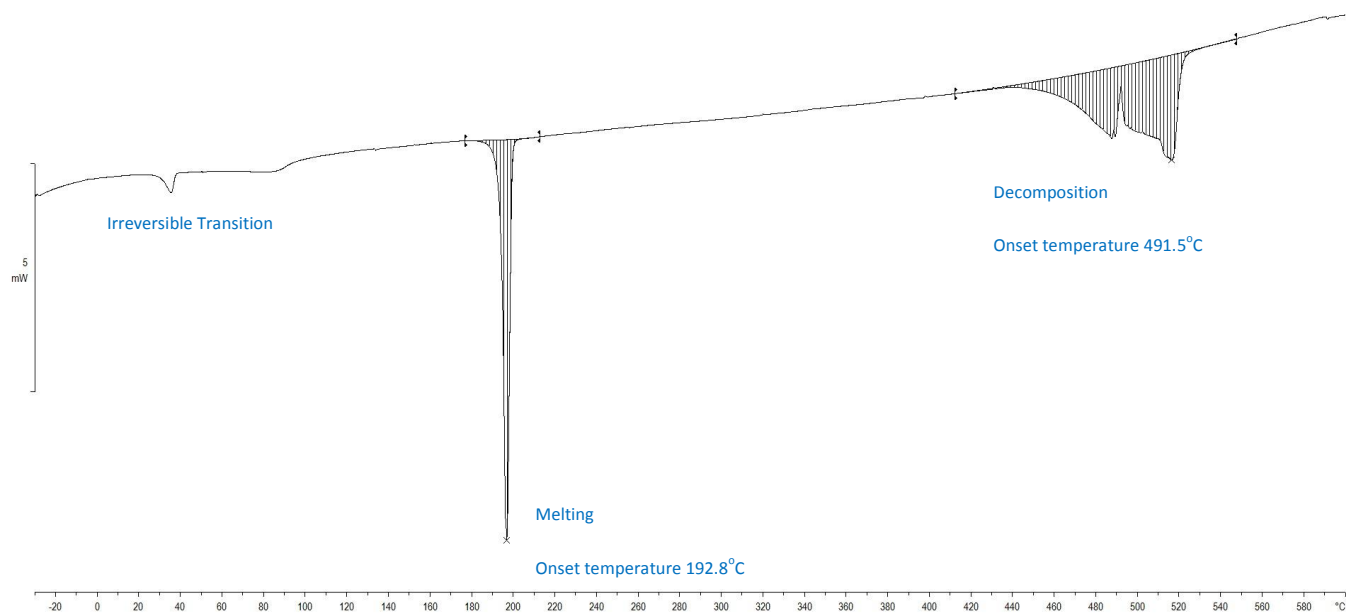


Figure S 247. Calorigram of Cesium Ethanoate determined by the DSC over the range of -30-600°C at 10°C·min<sup>-1</sup> heating rate and 100mL·min<sup>-1</sup> nitrogen flow.

## Cesium Propanoate

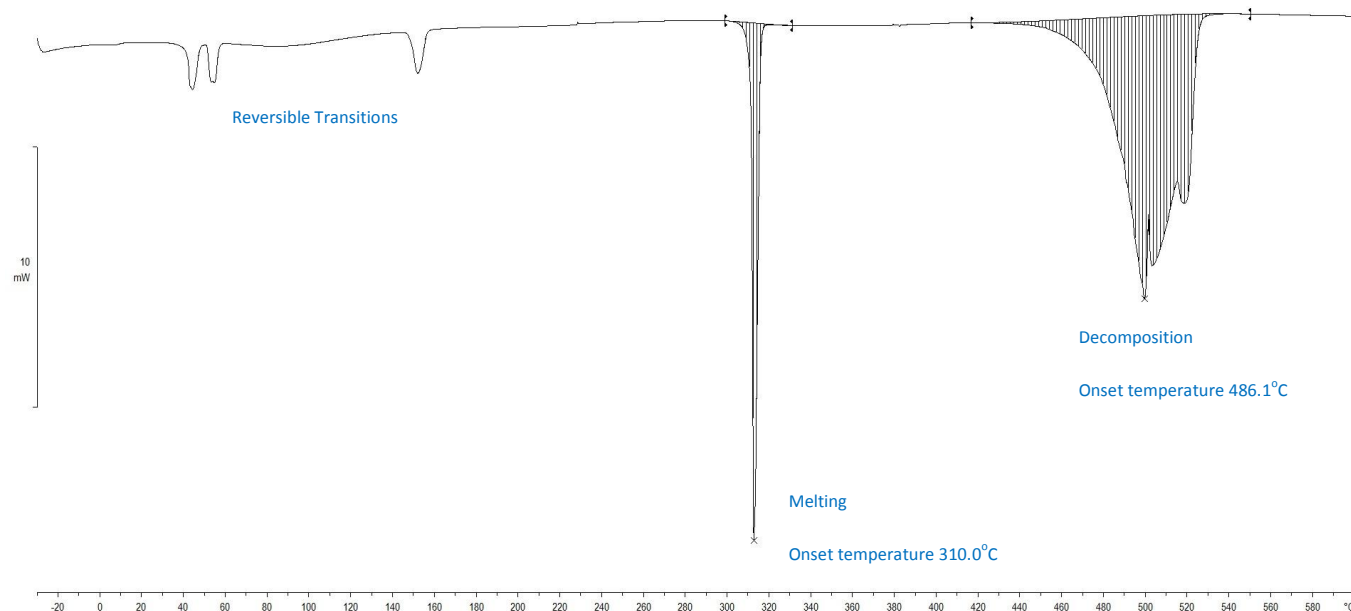


Figure S 248. Calorigram of Cesium Propanoate determined by the DSC over the range of -30-600°C at 10°C·min<sup>-1</sup> heating rate and 100mL·min<sup>-1</sup> nitrogen flow.

## Cesium Butanoate (butyrate)

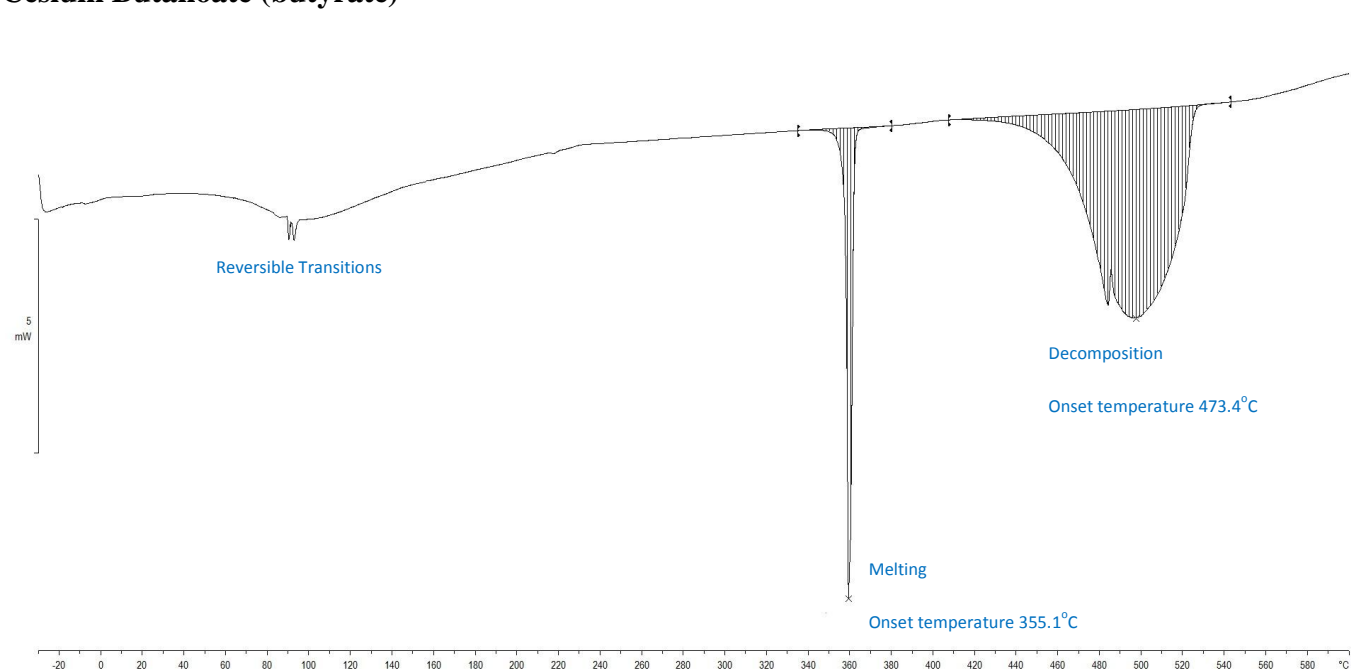


Figure S 249. Calorigram of Cesium Butanoate determined by the DSC over the range of -30-600°C at 10°C·min<sup>-1</sup> heating rate and 100mL·min<sup>-1</sup> nitrogen flow.

### Cesium Pentanoate (valerate)

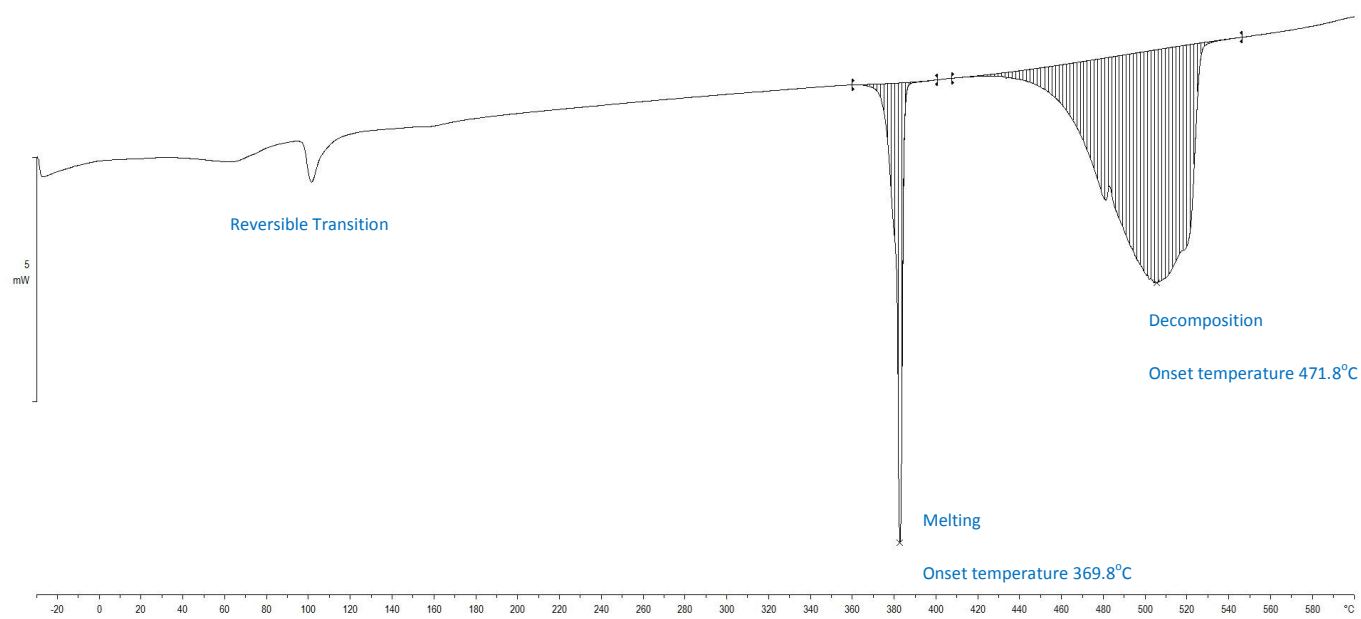


Figure S 250. Calorigram of Cesium Pentanoate determined by the DSC over the range of -30-600°C at 10°C·min<sup>-1</sup> heating rate and 100mL·min<sup>-1</sup> nitrogen flow.

### Cesium Hexanoate (caproate)

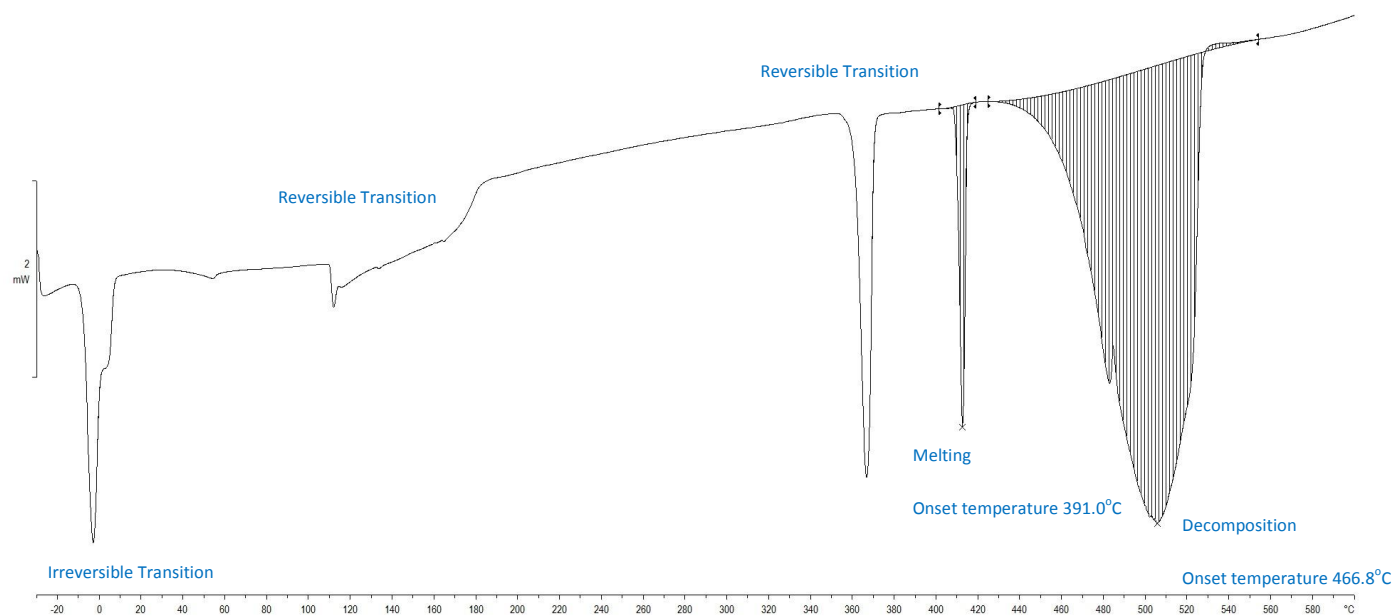


Figure S 251. Calorigram of Cesium Hexanoate determined by the DSC over the range of -30-600°C at 10°C·min<sup>-1</sup> heating rate and 100mL·min<sup>-1</sup> nitrogen flow.

## Cesium Heptanoate

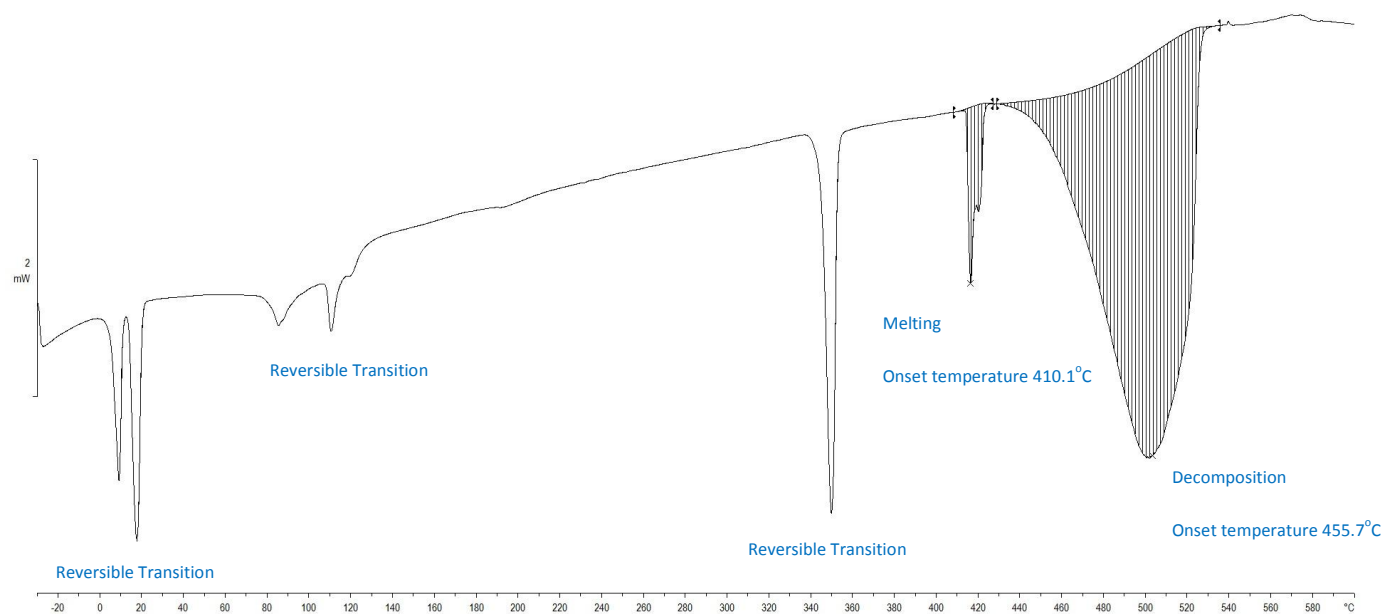


Figure S 252. Calorigram of Cesium Heptanoate determined by the DSC over the range of  $-30$ - $600^{\circ}\text{C}$  at  $10^{\circ}\text{C}\cdot\text{min}^{-1}$  heating rate and  $100\text{mL}\cdot\text{min}^{-1}$  nitrogen flow.

## Cesium Octanoate (caprylate)

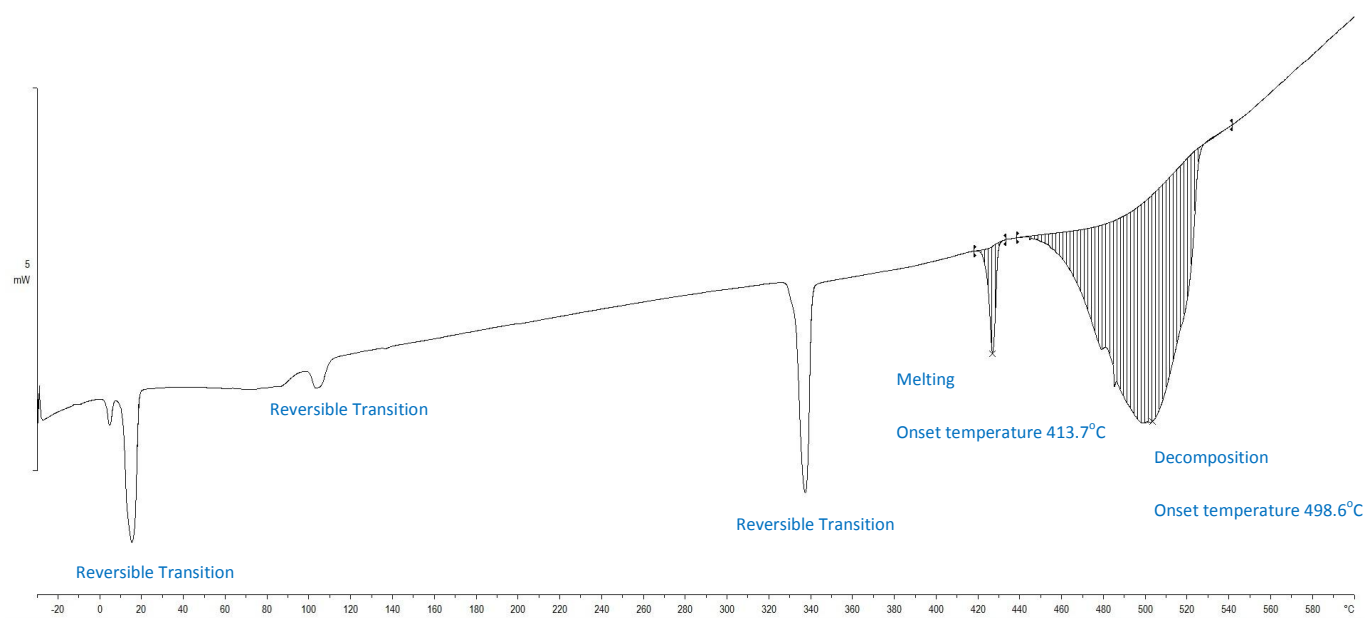


Figure S 253. Calorigram of Cesium Octanoate determined by the DSC over the range of  $-30$ - $600^{\circ}\text{C}$  at  $10^{\circ}\text{C}\cdot\text{min}^{-1}$  heating rate and  $100\text{mL}\cdot\text{min}^{-1}$  nitrogen flow.

## Cesium Nonanoate (pelargonate)

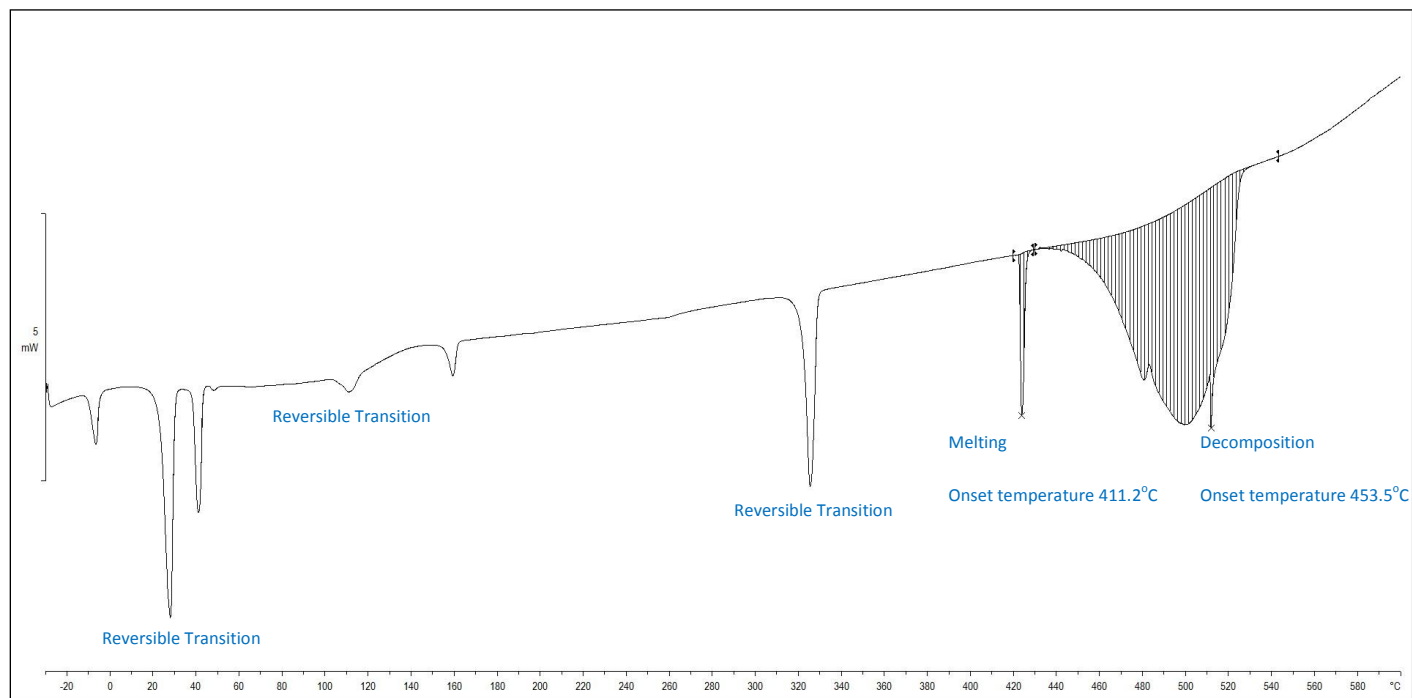


Figure S 254. Calorigram of Cesium Nonanoate determined by the DSC over the range of -30-600°C at 10°C min<sup>-1</sup> heating rate and 100mL min<sup>-1</sup> nitrogen flow.

## Cesium Decanoate (caprate)

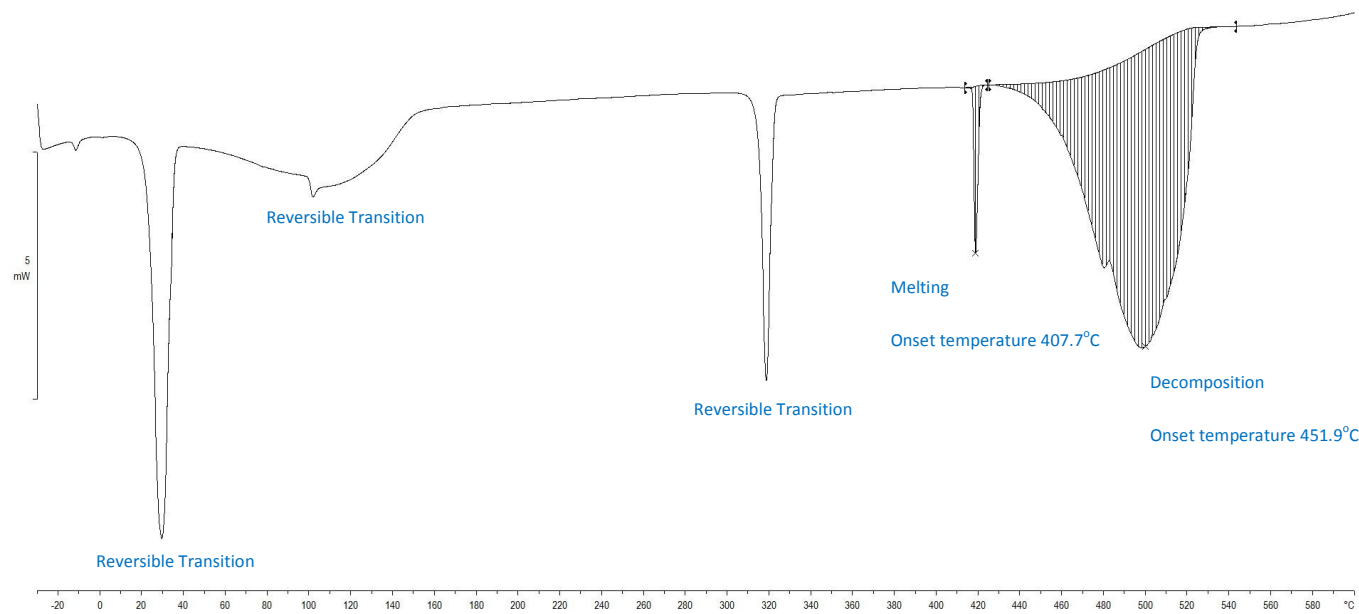


Figure S 255. Calorigram of Cesium Decanoate determined by the DSC over the range of -30-600°C at 10°C min<sup>-1</sup> heating rate and 100mL min<sup>-1</sup> nitrogen flow.

## Cesium Undecanoate

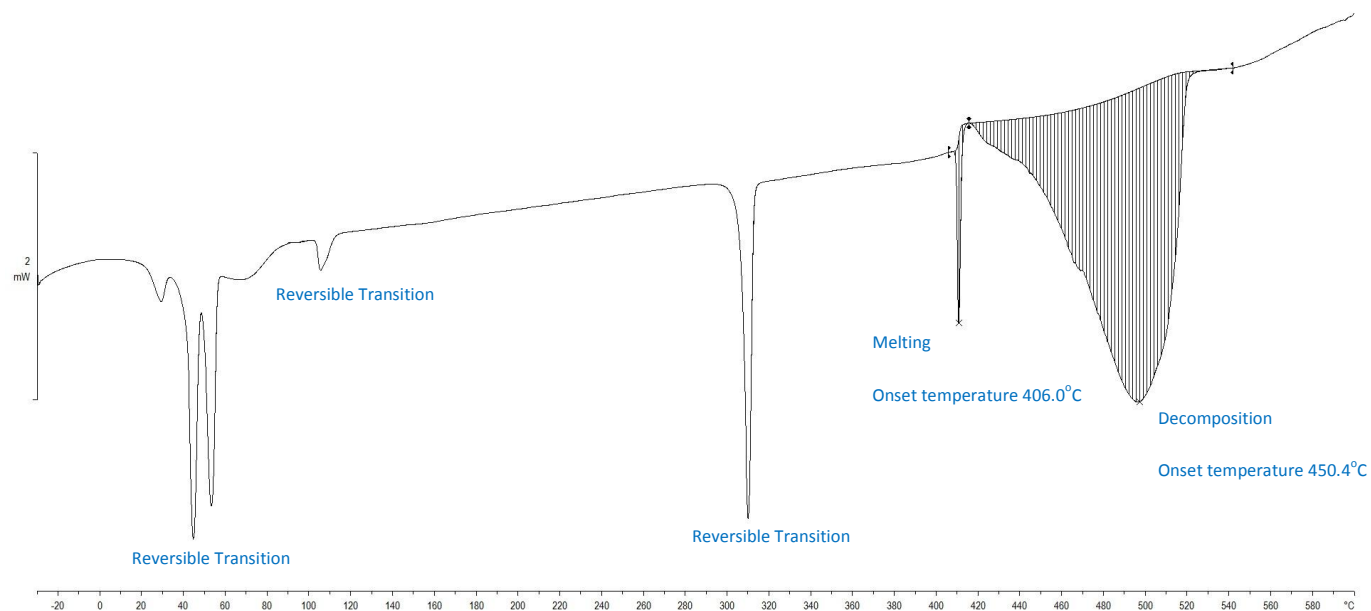


Figure S 256. Calorigram of Cesium Undecanoate determined by the DSC over the range of -30-600°C at 10°C·min<sup>-1</sup> heating rate and 100mL·min<sup>-1</sup> nitrogen flow.

## Cesium Dodecanoate (laurate)

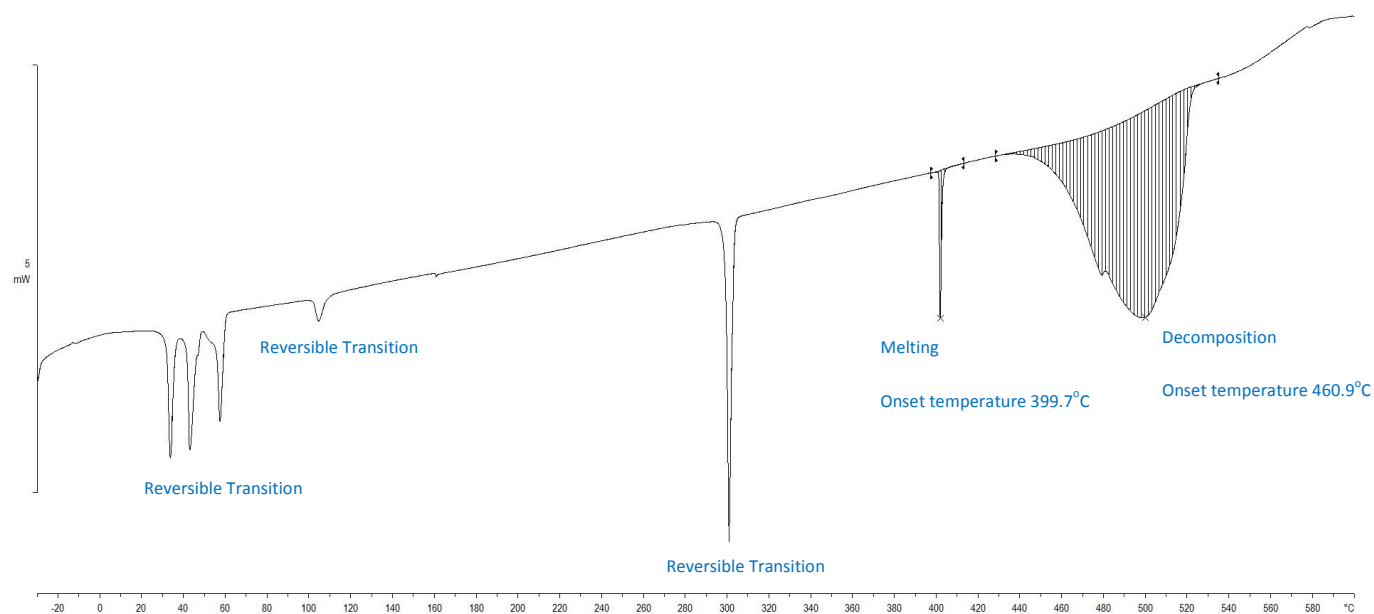


Figure S 257. Calorigram of Cesium Dodecanoate determined by the DSC over the range of -30-600°C at 10°C·min<sup>-1</sup> heating rate and 100mL·min<sup>-1</sup> nitrogen flow.

## Heat Capacity

### Cesium Methanoate

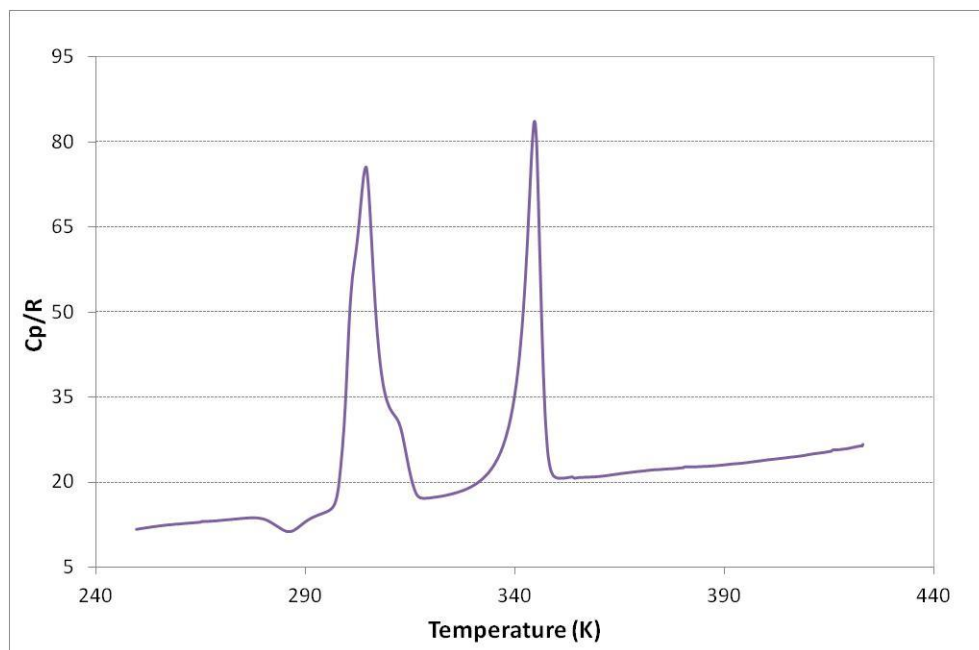


Figure S 258. Experimental molar heat capacities for Cs-methanoate ( $R = 8.31451 \text{ JK}^{-1}\text{mol}^{-1}$ )

### Cesium Ethanoate

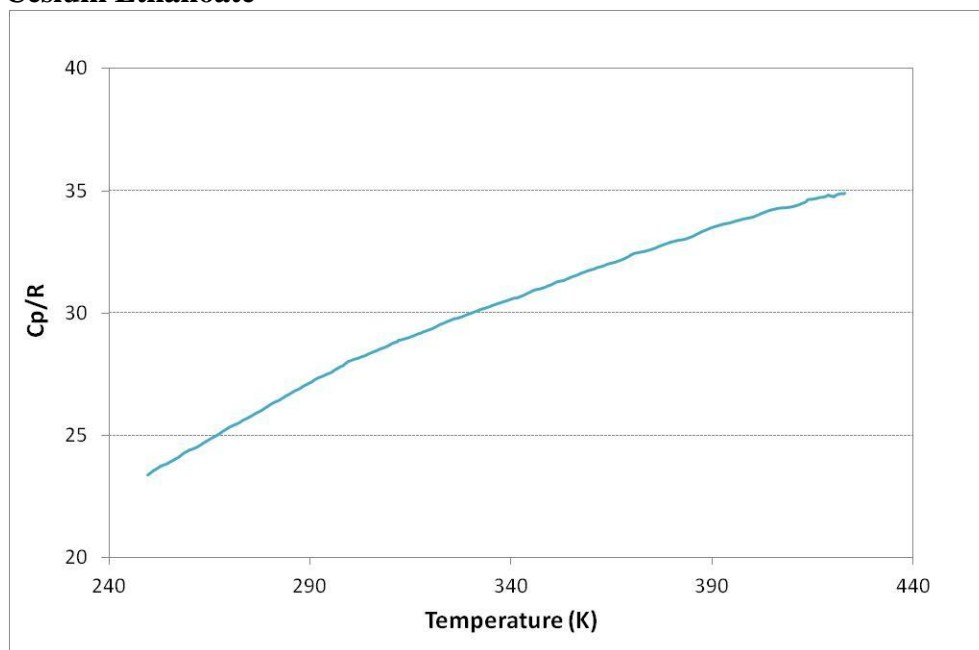


Figure S 259. Experimental molar heat capacities for Cs-ethanoate ( $R = 8.31451 \text{ JK}^{-1}\text{mol}^{-1}$ )

## Cesium Propanoate

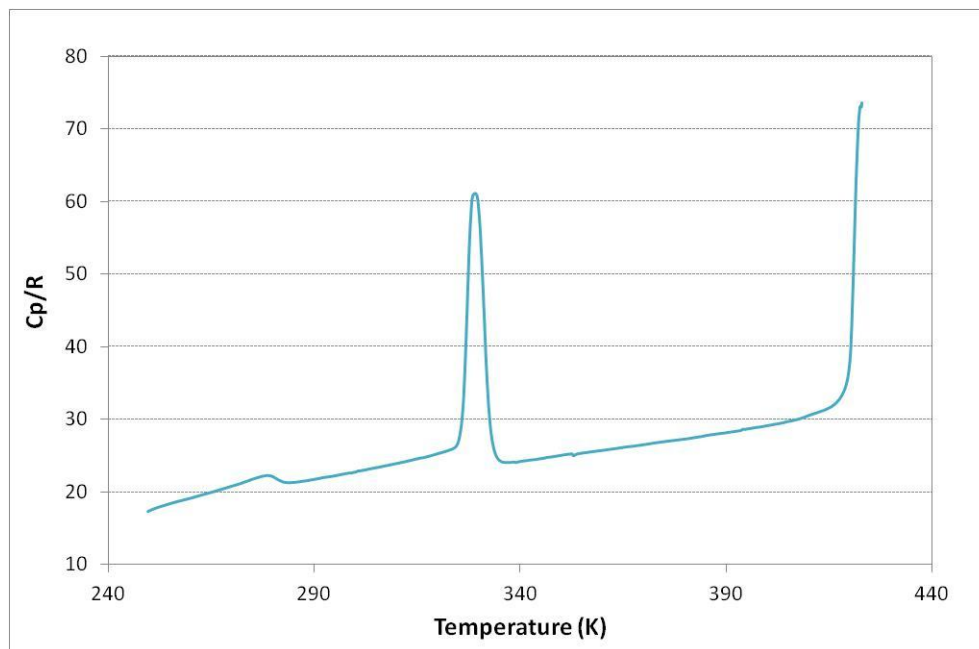


Figure S 260. Experimental molar heat capacities for Cs-propanoate ( $R = 8.31451 \text{ JK}^{-1} \text{ mol}^{-1}$ )

## Cesium Butanoate (butyrate)

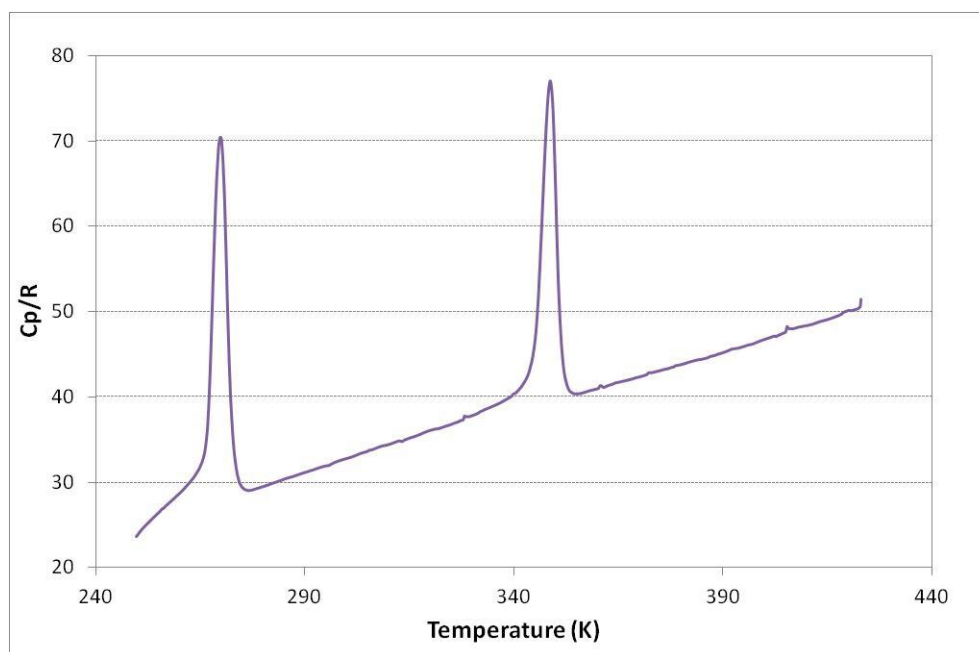


Figure S 261. Experimental molar heat capacities for Cs-butanoate ( $R = 8.31451 \text{ JK}^{-1} \text{ mol}^{-1}$ )

### Cesium Pentanoate (valerate)

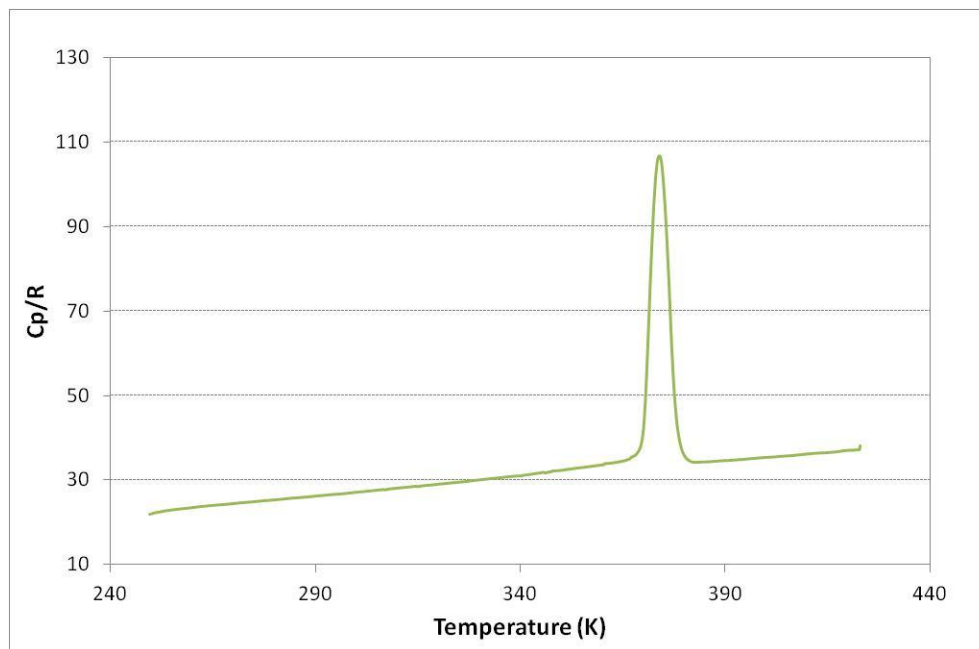


Figure S 262. Experimental molar heat capacities for Cs-pentanoate ( $R = 8.31451 \text{ JK}^{-1}\text{mol}^{-1}$ )

### Cesium Hexanoate (caproate)

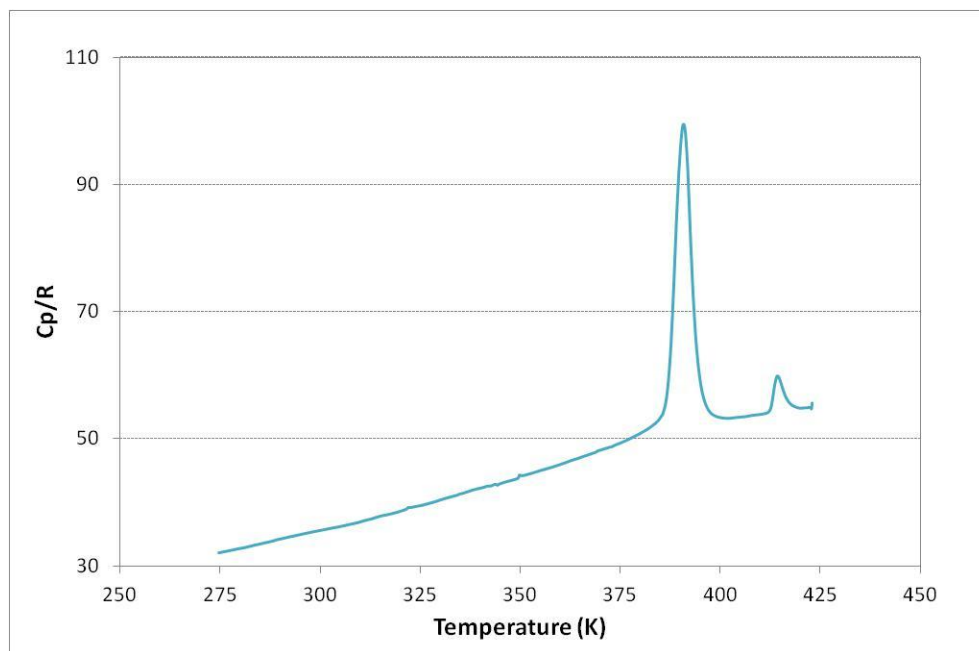


Figure S 263. Experimental molar heat capacities for Cs-hexanoate ( $R = 8.31451 \text{ JK}^{-1}\text{mol}^{-1}$ )

## Cesium Heptanoate

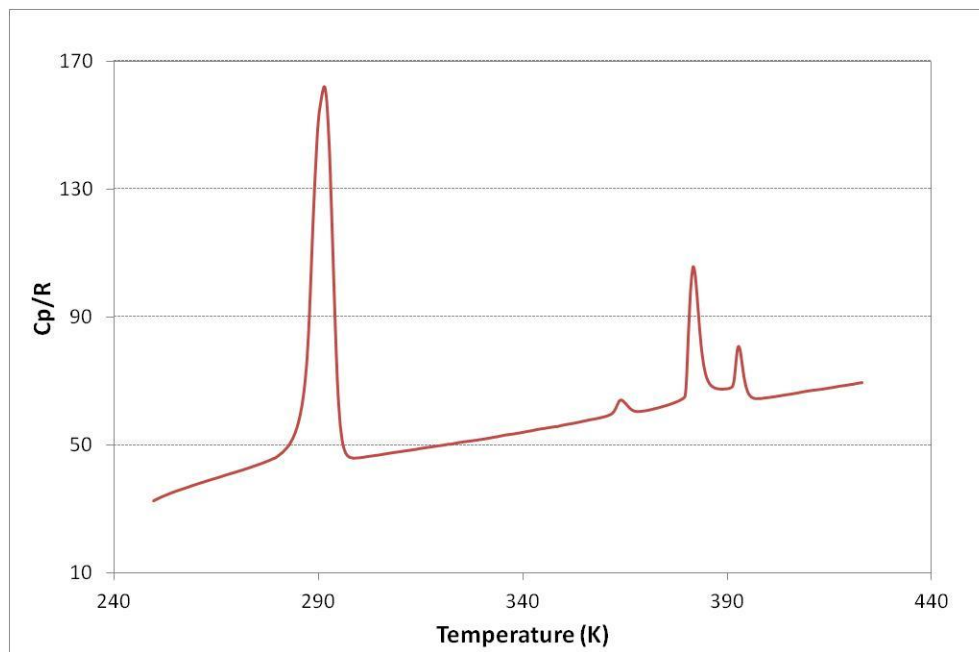


Figure S 264. Experimental molar heat capacities for Cs-heptanoate ( $R = 8.31451 \text{ JK}^{-1}\text{mol}^{-1}$ )

## Cesium Octanoate (caprylate)

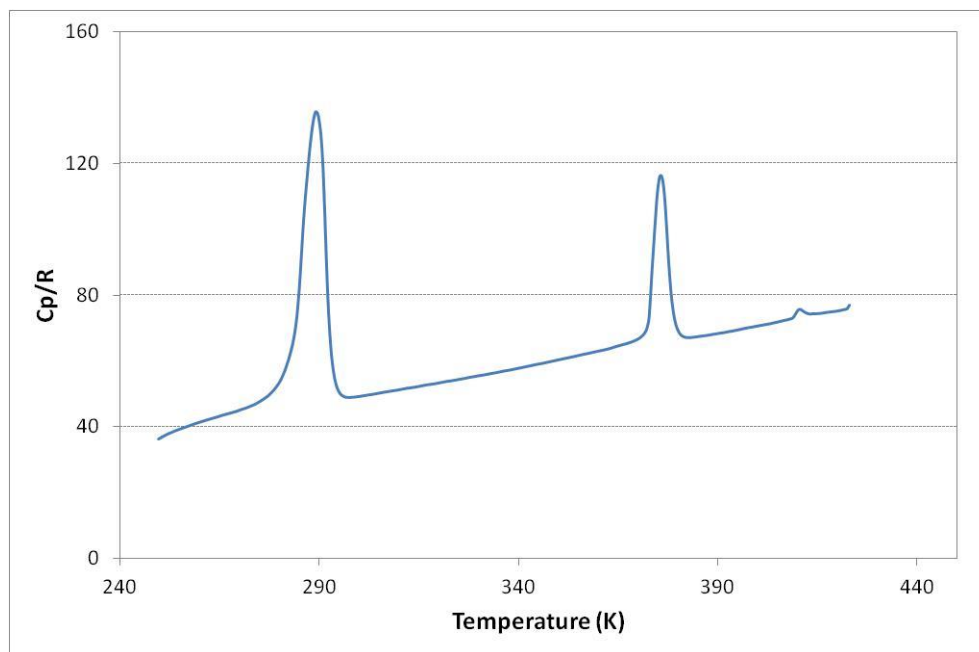


Figure S 265. Experimental molar heat capacities for Cs-octanoate ( $R = 8.31451 \text{ JK}^{-1}\text{mol}^{-1}$ )

### Cesium Nonanoate (pelargonate)

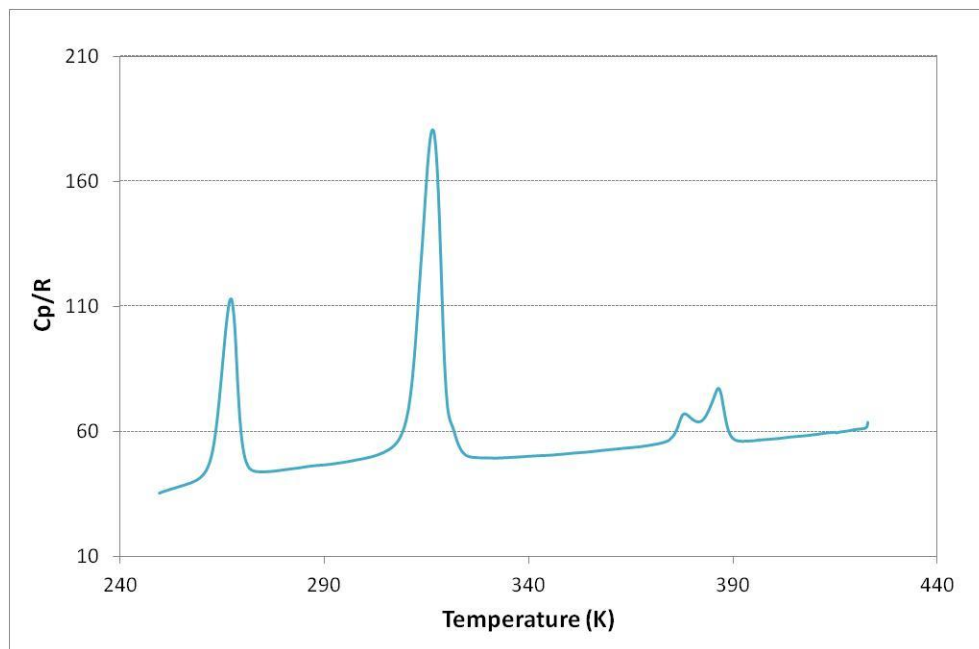


Figure S 266. Experimental molar heat capacities for Cs-nonanoate ( $R = 8.31451 \text{ JK}^{-1}\text{mol}^{-1}$ )

### Cesium Decanoate (caprate)

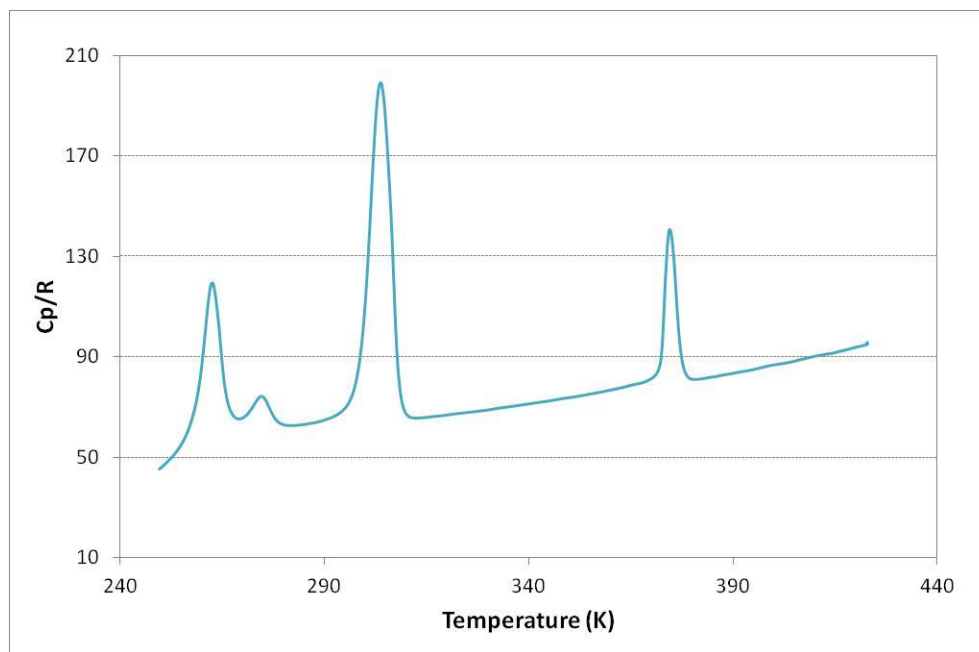


Figure S 267. Experimental molar heat capacities for Cs-decanoate ( $R = 8.31451 \text{ JK}^{-1}\text{mol}^{-1}$ )

## Cesium Undecanoate

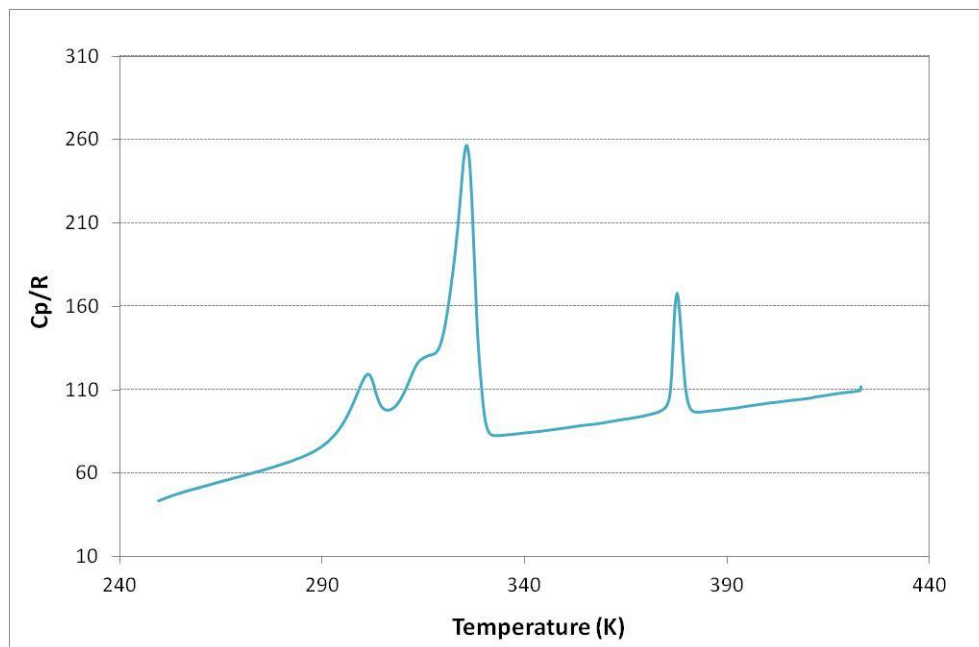


Figure S 268. Experimental molar heat capacities for Cs-undecanoate ( $R = 8.31451 \text{ JK}^{-1}\text{mol}^{-1}$ )

## Cesium Dodecanoate (laurate)

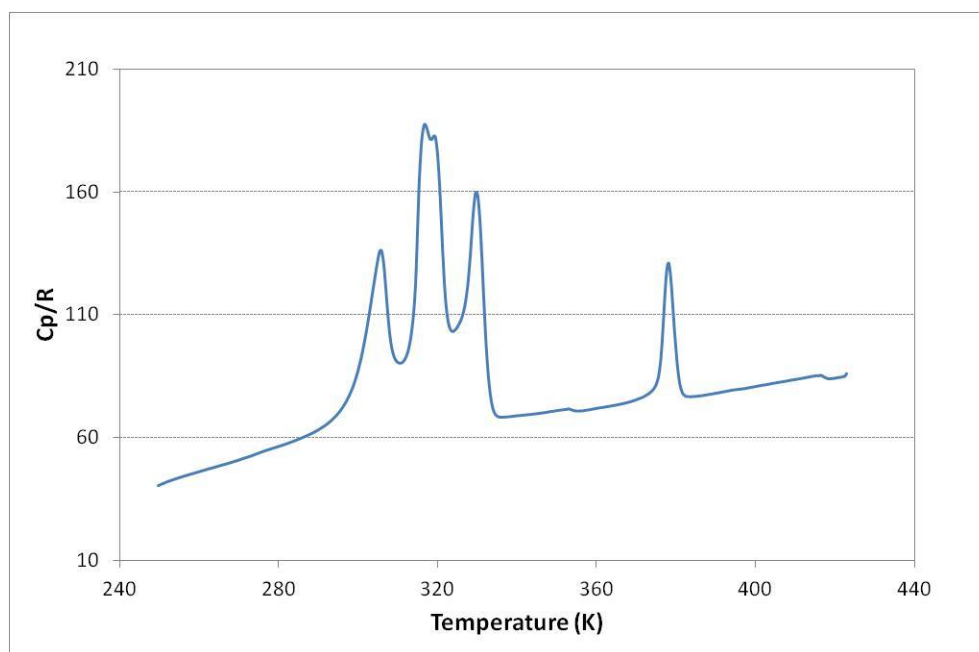


Figure S 269. Experimental molar heat capacities for Cs-dodecanoate ( $R = 8.31451 \text{ JK}^{-1}\text{mol}^{-1}$ )